AN INVESTIGATION OF NAADP-DEPENDENT CA^{2+} SIGNALLING MECHANISMS IN ARTERIAL SMOOTH MUSCLE

Nicholas P. Kinnear

A Thesis Submitted for the Degree of PhD
at the
University of St. Andrews

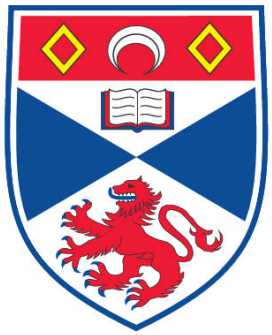

2007

An investigation on NAADP-dependent Ca^{2+} signalling mechanisms in arterial smooth muscle

Nicholas Patrick Kinnear

A thesis submitted to the University of St Andrews for the degree of Doctor of Philosophy

School of Biology
University of St Andrews

January 2007

Declarations

I, Nicholas Patrick Kinnear, hereby certify that this thesis, which is approximately 73,000 words in length, has been written by me, that it is the record of work carried out by me and that it has not been submitted in any previous application for a higher degree.

Date: Signature of candidate:

I was admitted as a research student in October 2001 and as a candidate for the degree of PhD in October 2002; the higher study for which this is a record was carried out in the University of St Andrews between 2001 and 2006.

Date: Signature of candidate:

I hereby certify that the candidate has fulfilled the conditions of the Resolution and Regulations appropriate for the degree of PhD in the University of St Andrews and that the candidate is qualified to submit this thesis in application for that degree.

Date: Signature of supervisor:

In submitting this thesis to the University of St Andrews I understand that I am giving permission for it to be made available for use in accordance with the regulations of the University Library for the time being in force, subject to any copyright vested in the work, not being affected thereby. I also understand that the title and abstract will be published, and that a copy of the work may be made and supplied to any *bona fide* library or research worker.

Date: Signature of candidate:

I confirm that the experiments described in this thesis were performed by me and me alone, with the one exception of those experiments highlighted in Chapter 3 which were performed in association with Dr. Francois-Xavier Boittin during my initial training in the use of the whole-cell patch clamp technique.

Date: Signature of candidate:

Acknowledgements

There are so many people who deserve thanks and I am really sorry to anyone I miss out!

Firstly I would like to thank Dr. Mark Evans for giving me this opportunity and for everything you have done for me over the course of my PhD. It has been a great journey for me and your support and encouragement have helped me get to the end.

To everyone else in the Evans group, starting with Chris and Jill. Thanks for helping me with my constant queries, along with your endless help, advice with my thesis and your technical expertise in the lab. You guys have been great to work with. To the newer members of the group, Elisa and Pete, cheers for putting up with my rants and grumpiness while I have been writing up. It comes to us all, I promise!! (Mocha cheesecake definitely helps in the dark times)

Thanks also to everyone who has helped me with technical support and advice in the Bute and the BMS over the course of my work, especially Dr. Francois Boittin for his patience while I learned to patch.

Grant Churchill, Justyn Thomas and everyone else that I worked with during my time in Oxford. For the help in the lab and making me feel so welcome I thank you guys so much, I loved every minute. It really is amazing how much binding can be achieved in the Rose and Crown!

Thanks to Madras Rugby club and everyone involved with it, thanks for the distraction, the banter, the friendship and the camaraderie during the past 4 years. If I couldn't have vented on the paddock I think I might have gone nuts!

To all the members of the Clan, I can't fit you all in here individually but thanks to every single one of you for the interest, kindness and endless encouragement you have given me.

Finally, the most important people through all of this:

Beccy, my time in St Andrews has been the hardest, but thanks to you, some of the happiest times I've ever known, you give me the belief in myself that I sometimes lack and for that I have to say "Cheers Dr. Dollface!"

Mum, Dad, Chris, Shona Ann, Jamie and Luke. The greatest family and the best influence anyone could ask for. I could never put into words just what you have done for me over the years but I think you have an idea of how much I appreciate everything. You have supported and encouraged me in everything I've ever done and for that I am eternally grateful.

This work was funded by the Biotechnology and Biological Sciences Research Council (BBSRC).

Abstract

Previous investigations on pulmonary artery smooth muscle cells have shown that nicotinic acid adenine dinucleotide diphosphate (NAADP) evokes highly localised intracellular Ca^{2+} bursts by mobilising thapsigargin-insensitive Ca^{2+} stores. Such localised Ca^{2+} signals may initiate global Ca^{2+} waves and contraction of the myocytes through the recruitment of ryanodine receptors (RyR) located on the sarcoplasmic reticulum (SR) via Ca^{2+}-induced Ca^{2+}-release (CICR). In this thesis I have shown that NAADP evokes localised Ca^{2+} signals through the mobilisation of a bafilomycin A1-sensitive, lysosome-related Ca^{2+} store. Lysosomal Ca^{2+} stores facilitate this process by colocalising with a subpopulation of RyRs on the surface of the SR to comprise a highly specialised trigger zone for Ca^{2+} signalling by NAADP. I have also shown that the proposed trigger zone for NAADP-dependent Ca^{2+} signalling may be formed between lysosomes and clusters of RyR subtype 3 (RyR3) located in close proximity to one another in the perinuclear region of cells. Localised Ca^{2+} bursts generated by NAADP-dependent Ca^{2+} release from acidic Ca^{2+} stores and subsequent CICR via RyR3 on the SR may then amplify Ca^{2+} bursts into a propagating Ca^{2+} signal by recruiting clusters of RyR subtype 2 (RyR2) located in the perinuclear and extra-perinuclear regions of the cell. The presence of this trigger zone may explain, in part, why Ca^{2+} bursts by NAADP induce, in an all-or-none manner, global Ca^{2+} signals by CICR via RyRs on the SR. Consitent with a role for NAADP and lysosomes as a discrete and agonist-specific Ca^{2+} signalling pathway utilised by vasoconstrictors, I have shown that endothelin-1 (ET-1), but not phenylephrine or prostaglandin-$F_{2\alpha}$, mobilises Ca^{2+} stores by NAADP, and that ET-1 initiates Ca^{2+} signalling by NAADP in a receptor subtype-specific manner through the activation of ETB receptors. These findings further advance our understanding of how that spatial organisation of discrete, organellar Ca^{2+} stores underpin the generation of differential Ca^{2+} signalling patterns by different Ca^{2+}-mobilising messengers.

Table of contents

Chapter 1: Introduction

1.1 The circulatory system

Blood vessels form an enclosed system which functions to transport blood throughout the body. These blood vessels form two systems of tubes which both begin and end at the heart. One system, the pulmonary circulation serves to transport deoxygenated blood from the right ventricle of the heart to the lungs and oxygenated blood back to the left atrium. The structure and function of the pulmonary circulation will be described in detail below. The other system, the systemic circulation, carries oxygenated blood from the left ventricle to the tissues in all other parts of the body before returning deoxygenated blood to the right atrium. Based upon their structure and function, blood vessels can be classified as either, arteries, capillaries or veins (Pugsley and Tabrizchi, 2000).

1.1.1 Arteries

Arteries function to carry blood away from the heart. Initially blood is pumped from the heart into large elastic arteries which branch into repeatedly smaller arteries whose internal diameter and wall thickness decrease as they approach the periphery. Arteries are also seen to change histologically as they branch. The aorta is predominantly an elastic structure which is ideally suited to receiving the surge in blood delivered by contraction of the heart. Peripheral arteries become increasingly more muscular until the arterioles, where the muscular layer predominates. In large arteries, frictional resistance is relatively small and as a result pressures are only slightly less than that found in the aorta. In contrast, small arteries offer moderate resistance to blood flow which reaches a maximal level in the arterioles. Adjustments in the degree of contraction of the circular muscle of these small blood vessels allows regulation of the blood flow to tissues and aids in the control of arterial blood pressure. Coupled with the reduction in pressure along the arterioles, there is also a change from the pulsatile arterial blood flow, due to the intermittent ejection of blood from the heart, to a steady flow of blood into capillaries. This

change in blood flow is achieved by a combination of factors, the compliance of large arteries and the frictional resistance in the small arteries and arterioles. Both the arteries and the veins are composed of the following three layers. The innermost layer, the tunica intima (also called tunica interna), is simple squamous epithelium, known as the endothelium, and is surrounded by a connective tissue basement membrane with elastic fibres. The middle layer, the tunica media, is primarily made up of smooth muscle and is usually the thickest of the three layers. The outermost layer, which attaches the vessel to the surrounding tissue, is the tunica externa or tunica adventitia. This layer consists of mostly connective tissue with varying amounts of elastic and collagenous fibers. The connective tissue is quite dense where it is adjacent to the tunica media, but it changes to loose connective tissue near the periphery of the vessel (Pugsley and Tabrizchi, 2000).

1.1.2 Capillaries and the microcirculation

The capillaries consist of a single layer of endothelial cells which permit rapid exchange of gases, water and solutes with interstitial fluid. The distribution of capillaries within the body varies between tissues. Metabolically active tissue such as cardiac muscle and glandular structures, have a high density of capillaries whereas less active tissue, such as subcutaneous tissue or cartilage have a low density of capillaries. Although blood flow through capillaries is not pulsatile, it is not uniform and depends chiefly upon the contractile state of arterioles (Pugsley and Tabrizchi, 2000).

1.1.3 The endothelium

For many years, the endothelium of blood vessels was regarded as an inert layer of cells which served solely as a passive filter permitting the movement of water and other small molecules across the blood vessel wall, while retaining blood cells and proteins within the vascular lumen. However, it is now clear that the endothelium plays an important role in regulating blood clot formation and is also an important source of a number of vasoactive substances such as Nitric oxide (NO), prostacyclin and endothelins, which can

cause contraction or relaxation of the underlying vascular smooth muscle (Berne, *et al.*, 2004).

Early studies showed that endothelial cells were able to release a labile factor, which was initially termed endothelium-derived relaxing factor (EDRF) which diffused to the adjacent smooth muscle layer to induce relaxation (Furchgott and Zawadski, 1980), at least in part through the formation of cGMP (Rapoport and Murad, 1983). Biochemical experiments showed that nitroglycerin elicits blood vessels relaxation following conversion to NO with the subsequent formation of cGMP (Moncada, *et al.*, 1991). Subsequent work provided strong evidence that NO was indeed very similar to EDRF (Ignarro, *et al.*, 1987; Palmer, *et al.*, 1987). NO is formed from its substrate L-arganine by nitric oxide synthase (NOS) producing NO and citrulline. There are two forms of NOS in cells, constitutive NOS (cNOS) and inducible NOS (iNOS). NO is continually produced by cNOS, the cNOS present in vascular endothelial cells is termed eNOS, the activity of which is regulated by the intracellular Ca^{2+} concentration. Thus, substances such as acetylcholine, bradykinin, histamine and insulin that induce increases in the intracellular Ca^{2+} concentration are able to stimulate the production of NO via cNOS. Another important regulator of NO production is shearing forces acting on the endothelium. Thus, an increase in blood flow velocity can stimulate extracellular Ca^{2+} influx and intracellular Ca^{2+} release in endothelial cells and an increase in NO production via cNOS. iNOS is not Ca^{2+}-dependent and is stimulated by the actions of a number of bacterial toxins and different cytokines such as tumour necrosis factor and a number of interleukins. Induction of iNOS occurs over several hours and results in NO production that may be up to 1000-fold greater than that produced by cNOS. This is an important mechanism in the pathogenesis of inflammation. Following formation of NO in an endothelial cell, it can readily diffuse into adjacent smooth muscle cells where it binds to a heme moiety on guanylyl cyclase, activating the enzyme to produce cGMP from GTP. Increased cGMP causes activation of a protein kinase, subsequently leading to the inhibition of Ca^{2+} influx into the smooth muscle cells, and a decrease in the stimulation of myosin light chain kinase (MLCK) by the Ca^{2+}:Calmodulin complex, this ultimately

leads to relaxation of the smooth muscle cell (Kiechle and Malinski, 1993; Gross and Wolin, 1995).

1.1.4 Veins

Veins function to return blood to the heart once it leaves the microcirculation. Upon leaving capillaries blood enters the smallest of veins, termed venules. From the venules, blood flows to progressively larger veins until reaching the heart. As described above, the walls of veins consist of the same three layers as arteries. However, veins have less smooth muscle and connective tissue than arteries thus the walls of veins appear much thinner. Although under a lower pressure than arteries, the internal diameter of veins can be altered by the vasomotor actions of the smooth muscle present in the vessel wall. These changes in resistance and the subsequent alterations in pressure within the lumen of the vessel may not be as great as the changes afforded by the thicker arteries, but they are believed to influence the pressure within the capillary vessel upstream (Milnor, 1982). Larger veins contain venous valves, similar to the semilunar valve in the heart, to maintain the direction of blood flow. These valves are especially important in the arms and legs, preventing backflow in response to the pull of gravity (Berne, *et al.*, 2004).

1. 2 Smooth muscle

Smooth muscle is found in all the hollow organs of the body from the intestine to the walls of the blood vessels. There are many differences between smooth muscle cells from different areas within the body, and even amongst different cells from within the same smooth muscle bed. Smooth muscle can be broadly classified into two types, phasic and tonic (Somlyo and Somlyo, 1968; Somlyo and Somlyo, 1990). Phasic smooth muscle generates action potentials and responds with fast, transient contractions to depolarisation of tissue with high K^+ solutions. Tonic smooth muscle on the other hand, does not usually generate action potentials and shows slow, sustained contraction in response to K^+-induced depolarisation (Somlyo and Somlyo, 1968). The vascular system

contains both phasic (e.g. portal vein) and tonic (e.g. pulmonary artery, aorta) smooth muscle (Jones, 1981).

Fluctuations in intracellular Ca^{2+} concentration are the main regulatory mechanism governing contraction of all muscle cells (Filo, *et al.*, 1965). The extracellular Ca^{2+} concentration and the Ca^{2+} concentration within the intracellular stores are significantly higher than that found in the cytoplasm of smooth muscle cells. Therefore, this results in an enormous concentration gradient which allows Ca^{2+} influx, or Ca^{2+} release to occur without the requirement for further energy expenditure. In vascular smooth muscle, fluctuations in cytosolic Ca^{2+} concentration are achieved through the opening of a variety of ion channels located on the plasma membrane or the membranes of intracellular Ca^{2+} stores allowing the influx/efflux of Ca^{2+}.

1.2.1 Excitation-contraction coupling in smooth muscle

The processes which govern contraction of smooth muscle are complex and a large volume of research has been carried out in order to gain an understanding of the mechanisms underlying "excitation-contraction coupling" in vascular smooth muscle. It would appear that excitation-contraction coupling in smooth muscle can be subdivided into two main processes, electromechanical coupling and pharmacomechanical coupling (Somlyo and Somlyo, 1968). Electromechanical coupling describes alterations in the plasma membrane potential and the subsequent effects this has on cytoplasmic Ca^{2+} concentration. The resting membrane potential of smooth muscle cells lies between -40 and -70 mV depending on the smooth muscle type. If the membrane potential becomes more positive (depolarises), this can lead to the opening of a number of ion channels, including voltage-gated Ca^{2+} channels (VGCCs), with resultant Ca^{2+} influx, increased intracellular Ca^{2+} concentration and contraction (Somlyo and Himpens, 1989). As the membrane potential becomes more negative, VGCCs are closed and the intracellular Ca^{2+} concentration decreases leading to relaxation of the smooth muscle.

In contrast to electromechanical coupling, pharmacomechanical coupling is initiated by the actions of a number of cell signalling pathways that may alter the force of contraction without necessarily altering the membrane

potential of the cell. The major mechanisms of pharmacomechanical coupling involve the production of the Ca^{2+} mobilising second messengers such as inositol 1, 4, 5-trisphosphate (IP_3), cyclic adenosine diphosphate ribose (cADPR) and nicotinic acid adenine dinucloetide phosphate (NAADP; Li, *et al.*, 2003). Initiation of pharmacomechanical coupling by these and related signalling cascades may also promote transmembrane Ca^{2+} influx via the activation of sarco/endoplasmic reticulum store-depletion activated influx to support store-refilling, and/or via the regulation of receptor-operated cation channels (Somlyo, *et al.*, 1999; Morano, 2003). These mechanisms will be discussed below.

1.2.2 The role of K^+ channels in the regulation of smooth muscle membrane potential

VGCCs act as a major source of contractile Ca^{2+} in a number of smooth muscle cells, including vascular smooth muscle and are activated by depolarisation of the plasma membrane. Thus, there exists a tight coupling between the membrane potential and the contractile state of smooth muscle cells. The membrane potential of smooth muscle cells is governed by a balance between depolarising and hyperpolarising ion channels present within the plasma membrane which can induce contraction and relaxation of cells, respectively. The depolarisation of smooth muscle cells is mediated by the activity of VGCCs, chloride channels and non-selective cation channels. K^+ channels function as the main source of hyperpolarising currents in smooth muscle and provide a precise negative feedback mechanism upon excitation of cells. Thus, K^+ channels can act to promote relaxation of cells by inhibiting Ca^{2+} influx through VGCCs in the plasma membrane (Nelson and Quayle, 1995). A number of types of K^+ channel have been identified as modulators of smooth muscle membrane potential and contractility including voltage-gated (Kv), large conductance Ca^{2+}-activated (BK_{Ca}), inward rectifier (Kir), ATP-sensitive (K_{ATP}) and two-pore domain K^+ channels (K_{2P}).

1.2.2.1 Voltage activated K^+ channels

As mentioned previously, Kv channels are activated by membrane depolarisation with activation thresholds in the range of basal membrane potentials reported for smooth muscle cells where they act to limit depolarisation of the plasma membrane and Ca^{2+} entry (Nelson and Quayle, 1995; Heppner, *et al.*, 1997; Koh, *et al.*, 1999). The blockade of Kv channels leads to the depolarisation and contraction of smooth muscle cells (Knot and Nelson, 1995). Kv currents have been recorded from a number of smooth muscle cells including vascular smooth muscle (Beech and Bolton, 1989; Aiello, *et al.*, 1995; Remillard and Leblanc, 1996; Smirnov, *et al.*, 2002). Kv currents in smooth muscle cells can be divided into 2 types based upon their rates of inactivation. Thus, they can be categorised as either slowly inactivating Kv currents that show little or no inactivation during depolarisations of 250 ms (delayed rectifier, K_{dr}) or fast inactivating Kv currents that inactivate within 100 ms (A-type). While K_{dr} have been identified in almost all smooth muscle cells studied, A-type currents tend to be expressed in phasic smooth muscle cells, such as the aorta (Halliday, *et al.*, 1995). A "non-inactivating" Kv current (I_{KN}) has also been identified in smooth muscle cells of the pulmonary artery which activates between -80 and -65 mV (Evans, *et al.*, 1996). Due to the non-inactivating nature of the I_{KN} currents it has been suggested that this current may provide a tonic hyperpolarisation of the smooth muscle resting membrane potential. Indeed, recent evidence suggests that these I_{KN} currents may be due to the actions of the twin-pore domain K^+ channel, TASK-1 (Gurney, *et al.*, 2003) and KCNQ class of Kv channels (Joshi, *et al.*, 2006).

The diversity in Kv currents in smooth muscle cells is achieved by tissue-specific differences in the expression and assembly patterns of members of the Kv channel superfamily composed of pore-forming α-subunit families Kv1 – Kv4. Members of the same Kv family assemble to form in a homo- or hetero-tetrameric manner functional channels. Kv5 – Kv11 α-subunit families are unable to form functional channels when expressed alone, but may form functional channels when co-assembled with either Kv2 or Kv3 to produce channels with distinct properties to channels composed of either Kv2 or Kv3

alone (Hugnot, *et al.*, 1996; Salinas, *et al.*, 1997; Kramer, *et al.*, 1998; Stocker, *et al.*, 1999).The diversity of Kv channels is further increased by the existence of modulatory β-subunits expressed in smooth muscle which co-assemble with pore-forming Kv subunits in smooth muscle to modulate the biophysical properties and trafficking of Kv channels to the membrane (Pongs, *et al.*, 1999).

1.2.2.2 Large conductance Ca^{2+}-activated K^+ channels

In a number of cell types, an increase in intracellular Ca^{2+} concentration is linked to membrane hyperpolarisation by Ca^{2+}-activated K^+ channels. On the basis of unitary conductance and pharmacological properties, and recently due to the identification of the relevant genes, there have been three types of Ca^{2+}-activated K^+ channels identified. These are the BK_{Ca}, the intermediate conductance (IK_{Ca}) and the small conductance (SK_{Ca}) channels.

BK_{Ca} channels have been observed in all types of smooth muscle cells examined to date, along with a number of other cell types (Nelson and Quayle, 1995). BK_{Ca} channels are voltage-activated K^+ channels, which are additionally activated by increases in the local cytoplasmic Ca^{2+} concentration. Binding of Ca^{2+} to the BK_{Ca} channels shifts the voltage at which channels are activated to more negative membrane potentials which lie within the physiological range of smooth muscle (Cox and Aldrich, 2000). BK_{Ca} channels function in a negative feedback role to help regulate smooth muscle membrane potential. Depolarisation-evoked Ca^{2+} entry via VGCCs activates BK_{Ca} channels resulting in hyperpolarisation and the prevention of further Ca^{2+} entry via VGCCs (Klockner and Isenberg, 1985; Guia, *et al.*, 1999).

Vasodialtors that activate adenylyl cyclase-coupled receptors, such as β-adrenoceptors, relax arterial smooth muscle by increasing cAMP levels and activating protein kinase A (PKA). Vasodilation by PKA-dependent signalling is mediated, in part, by BK_{Ca} channel activation and hyperpolarisation of the plasma membrane (Benham and Bolton, 1986; Kume, *et al.*, 1989; Nelson, *et al.*, 1995; Satake, *et al.*, 1996; Wang and Kotlikoff, 1996a; Knot, *et al.*, 1998b; Porter, *et al.*, 1998; Tanaka, *et al.*, 1998; Perez, *et al.*, 1999; Jaggar, *et al.*,

2000). There is evidence in the literature to suggest that PKA may activate these channels by phosphorylating the BK_{Ca} channel protein (Kume, *et al.*, 1989; Wang and Kotlikoff, 1996a; Jaggar, *et al.*, 2000) and/or RyRs located on the sarcoplasmic reticulum (SR) membrane (Valdivia, *et al.*, 1995; Jaggar, *et al.*, 2000), or via activation of the SR Ca^{2+} ATPase, increasing the SR Ca^{2+} concentration, thus increasing resting SR Ca^{2+} release in close proximity to the plasma membrane (Lindemann, *et al.*, 1983; Jaggar, *et al.*, 2000; Wellman, *et al.*, 2001). However, work from this laboratory has provided evidence in favour of an alternative mechanism by which adenylyl cyclase-coupled receptors may mediate vasodilation by cADPR-dependent Ca^{2+} release via RyRs in the SR (Boittin, *et al.*, 2003). This role for cADPR in mediating arterial vasodilation via BK_{Ca} channels is discussed in detail in section 1.5.7.

A role for BK_{Ca} channels in responses to cell stretching has been shown in a number of smooth muscle types including vascular smooth muscle (Kirber, *et al.*, 1992; Wellner and Isenberg, 1993; Wu and Davis, 2001). This activation by stretching may be induced by intracellular Ca^{2+} release (Ji, *et al.*, 2002), or via the influx of extracellular Ca^{2+} (Wu and Davis, 2001). Indeed, the activation of BK_{Ca} channels in response to increases in pressure/stretch would provide a mechanism to combat stretch-evoked depolarisation of smooth muscle cells.

The pore-forming subunit of BK_{Ca} channels is similar to that of the K_v channels (Wallner, *et al.*, 1996). Only 1 pore-forming α-subunit has been identified to date, producing a number of splice variants that may help to explain BK_{Ca} diversity (Vogalis, *et al.*, 1996). The diversity of BK_{Ca} channels is also provided by at least 4 different BK_{Ca} β-subunits which coassemble with the α-subunits to modulate the biophysical properties of BK_{Ca} channels (Uebele, *et al.*, 2000). Specifically the β_1-subunit is highly enriched in smooth muscle tissues and confers Ca^{2+} sensitivity to the α-subunit (McManus, *et al.*, 1995). When the α-subunit is co-expressed with the β_1-subunit, currents possess faster activation kinetics and are larger at negative membrane potentials, indicating a higher "open probability" at those potentials. The membrane potential needed to half-activate the channel shifts from 0 to near –100 mV with coexpression of the α- and β_1-subunits (Jiang, *et al.*, 1999).

The pore forming α-subunit of BK_{Ca} channels shares little sequence homology to the pore-forming protein of IK_{Ca} and SK_{Ca} channels. The IK_{Ca} channel (KCNN4) belongs to the same gene family as the SK_{Ca} and shares about 40% sequence homology. SK_{Ca} channels consist of three members, SK_{Ca}1, 2 and 3 (termed KCNN1, 2 and 3, respectively), which share 60-70% sequence homology (Kohler, *et al.*, 1996). These channels require CaM for Ca^{2+} sensitivity (unlike BK_{Ca} channels that have an intrinsic Ca^{2+} sensor). CaM binds constitutively to the proximal section of the C-terminus and acts as the Ca^{2+} sensor (Xia, *et al.*, 1998). A number of reports have suggested a role for SK_{Ca} and IK_{Ca} channels in regulation of vascular smooth muscle tone (Prieto, *et al.*, 1998; Crane and Garland, 2004; McNeish, *et al.*, 2006). Despite these reports, the distribution of these channels in human tissues is less than clear and it is still unknown which SK_{Ca} subtype is present on vascular smooth muscle.

1.2.2.3 Inward rectifier K^+ channels

Kir channels have been shown to be present in vascular smooth muscle cells isolated from small arteries and in segments of arterioles (Edwards, *et al.*, 1988; Quayle, *et al.*, 1993; Quayle, *et al.*, 1996). Indeed, Kir channels demonstrate a decrease in density as vessel size increases (Quayle, *et al.*, 1996) and are absent from large blood vessels (Quayle, *et al.*, 1997). Kir channels in vascular smooth muscle demonstrate a strong inward rectification, with an attenuated outward current at membrane potentials positive to the equilibrium potential of K^+ (~ -85 mV) and increased inward current negative to the K^+ equilibrium potential (Quayle, *et al.*, 1997; Bradley, *et al.*, 1999). The inward rectification of the channels is due to a mixture of intrinsic channel properties coupled with the internal blockade of the channels by Mg^{2+} and polyamines (Ruppersberg, 2000). Thus the current carried by Kir channels in vascular smooth muscle under resting membrane potentials (-30 to -60 mV) is very small indeed. Yet, Kir channels may be important when the concentration of extracellular K^+ increases, resulting in systemic arterial dilation (Quayle, *et al.*, 1997). This may occur as a result of the increase in external K^+ concentration

driving a positive shift in the reversal potential for K^+ ions across the plasma membrane which causes an increase in the outward Kir current occurring in the range of vascular smooth muscle membrane potential.

To date there have been 6 members of the Kir family of channels cloned (Kir1 – 6), of which the subfamily Kir2 demonstrate strong inward rectification (Quayle, *et al.*, 1997) consistent with native vascular smooth muscle (Edwards, *et al.*, 1988; Quayle, *et al.*, 1993; Quayle, *et al.*, 1996; Kamouchi, *et al.*, 1997). Kir2.1 has been implicated as the gene encoding vascular smooth muscle Kir currents and indeed Kir2.1 is the only member of the Kir2 family that is expressed in smooth muscle cells of the coronary, mesenteric and cerebral arteries, having markedly similar properties to the Kir currents observed in these smooth muscle cells (Bradley, *et al.*, 1999).

1.2.2.4 ATP-sensitive K^+ channels

K_{ATP} channels were first identified in cardiac muscle cells in the early 1980's (Noma, 1983) and have since been shown to play an important role in the control of smooth muscle contractility (Quayle, *et al.*, 1997). Gating of K_{ATP} channels is inhibited by the cytoplasmic concentration of ATP, with channels being activated in response to a decrease in cellular ATP concentration, as occurs in hypoxia or metabolic inhibition. They are activated by a number of K^+ channel openers, while they are inhibited by antidiabetic sulphonylurea drugs such as glibenclamide (Quayle, *et al.*, 1997). Indeed, the ability of K_{ATP} channel openers to hyperpolarise and cause relaxation has been demonstrated in smooth muscle from a number of tissues including the urinary bladder (Petkov, *et al.*, 2001) and blood vessels (Standen, *et al.*, 1989). K_{ATP} channels have been proposed to play a role in the maintenance of basal smooth muscle tone, as indicated by the ability of glibenclamide to depolarise the membrane potential and increase tone (Daut, *et al.*, 1994; Gardiner, *et al.*, 1996). Single-channel recordings of K_{ATP} channels from smooth muscle have demonstrated a large degree of variability, with conductance values ranging from 10 to 280 pS (Quayle, *et al.*, 1997). Single channel K_{ATP} channels recorded from rabbit portal vein, guinea-pig coronary and rat mesenteric artery smooth muscle cells have been termed K_{NDP} channels as, unlike other smooth

muscle K_{ATP} channels, they are activated by cytoplasmic nucleoside diphosphates, such as ADP and GDP (Kajioka, *et al.*, 1991; Beech, *et al.*, 1993a; Beech, *et al.*, 1993b; Dart and Standen, 1993; Dart and Standen, 1995; Zhang and Bolton, 1996). At the level of the single channel, K_{NDP} channels, but not the larger conductance K_{ATP} channels, are inhibited by PKC activation. This is consistent with the inhibition of whole-cell K_{ATP} currents by agonists leading to PKC activation (Kleppisch and Nelson, 1995; Bonev and Nelson, 1996).

It has recently been shown that mice lacking in the expression of the genes which encode smooth muscle K_{ATP} channels are hypertensive and die prematurely due to coronary artery vasospasm (Chutkow, *et al.*, 2002; Miki, *et al.*, 2002). K_{ATP} channels are formed by the co-assembly of the pore-forming Kir6 family members Kir6.1 or Kir6.2 and sulphonylurea receptor proteins SUR1, SUR2A or SUR2B (Aguilar-Brtyan, *et al.*, 1998). Recently Kir6.1 has been shown to be the pore-forming subunit responsible for K_{ATP} channels in vascular smooth muscle in studies carried out using Kir6.1 and Kir6.2 KO mice (Suzuki, *et al.*, 2001; Miki, *et al.*, 2002). Thus it would appear that K_{ATP} channels containing Kir6.1 subunits are the dominant channel type in vascular smooth muscle.

1.2.2.5 Two-pore domain K^+ channels

Background or 'leak' K^+ channels, as defined by having a lack of time- and voltage-dependency, are believed to play a key role in setting the resting membrane potential of excitable cells (Kim, *et al.*, 1998; Millar, *et al.*, 2000). K_{2P} channels have been shown to conduct several leak K^+ currents and are believed to be involved in the regulation of a number of other important cellular functions such as sensing of oxygen and pH (Patel and Honore, 2001) and mechanosensitivity of cells (Chemin, *et al.*, 2005). Selective pharmacology for K_{2P} channels is unavailable and detailed information regarding these channels has to be gleaned from studies carried out on cloned channels expressed in model cells.

K_{2P} channels consist of four transmembrane domains and 2 pore domains. In mammals there have been six distinct sub-families of K_{2P} channels

identified and 15 genes which encode K_{2P} channels (Sanders and Koh, 2006). To date there have been limited reports of K_{2P} channels in vascular smooth muscle cells. However, Gurney and colleagues have shown that TASK-1 channels are expressed in pulmonary artery smooth muscle of rabbits (Gurney, *et al.*, 2003). In their study they identified a functional conductance that was inhibited by extracellular pH, Zn^{2+} and anandamide. This conductance was insensitive to Ca^{2+}, 4-amino pyridine and quinine (Gurney, *et al.*, 2003). These pharmacological properties closely resemble the pharmacology of natively expressed TASK-1 channels and the authors concluded that TASK-1 channels may play an important role in regulation of resting membrane potential in pulmonary arteries. More recently, Olschewski and colleagues have shown that TASK-1 channels are functionally expressed in human pulmonary artery smooth muscle where they are also important in the regulation of resting membrane potential (Olschewski, *et al.*, 2006).

1.2.3 A role for Cl^- channels in modulation of smooth muscle membrane potential?

Both the molecular basis and the physiological role of chloride channels in smooth muscle are yet to be fully understood. However, it would appear that smooth muscle cells express both Ca^{2+}-activated Cl^- channels and volume sensitive Cl^- channels.

1.2.3.1 Ca^{2+}-activated Cl^- channels

Ca^{2+}-activated Cl^- channels have been shown to underlie transient inward currents elicited by agonist-mediated SR Ca^{2+} release in smooth muscle cells (Byrne and Large, 1988; Amedee, *et al.*, 1990; Fleischmann, *et al.*, 1997; Wang and Kotlikoff, 2000). It has also been shown that dialysis of arterial smooth muscle cells with Ca^{2+} activates Ca^{2+}-activated chloride currents which are regulated by Ca^{2+}-dependent phosphorylation/dephosphorylation mechanisms (Greenwood, *et al.*, 2001; Ledoux, *et al.*, 2003; Greenwood, *et al.*, 2004). Although Ca^{2+}-activated Cl^- channels are unable to gate the flux of Ca^{2+} ions, at resting membrane potentials in smooth muscle they can provide a

depolarising influence. It has been suggested that Ca^{2+}-activated Cl^- currents may provide the link between stimulations which mediate SR Ca^{2+} release and depolarisation of the plasma membrane, thus facilitating VGCC activity. Spontaneous transient inward currents mediated by Ca^{2+}-activated Cl^- channels have been identified in smooth muscle cells from a number of tissues, including vascular smooth muscle (Hogg, *et al.*, 1993a; Hogg, *et al.*, 1993b; Yuan, 1997; Craven, *et al.*, 2004).

1.2.3.2 Volume sensitive Cl^- channels

Cl^- currents that are sensitive to cellular volume and which are activated by cell swelling have been identified in a number of smooth muscle cells (Xu, *et al.*, 1997; Yamazaki, *et al.*, 1998). Like Ca^{2+}-activated Cl^- currents, these volume sensitive Cl^- currents are able to provide a depolarising inward current under normal physiological conditions. Thus, it has been suggested that swelling activated Cl^- channels may contribute to stretch/pressure induced contraction of smooth muscle via the activation of VGCCs. The mechanism which mediates activation of these volume sensitive Cl^- currents in vascular smooth muscle of pulmonary arteries is believed to involve protein kinase C (PKC) as PKC inhibitors increase, while PKC activators decrease swelling activated Cl^- currents (Zhong, *et al.*, 2002). Although the precise molecular identity of the volume-sensitive Cl^- channels has yet to be conclusively identified, the ClC-3 channel, a member of the voltage-dependent ClC Cl^- channel family (Jentsch, *et al.*, 2002), has been proposed as a candidate protein (Duan, *et al.*, 1997). ClC-3 has been identified in vascular smooth muscle of the aorta and the pulmonary artery (Yamazaki, *et al.*, 1998; Lamb, *et al.*, 1999). Indeed, ClC-3 has been recently implicated as having an important role in the proliferation, growth and volume regulation of vascular smooth muscle cells (Wang, *et al.*, 2002; Dai, *et al.*, 2005). However, the role of ClC-3 in regulation of arterial tone remains unclear (Nakazawa, *et al.*, 2001).

1.2.4 Ca^{2+} influx pathways in vascular smooth muscle

Mechanisms of Ca^{2+} flux must be highly regulated in order to effectively control a variety of discrete Ca^{2+}-sensitive processes within the cell. The main routes of Ca^{2+} influx into the cytoplasm from the extracellular environment are mediated via three main groups of channel proteins: (1) VGCCs, (2) Receptor-operated (or ligand-gated) Ca^{2+} channels (ROC), and (3) Store-operated Ca^{2+} channels (SOC).

VGCCs belong to a gene superfamily which includes voltage-dependent sodium and potassium channels (Jan and Jan, 1992; Catterall, 1993). They are activated by a conformational change caused by a depolarisation of the cell membrane. VGCC were first described in crustacean muscle (Fatt and Katz, 1953). These channels were then characterised according to their biophysical properties into low- and high-threshold voltage-activated channels (Carbone and Lux, 1984). Following this, studies identified a high-threshold voltage-activated current termed the 'long-lasting' or L-type channel, which was shown to be sensitive to the 1,4-dihydropyridine class of drugs (Hess, *et al.*, 1984; Nowycky, *et al.*, 1985). The L-type Ca^{2+} channels account for the vast majority of VGCCs expressed in vascular smooth muscle cells. VGCC are multimeric complexes which consist of up to four different subunits, namely the $\alpha1$, $\alpha2\delta$, $\beta2$ and γ subunits (Hoffmann, *et al.*, 1994). Of these subunits the $\alpha1$ subunit is the principal subunit, containing the voltage-gated ion pore. To date, there have been ten $\alpha1$ subunits cloned, four of which have been shown to constitute the family of L-type Ca^{2+} channels, namely $Ca_v1.1$, $Ca_v1.2$, $Ca_v1.3$ and $Ca_v1.4$ (Ertel, *et al.*, 2000).

Although these channels are regulated by membrane potential they can also be modulated by the concentration of intracellular Ca^{2+} and more directly by the influence of Ca^{2+}:calmodulin complex (CaM) . L-Type Ca^{2+} channels show two opposing responses to alterations in intracellular Ca^{2+} concentration. On one hand the channels inactivate rapidly with the rise in local Ca^{2+} concentration and, on the other hand, the channels can facilitate further Ca^{2+} entry (Zuhlke and Reuter, 1998; Peterson, *et al.*, 1999; Zuhlke, *et al.*, 1999). As mentioned above, the molecule responsible for the positive feedback, Ca^{2+}-

dependent facilitation of the opening of L-type Ca^{2+} channels has been suggested by a number of studies to be the calmodulin (CaM) activated, multifunctional serine/threonine kinase, calmodulin kinase (CaMK; Tiaho, *et al.*, 1994; Yuan and Bers, 1994; Wu, *et al.*, 1999; Dzhura, *et al.*, 2000). An early study carried out by Yuan and Bers (1994) showed that repetitive membrane depolarisations from -90 – 0 mV in ventricular myocytes from rabbit and ferrets caused a staircase in the Ca^{2+} current across cell membranes. This effect was completely blocked by the dialysis of cells with blockers of CaMK. Similar results to these were obtained by Anderson *et al.* (1994) in rabbit ventricular myocytes, where again, addition of CaMK inhibitory peptides prevented the augmentation in activity of L-type Ca^{2+} channels. That this facilitation of L-type channels is a direct effect of CaMK on the channels was shown in a study using inside-out patches from murine ventricular myocytes (Dzhura, *et al.*, 2000). The stimulatory effect of CaMK required ATP and was not mimicked by CaM alone, however the effect was knocked out by the addition of a CaMK inhibitor.

In contrast, a number of studies have suggested that CaM-dependent inactivation of L-Type Ca^{2+} channels may result from the dephosphorylation of the channel by the CaM-dependent phosphatase calcineurin (Chad and Eckert, 1986; Armstrong, 1989; Schuhmann, *et al.*, 1997). On the other hand however, a number of groups have proposed that CaM directly interacts with the α_1-subunit of the L-type channel and that channel phosphorylation is not involved (Pate, *et al.*, 2000; Peterson, *et al.*, 2000; Romanin, *et al.*, 2000; Zuhlke, *et al.*, 2000). A number of studies have in fact suggested that direct binding of CaM to the α_1-subunit is the critical step in both the Ca^{2+}-dependent activation and inactivation of L-Type Ca^{2+} channels. A mutation in the consensus CaM-binding IQ motif in the COOH-terminal tail of α_1 eliminates both forms of Ca^{2+}-dependent automodulation of Ca^{2+} channels (Zuhlke, *et al.*, 1999; Zuhlke, *et al.*, 2000).

Low-voltage-activated T-type Ca^{2+} channels have also been identified in vascular smooth muscle (Bean, *et al.*, 1986; Benham and Tsien, 1987). The T-type channels are encoded for by a family of genes, $Ca_v3.1$, $Ca_v3.2$ and $Ca_v3.3$ (Perez-Reyes, 2003), with $Ca_v3.1$ but not $Ca_v3.2$ being expressed in

vascular smooth muscle (Brueggemann, *et al.*, 2005). The three T-type channels encoded for by these genes display very similar functional properties and initial electrophysiological studies found it difficult to distinguish between these three subtypes. Recent analysis of cloned T-type channels has provided information on their differing kinetics and pharmacology (Lee, *et al.*, 1999; Martin, *et al.*, 2000; Michels, *et al.*, 2002). However, techniques to distinguish members of the Ca_v3 family at anything other than the molecular level remain limited.

Store-operated Ca^{2+} entry was first described in 1986 (Putney, 1986), although an earlier report had described a "Ca^{2+} readmission" response in acinar cells of the cockroach salivary gland (Ginsborg, *et al.*, 1980). The early work carried out on store-operated Ca^{2+} entry suggested that the level of Ca^{2+} within the stores was critical to controlling Ca^{2+} influx into non-excitable cells. This process was described as capacitative Ca^{2+} entry. The first direct evidence for this model was the identification of a Ca^{2+} current in mast cells which was termed the Ca^{2+} release-activated Ca^{2+} current, or I_{CRAC} (Hoth and Penner, 1992). SOC can be activated by any process which empties intracellular Ca^{2+} stores (Hoth and Penner, 1992; Parekh and Penner, 1997). A number of SOC from various different vascular beds have been reported in the literature such as the aorta (Trepakova, *et al.*, 2001), the portal vein (Albert and Large, 2002) and the pulmonary artery (Golovina, *et al.*, 2001). The molecular makeup of ROC and SOC in vascular smooth muscle remains unclear. However, a number of recent studies suggest a role for Transient Receptor Potential (TRP) channels in forming Ca^{2+}-permeable cation channels that can be activated by store depletion (Ma, *et al.*, 2000; Vasquez, *et al.*, 2001; Bergdahl, *et al.*, 2003), or by receptor activation (Boulay, *et al.*, 1997; Inoue, *et al.*, 2001; Trebak, *et al.*, 2002). Animal and human pulmonary artery smooth muscle cells have been shown to express transcripts of members of the canonical TRP superfamily (TRPC) TRPC1, TRPC4, TRPC5 and TRPC6 suggesting that these channels may form homo-or heterotetrameric channels that can be regulated by agonist-mediated receptor activation and/or store depletion in pulmonary artery smooth muscle cells (McDaniel, *et al.*, 2001; Sweeney, *et al.*, 2002; Yu, *et al.*, 2003). Recently a role for an interaction between the ER-Ca^{2+} sensor STIM1 and the pore forming membrane protein Orai1 in underlying store-operated Ca^{2+} entry

has been proposed (Luik, *et al.*, 2006; Prakriya, *et al.*, 2006; Wu, *et al.*, 2006). It is clear that further investigations are required in order to determine the true molecular identity of these store-operated Ca^{2+} influx mechanisms (Beech, *et al.*, 2004; Parekh and Putney, 2005).

1.2.5 The plasma membrane and Ca^{2+} extrusion mechanisms

The plasma membrane plays an extremely important role in intracellular Ca^{2+} homeostasis and the overall control of Ca^{2+} signalling within many excitable and non-excitable cells. Smooth muscle cells expel Ca^{2+} from the cytoplasm to the extracellular space through two main pumps, the plasma membrane Ca^{2+}-ATPase (PMCA), or via the Na^{+}/Ca^{2+} exchanger. The PMCA uses energy from ATP to pump Ca^{2+} ions up the steep electrochemical gradient which exists between the cytoplasm of the cell and the extracellular environment (Horowitz, *et al.*, 1996). The pump is electron neutral as it transports two H^{+} ions into the cell for every Ca^{2+} ion removed. Therefore, Ca^{2+} extrusion via this mechanism results in an increase in cytoplasmic H^{+} ion concentration which is corrected via the action of various transporter mechanisms such as the sodium/hydrogen exchanger (Hogue, *et al.*, 1991). To date there are no specific inhibitors for the PMCA although non-specific P-type transporter inhibitors have been shown to inhibit them (Carafoli, 1991). The PMCA are the products of a minimum of four different genes, and isoforms 1 to 4 are widely expressed (Carafoli, *et al.*, 1996). Although only coded for by four genes there are to date at least 32 splice variants of the genes that have been identified in mammalian tissues (Strehler and Zacharias, 2001) and these may be important in the targeting of the channels to specific areas of the cells through the interaction of residues found within the splice variants and other specific proteins within the cell (DeMarco and Strehler, 2001; Chicka and Strehler, 2003). For example, PMCA have been shown to localise in caveolae of smooth muscle cells, as well as endothelial cells and cardiac muscle cells (Fujimoto, 1993; Hammes, *et al.*, 1998) where they may be involved in the regulation of a number of signalling pathways. For example, in the cultured cell lines HEK-293 and neuro-2a cells overexpression of PMCA subtype hPMCA4b resulted in a reduction of nitric oxide NO production (Schuh, *et al.*,

2001). It was seen that this inhibition of NO synthesis was due to the interaction of the COOH-terminus of the hPMCA4b and the PDZ domain of neuronal nitric oxide synthase (nNOS). Studies have previously shown that nNOS is expressed within caveolae of vascular smooth muscle cells (Segal, *et al.*, 1999), and recent evidence suggests that in arterial smooth muscle cells of mice, an overexpression of the human PMCA subtype hPMCA4b is associated with enhanced vascular reactivity and an increase in blood pressure through the negative regulation of nNOS (Gros, *et al.*, 2003).

The second of these extrusion mechanisms is the Na^+/Ca^{2+} exchanger. In humans, The Na^+/Ca^{2+} exchanger is encoded for by two gene families, namely SLC8 (Quednau, *et al.*, 2004) and SLC24 (Schnetkamp, 2004). Both of these families of proteins, when expressed, can act in either the forward (Ca^{2+} extrusion) or reverse (Ca^{2+} entry) modes depending on ion concentration gradients and membrane potential (Blaustein and Lederer, 1999). The SLC8 gene family encode Na^+/Ca^{2+} exchangers (NCX) that function independently of K^+ ions. This gene family encodes for three genes, the NCX1, NCX2 and NCX3 exchangers which exchange 3 Na^+ ions for every Ca^{2+} ion (Reeves and Hale, 1984). NCX1 is the most widely studied of the three proteins and has been shown to be expressed ubiquitously with the expression of NCX2 and NCX3 limited to both the brain and skeletal muscle (Lee, *et al.*, 1994c; Nicoll, *et al.*, 1996). NCX have been shown to be expressed in vascular smooth muscle (Juhaszova, *et al.*, 1994), including NCX1 and NCX3 in human pulmonary artery smooth muscle (Zhang, *et al.*, 2005) and has been shown to have a role in cytoplasmic Ca^{2+} homeostasis in blood vessels (Slodzinski, *et al.*, 1995; Shimizu, *et al.*, 1997; Blaustein and Lederer, 1999; Arnon, *et al.*, 2000). The expression of NCX may be important for function in arterial smooth muscle as NCX has been shown to be located in areas where the SR is in close apposition to the plasma membrane (Moore, *et al.*, 1993; Juhaszova, *et al.*, 1994). In these areas of cells there is evidence to suggest that concentrations of Na^+ and Ca^{2+} ions exceed the average values within the cells, and within cardiac myocytes, this may enhance Ca^{2+} extrusion and cytoplasmic clearance through the NCX (Leblanc and Hume, 1990), or indeed Ca^{2+} influx if the concentration of Na^+ is high, i.e., the transporter is able to work in the reverse mode (Levesque, *et al.*, 1991).

There have been five SLC24 genes discovered in man, encoding for five different forms of the K^+-dependent Na^+/Ca^{2+} exchanger (NCKX). These have been termed NCKX1-5 with the distribution of NCKX1-4 well characterised, the distribution of NCKX5 is still unknown (Schnetkamp, 2004). These exchangers have been shown to transport 4 Na^+ for every 1 K^+ and 1 Ca^{2+} ion (Cervetto, *et al.*, 1989). The expression of the NCKX1 and 2 exchangers appears to be extremely tissue-specific with the NCKX1 expressed in rod cells within the eye and platelets, and the NCKX2 expressed mostly in the brain and other neuronal tissue (Schnetkamp, 2004). NCKX3 and 4 have been shown to be expressed in a number of different tissue types, including vascular smooth muscle (Schnetkamp, 2004). A number of studies have been carried out to characterize native exchangers, with the most detailed work being carried out on the NCKX1 (Schnetkamp, 1995), with more recent studies addressing the properties of heterologously expressed NCKX1 and NCKX2 proteins (Szerencsei, *et al.*, 2000; Dong, *et al.*, 2001). However, very little is known about the NCKX3 and NCKX4 exchangers.

1.3 Intracellular Ca^{2+} stores in arterial smooth muscle

1.3.1 The sarcoplasmic reticulum

The sarcoplasmic reticulum (SR) is recognised as being the major intracellular source and sink for Ca^{2+} within both smooth (Somlyo and Somlyo, 1991) and striated muscle (Ebashi, 1991). Ca^{2+} is sequestered into the lumen of the SR from the cytoplasm by the actions of specific sarcoplasmic/endoplasmic reticulum Ca^{2+}-ATPase (SERCA) pumps, which will be described below. The distribution of the SR is different amongst smooth muscle cells with the SR of phasic smooth muscle (e.g. vas deferens, portal vein) accounting for only 2-3 % of total cell volume, and being distributed mainly along the periphery of the cell (Villa, *et al.*, 1993; Nixon, *et al.*, 1994). The SR is much more abundant in tonic vascular smooth muscle where it accounts for around 5-7 % of total cell volume (Devine, *et al.*, 1972) with some of the surface of the SR being closely associated with the plasma membrane of the cell, but with a large proportion located centrally, and in close association with the nucleus.

The SR of vascular smooth muscle cells consists of two types of SR, rough SR and smooth SR. Smooth SR does not contain any ribosomes and is involved in a number of processes such as fatty acid synthesis and metabolism of phospholipids. Rough SR does possess ribosomes and is involved in the synthesis of many extracellular proteins such as elastin and collagen (Pozzan, *et al.*, 1994; Orallo, 1996).

Although there has been a large number of investigations carried out on it, many details of the SR Ca^{2+} stores organistation, and of the Ca^{2+} release and refilling processes are still poorly understood. It is widely accepted that there are two classes of Ca^{2+} release mechanisms, those associated with the Inositol 1,4,5-trisphosphate receptors (IP_3Rs) and those associated with the ryanodine receptors (RyRs; Somlyo and Somlyo, 1994). Whether these receptors are associated with a single, interconnecting Ca^{2+} store, or with functionally independent stores remains a controversial field of research.

The SR membrane is not freely permeable to Ca^{2+} ions. Therefore, as mentioned above, the SR uses specialised SERCA pumps to sequester Ca^{2+} from the cytosol of the cell. The SERCA pumps belong to the P-type family of ATPases, which form a phosphoprotein intermediate and undergo conformational changes during the course of ATP hydrolysis (de Meiss and Vianna, 1979; Jencks, 1992). These pumps use the energy supplied by the hydrolysis of ATP to drive the translocation of Ca^{2+} into the SR lumen. SERCA pumps were first visualised by means of electron microscopy in the late 1960's (Inesi and Asai, 1968). In this study the investigators noted that the there were distinct granules protruding from the cytosolic surface of the SR, which were linked by a narrow stalk to a membrane bound region. These granules have since been shown to correspond to the cytosolic region of the SERCA pump; a ~100 kDa protein which consists of 2 main regions, a hydrophilic region which protrudes into the cytosol of the cell (corresponding to the granules seen by Inesi and Asai (1968)), and a hydrophobic region imbedded in the SR membrane. The ATP binding site has been shown to be located within a groove formed on the cytosolic head of the pump (Yonekura, *et al.*, 1997). The residues that are involved in the hydrolysis of ATP are contained within the stalk section of the protein. SERCA pumps are able to bind and translocate 2 Ca^{2+} ions at a time, and work to generate and maintain a

Ca^{2+} gradient of about 10,000 fold between the lumen of the SR and the cytoplasm of the cell, which is achieved by the utilisation of the energy released by the hydrolysis of ATP, as mentioned previously. SERCA pumps reversibly cycle through a number of conformational states (Dode, *et al.*, 2003), of which four have been stabilised (E_1Ca_2, E_1~P(Ca_2), E_2-P and E_2; Fig. 1.1). The binding of 2 Ca^{2+} ions in the Ca^{2+} binding domain described previously is required for the formation of E_1Ca_2 (Fig. 1.1). This binding of Ca^{2+} ions activates conformational changes allowing the transfer of the γ-phosphoryl group of ATP to the aspartic acid residue at position 351. This phosphorylation induces further conformational changes (E_1Ca_2 to E_1~P(Ca_2) transition; Fig. 1.1) which translocates the two Ca^{2+} binding sites from the cytosolic side of the SR membrane to the luminal side of the SR membrane, this also lowers the affinity of the Ca^{2+} binding sites for Ca^{2+} by around three orders of magnitude. The conversion of E_1~P(Ca_2) to the ADP-insensitive low-energy E_2-P phosphoenzyme intermediate, the rate limiting step in Ca^{2+} translocation across the SR membrane (de Meiss and Vianna, 1979; Inesi, *et al.*, 1990), is accompanied by the loss of Ca^{2+} ions into the ER/SR lumen. This dissociation of Ca^{2+} ions from the pump promotes hydrolysis of Pi on the aspartic acid residue at position 351 of E_2-P and the regeneration of the high affinity Ca^{2+} binding sites open to the cytosolic environment completing the reversible Ca^{2+} transport cycle (Fig. 1.1).

There are three genes which encode for SERCA pumps, with two subtypes of the SERCA2 pump, SERCA2a and SERCA2b, having been identified. Most smooth muscle cells have been shown to express SERCA2b and SERCA3 isoforms of the pump (Wu, *et al.*, 1995). The different SERCA pump subtypes display varying sensitivities for Ca^{2+} and also display differences in their turnover rate, in other words they pump Ca^{2+} into the SR lumen at differing rates. The turnover of SERCA 1 is 2-fold faster than that of SERCA 2A (Sumbilla, *et al.*, 1999), although their affinities for Ca^{2+} would appear to be very similar (Lytton, *et al.*, 1992). Verboomen *et al.* (1992) using Ca^{2+} uptake by microsomes, revealed that the Ca^{2+} affinity of SERCA 2B is two fold higher than the affinity of SERCA 2A. However, SERCA 2B has a 2-

fold lower turnover rate for Ca^{2+} uptake relative to SERCA 2A (Lytton, *et al.*, 1992; Verboomen, *et al.*, 1994).

SERCA pump activation can be regulated by the proteins phospholamban (Arkin, *et al.*, 1997) and sarcolipin (Lee, 2002). Phospholamban (PLN), a small phosphoprotein, is the key regulator of SR Ca^{2+}

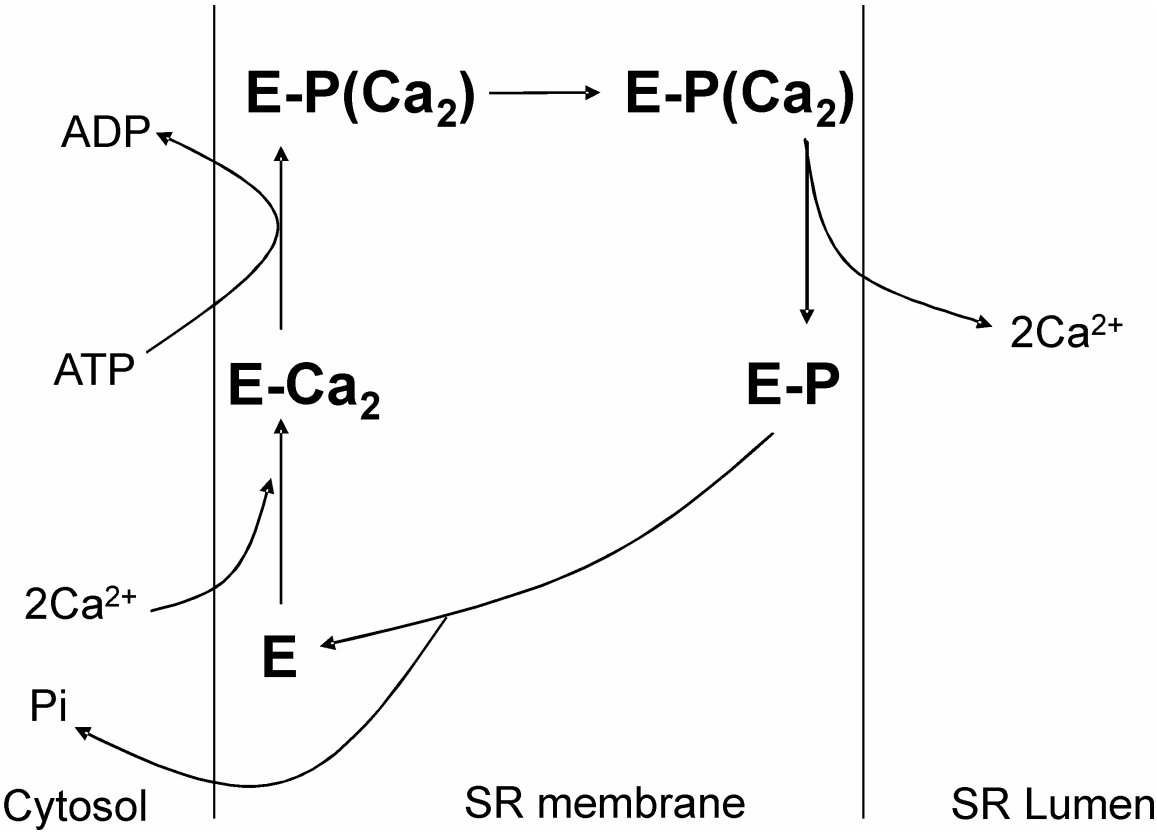

Fig. 1.1. **Translocation of Ca^{2+} into the SR:** Simple diagrammatic representation of the translocation of Ca^{2+} from the cytosol of the cell into theER/SR lumen by means of the action of SERCA pumps. Briefly, 2 Ca^{2+} ions bind to high affinity sites on the pump (**E**) resulting in a conformational change in the pump (**E-Ca_2**) Phosphorylation of ATP provides the energy for the next step and the inorganic phosphate (**Pi**) is bound to the pump inducing a further conformational change (**E-P(Ca_2)**) which has a much lower affinity for Ca^{2+} resulting in loss of Ca^{2+} to the SR lumen (**E-P**). Following this loss of Ca^{2+} to the lumen the pump undergoes a further change losing **Pi** to the cytosol and re-enetring its original conformation complete with high affinity Ca^{2+} binding sites.

cycling through its reversible inhibitory effect on SERCA pumps. It is present in cardiac, smooth and slow-twitch skeletal muscle. However, its regulatory effects have mainly been examined in cardiac muscle (Briggs, *et al.*, 1992). In

vitro investigations have identified three distinct sites at which PLN can be phosphorylated by various protein kinases: serine 10 by PKC; serine 16 by cAMP- or cGMP-dependent protein kinase; and threonine 17 by a Ca:CaM-dependent protein kinase. The phosphorylation of PLN is associated with stimulation of the initial rates of cardiac SERCA Ca^{2+} uptake at low Ca^{2+} concentrations which results in an overall increase in the affinity of the SERCA 2A for Ca^{2+} (Kim, *et al.*, 1990). This finding has led to the current view of PLN as a reversible inhibitor of the SERCA 2A activity. Sarcolipin (SLN) is a small SR membrane protein which interacts with, and inhibits SERCA pumps by lowering both their apparent Ca^{2+} affinity and V_{max}. The transmembrane sequence of SLN is similar to that of PLN, but it differs in its C-termini, where SLN ends with a more hydrophilic sequence than PLN. The structural similarity of the transmembrane domains of SLN and PLN indicates that SLN is a homologue of PLN (Odermatt, *et al.*, 1998). Other than its effects on the Ca^{2+} affinity and V_{max} of SERCA pumps, SLN is able to induce a superinhibitory effect of PLN to SERCA (Asahi, *et al.*, 2002). This is due, in part, to the fact that SLN can bind directly to PLN and prevent polymerisation of PLN resulting in an increase in the active form of PLN. PLN has a higher affinity for the SERCA binding sites than SLN. Thus, SLN may have additional interactions with the SERCA-PLN complex. Therefore, SLN can inhibit SERCA either by direct interaction with SERCA pumps, or through stabilisation of the SERCA-PLN complex.

After pumping into the SR, Ca^{2+} is bound by specific buffering proteins calrecticulin or calsequestrin. These two proteins are both able to bind large amounts of Ca^{2+}, allowing the Ca^{2+} store within the SR to reach concentrations of around 10-15 mM (Van Breemen and Saida, 1989). The binding of Ca^{2+} to these proteins allows for large amounts of Ca^{2+} to be contained within the SR without the problem of the precipitation of insoluble Ca^{2+} phosphate. The high capacity for Ca^{2+} storage is the result of the presence of Ca^{2+}-binding proteins. Calsequestrin is a binding protein first isolated from striated muscle SR. It has high binding capacity (50 binding sites per molecule) of low affinity (K_d = 1 mM; Campbell, *et al.*, 1983). Binding of Ca^{2+} to calsequestrin is believed to require only a pair of acidic residues, which is in contrast to more complex "EF-hands" which bind Ca^{2+} in other Ca^{2+} binding proteins (e.g. calmodulin).

Ca^{2+} binding is driven by a gain in entropy when molecules of water surrounding the Ca^{2+} ion are liberated during Ca^{2+} binding (Krause, *et al.*, 1991). Calsequestrin is a very acidic molecule, with 33-46 % of its residues being acidic. The C terminus of calsequestrin is believed to account for around 26 % of the total Ca^{2+} binding (Shin, *et al.*, 2001). A similar protein, calreticulin, has been found in the endoplasmic/sarcoplasmic reticulum of most other cells. This protein has 20 to 40 low affinity binding sites and one high affinity site (Michalak, *et al.*, 1992; Krause and Michalak, 1997; Michalak, *et al.*, 1999). These Ca^{2+} binding sites are also located in the C-domain, towards the C-terminus of the molecule which is a highly acidic region (Nakamura, *et al.*, 2001). Unfortunately no structural information is available at present for the C-terminal domain of calrecticulin. The low affinity of the Ca^{2+} binding sites within these two molecules, calrecticulin and calsequestrin, make the Ca^{2+} bound to them readily available for release from the ER/SR.

1.3.2 Mechanism of smooth muscle contraction

In smooth muscle binding of Ca^{2+} to Calmodulin and subsequent activation of myosin light chain kinase (MLCK), results in the phosphorylation of the serine residue at position 19 on MLC. This allows the activation of myosin ATPase by actin to occur and thereby contraction of the muscle (Sweeney, *et al.*, 1994). An eventual fall in the intracellular Ca^{2+} concentration will cause inactivation of myosin light chain kinase and dephosphorylation of the myosin light chain by myosin light chain phosphatase (MLCP), deactivation of the actomyosin ATPase and subsequent relaxation of the smooth muscle (Driska, *et al.*, 1989; Gong, *et al.*, 1992). Although the concentration of intracellular Ca^{2+} is an important determinant in mediating the contractile state of the cell, smooth muscle can generate tone in the presence of relatively low Ca^{2+} concentrations. Indeed, the active MLCK to active MLCP ratio is a major determining factor underlying the contractile state of a smooth muscle cell. The basis of contraction in smooth muscle is very similar to that of striated muscle. Smooth muscle contains cytoplasmic and membrane-bound dense bodies which correspond to the Z-lines seen in striated muscle, this is where actin binds (Somlyo and Somlyo, 1991). Smooth muscle myosin is a

hexamer consisting of two heavy chains and four light chains, two MLC_{20} and two LC_{17} chains. Smooth muscle and striated muscle vary in their energy metabolism. Unlike striated muscle, smooth muscle is able to maintain tone even in the presence of a lower Ca^{2+} concentration than that required for force development (Morgan and Morgan, 1982), and in the absence of significant MLC_{20} phosphorylation (Dillon, *et al.*, 1981). This is described as the 'Latch' theory (Fig. 1.2). In this proposal the dephosphorylation of MLC_{20} which has already formed a cross bridge with actin, does not result in the dissociation of the actin and myosin cross bridge, it merely alters the detachment rate by forming a relatively long lasting 'latch bridge' (Horowitz, *et al.*, 1996).

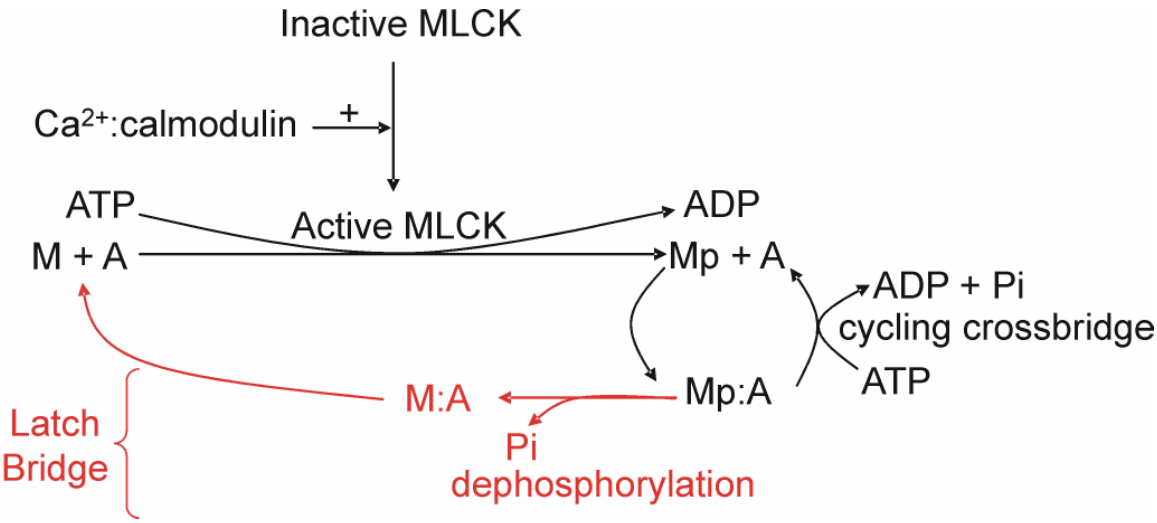

Fig. 1.2 **The 'latch bridge' theory of smooth muscle contraction:** The above diagram shows an overview of the processes involved in the contraction of smooth muscle. Highlighted in red is the process known as the latch bridge which allows smooth muscle to generate maximum contractile force with little energy expenditure. MLCK: myosin light chain kinase; M: myosin; A: actin.

1.3.3 Ca^{2+} sensitisation of smooth muscle

As mentioned above, contraction of smooth muscle cells is not entirely dependent upon a sustained elevation of cytoplasmic Ca^{2+} concentration. Indeed, the major determinant of cross-bridge cycling within smooth muscle is the activated MLCK to activated MLCP ratio. This ratio can be regulated by a number of signalling pathways which will be discussed below.

Investigations using Ca^{2+} sensitive fluorescent probes suggested that force generated at a given intracellular Ca^{2+} concentration could vary dependent upon the initial stimuli. Thus, a number of studies have shown that agonist-induced force is often higher than the force generated by depolarisation, induced by application of KCl, at similar or even lower intracellular Ca^{2+} concentrations in smooth muscle preparations (Bradley and Morgan, 1987; Himpens and Casteels, 1990). Studies in smooth muscle preparations that were permeabilised but retained G protein-coupled receptors confirmed that the mechanism underlying these observations was agonist-induced Ca^{2+} sensitisation of the contractile apparatus (Kitazawa, *et al.*, 1989). A number of investigations have shown that this sensitisation of the contractile apparatus is due to a decrease in the activity of MLCP via a number of pathways, indeed the RhoA : Rho kinase (ROK) pathway is believed to be the most important modulator of Ca^{2+} sensitivity in smooth muscle (Somlyo and Somlyo, 2003).

The Rho proteins are a subfamily of the small GTP-binding proteins which act as molecular "on-off" switches controlling a number of cellular processes (Etienne-Manneville and Hall, 2002). The Rho family of small G proteins have been implicated in a number of physiological processes involving changes in the actin cytoskeleton within cells, such as cell adhesion, motility, migration and contraction (Takai, *et al.*, 1995; Narumiya, *et al.*, 1997). There are, as yet, 20 identified members of the Rho family in mammalian cells (Burridge and Wennerberg, 2004). The Rho protein family can be further subdivided into three major classes: 1) Rho proteins, consisting of RhoA, RhoB and RhoC, 2) Rac proteins, consisting of Rac1, Rac2, Rac3 and 3), RhoG and Cdc42 proteins, consisting of Cdc42, TC10, TCL, Wrch1 and Chp/Wrch2. A number of studies carried out in cells utilising either constitutively active, or dominant-negative forms of Rho proteins suggest that RhoA regulates the assembly of contractile actomyosin filaments (Ridley and Hall, 1992), while Rac and Cdc42 regulate the polymerisation of actin to form specific peripheral structures within cells (Ridley, *et al.*, 1992; Nobes and Hall, 1995).

As previously mentioned, Rho proteins act as molecular switches which cycle between active-GTP bound and inactive GDP-bound forms. It is in the

GTP-bound form that they mediate cellular processes via interactions with downstream effectors. This cycle is under the control of three groups of regulatory proteins (Fig 1.3; Van Aelst and D'Souza-Schorey, 1997; Etienne-Manneville and Hall, 2002). In the inactive GDP-bound form, Rho proteins are locked in the cytosol by guanine dissociation inhibitors (GDIs) which prevent the cycle from occurring (Fig. 1.3). There are currently 4 GDIs identified within mammalian tissues (Etienne-Manneville and Hall, 2002) and they inhibit activation of Rho proteins by preventing translocation to the plasma membrane by binding Rho proteins at the prenylation site essential for insertion into the PM. They also mask the 'switch 1' and 'switch 2' regions of

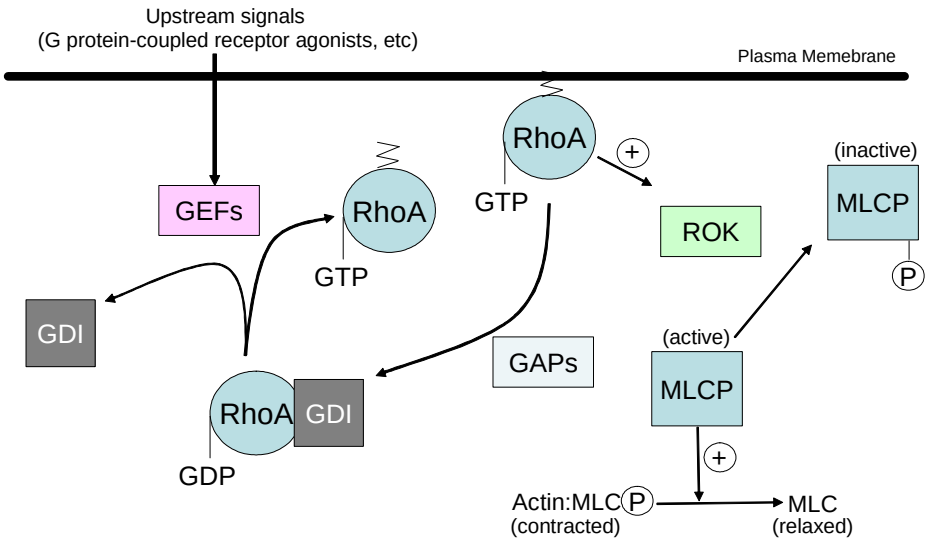

Fig. 1.3 **The RhoA:ROK pathway:** The above diagram shows a schematic representation of the processes involved in Ca^{2+} sensitisation as mediated by the small G protein RhoA and its downstream target ROK. GEF: guanine nucleotide exchange factors; GDI: guanine dissociation inhibitors; GAP: GTPase-activatiing proteins; MLCP: myosin light chain phosphatase; ROK: Rho kinase; MLC: myosin light chain.

Rho proteins required for the exchange of GDP for GTP. Activation of G protein coupled receptors (GPCR) and/or non-receptor tyrosine kinases (NRTK) leads to the activation of guanine nucleotide exchange factors (GEFs) which catalyse the exchange of GDP for GTP to activate Rho proteins (Fig.

1.3). To date, 50 GEFs have been identified in mammalian tissue (Etienne-Manneville and Hall, 2002). Activation of Rho proteins via exchange of GDP for GTP and translocation to the PM via unmasking of the prenylated carboxy terminus leads to activation of downstream effector molecules, such as Rho Kinases (ROK; Fig 1.3). Inactivation of Rho proteins occurs via the intrinsic GTPase activity of the molecules which can be accelerated via the action of GTPase-activating proteins (GAPs; Moon and Zheng, 2003). There are 70 GAPs identified so far in mammalian cells (Etienne-Manneville and Hall, 2002). To date, there have been over 60 downstream targets identified for Rho proteins in mammalian cells, highlighting the complexity and importance of the Rho signalling pathway in the regulation of cellular functions (Etienne-Manneville and Hall, 2002).

One of the most important targets of RhoA in vascular smooth muscle is the serine threonine protein kinase ROK. ROK is activated by the binding of activated GTP:RhoA to the C-terminus of ROK, thereby uncovering the catalytic phosphotransferase domain (Gong, *et al.*, 1997; Amano, *et al.*, 2000). Arachadonic acid is able to activate ROK independently of RhoA by binding at a separate site on ROK (Amano, *et al.*, 2000; Araki, *et al.*, 2001). Indeed arachadonic acid has been shown to contribute to agonist induced Ca^{2+}-sensitisation via Ca^{2+}-independent phospholipase A_2 (PLA_2; Araki, *et al.*, 2001) Once activated ROKs can act on a number of downstream targets including MLCP and LIM Kinase. ROK phosphorylates the 130kDa myosin binding site (MBS) of MLCP (Kimura, *et al.*, 1996). This inhibits MLCP as it prevents the catalytic subunit of MLCP (PP1c) from dephosphorylating MLC (Kimura, *et al.*, 1996; Somlyo and Somlyo, 2003). Thus, activation of ROK results in an increase in the activated MLCK to MLCP ratio, thereby increasing Ca^{2+} sensitivity within the smooth muscle cell. ROK is also able to inhibit MLCP by phosphorylating the PKC substrate CPI-17, a phospho-protein which acts as an inhibitory modulator of MLCP (Koyama, *et al.*, 2000). Also, ROK has been shown to be able to directly phosphorylate MLC itself to promote Ca^{2+}- and MLCP-independent constriction of vascular smooth muscle. However, the physiological relevance of this remains unclear (Kureishi, *et al.*, 1997). As mentioned above, ROK is also able to promote contraction of smooth muscle through an inhibitory interaction with LIM kinase which disrupts the actin

depolymerising protein cofilin resulting in stabilisation of filamentous actin (Maekawa, *et al.*, 1999). Thus, ROK is able to promote increased constriction of vascular smooth muscle and promote Ca^{2+} sensitisation through downstream effects on a number of molecular targets.

1.4 Ca^{2+} mobilising second messengers

It is clear that agonist-specificity is determined, in part, by the release of Ca^{2+} from intracellular stores in a manner dependent upon the generation and action of second messengers and their associated Ca^{2+} release channels. During the process of pharmacomechanical coupling in smooth muscle, it has long been accepted that many G protein-coupled receptors induce the cleavage of PIP_2 to produce diacyl glycerol and IP_3, the latter of which can lead to the activation of one or more of the known IP_3 receptor subtypes on the SR resulting in the release of Ca^{2+} from this store (Somlyo and Somlyo, 1994; Berridge, *et al.*, 2000). There is also now a growing body of evidence to support a role for pyridine nucleotides as Ca^{2+} mobilizing messengers within a number of cell types including smooth muscle (Li, *et al.*, 2003). Consistent with this proposal the enzymes for the synthesis and metabolism of NAADP (Wilson, *et al.*, 1998; Yusufi, *et al.*, 2002) and cADPR (Wilson, *et al.*, 2001) have been shown to be associated with smooth muscle, along with other cell types (Walseth, *et al.*, 1991). In addition to this evidence, a number of recent studies have suggested that the spatiotemporal pattern of Ca^{2+} signals may also be determined via the selection of different intracellular Ca^{2+} stores in a manner dependent on the nature of the Ca^{2+} mobilizing messenger(s) recruited by a given stimulus (Lee and Aarhus, 2000; Churchill, *et al.*, 2002; Masgrau, *et al.*, 2003; Mitchell, *et al.*, 2003).

1.4.1 Ca^{2+} mobilisation by IP_3

1.4.1.1 Synthesis and metabolism of IP_3

The Ca^{2+} mobilizing properties of IP_3 were first described in the blowfly salivary gland (Berridge, 1982), and in mammalian pancreatic acinar

cells (Streb, *et al.*, 1983). Since this discovery a large volume of research has been carried out and IP_3 is now firmly regarded as the 'classical' Ca^{2+} mobilizing messenger within many cell systems. As mentioned previously, IP_3 is generated from PIP_2 through the actions of phospholipase C (PLC) isoforms, PLC_β, PLC_γ and PLC_δ. PLC_β is activated by the actions of atypical $G\alpha_q$ subunits of membrane bound G-proteins (Rebecchi and Pentyala, 2000), while PLC_γ is activated through the phosphorylation of three tyrosine residues by receptor tyrosine kinases (Wahl, *et al.*, 1989a; Wahl, *et al.*, 1989b; Kim, *et al.*, 1991). PLC_δ lacks the SRC homology domains, these are highly conserved noncatalytical structural sequence domains detected initially in the src oncogene, which are important for the tyrosine kinase activation of PLC_γ. PLC_δ is activated by the $G\alpha_q$ subunits in a similar fashion to PLC_β. In addition to this, PLC_δ can also be activated by cytosolic Ca^{2+} concentrations (Ochocka and Pawelczyk, 2003). Once liberated IP_3 moves through the cytoplasm of the cell and binds to specific IP_3 receptors (IP_3Rs) in order to initiate Ca^{2+} mobilization (Marshall and Taylor, 1993). IP_3 can be inactivated by two known metabolic pathways. Either via phosphorylation by a phosphatidylinositol-3-kinase (Batty, *et al.*, 1985), or by dephosphorylation via the actions of a 5-phosphatase (Downes, *et al.*, 1982; Berridge, *et al.*, 1983).

1.4.1.2 Cells express different IP_3Rs, each with varying sensitivities to IP_3

The IP_3Rs are tetramers of subunits, each consisting of around 27,000 amino acids. They share a common evolutionary origin with other members of the family of intracellular Ca^{2+} release channels such as the ryanodine receptors (RyRs; Furuichi, *et al.*, 1989). The IP_3 binding domain is located at the N-terminal end of the IP_3Rs (Mignery and Sudhof, 1990), whilst the C-terminal end traverses the ER/SR membrane to form the Ca^{2+} channel domain (Michikawa, *et al.*, 1994). There are three known IP_3R isoforms, IP_3R1, IP_3R2 and the IP_3R3. Each of these Subtypes of IP_3R have been shown to express a single IP_3 binding site consisting of two linked domains located towards the N-terminus of the subunit. One of these domains expresses IP_3 binding capability, while the other potentiates this binding but cannot bind IP_3 alone (Yoshikawa,

et al., 1999). Basic conserved residues within these sites are likely to mediate the interaction between the IP_3R subunits and the phosphate groups of IP_3 (Yoshikawa, *et al.*, 1999). Most investigations into the effects of IP_3 on the Ca^{2+} release mediated through the opening of IP_3Rs have shown a requirement for IP_3 binding to several, if not all of the subunits of the receptor in order for the channel to open (Meyer, *et al.*, 1988; Dufour, *et al.*, 1997; Marchant and Taylor, 1997).

The IP_3R subtypes differ in their affinities for IP_3 with the sensitivity of the receptors to IP_3 being in the order of $IP_3R2 > IP_3R1 > IP_3R3$ (Miyakawa, *et al.*, 1999). The IP_3R subtypes have been shown to form both homotetrameric and heterotetrameric channels. However, the evidence that IP_3R subunits form heterotetramers is limited to studies of reconstituted receptors in cell lines and, as yet, heterotetrameric compositions of the receptor have not been described in wild type cells (Patel, *et al.*, 1999; Taylor, *et al.*, 1999). Although IP_3R subtypes are co-expressed in the majority of cells, the relative amount varies between tissues and has also been shown to change during development (Newton, *et al.*, 1994; Wojcikiewicz, 1995). Smooth muscle has been shown to express the IP_3R1 in high amounts. In phasic smooth muscle, for example that of the *vas deferens*, IP_3R1 is located mainly in the peripheral SR (Villa, *et al.*, 1993; Nixon, *et al.*, 1994). Tonic smooth muscle, such as arterial smooth muscle cells, have been shown to express a greater amount of central SR than phasic smooth muscle, and, with this a larger amount of IP_3R1 being expressed upon the central SR membrane than upon the peripheral SR (Nixon, *et al.*, 1994). The other IP_3R subtypes are also expressed in arterial smooth muscle, but this expression appears to be dependent on the developmental status of the tissue. IP_3R3 is the predominant receptor subtype in neonatal smooth muscle but its levels decline and IP_3R1 expression levels increase as the animal develops (Tasker, *et al.*, 1999). IP_3R2 has also been shown to be higher in neonatal smooth muscle cells (Tasker, *et al.*, 2000). The cellular distribution of the different subtypes has been shown to differ in studies carried out using primary cultures of rat aorta smooth muscle cells (Sugiyama, *et al.*, 2000), and freshly isolated rat aorta smooth muscle (Tasker, *et al.*, 2000). In these studies it was shown that IP_3R1 is found throughout the cytoplasm, with higher IP_3R2 expression around the plasma membrane and perinuclear area and IP_3R3 found

mostly in the perinuclear region (Sugiyama, *et al.*, 2000; Tasker, *et al.*, 2000). However, expression of receptors increases in proliferating cultured cells when compared to freshly isolated non-proliferative cells, particularly with respect to type 2 and type 3 receptors (Tasker, *et al.*, 2000). This evidence suggests that the IP_3R2 and IP_3R3 receptors may have an important role in arterial smooth muscle development.

1.4.1.3 Regulation of IP_3Rs by cytoplasmic Ca^{2+} and IP_3

IP_3Rs are not only under the influence of the IP_3 concentration within the cell, but can also be influenced by the cytoplasmic Ca^{2+} concentration within the cell in either a stimulatory or inhibitory manner (Hirata, *et al.*, 1984; Iino, 1990) . The exact area to which Ca^{2+} binds to exert its stimulatory/inhibitory effects on the IP_3R, and the exact interplay between IP_3 and Ca^{2+} in gating IP_3R activity remains an area of keen debate in the field (Taylor and Laude, 2002). As early as 1984, Hirata and colleagues showed that the release of Ca^{2+} from IP_3Rs in macrophages could be inhibited by micromolar concentrations of Ca^{2+} (Hirata, *et al.*, 1984). A number of years after this, Iino and colleagues showed that low concentrations of Ca^{2+} were able to potentiate the Ca^{2+} release elicited by IP_3 and that the Ca^{2+} mobilised via IP_3R activation was under biphasic regulation (Iino, 1990). This biphasic regulation of IP_3Rs allows the Ca^{2+} liberated through receptor activation to regulate further Ca^{2+} release, thus presenting an extremely rapid, and very useful feedback mechanism to the cell (Iino and Endo, 1992).

1.5 Ca^{2+} mobilization by pyridine nucleotides

1.5.1 An historical overview

Four years after the discovery of the Ca^{2+} mobilizing messenger IP_3 by Berridge and colleagues (Streb, *et al.*, 1983), Lee and co-workers identified two further mechanisms of Ca^{2+} mobilisation in the sea urchin egg, using purified microsomes and egg homogenates (Clapper, *et al.*, 1987). One of these mechanisms was initiated by the addition to sea urchin egg homogenate of β-

nicotinamide adenine dinucloetide (β-NAD^+), whilst the other was initiated by β-nicotinamide adenine dinucloetide phosphate (β-$NADP^+$). Each of these mechanisms proved unique as they were shown to be independent of mitochondria and of IP_3-dependent Ca^{2+} release mechanisms. One of the most significant findings was that the addition of β-NAD^+ caused endoplasmic reticulum (ER) Ca^{2+} release after a significant delay of around 1 – 2 minutes. This delay indicated that a β-NAD^+ metabolite initiated ER Ca^{2+} release. Two years after this study, the molecular formula of the β-NAD^+ metabolite was elucidated (Lee, *et al.*, 1989) and the novel cyclic structure of the metabolite was finally characterized and shown to be cADPR four years after this (Kim, *et al.*, 1993; Lee, *et al.*, 1994b). By this time, cADPR and the enzymes which are responsible for its synthesis and subsequent metabolism had already been shown to exist in a number of mammalian tissues (Walseth, *et al.*, 1991). The Ca^{2+} release mediated by cADPR had also been characterized as utilising ER Ca^{2+} stores through the activation of RyRs (section 1.5.2). The Ca^{2+} release mediated by β-$NADP^+$ occurred without the delay seen with β-NAD^+. It was, however, facilitated by an alkaline pH, suggesting that Ca^{2+} release in sea urchin eggs in response to the addition of β-$NADP^+$ was initiated by an active metabolite of β-$NADP^+$ (Clapper, *et al.*, 1987). Studies on this active metabolite revealed that it was NAADP (Lee and Aarhus, 1995). This differs from β-$NADP^+$ only by the substitution of a carboxyl group for the amide group of the nicotinamide moiety, and was shown to be a contaminant present in the original β-$NADP^+$ preparations used by Clapper and colleagues (1987). NAADP had been identified a number of years previously but with no function attributed to it (Bernofsky, 1980). The receptor for NAADP and the exact mechanisms by which NAADP facilitates Ca^{2+} release within cells have yet to be fully characterised. It is clear, however, that NAADP initiates Ca^{2+} release from cellular stores other than the SR or mitochondria (Lee and Aarhus, 1995; Genazzani and Galione, 1996; Churchill and Galione, 2001; Boittin, *et al.*, 2002; Churchill, *et al.*, 2002).

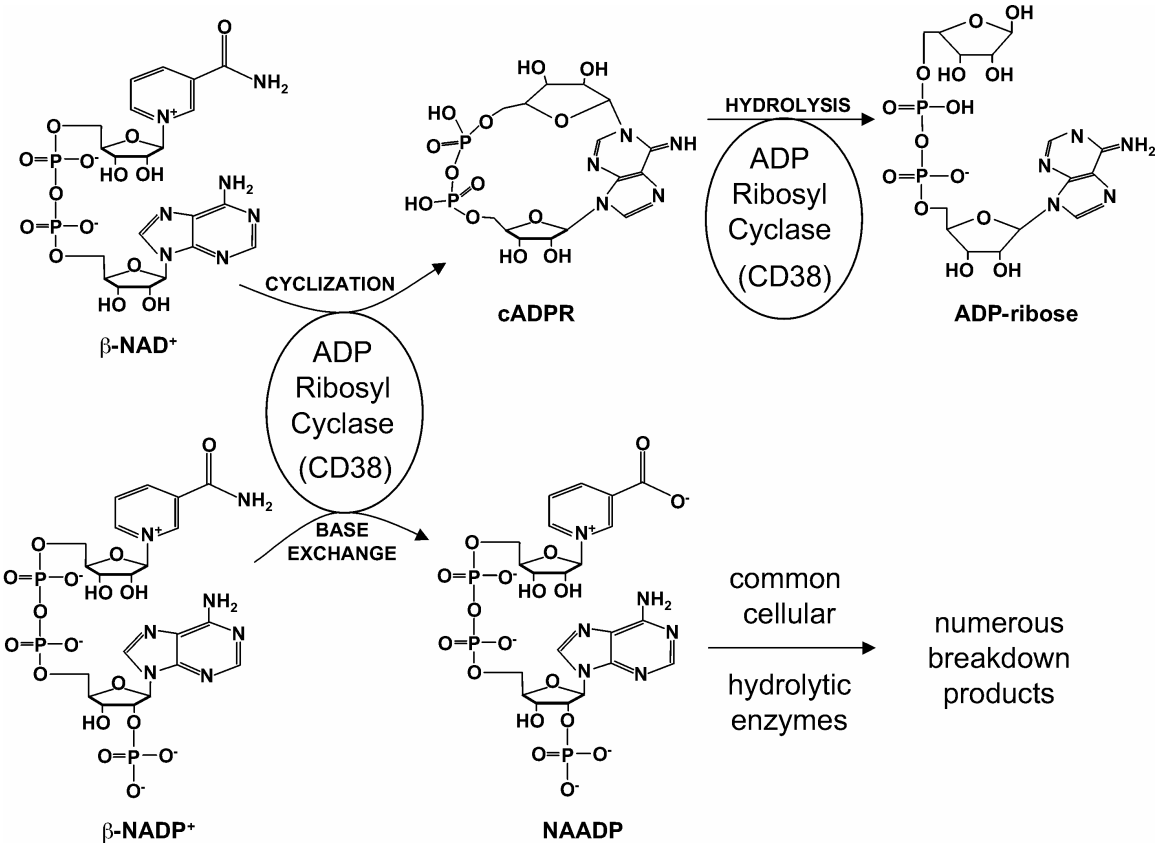

Fig. 1.4 **Possible intracellular routes of synthesis and metabolism for cADPR and NAADP.**

The enzymes which synthesise and metabolise cADPR and NAADP have been isolated and shown to be present in a number of preparations other than the sea urchin egg, including all major mammalian organs (Rusinko and Lee, 1989; Lee and Aarhus, 1993; Chini and Dousa, 1995; Wilson, *et al.*, 1998; Wilson, *et al.*, 2001). The enzyme in question was named ADP-ribosyl cyclase due to the fact that it removes nicotinamide from β-NAD^+ to yield cADPR (Lee and Aarhus, 1991). From this growing family of enzymes the first one to be sequenced was a soluble ADP-ribosyl cyclase of approximately 36 kDa. It was isolated from the ovotestis of the sea-slug *Aplysia californica*. Following this a type II membrane glycoprotein CD38 was identified as a mammalian homolog to the *Aplysia* cyclase (States, *et al.*, 1992; Howard, *et al.*, 1993). Hot on the heals of this discovery was the identification of a second cell surface antigen with ADP-ribosyl cyclase activity, CD157 (Hirata, *et al.*, 1994; Itoh, *et al.*, 1994). Most recently, a membrane bound ADP-ribosyl cyclase was isolated

from the microscopic unicellular organism *Euglena* (Masuda, *et al.*, 1999). However, the sequence of this cyclase has yet to be identified.

Of the two mammalian homologs of the *Aplysia* cyclase CD38 and CD157, more is known about CD38. As mentioned previously, it is a type II membrane glycoprotein originally identified as a lymphocyte antigen important in cell-cell interactions and in the activation of natural killer cells (Deaglio, *et al.*, 2002). It has a single membrane-spanning domain located at the N terminus, with the ADP-ribosyl cyclase site situated in the extracellular domain. Given that the ADP-ribosyl cyclase site is expressed on the external surface of the plasma membrane, this would seem to preclude the enzyme from a role in intracellular Ca^{2+} signalling. However, a number of studies have provided data to support two hypotheses consistent with this idea. It has been suggested that CD38 may act as a cADPR transporter during the catalytic process allowing newly synthesized cADPR to be delivered to the intracellular environment leading to subsequent Ca^{2+} release (Franco, *et al.*, 1998). Supporting this hypothesis are the findings that extracellular application of β-NAD^{+} leads to the mobilization of intracellular Ca^{2+} stores in cerebellar granule cells (De Flora, *et al.*, 1996), astrocytes (Verderio, *et al.*, 2001) and fibroblasts (Franco, *et al.*, 2001). In osteoclasts, the extracellular application of β-NAD^{+} leads to the mobilization of Ca^{2+} stores and subsequent bone resorption which is blocked by the application of anti-CD38 antibodies (Sun, *et al.*, 1999). A second suggestion is that CD38 may be internalized upon the binding of β-NAD^{+} which would deliver newly synthesised cADPR directly to the cytoplasm (Zocchi, *et al.*, 1996; Franco, *et al.*, 2001). A significant finding to support a role for CD38-derived cADPR in intracellular Ca^{2+} signalling is the finding that CD38 is expressed on the surface of intracellular organelles (Yamada, *et al.*, 1997) such as the nuclear membrane (Adebanjo, *et al.*, 1999; Khoo, *et al.*, 2000). The stable expression of CD38 in the 3T3 and HeLa cell lines is accompanied by the consumption of β-NAD^{+}, cADPR synthesis and the mobilization of ER Ca^{2+} stores (Zocchi, *et al.*, 1998). Moreover, studies on CD38 knockout mice have shown a decrease in endogenous cADPR levels in a number of tissues (Kato and Staub, 1966; Cockayne, *et al.*, 1998). Also, cADPR-dependent Ca^{2+} signalling pathways in pancreatic acinar cells and

pancreatic β-cells are defective in CD38 knockout mice, although these cells respond normally to the intracellular application of cADPR (Kato, *et al.*, 1999; Fukushi, *et al.*, 2001). Takahashi and colleagues have recently reported that cADPR levels in CD38 knockout mice are one tenth of the level found in wild type mice, which may be associated with abnormalities in the Ca^{2+} handling capabilities and contractility of cardiac myocytes (Takahashi, *et al.*, 2003). This finding appears to conflict with previous reports suggesting that CD38 knockout mice showed no deficiency in cADPR synthesis in cardiac and brain tissue (Partida-Sanchez, *et al.*, 2001). The latter report suggests that significant cADPR synthesis may still occur in CD38 knockout mice and that there may be an unidentified ADP-ribosyl cyclase present in mammalian tissue which may be important in the regulation of cardiovascular function. Consistent with this hypothesis is the finding in arterial smooth muscle that the predominant ADP-ribosyl cyclase is associated with the microsomal fraction and not the plasma membrane, nuclear or cytosolic fractions (Wilson, *et al.*, 2001). This cyclase remains to be identified as does the cyclase that has been shown to be associated with the SR of cardiac muscle (Meszaros, *et al.*, 1997), the mitochondria of liver (Ziegler, *et al.*, 1997) and the cytosolic fractions isolated from sea urchin eggs, mammalian brain (Matsumura and Tanuma, 1998) and from T-lymphocytes (Guse, *et al.*, 1999). However, it has been suggested that CD38 isoforms may represent the intracellular ADP-ribosyl cyclase in mammalian cells (Howard, *et al.*, 1993).

Of the four members of this family, which have been characterised, three have been shown to be multi-functional enzymes. CD38 and CD157 have both been shown to catalyse the synthesis of cADPR from β-NAD^+ and the subsequent hydrolysis of cADPR to ADP-ribose (Howard, *et al.*, 1993; Hirata, *et al.*, 1994). The primary product of both cyclases is ADP-ribose due to the fact that the hydrolase activity within each is dominant. However, a net increase in cADPR levels is accumulated from β-NAD^+. Given that a net increase in cADPR was seen but the hydrolase activity is dominant, it has been suggested that an increase in ADP-ribose production could inhibit, by a negative feedback mechanism, cADPR hydrolase activity of the cyclase thereby increasing cADPR levels (Genazzani, *et al.*, 1996a). Although the

known ADP-ribosyl cyclases function in a stereospecific manner, a number of β-NAD^+ analogues can be efficiently cyclised in order to produce stable or fluorescent products that may be used in order to study enzyme regulation (Graeff, *et al.*, 1994). These products may also be used as cADPR antagonists or mimetics (Walseth and Lee, 1993; Sethi, *et al.*, 1997; Walseth, *et al.*, 1997). Conversely the hydrolase activity is extremely substrate specific with closely related analogues to cADPR being resistant to hydrolysis (Graeff, *et al.*, 1994; Sethi, *et al.*, 1997; Wong, *et al.*, 1999). By contrast, cADPR is also uniquely stable when faced with common hydrolytic enzymes found within the cells.

Along with their ability to produce and degrade cADPR, the *Aplysia* cyclase and CD38 have also been shown to synthesise NAADP through the substitution of nicotinic acid for the nicotinamide group of β-$NADP^+$ (Aarhus, *et al.*, 1995). Along with this finding it has been shown that the microsome associated ADP-ribosyl cyclase isolated from homogenates of pulmonary artery smooth muscle has the ability to synthesise and hydrolyse cADPR, and to synthesise NAADP (Wilson, *et al.*, 1998; Wilson, *et al.*, 2001). In contrast to cADPR, NAADP does not appear to be metabolized by any of the known ADP-ribosyl cyclases. However, alkaline phosphatases within the cell metabolise NAADP to yield NAAD (Kontani, *et al.*, 1993), and nucleotide pyrophosphatase yields 2'-phospho-AMP and nicotinic acid mononucleotide (De Flora, *et al.*, 2000).

1.5.2 Ca^{2+} mobilization by cADPR via ryanodine receptors

RyRs were first identified by the ability of the plant alkaloid ryanodine to block Ca^{2+} mobilization from the SR/ER alone. Since their discovery they have been shown to be present in a number of cell types including skeletal (Inui, *et al.*, 1987a), cardiac (Inui, *et al.*, 1987b) and smooth muscle (Herrmann-Frank, *et al.*, 1991). There have to date been three mammalian subtypes of the RyR identified, namely RyR1 (Inui, *et al.*, 1987b; Lai, *et al.*, 1988; Takeshima, *et al.*, 1995), RyR2 (Inui, *et al.*, 1987a; Takeshima, *et al.*, 1998) and RyR3 (Hakamata, *et al.*, 1992; Sorrentino, *et al.*, 1993; Takeshima, *et al.*, 1996) with all three having been shown to be present in vascular smooth

muscle (Herrmann-Frank, *et al.*, 1991; Neylon, *et al.*, 1995; Jeyakumar, *et al.*, 1998; Coussin, *et al.*, 2000; Mironneau, *et al.*, 2001).

Ca^{2+} may activate RyRs in its own right or facilitate further Ca^{2+} release via RyRs by positive feedback, or Ca^{2+}-induced Ca^{2+}-release (CICR; Endo, *et al.*, 1970; Ford and Podolsky, 1970; Fabiato and Fabiato, 1975; Fabiato, 1983; Sutko and Airey, 1996a). CICR offers cells the facility to amplify small, highly localized Ca^{2+}signals into global Ca^{2+}waves via the recruitment of neighbouring RyR complexes (Fig. 1.3), and with a high margin of safety due to the limitations placed on Ca^{2+} diffusion ($\leq$ 5μm; Allbritton, *et al.*, 1992) by the buffering capacity within the cytoplasm. Thus, CICR may recruit, in concert, discrete clusters of RyRs to initiate highly localized, elementary Ca^{2+} release events such as Ca^{2+} sparks (Cheng, *et al.*, 1993; Niggli, 1999; Jaggar, *et al.*, 2000). Alternatively, once a given threshold concentration is breached, Ca^{2+} may induce a propagating global Ca^{2+} wave by the progressive recruitment of RyR clusters distant from the site of initiation by CICR. As mentioned previously, cADPR is an endogenous regulator of RyRs (Galione, *et al.*, 1991) and may either activate RyRs directly or may facilitate CICR via RyRs (Fig. 1.5; Galione, *et al.*, 1991; Meszaros, *et al.*, 1993). Not surprisingly, given this fact, Ca^{2+} has also been shown to sensitise RyRs to activation by cADPR (Tanaka and Tashjian, 1995; Panfoli, *et al.*, 1999). Therefore, when studying the regulation by cADPR of RyRs in a given cell type, consideration of the combinatorial effects of Ca^{2+} and cADPR is of fundamental importance, particularly when it comes to determining the threshold for activation of RyRs by either agent. Given that RyR activation by cytoplasmic Ca^{2+} is augmented by the luminal Ca^{2+} concentration of the SR via a luminal Ca^{2+} sensor (Gilchrist, *et al.*, 1992; Tripathy and Meissner, 1996; Gyorke and Gyorke, 1998; Ching, *et al.*, 2000; Beard, *et al.*, 2002), the luminal Ca^{2+} concentration of the SR may also influence cADPR-dependent regulation of RyR function (Sitsapesan and Williams, 1995).

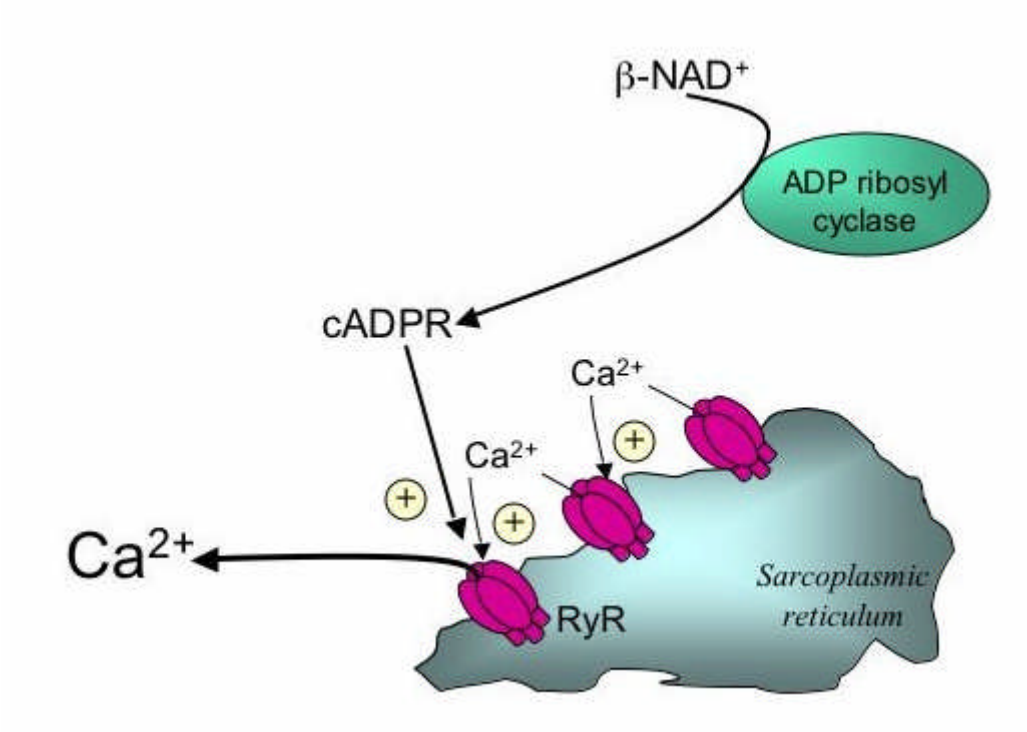

Fig. 1.5 **Schematic diagram depicting the regulation of Ca^{2+}-induced Ca^{2+}-release via RyRs by cADPR.**

The three subtypes of RyR have distinct functions and tissue-specific distributions have been identified. Furthermore, it has been suggested that each subtype may offer, in part, the functional diversity required of Ca^{2+} signals within a single cell type (Yamazawa, *et al.*, 1996). It is significant, therefore, that RyR1, RyR2 and RyR3 may all be present in vascular smooth muscle (Herrmann-Frank, *et al.*, 1991; Neylon, *et al.*, 1995; Jeyakumar, *et al.*, 1998; Coussin, *et al.*, 2000; Mironneau, *et al.*, 2001), not least because all three subtypes of the receptor can be expressed in a cADPR-sensitive form (Giannini, *et al.*, 1992; Sonnleitner, *et al.*, 1998; Cui, *et al.*, 1999). Thus different RyR subtypes may not only coordinate differential Ca^{2+} signals in arterial smooth muscle, but might mediate distinct Ca^{2+} signals to elicit different functional responses in a single smooth muscle cell. Support for this view may be derived from the fact that different RyR subtypes exhibit different sensitivities to Ca^{2+} and cADPR, respectively (Chu, *et al.*, 1993; Sierralta, *et al.*, 1996; Chen, *et al.*, 1997a; Jeyakumar, *et al.*, 1998; Sonnleitner, *et al.*, 1998; Cui, *et al.*, 1999; Murayama, *et al.*, 2000).

1.5.3 cADPR does not bind directly to ryanodine receptors

High affinity, binding sites specific for cADPR have been shown to exist in the sea urchin egg (Lee, 1991), and in smooth muscle from mammals (Kuemmerle and Makhlouf, 1995). However, a number of photoaffinity labelling studies have suggested that the polypeptides in question are, in fact, far too small to be RyRs (Walseth and Lee, 1993). To add to this, detailed characterization of cADPR binding sites within the sea urchin egg have revealed no correlation between [^{32}P]cADPR binding and the effects of a number of known regulators of RyR function (Thomas, *et al.*, 2001). This would suggest that the RyR is a down-stream target of the cADPR receptor.

Calmodulin is known to have both inhibitory and stimulatory effects on RyR function (Balshaw, *et al.*, 2002). In its Ca^{2+}-free state it can stimulate RyR opening (Rodney, *et al.*, 2001; Samso and Wagenknecht, 2002). Whilst in its Ca^{2+}-bound state it appears to be inhibitory (Meissner and Henderson, 1987). Also, the Ca^{2+} dependency of calmodulin mirrors the bell-shaped response of RyRs to Ca^{2+}, with low concentrations of Ca^{2+} activating and high concentrations of Ca^{2+} inhibiting. Furthermore, the removal of calmodulin from RyRs in a cell free system has been shown to abolish the activation of RyRs by cADPR (Lee, *et al.*, 1994a). Thus, it was suggested that calmodulin may be required for cADPR-mediated modulation of CICR within cells. Indeed, the presence of calmodulin does sensitize RyRs to activation by cADPR, Ca^{2+} and other classical modulators of RyR function (Lee, *et al.*, 1995; Tanaka and Tashjian, 1995; Fruen, *et al.*, 2000; Thomas, *et al.*, 2001).

A number of recent investigations have suggested a role for the FK-506 binding proteins as the potential cADPR binding protein. These proteins are known to bind to and modulate RyR function (Timerman, *et al.*, 1993; Timerman, *et al.*, 1995; Ahern, *et al.*, 1997). They bind to RyRs and modulate their function in a way that may be important in the co-ordination of Ca^{2+} signalling (Brillantes, *et al.*, 1994; Marx, *et al.*, 1998). It has been reported that the blockade, removal or dissociation of FKBP12.6 from RyRs results in the abolition of activation by cADPR in pancreatic islets (Noguchi, *et al.*, 1997) and coronary artery smooth muscle cells (Tang, *et al.*, 2002). Therefore, it has

been proposed that FKBP12.6 dissociates from the RyR upon binding of cADPR (Noguchi, *et al.*, 1997; Tang, *et al.*, 2002). However, the binding affinity of recombinant FKBPs to RyR3 was unaffected by cADPR addition (Bultynck, *et al.*, 2001). Also, it has been noted that the FKBP antagonists rapamycin and FK-506 (Harding, *et al.*, 1989; Ahern, *et al.*, 1997) were without effect on cADPR binding in sea urchin eggs (Thomas, *et al.*, 2001). Therefore, it would appear that if the FKBP proteins do represent a cADPR binding protein, they may act as such in a cell-specific or RyR subtype/splice variant specific manner.

1.5.4 cADPR-dependent Ca^{2+} signalling in vascular smooth muscle

Studies with homogenates of smooth muscle have shown that both the synthesis of cADPR from β-NAD^+, and its metabolism to ADP-ribose, occurs in arterial smooth muscle from a number of vascular beds: coronary (Li, *et al.*, 1999; Ge, *et al.*, 2003), renal (Li, *et al.*, 2000), pulmonary (Wilson, *et al.*, 1998) and aorta (de Toledo, *et al.*, 1997). In smooth muscle of the pulmonary artery (Wilson, *et al.*, 1998), and the coronary artery (Li, *et al.*, 1999; Ge, *et al.*, 2003), ADP-ribosyl cyclase and cADPR hydrolase activities were shown to be associated with the microsomal fraction, but absent from the cytosolic fraction. This work suggests that the ADP-ribosyl cyclase found in vascular smooth muscle would appear to be membrane bound. It is noteworthy that there was only limited association of these enzymes with the plasma membrane fraction, and that the activity found within the microsomal fraction was not due to contamination of the sample with plasma membrane (Wilson, *et al.*, 2001). Thus, the majority of the cyclase/hydrolase activity in arterial smooth muscle is not conferred by plasma membrane bound CD38. In a separate study, the removal of CD38 from coronary artery smooth muscle homogenates did not result in loss of the total cyclase/hydrolase activity of the tissue (Li, *et al.*, 2002b). This suggests that arterial smooth muscle may express a membrane bound, microsomal associated ADP-ribosyl cyclase other than CD38. However, an as yet unidentified isoform of CD38 may be targeted to membranes of intracellular organelles (Yamada, *et al.*, 1997; Santella, *et al.*,

1998; Adebanjo, *et al.*, 2000). Therefore, there is little evidence in arterial smooth muscle to support the role of plasma membrane bound CD38 in cADPR mediated Ca^{2+} signalling.

The ADP-ribosyl cyclase/cADPR hydrolase activities are not universal within the vasculature and these appear to be differentially expressed in smooth muscle from different vascular beds. For example, these enzyme activities were shown to be considerably higher in pulmonary arterial homogenates than in the mesentery or aortic beds. This study also showed that the activity within the pulmonary vasculature was inversely proportional to the artery diameter i.e. the smaller the diameter, the greater the activity (Wilson, *et al.*, 2001). Furthermore, in the renal vasculature higher activity was seen in pre-glomerular arteries than in post-glomerular vas recta (Li, *et al.*, 2000). It is possible therefore, that cADPR-dependent Ca^{2+} signalling may perform discrete roles in different vascular beds, a viewpoint that is now supported by functional studies (see below).

To date, there have only been two studies that have measured the levels of endogenous cADPR in vascular smooth muscle. In rat pulmonary artery the resting measurement of cytoplasmic concentration of cADPR provided estimates in the range of 0.2 μM-0.5 μM (Wilson, *et al.*, 2001), which is consistent with measurements obtained previously from a range of mammalian tissues (Walseth, *et al.*, 1991). Coronary arteries appear to express a lower resting level of cADPR, of around 150 nM (Li, *et al.*, 1997). It is worthy of note, however, that when interpreting these results that they are likely to be underestimates of the true intracellular concentration of cADPR. This is because values were initially normalized to protein content of the sample that does not exclude protein that is unassociated with smooth muscle (e.g. connective tissue). Perhaps most significantly, these measures do not take into account possible spatial compartmentalization at the site of cADPR production within the cell.

1.5.5 Ca^{2+} mobilization by cADPR in arterial smooth muscle

The first report of Ca^{2+} mobilization by cADPR from the SR came in 1995 (Kuemmerle and Makhlouf, 1995). The following year Kannan and colleagues reported that the application of cADPR led to the release of Ca^{2+} from SR stores in β-escin permeabilised coronary artery smooth muscle cells (Kannan, *et al.*, 1996). This work is now supported by a number of studies showing the release of Ca^{2+} from SR stores in response to cADPR application in coronary (Yu, *et al.*, 2000), pulmonary (Wilson, *et al.*, 2001) and renal artery smooth muscle cells (Li, *et al.*, 2000). There is also a great deal of evidence suggesting that Ca^{2+} mobilization by cADPR is abolished by the blockade of RyRs with ryanodine or by blocking the action of cADPR by using the membrane permeant cADPR antagonist 8-bromo-cADPR (8-Br-cADPR; Sethi, *et al.*, 1997).

Contrary findings have, however, been reported in colonic smooth muscle. Bradley and colleagues reported that flash-photolysis of caged cADPR did not result in SR Ca^{2+} mobilization, or facilitation of CICR induced by voltage-gated Ca^{2+} influx (Bradley, *et al.*, 2003). When examining the effects of cADPR, therefore, we must always consider the possibility that cADPR may not initiate Ca^{2+} mobilization in all cell types.

1.5.6 cADPR and vasoconstriction

1.5.6.1 Does cADPR mediate vasoconstrictor-induced sarcoplasmic reticulum Ca^{2+} release in arterial smooth muscle?

There are only a handful of reports that study the role of cADPR in mediating vasoconstriction. This may be due to the fact that most studies have focused on establishing the presence or absence of ADP-ribosyl cyclase and on the mobilization of SR stores by application of cADPR. However, it has been suggested that cADPR, in part, mediates vasoconstriction via M1 muscarinic acetylcholine receptors (Ge, *et al.*, 2003). Studies on tracheal smooth muscle have also suggested a role for cADPR in mediating Ca^{2+} signals in response to

the activation of muscarinic receptor activation (Prakash, *et al.*, 1998). In this study it was shown that treatment of tracheal smooth muscle with acetylcholine resulted in Ca^{2+} oscillations whose frequency was increased upon addition of 1 μM cADPR. The acetylcholine-induced Ca^{2+} oscillations were shown to be abolished by the application of 20 μM 8-amino-cADPR, a known antagonist of cADPR effects, suggesting that cADPR was involved in agonist-induced Ca^{2+} mobilization within tracheal smooth muscle. However, consideration of the literature suggests the involvement of a more complex mechanism than cADPR-dependent Ca^{2+} mobilisation alone. Earlier studies had already established that acetylcholine induced a biphasic Ca^{2+} signal in smooth muscle of the trachea. It was thought that an initial transient response was mediated by phospholipase C coupled M3 receptors and IP_3-dependent SR Ca^{2+} release through IP_3R activation (Coburn and Baron, 1990; Shieh, *et al.*, 1991; Sims, *et al.*, 1996). The signal was then proposed to be maintained by CICR from the SR via RyRs in a manner dependent upon Ca^{2+} influx, possibly via a store-refilling current (Murray and Kotlikoff, 1991; Shieh, *et al.*, 1991; Murray, *et al.*, 1993; Kannan, *et al.*, 1997; Prakash, *et al.*, 1997). However, cADPR antagonists have now been shown to block the maintained phase of SR Ca^{2+} release in response to acetylcholine (Prakash, *et al.*, 1998). This suggests that cADPR possibly serves to amplify the initial Ca^{2+} signal generated through IP_3R activation by sensitizing RyRs to CICR and maintain the initial Ca^{2+} signals by sensitizing CICR via RyRs in a similar fashion to the way cADPR might amplify Ca^{2+} signals during cholesystokinin-dependent activation of pancreatic acinar cells (Cancela, *et al.*, 1999; Cancela, *et al.*, 2000; Cancela, *et al.*, 2002).

1.5.6.2 Does cADPR facilitate Ca^{2+}-induced Ca^{2+}-release in response to voltage-gated Ca^{2+} influx?

As mentioned previously, CICR is fundamental to excitation-contraction coupling in cardiac muscle. In ventricular myocytes there is growing evidence to support a role for cADPR in modulating CICR (Meszaros, *et al.*, 1993; Rakovic, *et al.*, 1996; Cui, *et al.*, 1999; Rakovic, *et al.*, 1999; Xin,

et al., 2002). However, this is not clear cut in arterial smooth muscle. The amplification of voltage-gated Ca^{2+} influx by CICR does not appear to be universal in vascular smooth muscle. In rat cerebral arteries there is significant amplification of voltage-gated Ca^{2+} influx by CICR (Kamishima and McCarron, 1997), whereas voltage-gated Ca^{2+} influx fails to trigger CICR from the SR of smooth muscle cells isolated from the rat femoral artery, or rat portal vein (Kamishima and McCarron, 1996; Kamishima, *et al.*, 2000). In guinea-pig coronary artery smooth muscle cells CICR is only observed when voltage-gated Ca^{2+} influx is enhanced (Ganitkevich and Isenberg, 1995). One report has suggested that the initiation of CICR may be determined by the magnitude of the voltage-gated Ca^{2+} current and, therefore, Ca^{2+} influx (Kamishima and McCarron, 1997). The spatial compartmentalization of voltage-gated Ca^{2+} channels and RyRs, however, may determine whether or not there is functional coupling. In guinea-pig bladder smooth muscle voltage-gated Ca^{2+} channels in the plasma membrane co-localize with RyRs in the SR (Carrington, *et al.*, 1995), and CICR is triggered by voltage-gated Ca^{2+} influx (Ganitkevich and Isenberg, 1995). Consistent with the tissue-dependency of CICR control by voltage-gated Ca^{2+} influx, the small amount of information available suggests that the modulation of CICR by cADPR in response to voltage-gated Ca^{2+} influx may also be specific to different vascular beds. In bovine coronary arteries depolarization-induced vasoconstriction can be attenuated by 8-Br-cADPR (Zhang, *et al.*, 2002). In contrast, it has been shown that constriction by depolarization-gated Ca^{2+} influx in both rat and rabbit pulmonary artery smooth muscle is unaffected by 8-Br-cADPR or by block of ryanodine-sensitive SR Ca^{2+} stores with ryanodine and caffeine (Dipp and Evans, 2001; Dipp, *et al.*, 2001; Wilson, *et al.*, 2001).

1.5.7 Ca^{2+}-dependent vasodilation by cADPR

Although there is little evidence as yet to suggest a role for cADPR in determining resting tone in arterial smooth muscle, it is clear that cADPR-dependent SR Ca^{2+} release via RyRs can lead to the activation of BK_{Ca} channels, an increase in STOC frequency and consequent membrane hyperpolarisation in arterial smooth muscle (Wilson, *et al.*, 2001; Boittin, *et*

al., 2003; Cheung, 2003). Therefore, cADPR may play a role in mediating smooth muscle relaxation in response to known vasodilators.

As mentioned previously, a variety of transmitters relax smooth muscle by increasing cAMP levels and thereby activating PKA. In arteries, trachea, human airway and lymphatic vessels, PKA-dependent smooth muscle relaxation is mediated, in part, by the opening of BK_{Ca} channels and membrane hyperpolarisation (Allen, *et al.*, 1986; Kume, *et al.*, 1989; Nelson, *et al.*, 1995; Wang and Kotlikoff, 1996b; Jaggar, *et al.*, 2000). In arterial smooth muscle adenylyl cyclase-coupled receptors such as β-adrenoceptors open BK_{Ca} channels by evoking Ca^{2+} signals via RyRs in the SR proximal to the plasma membrane, leading to smooth muscle cell hyperpolarisation and a consequent reduction in blood pressure through vasodilation (Benham and Bolton, 1986; Nelson, *et al.*, 1995; Knot, *et al.*, 1998a; Jaggar, *et al.*, 2000). Despite the wealth of information linking RyR activation to vasodilation by adenylyl cyclase coupled receptors and the role of cADPR as a regulator of RyR function (Lee, 1997), little attention has been paid to the possible role of cADPR in this process. However, investigations by this laboratory into this hypothesis have provided strong evidence to support a role for cADPR in this process (Boittin, *et al.*, 2003).

Intracellular dialysis (from a patch-pipette) of low concentrations of cADPR (20 μM) increased cytoplasmic Ca^{2+} concentration at the perimeter of isolated pulmonary artery smooth muscle cells and concomitant membrane hyperpolarisation. Hyperpolarisation was reversed by the highly selective BK_{Ca} channel antagonist iberiotoxin, which demonstrates that BK_{Ca} channel activation underpins cADPR-dependent hyperpolarisation (Boittin, *et al.*, 2003). Furthermore, SR Ca^{2+} release via RyRs was shown to be a pre-requisite for this response, because hyperpolarisation by cADPR was abolished by chelating intracellular Ca^{2+} with BAPTA, by selective block of RyRs with ryanodine and by depletion of SR Ca^{2+} stores with cyclopiazonic acid. Most importantly, hyperpolarisation by cADPR was blocked by the cADPR antagonists 8-amino-cADPR and 8-bromo-cADPR, whilst hyperpolarisation by caffeine remained unaffected. This is consistent with the cADPR antagonists

blocking the action of cADPR, but not the activation of RyRs *per se.* (Boittin, *et al.*, 2003).

Consistent with previous studies on smooth muscle from a variety of tissues (for review see (Jaggar, *et al.*, 2000), investigations from this laboratory found that isoprenaline and cAMP induced hyperpolarisation in isolated pulmonary arterial smooth muscle cells, and demonstrated that in each case hyperpolarisation exhibited similar pharmacology to hyperpolarisation by cADPR i.e. abolished by intracellular BAPTA, ryanodine, 8-amino-cADPR and iberiotoxin. Strikingly, the selective PKA antagonist H89 blocked hyperpolarisation by both isoprenaline and cAMP, but was without effect on hyperpolarisation by cADPR. Thus, it would appear that cADPR is a downstream element in this signalling cascade. Hyperpolarisation by β-adrenoceptors in pulmonary artery smooth muscle cells may therefore result, at least in part, from activation of adenylyl cyclase, increased cytoplasmic cAMP levels and activation of PKA, leading to activation of ADP-ribosyl cyclase, increased cADPR synthesis, consequent SR Ca^{2+} release via RyRs and hyperpolarisation by BK_{Ca} channel activation. Further support for this proposal was derived from studies on isolated artery rings without endothelium. Vasodilation evoked due to β–adrenoceptor activation by isoprenaline was inhibited by approximately 50% by blocking cADPR with the membrane permeant antagonist 8-bromo-cADPR, by block of RyRs with ryanodine and by depletion of SR Ca^{2+} stores by cyclopiazonic acid. Importantly, 8-bromo-cADPR was without effect on residual dilation by isoprenaline after blocking BK_{Ca} channels with iberiotoxin. Thus, 8-bromo-cADPR reverses isoprenaline-induced dilation by blocking cADPR-dependent SR Ca^{2+} release and, therefore, BK_{Ca} channel activation, because 8-bromo-cADPR does not block BK_{Ca} channel activation *per se*. It is interesting to note, however, that iberiotoxin inhibited dilation by isoprenaline by approximately 78% compared with 50-60% reversal by 8-bromo-cADPR, ryanodine and cyclopiazonic acid, respectively. It would appear, therefore, that cADPR-dependent Ca^{2+} signalling via a cyclopiazonic acid-sensitive SR store is responsible for approximately 80% of BK_{Ca}–dependent vasodilation by isoprenaline in isolated pulmonary arteries. The residual 20% may depend on a mechanism independent of SR

Ca^{2+} release, such as PKA-dependent phosphorylation of the BK_{Ca} channel or an accessory protein (Kume, *et al.*, 1989; Kume, *et al.*, 1994). Support for a role for cADPR in mediating arterial dilation may also be taken from a recent report which suggested that cADPR may mediate vasodilation by urocortin in renal arteries from female, but not male rats (Sanz, *et al.*, 2003).

Previous studies on coronary artery smooth muscle have suggested that increased synthesis of ADP-ribose, a cADPR metabolite, may mediate BK_{Ca}-dependent vasodilation by 11,12-epoxyeicosatrienoic acid (Li, *et al.*, 2002a). By contrast, however, this laboratory found equivalent concentrations of ADP-ribose to be without effect on membrane potential in pulmonary artery smooth muscle cells.

A further variation on the theme comes from the proposal that NO may mediate vasodilation by inhibiting cADPR formation (Geiger, *et al.*, 2000; Yu, *et al.*, 2000). In marked contrast to previous studies on sea urchin egg homogenates (Galione, *et al.*, 1993), NO appeared to act directly upon ADP-ribosyl cyclase in arterial smooth muscle and in a manner independent of guanylyl cyclase and cGMP (Yu, *et al.*, 2000). Thus, cADPR synthesis in coronary artery homogenates was inhibited by the NO donor SNP, with inhibition being reversed by NO scavengers but not by guanylyl cyclase inhibitors. Furthermore, subsequent studies on recombinant CD38 suggested that NO may inhibit ADP-ribosyl cyclase via *S*-nitrosylation of sulphydryl groups (White, *et al.*, 2002), which may impact on dimerisation (Berruet, *et al.*, 1998; Chidambaram and Chang, 1998).

The aforementioned studies suggest, therefore, that the mechanism by which regulators of pyridine nucleotide signalling promote relaxation of arterial smooth muscle may vary in a manner dependent on the nature of the vasodilator and / or the vascular bed under investigation.

1.5.8 NAADP as a Ca^{2+} mobilizing messenger

1.5.8.1 Ca^{2+} mobilization by NAADP occurs from a non-ER/SR Ca^{2+} store

As mentioned previously there is significant evidence that the molecular target for NAADP is distinct from that for IP_3 or cADPR. In

homogenates of sea urchin egg which have active Ca^{2+} stores, addition of NAADP was seen to cause concentration-dependent Ca^{2+} release (Chini, *et al.*, 1995; Lee and Aarhus, 1995). This NAADP-mediated Ca^{2+} release was shown to undergo homologous desensitization, which was without effect upon Ca^{2+} mobilisation in response to the application of either IP_3 or cADPR (Chini, *et al.*, 1995; Lee and Aarhus, 1995). In these studies NAADP-mediated Ca^{2+} release was also shown to be insensitive to a known inhibitor of IP_3-mediated Ca^{2+} release, heparin (Chini, *et al.*, 1995; Lee and Aarhus, 1995), or to known inhibitors of cADPR-mediated Ca^{2+} release, 8-amino-cADPR (Lee and Aarhus, 1995) or Ruthenium Red (Chini, *et al.*, 1995). Lee and Aarhus (1995) proposed that the NAADP-sensitive Ca^{2+} store was separate from those stores accessed by either IP_3 or cADPR. In support of this view, NAADP-mediated Ca^{2+} release was shown to occur in different fractions of sea urchin egg homogenates than that mediated by either IP_3 or cADPR, when homogenates were separated by the use of Percoll density gradients. Whilst the IP_3- and cADPR-sensitive Ca^{2+} stores were located in fractions with a high abundance of ER membrane markers, the NAADP-sensitive Ca^{2+} store was seen to be located in separate fractions, with little or no cross-over between these different stores (Lee and Aarhus, 1995). These fractionation studies also showed that the NAADP-sensitive Ca^{2+} store within sea urchin eggs was unlikely to be the mitochondria, as NAADP-sensitive Ca^{2+} stores were distant to the mitochondrial marker cytochrome c oxidase (Lee and Aarhus, 1995).

The NAADP-sensitive Ca^{2+} store has also been reported to be pharmacologically distinct to the Ca^{2+} stores mobilised by either IP_3 or cADPR. Thapsigargin, a plant-derived sesquiterpine lactone (Thastrup, *et al.*, 1990) known to bind potently to and inhibit uptake of Ca^{2+} into the ER/SR via SERCA pumps (Lytton, *et al.*, 1991), leading to depletion of ER/SR Ca^{2+} stores, has been shown to abolish both cADPR- and IP_3-mediated Ca^{2+} release (Genazzani and Galione, 1996). NAADP-mediated Ca^{2+} signals, however, remained unaffected after the depletion of microsomal Ca^{2+} stores in sea urchin egg homogenates by thapsigargin (Genazzani and Galione, 1996; Churchill and Galione, 2001). This led to the proposal that NAADP mobilized a thapsigargin-insensitive Ca^{2+} store other than the ER. The precise nature of the store accessed by NAADP and the molecular target of NAADP remained elusive.

However, in sea urchin egg homogenates NAADP-mediated Ca^{2+} release has been shown to be inhibited by the L-type Ca^{2+} channel antagonists verapamil and diltiazem (Genazzani, *et al.*, 1996b), The NAADP-dependent Ca^{2+}release channel is unlikely to be an L-type Ca^{2+}channel though, as the L-type Ca^{2+} channel agonist, BAY K8844 also inhibits NAADP-mediated Ca^{2+} release in sea urchin egg homogenates (Genazzani, *et al.*, 1996b). NAADP-mediated Ca^{2+} release also remains unaffected by pH (Genazzani, *et al.*, 1997; Chini, *et al.*, 1998). In their study, Genazzani *et al.* (1997) showed that Ca^{2+} release by NAADP remained unaffected by changes in cellular pH between normal (pH 7.2), acidic (pH 6.7) and alkaline (pH 8.0) conditions, while IP_3-mediated Ca^{2+} release and cADPR-mediated Ca^{2+} release were undetectable under acidic conditions, thus providing further evidence in support of the view that NAADP mediates Ca^{2+} release from a separate channel to cADPR or IP_3. Another important feature of NAADP-mediated Ca^{2+} release is the lack of an effect of Ca^{2+} on the release mechanism. In sea urchin egg homogenates (Chini and Dousa, 1996; Genazzani and Galione, 1996), brain microsomes (Bak, *et al.*, 1999) and microsomes isolated from higher plants, such as cauliflower and red beet (Navazio, *et al.*, 2000) Ca^{2+} concentration was shown to be ineffective in regulating the amount of Ca^{2+} released by NAADP application. This contrasts sharply with the findings that both IP_3R and RyR channels are biphasically regulated by Ca^{2+}.

Subsequent to these pharmacological studies, the NAADP-sensitive Ca^{2+} store was shown to be visibly separate from either the IP_3- or cADPR-sensitive stores following stratification of intact sea urchin eggs (Lee and Aarhus, 2000). Stratification refers to a process where the intracellular organelles within intact cells can be separated by centrifugation at 7 – 8000 g on a desktop microfuge. Using the fluorescent Ca^{2+} indicator dye, Fluo-3, to visualise the intracellular Ca^{2+} concentration it was seen that flash-photolysis of caged NAADP mobilised Ca^{2+} from the opposite pole of the eggs when compared to photolysis of either caged IP_3 or caged cADPR (Lee and Aarhus, 2000). The separation of stores accessible to NAADP and IP_3 has been shown in mammalian cells as well. In the highly polarised pancreatic acinar cells flash photolysis of NAADP has been shown to initiate $Ca^{2+}$from the opposite pole of cells to IP_3 (Krause, *et al.*, 2002).

1.5.8.2 Inactivation of NAADP-induced Ca^{2+} release

An interesting and remarkable feature of the NAADP-mediated Ca^{2+} release mechanism is the manner in which it can be inactivated. In sea urchin eggs exposure to low concentrations of NAADP attenuates Ca^{2+} release in response to an otherwise normally maximal concentration of NADDP (Aarhus, *et al.*, 1996a; Genazzani, *et al.*, 1996b). This in itself is not too unusual. However, it is when we consider that this attenuation of the response is seen to happen at sub-threshold concentrations of NAADP that this mechanism becomes more intriguing (Aarhus, *et al.*, 1996a; Genazzani, *et al.*, 1996b). This inactivation appears to be both time-and concentration-dependent. In the presence of fixed sub-threshold concentrations of NAADP, the Ca^{2+} response elicited by the maximal NAADP concentration is seen to decline steadily as the time between the two NAADP applications increases (Aarhus, *et al.*, 1996a; Genazzani, *et al.*, 1996b). Inactivation requires around 2 minutes in order to reach a plateau and it appears to be independent of the NAADP concentration used (Aarhus, *et al.*, 1996a; Genazzani, *et al.*, 1996b). This process of inactivation can be described in a simple model which proposes that NAADP receptors posses two separate NAADP binding sites, a low affinity site which mediates channel opening and a high affinity site which mediates channel inactivation. When the NAADP concentration within the system is low, the high affinity site will be occupied, leading to inactivation of the release mechanism. If the NAADP concentration is then raised, a subsequent challenge will be unable to mediate any Ca^{2+} release, as the receptor will stay inactivated. The inactivation process must be a relatively slow process. If it were not the channels would not open in homogenate preparations treated with higher NAADP concentrations, as both sites would be occupied. Given that the rate of inactivation of Ca^{2+} release in response to NAADP is independent of the concentration of NAADP, it suggests that the rate-limiting step which governs channel function is the inactivation process itself and not binding of NAADP to the receptor (Aarhus, *et al.*, 1996a; Genazzani, *et al.*, 1996b). Since the binding of NAADP to its target in sea urchin eggs is irreversible (Aarhus, *et al.*, 1996a; Billington and Genazzani, 2000b; Patel, *et al.*, 2000a), it is conceivable that

binding of NAADP to the high affinity site results in the conversion of the receptor to its inactivated state.

The target for NAADP in mammalian cells has also been shown to inactivate prior to activation. However, the mammalian receptors do so in a fundamentally different fashion to the binding sites in sea urchin eggs. The concentration-effect relationships to NAADP mediated Ca^{2+} release examined in several cell types appear to be biphasic in nature. This was first seen in the pancreatic acinar cell (Cancela, *et al.*, 1999). In this study nanomolar concentrations of NAADP mediated complex Ca^{2+} signals, whereas concentrations of NAADP in the micromolar range were seen to be ineffective (Cancela, *et al.*, 1999). The evidence presented within the study of Cancela *et* al (1999) showed that inactivation of the NAADP-mediated Ca^{2+} release mechanism occurred prior to activation. However, in contrast to the sea urchin egg, this inactivation occurred at concentrations much higher than the threshold concentration for Ca^{2+} release. Studies into the effect of differing concentrations of NAADP have been carried out other cell types, including T lymphocytes (Berg, *et al.*, 2000), human pancreatic beta cells (Johnson and Misler, 2002), and the clonal cell line MIN-6 (Masgrau, *et al.*, 2003). These studies indicate a clear bell shaped activation curve for the 'NAADP-receptor'. However, since these studies were carried out using microinjection techniques, the absolute concentration of NAADP at the target molecule within the cells cannot be accurately determined. Recent evidence from this laboratory has shown that lower concentrations of NAADP (10 nM) are much more effective in activating Ca^{2+} release within individual smooth muscle cells isolated from pulmonary arteries than higher concentrations (100 μM; Boittin, *et al.*, 2002). These inactivation and activation properties of the mammalian NAADP receptor can also be described by the use of a high-and low-affinity binding site model. In contrast to the model proposed for the sea urchin egg it has been proposed that the low affinity binding site mediates channel inactivation within mammalian cells (Patel, 2004). This model does not require irreversible NAADP binding in mammalian cells, as is the case with the sea urchin eggs, and there is evidence to suggest that the binding of NAADP to its molecular target is reversible in mammalian cells (Patel, *et al.*, 2000b; Bak, *et al.*, 2001).

1.5.8.3 The NAADP receptor

The sequence of the NAADP receptor has yet to be identified. However, high affinity binding sites for NAADP have been isolated from the sea urchin egg and from mammalian cells (Billington and Genazzani, 2000b; Patel, *et al.*, 2000a; Patel, *et al.*, 2000b). In sea urchin eggs, studies involving the purification and solubilisation have thus far taken advantage of the fact that NAADP binding to its receptor appears to be irreversible in the presence of physiological concentrations of K^+ (Dickinson and Patel, 2003). Therefore, NAADP radio-labeled with [^{32}P] has been used to tag receptors through the process of purification (Billington and Genazzani, 2000b; Berridge, *et al.*, 2002). What we can identify from protein purification is that the NAADP receptor may be an oligomeric structure of around 450 kDa in size, derived from subunits with molecular weights of about 150 kDa each (Berridge, *et al.*, 2002). Therefore, this suggests that the NAADP receptors may be smaller than either the IP_3Rs or the RyRs.

1.5.8.4 Co-operative Ca^{2+} signalling between NAADP, IP_3 and cADPR

There is a large volume of evidence which demonstrates that NAADP mediates the release of Ca^{2+} from a dedicated and, as yet, unknown NAADP receptor located on a store separate from the ER/SR stores accessed by IP_3 and cADPR. However, it appears that although separate from the ER/SR, the NAADP receptors do not act in isolation, and a number of studies have demonstrated a degree of cross-talk between these different Ca^{2+} release mechanisms. This phenomenon has been termed 'channel chatter' (Patel, *et al.*, 2001), with the pancreatic acinar cell presenting one of the best examples of it. Ca^{2+} signalling within the pancreatic acinar cell is well characterised and it has been known for some time that different agonists evoke very different Ca^{2+} signalling patterns (Cancela, 2001). For example, the brain/gut peptide cholecystokinin produces a mixture of short-and long-term Ca^{2+} oscillations that correspond to Ca^{2+} increases within the secretory pole and global signals which are able to travel through the entire cell (Cancela, 2001). The application

of NAADP to the cells through a patch pipette was able to mimic these effects, however, the application of either IP_3 or cADPR were not able to mimic these responses (Cancela, *et al.*, 1999). Interestingly, in pancreatic acinar cells, Ca^{2+} spikes induced by NAADP were seen to be abolished by the combination of heparin and 8-amino-cADPR, known antagonists of the IP_3- and cADPR-mediated Ca^{2+} release, respectively (Cancela, *et al.*, 1999). However, the abolition of NAADP-mediated Ca^{2+} release by inactivation of NAADP-mediated Ca^{2+} release, with 100 μM NAADP, did not affect the production of Ca^{2+} spikes in response to either IP_3 or cADPR (Cancela *et al.*, 1999). Due to these findings, it was suggested that NAADP triggers an initial phase of Ca^{2+} release, which is then amplified into a global Ca^{2+} response via CICR from IP_3Rs and RyRs (Cancela, *et al.*, 1999).

Further evidence of a clear coupling between the NAADP-, IP_3-and cADPR-mediated Ca^{2+} release mechanisms has also been provided by studies carried out on sea urchin eggs (Churchill and Galione, 2000), and starfish oocytes (Santella, *et al.*, 2000). In both of these preparations Ca^{2+} signals generated in response to NAADP are inhibited by a combination of heparin and 8-NH_2-cADPR. Similar to the pancreatic acinar cell, responses in the starfish oocytes in response to NAADP are abolished by this combination of antagonists (Santella *et al.*, 2000). However, Ca^{2+} release, although inhibited, is still observed in response to NAADP following treatment of sea urchin eggs with heparin and 8-NH_2-cADPR (Churchill and Galione, 2000). The mechanism underlying these observed differences in response to NAADP following inhibition of IP_3- and cADPR-mediated Ca^{2+} release remains unclear.

1.5.8.5 Acidic Ca^{2+} stores, the source of NAADP-mediated Ca^{2+} signals?

Recently, reserve granules have been identified as the NAADP-sensitive Ca^{2+} store in sea urchin eggs (Churchill, *et al.*, 2002). Churchill *et al* showed that NAADP-mediated Ca^{2+} release was selectively abolished by pre-treatment of sea urchin eggs with glycyl-phenylalanyl-napthylamide (GPN), a known substrate of the lysosomal exopeptidase cathepsin C. Upon entering the

lysosome GPN is hydrolysed to free amino acids by the actions of the cathepsin C. These resultant amino acids are unable to exit the lysosome and, therefore, their accumulation causes an increase in osmotic pressure, eventually leading to rupture of the compartment (Berg, *et al.*, 1994). In order to determine that this loss of NAADP responsiveness was due to an effect of GPN on reserve granules, sea urchin eggs were loaded with the fluorescent weak base, LysoTracker Red. LysoTracker Red accumulates in acidic stores, and following pre-treatment of cells with LysoTracker Red, acidic organelles were seen to be diffusely distributed throughout sea urchin eggs. LysoTracker fluorescence was lost in a time-dependent manner after the application of GPN to eggs suggesting that the effects of GPN on NAADP-mediated Ca^{2+} signals were down to a disruption of a lysosome-related, acidic Ca^{2+} store (Churchill, *et al.*, 2002). In sea urchin eggs loaded with fluorescent Ca^{2+} indicator dye, GPN was seen to cause localized Ca^{2+} release events, consistent with a role for lysosome-related acidic Ca^{2+} stores (Churchill, *et al.*, 2002). Following these observations, stratification of sea urchin eggs showed that acidic organelles were depleted in the pole of the egg containing the nucleus and the ER, and were enriched in the opposite pole (Churchill, *et al.*, 2002). This finding was consistent with the Ca^{2+} release previously described in stratified sea urchin eggs in response to NAADP, cADPR and IP_3 (Lee and Aarhus, 2000). In their study, Churchill *et al.* (2002) carried out further experiments on crude, subcellular fractions in order to further characterise the mechanism of NAADP-mediated Ca^{2+} release. It was shown that subcellular fractionation produced fractions that responded predominantly to NAADP. Occasional responses within these fractions to cADPR and IP_3 were removed by separation of the fraction further on a Percol density gradient. This method of separation had been previously described as an accurate and reliable method of isolating reserve granules (McNeil, *et al.*, 2000), the functional equivalent of mammalian lysosomes within sea urchin eggs (Armant, *et al.*, 1986). After separation, the fraction that only responded to NAADP was shown to express larger amounts of lysosomal membrane markers, such as acid phosphatase, glucosaminadase and β-galactosidase, than those fractions insensitive to NAADP. This suggested that the NAADP-sensitive Ca^{2+} store was lysosomal

in nature (Churchill, *et al.*, 2002). This fraction only possessed a NAADP-sensitive store, as no Ca^{2+} release was triggered by cADPR, IP_3 or thapsigargin. Churchill and colleagues were therefore able to characterise the mechanism of Ca^{2+} uptake into this Ca^{2+} store (Churchill, *et al.*, 2002). Ca^{2+} uptake into these compartments was found to be prevented by treatment of fractions with apyrase, an agent that induces the hydrolysis of ATP, suggesting that Ca^{2+} uptake into the NAADP-sensitive Ca^{2+} stores was ATP-dependent. This NAADP-sensitive store also seemed to have some requirement for protons, as Ca^{2+} uptake into this store was also seen to be abolished by treatment of the fraction with various protonophores. This proton requirement suggested that a proton gradient across the store was required for Ca^{2+} uptake, a finding confirmed by treatment of fractions with the K/H^+ exchanger, nigericin, or the weak base NH_3 (Churchill, *et al.*, 2002). Ca^{2+} uptake was also abolished by treatment of NAADP-sensitive fractions with the inhibitor of the vacuolar proton pump ($V\text{-}H^+$ ATPase) Bafilomycin A1, which had previously been shown to collapse proton gradients within lysosomes (Christensen, *et al.*, 2002). Thus, a $V\text{-}H^+$ ATPase is required for maintenance of a proton gradient. This proton gradient was shown to drive Ca^{2+} uptake into NAADP-sensitive stores through a Ca^{2+}/H^+ ATPase as Ca^{2+} uptake was also inhibited by vanadate, previously shown to be an inhibitor of these Ca^{2+}/H^+ exchangers (Rooney and Gross, 1992). This led Churchill and colleagues to propose that the NAADP-sensitive Ca^{2+} stores within sea urchin eggs are the reserve granules (Churchill, *et al.*, 2002). Further investigations have suggested that NAADP mediates initial Ca^{2+} release from acidic stores in mammalian cells. NAADP has been shown to mediate initial Ca^{2+} signals from an acidic, lysosome-related Ca^{2+} store in murine pancreatic acinar cells and a clonal pancreatic beta cell line, MIN-6 (Yamasaki, *et al.*, 2004). Indeed, in this study Yamasaki *et al.* showed that different agonists mediate their effects through recruitment of different second messengers. In pancreatic acinar cells responses generated to acetylcholine and bombesin recruit ER Ca^{2+} stores, while cholecystokinin recruits an acidic, lysosome-related Ca^{2+} store (Yamasaki, *et al.*, 2004). Calcium signals in response to cholecystokinin have been shown to require Ca^{2+} signals generated by NAADP and cADPR acting in concert. Activation of cholecystokinin receptor A on pancreatic acinar cells results in an

initial, transient increase in NAADP levels, followed by a slower rising, sustained increase in cADPR levels (Yamasaki, *et al.*, 2005). NAADP has also been shown to be important in neurite outgrowth in rat cortical neurons. Application of NGF to neurons has been shown to elicit Ca^{2+} signals through NAADP-mediated acidic Ca^{2+} release and subsequent Ca^{2+} release via both IP_3Rs and RyRs (Brailoiu, *et al.*, 2005).

That NAADP mediates Ca^{2+} release through a distinct channel located on a store other than the ER/SR is not a universally accepted proposal. It has been proposed that NAADP directly activates RyRs. Hohenegger *et al*. (2002) described NAADP-induced Ca^{2+} release in microsomes isolated from skeletal muscle where the regulation of NAADP-mediated Ca^{2+} release by Ca^{2+}, and the abolition of responses to NAADP by ryanodine, are consistent with direct activation of RyR subtype 1 by NAADP (Hohenegger, *et al.*, 2002). In this study NAADP was seen to modulate the opening of single channels of purified RyRs reconstituted into lipid bilayers (Hohenegger, *et al.*, 2002). NAADP has also been suggested to regulate the opening of RyR subtype 2 isolated from cardiac microsomes and expressed in lipid bilayers (Mojzisova, *et al.*, 2001). However, another study carried out on RyR subtype 1, isolated from skeletal muscle, and RyR subtype 2, isolated from cardiac muscle, both reconstituted in lipid bilayers, showed that NAADP did not influence the opening of these receptors (Copello, *et al.*, 2001).

Despite these latter findings, however, that controversy surrounding the nature of the NAADP receptor continues. In an examination of the nuclear envelope Ca^{2+} store within pancreatic acinar cells, Gerasimenko *et al* (2003) suggest that NAADP activates RyRs present on the nuclear envelope. In this study the application of pharmacological agents which disrupt Ca^{2+} handling within acidic stores such as nigericin and Bafilomycin A1 were seen to be ineffective at inhibiting Ca^{2+} release induced by NAADP. The investigators also showed that NAADP-mediated Ca^{2+} release was abolished in these isolated nuclei after treatment with blockers of RyRs ryanodine and ruthenium red. Ca^{2+} release by NAADP was also shown to be unaffected by the treatment of nuclei with blockers of IP_3Rs, which led the investigators to suggest that NAADP mediates Ca^{2+} release into the nucleoplasm through RyRs in the nuclear envelope of pancreatic acinar cells (Gerasimenko, *et al.*, 2003). In

intact pancreatic acinar cells, Yamasaki *et al.* (2004) have shown that NAADP-mediates Ca^{2+} release from an acidic, lysosome-related Ca^{2+} store. Ca^{2+} signals generated in response to NAADP were abolished by preincubation of cells with either Bafilomycin A1 or GPN, but were only partially inhibited by depletion of SR Ca^{2+} stores by thapsigargin.

NAADP has also been shown to be a potent Ca^{2+} mobiliser in Jurkat T-cells, a cell line derived from human T-lymphocytes (Berg, *et al.*, 2000). In their investigation, Berg *et al* (2000) showed that NAADP invoked Ca^{2+} signals independently of either cADPR or IP_3, as antagonists of both cADPR- and IP_3-mediated Ca^{2+} release did not affect NAADP-mediated Ca^{2+} signals. However, the application of high concentrations of NAADP, in order to inactivate the NAADP-release mechanism, caused a marked inhibition of Ca^{2+} signals generated in response to either cADPR or IP_3 (Berg, *et al.*, 2000). Therefore, the authors proposed that cADPR- and IP_3-mediated Ca^{2+} release was required for a functional NAADP-mediated Ca^{2+} release system (Berg, *et al.*, 2000). Further investigations by Guse and colleagues have suggested that Ca^{2+} signals in response to NAADP in Jurkat T-cells are initiated by RyR-mediated Ca^{2+} release which is amplified by Ca^{2+} influx from the extracellular environment (Langhorst, *et al.*, 2004). Most recently, Guse and colleagues have presented evidence suggesting that the NAADP acts directly upon RyRs in Jurkat T-cells to cause Ca^{2+} release, rather than a separate, putative NAADP receptor (Dammermann and Guse, 2005). Given these varied and often conflicting reports it is clear that the precise mechanism through which NAADP affects Ca^{2+} release is still an area great uncertainty, and further investigation is required in order to determine the precise mechanisms involved.

1.5.8.6 A role for NAADP-dependent Ca^{2+} signalling in vascular smooth muscle

Despite a number of investigations on other cell types into the mechanisms of NAADP-dependent Ca^{2+} signalling, our knowledge on the role of this Ca^{2+} mobilising messenger in vascular smooth muscle is extremely limited. Only a handful of studies have been carried out, and from these very

little is known. It has been shown that the enzymes for the synthesis and metabolism of NAADP are present in vascular smooth muscle (Wilson, *et al.*, 1998; Yusufi, *et al.*, 2001), and microsomes prepared from rat aortic vascular smooth muscle have been shown to release Ca^{2+} in a concentration dependent manner in response to NAADP (Yusufi, *et al.*, 2001). In these microsomes, IP_3-, cADPR- and NAADP-mediated Ca^{2+} release mechanisms were seen to function independently of each other (Yusufi, *et al.*, 2002). Blockade of IP_3Rs with heparin only inhibited IP_3-mediated signals, while blockade of RyRs with ruthenium red was seen to only inhibit Ca^{2+} signals mediated by cADPR. Consistent with findings in other cell types (Genazzani, *et al.*, 1996b), NAADP-mediated Ca^{2+} signals were seen to be inhibited by the treatment of microsomes with L-type Ca^{2+} channel blockers, which were without effect on IP_3- or cADPR-mediated Ca^{2+} signals (Yusufi, *et al.*, 2002).

1.6 The pulmonary circulation

1.6.1 Pulmonary blood flow

Blood enters the pulmonary circulation from the right ventricle of the heart and returns to the left atrium. Partially or fully deoxygenated blood enters the right ventricle from the systemic circulation via the superior or inferior vena cavae; it is then pumped into the main pulmonary artery. The main pulmonary artery, which is about 5 cm in length in man, then divides into two branches (left and right) that supply the blood to each of the lungs. These branches then further divide into smaller resistance arteries (<1 mm internal diameter), which themselves further divide into even smaller capillary vessels (<10 μm internal diameter). If the lobe of the lung is placed with its parietal surface facing upwards, the artery is seen to be located directly below the airway, which also branches and divides. The trachea branches into bronchi, bronchioles and finally, alveoli. An extremely dense network of capillaries, which surround the alveoli, allows the gaseous exchange to occur between alveoli and pulmonary capillaries (Gray, 1858).

The pulmonary circulation is in series with the systemic circulation and is therefore required to take the entire cardiac output. It is unable to adjust its own blood flow, without altering the blood flow of the entire systemic circulation. It does manage, however, to regulate local blood flow within the system depending on which areas of the lung are oxygenated by the mechanism of hypoxic pulmonary vasoconstriction (HPV), as will be discussed in more detail later.

1.6.2 Pulmonary arteries

The pulmonary arteries are shorter in length, larger in diameter and thinner than their systemic counterparts. They have more distensible walls which contain less smooth muscle and elastin resulting in the pulmonary circulation having a high compliance. Second order branches of the pulmonary artery have a relatively small lumen (<2 mm internal diameter in humans) and a thick wall consisting primarily of elastic tissue and smooth muscle (up to about three quarters of its total mass). The even smaller resistance arteries (<1 mm internal diameter in humans) are composed almost entirely of smooth muscle (Gray, 1858).

1.6.3 Pulmonary veins

Pulmonary veins are composed of the same elements as the pulmonary arteries as described above. However, the proportions are different, with the vein being thinner with much less elastic tissue and smooth muscle than the artery. The veins of the pulmonary system are far more variable than arteries with respect to their branching pattern (Brock, 1942). The pulmonary veins accompany the bronchi and pulmonary arteries, located centrally within each segment, however, the pulmonary veins also run between segments of the lung and below visceral pleura, unlike the arteries and the bronchi.

1.6.4 Pulmonary capillaries

The capillaries are the most abundant blood vessels within the body. The pulmonary capillary bed in humans is believed to consist of an area of around 30 m^2 (Weibel, 1963). The primary function of all capillaries is gaseous exchange, primarily between oxygen and carbon dioxide, which is a role that capillaries are exceptionally well adapted to perform. The walls of the capillary vessels are composed almost entirely of simple endothelial cells and provide a diffusion barrier of as little as 0.5 μm. A characteristic of pulmonary capillaries which distinguishes them from their systemic counterparts is a greater compliance. This is associated with the fact that they are surrounded by air, rather than tissue (Fung and Sobin, 1972).

1.6.5 Nervous innervation

On the whole, it appears that local mechanisms regulate local blood flow while nervous control regulates global blood flow (control of arterial pressure, redistribution to an area of the body, increase in heart and force of contraction; Williams (1995)). However, the possibility of local effects by nervous control cannot be dismissed. The innervation of pulmonary blood vessels is by efferent autonomic fibres controlled by the sympathetic nervous system. All blood vessels, with the exception of most capillaries (and the small resistance pulmonary arteries of the rat) are innervated by sympathetic vasomotor nerve fibres which exit the spinal cord through the thoracic and first two lumbar spinal nerves (Gray, 1858).

As mentioned previously, a number of studies have suggested that the pulmonary innervation plays little role in ventilation/perfusion matching through the mechanism of HPV (Nissel, 1948; Tucker, 1979). This has led to the suggestion that control of vascular permeability rather than control of vascular resistance is the role of the nervous innervation found within the pulmonary circulation (Beckman and Metha, 1996). However innervation of the pulmonary vasculature may also play a role in regulating the compliance of large conduit vessels where there is a lot of innervation; however this role may

become less important as innervation decreases further down the vascular tree (McLean, *et al.*, 1985).

1.7 Hypoxic pulmonary vasoconstriction

HPV was first described in 1894 when Bradford and Dean noted that upon asphyxia there was a significant rise in pulmonary arterial pressure (Bradford and Dean, 1894). Fifty years later, von Eular and Liljestrand (1946) showed, in the feline circulation, hypoxia alone (without hypercapnia) was able to constrict vessels from the pulmonary system. They also hypothesised in this study that this constriction may aid ventilation/perfusion matching at the alveolar level (von Euler and Liljestrand, 1946). An important discovery in this field was then made when it was shown that the hypoxic response in the isolated perfused feline lung was a local response and was not mediated by the autonomic nervous system (Nissel, 1948).

As mentioned previously, the mechanism of HPV acts to divert blood flow from poorly ventilated areas of the lung to better ventilated regions, i.e. it matches local perfusion to ventilation (von Euler and Liljestrand, 1946). Systemic arteries, however, tend to dilate or show no response to hypoxia (Szidon, *et al.*, 1969). When it occurs, systemic artery dilation by hypoxia serves to match local perfusion to local metabolism (Roy and Sherrington, 1890; Lassen, *et al.*, 1978). The mechanism by which HPV occurs is not fully understood and remains a topic of great debate and research.

The final step for all stimuli which induce pulmonary vasoconstriction involves the activation of the cellular contractile apparatus. There is little evidence in the literature to suggest that the contractile apparatus within the pulmonary artery is unique and most agents which induce constriction of pulmonary arteries cause concurrent systemic vasoconstriction. Notable exceptions to these are hypoxia and mitochondrial electron transport chain (ETC) inhibitors (Archer, *et al.*, 1993). It appears that this restriction of hypoxic vasoconstriction to the resistance pulmonary arteries is due to a unique property of pulmonary artery smooth muscle and endothelial cells. The precise nature of this unique ‘sensor’ is still steeped in uncertainty and controversy, with a number of likely candidates having been championed.

1.7.1 Mechanism involved in the initiation of hypoxic pulmonary vasoconstriction

Relatively mild hypoxia has been shown to inhibit mitochondrial oxidative phosphorylation in O_2-sensing cells and it has been suggested that this may underpin, at least in part, cell activation (Mills and Jobsis, 1972; Rounds and McMurtry, 1981; Duchen and Biscoe, 1992a; Wyatt and Buckler, 2004). Thus, depolarisation of the mitochondrial membrane potential and/or an increase in β-NAD(P)H levels has been reported in all O_2-sensing cells examined (Archer, *et al.*, 1986; Duchen, 1992); Youngson, *et al.*, 1993; Shigemori, *et al.*, 1996; Leach, *et al.*, 2001) and over a range of P_{O_2} that elicits no such response in other cell types (Duchen and Biscoe, 1992b). There are currently three theories within the field that have been proposed to couple mitochondria to HPV. These theories are outlined below.

A number of investigations on HPV have suggested that inhibition of mitochondrial oxidative phosphorylation by hypoxia elicits a decrease in the production of reactive oxygen species (ROS) and an associated increase in reduced redox couples (Archer, *et al.*, 1986; Archer, *et al.*, 1989; Archer, *et al.*, 1993; Paky, *et al.*, 1993), and that these events lead to the initiation of HPV (Archer, *et al.*, 1986; Reeve, *et al.*, 1995).

However, there is evidence in the literature to suggest that hypoxia results in a paradoxical increase in ROS in pulmonary artery smooth muscle (Marshall, *et al.*, 1996; Waypa, *et al.*, 2001; Liu, *et al.*, 2003), calling into question the validity of the redox model proposed by Archer and colleagues. This converse theory involving ROS suggests that the increase in ROS results in a shift in the cellular redox status to a more oxidized state, triggering HPV. It is still open to question whether or not ROS or reduced redox couples act as mediators of HPV.

Recently, work from this laboratory has suggested that AMP-activated protein kinase (AMPK) may function to couple mitochondrial oxidative phosphorylation to Ca^{2+} signalling mechanisms underpinning HPV in pulmonary artery smooth muscle cells (Evans, *et al.*, 2005).

Within the last ten years, AMPK, a serine threonine kinase, has come to prominence as a metabolic fuel gauge which monitors the cellular AMP/ATP ratio within cells as an indicator of metabolic stress (Hardie, *et al.*, 2006). It is activated in response to a number of metabolic stresses (e.g. hypoxia, glucose deprivation, excercise) that either increase cellular ATP consumption or reduce ATP supply via mitochondrial oxidative phosphorylation. AMPK activation is consequent to the action of adenylate kinase, which catalyses the conversion of 2 molecules of ADP to ATP + AMP, countering a reduction in ATP supply. AMPK then catalyses the production of ATP from AMP to help further maintain the cellular ATP supply (Hardie, *et al.*, 2006). Activation of AMPK promotes catabolic pathways in order to maintain ATP supply, whilst also switching off non-essential ATP-consuming pathways (Hardie, *et al.*, 2006). However, far from being solely a mediator of energy metabolism, it is now clear that AMPK can also target non-metabolic processes within cells (Hardie, 2005). Consistent with this proposal work from this laboratory has provided evidence which supports a role for AMPK in mediating Ca^{2+} signals in response to hypoxia in pulmonary artery smooth muscle cells (Evans, *et al.*, 2005).

1.7.2 Increases in intracellular Ca^{2+} concentration and the generation of hypoxic pulmonary vasoconstriction

HPV had been presumed to be mediated by inhibition of K_v channels, subsequent membrane depolarisation and voltage-gated Ca^{2+} influx (Michelakis, *et al.*, 2004). However it is now clear that constriction of pulmonary artery rings by hypoxia may be induced in the absence of extracellular Ca^{2+}, i.e. under conditions where voltage-gated Ca^{2+} influx is abolished (Dipp, *et al.*, 2001).

In isolated pulmonary artery rings, HPV is biphasic (Fig. 1.6) when induced by switiching from normoxia (155-160 Torr) to hypoxia (16-21 Torr). Thus, hypoxia induces an initial transient constriction (Phase 1) followed by a slow tonic constriction (Phase 2; Salvaterra and Goldman, 1993; Leach, *et al.*, 1994; Robertson, *et al.*, 1995; Dipp and Evans, 2001; Dipp, *et al.*, 2001; Wilson, *et al.*, 2001). In arteries without endothelium, this laboratory has

shown that the initial transient constriction is followed by a maintained plateau constriction, which persists for the duration of exposure to hypoxia (Dipp and Evans, 2001; Dipp, *et al.*, 2001). Thus, the development of the slow tonic constriction is endothelium dependent (Dipp, *et al.*, 2001), whilst the initial transient constriction and maintained plateau are mediated by mechanisms

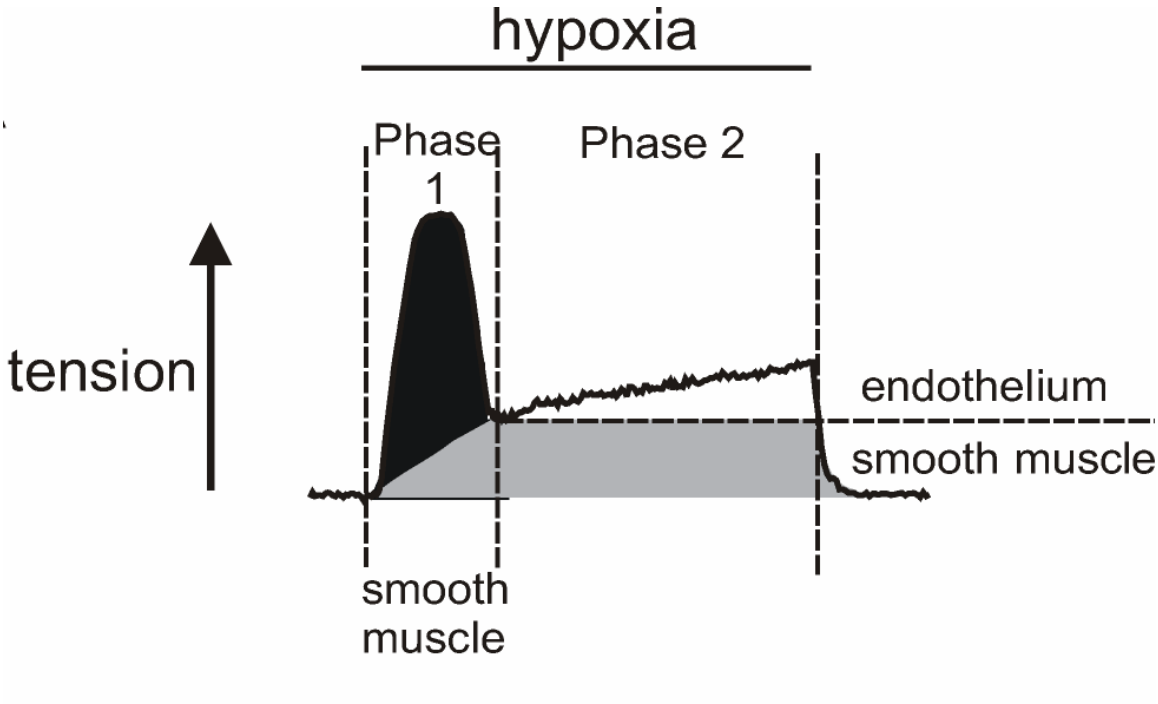

Fig. 1.6 **The response of pulmonary arteries to hypoxia consists of 2 phases:** Black indicates cADPR-independent constriction driven by smooth muscle SR ca^{2+} release; grey indicates the constriction driven by cADPR-dependent smooth muscle SR Ca^{2+} release; and white indicates endothelium-dependent component.

intrinsic to the smooth muscle (Fig. 1.6; Dipp and Evans, 2001; Dipp, *et al.*, 2001; Wilson, *et al.*, 2001). Indeed, these investigations provide compelling evidence in support of a pivotal role for continued smooth muscle SR Ca^{2+} release in the maintenance of sustained HPV in isolated pulmonary arteries both with and without endothelium (Dipp and Evans, 2001; Dipp, *et al.*, 2001; Wilson, *et al.*, 2001). Consistent with these findings, a growing body of evidence now suggests that acute HPV is primarily initiated and maintained by the release of Ca^{2+} from smooth muscle SR stores via RyRs (Salvaterra and Goldman, 1993; Jabr, *et al.*, 1997; Dipp and Evans, 2001; Morio and

McMurtry, 2002) and by consequent Ca^{2+} influx via a store-refilling current (Kang, *et al.*, 2003; Ng, *et al.*, 2005; Wang, *et al.*, 2005).

1.7.2.1 A role for cADPR in hypoxic pulmonary vasoconstriction

Given that both Phases 1 and 2 of HPV are abolished by block of SR Ca^{2+} release with ryanodine and caffeine (Dipp and Evans, 2001; Dipp, *et al.*, 2001) a possible role for cADPR in mediating SR Ca^{2+} release was considered. Previous work from this laboratory has shown that the enzymes for both the synthesis and metabolism of cADPR are around 1 order of magnitude higher in homogenates of pulmonary artery when compared to homogenates of aorta or mesenteric artery (Wilson, *et al.*, 2001). Also in this study, an increase in the levels of cADPR was observed in response to hypoxia, by 2-fold in 2^{nd} order pulmonary artery branches and 10-fold in 3^{rd} order pulmonary artery branches. Furthermore, the cADPR antagonist 8-Br-cADPR was shown to abolish acute HPV induced by alveolar hypoxia in isolated rat pulmonary artery rings and in the isolated, ventilated and perfused rat lung (Dipp and Evans, 2001). Therefore, an increase in smooth muscle cADPR levels and cADPR-dependent SR Ca^{2+} release may be a prerequisite for maintained HPV by alveolar hypoxia in the lung irrespective of the other mechanisms that may be activated by hypoxia (Dipp and Evans, 2001). The effects of 8-Br-cADPR on HPV in isolated pulmonary arteries were, however, quite different to the effects of blocking SR Ca^{2+} release via RyRs with ryanodine and caffeine. In arteries with and without endothelium, 8-Br-cADPR had no effect on Phase 1 of HPV. However, it abolished Phase 2 in the presence of endothelium and blocked maintained constriction observed in arteries without endothelium (Dipp and Evans, 2001; Wilson, *et al.*, 2001). Therefore, while cADPR-dependent SR Ca^{2+} release may maintain acute HPV in isolated pulmonary artery rings, it does not mediate the phase 1 constriction (Fig. 1.6; Dipp and Evans, 2001; Wilson, *et al.*, 2001). Interestingly, the SERCA pump antagonist cyclopiazonic acid (CPA) was shown to have the reverse of the effect of 8-Br-cADPR, in that it blocked Phase 1 of HPV without effect on Phase 2 in pulmonary arteries with or without endothelium (Dipp, *et al.*, 2001), despite the fact that Ca^{2+} release from ryanodine-sensitive SR stores in the smooth muscle underpins both

phases of HPV. Thus, it is possible that Phase 1 may be mediated by the mobilization of an SR compartment served by CPA-sensitive SERCA pumps that may be inhibited by hypoxia due to a fall in ATP supply (Dipp and Evans, 2001), and that this may lead to the attenuation of vasodilation mechanisms that might oppose HPV (as described previously in Section 1.5.7). If this were to be achieved while allowing for the second phase of maintained cADPR-dependent SR Ca^{2+} release, it would require the presence of a second spatially segregated SR Ca^{2+} store that is served by a discrete, CPA-insensitive SERCA pump (Dipp and Evans, 2001).

1.7.3 The involvement of the endothelium and myofilament Ca^{2+} sensitisation in hypoxic pulmonary vasoconstriction

Increased tension generation during phase 2 of HPV is dependent on an intact endothelium and the generation of endothelium-derived factors (Robertson, *et al.*, 1995; Ward and Robertson, 1995; Dipp, *et al.*, 2001; Liu, *et al.*, 2001). The 21-amino acid peptide endothelin 1 (ET-1) is secreted by endothelial cells and is considered to be a contributing mediator of phase 2 of HPV. At low concentrations (~10^{-10} M) ET-1 increases the sensitivity of the contractile response to the hypoxia-induced increase in intracellular Ca^{2+} concentration, while at higher doses (~10^{-8} M) it directly increases the intracellular Ca^{2+} concentration in pulmonary artery smooth muscle cells (Shimoda, *et al.*, 2000). Whether endothelium-derived ET-1 increases Ca^{2+} sensitivity and/or the intracellular Ca^{2+} concentration in pulmonary artery smooth muscle cells during hypoxia remains to be resolved. However, hypoxia has been shown to increase the ET-1 expression and secretion from cultured endothelial cells (Yamashita, *et al.*, 2001). Moreover, the ET-1 receptor A (ETA) antagonist BQ-123 has been shown to attenuate phase 2 of HPV in isolated vessels and whole lungs (Sato, *et al.*, 2000; Liu, *et al.*, 2003).

The possibility that endothelium-derived factors in addition to ET-1 may exist was suggested by studies involving the inhibition of ETA and ETA/Endothelin receptor B (ETB) which did not always attenuate the sustained contractile response seen in phase 2 of HPV (Robertson, *et al.*, 1995; Lazor, *et al.*, 1996; Robertson, *et al.*, 2003). To date, the identity of these

additional hypoxia-induced, endothelium-derived factors is still unclear, however a vasoconstrictor(s) has been isolated (Robertson, *et al.*, 2001; Evans and Dipp, 2002). The vasoconstrictor is heat stable and pulmonary selective (Robertson, *et al.*, 2001), and may promote constriction by increasing myofilament sensitivity via the activation of ROK (Robertson, *et al.*, 2001; Evans and Dipp, 2002).

There is compelling evidence that the mechanism of Ca^{2+} sensitisation via the RhoA:ROK pathway is more important in pulmonary resistance vessels than in systemic arteries. Thus, the ROK inhibitor Y-27632 produced significantly greater relaxation in pulmonary artery rings preconstricted with phenylephrine than was observed in aortic rings (Hyvelin, *et al.*, 2004). The increased role of ROK in pulmonary arteries may be of fundamental importance given that Ca^{2+} sensitisation is an integral component of sustained HPV. Ca^{2+} sensitisation in response to hypoxia appears to occur independently of PKC (Robertson, *et al.*, 1995). However, there is compelling evidence to suggest that activation of RhoA and ROK is a central component of this mechanism (Robertson, *et al.*, 2001). Robertson and colleagues showed that Y-27632 inhibited both the sustained phase of HPV in isolated rat intrapulmonary arteries and the hypoxic pressor response in perfused lungs in a concentration-dependent manner (Robertson, *et al.*, 2001). Inhibition of ROK with Y-27362 has also been shown to inhibit acute HPV in isolated mouse lung (Fagan, *et al.*, 2004). Recently, ROK activity has been shown to increase by around ~260 % in isolated pulmonary arteries of rat in response to sustained HPV (Robertson, *et al.*, 2005). This activation of ROK in rat pulmonary arteries was endothelium-dependent, as in endothelium-denuded arteries the increase in ROK (~ 40%) was similar to the reported increase in ROK activity previously observed in cultured smooth muscle cells (Wang, *et al.*, 2001). Although there is compelling evidence of an involvement for the RhoA:ROK pathway in Ca^{2+} sensitisation and HPV, there is evidence of an involvement of a number of other cellular kinases such as mitogen-activated protein kinase and non receptor tyrosine kinase in mediating both Ca^{2+} sensitisation (Somlyo and Somlyo, 2003) and HPV (Ward, *et al.*, 2004). However, the complexities of these pathways and the possible interactions between them will not be discussed here.

1.7.4 Chronic hypoxia and hypoxic pulmonary hypertension

Sustained HPV leads to hypoxic pulmonary hypertension (HPH) and an increase in pulmonary vascular resistance (PVR). Ultimately, this increased PVR results in right heart failure and death, due to an excessive work load placed on the heart in order to maintain blood flow through the restricted pulmonary vasculature. Thus, chronic HPH results from sustained vasoconstriction and structural alterations to the pulmonary vascular bed. Following a swift return to the a normal PO_2 the immediate fall in arterial pressure is slight and leaves the arterial pressure elevated substantially above normal levels (Sime, *et al.*, 1971; Lockhart, *et al.*, 1976; Fried, *et al.*, 1983) . These observations suggested that structural changes occurring in the pulmonary vascular bed are the major determinant of the increased vascular resistance. Structural changes that underlie the increase PVR in HPH can be roughly categorised into two processes: 1) remodelling of the pulmonary resistance vessels; and 2) a reduction in the number of blood vessels within the lung, which is often referred to as rarefaction or pruning.

Pulmonary vascular remodelling results in thickening of the arterial wall and is believed to increase vessel resistance by causing encroachment of the vessel into the lumen, therefore reducing the internal diameter of the vessel. This remodelling of the vascular wall is due to muscularisation of previously non-muscular arteries, increased medial thickness of previously partially or completed muscularised arteries, adventitial hypertrophy and deposition of additional matrix components (e.g. collagen and elastin) in the vascular walls (Rabinovitch, *et al.*, 1979; Stenmark and Mecham, 1997; Rabinovitch, 2001).

The second major structural modification which occurs due to chronic HPV is the loss of small blood vessels. This is believed to increase PVR by reducing the extent of parallel vascular pathways through the lung (Hislop and Reid, 1976; Hislop and Reid, 1977; Rabinovitch, *et al.*, 1979; Partovian, *et al.*, 2000). This loss of blood vessels has been detected as a decrease in the ratio of the number of blood vessels to the number of alveoli in the gas-exchange regions of the lung. However, not all investigators agree with the view that HPH reduces the number of vessels in the pulmonary vasculature. Indeed, several investigations have shown that there is no decrease, while other

investigators report an increase in the number of vessels (Kay, *et al.*, 1982; Finlay, *et al*., 1986; Howell, *et al.*, 2003).

1.8 NAADP-dependent Ca^{2+} signalling in pulmonary artery smooth muscle

A recent study from this laboratory has demonstrated that global Ca^{2+} release and contraction of isolated pulmonary artery smooth muscle cells occurred in response to the intracellular dialysis of NAADP (Boittin, *et al.*, 2002). Consistent with the proposal of Churchill and Galione (2001), it was shown that NAADP generated global Ca^{2+} signals via a two pool mechanism in pulmonary artery smooth muscle. Intracellular dialysis of NAADP from a patch pipette under whole-cell conditions and in current clamp mode (I = 0) was seen to mediate spatially restricted Ca^{2+} release events, which were termed 'Ca^{2+} bursts'. These Ca^{2+} bursts were seen to either decline to basal levels, or precede and then trigger a global Ca^{2+} wave and contraction of the smooth muscle cells. Ca^{2+} bursts were seen to generate global Ca^{2+} waves only if they breached a threshold Ca^{2+} concentration of approximately 400 nM (Boittin, *et al.*, 2002). In this study, no detectable Ca^{2+} mobilisation was seen to the intracellular dialysis of NAADP when the fast calcium chelator BAPTA was present in the pipette solution. However, when BAPTA was added to the extracellular solution and Ca^{2+} was removed, there was no effect on NAADP-mediated Ca^{2+} mobilization. These results show that NAADP releases Ca^{2+} from an intracellular Ca^{2+} store. Boittin *et al.* dismissed the SR as the site of NAADP mediated Ca^{2+} release. Consistent with previous investigations in other cell types (Genazzani and Galione, 1996; Churchill and Galione, 2000; Churchill and Galione, 2001), preincubation of isolated pulmonary artery smooth muscle cells with the SERCA pump inhibitor thapsigargin did not abolish NAADP-mediated Ca^{2+} bursts. Global Ca^{2+} waves were abolished however, suggesting a role for the SR Ca^{2+} stores in the amplification of initial Ca^{2+} release events into global Ca^{2+} signals. However, in contrast to studies in sea urchin eggs (Churchill and Galione, 2001), the Ca^{2+} bursts mediated by NAADP were seen to be insensitive to blockers of IP_3Rs. Following the blockade of IP_3Rs on the SR with xestospongin C, NAADP-mediated Ca^{2+}

signals remained unaffected (Boittin, *et al.*, 2002). However, prevention of Ca^{2+} release through RyRs with ryanodine resulted in a loss of global Ca^{2+} signals to NAADP, while spatially restricted Ca^{2+} bursts were still detected. Therefore, it was concluded that NAADP mobilises Ca^{2+} from an non-SR Ca^{2+} store in isolated pulmonary artery smooth muscle cells, which is then amplified to global Ca^{2+} signals by CICR via RyRs located on the SR (Boittin, *et al.*, 2002). Given that cADPR sensitises RyRs to CICR, this raised the possibility that NAADP and cADPR may act in concert to mediate HPV, which in a similar manner to global Ca^{2+} waves induced by NAADP, is initiated in an all-or-none manner. I therefore sought to characterise in more detail the mechanisms that underpin Ca^{2+} signals mediated by NAADP in pulmonary artery smooth muscle.

1.9 Aims of this thesis

1. Investigate the nature of the Ca^{2+} store accessed by NAADP in smooth muscle cells of the rat pulmonary artery.

2. Investigate the relationship between the NAADP-sensitive Ca^{2+} store and RyRs in an effort to build a model to explain Ca^{2+} signalling by NAADP in smooth muscle of the pulmonary artery.

3. Investigate and identify a vasoconstrictor mechanism which couples to NAADP-dependent Ca^{2+} signalling in an effort to demonstrate that NAADP is indeed a true Ca^{2+} mobilising messenger in arterial smooth muscle.

Chapter 2: Materials and methods

2.1 Dissection and identification of intrapulmonary arteries

All experiments were performed in accordance with the *United Kingdom Animals (Scientific Procedures) Act 1986*. Adult male Wistar rats (150-300g) were sacrificed via a Schedule 1 procedure and the heart and lungs were removed *en bloc* and placed into cold (4^{o}C) HEPES buffered salt solution (HBSS) of the following composition (mM): 130 NaCl, 5.2 KCl, 1 $MgCl_2$, 1.7 $CaCl_2$, 10 glucose, 10 Hepes, pH 7.4. Individual lobes were constantly bathed in cold HBSS during dissection of intrapulmonary arteries. All subsequent dissection was carried out under a dissection microscope (model PZM , World Precision Instruments, Fl, USA). Individual lobes were pinned out on a Sylgard-lined dissection dish with the parietal surface facing upwards. The airway was cut open from where the trachea entered the lobe of the lung, and was cut open moving away from the initial cut until the far end of the lobe was reached. The intrapulmonary artery was identified as running below and parallel to the trachea. Once the pulmonary artery was identified, dissection was carried out in order to ensure as little damage as possible was done to the artery. All tissue was removed above the artery, as it was seen looking down the microscope, and parenchyma on either side of the artery was also carefully removed in order to expose the artery. A small piece of parenchyma was left attached to the artery at one end, close to where the artery entered the lobe. Following this the artery was removed by cutting the remaining connective tissue and handled only by remaining parenchyma.

2.2 Isolation of pulmonary artery smooth muscle cells

2nd order branches of the pulmonary artery were identified and dissected free from their lobe as described in section 2.1. Following this they were then cut open lengthways from end to end. Arteries were then placed into cold (4 ^{o}C) low Ca^{2+} 'dissociation solution' (DS) of the following composition (mM): 124 NaCl, 5 KCl, 1 $MgCl_2$, 0.5 NaH_2PO_4, 0.5 KH_2PO_4, 15 $NaHCO_3$,

0.16 $CaCl_2$, 0.5 EDTA, 10 glucose, 10 Taurine, 10 Hepes, pH 7.4. After ten minutes arteries were transferred to low Ca^{2+} solution containing 0.5 mg/ml papain and 1 mg/ml bovine serum albumin. Papain is a proteolytic enzyme which requires a free sulfhydryl group in order to work. It was first isolated in the 1930s, from the latex of the green fruit and the leaves of the plant *Carica papaya* (Buhling, *et al.*, 2000). The arteries were then kept in this solution at 4°C overnight to allow the protease adequate time in which to penetrate into the tissue. The following day, 0.2mM 1, 4-Dithio-DL-thretiol (DTT) was added to activate the protease, and the preparation was then incubated for one hour at room temperature (22°C). DTT, often referred to as Cleland's Reagent, was used in order to maintain sulfhydryl groups in a reduced state and thereby activate the papain. After this time the arteries were washed 5 times in 1.5 ml of fresh cold (4°C) DS free from enzymes and placed in 2 ml of fresh DS. Single smooth muscle cells were then isolated by gentle trituration using a fire polished Pasteur pipette. The cell suspension was then kept at 4°C until required.

2.3 Fluorescent labelling of sub-cellular structures in freshly isolated pulmonary artery smooth muscle cells

2.3.1 Labelling of ryanodine receptors in freshly isolated pulmonary artery smooth muscle cells

Cells were isolated as described in section 2.2. Following dissociation, 200 μl of the cell suspension was incubated for 60 minutes in the dark at room temperature (~20 °C) with 1 μM BODIPY-FL ryanodine (Fig. 2.1). The dipyrometheneboron difluoride (BODIPY)-FL group is an amine reactive group and has an advantage over other BODIPY tags in that it mainly produces non-polar compounds. It is a fluorescent protein with an excitation wavelength of 505 nm and an emission wavelength of 515 nm (Fig. 2.1)

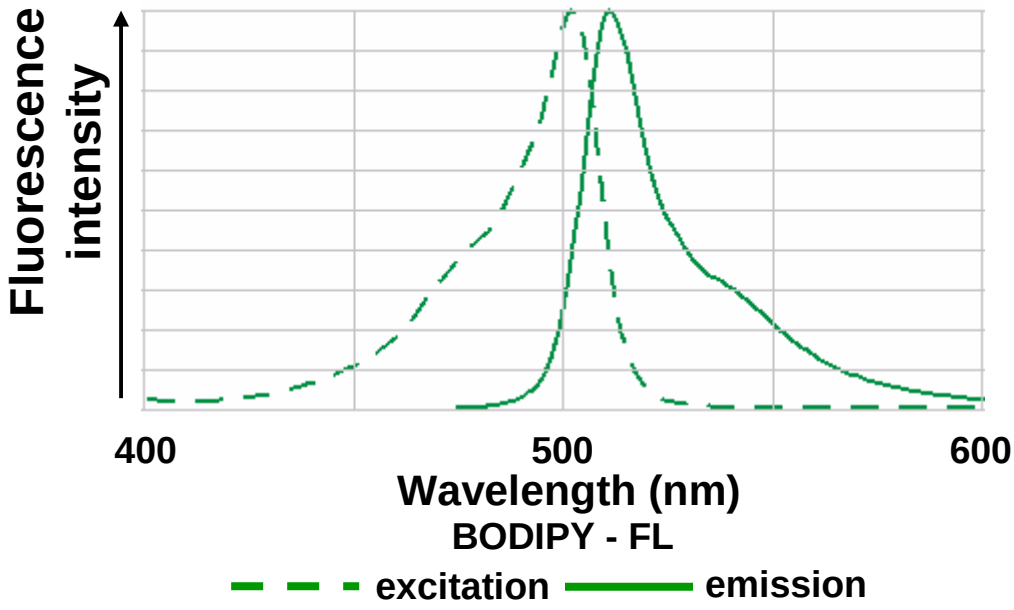

Fig. 2.1: **Excitation and emission spectra for the fluorescent probe BODIPY-FL.**

BODIPY-FL has been shown to be a better probe than the more established fluorescein dyes for a number of reasons. Unlike fluorescein, the spectra of BODIPY-FL is relatively insensitive to polarity, and to changes in pH in its surroundings (Karolin, *et al.*, 1994). BODIPY-FL ryanodine has been identified as being a good label for ryanodine receptors (RyR; Holz, *et al.*, 1999; Abrenica and Gilchrist, 2000; Coussin, *et al.*, 2000). When ryanodine is joined to the BODIPY-FL molecule on carbon 10 there is minimal change to the dissociation constant when compared to that of ryanodine (Humerickhouse, *et al.*, 1994).

2.3.2 Labelling of lysosomes within freshly isolated pulmonary artery smooth muscle cells

After fifteen minutes of incubation with BODIPY-FL ryanodine, 0.5 - 2 nM of LysoTracker Red was added to the cells. Cells were then incubated in the dark for the last 30 minutes at room temperature (~20 ^{o}C). All cells loaded with BODIPY-FL ryanodine were colabelled with LysoTracker Red (Chapter 4), however, initial experiments were carried out in cells labelled with LysoTracker Red alone (Chapter 3). LysoTracker Red is a fluorescent

molecule with an excitation wavelength of 577 nm and an emission wavelength of 590 nm (Fig. 2.2). It consists of a weak base linked to a fluorophore and is partially protonated at neutral pH, allowing it to move freely across the cells membrane and accumulate in acidic organelles, however, the exact mechanism of retention is unclear.

Cells were then transferred to a glass bottomed Petri dish for the last twenty minutes of the incubation period to allow the cells to adhere. After this time the volume within the dish was made up to 2 ml using fresh HBSS at room temperature (~22 ^{o}C; pH 7.4) and washed with 5 x 2ml fresh HBSS. Cells were left to equilibrate in the dark before commencement of the imaging protocol. In experiments involving glycyl-L-phenylalanine 2-napthylamide (GPN), cells were pre-treated for 15 minutes with the myosin light chain kinase inhibitor 1-(5-chloronapthalene-1-sulfonyl)-1-H-hexahydro-1, 4-diazepine (ML-9; 10 μM) in order to prevent contraction of the cells (Saitoh, *et al.*, 1986).

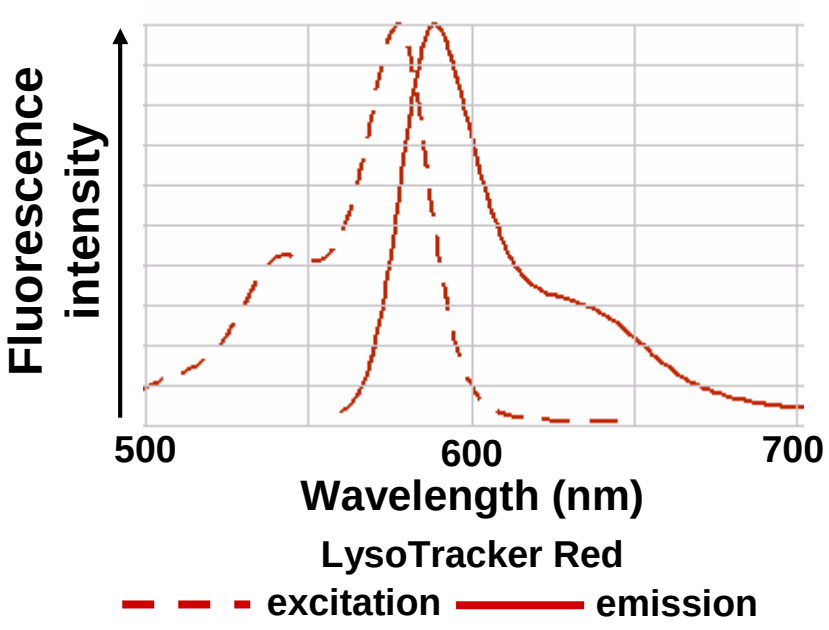

Fig. 2.2: **Excitation and emission spectra for the fluorescent probe LysoTracker Red.**

LysoTracker Red and BODIPY-FL ryanodine were deemed suitable for colabelling studies due to the lack of overlap in their excitation and emission spectra (Fig. 2.3)

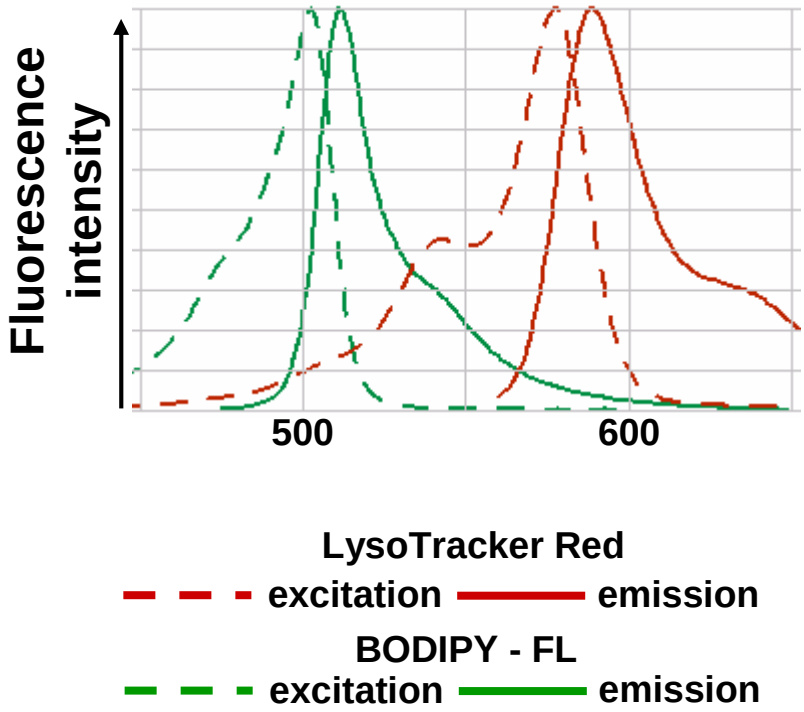

Fig. 2.3: **comparison of excitation and emission spectra for the fluorescent probes LysoTracker Red and BODIPY-FL.**

2.3.3 Procedure for imaging sub-cellular structures in isolated pulmonary artery smooth muscle cells

Cells were excited by the light from a 100W mercury arc lamp. Beamsplitter filters were used to accurately control the required wavelength for illumination. Images were captured using a Deltavision microscope system (Applied Precision) consisting of an inverted microscope (Olympus IX70) with a 60X 1.4-numerical aperature oil immersion objective lens (Olympus) and a Photometric CH300 charge-coupled device camera (CCD camera).

A CCD camera consists of a large array of photodiodes on a silicon substrate which form individual areas of the picture, or picture elements (pixels). Utilising the photoelectric effect, a photon of light falling upon a given photodiode causes the release of an electron. Therefore, light falling on a

pixel is converted into a charge pulse, which is measured by the CCD electronics and is represented by a number in the analysis software, in the case of the Deltavision system this is the Softworx acquisition and analysis software (Applied precision) on a Silicon Graphics O_2 workstation (Silicon Graphics Inc., CA, USA). Within the acquisition and analysis software a digital image is constructed from the collection of light intensity numbers from all the photodiodes making up the CCD camera. The computer software reconstructs the image by varying the digital intensity for each pixel in a manner proportional to the charge pulse number recorded. The images from each pixel are displayed on the computer monitor in the correct order. Digital computers process binary information. If we wish to process an analogue image, in this case a picture of our cell of interest, we must convert the image into a data set the computer can understand. The analogue picture is converted into a digital image using the following principal. Photographic images are analogue images and the colours are expressed on a continuous scale, which has an infinite number of possible colours. In order to process these images effectively the computer does not use this continuous scale, rather it converts it into a number of discreet levels based on intensity of light within the image. The computer uses a scale that comprises of 256 levels of grey from white through to black. Therefore, the different intensities of light in each pixel will be given a different grey value and from this it is possible to build up a picture. The fluorescence intensity within a sample is displayed as a range of grey levels.

Images were collected as single Z sections of 0.28 μm in depth, or as a series of Z sections through the cell at 0.2 μm intervals. This provides a series of 2D images containing information on all the staining throughout the cell. However, given that the microscope will pick up a great deal of out of focus light at each Z step we need a way to remove the out of focus light and leave us with the information for the given Z section we are looking at. This is done by the process of deconvolution, which describes a number of software techniques for ‘de-blurring’ a given image.

2.3.4 Deconvolution of images of isolated pulmonary artery smooth muscle cells

The Deltavision system employs a sophisticated method known as 'constrained-iterative deconvolution' to reassign out of focus light to its original location. Within this process the use of point spread function (PSF) data allows the conservation of data commonly lost by other methods of deconvolution. PSF refers to the imaging characteristics of the lens employed for imaging. No microscope objective is able to perfectly reproduce an image of an object. The PSF describes the degree to which a point of light is altered in three dimensions as it passes through the lens and relay optics of the microscope. The PSF will differ for each lens and microscope system combination and the Deltavision system is carefully calibrated to ensure an accurate value for the PSF of the lens within the system. Therefore, the PSF is corrected for in the deconvolution process, allowing for a more accurate redistribution of light within an image.

Following deconvolution, Softworx software or Volocity software (Improvision, UK) was employed to produce 3 dimensional reconstructions of imaged cells for off-line analysis.

2.4 Fluorescent labelling of intracellular proteins in isolated pulmonary artery smooth muscle cells

2.4.1 Fixation and labelling of lysosomal membrane protein αlgp120 and ryanodine receptor subtypes 1, 2 and 3 in isolated pulmonary artery smooth muscle cells

Sequence specific antibodies to the RyR subtypes 1, 2, and 3 were a gift from Professor Sidney Fleischer and have previously been shown to be highly sequence specific for their individual targets on the different RyR subtypes (Lesh, *et al.*, 1992; Jeyakumar, *et al.*, 1998; Jeyakumar, *et al.*, 2001); Table 2.1). GM10 antibodies (Grimaldi, *et al.*, 1987), raised against the lysosomal glycoprotein antigen αlgp120 (Lewis, *et al.*, 1985) were a gift from Professor Paul Luzio. The antigen αlgp120 has previously been shown to be

preferentially associated with the membrane of lysosomes (Lewis, *et al.*, 1985; Howe, *et al.*, 1988).

Antibody	Raised in	Dilution Immunocyt.	Dilution Westerns	Target sequence	References
RyR1	Rabbit	1:500	1:500	Residues 4476-4486	Lesh *et al*, 1993
RyR2	Rabbit	1:500	1:500	Residues 1344-1365	Jeyakumar *et al*, 2001
RyR3	Rabbit	1:500	1:500	Residues 4236-4336	Jeyakumar *et al*, 1998

Table 2.1: **Dilution factors, sequence specifics and initial references relating to anti-ryanodine receptor (RyR) antibodies for immunocytochemistry (Immunocyt.) and Western blotting (Westerns) investigations.**

200 µl of freshly dissociated cell suspension was put onto poly-d-lysine coated glass coverslips and cells were allowed to settle for 1 hour at room temperature (~22 ^{o}C). Coverslips were covered in Poly-D-lysine to coat the surface with a net negative charge in order to enhance cell adhesion. After 1 hour, excess solution was removed and the coverslips placed in freezing cold methanol for 15 minutes to fix the cells. Methanol fixation works by removing lipids and dehydrating the cell while denaturing and precipitating proteins on the cellular architecture. This method allows for quick fixation of the cells; however it can result in the loss of diffuse proteins, i.e. those proteins which are not anchored to membranes and are free to move within the cytoplasm of the cell. Once fixation was complete cells were removed from the methanol and were permeabilised by three, five minute washes in phosphate buffered saline (PBS; pH 7.4) containing the non-ionic detergent Triton X-100 (polyethyrene glycol mono-p-iso-octylphenyl ether; 0.3%). Triton X-100 causes the formation of pores in the membranes of cells, thus allowing access of specific antibodies to the inside of the cell. After this cells were washed 3 x 5 minutes with blocking solution (1% bovine serum albumin (BSA), 4% goat serum and 0.1% Triton X-100). Blocking solution contains goat serum and BSA to prevent any non- specific binding of the primary antibodies within the cell. This significantly improves signal to noise ratio within the sample. Triton X-100 is included in the solution to aid the penetration of goat serum, BSA and primary antibodies. Cells were then incubated overnight at 4 ^{o}C with antibodies raised in rabbit to sequences of one of the RyR subtypes and with GM10

antibodies. These antibodies were diluted in blocking solution to help minimize non specific binding (Table 2.1).

The following day cells were washed three times for five minutes in fresh blocking solution of the same composition of that used previously. In order to determine where the primary antibody has bound within the cell it is necessary to employ some means of being able to visualize it. This was achieved by employing a secondary antibody raised against immunoglobulins of the species that the primary antibody is raised in. Secondary antibodies are conjugated to a fluorescent molecule, allowing for visualisation. Following the washing step, cells were incubated for two hours in the dark at room temperature (~20 ^{o}C) with fluorescently labelled secondary antibodies. In order to visualize the primary antibodies raised in rabbit against RyRs an anti-rabbit antibody raised in goat was used. This antibody was conjugated with the red fluorescent dye Texas Red (excitation 555 nm, emission 617 nm) and diluted 1:200 with blocking solution. The primary antibody, GM10, raised against the lysosomal membrane glycoprotein αlgp120, was visualised using an anti-mouse secondary antibody raised in goat and conjugated to the green fluorescent dye FITC (excitation 490 nm, emission 528nm; diluted 1:200 with blocking solution). These two dyes are suitable to use for co-labelling studies as their excitation and emission spectra show very little overlap (Fig. 2.4).

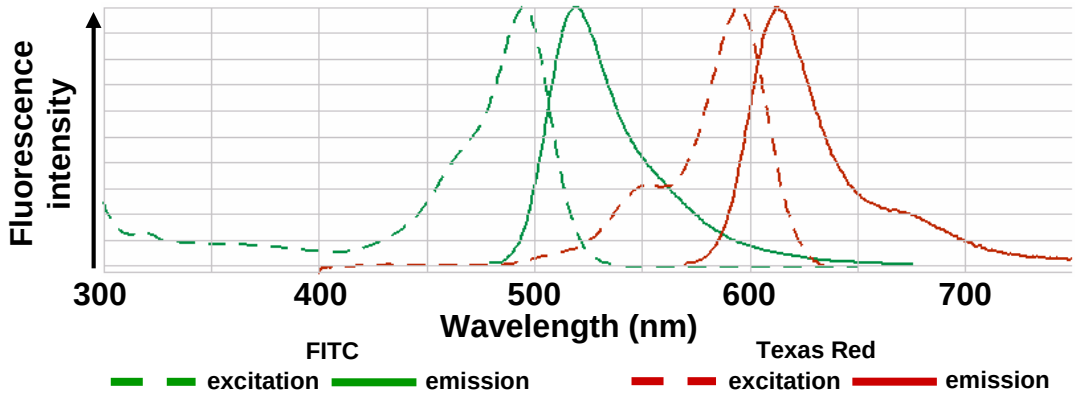

Fig. 2.4 **Diagram of excitation and emission spectra for the fluorescent probes FITC and Texas Red showing the lack of overlap between the two**

Cells were washed five times for five minutes each in the dark with fresh PBS (pH 7.4) following the two hour incubation. Cells were then attached

to microscope slides using hard setting, anti-fade mountant containing the fluorescent nuclear dye 4'6-diamidino-2-phenylindole (DAPI; excitation 360 nm, emission 457 nm). DAPI has been shown to associate with the minor groove of double stranded DNA, preferentially binding to AT clusters (Kubista, *et al.*, 1987). The binding of DAPI to the minor groove produces around a 20 fold increase in fluorescence under excitation allowing for accurate visualization of the nuclear region of the cell (Barcellona, *et al.*, 1990).

The slides were then left for 2 hours in the dark at room temperature (20^{o}C) to allow the mountant to set. Slides were then stored in the dark at 4 ^{o}C until examined.

2.4.2 Preparation of control slides for use in immunocytochemical investigations

In order to remove background fluorescence and allow for examination of the binding of secondary antibodies within cells, two sets of control slides were prepared in parallel to test slides.

The first control slides differed from test slides in that these control slides were not incubated with primary antibodies overnight. This allowed me to examine the fluorescence intensity of background fluorescence associated with the presence of secondary antibodies within the fixed cells (Fig. 2.5A). By determining the level of intensity of secondary antibody fluorescence in control slides, following deconvolution using Softworx software (Chapter 2, Section 2.3.4), it was possible to determine a 'threshold' fluorescence intensity level in order to remove background fluorescence from test slides, enabling visualization of specific labelling within the test cells (Fig. 2.5B).

The second set of control slides were prepared to confirm the specificity of the primary antibodies by incubating a given concentration of primary antibodies with a 10X concentration of the specific sequence the primary antibodies are raised against. Following three hours of incubation of the primary antibodies with their 'blocking peptide', slides were prepared as described above. The fluorescence intensity of these control slides were then examined for comparison against test slides. The absence of fluorescent

labelling above the 'threshold' fluorescence intensities determined from control slides prepared in the absence of primary antibody confirmed the specificity of primary antibodies.

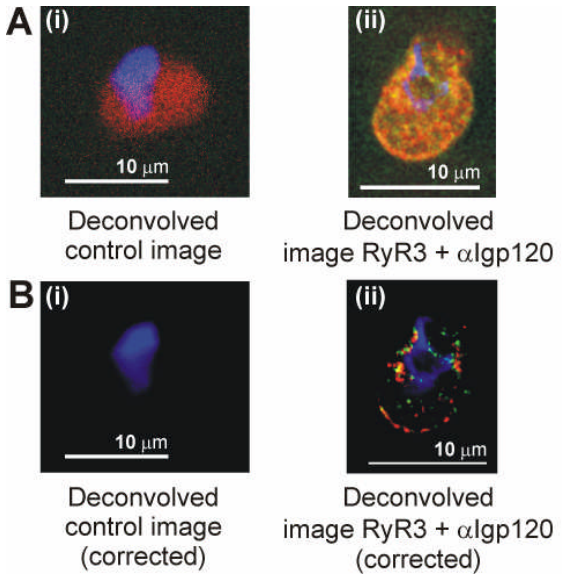

Fig. 2.5: **Elimination of background fluorescence from images obtained on the Deltavision system:** ***Panel A(i)*** shows a deconvolved Z-section (depth 0.28 μm) taken through an isolated pulmonary artery smooth muscle cell from a control slide not incubated with primary antibody against RyRs or lysosomes. The cell has been incubated with fluorescent-conjugated secondary antibody (red/green) and is labelled to show the position of the nucleus (blue). ***A(ii)*** shows a deconvolved Z-section (depth 0.28 μm) through a different isolated pulmonary artery smooth muscle cell that was incubated with primary antibody against RyRs or lysosomes. Binding of fluorescent-conjugated secondary antibodies shows the distribution of RyR3 (Red) and the lysosomes (green), although considerable background fluorescence is still seen. The position of the nucleus is indicated in blue. ***Panel B(i)*** shows the same cell as in ***A(i)*** following adjustment to remove background fluorescence, the position of the nucleus is still apparent (blue). ***B(ii)*** shows the same cell as in ***A(i)*** following adjustment to remove background fluorescence, the distribution of RyRs (red) and lysosomes (green) can be easily determined in relation to the position of the nucleus (blue).

2.4.3 Visualisation of labelling in methanol-fixed, isolated pulmonary artery smooth muscle cells

Fluorescent labelling in methanol-fixed, isolated pulmonary artery smooth muscle cells were visualised using the Applied Precision Deltavision imaging system as described in Chapter 2, Section 2.3.3. Z-series of images

were captured at 0.2 μm steps in the Z-direction. Captured images were deconvolved using the method of deconvolution contained within the Deltavision software, described in Chapter 2, Section 2.3.4. Volumetric analysis of fluorescent labelling was carried out using Volocity Software (Improvision, UK).

2.5 Detection of proteins in pulmonary artery smooth muscle by use of Western blotting

2.5.1 Preparation of protein samples for use in assays

2nd order branches of the pulmonary artery were identified as described in section 2.1 and dissected clear of surrounding parenchyma. Arteries were then cut open longitudinally and the endothelium was removed by gently rubbing of the luminal wall with a cotton bud. The brain of the animal was removed from the skull and cut into pieces, as was the heart and skeletal muscle (the vastus lateralis from the hind leg). All tissue was snap frozen immediately after removal in liquid nitrogen and stored at -80 ^{o}C until required. Tissue was placed into a small cooled mortar containing liquid nitrogen, once most of the liquid nitrogen had evaporated a cooled pestle was used to grind the tissue into a fine powder. The crushed tissue was then placed in a cooled microcentrifuge tube and buffer was added (3 μl per 1 mg tissue) of the following composition (mM): 50 Tris base, 150 NaCl, 50 NaF, 5 Na pyrophosphate, 1 EDTA, 1 EGTA, 1 DTT, 0.1 benzamidine, 0.1 % (v/v) Triton X-100, 0.1 PMSF, 0.25 mannitol, pH 7.4. After two minutes a motorised pestle was used to ensure a smooth homogenate was formed. Once formed the homogenate was left on ice for 30 minutes after which time the homogenate was spun on a desktop centrifuge for 5 minutes at 10,000 g, this was carried out at 4^{o}C. The supernatant containing the protein fraction was removed to a cooled eppendorf tube and both the supernatant and the pellet containing cell debris were retained at -80 ^{o}C until required.

2.5.2 Bradford assay of protein content

Since it was first described in 1976, the Bradford assay has become a widely used protein assay method as it is simple, rapid, inexpensive and sensitive (Bradford, 1976). The Bradford assay takes advantage of the absorbance shift of Coomassie brilliant blue G-250 (CBBG) when it binds to proteins at specific amino acid residues, namely arganine, tryptophan, tyrosine, histadine and phenylalanine residues. CBBG binds to these residues in its anionic form which has an absorbance maximum of 595 nm. The free dye in solution is found in the cationic form, with an absorbance maximum at 470 nm. The assay is read at 595 nm in the spectrophotometer which gives a measure of the CBBG complex with the protein.

Appropriate volumes (1-10 μl) of each protein sample were added to different plastic cuvettes. To each cuvette 2 ml of Bradford reagent was added, cuvettes were then shaken to mix contents. Bradford reagent consists of Coomassie brilliant blue G-250, 95 % ethanol and 85 % orthophosphoric acid. The spectrophotometer (CE 393 Digital Grating Spectrophotometer, Cecil Instruments Ltd., UK) was turned on and allowed to warm up for fifteen minutes in order to allow for a consistent reading. Protein concentrations are determined by extrapolation from a standard curve of protein concentrations. This was produced using a BSA stock solution (1.45 mg/ml) diluted to the following concentrations, in pure-filtered H_2O (mg protein/ml): 0, 0.1, 0.25, 0.5, 0.75, 1, and 1.45. The standards and the protein samples were both read on the spectrophotometer and the protein concentrations of the tissue samples were determined via interpolation using Prism software described in section 2.6.6.

2.5.3 SDS-polyacrylamide gel electrophoresis

SDS- polyacrylamide gel electrophoresis (SDS- PAGE) is a method for separating and identifying proteins according to their molecular weight. The proteins move through the gel due to the influence of an electric current and the proteins migrate towards the anode, the positive electrode.

The pores within the gel restrict the passage of the proteins in proportion to their molecular weight so that the low molecular weight proteins move more rapidly. In this system gels of two different pore sizes are used: the stacking gel has a lower pH (6.8) and a larger pore size than the resolving gel (pH 8.8). This results in the concentration of the proteins at the interface between the two gels, thus giving a better resolution. Effectively, the gels are made by chemical polymerisation of a mixture of acrylamide and bis-acrylamide (a cross linker), with ammonium persulphate which catalyses and TEMED which initiates the polymerisation reaction. The final concentration of acrylamide depends on the molecular weight range desired, high concentration gives good resolution of low molecular weight proteins and vice versa. Resolution of proteins was performed using 6 % bis- acrylamide gels cast in Novex gel cassettes (Invitrogen, UK) with five lanes. The resolving gel mix (6 % acrylamide, 0.375 M Tris, 0.1 % w/v SDS, 0.05 % w/v APS and 0.05 % TEMED) was poured into the gel cassette. The mix was overlaid with pure-filtered H_2O and left to polymerise for 30 minutes. Once the gel had polymerised, removal of any unpolymerised gel mix was achieved by washing with distilled H_2O. After this the stacking gel (4.2 % acrylamide, 1 % w/v SDS/ 0.125 M Tris, 0.05 % w/v APS and 0.08 % TEMED) was poured over the resolving gel and a 10 well comb was inserted to create lanes. The gel was then allowed to polymerise again for approximately 30 minutes.

Proteins are boiled in Laemmli buffer containing SDS, a reducing agent (β-mercapotethanol), glycerol and the marking dye bromophenol blue. Sodium dodecyl- sulphate (SDS) is a detergent with a strong negative charge, which binds avidly to all proteins, hence all proteins, whatever their original charge, are converted to complexes that have a strong negative charge. Also, the three dimensional shape of the protein is converted into a rod-like structure. Since the SDS molecules bind to polypeptides with a constant weight ratio, the charge per unit weight is constant and electrophoretic motility becomes a function of molecular weight. The reducing agent breaks the disulphide bonds (-S-S-) within the proteins which aids in the conversion of the proteins 3-dimensional structure into a rod- like structure and prevents it from converting back. The presence of the marking dye allows control over the distance of

migration of proteins. Using the protein concentrations determined from the Bradford assay, protein samples were made up to a final concentration of 1 mg/ml in the appropriate volumes of sample buffer (composition (mM): 63 Tris pH6.8, 139 SDS, 3.3 % glycerol, 1 % bromophenol blue, 5 % β-mercaptoethanol) and 50 mM Tris. The resultant mixture was heated to 95 ^{o}C for five minutes after which 50 μg of sample was loaded onto the gel. The gels were then run using an XCell *surelock* Mini-Cell system (Invitrogen, UK). In order to allow size discrimination of the resolved proteins, 5 μl of Broad Range Prestained protein markers (Bio-Rad, UK) were also loaded into one lane. The gels were run for 0.5 hours at 50 V to allow protein to concentrate at the gel interface. Following this, gels were then run at 125 V for 2.5 hours.

2.5.4 Immunoblotting

Following SDS- PAGE the gels were removed from the cassettes and placed into transfer buffer of the following composition (mM): 42.9 Tris, 38.9 glycine, 0.038 % w/v SDS, 20 % methanol. Grade 1F electrode filter paper and Hybond ECL nitrocellulose membranes were cut to the size of the gel and pre-soaked in the transfer buffer. Proteins were transferred onto nitrocellulose membranes using an XCell II blot module Mini Cell system (Invitrogen, UK). A stack was built in order to transfer the proteins. On top of a piece of filter paper was placed the gel. The 'sticky' nitrocellulose membrane was placed onto the gel and a further piece of filter paper was placed on top of this. Trapped air was removed from the stack by gently rolling a glass rod across the top. Two blotting pads soaked in transfer buffer were placed on the cathode and the stack was placed on top of this. A further 2-3 blotting pads were placed on top of the stack and the anode was placed on top of the stack. Following this the gels were blotted for 1.5 hours at 25 V (~ 100mA).

2.5.5 Immunodetection

After transfer, the nitrocellulose membranes were blocked with 5 % blocking buffer of the following composition (mM): 20 Tris base, 150 NaCl,

0.1 % Tween 20, 5 % non- fat milk powder, pH 7.5) for 1 hour at room temperature. The blocking buffer acts to bind to the remaining sticky areas of the membrane in order to prevent any non- specific protein interactions between the membrane and the antibody protein. Following this, the membranes were washed in TBST of the following composition (mM): 20 Tris base, 150 NaCl, 0.1 % Tween 20, pH 7.5) three times for 10 minutes. The blots were incubated with the primary antibody diluted in 1 % Blocking buffer of the following composition (mM): 20 Tris base, 150 NaCl, 0.1 % Tween 20, 1 % non- fat powder milk, pH 7.5) overnight at 4 ^{o}C.

The following day the membranes were washed 2 X 5 minutes and 1 X 15 minutes with TBST to remove any unbound primary antibody. Secondary HRP- conjugated anti-rabbit antibodies diluted in 1% blocking buffer at 1:1000 were incubated with the membranes for 2 hours. The secondary antibody is linked to horseradish peroxidase (HRP), which can be used to allow visualization of the protein of interest on the membrane. The membranes were then washed for 2X 5 minutes and 1 X 15 minutes in TBST. The binding of the primary antibody was detected using a chemiluminescence detection system. The membrane was incubated with the substrate for the HRP, luminol, which is a diacylhydrazide. This reaction was carried out in the presence of chemical enhancers such as phenols which increase the light output and extend the time of light emission. The HRP catalyses the oxidation of luminol which excites an electron, moving it to a higher energy state. This electron then decays back to its resting ground state which emits a photon of light. The maximum emission is at the wavelength 428 nm that can be detected by a short exposure to blue-light sensitive autoradiography film. The chemiluminescence system used was the ECL Western blotting detection reagents (Amersham Bioscince, UK). The membranes were incubated with a 1:1 mixture of Reagents 1 and 2 for 1 minute. Following this, the membranes were exposed to ECL Hyperfilm (Amersham, UK) in a dark room. Exposure times ranged from 1 minute to 5 minutes depending on the strength of the signal. The X-ray films were developed using a Fuji film X-ray processor (Model RGII).

2.6 Fluorescence imaging of Ca^{2+} within isolated pulmonary artery smooth muscle cells

2.6.1 Isolation of single pulmonary artery smooth muscle cells

2^{nd} order branches of the pulmonary artery were identified and dissected out as described in section 2.1. Single smooth muscle cells were then isolated using proteolytic cleavage as described in section 2.2.

2.6.2 Fluorescent Ca^{2+} indicating dyes

Fluorescent dyes can be used to indicate the presence of specific molecules and also to reveal their position within a given preparation, in this case Ca^{2+} in the isolated pulmonary artery smooth muscle cell. The fluorescent dye molecule, which I shall refer to as the indicator from here-on in, becomes excited by the absorption of a single photon of light. This raises the energy state of an electron within the indicator to a new excited 'singlet' state from which the molecule decreases in energy until a radiative transition occurs and the electron returns to its ground state with the emission of a photon (See Fig 2.6). Alternatively, the emitted photon can be reabsorbed by the indicator or the excited state may be quenched, or lost, through the collision of the excited indicator with another molecule. Either of these processes occurring will result in the number of emitted photons being considerably less than the number of absorbed photons and the ratio between the two is referred to as the quantum efficiency of the indicator. The energy of the emitted photon is ordinarily lower than that of the absorbed photon and is therefore of a longer wavelength. It must be noted, however, that at periods of very high light intensity it is possible for the indicator to absorb 2 long wavelength protons in quick succession, simulating the absorption of a single photon of half their wavelength. When in this high energy state, the indicator molecule is more likely to be oxidised resulting in a loss of fluorescence, this process is known as photo-bleaching. If the wavelengths of the light used for excitation and emission are suitably far apart then it is possible to use filters to block the excitation light from reaching

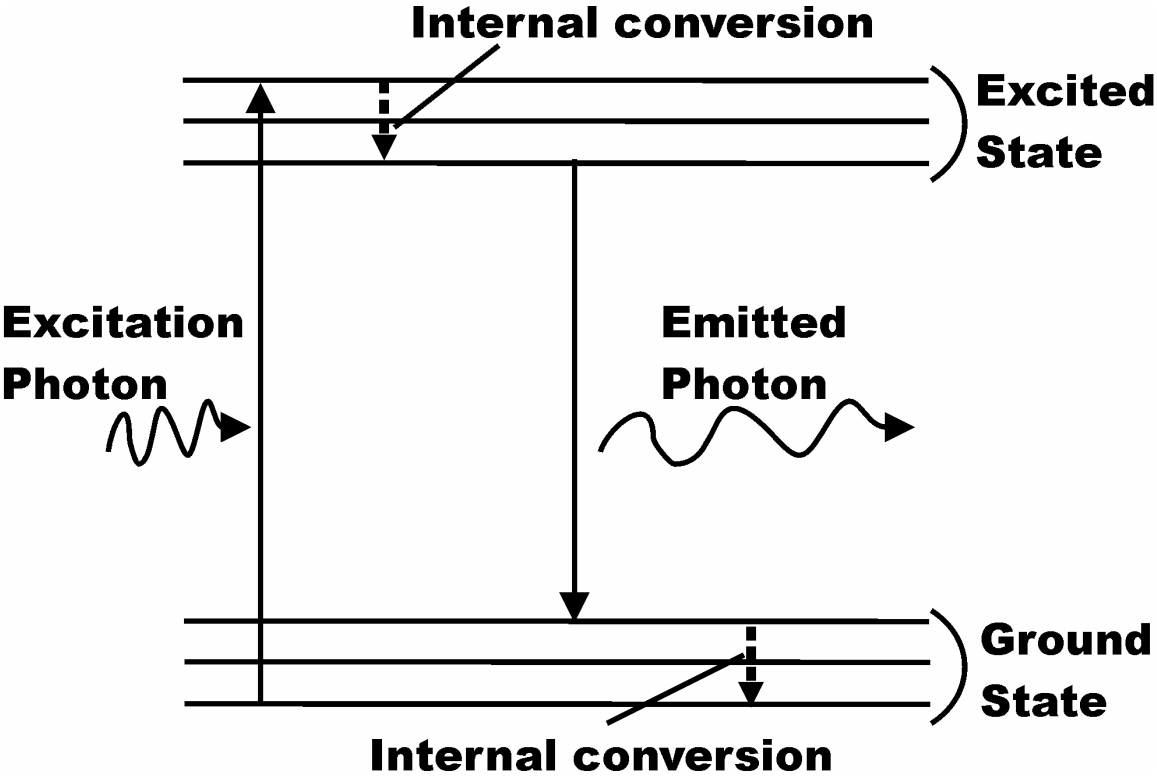

Fig 2.6: **Schematic energy state diagram depicting the excitation of an electron from a ground state to an excited energy state after absorption of a photon of excitation light**. Following excitation, this electron loses energy and eventually falls from the excited state back to ground state with the emission of a photon of light.

the detector, this allows for the emission to be measured against a black background. In reality, however, the background is seldom black, as other components of the cell will fluoresce to some extent. This is known as auto-fluorescence, however, this can be corrected for using a process known as dark subtraction, which will be discussed below.

Ion specific fluorescent indicators are generated by attaching groups that bind ions to the fluorescent section of the molecule. The binding of an ion then alters the electronic configuration of the molecule, which in turn alters the fluorescence of the molecule. The commonly available Ca^{2+} indicator dyes fall into two main classes, the single-wavelength intensity-modulating dyes, and the dual-wavelength ratiometric dyes, which are referred to as single-wavelength indicators and ratiometric indicators respectively.

For single-wavelength indicators, changes in the concentration of Ca^{2+} results in changes in the intensity of their fluorescence excitation and emission

spectra while the spectral maxima remains unchanged. The excitation spectra are determined by monitoring the fluorescence emission intensity at a fixed wavelength while the excitation light is scanned through a range of wavelengths at which the sample can absorb light. The emission intensity detected is then plotted as a function of excitation wavelength. An example of excitation spectra is given for the ratiometric Ca^{2+} indicator Fura-2 in Fig. 2.7. The opposite is true if we wish to obtain an emission spectrum. This time excitation light is delivered at a constant wavelength but the emission intensity of the sample is monitored over a wavelength range. In this case emission intensity is plotted as a function of emission wavelength (Fig. 2.7). An example of a single-wavelength indicator is fluo-3. Fluo-3 has a calcium co-ordination site based upon the Ca^{2+} chelator BAPTA and its fluorescent group is attached to one side of this BAPTA backbone. Put simply, the binding of Ca^{2+} to Fluo-3

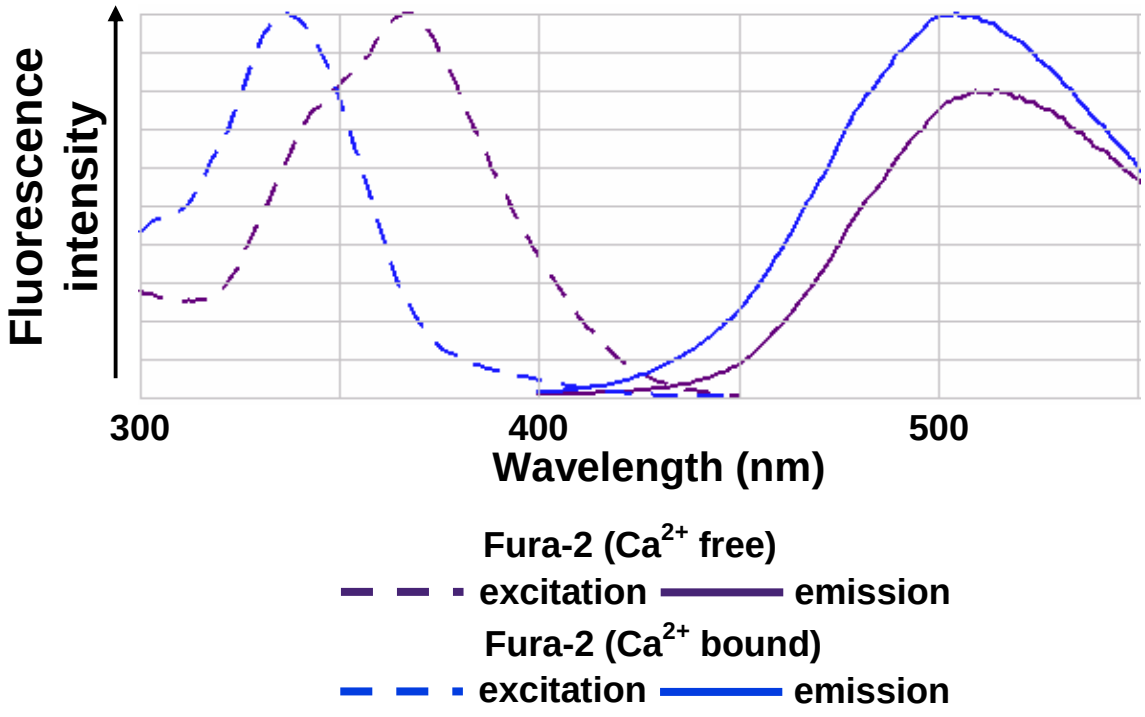

Fig 2.7: **Excitation and emission spectra of the Ca^{2+}-bound and Ca^{2+}-free forms of the fluorescent Ca^{2+} indicator dye Fura-2.**

draws electrons from the BAPTA rings, which will in turn draw electrons from the rings of the fluorescent group which results in an increase in fluorescence

of the molecule. To determine changes in ion levels with a single-wavelength indicator all that is required is the measurement of fluorescence at a suitable wavelength for both excitation and emission. Unfortunately the raw signal detected would not be quantitative because the absolute fluorescence of the dye depends upon a number of factors. Firstly, the absolute concentration of the indicator will affect the signal generated. Secondly, the volume of the cell or how far the light has to travel will affect the absolute fluorescence, as will the intensity of the excitation light and the variables within ones detection system. Auto-fluorescence within the cell of interest can also affect the signal, as can the Ca^{2+} concentration itself. The variation in Ca^{2+} concentration is the only variable of real interest. There are a number of ways to compensate for the unwanted variables occurring, although these will not be discussed here.

It is possible that the binding of the target ion by the fluorescent indicator will cause a shift in the fluorescence spectra rather than a simple modification in intensity of emission as discussed for Fluo-3. In principle, this concept is straightforward enough but its consideration can be complicated by the possibility that either, or both, of the excitation and emission spectra may be shifted upon binding of the target ion. The commonly used Ca^{2+} indicator molecule Fura-2, like Fluo-3, has a calcium coordination site which is based upon BAPTA, with the fluorescent group attached to this (Grynkiewicz, *et al.*, 1985). Alteration within the electronic structure of the molecule which occurs upon Ca^{2+} binding by Fura-2 results in a shift in the excitation spectra of Fura-2 to shorter wavelengths (Grynkiewicz, *et al.*, 1985). Such a shift in the spectra are desirable as they allow the concentration of Ca^{2+} to be estimated from the levels of fluorescence detected at two different wavelengths. This technique is known as ratiometric fluorescence measurement.

The use of ratiometric Ca^{2+} indicators can lead to a reduction in the factors compounding the measurements that we see with single- wavelength dyes such as Fluo-3. As ratiometric Ca^{2+} imaging is not reliant on the concentration of the indicator in the cell, or the volume of the cell, it reduces the artefacts introduced due to cell contraction or extrusion of dye from the cell. Thus, ratiometric Ca^{2+} imaging was used in my investigations as they were carried out in contracting cells.

2.6.3 Loading of isolated pulmonary artery smooth muscle cells with fluorescent Ca^{2+} indicator dye Fura-2.

0.5ml of cell suspension was incubated for 30 minutes at room temperature (~20 ^{o}C) in the dark with the ratiometric Ca^{2+} indicator dye Fura-2-AM (5 μM) and 1% pluronic F-127 acid that had been previously dissolved in 1 ml of DMSO, in order to help the loading of the dye into cells at room temperature.

The fluorescent Ca^{2+} indicator dye Fura-2 was first described by Grynkiewicz and colleagues (1985). Fura-2 shows a maximum fluorescence emission at 510 nm when excited at 380 nm in its Ca^{2+} free form. Once all 4 Ca^{2+} binding sites on a molecule of Fura-2 are occupied, spectral shift occurs and the maximum intensity of emission is achieved by excitation at 340 nm (Fig. 2.7). By measuring the relative intensity at these two wavelengths over the course of an experiment and expressing them as the ratio of light emitted on excitation at 340 nm divided by that emitted at 380 nm (340 nm/380 nm), it is possible to detect changes in intracellular Ca^{2+}. Fura-2 is a polycarboxylate anion, which is unable to cross the lipid bilayer of the cell membrane and enter the cytoplasm. In order to enter the cell Fura-2 can be put into a cell by microinjection or by complex permeabilisation procedures that require specialised equipment and skill. It can, however, enter a cell when attached to a molecule that masks the negatively charged carboxyl groups. The molecule used for this procedure is acetoxymethyl (AM) ester; it binds to fura-2 to produce an uncharged product that is able to cross the cell membrane.

The AM ester is removed by enzymatic digestion by the many cellular esterases. Once freed from the AM ester Fura-2 is trapped inside the cell and is free to bind Ca^{2+} ions. Pluronic F-127 acid is a non-ionic and non-denaturing detergent which helps Fura-2 loading of cells by dispersing the Fura-2 throughout the loading medium, increasing the possibility of uptake into cells (Kao, 1994).

After twenty minutes the cell suspension was added to a glass coverslip in an experimental chamber (2ml open to the air) and left for the final ten minutes of loading to adhere to the glass coverslip. Following this, cells were

then washed by superfusion with HBSS at room temperature (22 ^{o}C) for a further twenty minutes before experimentation commenced.

2.6.4 Imaging of changes in Ca^{2+} in isolated pulmonary artery smooth muscle cells

Excitation light was from a monochromator, TILL Photonics Polychrome II (TILL Photonics, Germany) which emitted previously selected wavelengths (340 and 380 nm) of light. The monochromator works by taking a white light source, in this case a Xenon lamp, and passing the light through a slit at the entrance to the monochromator. This slit ensures that the light passing into the system is as parallel as possible in order to limit problems further on in the process. The light that enters the system is then redirected by a mirror to the diffraction grating. This then redirects the light at slightly different angles depending on its wavelength to another mirror. The diffraction grating consists of many small parallel grooves that cause interference patterns resulting in the light being 'bent' and split into its constitutive components, for example blue light is bent least, while red light is bent the most. By the time the light hits the next mirror each of the wavelengths are some distance apart. The next mirror reflects the light towards the exit slit, with the wavelengths of light being further separated by the time they reach it, causing them to fall like a rainbow upon the exit. The fine slit in the exit allows selection of a single wavelength of light by adjusting the position of the diffraction grating to alter the position of the rainbow on the exit slit. The selected wavelength of light is then passed to the microscope by use of an optical fibre which prevents loss of light during transfer.

Emitted fluorescence from smooth muscle cells was monitored using a Hammamatsu 4880 image intensifying CCD camera, set to external (synchronous) high-speed acquisition, with 2 X 2 binning. The CCD camera was attached to an inverted microscope (Leica, DMIRBE) equipped with a 40X, 1.3 n.a. oil immersion lens (Zeiss). The fluorescence intensity was recorded and analyzed using Openlab imaging and analysis software (Improvision, UK) on an Apple Macintosh G4 personal computer.

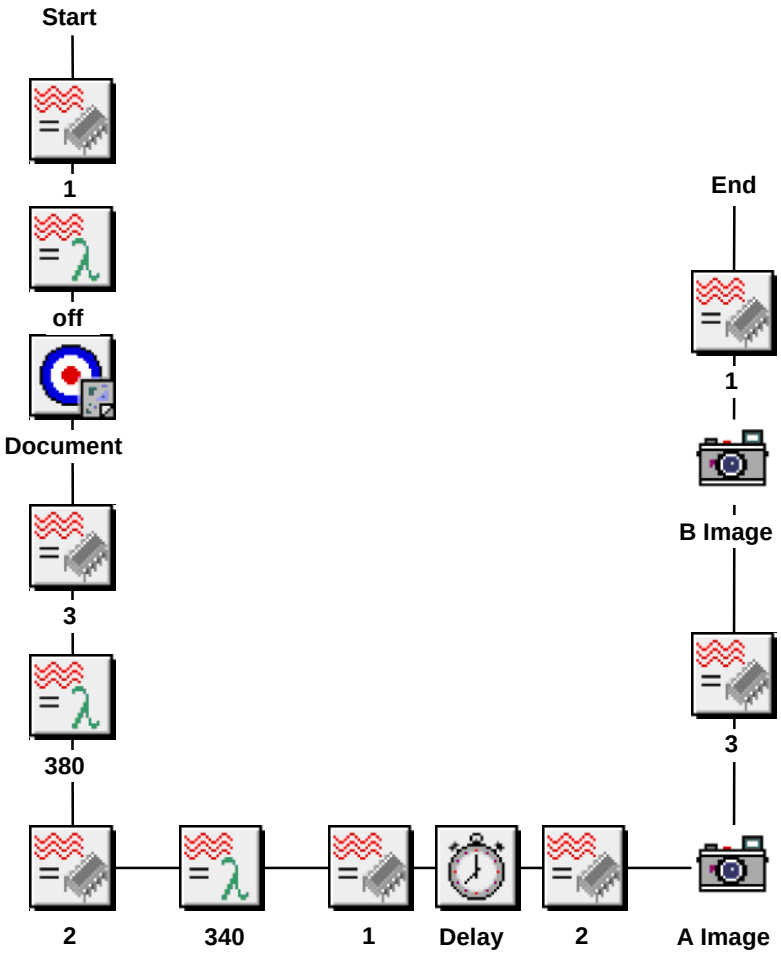

Fig. 2.8 **Diagram of the automation used to obtain background levels of fluorescence in order to correct images captured in experiments by means of 'dark subtraction'.** At the beginning of the automation the monochromator is switched off (1) and no light is transmitted to the signal. The monochromator is then switched on and light at 340 nm is transmitted (2). An image is captured by the CCD camera (A image). The light emitted by the monochromator is switched to 380 nm (3) and a second image is captured (B image). These images are then stored and used to carry out background subtraction.

To interpret the images captured on Openlab, it was necessary to correct them for any background fluorescence. This was achieved by a method known as dark subtraction, as mentioned previously, using an automation written for the Openlab software (A. M. Evans, Bute medical Building, University of St Andrews; Fig. 2.8). The lens is moved so that the cells in the experimental chamber are outside the focal plane, so that the camera does not detect any fluorescence from the cells when exposed to 340 nm or 380 nm light. Images at these two wavelengths are then captured and are used as a measure of the background light the camera will pick up during the

experiment. These background images are subtracted from the images captured during the experiment in order to give a true representation of the Fura-2 fluorescence detected by the CCD camera within each cell.

Using the Openlab software I was able to control the excitation wavelength, camera exposure, the number of images acquired and ratioing of the Fura-2 images by means of a pre-written automation (A. M. Evans, Bute Medical Building, University of St Andrews; Fig. 2.9). Initially, the automation checks to ensure that the monochromator is switched off, with no light being shone on the cells in the chamber. The required number of images is inputted telling the software how often to repeat the main loop of the automation. The main loop has three main parts. Firstly, the monochromator is switched on to shine 340 nm light on the sample for a predetermined period of time, and the emitted fluorescence is captured by the CCD camera using a predetermined exposure time (30 ms). The captured image is saved as image A. The monochromator is then signalled to change its output to 380 nm. Emitted fluorescence is once again captured by the camera using the same exposure time as for the 340 nm image and the second image is then saved as image B. Secondly, the software uses the background images captured previously to remove any background light from the captured images. A ratio image is determined for this loop of the automation by dividing the intensity of light in each pixel of the 340 nm image by the intensity of light within each corresponding pixel of the 380 nm image. This gave the computer a 340/380 nm ratio value for each pixel which is displayed as a grey scaled image. Grey-scale images were converted to a pseudocolour representation to allow easy visualisation of changes in Fura-2 fluorescence ratio to be easily mapped as distinguishable colour changes. Threshold values for each wavelength can be set in order to eliminate any haze or fluorescent glow remaining after the application of the dark subtraction method. In doing this we can eliminate all fluorescent light below a certain fluorescence intensity, allowing for a more accurate representation of what is occurring over the time course of the experiment within the cells of interest. This is achieved by setting the Rmin and Rmax values for the pseudocolour display. The computer applies a colour range to the grey scale, with each grey level represented by a different colour,

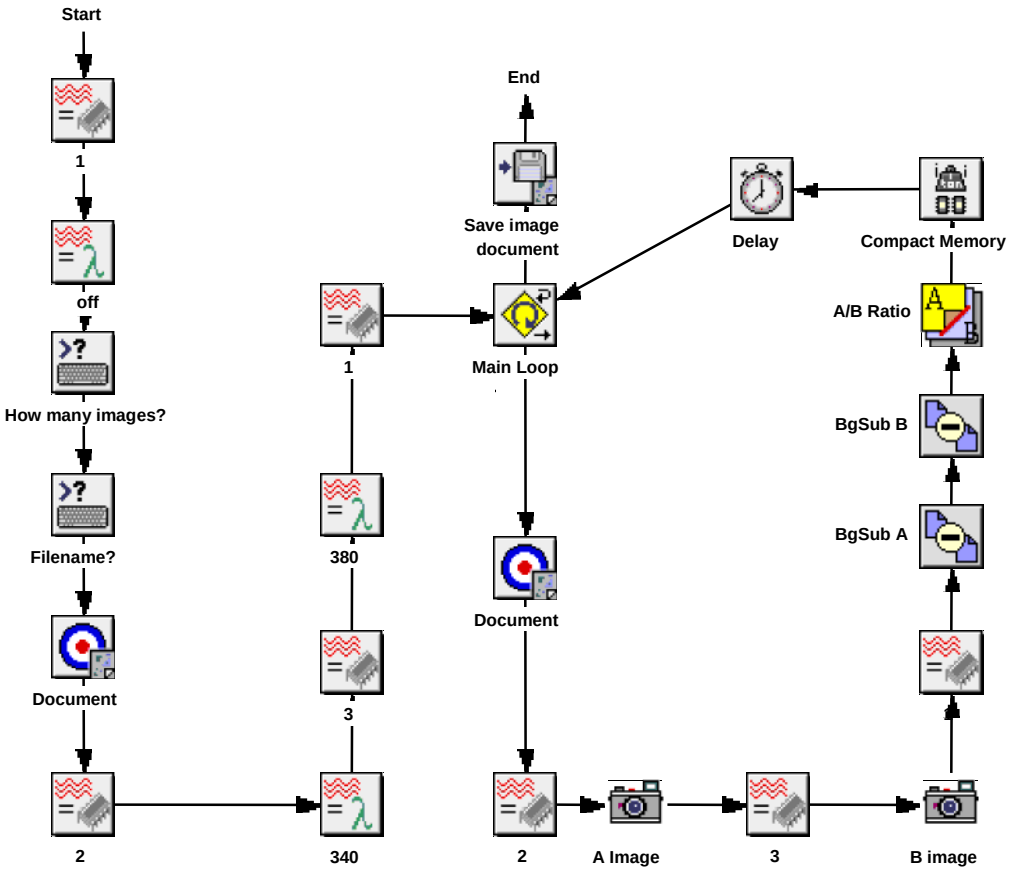

Fig. 2.9 **Diagram of the automation used to obtain Fura-2 fluorescence ratios from isolated pulmonary artery smooth muscle cells.** At the beginning of the automation the monochromator is switched off (1) and no light is transmitted to the signal. The monochromator is then switched on and light at 340 nm is transmitted (2). An image is captured by the CCD camera (A image). The light emitted by the monochromator is switched to 380 nm (3) and a second image is captured (B image). Following background subtraction (BgSub A,B), the 340/380 ratio value for each pixel of the image is calculated (A/B ratio). Following a user-defined time delay the main loop is repeated until the required number of ratio images have been collected.

in my experiments this was a rainbow (Fig. 2.10), with any value below the set Rmin as black and any value above the Rmax as being white, an example of the pseudocolour representation used in the experiments is shown in Fig. 2.8.

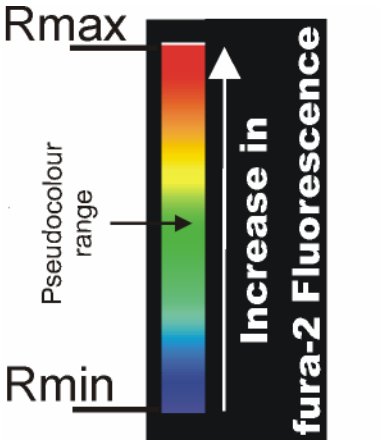

Fig 2.10 **Pseudocolour range applied to grey scale images of Fura-2 fluorescence:** Depiction of the pseudocolour range applied to ratio images using Openlab software. The Rmin and Rmax values represent the user defined cut off points for visualization of the fura-2 fluorescence ratio within isolated pulmonary artery smooth muscle cells.

In the final step of the automation, the software engages a user-defined sample interval after which the sequence is repeated until the required number of ratio images have been acquired (Fig. 2.9).

2.6.5 Extracellular application of pharmacological agents

For experiments on the effects of intracellular dialysis of NAADP and IP_3, pharmacological agents were applied directly to the bath solution. During investigations into the effects of Bafilomycin A1, phenylephrine, prostaglandin $F_{2\alpha}$ and endothelin-1, these and other pharmacological agents were applied by the use of a microsuperfusion system (Langton, 1993)). The miniature flow system consisted of seven lines which fed a common outflow pipe positioned close to the cells under study. The flow of each of these lines was controlled by the use of electrical switched solenoid valves (lee, USA). The diameter of the flow system tubing was approximately 200 μm, the tip was approximately 500 μm and the dead volume of the system was less than 5 μl, this allowed for switching of solutions to occur within 2 s (Langton, 1993). The tip of the flow pipe was positioned approximately 100 μm away from the cells of interest at the edge of the field of view as seen through the microscope objective.

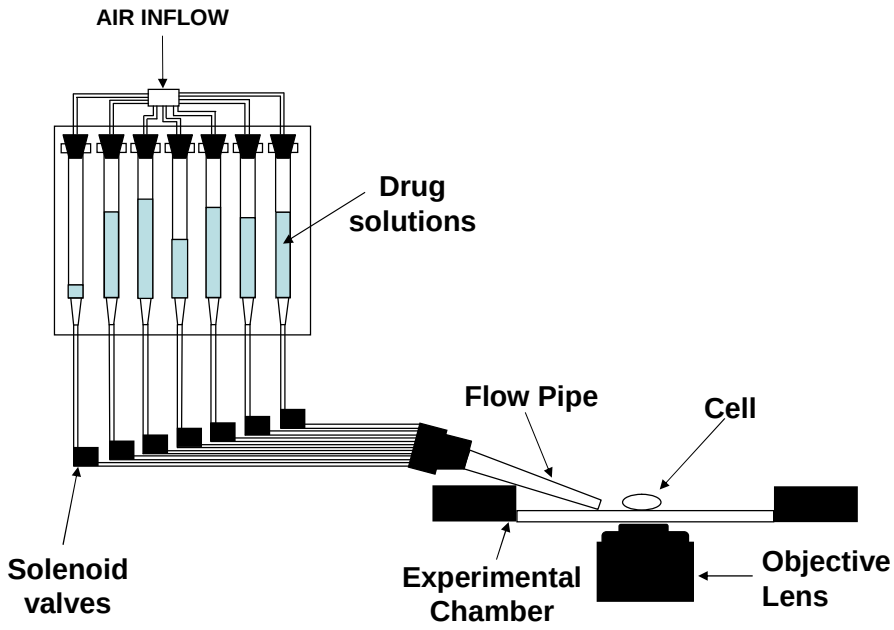

Fig 2.11: **Simple diagrammatic representation showing the miniature flow system used to deliver pharmacological agents extracellularly during fluorescence imaging experiments:** A common air supply was fed to each of the seven reservoirs containing drug solutions, user controlled electrical solenoid valves were used to mediate application of solutions from different reservoirs. Solutions were applied to the experimental chamber and the cells of study using a flow pipe placed within 100 μm of the cells under study.

2.6.6 Ca^{2+} calibration curve

The concentration of Ca^{2+} represented by a given Fura-2 fluorescence ratio was determined through the use of a Fura-2 calcium calibration kit (Molecular probes, Invitrogen Inc.CA, USA). The kit consists of a range of known Ca^{2+} concentrations (0 – 10 mM) buffered with the Ca^{2+} chelator EGTA, made up in solution along with 50 μM Fura-2. Each solution also contains a number of 15 μM unstained polystyrene beads. 50 μl of each solution from the kit was put on different glass coverslips marked with a solid black line in order to determine focal plane. A small circular glass coverslip was then placed on top of the solution. The presence of the polystyrene beads

means that the distance between the 2 coverslips will be consistent throughout. Clear nail varnish was then dabbed around the outside of the circular coverslips in order to prevent any dye leakage from between the coverslips. Clear nail varnish was used as it generates little or no auto-fluorescence under the wavelength of light used in the experiments. Following this, coverslips were placed on the imaging microscope and imaged with a camera exposure of 30 ms at 340 nm and 380 nm as described in Section 2.4.4. Background subtraction was carried out using calibration solution which contained 10 μM CaEGTA but no Fura-2. Ratio values were then determined for each different Ca^{2+} concentration using Openlab software (Improvision, UK; Section 2.6.4), and a standard curve was then produced using Prism analysis software (Graphpad, CA, USA). Ca^{2+} concentrations were then determined by interpolation using Fura-2 fluorescence ratios gathered from Ca^{2+} imaging experiments (Fig. 2.12). Prism analysis determined the Hill Slope values from a form of non-linear regression known as sigmoidal dose response curves with variable slope. This uses the following calculation to calculate the EC_{50} and Hill slope values (Equation 2.3):

$$Y = \text{Bottom} + \frac{(\text{Top}-\text{Bottom})}{1+10^{(\text{Log EC50}-X)\text{Hillslope}}} \qquad \textit{Equation 2.3}$$

where Y = Response

X = Log (agonist concentration)

Top = Y value at the top of the plateau

Bottom = Y value at the bottom of the plateau

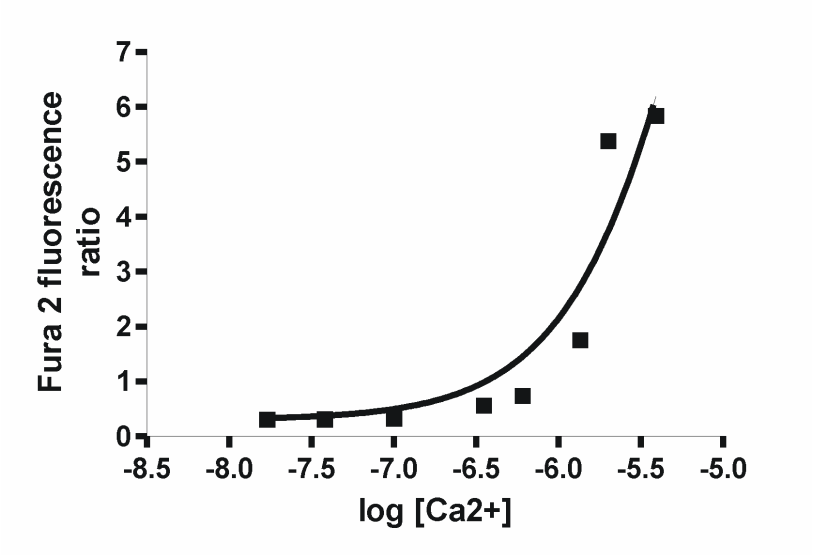

Fig. 2.12: **Example of standard curve used to interpolate Ca^{2+} concentrations from Fura-2 fluorescence ratio values obtained from ratiometric imaging in isolated pulmonary artery smooth muscle cells**

2.7 Whole-cell patch-clamping

Not all pharmacological agents are able to cross the plasma membrane and must therefore be delivered directly to the cytoplasm of the cell. In order to achieve this goal I used the technique of whole-cell patch clamping. In this technique the pharmacological agent of interest is dissolved in a media of an ionic composition close to that of the cytoplasm found in the cell. This media is loaded into a freshly prepared glass electrode, or patch-pipette which is then used to form a tight seal with the cell of interest. Upon formation of this tight seal, negative pressure is applied and the area of membrane directly below the pipette is ruptured allowing the freedom to deliver the pharmacological agent to the intracellular environment (Hamill, *et al.*, 1981).

Pharmacological agents were delivered to the cell at the required final concentration by means of the whole-cell configuration of the patch clamp technique and in current clamp mode (I = 0) using a CV 203BU headstage (axon Instruments, Molecular Devices, USA) attached to an axopatch 200B integrating patch- clamp unit (Axon Instruments, Molecular Devices, USA). Carrying out the delivery of NAADP under current clamp mode allows us to

mimic the situation found in an intact cell, where the membrane potential is allowed to vary and is not held constant.

2.7.1 Preparation of patch pipettes

Filamented boroscilicate glass capillaries (1.5 mm O.D., 0.86 mm I.D.; Harvard Apparatus, UK) were used to generate patch pipettes (2 – 3 MΩ resistance) using a pipette puller (Model pp-830, Narishige, Japan) with a double pull technique. The glass capillaries are anchored above and below a heating coil. Once anchored the heating coil is switched on and the middle of the capillary is heated. As the temperature of the glass increases it becomes more malleable and is pulled apart by the force of gravity pulling the weighted

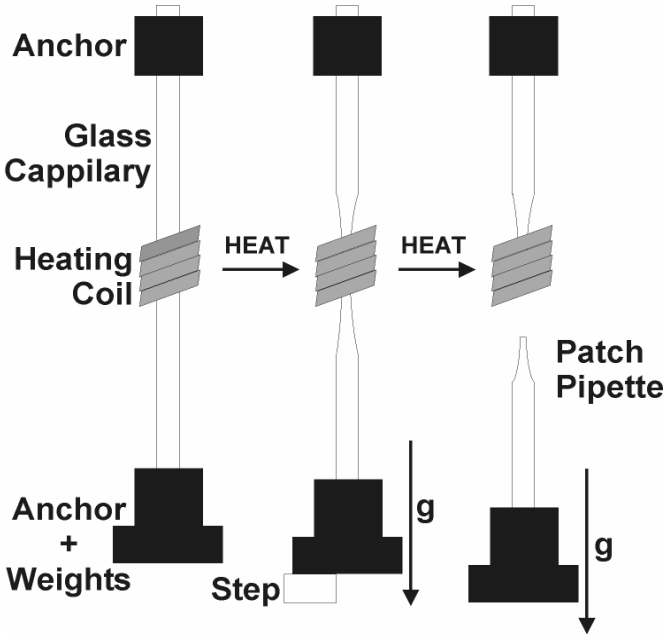

Fig. 2.13: **Simple diagrammatic representation of the double pull technique used to produce patch pipettes:** First, a borosilicate glass capillary is anchored above and below a heating coil. Once turned on the heating coil warms the glass until it is no longer strong enough to resist the pull of gravity (g) on the weights attached to the lower anchor pulling the glass apart and stopping when it comes into contact with a step. The coil is turned off and the glass allowed to cool down. Following this the step is removed, the heating coil is once again turned on and once the capillary is sufficiently warmed the weights again pull the glass apart until the two ends come apart leaving two patch pipettes.

lower anchor down. This continues until the lower anchor comes into contact with a step. The heating coil switches off and the capillary cools down. Following this the heating coil is switched on at a lower heat and the step is removed. This allows the second anchor to pull apart the two halves of the capillary as the glass is gently heated generating two patch pipettes with smooth tips (Fig 2.13).

2.7.2 Generation of a seal and delivery of pharmacological agents

Smooth muscle cells were isolated from the second order branches of pulmonary arteries taken from adult male Wistar rats as described in detail in section 2.2. Following enzymatic isolation with papain, cells were loaded with the ratiometric Ca^{2+} indicator dye Fura-2 as described previously in section 2.6. Cells were then put in an experimental chamber (2 ml final bath volume) in order to undertake investigations. Patch pipettes were filled with pipette solution of the following composition (mM): 140 KCl; 10 HEPES; 1 $MgCl_2$; 5 μM Fura-2 free acid, corrected to pH 7.2 with NaOH. The addition of Fura-2 free acid to the patch pipette prevents loss of fluorescence signal due to the dilution of Fura-2 in the cytoplasm by pipette solution upon entering the whole cell-configuration.

Filled patch-pipettes were placed onto the electrode holder attached to the headstage. Pipette solution was in electrical contact with the headstage via a Ag/AgCl wire located inside the pipette once it was secured to the headstage. The patch-pipette was placed over the electrode wire until it had reached the top of the pipette holder, a cap was then tightened around the base of the patch-pipette which secured it in position by compressing a rubber O-ring. The pipette holder was attached to the headstage that was in turn attached to the patch-clamp amplifier. The amplifier was in electrical contact with the extracellular solution via the Ag/AgCl bath electrode. A length of silicon tubing was attached to electrode holder in order to apply negative pressure to the pipette solution. The patch-pipette was then positioned several microns above the cell of interest, using a three plane piezoelectric micromanipulator (PCS 5000 series, EXFO Burleigh, Canada). The piezoelectric

micromanipulator uses solid ceramic actuators which expand under applied voltages. These provide very precise, fast and stable positioning with extremely low levels of drift during experimentation.

When there are differences in the ionic compositions between the bath solution and the pipette solution it is important to correct for the junction potential which arises at the interface between the two solutions. The potential develops due to differences in concentration and mobility of the ions within the two solutions and maintains electroneutrality across the boundary between the solutions. Once the patch-pipette is put into the bath solution, the current flowing into the pipette is driven by the difference between the bath potential and the pipette potential. This is zeroed before formation of the seal by adjusting the V_{ref} (which sets the pipette potential with reference to the bath potential) using the control on the amplifier. In order to form a seal on an isolated pulmonary artery smooth muscle cell, the tip of the patch- pipette was gradually lowered towards the cell membrane using the piezoelectric micromanipulator. Before contact was made with the cell membrane the integrator unit was set to voltage-clamp mode, holding potential, thus, the voltage that the membrane was to be clamped at was set to 0 mV, with a 5 mV voltage pulse applied at 50 Hz. This voltage pulse evoked a square wave current step (Fig. 2.14A) which was observed on an oscilloscope located in the amplifier unit, allowing the pipette resistance to be calculated (resistance can be calculated using Ohm's law, where resistance (R) is equal to the potential difference across the resistor, the voltage (V) divided by the current (I) passing through it, therefore: $R = V / I$). Contact with the cell membrane resulted in an increase in the resistance of the patch-pipette, which was observed as a decrease in the amplitude of the current step (Fig. 2.14B). Negative pressure was then applied to the pipette solution by use of a syringe attached via a three way valve to the silicon tubing. As the seal improved, electrode resistance increased further, corresponding with a further decrease in amplitude of the current trace on the oscilloscope. Further careful suction was then applied until a gigaohm resistance seal was obtained.

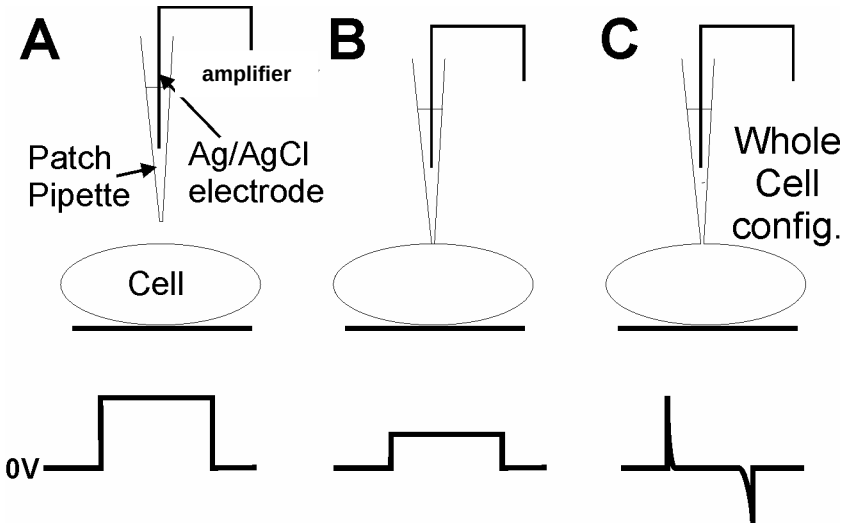

Fig. 2.14: **Schematic diagram showing stages involved in generation of a whole cell seal:** the upper panel of ***A*** shows a patch pipette above the cell of interest filled with pipette solution and containing the Ag/ AgCl electrode, prior to lowering to form a seal. The lower panel of ***A*** shows the image displayed on the oscilloscope screen showing the voltage step applied which allows for calculation of the pipette resistance. The upper panel of ***B*** shows the patch- pipette as it comes into contact with the membrane of the cell prior to entering the whole- cell configuration. The lower panel in ***B*** shows the decrease in the amplitude of the current step associated with the contact between the patch- pipette and the cell. The upper section in Panel ***C*** shows the whole- cell configuration of the patch- clamp technique after the membrane below the patch- pipette has been removed by the application of negative pressure. The lower section in ***C*** shows the capacitance transients characteristic after entering of the whole- cell configuration.

Capacitive transients caused by stray capacity to ground to the pipette wall, seen at the beginning and the end of the voltage step, were compensated for using the fast and slow capacitance compensation facilities on the integrator unit. Further suction was then applied via the syringe in order to rupture the patch of the membrane under the patch- pipette. The development of large membrane capacitive transients at either end of the current step was indicative of the whole- cell configuration being achieved (Fig. 2.14C).

Fluorescent Ca^{2+} imaging of changes in intracellular Ca^{2+} concentration caused by intracellular dialysis of pharmacological agents were imaged using Openlab software as described in Section 2.6.4.

Within the experiments described in this thesis involving the intracellular dialysis of pharmacological agents utilising the patch clamp

technique, the seal resistance was ≥ 3 GΩ, whereas the series resistance and the pipette resistrance were ≤ 10 MΩ and 2 – 3 MΩ, respectively.

2.8 Radioligand binding assay for the determination of NAADP levels in pulmonary artery smooth muscle

2.8.1 Preparation of arteries for radioligand binding assays

2nd and 3rd order branches of the intrapulmonary artery were identified and dissected free of the lung as described in Section 2.1. The arteries were then cut open lengthways and the endothelium was removed from the preparation by gentle rubbing of the luminal wall of the vessel with a cotton bud. Tissue was then placed in HBSS at 37°C (pH 7.4) for a period of equilibration (30 min).

2.8.2 Preparation of sea urchin egg homogenates

Unfertilized *Lytechinus pictus* sea urchin eggs were collected during the gravid season between the months of May and September. Urchins were shipped from California and collection of gametes occurred immediately upon arrival. Eggs were obtained by stimulating ovulation of female sea urchins with an intracoelomic injection of KCl (0.5M; up to 0.5 ml total volume). Eggs were collected in artificial sea-water (ASW), of the following composition (mM): NaCl 435, $MgSO_4$ 15, $CaCl_2$ 11, KCl 10, $NaHCO_3$ 2.5 and EDTA 1.0 at pH 8.0.

Homogenates (50% v/v) of unfertilized sea urchin eggs were prepared in a similar manner to that described previously (Clapper, *et al.*, 1987; Dargie, *et al.*, 1990). Eggs were dejellied in ASW by filtering through 85-mm Nitex mesh (Plastok Associates Ltd, Merseyside, UK). Dejellied eggs were immediately washed by centrifugation at 800 g and 10 °C in approximately 10 times their volume of AWS. Eggs were washed twice in Ca^{2+}-free ASW with EGTA and twice in Ca^{2+}-free ASW composed of (mM): NaCl 470, $MgCl_2$ 27, $MgSO_4$ 28, KCl 10 and $NaHCO_3$ 2.5 at pH 8.0, or including EGTA 1.0.

Finally, eggs were washed with an 'intracellular medium' (IM), composed of (mM): potassium gluconate 250, N-methylglucamine 250, HEPES 20 and $MgCl_2$ 1. The pH was adjusted to 7.2 using acetic acid.

Eggs were then homogenised in IM plus 2 mM ATP, 20 U/ml creatine phosphokinase (CPK), 20 mM phosphocreatine, 50 μg/ml leupeptin, 20 μg/ml aprotinin and 100 μg/ml SBTI (Soya bean trypsin inhibitor), using a dounce glass tissue homogeniser, size 'A' pestle. Cortical granules were removed and discarded by centrifugation at 13,000 *g* for 10 seconds at 4 °C. Homogenates were aliquoted (1 ml) into microcentrifuge tubes and stored at -80 °C, until used for radioligand binding assays.

2.8.3 Preparation of tissue and acid extraction of endogenous NAADP from pulmonary artery smooth muscle

Tissue was dissected as described in section 2.8.1, and placed in HBSS at 37 ^{o}C (pH 7.4) for 30 minutes to equilibrate. Tissue was then placed into fresh HBSS at 37 ^{o}C as a control, or in HBSS containing test compound. After a given period of time tissue was removed from the HBSS, dried by quickly running the tissue over tissue paper, weighed and snap frozen in liquid nitrogen within 5 seconds of removal from HBSS and stored at -80 ^{o}C until required for extraction of nucleotides.

The extraction of endogenous NAADP from tissue samples was carried out using a variation of a method previously described (Walseth, *et al.*, 1991). Tissue samples were diluted 1:4 with ice cold perchloric acid (PCA; 1.5 M) in order to prevent any degradation of the nucleotides by enzymes in the samples and to precipitate proteins out of the solution. Tissues were then homogenized by sonicating the tissue five times for ten second bursts while on ice to prevent any overheating of the samples (Jencons Vibracell at amplitude 60). Samples were then left in an ice bath for twenty minutes in order to allow for full separation of the nucleotides from the protein sample. After this time samples were spun on a desktop centrifuge (13 000 g) for ten minutes in order to remove precipitated proteins. After centrifugation, the supernatant was

removed and the protein fraction was stored at -80 ^{o}C until the level of protein within the samples could be determined as described in section 2.8.6.

The supernatant was then neutralized with a 1:1 addition of potassium bicarbonate ($KHCO_3$, 2 M) and placed in an ice bath for 20 minutes. After this time the samples were centrifuged at 13 000g for ten minutes to separate the nucleotide containing supernatant from the precipitated $KClO_4$. The supernatant was then removed and frozen at -80^{o}C until required for binding.

2.8.4 Preparation of [^{32}P]NAADP for use in radioligand binding assay

The synthesis of [^{32}P]NAADP was carried out in a two-step reaction as described previously (Aarhus, *et al.*, 1996b; Patel, *et al.*, 2000a). Firstly, [^{32}P]NADP was synthesised by incubating [^{32}P]NAD with 0.5 U/ml human NAD kinase, 5 mM MgATP, and 100 mM HEPES for 1 hour. 100 mM nicotinic acid and 1 μg/ml ADP-ribosyl cyclase were added to commence the second step, which was allowed to proceed for one further hour. The resulting mixture was pumped onto a high pressure liquid chromatography (HPLC) column. Separation was carried out on an anion-exchange resin (AGMP1, Biorad) using a concave upwards gradient of trifluoroacetic acid (TFA) as described previously (Aarhus, *et al.*, 1996b; Billington and Genazzani, 2000a; Galione, *et al.*, 2000; Patel, *et al.*, 2000a). The NAADP fraction was then stored for use in the assay.

2.8.5 Radioligand binding assay to determine levels of NAADP within pulmonary artery smooth muscle

Endogenous levels of NAADP within the tissue were determined using a variation of a technique previously described (Masgrau, *et al.*, 2003). Sea urchin egg homogenate was made up to a final concentration of 1.25% in IM. [^{32}P]NAADP (50 000 CPM) and known concentrations of unlabelled NAADP (0.001 – 300 nM) or unknown samples were added to 200 μl of homogenate to make a final volume of 250 μl in the reaction vessel. Due to the irreversible binding of NAADP to its target in sea urchin egg (Aarhus, *et al.*, 1996a;

Billington and Genazzani, 2000a; Patel, *et al.*, 2000a) it is important that the homogenate is exposed to both the radiolabelled and unlabelled NAADP simultaneously otherwise one will not displace the other. Once mixed the samples were left for 15 minutes at room temperature (22 ^{o}C) to allow binding to reach equilibrium. Binding was terminated by rapid filtration through glass microfibre (GF/B) filters (Whatman, US) using a Brandell cell harvester. Filters were washed immediately prior to binding with ice-cold HEPES-EDTA solution of the following composition (mM): HEPES 10, EDTA 1, pH 7.2. Following filtration, filters were washed four times with 4 – 5 ml of HEPES-EDTA solution. Filters were then removed and retained [^{32}P]NAADP was determined using either Cerenkov Spectrometry or storage phosphor screen autoradiography.

In storage phosphor screen autoradiography, filters are exposed to a storage phosphor screen (General purpose storage phosphor screen, 35 x 43 cm, Amersham Bioscience, UK) within an exposure cassette (Amersham Bioscience, UK) for thirty minutes. During this time an imprint of the retained radiation within the filters is created on the screen. The phosphor screen is composed of fine crystal of BaFBR:Eu^{2+} contained within an organic binder. The radiation from the filters causes the oxidation of Eu^{2+} to Eu^{3+} and the reduction of BaFBr to $BaFBr^{-}$. These ions remain oxidized and reduced after removal of the screen from the filters, and thereby retains the energy of the ionizing radiation. The release of the stored energy occurs when the storage phosphor is stimulated by light of an appropriate wavelength. The screen is stimulated by red light (wavelength: 633 nm) which is absorbed by the $BaFBr^{-}$ complex. This frees electrons and reduces the Eu^{3+} to Eu^{2+*} (a Eu^{2+} ion with an excited electron). As this excited electron falls to the ground state it releases energy in the form of blue light (emission maxima: 390 nm). The Typhoon scanner system (Amersham Biosciences, UK) uses a band- pass filter, allowing light around 390 nm to pass through to the detector. The light is then collected and measured by the detector. Therefore the emitted light intensity is proportional to the radioactivity. An image of the filter is then displayed on the computer screen with the detected light depicted in a grey scale. Therefore, the more light detected the darker the image. The image is then quantified using

densitometry analysis (ImageQuant software, Amersham Biosciences, UK) and analyzed using Prism software as described below.

Total binding of [^{32}P]NAADP to sea urchin egg homogenate was determined in the absence of unlabelled NAADP and unknown sample. The amount of [^{32}P]NAADP retained on the filters after filtration decreased as the concentration of unlabelled NAADP increased as they compete for the same binding site. This allowed for the construction of a dissociation curve for [^{32}P]NAADP binding to sea urchin egg homogenate. Non-specific binding was determined as being the amount of radiation (CPM) retained in the presence of 1 μM NAADP. This value was subtracted from the values obtained for the known concentrations of NAADP or unknown samples in order to determine specific binding. By obtaining the values for the retained radiation against various concentrations of NAADP and plotting them as a graph of CPM versus concentration of NAADP it was possible to fit a curve to the data using non-linear regression and fitting a sigmoidal concentration displacement curve with

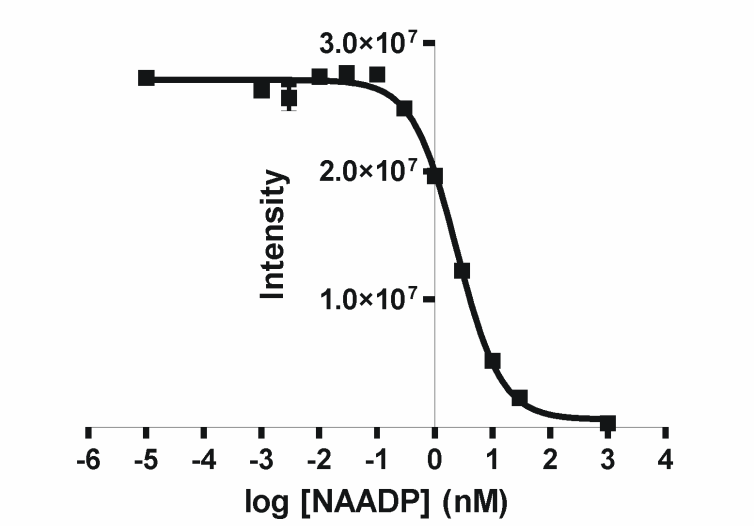

Fig. 2.15 **Example of dissociation curve used to determine the concentration of NAADP levels within pulmonary arteries.**

variable slope fitted using Equation 2.3 (Section 2.6.7) using Prism analysis software (Fig. 2.15; Graphpad, CA, USA). Using this curve it was possible to extrapolate the concentration of NAADP in the unknown samples by determining their position on the dissociation curve. Binding of NAADP to its receptor has been shown to be affected by the presence, or absence of K^+ ions

(Dickinson and Patel, 2003). In order to minimize any effects caused by a differing concentration of K^+ ions in the reaction mixture the samples of known NAADP concentration were subjected to the same acid extraction protocol as the unknown samples.

2.8.6 BCA protein assay and determination of concentrations of NAADP within artery smooth muscle

The protein concentrations of the tissues from which NAADP were extracted for the radioligand binding were determined spectrophotometrically using the bicinchonic acid (BCA) assay according to the manufacturers instructions (Sigma-Aldrich, Dorset, UK). This assay relies on the alkaline reduction of Cu^{2+} to Cu^+ by proteins and on the fact that the bicinchonic acid:Cu^+ complex has absorption maxima of 562 nm. Samples containing 10-50 μg protein in a volume of 50 μl were incubated with 1 ml BCA solution and 0.08 % copper sulphate pentahydrate for 30 minutes at 37 ^oC. Incubations were then given five more minutes at room temperature (20 ^oC), after which their absorbance was measured at 563 nm. Standard protein concentrations of BSA were used to construct a standard curve using Prism analysis software (Graphpad, CA, USA), from which protein concentrations from tissue samples could be determined by interpolation. Following this, concentrations of NAADP were corrected for the dilutions during acid extraction and using these data the concentration of NAADP were expressed as pmol per mg of protein.

2.9 Drugs and chemicals

Fura-2 pentapotassium salt, Fura-2 AM, DAPI, LysoTracker Red and BODIPY-FL ryanodine which were obtained from Molecular probes (Invitrogen Ltd., USA). Anti-RyR antibodies were a kind gift from Professor Sidney Fleischer. Anti-algp120 antibodies were a kind gift from Professor Paul Luzio. Fluorescently conjugated secondary antibodies were obtained from Jackson ImmunoResearch (USA). NAD (^{32}P-radiolabelled) was obtained from Amersham Biosciences (UK). All other compounds were obtained from

Sigma-Aldrich (Poole, Dorset). Stock solutions of ryanodine and thapsigargin were made up in Me_2SO as the solvent. The minimum dilution of Me_2SO was 1:1000 in HBSS, at which concentration Me_2SO alone was without effect on the responsiveness of the preparation. All other stock solutions were made up in double distilled H_2O before further dilution in HBSS.

2.10 Statistical analysis

Data from investigations is summarised as the mean and standard error of the mean (S.E.M. ±) for 'n' experiments. Comparisons between groups were carried out using one-way analysis of variance (ANOVA) in Minitab 14 (Minitab Inc. USA). Differences between groups were considered statistically significant if $P \leq 0.05$.

One-way ANOVA tests were used consistently throughout investigations as it is a robust enough statistical test to be used with data that is not sampled from a normally distributed population. The validity of the results gained from ANOVA tests are only marginally affected by considerable deviations from normality with respect to the assumption of the normality of the distribution of the underlying population (Zar, 1999).

Chapter 3: NAADP mobilises Ca^{2+} from lysosome-related stores in pulmonary artery smooth muscle

3.1 Introduction

NAADP has been shown to mobilise Ca^{2+} from a number of cell types, including vascular smooth muscle (Chini, *et al.*, 1995; Lee and Aarhus, 1995; Genazzani and Galione, 1996; Cheng, *et al.*, 2001; Boittin, *et al.*, 2002). Furthermore, the location of the NAADP-sensitive Ca^{2+} store has recently been identified in the sea urchin egg (Churchill, *et al.*, 2002). In a number of elegant experiments Churchill *et al.* identified reserve granules as the site of NAADP-mediated Ca^{2+} release (Churchill, *et al.*, 2002). Consistent with these findings, recent studies on mammalian cells have suggested that NAADP mobilises Ca^{2+} from an acidic, lysosome-related store, the functional equivalent of reserve granules (Mitchell, *et al.*, 2003; Yamasaki, *et al.*, 2004). This proposal gains further support from prior studies which identified lysosomes as a Ca^{2+} store in snail neurons (Sugaya and Onozuka, 1978) and Madin-Darby canine kidney cells (Haller, *et al.*, 1996).

As described in detail in Chapter 1 (Section 1.8), a previous study from this laboratory has shown that NAADP mobilises Ca^{2+} from a thapsigargin-insensitive, non-SR Ca^{2+} store in pulmonary artery smooth muscle cells. The aim of this chapter is, therefore, to identify the nature of the Ca^{2+} store accessed by NAADP in pulmonary artery smooth muscle by employing a number of the pharmacological agents identified by Galione and colleagues (Churchill, *et al.*, 2002; Yamasaki, *et al.*, 2004), namely Bafilomycin A1, GPN and LysoTracker Red.

3.2 Results

3.2.1 NAADP induces global Ca^{2+} waves in isolated pulmonary artery smooth muscle cells

In order to examine whether or not nicotinic adenine dinucleotide phosphate (NAADP) functions as a Ca^{2+} mobilizing messenger in pulmonary arterial smooth muscle, a fixed concentration of NAADP (10 nM) was applied intracellularly by dialysis from a patch-pipette in the whole-cell configuration of the patch-clamp technique under current clamp conditions (I = 0). Changes in intracellular Ca^{2+} concentration were reported by changes in the Fura-2 fluorescence ratio (F_{340}/F_{380}). A representative experiment is shown in Fig. 3.1. (Note, the cell represented in Fig. 3.1 was obtained as a control cell for a paired cell pre-incubated with Bafilomycin A1 (see Fig. 3.7)). Ca^{2+} bursts initiated by the intracellular dialysis of NAADP either declined to basal levels (Fig. 3.1, image 2), or proceeded to trigger a global Ca^{2+} wave (Fig. 3.1, images 4 – 7). The findings of this investigation were in agreement with the investigation of Boittin *et al.* (2002) as regards the generation of Ca^{2+} bursts prior to the initiation of a global Ca^{2+} wave. It is notable that Ca^{2+} bursts were initially evoked in isolation (Fig. 3.1, image 2). In other words, the Ca^{2+} burst initiated by NAADP may arise and subsequently decay without the generation of a global Ca^{2+} wave. It would appear, therefore, that the initial Ca^{2+} burst in response to NAADP may need to breech a given threshold, determined by the local Ca^{2+} concentration (Boittin, *et al.*, 2002). Analysis of all cells studied showed that NAADP increased the Fura-2 fluorescence ratio from 0.7 ± 0.1 to 1.9 ± 0.1 (n = 17; 16 cells acquired by Dr. F.-X. Boittin; Appendix 1, Table 3.1). This equates to an increase in the intracellular Ca^{2+} concentration from ~200 nM to ~700 nM as determined by the use of a standard *in vitro* Ca^{2+} calibration curve described in Chapter 2, Section 2.6.6. NAADP-induced Ca^{2+} signals were associated with an initial hyperpolarisation and subsequent oscillating membrane potential depolarisations (not shown).

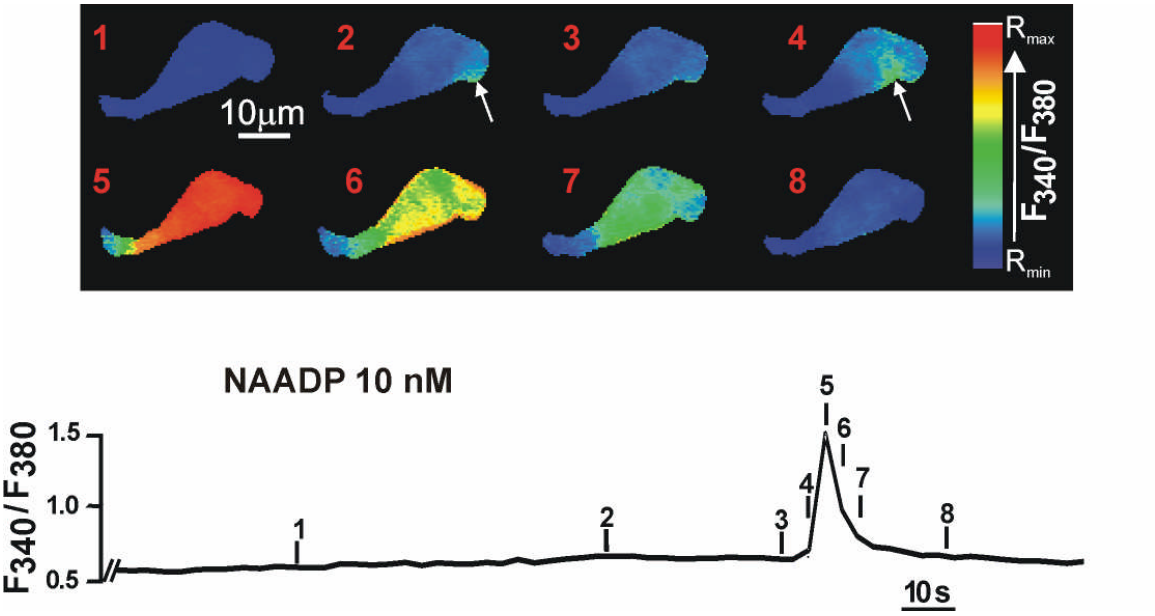

Fig. 3.1: **Intracellular dialysis of NAADP evokes global Ca^{2+} signals in isolated pulmonary artery smooth muscle cells:** ***Upper panel*** shows a series of pseudocolour representations of the change in Fura-2 fluorescence ratio (F_{340}/F_{380}) within an isolated pulmonary artery smooth muscle cell in response to the intracellular dialysis of NAADP (10 nM) from a patch- pipette. The arrows indicate spatially restricted Ca^{2+} bursts which occur prior to the global Ca^{2+} wave and contraction of the cell. ***Lower panel*** shows a record of the Fura-2 fluorescence ratio against time recorded from the same cell as in the upper panel.

In contrast to the global Ca^{2+} waves, spatially restricted Ca^{2+} bursts evoked by NAADP were of a much lower magnitude. Careful consideration was given to analyzing the Ca^{2+} bursts further in order to determine the difference in magnitude between those Ca^{2+} bursts which triggered a global Ca^{2+} wave and those which did not, as any difference in magnitude could support this laboratory's view that Ca^{2+} bursts must breach a threshold concentration in order to elicit a global Ca^{2+} wave. However, the increase in Fura-2 fluorescence observed was small, highly variable and likely represented the average rise in Ca^{2+} concentration achieved through a number of Ca^{2+} release events rather than the absolute maximum achieved at any given point. These confounding influences prevented discrimination between those Ca^{2+} burst events that initiated global Ca^{2+} waves and those that did not on the grounds of local Ca^{2+} concentration. However, future investigations using

confocal microscopy may allow for more accurate assessment of local Ca^{2+} release events evoked by NAADP.

3.2.2 The role of the sarcoplasmic reticulum and other Ca^{2+} stores in mediating global Ca^{2+} signals in response to NAADP

Previous investigations from this laboratory (Boittin, *et al.*, 2002) have established that subsequent to the Ca^{2+} burst evoked by NAADP, a global Ca^{2+} wave is induced by Ca^{2+}-induced Ca^{2+}-release (CICR) via RyRs on the SR. Thus, (1) the magnitude of global Ca^{2+} waves induced by the intracellular dialysis of NAADP were unaffected by the removal of extracellular Ca^{2+} in the presence of the fast calcium chelator BAPTA (1 mM); (2) Ca^{2+} bursts and global Ca^{2+} waves were abolished when 1 mM BAPTA was included with NAADP in the intracellular pipette solution; (3) global Ca^{2+} waves, but not local Ca^{2+} bursts in response to NAADP, were abolished after depletion of SR Ca^{2+} stores in isolated pulmonary artery smooth muscle cells by pretreatment (20 min) with thapsigargin; (4) block of RyRs with ryanodine, but not the block of IP_3Rs with xestospongin C, abolished global Ca^{2+} waves but did not affect localized Ca^{2+} bursts (Boittin, *et al.*, 2002). These findings suggest that NAADP evokes global Ca^{2+} waves in arterial smooth muscle via a two pool mechanism. Briefly, it was concluded that NAADP induced Ca^{2+} release from a thapsigargin-insensitive, non-SR store that was subsequently amplified into a global Ca^{2+} wave by CICR via RyRs located on the SR. However, the nature of the non-SR Ca^{2+} store mobilised by NAADP remained to be defined (Boittin, *et al.*, 2002).

In a recent investigation, Churchill *et al.* (2002) identified reserve granules in the sea urchin egg as a possible NAADP-sensitive Ca^{2+} store.

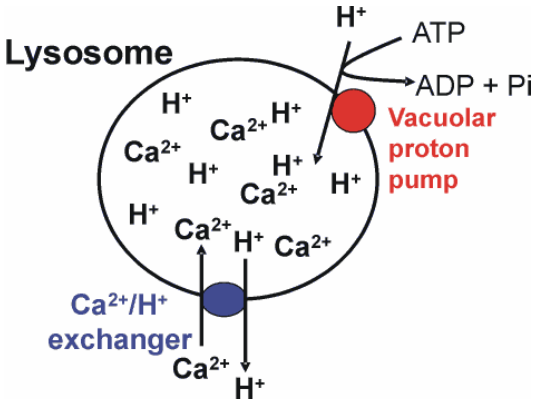

Fig 3.2: **Diagrammatic representation of the two-stage process by which lysosomes are believed to maintain a Ca^{2+} store.** Firstly, protons are pumped into the lysosome via a vacuolar proton pump. Following this, protons are pumped out and Ca^{2+} is pumped in via the actions of a Ca^{2+}/H^{+} exchanger (Christensen, *et al.*, 2002).

Reserve granules represent the functional equivalent of lysosomes in mammalian cells. Previous studies carried out in cultured bone-marrow-derived macrophages from C57B1/6 mice have established that lysosomes maintain a Ca^{2+} store via a two-stage transport system (Christensen, *et al.*, 2002). Firstly, a proton gradient is generated across the lysosomal membrane by the action of the vacuolar proton pump ($V\text{-}H^{+}$- ATPase). This then allows for the uptake of Ca^{2+} into the lumen of the lysosome through the actions of a Ca^{2+}/H^{+} exchanger (Fig 3.2; Christensen, *et al.*, 2002). Churchill *et al* (2002) demonstrated in the sea urchin egg that inhibition of the vacuolar proton pump with Bafilomycin A1 prevented refilling of NAADP-sensitive Ca^{2+} stores following NAADP-mediated Ca^{2+} mobilisation as subsequent uncaging of caged NAADP by flash photolysis did not induce further Ca^{2+}release. The effects of Bafilomycin A1 were without effect on Ca^{2+} mobilisation by either cADPR or IP_3 (Churchill *et al*., 2002). I, therefore, investigated the possibility that lysosomes may represent the NAADP-sensitive Ca^{2+} store in pulmonary artery smooth muscle cells using Bafilomycin A1 as a key pharmacological tool.

3.2.3 The effects of Bafilomycin A1 on intact pulmonary artery smooth muscle cells

Surprisingly, when Bafilomycin A1 (100 - 300 nM) was applied extracellularly to isolated pulmonary smooth muscle cells a pronounced and global Ca^{2+} wave was triggered. Fig. 3.3 shows a representative cell. The increase in Fura-2 fluorescence ratio in response to Bafilomycin A1 (100 – 300 nM) was seen to peak within 300 s. The Fura-2 fluorescence ratio then returned

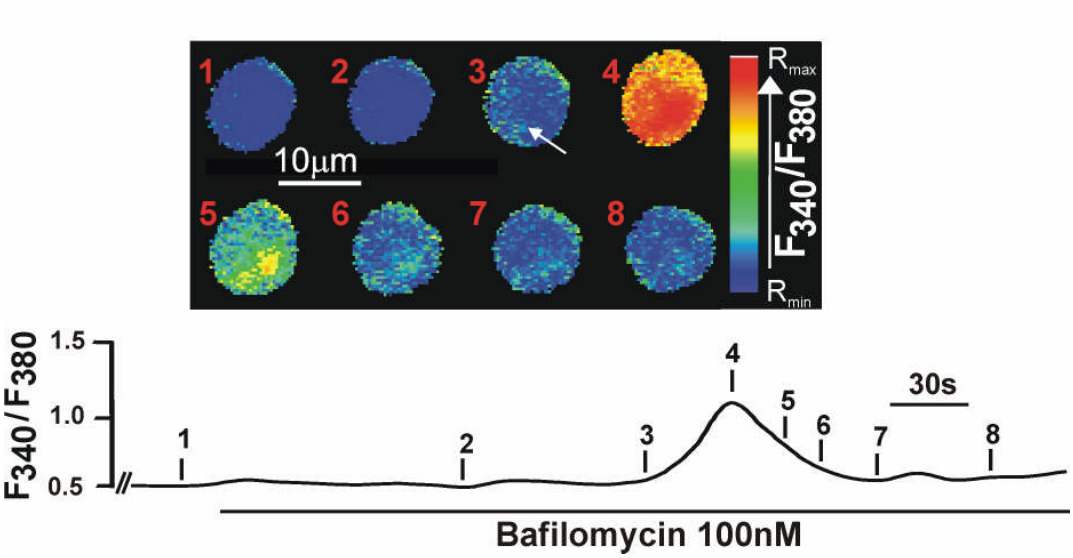

Fig. 3.3: **Bafilomycin A1 induces global Ca^{2+} signals in isolated pulmonary artery smooth muscle cells:** ***Upper panel*** shows a series of pseudocolour representations of the change in Fura-2 fluorescence ratio (F_{340}/F_{380}) within an isolated pulmonary artery smooth muscle cell in response to the extracellular application of Bafilomycin A1 (100 nM). The arrow in image 3 indicates a localised increase in Ca^{2+} generated prior to the global Ca^{2+} response. ***Lower panel*** shows a record of the Fura-2 fluorescence ratio against time recorded in the same cell.

to a resting level within 45 minutes. Bafilomycin A1 induced an increase in the Fura-2 fluorescence ratio from 0.63 ± 0.05 to 1.04 ± 0.07, which relates to a rise in intracellular Ca^{2+} concentration of ~150 nM to ~600 nM (n = 20; Appendix 1, Table 3.2). Interestingly, initial Ca^{2+} release events in response to the application of Bafilomycin A1 (100 – 300 nM) were seen to be similar in nature to Ca^{2+} bursts initiated by intracellular dialysis of NAADP (10 nM). Upon extracellular application of Bafilomycin A1 to cells spatially restricted

rises in F_{340}/F_{380} fluorescence ratio were observed within the cells, as indicated in Fig. 3.3, image 3. However, unlike the NAADP-mediated Ca^{2+} bursts, localized rises in Ca^{2+} concentration elicited by Bafilomycin A1 did not appear to decay before a global Ca^{2+} wave was initiated. Rather these responses appeared to rise to a point at which they initiated a global Ca^{2+} response (Fig. 3.3). Therefore, it would appear that treatment of isolated pulmonary artery smooth muscle cells with the V-H^+- ATPase inhibitor Bafilomycin A1 may mobilise a Ca^{2+} store in its own right without the requirement for NAADP, as was previously observed in sea urchin eggs (Churchill, *et al.*, 2002).

3.2.4 Comparison of the pharmacology of Ca^{2+} release mediated by NAADP and Bafilomycin A1

To determine whether or not Bafilomycin A1 mobilised the NAADP-sensitive Ca^{2+} store in pulmonary artery smooth muscle, I then examined the pharmacology of Bafilomycin A1-mediated Ca^{2+} release. As mentioned previously, recent work from this laboratory has shown that preincubation (20 min) of isolated pulmonary artery smooth muscle cells with thapsigargin (1 μM) significantly attenuated Ca^{2+} signals generated by the intracellular dialysis of NAADP (10 nM; Boittin, *et al.*, 2002). In these cells, however, spatially restricted Ca^{2+} bursts were still detected in all the cells examined (Boittin, *et al.*, 2002). In a similar fashion, preincubation (20 min) of isolated pulmonary artery smooth muscle cells with thapsigargin (1 μM) eliminated global Ca^{2+} signals in response to the extracellular application of Bafilomycin A1 (100 – 300 nM). However, small spatially restricted and asynchronus Ca^{2+} transients were observed in 8 out of 11 cells (Fig. 3.4, Appendix 1, Table 3.3). In these 8 cells a region of interest (ROI) was drawn around the area covered by this spatially localised release event (Fig. 3.4, image 7). The increase in Fura-2 fluorescence ratio within this ROI was then determined. On average, these spatially restricted increases in the Fura-2 fluorescence ratio were seen to rise from 0.72 ± 0.03 to 0.91 ± 0.02 (Appendix 1, Table 3.3, results indicated with an asterisk (*)), an increase in the intracellular Ca^{2+} concentration from ~210 nM to ~310 nM (Fig 3.4). In the remaining 3 cells of the 11 examined, the

increase in Fura-2 was seen as a non-uniform increase in Fura-2 fluorescence ratio across the entire cell. As the increase in Fura-2 fluorescence ratio within these 3 cells did not occur in a spatially restricted fashion, an ROI was drawn around the entire cell and the increase in Fura-2 fluorescence measured. The

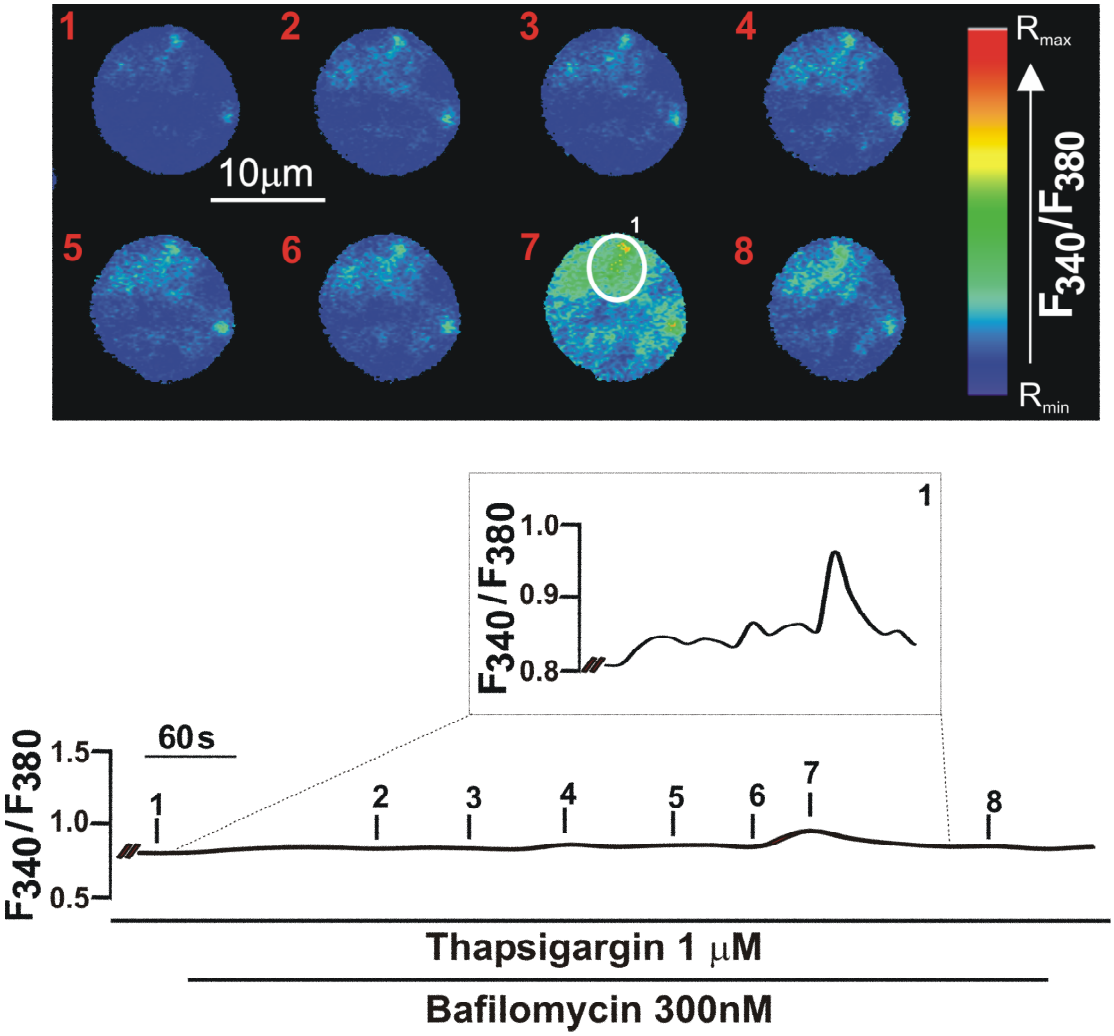

Fig. 3.4: **Thapsigargin abolishes global Ca^{2+} waves in response to Bafilomycin A1, but not localized Ca^{2+} release events:** ***Upper panel:*** shows a pseudocolour representation of the changes in Fura-2 fluorescence ratio within an isolated pulmonary artery smooth muscle cell after preincubation (20 min) with thapsigargin (1 µM) in response to the extracellular application of Bafilomycin A1 (300 nM). Note, the spatially restricted Ca^{2+} burst indicated by the ROI in pseudocolour image 7. ***Lower panel:*** shows the average Fura-2 fluorescence ratio against time within the entire cell shown in the upper panel, the insert shows the Fura-2 fluorescence ratio against time on an expanded scale for the ROI indicated in pseudocolour representation in image 7.

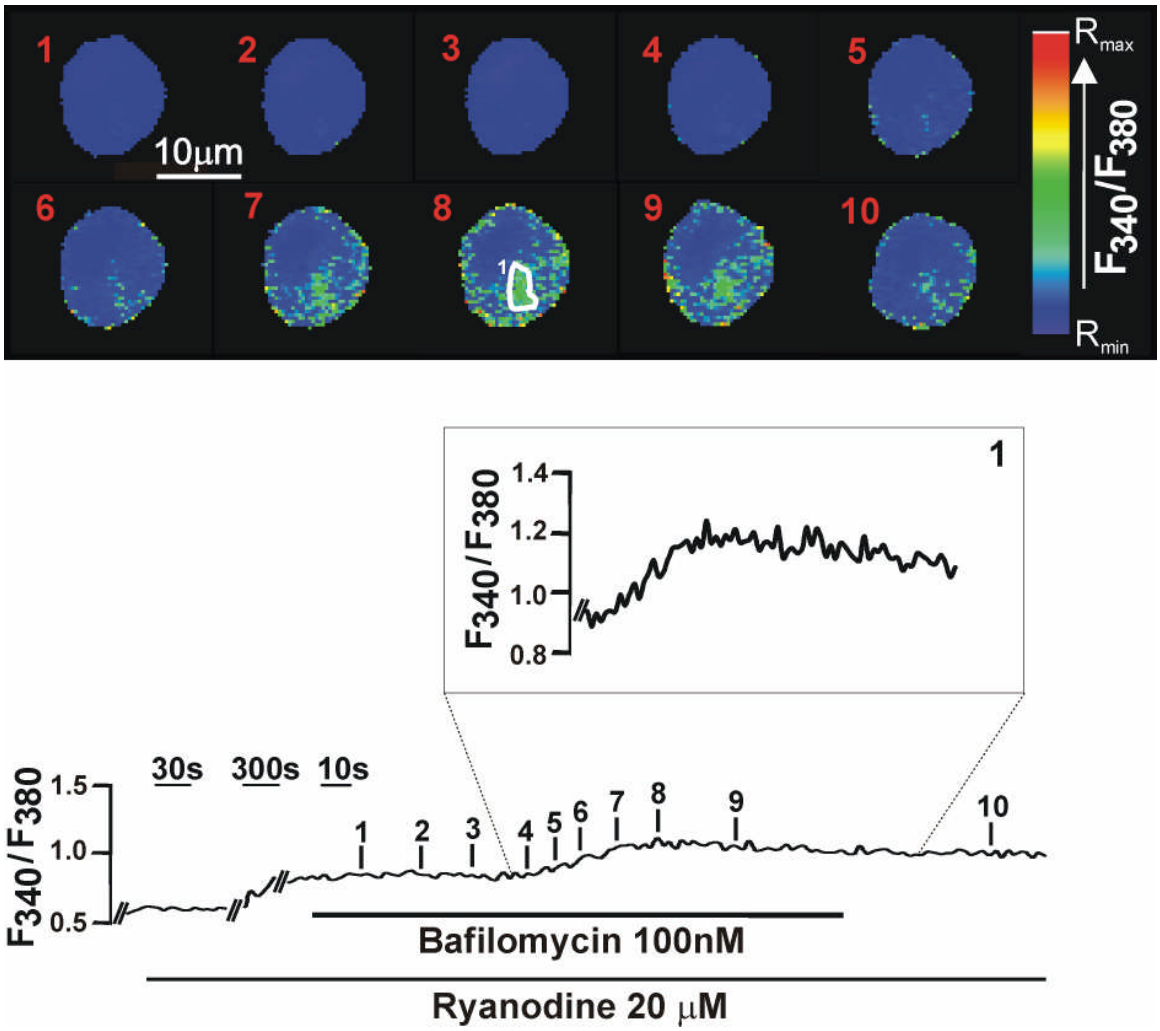

Fig. 3.5: **Ryanodine abolishes global Ca^{2+} waves in response to Bafilomycin A1, but not localized Ca^{2+} release events.** ***Upper panel:*** shows a pseudocolour representation of the changes in Fura-2 fluorescence ratio within an isolated pulmonary artery smooth muscle cell after preincubation (20 min) with ryanodine (20 μM) in response to the extracellular application of Bafilomycin A1 (100 nM). Note, the spatially restricted Ca^{2+} release event indicated by an ROI in pseudocolour image 8. ***Lower panel:*** shows the average Fura-2 fluorescence ratio against time in the entire cell shown in the upper panel. The insert shows the Fura-2 fluorescence ratio against time on an expanded scale for the ROI indicated in pseudocolour representation 8.

average rise in Fura-2 fluorescence ratio in all 11 cells examined was from 0.64 ± 0.05 to 0.79 ± 0.06 (n = 11, Appendix 1, Table 3.3), an increase in intracellular Ca^{2+} from ~200 nM to ~250 nM. Statistical comparison of the increase in Fura-2 fluorescence ratio observed in response to the application of Bafilomycin A1 following preincubation of cells with thapsigargin (0.16 ±

0.02, n = 11; Appendix 1, Table 3.4) against the increase in Fura-2 fluorescence in cells to the application of Bafilomycin A1 in the absence if thapsigargin (0.42 ± 0.04, n = 20; Appendix 1, Table 3.4), by means of a one-way ANOVA test, showed there was a significant difference between the test and control groups (P = <0.0001; Appendix 1, Table. 3.4). The results of experiments in isolated pulmonary artery smooth muscle cells preincubated with thapsigargin suggest, therefore, that Bafilomycin A1, like NAADP, causes an initial phase of Ca^{2+} release from a non-SR Ca^{2+} store, that is amplified into a global Ca^{2+} signal by SR Ca^{2+} release.

Given that amplification of NAADP-mediated Ca^{2+} bursts into global Ca^{2+} waves requires amplification via CICR from RyRs on the SR, I next sought to determine whether or not CICR via RyRs was required for the generation of global Ca^{2+} signals by Bafilomycin A1. When isolated pulmonary artery smooth muscle cells were preincubated with ryanodine (20 μM, 20 min), the extracellular application of Bafilomycin A1 (100 – 300 nM) failed to induce global Ca^{2+} waves. However, in 5 out of 8 cells examined under these conditions localized Ca^{2+} release events were observed (Fig. 3.5). ROI's were drawn to encompass localised Ca^{2+} release events and the increase in Fura-2 fluorescence ratio was measured. Within a given ROI in cells preincubated with ryanodine, Bafilomycin A1-induced Ca^{2+} release events increased the Fura-2 fluorescence ratio from 0.66 ± 0.06 to 0.88 ± 0.09 (Fig 3.5, Appendix 1, Table 3.5, results marked with asterisk (*)). This equated to an increase in the cytoplasmic Ca^{2+} concentration within these regions from ~180 nM to ~300 nM. In the remaining 3 cells the increase in Fura-2 fluorescence ratio was observed as a non-uniform increase across the entire cell. As there was no clear spatial definition to these rises, ROI's were drawn to encompass the entire cell. Following this the increase in Fura-2 fluorescence ratio was determined. On average, the Fura-2 fluorescence ratio was seen to increase from 0.61 ± 0.05 to 0.79 ± 0.08 across all the cells examined, corresponding to an increase in intracellular Ca^{2+} concentration from ~160 nM to ~300 nM. As was the case in cells preincubated with thapsigargin, the inhibition by ryanodine of the increase in Fura-2 fluorescence ratio in response to the application of Bafilomycin A1 (0.18 ± 0.03, n = 8; Appendix 1, Table

3.6) was significantly lower than the increases in Fura-2 fluorescence ratio within control cells exposed to Bafilomycin A1 in the absence of ryanodine (0.42 ± 0.04, Appendix 1, Table 3.6) using a one-way ANOVA test (P = < 0.0001, Appendix 1, Table 3.6).

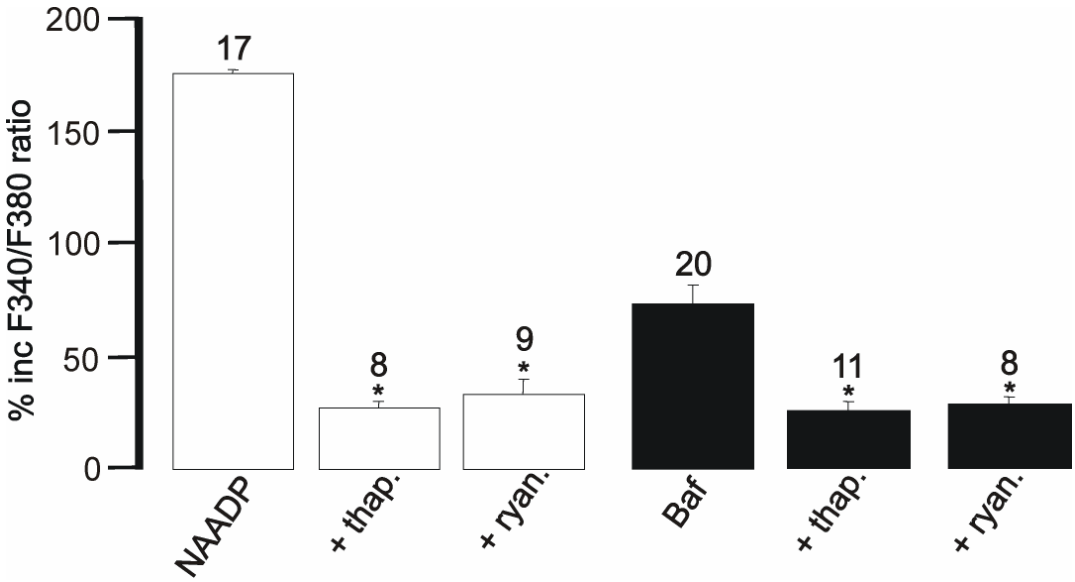

Fig. 3.6: **Bar chart showing the similarity in the pharmacology underlying Ca^{2+} signalling in isolated pulmonary artery smooth muscle cells in response to NAADP (10 nM) and Bafilomycin A1 (100 – 300 nM).**

Fig. 3.6 compares the pharmacological profile of Ca^{2+} signals generated by NAADP and Bafilomycin A1, respectively. On the basis of the similarities in this pharmacology, I conclude that both NAADP and Bafilomycin A1 generate Ca^{2+} bursts from a thapsigargin- and ryanodine-insensitive Ca^{2+} store, that are then amplified into global Ca^{2+} waves by CICR via RyRs located on the SR (Fig. 3.6).

3.2.5 Bafilomycin A1 abolishes Ca^{2+} release mediated by NAADP without affecting Ca^{2+} release from sarcoplasmic reticulum Ca^{2+} stores

In association with Dr. Francois Boittin, I next examined the possibility that the thapsigargin- and ryanodine-insensitive Ca^{2+} store mobilised by NAADP in pulmonary artery smooth muscle cells may be an acidic, lysosome-

related Ca^{2+} store. Isolated pulmonary artery smooth muscle cells were preincubated for 50 minutes with Bafilomycin A1 (100 nM) prior to the intracellular dialysis of NAADP (10 nM) from a patch-pipette.

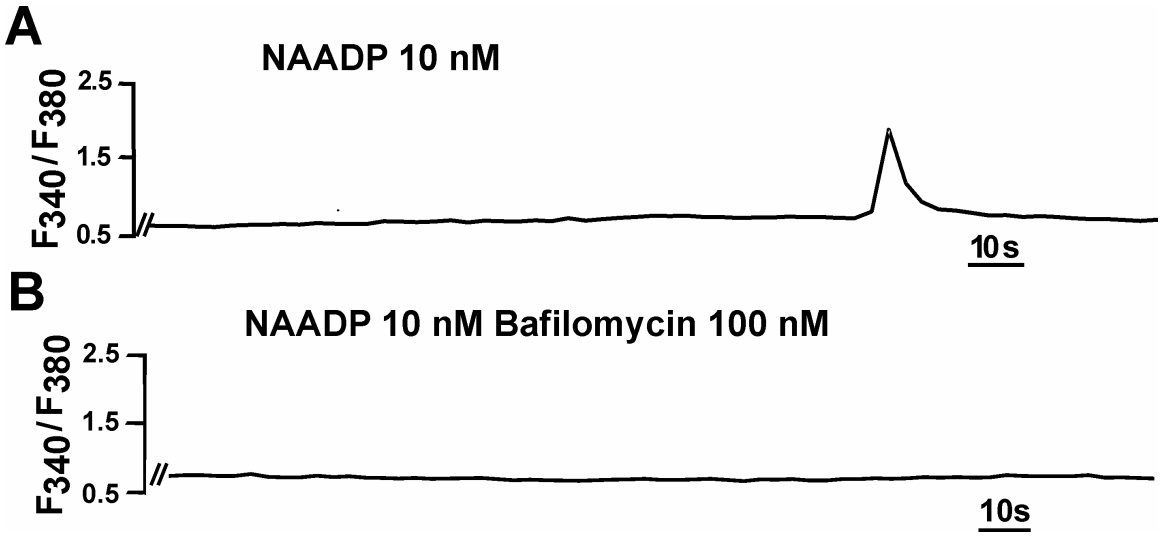

Fig. 3.7: **Bafilomycin A1 abolishes Ca^{2+} signals to NAADP in isolated pulmonary artery smooth muscle cells:** ***Panel A*** Record of the Fura-2 fluorescence ratio against time in an isolated pulmonary artery smooth muscle cell in response to the intracellular dialysis of NAADP (10 nM). ***Panel B***, Record of the Fura-2 fluorescence ratio against time in a paired isolated pulmonary artery smooth muscle cell in response to the intracellular dialysis of NAADP (10 nM) following the preincubation (50 min) of the cell with the $V\text{-}H^{+}$- ATPase inhibitor Bafilomycin A1 (100 nM).

This allowed for mobilisation, or depletion of the Bafilomycin A1-sensitive Ca^{2+} store; as indicated by the rise in the Fura-2 fluorescence ratio and subsequent decline back to levels seen under control conditions. Following this, intracellular dialysis of NAADP (10 nM) had little or no effect on the Fura-2 fluorescence ratio, whilst initiating a global Ca^{2+} wave in paired cells that had not been exposed to Bafilomycin A1 (100 nM; Fig. 3.7 and Appendix 1, Table 3.7). Thus, Ca^{2+} signalling by NAADP was abolished by preincubation of cells with Bafilomycin A1. Not surprisingly then, the response of cells to the intracellular dialysis of NAADP after preincubation of cells with Bafilomycin A1 (0.17 ± 0.03; $n = 7$) was significantly lower than that observed under control conditions (1.3 ± 0.2; $n = 17$; $P = <0.0001$; Appendix 1, Table 3.8).

Importantly, we found that the incubation of cells with Bafilomycin A1 did not affect other mechanisms of Ca^{2+} release from SR Ca^{2+} stores of isolated

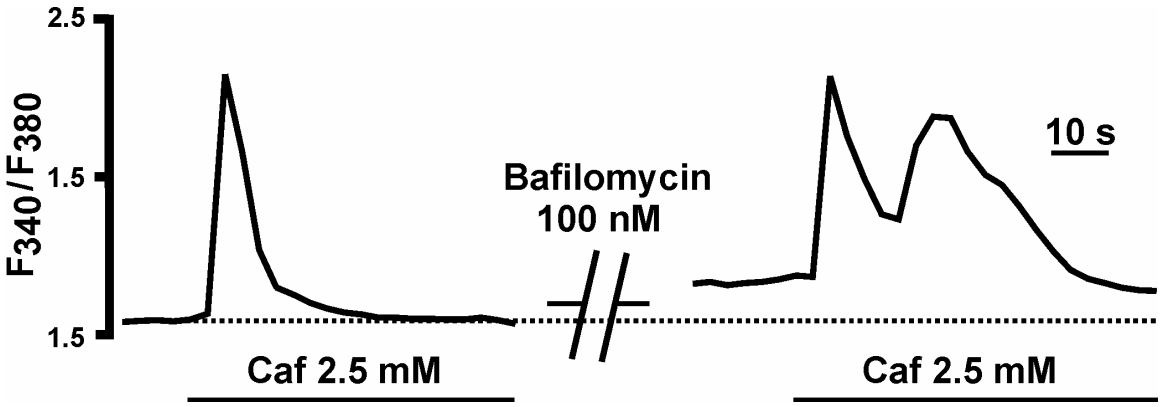

Fig. 3.8: **Changes in Fura-2 fluorescence ratio in response to Caffeine in the presence and absence of Bafilomycin A1**.Record of the change in the Fura-2 fluorescence ratio against time in an isolated pulmonary artery smooth muscle cell in response to the extracellular application of caffeine (2.5 mM) both before and after preincubation (50 min) of the cell with Bafilomycin A1 (100 nM).

pulmonary artery smooth muscle cells. Thus, preincubation (50 mins) of isolated pulmonary artery smooth muscle cells with Bafilomycin A1 did not affect the Ca^{2+} signals generated by the extracellular application of caffeine (2.5 mM; Fig. 3.8) to induce RyR-mediated Ca^{2+} release. It was seen that the extracellular application of caffeine to pulmonary artery smooth muscle cells in the absence of Bafilomycin A1 resulted in an increase in the Fura-2 fluorescence ratio from 0.68 ± 0.06 to 2.22 ± 0.2 (n = 4; Appendix 1, Table 3.9) which is equal to an increase in intracellular Ca^{2+} concentration from ~200 nM to ~900 nM. After pre-incubation (50 mins) with Bafilomycin A1 (100 nM) the response to caffeine was not significantly different from control (P = 0.7; Appendix 1, Table 3.11), as shown by the fact that the Fura-2 ratio increased from 0.71 ± 0.02 to 2.18 ± 0.06 (Appendix 1, Table 3.10), equating to an increase in Ca^{2+} concentration from ~210 nM to ~900 nM.

Similarly, experiments carried out in association with Dr. Francois Boittin showed that preincubation of isolated pulmonary artery smooth muscle cells with Bafilomycin A1 was without effect on Ca^{2+} signals generated by the release of Ca^{2+} from the SR via IP_3Rs mediated by the intracellular dialysis of

IP_3 (1 μM; Fig 3.9). Intracellular dialysis of IP_3 (1 μM) from a patch-pipette was seen to induce a transient depolarisation in the membrane potential and an increase in the Fura-2 fluorescence ratio from 0.61 ± 0.04 to 1.83 ± 0.38 (n = 4; Appendix 1, Table 3.12) in the absence of Bafilomycin A1, and from 0.68 ± 0.06 to 2.22 ± 0.19 (n = 4; Appendix 1, Table 3.13) following preincubation (50 mins) of paired cells with Bafilomycin A1 (100 nM). This equated to an increase in the Ca^{2+} concentration within the cells from ~170 nM to ~700 nM and from ~200 nM to ~900 nM, respectively. Statistical analysis of these data sets clearly showed that there was no significant difference (P = 0.4; Appendix 1, Table 3.14) between the changes in Fura-2 fluorescence ratio under control or test conditions.

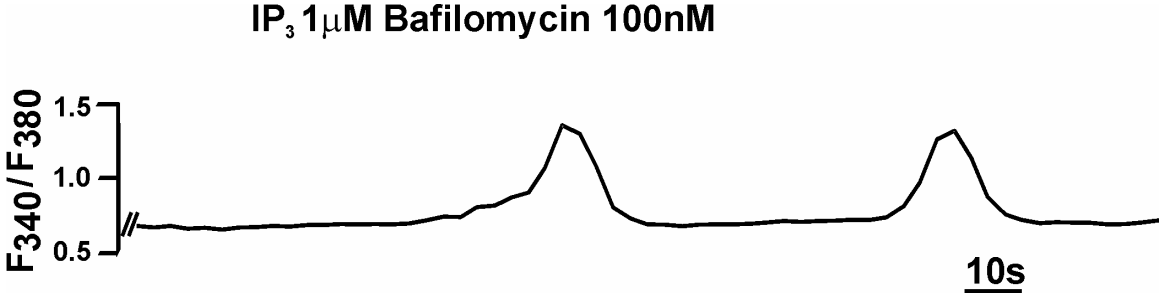

Fig. 3.9: **IP_3 induces global, regenerative Ca^{2+} signals following preincubation of isolated pulmonary artery smooth muscle cells with Bafilomycin A1:** Record of the change in the Fura-2 fluorescence ratio in an isolated pulmonary artery smooth muscle cell in response to intracellular dialysis of IP_3 (1 μM) after preincubation (50 min) of the cell with Bafilomycin A1 (100 nM).

3.2.6 Lysosomes form tight clusters within isolated pulmonary artery smooth muscle cells

The finding that NAADP mediates Ca^{2+} bursts by mobilizing Ca^{2+} from non-SR stores (Boittin, *et al.*, 2002) which are Bafilomycin A1-sensitive provides evidence in support of the view that acidic, lysosome-related Ca^{2+} stores represent an NAADP-sensitive Ca^{2+} store in pulmonary artery smooth muscle cells (Kinnear, *et al.*, 2004). In order to further examine this proposal I investigated whether there was any evidence to suggest that the distribution of lysosomes within these cells may underlie the generation of the Ca^{2+} bursts

evoked by NAADP and the spatially restricted Ca^{2+} release events evoked by Bafilomycin A1. In order to do this I used the fluorescent indicator dye LysoTracker Red. As mentioned previously, LysoTracker Red is a weak base and accumulates within acidic organelles, such as lysosomes (see Chapter 2, Section 2.3.2). This allowed me to determine the spatial organisation of these sub-cellular organelles.

In deconvolved Z-sections (focal depth 0.28 μm) taken through isolated pulmonary artery smooth muscle cells loaded with LysoTracker Red (0.5 – 2 nM, 30 min) the distribution of LysoTracker Red labelling revealed that the acid organelles formed clusters that were either located in a ring around the perimeter of the cell, or as spatially restricted clusters located close to the centre of the cell. However, it was noted that smaller clusters/individual lysosomes were also observed in other parts of the cell. Two typical examples of the cellular distribution of LysoTracker Red labelling are shown in Fig. 3.10. It was important to determine whether or not the organelles that were being labelled with LysoTracker Red were indeed lysosomes and, in order to

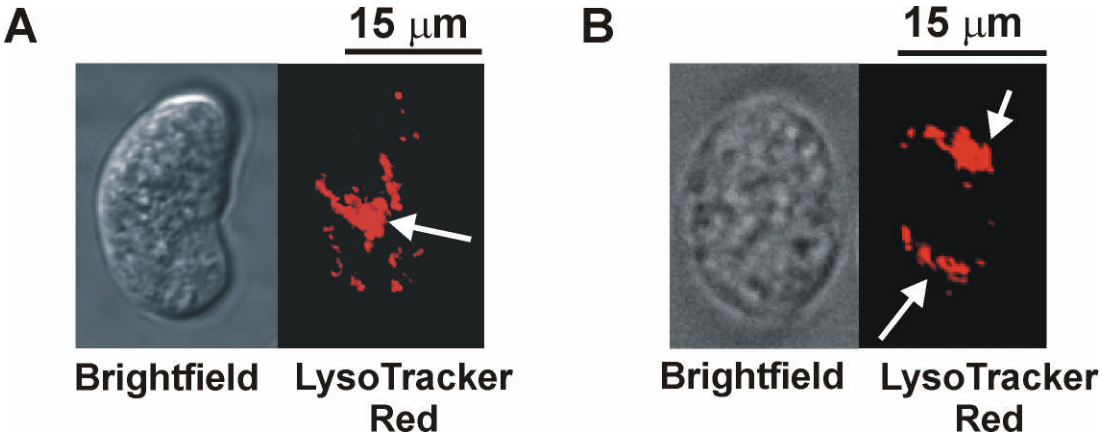

Fig. 3.10: **LysoTracker Red fluorescent labelling of acidic organelles in isolated pulmonary artery smooth muscle cells.** ***Panel A***, left-hand image shows a brightfield image of the cell under investigation. The right-hand panel shows the corresponding LysoTracker Red (excitation 577 nm, emission 590 nm) fluorescence image from a deconvolved Z section (depth 0.28 μm) taken through the centre of the cell. Note, the largest area of clustering located centrally within the cell as indicated by the arrow; ***Panel B***, left-hand image shows a brightfield image of the cell under investigation. The right-hand panel shows the corresponding LysoTracker Red fluorescence image from a deconvolved Z section taken through the centre of the cell. Note, the cell shows areas of lysosomal clustering associated at the perimeter of the cell, as indicated by the arrows.

do this, I carried out investigations using the compound glycl-L-phenylalanine 2-napthylamide (GPN). GPN is a substrate of cathepsin C, which leads to rupturing of lysosomes via osmotic lysis. Cathepsin C is a lysosomal cysteine protease and it can sequentially remove dipeptides from the N- termini of various peptides and proteins (Coffey and de Duve, 1968). It breaks GPN down into its component amino acids which, due to their polarity, are unable to exit the lysosome, leading to increased osmotic stress until eventually the lysosome ruptures (Jadot, *et al.*, 1984; Berg, *et al.*, 1994). Cathepsin C has previously been shown to only be expressed in end stage lysosomes (Jadot, *et al.*, 1984; Berg, *et al.*, 1994; Jadot and Wattiaux, 1995). Therefore, addition of GPN to cells will only lead to rupture of end stage lysosomes and subsequent loss of fluorescence from these organelles.

That LysoTracker Red labelled organelles lost fluorescence in a time-dependent manner following addition of GPN to the experimental chamber confirmed that these LysoTracker Red labelled organelles were indeed lysosomes. The osmotic lysis of lysosomes caused by the application of GPN may induce contraction of the cells due to the release of lysosomal Ca^{2+} stores or as a result of altering cellular pH, which can alter Ca^{2+} homeostasis within the cell. In order to prevent any misinterpretation of results which may arise due to movement of cells as a result of contraction, cells were incubated for fifteen minutes with the compound ML-9, an inhibitor of myosin light chain kinase, which has previously been shown to prevent contraction of smooth muscle cells (Saitoh, *et al.*, 1986). GPN has previously been shown to trigger a loss of LysoTracker Red fluorescence from acidic vesicles in a time-dependent manner, and subsequently abolish NAADP-mediated Ca^{2+} release from these vesicles in sea urchin eggs (Churchill, *et al.*, 2002). Consistent with the findings by Churchill *et al*. in sea urchin eggs, it was noted that GPN (200 μM), eliminated LysoTracker Red fluorescence within 15 minutes of application to pulmonary artery smooth muscle cells (Fig. 3.11; n = 6), which is consistent with the labelled organelles being lysosomes. The spatial distribution of Ca^{2+} burst events have been shown to be manifested in two primary forms (Boittin, *et al.*, 2002). Firstly, Ca^{2+} bursts were seen to generate

a ring of Ca^{2+} release around perimeter of the cell, proximal to the plasma membrane, or were seen as spatially restricted focal Ca^{2+} bursts covering an

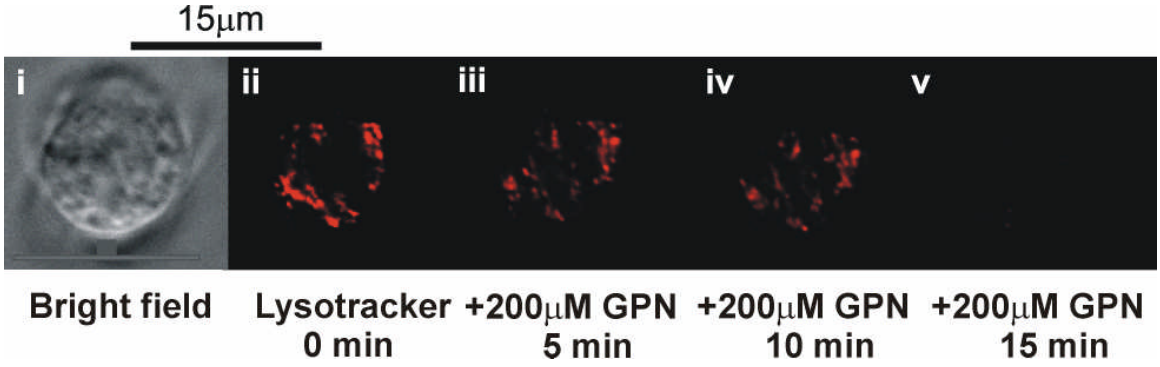

Fig. 3.11: **GPN depletes LysoTracker Red labelling of lysosomes in a time dependent manner:** ***(i)*** Shows a brightfield image of an isolated pulmonary artery smooth muscle cell, ***(ii)*** corresponding LysoTracker Red fluorescence in a deconvolved Z section (depth 0.28 μm) taken through the centre of the cell in (i). ***(iii – iv)*** LysoTracker Red fluorescence 5 ***(iii)***, 10 ***(iv)*** and 15 ***(v)*** minutes after application of glycylphenylalanine 2- napthylamide (GPN; 200 μM).

area of between 2 – 10 μm across the cell. Consistent with the spatial distribution of the Ca^{2+} bursts generated in response to NAADP (Fig 3.12; A (ii) and B(ii), experiments carried out by Dr. F.X. Boittin), the large areas of LysoTracker Red labelling observed within isolated pulmonary artery smooth muscle cells appeared in either one or two distinct forms. Firstly, the LysoTracker Red staining was seen to form a "ring" proximal to the plasma membrane of the cell (Fig 3.12A(i)). This ring was seen to be approximately 2 μm in diameter in the cells examined (n = 5). Secondly, LysoTracker Red fluorescence was seen to form spatially restricted units that were primarily located in the centre of the cell, close to a large area devoid of labelling which may indicate the position of the nucleus within the cell (Fig. 3.12B(i)). These tight lysosomal clusters were seen to be approximately 2 – 6 μm across (n = 6). Thus, we may conclude that the spatial organisation of lysosomes in pulmonary arterial smooth muscle cells approximates that of the primary forms of Ca^{2+} bursts induced by NAADP.

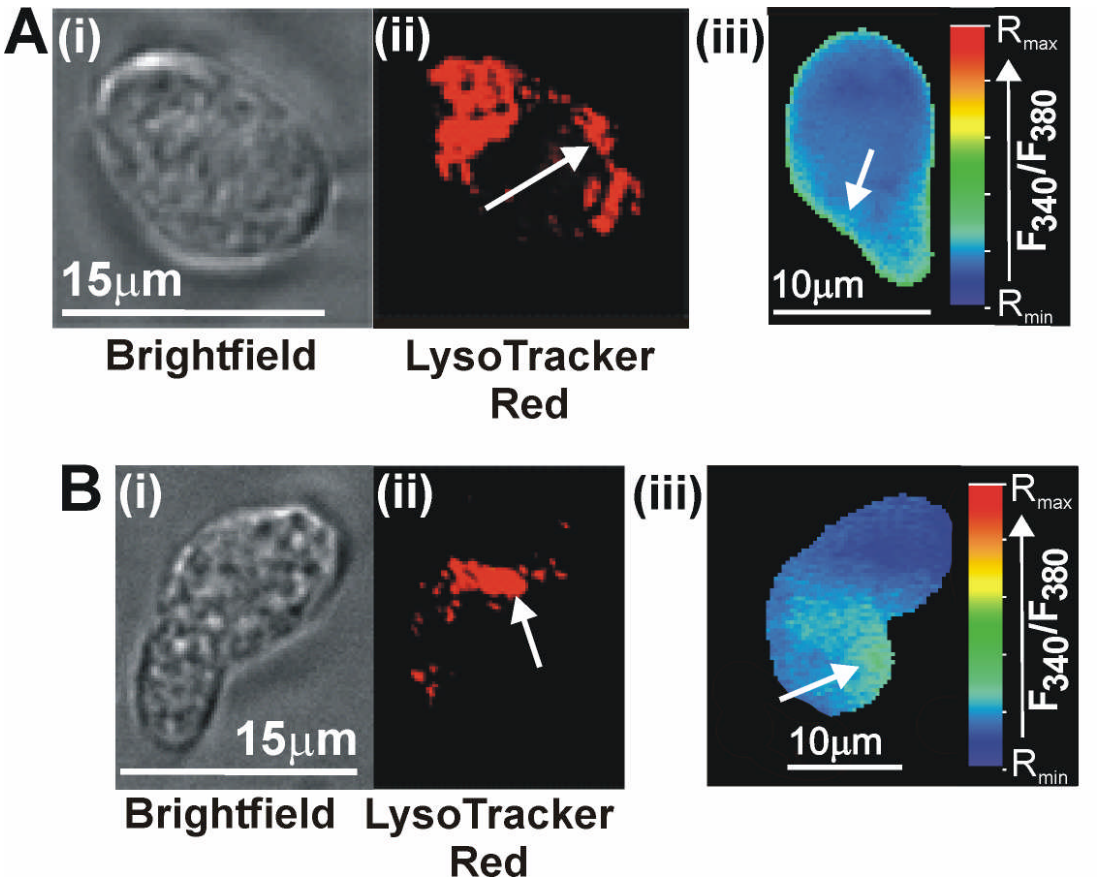

Fig 3.12: **Distribution of lysosomal clusters closely mirrors NAADP-mediated Ca^{2+} bursts in isolated pulmonary artery smooth muscle cells *Panel A*: *(i)*** Shows a bright field image of an isolated pulmonary artery smooth muscle cell and ***(ii)*** the corresponding LysoTracker Red fluorescent image in a deconvolved Z section (depth 0.28 μm) taken through the cell. The arrow indicates LysoTracker staining running proximal to the plasma membrane. ***(iii)*** shows a pseudocolour representation of a Ca^{2+} burst (indicated by the arrow) arising proximal to the plasma membrane in response to intracellular dialysis of NAADP (10 nM) in a different pulmonary artery smooth muscle cell. ***Panel B*: *(i)*** Shows a bright field image of a different isolated pulmonary artery smooth muscle cell and, ***(ii);*** the corresponding LysoTracker Red fluorescent image in a deconvolved Z section (depth 0.28 μm) taken through the cell. The arrow indicates a spatially restricted lysosomal cluster located in the centre of the cell. ***(iii)*** Shows a pseudocolour representation of a spatially restricted Ca^{2+} burst elicited in response to NAADP (10 nM) in a different isolated pulmonary artery smooth muscle cell as indicated by the arrow.

Following 3D reconstruction of deconvolved Z stacks (depth 0.28 μm, Z-step 0.2 μm) using the Softworx software (Fig. 3.13(iii)) I was able to examine the volume occupied by the spatially restricted primary lysosomal clusters within cells (Fig. 3.13(iv) and Appendix 1, Table 3.15). 3- dimensional

reconstructions of cells were rotated around the X- or Y-axis through 0^o, 90^o, 180^o and 270^o. At each point of rotation, measurements were taken of length and height of the largest discernable lysosome clusters (Fig. 3.12(v – viii). The volumes of the lysosomal clusters were then determined. In order to limit the amount of dead space in the volume measurements, clusters which appeared cylindrical upon rotation volumes were determined using the equation for the volume of a cylinder:

$$\text{Volume} = h \times \pi \times r^2 \qquad \textit{Equation 3.1}$$

Where h is the height of the cluster measured in μm, π is taken to be equal to 3.14, and r^2 is the square of the radius. The radius is equal to half of the diameter, and the diameter is taken to be the length across the cluster, measured in μm, when viewed face on. Lysosomal clusters which were not seen to be cylindrical in appearance had there volume determined by applying the equation used to determine the volume of a box:

$$\text{Volume} = l \times b \times h \qquad \textit{Equation 3.2}$$

Where l is the length of the cluster in μm, b is the width of the cluster in μm and h is the depth of the cluster in the Z-plane measured in μm. These measurements allowed for calculation of the approximate volume occupied by the lysosomal clusters. From the measurements gathered from these cells, the volume occupied by the largest separable lysosomal clusters identified in each cell studied, was seen to range from 7.84 μm^3 to 42.83 μm^3. This represented a mean volume of 27.42 ± 10μm^3 (n = 3, Appendix 1, Table 3.15).

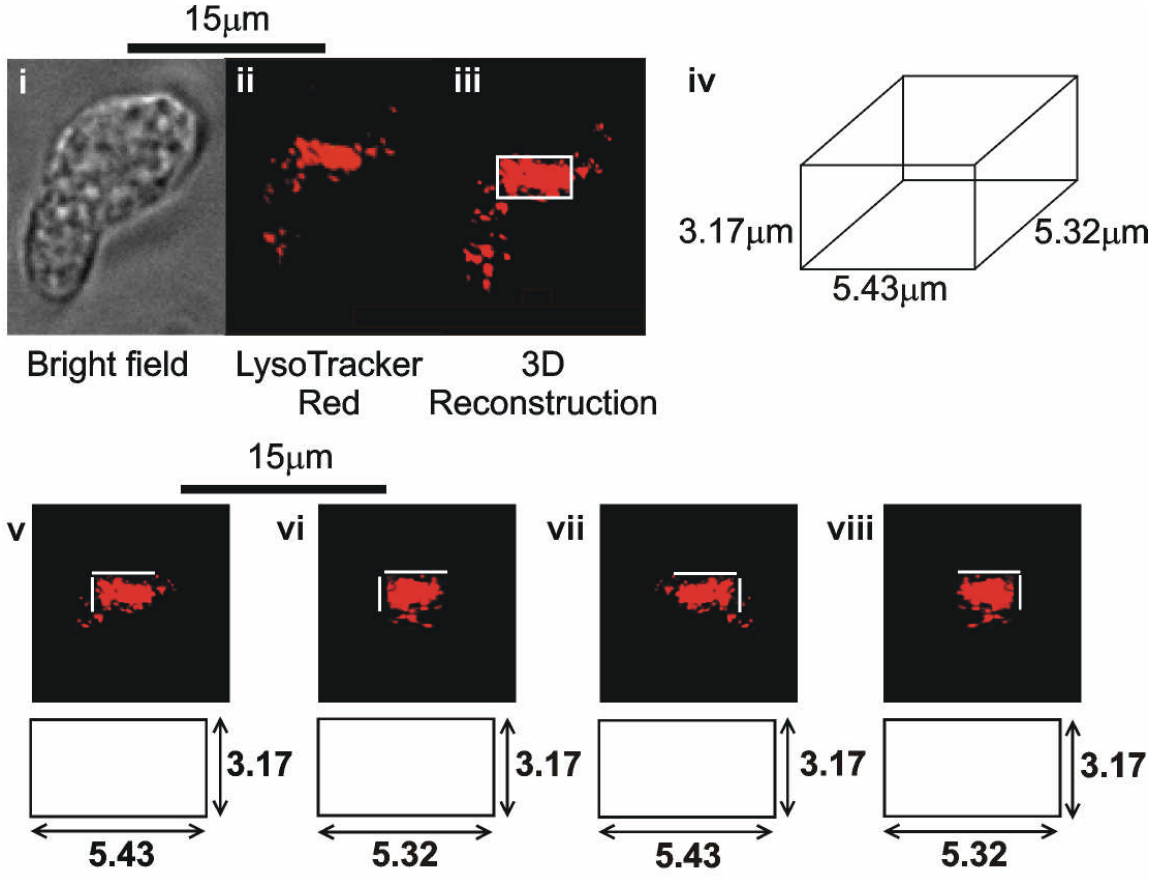

Fig. 3.13: **Measurement of the largest individual cluster of lysosomes in an isolated pulmonary artery smooth muscle cell:** ***(i)*** shows a bright field image of an isolated pulmonary artery smooth muscle cell, ***(ii)*** the corresponding deconvolved LysoTracker Red fluorescence image from a Z section (depth 0.28 μm) through the middle of the cell, ***(iii)*** the corresponding 3- dimensional reconstruction of deconvolved stack of Z sections (40 Z's, depth 0.28 μm, Z-step 0.2 μm); note lysosomes form a spatially restricted cluster ~ 6 μm across as indicated by the white rectangle; ***(iv)*** shows a schematic diagram of the volume occupied by the largest lysosomal cluster in the cell shown in (iii), as indicated by the white rectangle; ***(v – viii)*** three dimensional reconstruction of the largest lysosomal cluster in the cell shown in panel (iii) as indicated by the white rectangle , measured for volume through 0^{o} ***(v)***, 90^{o} ***(vi)***, 180^{o} ***(vii)*** and 270^{o} ***(viii)***; white lines indicate the distance measured for volume measurements in micrometers (μm).

These data show that lysosome-related organelles in pulmonary artery smooth muscle cells form dense clusters that may provide an NAADP-sensitive Ca^{2+} store with a high degree of spatial organisation. Thus, the spatial organisation of these acidic organelles within isolated pulmonary artery smooth muscle cells is quite different to the granular pattern of discrete vesicles observed in sea urchin eggs (Churchill, *et al.*, 2002).

3.3 Discussion

The data presented in this chapter provide evidence in support of this laboratory's assertion that NAADP acts as a discrete and potent Ca^{2+}-mobilising messenger in arterial smooth muscle (Boittin *et al.*, 2002). Perhaps most significantly, this investigation provides direct evidence in support of the proposal (Churchill *et al.*, 2002; Yamasaki *et al.*, 2004) that NAADP may selectively elicit Ca^{2+} signals from a lysosome-related store alone, which may then be amplified by CICR via RyRs on the SR.

3.3.1 Bafilomycin A1 induces global Ca^{2+} waves and smooth muscle contraction in similar manner to NAADP

Extracellular application of Bafilomycin A1 to isolated pulmonary artery smooth muscle cells caused global Ca^{2+} waves and cell contraction. In a similar fashion to the global Ca^{2+} waves initiated by NAADP, Bafilomycin A1-evoked global Ca^{2+} signals were preceded by spatially restricted Ca^{2+} release events. It was also noted that global Ca^{2+} waves induced by Bafilomycin A1 shared a similar pharmacological profile to global waves induced by NAADP (Boittin *et al.*, 2002). Thus, global Ca^{2+} waves in response to Bafilomycin A1 were inhibited by depletion of SR Ca^{2+} stores in isolated pulmonary artery smooth muscle cells by inhibition of SERCA pumps with thapsigargin, however, spatially restricted Ca^{2+} release events were still observed. Furthermore, global Ca^{2+} signals in response to Bafilomycin A1 were abolished when ryanodine receptors were blocked with ryanodine. Once more, spatially restricted Ca^{2+} release events were observed. Therefore, consistent with the mechanism of action of NAADP (Boittin *et al.*, 2002), Bafilomycin A1 initiates spatially restricted Ca^{2+} release events that are subsequently amplified into global Ca^{2+} waves by CICR via RyRs on the SR. These data suggest that, like NAADP, Bafilomycin A1 triggers global Ca^{2+} waves via a 'two-pool' mechanism initiated by the depletion of a non-SR Ca^{2+} store. The source of this Ca^{2+} store is likely to be acidic in nature, as Bafilomycin A1 is an inhibitor of the V-H^+ ATPase (Docampo and Moreno, 1999). Therefore, the apparent similarity in the mechanisms of Ca^{2+} release exhibited by Bafilomycin

A1 and NAADP in isolated pulmonary artery smooth muscle cells provides indirect evidence for a possible role for an acidic Ca^{2+} stores as being those accessed by NAADP.

3.3.2 Bafilomycin A1 eliminates Ca^{2+} signals in response to NAADP without affecting sarcoplasmic reticulum-mediated Ca^{2+} release mechanisms

Direct evidence in support of the proposal that an acidic Ca^{2+} store is the source of NAADP-mediated Ca^{2+} signals in vascular smooth muscle was gained through further experiments on the effect of Bafilomycin A1 on Ca^{2+} signals evoked by NAADP. Given the similarity in Ca^{2+} signals evoked by NAADP and Bafilomycin A1, in association with Dr. F.X. Boittin, I examined whether or not depletion of Bafilomycin A1-sensitive Ca^{2+} stores attenuated Ca^{2+} signals in response to NAADP. Strikingly, preincubation of isolated pulmonary artery smooth muscle cells with Bafilomycin A1 was seen to completely abolish Ca^{2+} signals in response to the intracellular dialysis of NAADP. Consistent with previous studies which have shown Bafilomycin A1 to be selective for vacuolar proton pumps (Bowman, *et al.*, 1988), preincubation of cells with Bafilomycin A1 was without effect on the mobilisation of SR Ca^{2+} stores by the activation of RyRs via caffeine, or the activation of IP_3Rs by intracellular dialysis of IP_3. These positive controls (caffeine and IP_3) indicate that depletion of Bafilomycin A1-sensitive Ca^{2+} stores selectively disrupts Ca^{2+} mobilisation by NAADP, without any discernable effect on Ca^{2+} uptake via SERCA pumps and subsequent SR Ca^{2+} release via RyRs and IP_3Rs. These findings are consistent with findings in sea urchin eggs (Churchill, *et al.*, 2002), pancreatic acinar cells (Yamasaki, *et al.*, 2004), the clonal pancreatic β cell line (MIN6; Yamasaki, *et al.*, 2004) and cortical neurons (Brailoiu, *et al.*, 2005), in which NAADP has been suggested to initiate Ca^{2+} signals from acidic organelles only in the presence of a proton gradient generated by the actions of the vacuolar proton pump.

Although NAADP appears to mobilise an acidic Ca^{2+} store in both sea urchin eggs and pulmonary artery smooth muscle cells, there appears to be a

significant difference between the responses to Bafilomycin A1 within these cells. Thus, Bafilomycin A1 did not deplete the NAADP-sensitive Ca^{2+} store in sea urchin eggs, as application of NAADP induced a robust Ca^{2+} signal in the presence of Bafilomycin A1. However, Bafilomycin A1 prevented refilling of this store, because there was no Ca^{2+} signal in response to a further challenge by NAADP (Churchill *et al*., 2002). This is in marked contrast to the observations described here in pulmonary artery smooth muscle cells, where Bafilomycin A1 abolished Ca^{2+} signals in response to the initial application of NAADP. It is conceivable that this difference in response may be due to the existence of different NAADP receptors in the two preparations. Whereas the NAADP receptor in sea urchin eggs may remain in a closed state until activation by NAADP, the NAADP receptor expressed in vascular smooth muscle may be tonically active at rest. This could render the lysosomal Ca^{2+} stores in this tissue 'leaky', with a constant turnover of Ca^{2+}. If this were the case, it suggests that the blockade of Ca^{2+} uptake as a result of Bafilomycin A1 treatment alters the equilibrium between Ca^{2+} uptake and Ca^{2+} release in these stores, causing Ca^{2+} release which ultimately results in the depletion of lysosomal Ca^{2+} stores in much the same manner as thapsigargin depletes SR Ca^{2+}stores. This may explain why Bafilomycin A1 induced global Ca^{2+} waves in pulmonary artery smooth muscle cells, but elicited no Ca^{2+} signals in sea urchin eggs (Churchill *et al*., 2002). Consistent with this proposal, disruption of reserve granules in the sea urchin egg by osmotic lysis via the actions of GPN was, unlike Bafilomycin A1, shown to elicit spatially restricted Ca^{2+} signals (Churchill *et al*., 2002). Furthermore, a previous investigation in cultured bone-marrow-derived macrophages showed a decrease in the luminal Ca^{2+} concentration within lysosomes in response to Bafilomycin A1 (Christensen, *et al.*, 2002), whilst a 'non-leaky' acidic Ca^{2+} store similar to that described previously by Churchill *et al.* (2002) may also be present in fibroblasts where the Ca^{2+} concentration within end stage lysosomes remains unaffected by treatment of cells with Bafilomycin A1 (Gerasimenko, *et al.*, 1998). It is entirely possible, therefore, that the nature of Ca^{2+} cycling via NAADP receptors may vary in a cell- and function-specific manner.

Despite the growing evidence in support of the view that NAADP-mobilises Ca^{2+} from acidic Ca^{2+} stores in some tissue, this is not a universally

held opinion within the field. Indeed a number of groups have proposed that NAADP mobilises Ca^{2+} from ER/SR stores by directly activating RyRs. In isolated nuclear preparations from pancreatic acinar cells it has been shown that NAADP- (and cADPR-) mediated Ca^{2+} signals were blocked by the RyR inhibitors ryanodine and ruthenium red, but not by caffeine (Gerasimenko, *et al.*, 2003), whilst IP_3 mediated-Ca^{2+}release was seen to be inhibited by caffeine, but not by ruthenium red (Gerasimenko, *et al.*, 2003). Gerasimenko *et al.* concluded that NAADP, like cADPR, mobilises Ca^{2+} from nuclear envelope Ca^{2+} stores through direct activation of RyRs. NAADP has also been proposed to directly activate RyR subtype 1 purified from skeletal muscle and reconstituted into lipid bilayers (Hohenegger, *et al.*, 2002). Also, it has been suggested that NAADP directly activates RyR subtype 2 isolated from cardiac muscle and reconstituted into lipid bilayers (Mojzisova, *et al.*, 2001). However, there has been a contradictory report which suggests that NAADP is without affect on all three RyR subtypes, as examined in lipid bilayer recordings of RyR1- and RyR3-subtypes isolated from rabbit skeletal muscle and bovine diaphragm muscle, respectively, or on crude microsome preparations from canine heart ventricles containing RyR2 receptors (Copello, *et al.*, 2001). Furthermore, a more recent study carried out in Jurkat T-cells utilising mRNA technology to knockdown the expression of RyRs showed that NAADP mediated Ca^{2+} signalling in these cells was inhibited but not abolished (Langhorst, *et al.*, 2004).

Therefore, there are clearly contradictory reports in the literature regarding NAADP regulation of RyRs. Whilst some studies show evidence to support direct activation of RyRs by NAADP, others provide clear evidence that RyR subtypes are not regulated by NAADP. These differences in opinion may arise from the fact that it is extremely difficult to separate ER/SR compartments with RyRs from closely associated lysosomes, as has been shown in the sea urchin egg where cADPR- and IP_3-sensitive ER fractions were contaminated with NAADP-sensitive reserve granule stores following separation on a Percoll density gradient (Lee and Aarhus, 1995). Furthermore, it may be extremely difficult to resolve Ca^{2+} signals generated via NAADP receptors following blockade of RyRs. However, the findings presented here clearly demonstrate that NAADP elicits spatially restricted Ca^{2+} signals from

bafilomycin-sensitive, lysosome-related organelles that are subsequently amplified by CICR via RyRs located on the SR in pulmonary artery smooth muscle cells.

3.3.3 Lysosomes form discrete clusters in pulmonary artery smooth muscle cells

In isolated pulmonary artery smooth muscle cells lysosomes were seen to form; (1) distinct clusters in the centre of cells, possibly close to the nucleus, or as (2) a ring located close to the perimeter of cells, consistent with the two forms of Ca^{2+} burst observed in response to NAADP (Boittin *et al*., 2002). The application of GPN to cells eliminates end-stage lysosomes confirmed that LysoTracker Red labelled lysosomes within pulmonary artery smooth muscle cells. Tight clustering of LysoTracker Red labelled organelles is in contrast to the diffuse granular distribution of acidic vesicles reported in the sea urchin egg (Churchill, *et al.*, 2002) and a clonal pancreatic β cell line (MIN6; Yamasaki, *et al.*, 2004). Clustering of LysoTracker Red labelled acidic stores which correspond to the location of initial Ca^{2+} signals in response to NAADP have, however, been reported in isolated pancreatic acinar cells (Yamasaki *et* al., 2004). In pancreatic acinar cells LysoTracker Red labelling was restricted to the basolateral pole of cells, while the liberation of NAADP by flash photolysis of caged NAADP resulted in the initiation of Ca^{2+} signals within this region of cells (Yamasaki *et al*., 2004). Thus, the visualisation of initial Ca^{2+} signals in isolated pulmonary artery smooth muscle cells and isolated pancreatic acinar cells in response to NAADP may be directly due to the clustering of the NAADP-sensitive Ca^{2+} stores. The obvious Ca^{2+} bursts in pulmonary artery smooth muscle cells or the initiation of Ca^{2+} signalling in the basolateral pole of pancreatic acinar cells may, therefore, be due to the summation of a great many individual Ca^{2+} release events from channels on acidic stores located within these clusters of lysosome-related organelles. These contrary findings suggest that lysosomal Ca^{2+} stores may be distributed in a manner that meets the functional requirement of a given cell type.

In summary, the results presented in this chapter suggest a role for acidic, lysosome-related organelles in arterial smooth muscle as a Ca^{2+} store that may be mobilised by NAADP, but not by direct activation of IP_3Rs or RyRs. These findings are consistent with the proposal of Galione and colleagues that reserve granules in sea urchin eggs may act as an NAADP-sensitive Ca^{2+} store (Churchill *et al*., 2002). However, in contrast with previous investigations showing a diffuse granular distribution of lysosome-related organelles in both sea urchin eggs (Churchill *et al*., 2002) and MIN-6 cells (Yamasaki *et al*., 2004), the investigations presented in this chapter suggest that lysosomes form highly organised clusters in pulmonary artery smooth muscle which may underpin the generation of Ca^{2+} signals with a discrete spatiotemporal pattern.

Chapter 4: Spatial distribution of ryanodine receptor subtypes and lysosomes in pulmonary artery smooth muscle

4.1 Introduction

Previous investigations from this laboratory has shown that NAADP mediates Ca^{2+} bursts from an acidic, lysosome-related Ca^{2+} store, which may then be amplified by CICR from the SR via RyRs, but not CICR via IP_3Rs (Boittin, *et al*, 2002; Chapter 3). These observations are contrary to previous reports in other cell types, which have suggested CICR via both RyR and IP_3R participates in the generation of global Ca^{2+} signals in response to NAADP (Cancela, *et al.*, 1999; Cancela, 2001; Patel, *et al.*, 2001). Therefore, cells may co-ordinate and restrict the relationship between lysosomal Ca^{2+} stores and the SR/ER in a manner suited to their function. Consistent with this proposal, and in marked contrast to previous investigations which have shown a diffuse, granular pattern of lysosome-related organelles in both sea urchin eggs (Churchill, *et al*, 2002) and MIN 6 cells (Yamazaki, *et al*, 2004), I have presented evidence in Chapter 3 of this thesis that lysosomes, visualised using LysoTracker Red, form highly organised and spatially restricted clusters in arterial smooth muscle. Furthermore, examination of these lysosomal clusters indicated that their spatial organisation was consistent with that of NAADP-mediated Ca^{2+} bursts (Chapter 3, Section 3.2.6).

Given that CICR via RyRs is a prerequisite for the generation of global Ca^{2+} waves in response to NAADP in pulmonary artery smooth muscle cells (Boittin, *et al*, 2002), the aim of this chapter is to determine whether or not lysosomes colocalise with RyRs on the surface of the SR to facilitate the generation of global Ca^{2+} signals in response to NAADP.

4.2 Results

4.2.1 Ryanodine receptors and lysosomal clusters colocalise to form tight junctions in pulmonary artery smooth musclecells

Given that NAADP has been shown to mediate Ca^{2+} bursts from a lysosome-related Ca^{2+} store that are then amplified into global Ca^{2+} waves through CICR via RyRs on the SR, I used the fluorescent probes LysoTracker Red (0.5 – 2 nM; excitation 577 nm, emission 590 nm) and BODIPY-FL ryanodine (1 μM; excitation 480 nm, emission 510 nm) to examine whether there was an underlying structural basis for this mechanism of Ca^{2+} signalling within freshly isolated pulmonary artery smooth muscle cells. To this end I examined whether or not lysosomes colocalised with RyRs expressed on the SR.

Fig. 4.1 shows 2 typical representations of the distribution of lysosomes and RyRs in isolated pulmonary artery smooth muscle cells. Fig. 4.1A(i) shows a transmitted light image of an isolated pulmonary artery smooth muscle cell. Fig. 4.1A(ii) shows the corresponding LysoTracker Red fluorescence, visualised in red, in a single deconvolved Z-section (focal depth 0.28 μm) acquired through the centre of the cell shown in Fig. 4.1A(i). In this cell, there is clear evidence of a number of small lysosomal clusters diffusely distributed throughout the cytoplasm, with the largest area of lysosomal clustering positioned in the centre of the cell, as highlighted by arrow 1. Fig. 4.1A(iii) shows BODIPY-FL ryanodine fluorescence, visualised in green, acquired in a deconvolved Z-section (focal depth 0.28 μm), acquired at the same Z-depth as A(ii). BODIPY-FL ryanodine labelling was seen throughout the cytoplasm in all cells studied, as would be expected given that RyRs have previously been shown to be located upon both peripheral and central sarcoplasmic reticulum (SR) in vascular smooth muscle cells (Lesh, *et al.*, 1998; Gordienko, *et al.*, 2001; Yang, *et al.*, 2005). In isolated pulmonary artery smooth muscle cells BODIPY-FL ryanodine labelling was seen to form ‘ribbons’ weaving through the cytoplasm, an example of which is highlighted by arrow 2 in Fig. 4.1A(iii).

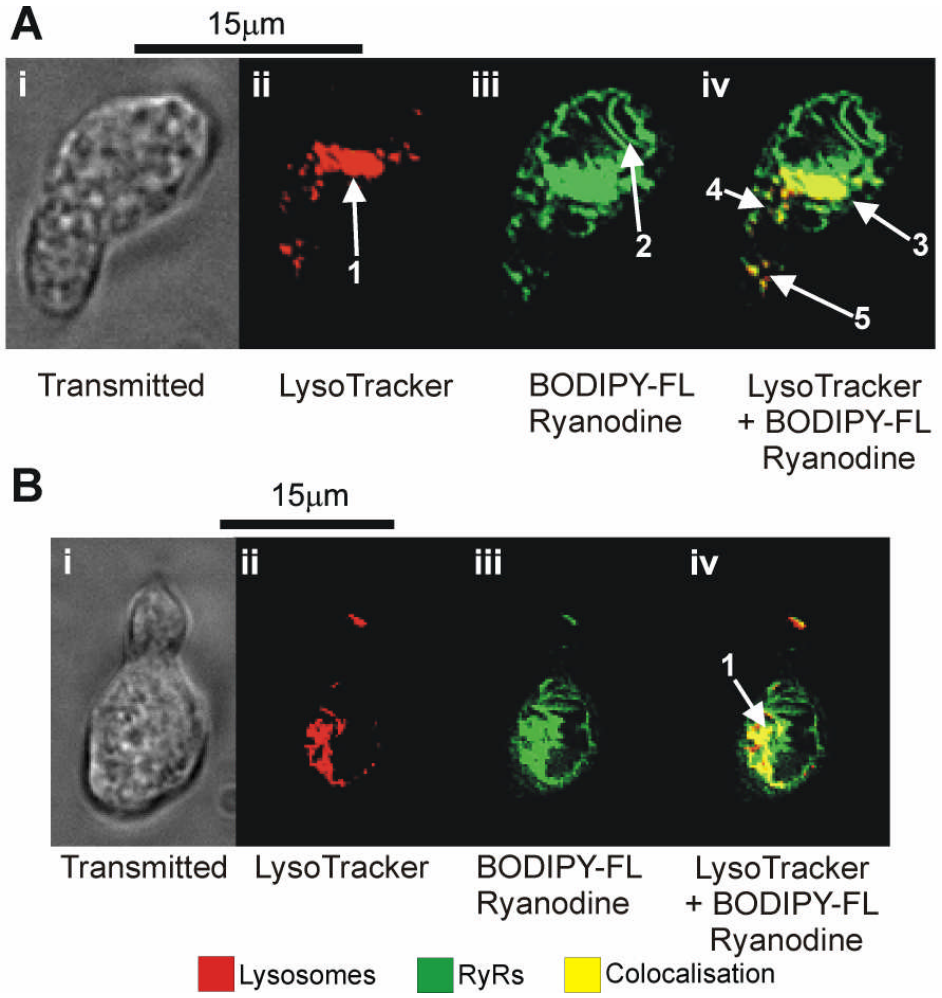

Fig. 4.1 **Lysosomes and RyRs colocalise in arterial smooth muscle cells:** ***Panel A(i)*** transmitted light image of an isolated pulmonary artery smooth muscle cell.; ***Panel A(ii)*** deconvolved Z-section (focal depth 0.28 μm) through the same cell as in ***A(i)*** shows lysosomes labelled with LysoTracker Red (0.5 nM, 45 min. incubation). A large area of lysosomal clustering is indicated with arrow 1; ***A(iii)*** deconvolved Z-section through the same cell as in ***A(i)*** shows the distribution of ryanodine receptors (RyRs) labelled with BODIPY-FL ryanodine (1 μM, 60 min incubation). Arrow 2 indicates a ribbon of BODIPY-FL ryanodine labelling; ***A(iv)*** composite image of ***A(ii)*** and ***A(iii)*** shows close association, as indicated by arrow 3, 4 and 5, of lysosomes and a subpopulation of RyRs. ***Panel B(i)*** transmitted light image of a different isolated pulmonary artery smooth muscle cell. ***B(ii)*** deconvolved Z-section (focal depth 0.28 μm) through the same cell as in ***B(i)*** shows lysosomes labelled with LysoTracker Red (1 nM, 45 min. incubation). ***B(iii)*** deconvolved Z-section through the same cell as in ***B(i)*** shows the distribution of RyRs labelled with BODIPY-FL ryanodine (1 μM, 60 min. incubation). ***B(iv)*** composite image of ***B(ii)*** and ***B(iii)*** shows close association between lysosomes and RyRs, arrow 1 indicates an area of close association between lysosomes and a subpopulation of RyRs.

These ribbons of BODIPY-FL ryanodine labelling are consistent with the distribution of the SR previously described within vascular smooth muscle cells (Devine, *et al.*, 1972). Images of LysoTracker Red labelling and BODIPY-FL ryanodine were then superimposed upon one another. From this it was clear that there was an extremely close association, within certain areas of the cells, between lysosomes and a subset of RyRs. Areas of colocalisation are visualised in yellow (Fig. 4.1A(iv)). A large, dense area of colocalisation can be seen between the largest cluster of lysosomal labelling and RyRs in the centre of the cell indicated by arrow 3 in Fig. 4.1A(iv). The largest area of colocalisation within the cells examined was seen to be located next to an area largely devoid of labelling. The lack of labelling of RyR or lysosomes within this region may be indicative of the position of the nucleus. It is also worthy of note that while dense areas of colocalisation were observed within cells, a number of smaller areas of colocalisation were observed throughout the cytoplasm of the cell, as shown in the areas surrounding arrows 4 and 5 in Fig. 4.1A(iv). A second example showing the close association between LysoTracker Red- and BODIPY-FL ryanodine-labelling in a different isolated pulmonary artery smooth muscle cell can be seen in Fig. 4.1B(i). Once again, the colocalisation between dense lysosomal labelling and RyRs is evident within this cell as indicated by arrow 1 in Fig. 4.1B (iv). As with the example shown in Fig. 4.1A, the largest area of colocalisation in Fig. 4.1B(iv) is located close to an area devoid of labelling which may indicate the positioning of the nucleus of the cell.

Given that lysosomes represent a discrete, sub-cellular organelle, and that RyRs are expressed on the SR, the distance between these two sites of Ca^{2+} release could have important functional implications. I therefore sought to determine the maximal distance between lysosomes and RyRs that existed within the same focal plane. To achieve this I examined 3-dimensional reconstructions of a series of deconvolved Z-sections acquired from isolated pulmonary artery smooth muscle cells (focal depth 0.28 μm, Z-step 0.2 μm) labelled with LysoTracker Red and BODIPY-FL ryanodine. An example of a 3-dimensional reconstruction of deconvolved Z-sections is shown in Fig. 4.2(i). In this cell a dense central plaque of lysosome and RyR colocalisation is

clearly evident, while a number of smaller areas of colocalisation can be seen throughout the cytoplasm of the cell. Following the generation of the 3-dimensional (3D) reconstruction, each area of colocalisation was examined and the cell was rotated in 1^{o} steps through 360^{o} around the X- and Y-axis in order to determine whether, at any point, the two fluorescent labels could be separated from one another in the same focal plane (Fig. 4.2(ii)). When the two fluorescent labels could be separated, the cell was rotated to determine the point at which they lay within the same plane (Fig. 4.2(iii)a). In order to achieve this aim the cell was rotated until the lysosomal labelling was seen to

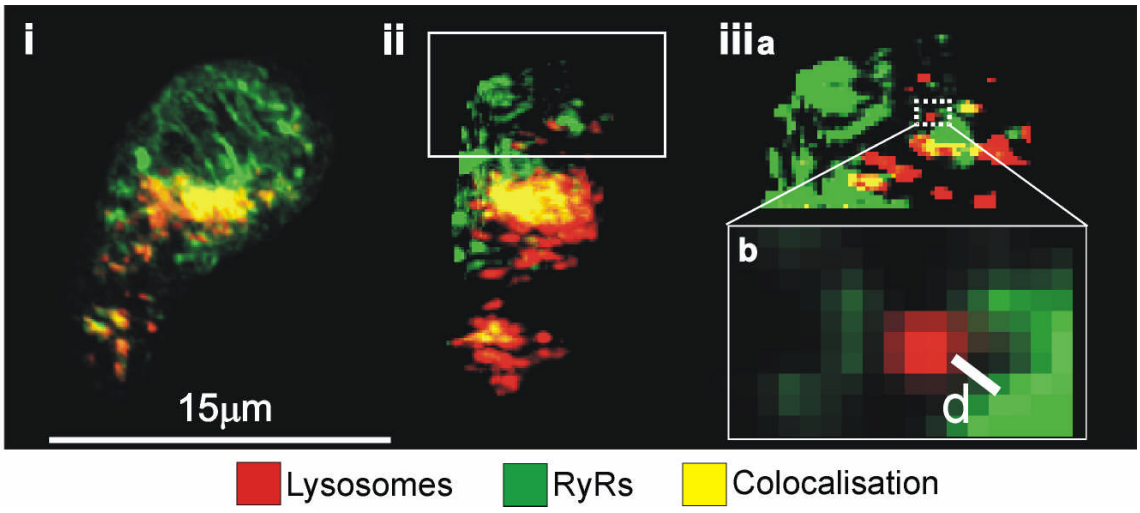

Fig. 4.2. **Formation of trigger zone between closely associated lysosomes and RyRs:** ***(i)*** 3D reconstruction of deconvolved Z-sections (depth 0.28 µm, Z-step 0.2 µm) taken through an isolated pulmonary artery smooth muscle cell shows close association of lysosomes labelled with LysoTracker Red (0.5 nM, 45 min. incubation) and a subpopulation of ryanodine receptors (RyRs) labelled with BODIPY-FL ryanodine (1 µM, 60 min. incubation); ***(ii)*** shows the cell in ***(i)*** rotated 284° around the *y* axis; ***(iii)*** two sequential enlargements (***a*** and ***b***) of the section of the cell in **(ii)** indicated with a *white rectangle*: ***(iii) b*** selected area shows distance (*d* = ≤ 0.4 µm) measured between a LysoTracker Red-labelled organelle and RyRs labelled with BODIPY-FL ryanodine colocalised in the same focal plane.

be located directly above the RyR labelling, and a note of the extent of rotation was taken. After this, the cell was again rotated until the RyR labelling was positioned directly above the lysosomal labelling; once more the degree of rotation was noted. From these measurements the point at which the fluorescent labels were positioned side by side at the same focal depth was determined and the cell was rotated to this point. A measurement of the distance between the BODIPY-FL ryanodine and the LysoTracker Red fluorescence was then taken using the SoftWorx software (Fig. 4.2(iii)b;

Appendix 2, Table 4.1). From the measurements taken, it was seen that RyRs and lysosomes that were closely associated within the same focal plane were separated by a distance of ≤ 0.4 μm (Fig. 4.2(iii)b; Appendix 2, Table 4.1; n = 12 areas from 9 cells). However, the majority of areas of colocalisation between RyRs and lysosomes were much smaller than could be resolved using the techniques at my disposal. Thus, it would appear that the junction or cleft between lysosomes and RyRs represents a very tight association between these elements. This close association between lysosomes and RyRs is well within the estimated maximum distance that Ca^{2+} may diffuse within the cytoplasm of cells (≤ 5 μm; Allbritton, *et al.*, 1992). Therefore, this close association is ideally suited to a role in RyR-dependent amplification of lysosomal Ca^{2+} signals.

It is clear from these experiments that a large proportion of BODIPY-FL ryanodine labelled RyRs are not associated with LysoTracker Red labelled organelles. There are three known subtypes of RyRs found in mammalian cells, namely; RyR1 (Inui, *et al.*, 1987b; Lai, *et al.*, 1988; Takeshima, *et al.*, 1995), RyR2 (Inui, *et al.*, 1987a; Takeshima, *et al.*, 1998) and RyR3 (Hakamata, *et al.*, 1992; Sorrentino, *et al.*, 1993; Takeshima, *et al.*, 1996). All three of these RyR subtypes have previously been shown to be expressed in several types of vascular smooth muscle, including pulmonary artery smooth muscle (Herrmann-Frank, *et al.*, 1991; Neylon, *et al.*, 1995; Jeyakumar, *et al.*, 1998; Coussin, *et al.*, 2000; Mironneau, *et al.*, 2001; Yang, *et al.*, 2005). Thus, a particular subpopulation of RyRs may colocalise with lysosomes to form a trigger zone for Ca^{2+} signalling by NAADP. Therefore, I sought to determine whether or not a specific subtype of RyR colocalised with lysosomes in order to comprise the proposed trigger zone for NAADP-mediated Ca^{2+} signalling.

4.2.2 Examination of lysosomal distribution in methanol-fixed pulmonary artery smooth muscle cells via visualisation of the lysosomal membrane protein αlgp120

4.2.2.1 Regionalisation of isolated pulmonary artery smooth muscle cells in order to determine the sub-cellular distribution of fluorescent labelling

In order to determine the sub-cellular distribution of fluorescent labelling within isolated pulmonary artery smooth muscle cells, each cell was divided into four regions. These regions were termed the 'nuclear region' 'perinuclear region', the 'extra-perinuclear region' and the 'sub-plasmalemmal region', as depicted in the schematic diagram of a cell shown in Fig. 4.3. The processing applied to pulmonary artery smooth muscle cells in order to define these regions and quantify the fluorescent labelling within each is outlined below.

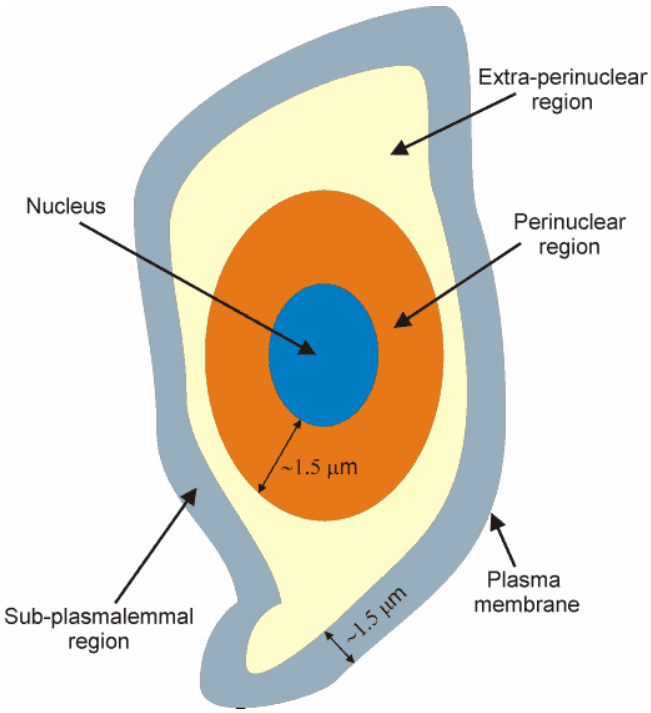

Fig. 4.3 **Designation of regions within a model isolated pulmonary artery smooth muscle to allow for examination of the spatial distribution of fluorescent labelling.**

Volumetric analysis of cells was carried out using Volocity software (Improvision, UK). Measurements of cellular volume were achieved by drawing a region of interest (ROI) around the perimeter of the cell and measuring its volume. Pulmonary artery smooth muscle cells were seen to occupy a volume of 1754.1 ± 258.4 μm^3 (n = 24; Appendix 2, Table 4.2).

The volume of the nucleus of the cell was defined by initially measuring the labelling of the fluorescent probe DAPI (excitation 360 nm, emission 457 nm). DAPI binds to the major groove of the double helix of DNA, once bound it fluoresces in response to ultraviolet light (Barcellona, *et al.*, 1990); note, accurate measurements of the volume of DAPI, and all other fluorescent probes, was achieved through the application of threshold filters to exclude any labelling with fluorescence intensities lower than the background levels (Chapter 2, section 2.4.2). Following this, an ROI was drawn around DAPI labelling to define the boundary of the nucleus. The volume of this ROI was measured and the nucleus was seen to occupy 105.7 ± 13.4 μm^3 of the volume of cells (n = 24, Appendix 2, Table 4.2). The volume of the nucleus, and any fluorescent labelling contained within, were excluded from all subsequent analyses (see below).

Once the nuclear boundary had been established, an ROI was drawn in the cytoplasm within 1.5 μm of the nucleus and termed the perinuclear ROI. The volume of the perinuclear region was then determined by subtracting the volume of the nucleus from the volume of the perinuclear ROI. The perinuclear region of cells occupied a volume 580.4 ± 103.9 μm^3 (n = 24; Appendix 2, Table 4.2).

A second ROI was then drawn within the cytoplasm of the cell and was termed the non sub-plasmalemmal ROI. This ROI included both the perinuclear and nuclear regions of the cell, but excluded the sub-plasmalemmal region. Subtraction of the volumes of the perinuclear and nuclear regions of cells, from the measures obtained from the non sub-plasmalemmal ROI provided a measure of the volume of the extra-perinuclear region of cells. The extra-perinuclear region occupied a volume of 418 ± 75 μm^3 (n = 24; Appendix 2, Table 4.2).

The sub-plasmalemmal region of the cell was determined as being the area of cytoplasm located within 1.5 μm of the plasma membrane of the cell. Subtraction of the volume of the non sub-plasmalemmal ROI from the ROI encompassing the whole cell gave a measure of the volume of the sub-plasmalemmal region of cells. The sub-plasmalemmal region of cells occupied a volume of 673.2 ± 135.2 μm^3 of cells (n = 24; Appendix 2, Table 4.2).

In areas of cells where the plasma membrane encroached within 1.5 μm of the nucleus, the distance that the perinuclear region extended from the nucleus was altered in order to prevent misleading calculations of the distribution of labelling. In order to do this, the distance from the edge of the nucleus to the plasma membrane of the cell was measured. The boundary of the perinuclear region was then readjusted to extend half the distance from the nucleus to the plasma membrane of the cell at that point. Therefore, if the nucleus was positioned 1 μm from the plasma membrane at a given point, the perinuclear region was readjusted to extend 0.5 μm from the nucleus at that point. Similarly, the boundary of the sub-plasmalemmal region was altered to extend half the distance from the nucleus to the plasma membrane within these regions. Therefore, within these regions the sub-plasmalemmal and perinuclear regions bordered one another, with exclusion of the extra-perinuclear region. In some cells, the distance between the nucleus and the plasma membrane was smaller than the accurate resolution limit of the imaging system. Therefore, any fluorescent labelling located within these areas of cells was excluded from analysis as it could not be confidently assigned to a given region of the cell.

As illustrated in Table 4.2 (Appendix 2), the volume of cells was not distributed evenly between the three regions. To allow comparison of measurements of fluorescent labelling between regions, a process of normalisation was applied to the labelling within each region of the cell. To achieve this, the volume of fluorescent labelling within a given region was divided by the volume occupied by that region in order to provide the volume of fluorescent labelling per μm^3 of a given region of the cell. Thus, the density of fluorescent labelling in a given region was measured, thereby allowing direct comparison of the distribution of labelling between different regions and between cells.

4.2.2.2 Determination of lysosomal distribution in methanol-fixed isolated pulmonary artery smooth muscle cells

The distribution of Lysosomes within immunocytochemical investigations was visualised through the use of an antibody raised in mouse against the integral lysosomal membrane glycoprotein, αlgp120 (GM10; Grimaldi, *et al.*, 1987). The glycoprotein αlgp120 has previously been shown to be expressed predominantly on the membrane of lysosomes, with little expression detected on endosomes, the plasma membrane, or within the golgi cisternae (Lewis, *et al.*, 1985). Binding of this primary antibody was visualised via the binding of goat anti-mouse secondary antibody conjugated to the fluorescent probe FITC (excitation 490 nm, emission 528 nm).

A typical example of the distribution of αlgp120-labelling within isolated pulmonary artery smooth muscle cells is shown in Fig. 4.4. Fig. 4.4(i) shows a transmitted light image of an isolated pulmonary artery smooth muscle cell, while Fig. 4.4(ii) shows a deconvolved Z-section (focal depth 0.28 μm) through the cell, corrected to remove background fluorescence, as determined from matched control slides (Chapter 2, Section 2.4.2). Lysosomal distribution and the position of the nucleus are visualised in green and blue, respectively. Consistent with the other cells examined, intense areas of lysosomal labelling are located in close proximity to the nucleus of the cell shown in Fig. 4.4(ii) and an example of one of these areas of labelling is indicated by arrow 1. Lysosomal labelling located further from the nucleus of the cell is evident; however, these areas are fewer in number and appear to be more diffuse than elements located close to the nucleus (Fig. 4.4(ii) arrows 2 and 3). Fig. 4.4(iii) shows a 3-dimensional (3D) reconstruction of a series of deconvolved Z-sections (focal depth 0.28 μm, Z step 0.2 μm) obtained through the cell. It can be seen that the densest areas of lysosomal labelling appear to be located close to the nucleus of the cell. Analysis of cells was then carried out to determine the volume of labelling present within cells. Under carefully controlled ‘optimal’ experimental conditions, the DeltaVision imaging system is able to accurately resolve elements of labelling smaller than 0.2 μm in size in each of

the X-, Y- and Z-planes. However, the precisely controlled environment under which these 'optimal' measurements are obtained cannot be recreated under the experimental conditions in my experiments. Therefore, in these and all subsequent analyses, I set a more conservative value on the limit of resolution in my experiments. To this end, I included only those volumes of labelling measuring ≥ 0.5 μm in the X-, Y- and Z-planes (volume ≥ 0.125 μm^3) and any element of labelling smaller than these limits were excluded from consideration. Fig. 4.4(iv) shows a 3D representation of the positioning of each individual volume ≥ 0.125 μm^3, in purple, of lysosomal labelling measured from the cell. Thus, examination of cells showed that αlgp120- labelling

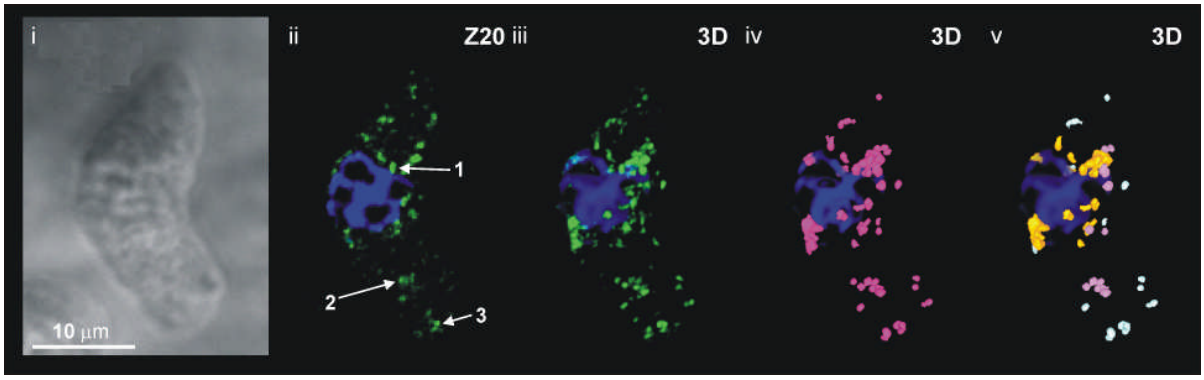

Fig. 4.4 **Visualisation of αlgp120 labelling within an isolated pulmonary artery smooth muscle cell:** ***(i)*** transmitted light image of an isolated pulmonary artery smooth muscle cell. ***(ii)*** deconvolved Z-section (focal depth 0.28 μm) taken through the cell shown in ***(i)*** showing the distribution of αlgp120 labelling, indicative of the distribution of lysosomes in *green*. The nucleus of the cell is shown in *blue*. Arrows 1 – 3 indicate areas of lysosomal labelling. ***(iii)*** 3D reconstruction of a series of Z-sections (focal depth 0.28 μm, Z step 0.2 μm) obtained through the cell shown in ***(i)*** showing the distribution of αlgp120 labelling in *green*. The nucleus of the cell is shown in *blue*. ***(iv)*** 3D representation of the distribution of individual volumes ≥ 0.125 μm^3 (in *purple*) of αlgp120 labelling measured in cells. Individual volumes of labelling were determined using Volocity software (Improvision, UK). ***(v)*** shows the individual volumes of αlgp120 labelling as in ***(iv)*** coloured to indicate the region of the cell in which they are located; volumes within the perinuclear, extra-perinuclear and sub-plasmalemmal regions are shown in *orange*, *pink* and *blue*, respectively.

occupied a volume of 29.84 ± 3.47 μm^3 in pulmonary artery smooth muscle cells (n = 24; Appendix 2, Table 4.3). This equated to a density of labelling

within cells of 0.019 ± 0.003 μm^3 of labelling per μm^3 of cell volume (n = 24; Appendix 2, Table 4.3). The spatial distribution of these volumes of labelling was then examined to provide a measure of the fluorescent labelling within each of the three different regions of the cell. Fig. 4.4(v) shows a 3D visual representation of the regionalised distribution of each individual volume of labelling within the cell shown in Fig. 4.4(iv). Each volume of labelling in Fig. 4.4(v) is coloured to indicate the region of the cell in which it is located. Thus, volumes of lysosomal labelling located in the perinuclear, extra-perinuclear and sub-plasmalemmal regions are visualised in orange, pink and light blue, respectively. Volumetric analysis of the lysosomal labelling located within the three different regions of cells indicated that both the volume and the density of labelling were greater in the perinuclear region of cells than either the extra-perinuclear or sub-plasmalemmal regions. Lysosomal labelling occupied a volume of 16.25 ± 3.18 μm^3 in the perinuclear region of cells (n = 24; Appendix 2, Table 4.4). This equated to a density of 0.032 ± 0.006 μm^3 of labelling per μm^3 of the perinuclear region (Fig. 4.5; Appendix 2, Table 4.4). In contrast, lysosomal labelling in the extra-perinuclear region occupied a volume of 6.72 ± 1.47 μm^3 (n = 24; Appendix 2, Table 4.5), accounting for a density of 0.018 ± 0.006 μm^3 of labelling per μm^3 of the region (Fig. 4.5; Appendix 2, Table 4.5). The sub-plasmalemmal region of cells contained both the lowest volume and the lowest density of lysosomal labelling measured in cells. In the sub-plasmalemmal region, lysosomal labelling occupied volume of 5.93 ± 1.68 μm^3 (n = 24; Appendix 2, Table 4.5) and a density of 0.01 ± 0.003 μm^3 of labelling per μm^3 of the region (Fig. 4.5; Appendix 2, Table 4.6).

A direct comparison between the densities of lysosomal labelling within the three regions of the cells examined is indicated in the bar chart in Fig. 4.5. Statistical comparison of the densities of labelling confirmed that a significantly greater density of labelling was present in the perinuclear region than either the extra-perinuclear ($P = < 0.05$; Appendix 2, Table 4.7) or the sub-plasmalemmal regions of cells ($P = < 0.05$; Appendix 2, Table 4.7). Furthermore, the density of labelling within the sub-plasmalemmal region of cells was significantly lower than that detected in the extra-perinuclear region ($P = < 0.05$; Appendix 2, Table 4.7). Therefore, these data suggest not only that

lysosomal labelling predominates within the perinuclear region but also that the density of labelling declines progressively as one moves from the nucleus to the plasma membrane of cells.

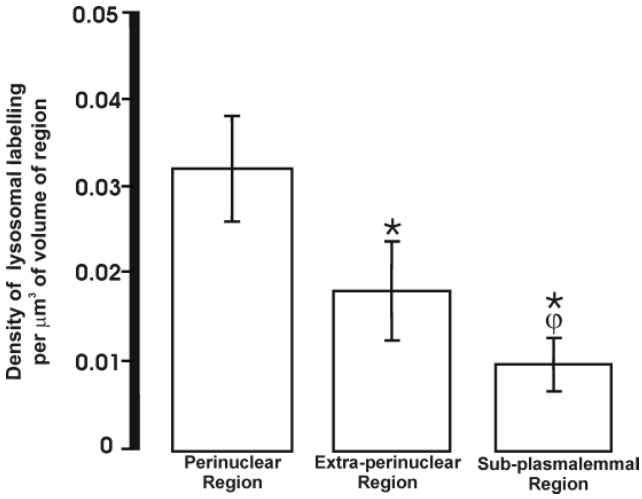

Fig. 4.5 **Comparison of the density (μm^3 of labelling per μm^3 of region) of lysosomal labelling within the 3 regions of isolated pulmonary artery smooth muscle cells. * indicates statistical difference (P = ≤ 0.05) when compared to the perinuclear region. φ indicates statistical difference (P = ≤ 0.05) when compared to the extra-perinuclear region (n = 24).**

A comparison was then carried out to examine whether there was a difference in the mean volumes of individual elements of lysosomal labelling within the different regions of cells. Separate elements of fluorescent labelling which are closer together than can be resolved with the imaging system used to acquire data are recorded as single elements of labelling. Thus, the larger the individual volumes of αlgp120 labelling detected, the larger the degree of lysosomal clustering. The difference between the mean volumes of labelling within the regions of the cell is indicated in the bar chart in Fig. 4.6. The mean volume of labelling within the perinuclear region of cells was 0.76 ± 0.14 μm^3 (n = 24; Fig. 4.6; Appendix 2, Table 4.4). The mean volumes of labelling were seen to decrease out with the perinuclear region of cells. Thus, the mean volume of labelling within the extra-perinuclear region of cells was 0.59 ± 0.13 μm^3 (n = 24; Fig. 4.6; Appendix 2, Table 4.5), while the mean volume of

elements of lysosomal labelling within the sub-plasmalemmal region of cells was 0.32 ± 0.06 μm^3 (n = 24; Fig. 4.6; Appendix 2, Table 4.6).

Although Fig. 4.6 shows a clear trend for a decrease in the mean volume of elements of labelling between the perinuclear and extra-perinuclear regions of cells, this decrease was not statistically significant (P = > 0.05, Appendix 2, Table 4.8). However, the mean volume of individual elements of labelling within the sub-plasmalemmal region of cells was significantly smaller than those observed in either the perinuclear (P = < 0.05; Appendix 2, Table 4.8) or extra-perinuclear regions (P = < 0.05; Appendix 2, Table 4.8). Therefore, the mean volume of individual elements of lysosomal labelling appeared to decrease across the cell from the perinuclear region to the sub-plasmalemmal region (Fig. 4.6).

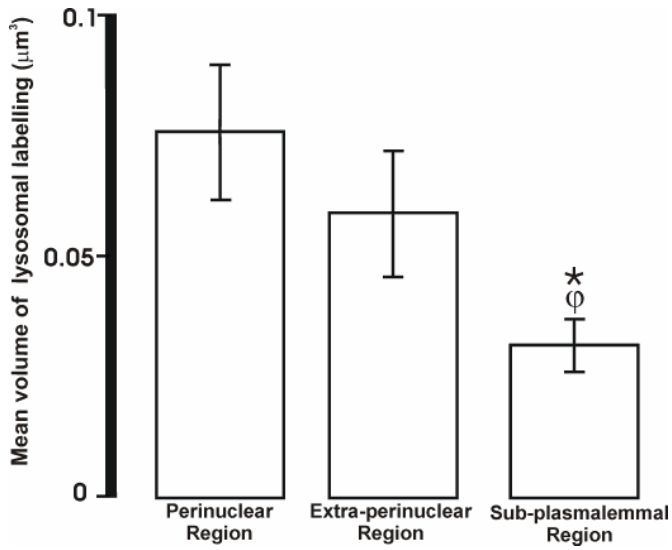

Fig. 4.6 **Comparison of the mean volume (μm^3) of lysosomal labelling within the 3 regions of isolated pulmonary artery smooth muscle cells. * indicates statistical difference (P = ≤ 0.05) when compared to the perinuclear region. φ indicates statistical difference (P = ≤ 0.05) when compared to the extra-perinuclear region (n = 24).**

I can conclude, therefore, that the density of lysosomes was greatest in the perinuclear region of pulmonary artery smooth muscle cells, where a high degree of lysosomal clustering was also evident. Given these data, coupled with the finding that lysosomal clusters colocalised with a subpopulation of RyRs in pulmonary artery smooth muscle cells (Section 4.3.1), I proceeded to

examine whether areas of colocalisation were formed between lysosomes and a specific subtype of RyRs.

4.2.3 Spatial distribution of ryanodine receptor subtypes within pulmonary artery smooth muscle cells

4.2.3.1 Identification of ryanodine receptor subtypes in pulmonary artery smooth muscle cells

The presence of RyR subtypes was investigated in pulmonary artery smooth muscle via the use of affinity-purified antibodies raised against specific amino acid sequences within each of the 3 different RyR subtypes namely, RyR1 (Lesh, *et al.*, 1993), RyR2 (Jeyakumar, *et al.*, 2001) and RyR3 (Jeyakumar, *et al.*, 1998), for target sequences see Chapter 2, section 2.4.1. Samples of protein isolated from the pulmonary artery were run alongside positive controls consisting of protein extracted from various tissues previously shown to express a high level of a specific RyR subtype: RyR1, skeletal muscle (Inui, *et al.*, 1987b); RyR2, cardiac muscle (Inui, *et al.*, 1987a); RyR3, brain (Hakamata, *et al.*, 1992). RyRs are large tetrameric ion channels composed of polypeptide subunits with molecular masses between 500 and 600 kDa (Sutko and Airey, 1996b). Therefore, one would expect to see bands corresponding to RyRs positioned above the 250 kDa marker which was the largest molecular weight marker used in this study. All three subtypes of RyR were identified in pulmonary arteries, denuded of their endothelia, by Western blot (Figs. 4.7), which is consistent with a recent investigation in rat pulmonary arteries, utilising the same sequence specific anti-RyR antibodies (Yang, *et al.*, 2005).

Fig. 4.7 shows representative blots probed with sequence-specific antibodies raised against RyR1 (Fig. 4.7A), RyR2 (Fig. 4.7B) and RyR3 (Fig. 4.7C). For all 3 RyR subtypes a band was identified that was > 250 kDA in the pulmonary artery. These bands corresponded with bands in the respective positive controls, thus demonstrating the presence of RyR1, RyR2 and RyR3 in the pulmonary artery. It is worthy of note that the blots shown here showed multiple bands in all tissues following probing with a given RyR subtype antibody. The presence of these multiple bands may be a due to the degradation

of RyRs during processing, as described previously in studies carried out in both pulmonary and aortic smooth muscle (Lesh, *et al.*, 1998; Yang, *et al.*, 2005).

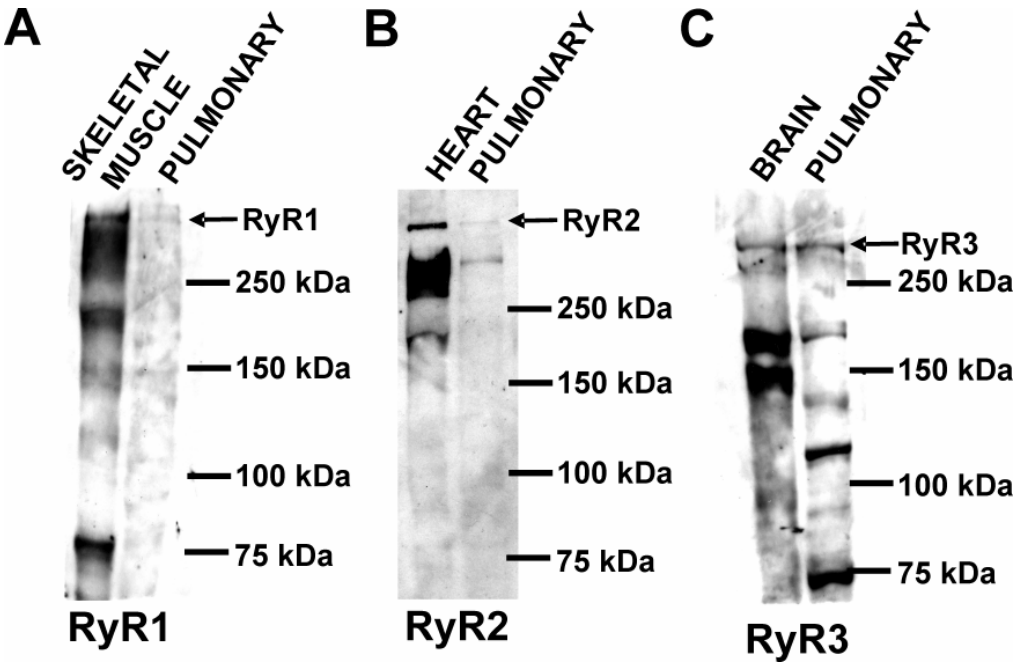

Fig. 4.7 **Pulmonary artery smooth muscle expresses all 3 RyR subtypes:** ***A*** specific antibody for Ryanodine receptor (RyR) subtype 1 immunoblotted against cytoplasmic homogenates from second order branches of rat pulmonary artery and rat skeletal muscle. 20 μg of protein were loaded to each lane. A specific band > 250 KDa of labelling representing RyR subtype 1 was identified in each lane. ***B*** specific antibody for RyR subtype 2 immunoblotted against cytoplasmic homogenates from second order branches of rat pulmonary artery and rat heart. 20 μg of protein were loaded to each lane. A specific band > 250 KDa of labelling representing RyR subtype 2 was identified in each lane. ***C*** specific antibody for RyR subtype 3 immunoblotted against cytoplasmic homogenates from second order branches of rat pulmonary artery and rat brain. 20 μg of protein were loaded to each lane. A specific band of labelling >250 KDa representing RyR subtype 3 was identified in each lane.

4.2.3.2 Distribution of ryanodine receptor subtypes in methanol-fixed pulmonary artery smooth muscle cells

Labelling of RyR subtypes was visualised in methanol-fixed pulmonary artery smooth muscle cells via secondary antibodies conjugated to the fluorescent probe, Texas Red (excitation 555 nm, emission 617 nm). Volumetric analysis suggests that the distribution within pulmonary artery

smooth muscle cells of the three RyR subtypes was markedly different. This is exemplified by typical examples of distribution of labelling of RyR1, RyR2 and RyR3 in Figs. 4.10, 4.13 and 4.16, respectively, within different isolated pulmonary artery smooth muscle cells.

4.2.3.2.1 Spatial distribution of ryanodine receptor subtype 1 labelling in pulmonary artery smooth muscle cells

Fig. 4.8(i) shows a transmitted light image of an isolated pulmonary artery smooth muscle cell, while Fig. 4.8(ii) shows a deconvolved Z-section (focal depth 0.28 μm) through the cell, corrected to remove background fluorescence, as determined from matched control slides (Chapter 2, Section 2.4.2). The distribution of RyR1 and the position of the nucleus are visualised in red and blue, respectively. Fig. 4.8(iii) shows a 3D reconstruction of a series of deconvolved Z-sections (focal depth 0.28 μm, Z step 0.2 μm) obtained through the cell. Analysis of the labelling within cells, excluding areas of labelling ≤ 0.5 μm in the X-, Y- and Z-planes was then carried out. Fig. 4.8(iv) shows a 3D representation of the positioning of each individual volume ≥ 0.125 μm^3, in purple, of RyR1 labelling measured from the cell.

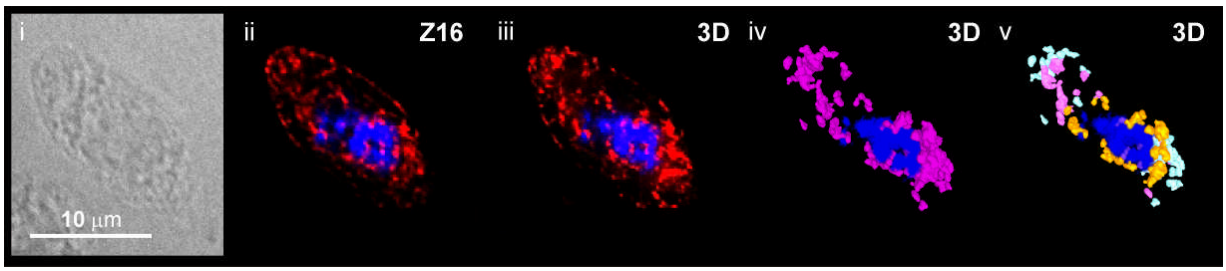

Fig. 4.8 **Visualisation of RyR1 labelling within an isolated pulmonary artery smooth muscle cell:** ***(i)*** transmitted light image of an isolated pulmonary artery smooth muscle cell. ***(ii)*** deconvolved Z-section (focal depth 0.28 μm) taken through the cell shown in ***(i)*** showing the distribution of RyR1 labelling in *red* and the nucleus in *blue*. ***(iii)*** 3D reconstruction of a series of Z-sections (focal depth 0.28 μm, Z step 0.2 μm) obtained through the cell shown in ***(i)*** fluorescently labelled as in ***(ii)***. ***(iv)*** 3D representation of the distribution of individual volumes ≥ 0.125 μm^3 (in *purple*) of RyR1 labelling. ***(v)*** individual volumes of RyR1 labelling as in ***(iv)*** coloured to indicate the region of the cell in which they are located; i.e. the perinuclear (*orange*), extra-perinuclear (*pink*) and sub-plasmalemmal (*light blue*).

Examination of labelled cells showed that RyR1 labelling occupied a volume of 50.77 ± 7.6 μm^3 in pulmonary artery smooth muscle cells (n = 8; Appendix 2, Table 4.9). This equated to a density of labelling within cells of 0.03 ± 0.004 μm^3 of labelling per μm^3 of cell volume (n = 8; Appendix 2, Table 4.9). Fig. 4.8(v) shows a 3D visual representation of the spatial distribution of each individual volume of labelling within the cell shown in Fig. 4.8(iv), following regionalisation. Each volume of labelling is coloured to indicate the region of the cell in which it is located. Thus, volumes of RyR1 labelling located in the perinuclear, extra-perinuclear and sub-plasmalemmal regions are visualised in orange, pink and light blue, respectively. RyR1 labelling can be seen throughout the cytoplasm of the cell shown in Fig. 4.8(v), with no obvious predominance in any given region. RyR1 labelling was measured as occupying a volume of 15.77 ± 3.7 μm^3 in the perinuclear region of cells (n = 8; Appendix 2, Table 4.10), equating to a density of 0.033 ± 0.008 μm^3 of labelling per μm^3 of the perinuclear region (n = 8; Fig. 4.9; Appendix 2, Table 4.10). Both the volume and density of labelling appeared to be lower in the extra-perinuclear region when compared to the perinuclear region. Thus, in the extra-perinuclear region RyR1 labelling occupied a volume of 9.38 ± 2.36 μm^3 (n = 8; Appendix 2, Table 4.11), accounting for a density of 0.018 ± 0.003 μm^3 of labelling per μm^3 of the region (n = 8; Fig 4.9; Appendix 2, Table 4.11). However, the volume and density of RyR1 labelling in the sub-plasmalemmal region was comparable to that observed in the perinuclear region. Thus, volumetric analysis of RyR1 labelling showed that there was 19.82 ± 3.24 μm^3 (n = 8; Appendix 2, Table 4.12) and a density of 0.031 ± 0.007 μm^3 of labelling per μm^3 of the region (n = 8; Fig 4.9; Appendix 2, Table 4.13). A statistical comparison of the density of labelling between the perinuclear, extra-perinuclear and sub-plasmalemmal regions showed that the apparent differences between the density of labelling between regions were not statistically significant ($P > 0.05$; Appendix 2, Table 4.14). Therefore, RyR1 labelling was distributed evenly throughout pulmonary artery smooth muscle cells.

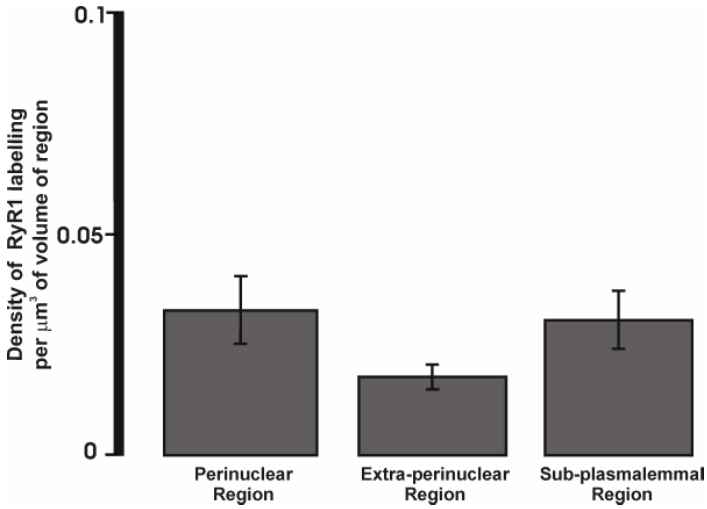

Fig. 4.9 **Comparison of the density (μm^3 of labelling per μm^3 of region) of RyR1 labelling within the 3 regions of isolated pulmonary artery smooth muscle cells (n = 8).**

As with lysosomal labelling, a measurement was made of the mean volume of individual elements of RyR1 labelling within cells. As described previously, a greater mean volume of RyR1 labelling within a given region of cells would be indicative of a greater degree of clustering of the receptor within that region. Measurements of RyR1 labelling in the perinuclear region of cells indicated that elements of RyR1 labelling had a mean volume of 1.17 ± 0.36 μm^3 (n = 8; Fig. 4.10; Appendix 2, Table 4.10). The mean volume of elements of labelling in the perinuclear region appeared larger than those measured in the extra-perinuclear region of cells, where the mean volume of individual elements of RyR1 labelling was 0.81 ± 0.29 μm^3 (n = 8; Fig. 4.10; Appendix 2, Table 4.11). The smallest clusters of RyR1 labelling appeared to be located in the sub-plasmalemmal region, where the mean volume was measured at 0.53 ± 0.11 μm^3 (n = 8; Fig. 4.10; Appendix 2, Table 4.12). However, as was observed for the density of RyR1 labelling within the three regions of cells, although there appeared to be a trend for a decrease in the mean volumes of RyR1 labelling from the perinuclear to the extra-perinuclear and sub-plasmalemmal regions of cells, there was no significant difference between the measures ($P > 0.05$; Appendix 2, Table 4.14). Therefore, these results show that the mean volume of RyR1 labelling was fairly uniform across the perinuclear, extra-perinuclear and sub-plasmalemmal regions of pulmonary artery smooth muscle cells.

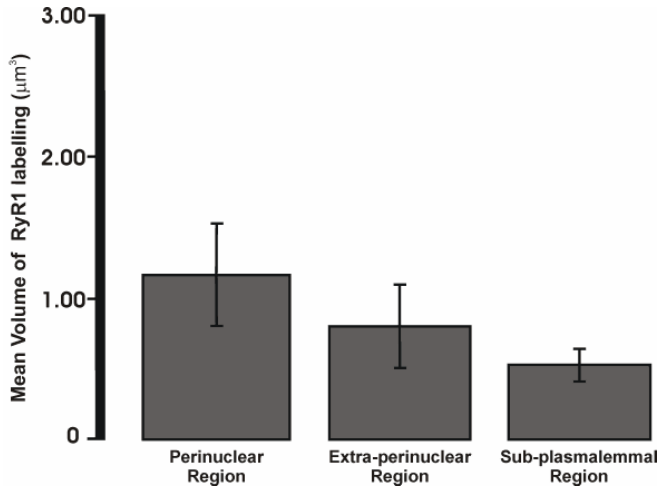

Fig. 4.10 **Comparison of the mean volume (μm^3) of RyR1 labelling within the 3 regions of isolated pulmonary artery smooth muscle cells (n = 8).**

4.2.3.2.2 Spatial distribution of ryanodine receptor subtype 2 labelling in pulmonary artery smooth muscle cells

An example of the distribution of RyR2 labelling within pulmonary artery smooth muscle cells is shown in Fig. 4.11. Fig. 4.11(i) shows a transmitted light image of an isolated pulmonary artery smooth muscle cell, while Fig. 4.11(ii) shows a deconvolved Z-section (focal depth 0.28 μm) obtained through the cell, corrected to remove background fluorescence. The distribution of RyR2 labelling and the position of the nucleus are visualised in red and blue, respectively. Fig. 4.11(iii) shows a 3D reconstruction of a series of deconvolved Z-sections (focal depth 0.28 μm, Z step 0.2 μm) obtained through the cell. Fig. 4.11(iv) shows a 3D representation of the positioning of each individual volume ≥ 0.125 μm^3, in purple, of RyR2 labelling measured from the cell in Fig. 4.11. RyR2 labelling occupied a volume of 48.92 ± 3.61 μm^3 in pulmonary artery smooth muscle cells (n = 8; Appendix 2, Table 4.15), equating to a density of labelling within cells of 0.03 ± 0.006 μm^3 of labelling per μm^3 of cell volume (n = 8; Appendix 2, Table 4.15). Fig. 4.11(v) shows a 3D visual representation of the spatial distribution of each individual volume of labelling within the cell shown in Fig. 4.11(iv) following regionalisation.

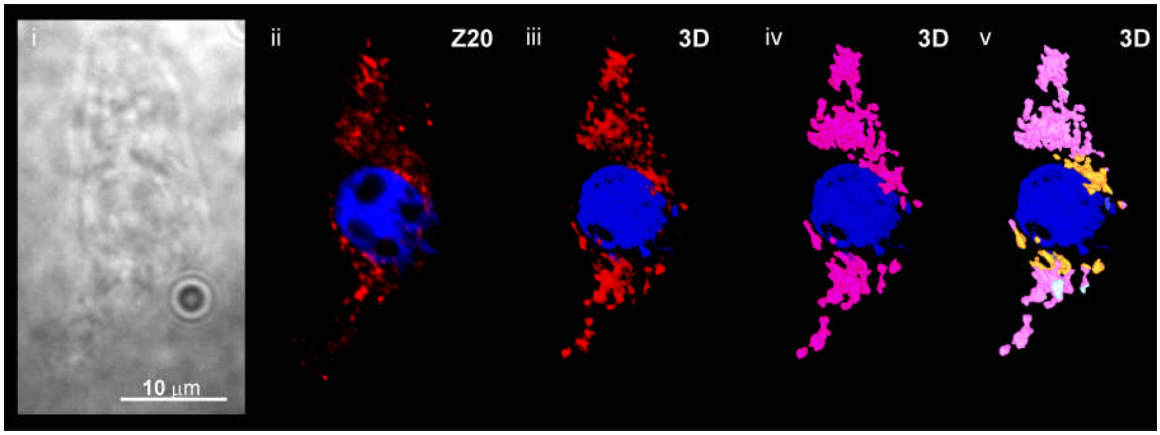

Fig. 4.11 **Visualisation of RyR2 labelling within an isolated pulmonary artery smooth muscle cell:** ***(i)*** transmitted light image of an isolated pulmonary artery smooth muscle cell. ***(ii)*** deconvolved Z-section (focal depth 0.28 μm) taken through the cell shown in ***(i)*** showing the distribution of RyR2 labelling in *red* and the nucleus in *blue*. ***(iii)*** 3D reconstruction of a series of Z-sections (focal depth 0.28 μm, Z step 0.2 μm) obtained through the cell shown in ***(i)*** fluorescently labelled as in ***(ii)***. ***(iv)*** 3D representation of the distribution of individual volumes ≥ 0.125 μm^3 (in *purple*) of RyR2 labelling. ***(v)*** individual volumes of RyR2 labelling as in ***(iv)*** coloured to indicate the region of the cell in which they are located; i.e. the perinuclear (*orange*), extra-perinuclear (*pink*) and sub-plasmalemmal (*light blue*).

Individual volumes of RyR2 labelling in the perinuclear, extra-perinuclear and sub-plasmalemmal regions are visualised as orange, pink and light blue, respectively. RyR2 labelling was located throughout the cell. However, volumetric analysis of RyR2 labelling suggested that RyR2 labelling was predominant in the extra-perinuclear region over the perinuclear and sub-plasmalemmal regions (Fig. 4.12). Thus, RyR2 labelling occupied a volume of 14.09 ± 2.16 μm^3 in the perinuclear region of cells (n = 8; Appendix 2, Table 4.16), equating to a density of 0.037 ± 0.0013 μm^3 of labelling per μm^3 of the perinuclear region (n = 8; Fig. 4.12; Appendix 2, Table 4.16). The labelling of RyR2 appeared to increase in the extra-perinuclear region, where it was seen to occupy a volume of 24.99 ± 4.97 μm^3 (n = 8; Appendix 2, Table 4.17), accounting for a density of 0.066 ± 0.0012 μm^3 of labelling per μm^3 of the region (n =8; Fig. 4.12; Appendix 2, Table 4.17). Thus, a two-fold greater density of RyR2 labelling was measured in the extra-perinuclear region when compared to the perinuclear region. RyR2 labelling was seen to decline to its lowest level in the sub-plasmalemmal region of cells, where it measured a volume of 7.36 ± 1.58 μm^3 (n = 8; Appendix 2, Table 4.18), equating to a

density of 0.012 ± 0.003 μm^3 of labelling per μm^3 of the region (n = 8; Fig. 4.12; Appendix 2, Table 4.18). Although there appeared to be a greater density of RyR2 labelling in the extra-perinuclear region of cells in comparison to the perinuclear region, this difference was not statistically significant (P = > 0.05; Appendix 2, Table 4.19). The density of RyR2 labelling within the perinuclear and extra-perinuclear regions of cells were, however, significantly greater than that observed in the sub-plasmalemmal region of cells (P = ≤ 0.05; Appendix 2, Table 4.19). Therefore, RyR2 labelling was seen to be distributed throughout the cytoplasm of cells. However, there was a marked decrease in the density of RyR2 labelling in the sub-plasmalemmal region.

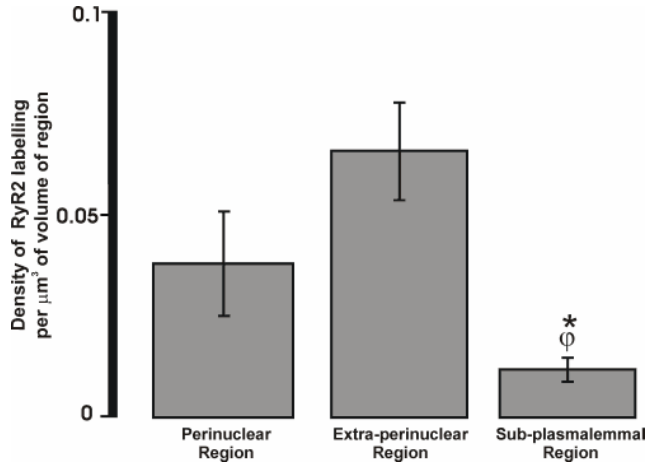

Fig. 4.12 **Comparison of the density (μm^3 of labelling per μm^3 of region) of RyR2 labelling within the 3 regions of isolated pulmonary artery smooth muscle cells. * indicates statistical difference (P = ≤ 0.05) when compared to the perinuclear region. φ indicates statistical difference (P = ≤ 0.05) when compared to the extra-perinuclear region (n = 8).**

Differences were also observed within cells with regard to the mean volumes of RyR2 labelling. Elements of RyR2 labelling in the perinuclear region of cells had a mean volume of 0.94 ± 0.23 μm^3 (n = 8; Fig. 4.13; Appendix 2, Table 4.16), while the mean volumes of elements of RyR2 labelling in the extra-perinuclear region appeared to be almost double this, measuring 1.71 ± 0.47 μm^3 (n = 8; Fig. 4.13; Appendix 2, Table 4.17). Furthermore, the mean volume of RyR2 labelling in the sub-plasmalemmal region of cells was considerably smaller than was observed in either the perinuclear or extra-perinuclear regions. Therefore, the mean volume of RyR2

labelling in the sub-plasmalemmal region of cells was 0.4 ± 0.036 μm^3 (n = 8; Fig. 4.13; Appendix 2, Table 4.18). Statistical comparison of the mean volume of RyR2 labelling within the three different regions indicated that there was no significant difference between the mean volumes in the perinuclear and extra-perinuclear regions of cells (P > 0.05; Appendix 2, Table 4.20). There was,

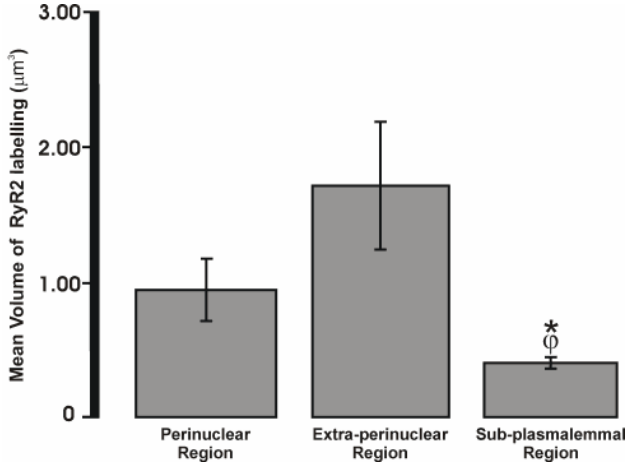

Fig. 4.13 **Comparison of the mean volume (μm^3) of RyR2 labelling within the 3 regions of isolated pulmonary artery smooth muscle cells. * indicates statistical difference (P = ≤ 0.05) when compared to the perinuclear region. φ indicates statistical difference (P = ≤ 0.05) when compared to the extra-perinuclear region (n = 8).**

however, a significant decrease in the mean volume of elements of RyR2 labelling within the sub-plasmalemmal region when compared to the perinuclear and extra-perinuclear regions (P ≤ 0.05; Appendix 2, Table 4.20). These results, therefore, suggest that larger clusters of RyR2 labelling are located primarily in the extra-perinuclear and perinuclear regions with significantly smaller aggregations of RyR2 close to the plasma membrane of cells.

4.2.3.2.3 Spatial distribution of ryanodine receptor subtype 3 labelling in pulmonary artery smooth muscle cells

A typical example of the distribution of RyR3 labelling within pulmonary artery smooth muscle cells is shown in Fig. 4.14. Fig. 4.14(i) shows a transmitted light image of an isolated pulmonary artery smooth muscle cell, while Fig. 4.14(ii) shows a deconvolved Z-section (focal depth 0.28 μm)

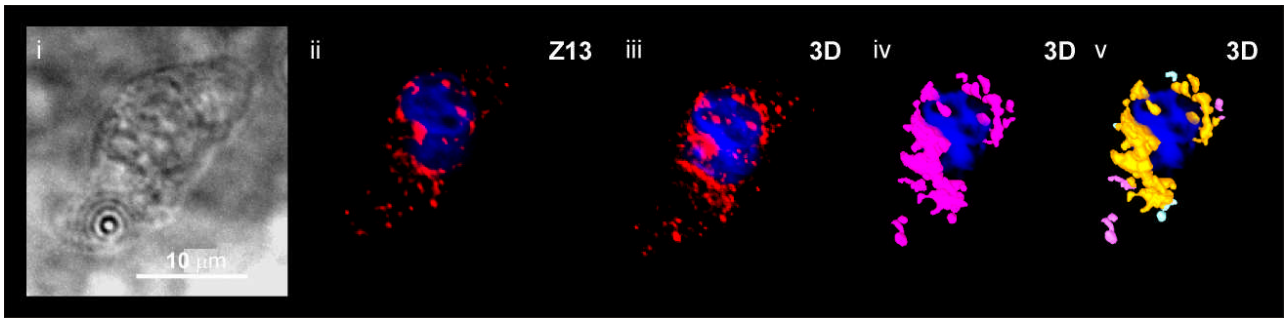

Fig. 4.14 **Visualisation of RyR3 labelling within an isolated pulmonary artery smooth muscle cell:** ***(i)*** transmitted light image of an isolated pulmonary artery smooth muscle cell. ***(ii)*** deconvolved Z-section (focal depth 0.28 µm) taken through the cell shown in ***(i)*** showing the distribution of RyR3 labelling in *red* and the nucleus in *blue*. ***(iii)*** 3D reconstruction of a series of Z-sections (focal depth 0.28 µm, Z step 0.2 µm) obtained through the cell shown in ***(i)*** fluorescently labelled as in ***(ii)***. ***(iv)*** 3D representation of the distribution of individual volumes ≥ 0.125 μm^3 (in *purple*) of RyR3 labelling. ***(v)*** individual volumes of RyR3 labelling as in ***(iv)*** coloured to indicate the region of the cell in which they are located; i.e. the perinuclear (*orange*), extra-perinuclear (*pink*) and sub-plasmalemmal (*light blue*).

through the cell, corrected to remove background fluorescence. The distribution of RyR3 labelling and the position of the nucleus are visualised in red and blue, respectively. Fig. 4.14(iii) shows a 3D reconstruction of a series of deconvolved Z-sections (focal depth 0.28 µm, Z step 0.2 µm) obtained through the cell. RyR3 labelling showed the least diffuse distribution of all three RyR subtypes. Fig. 4.14(iv) shows a 3D representation of the positioning of each individual volume ≥ 0.125 μm^3, in purple, of RyR3 labelling measured from the cell. RyR3 labelling occupied a volume of 47.13 ± 5.88 μm^3 in pulmonary artery smooth muscle cells (n = 8; Appendix 2, Table 4.21), equating to a density of labelling within cells of 0.029 ± 0.003 μm^3 of labelling per μm^3 of cell volume (n = 8; Appendix 2, Table 4.21). Fig. 4.14(v) shows a 3D visual representation of the spatial distribution of each individual volume of labelling within the cell shown in Fig. 4.14(iv) following regionalisation. Individual volumes of RyR3 labelling located in the perinuclear, extra-perinuclear and sub-plasmalemmal are visualised in orange, pink and light blue, respectively. RyR3 labelling occupied a volume of 37.25 ± 5.13 μm^3 in the perinuclear region of cells (n = 8; Appendix 2, Table 4.22), equating to a

density of 0.066 ± 0.001 μm^3 of labelling per μm^3 (n = 8; Fig. 4.15; Appendix 2, Table 4.22). In marked contrast, RyR3 labelling was 3-fold lower in the extra-perinuclear region with a volume of 5.75 ± 2.09 μm^3 (n = 8; Appendix 2, Table 4.23), and a density of 0.017 ± 0.005 μm^3 of labelling per μm^3 of the region (n = 8; Fig. 4.15; Appendix 2, Table 4.23), and 6-fold lower within the sub-plasmalemmal region in which there was a total volume of 3.14 ± 1.58 μm^3 (n = 8; Appendix 2, Table 4.24) and a density of 0.006 ± 0.002 μm^3 of labelling per μm^3 of the region (n = 8; Fig. 4.15; Appendix 2, Table 4.24). There was a greater density of RyR3 labelling in the perinuclear region of cells when compared to both the extra-perinuclear ($P = \leq 0.05$; Appendix 2, Table 4.25) and sub-plasmalemmal regions of cells ($P = \leq 0.05$; Appendix 2, Table 4.25). Therefore, it is clear from this regionalisation of RyR3 labelling that there was a much greater density of labelling within the perinuclear region of cells than was observed in either the extra-perinuclear or sub-plasmalemmal regions.

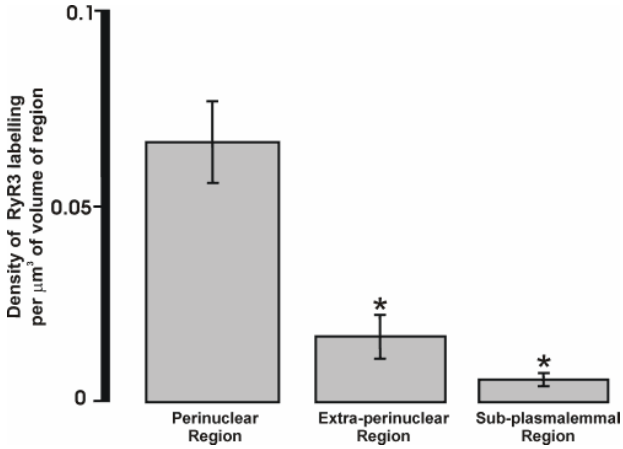

Fig. 4.15 **Comparison of the density (μm^3 of labelling per μm^3 of region) of RyR3 labelling within the 3 regions of isolated pulmonary artery smooth muscle cells. * indicates statistical difference ($P = \leq 0.05$) when compared to the perinuclear region (n = 8).**

As with the labelling of the other RyR subtypes, an examination of the mean volume of RyR3 was carried out to determine the extent to which RyR3 was clustered in the perinuclear, extra-perinuclear and sub-plasmalemmal regions. Elements of RyR3 labelling in the perinuclear region of cells had a mean volume of 2.33 ± 0.45 μm^3 (n = 8; Fig. 4.16; Appendix 2, Table 4.22), compared to 0.79 ± 0.2 μm^3 in the extra-perinuclear (n = 8; Fig. 4.16;

Appendix 2, Table 4.23) and 0.45 ± 0.12 μm^3 in the sub-plasmalemmal region (n = 8; Fig. 4.16; Appendix 2, Table 4.24). Statistical analysis of the mean volumes of RyR3 labelling indicated that the mean volume of labelling was significantly larger in the perinuclear region when compared to the extra-perinuclear (P = ≤ 0.05; Appendix 3, Table 4.26) and the sub-plasmalemmal region (P = ≤ 0.05; Appendix 2, Table 4.26). Therefore, RyR3 forms large clusters in the perinuclear region with much smaller clusters out with the perinuclear region.

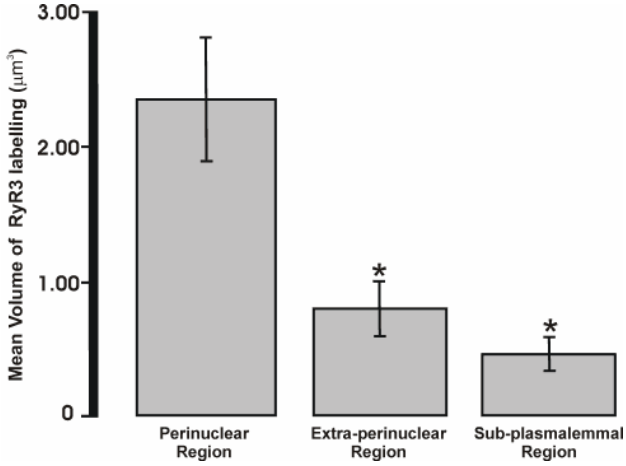

Fig. 4.16 **Comparison of the mean volume (μm^3) of RyR3 labelling within the 3 regions of isolated pulmonary artery smooth muscle cells. * indicates statistical difference (P = ≤ 0.05) when compared to the perinuclear region (n = 8).**

4.2.3.2.4 Comparison between the spatial distribution of labelling of the different ryanodine receptor subtypes in pulmonary artery smooth muscle cells

A direct comparison between the distributions of the three subtypes of RyR labelling in the perinuclear, extra-perinuclear and sub-plasmalemmal regions of cells is shown in the bar chart in Fig. 4.17. Comparison of the density of RyR subtype labelling in the perinuclear region of cells showed that there was a significantly greater density of RyR3 labelling within this region than was observed for RyR1 (P = ≤ 0.05; Appendix 2, Table 4.27). There was also a larger density of RyR3 labelling within the perinuclear region than for RyR2, but this was not statistically significant (P = > 0.05; Appendix 2, Table

4.27). These data suggest that RyR3 represents the predominant RyR subtype within the perinuclear region of cells.

In marked contrast to my findings with respect to the perinuclear region of cells, comparison of the labelling for the three RyR subtypes within the extra-perinuclear region indicated that there was a significantly greater density of RyR2 labelling compared to either RyR1 ($P = \leq 0.05$; Appendix 2, Table 4.28) or RyR3 labelling ($P = \leq 0.05$; Appendix 2, Table 4.28). Therefore, RyR2 is the predominant subtype of RyR expressed within the extra-perinuclear region of pulmonary artery smooth muscle cells.

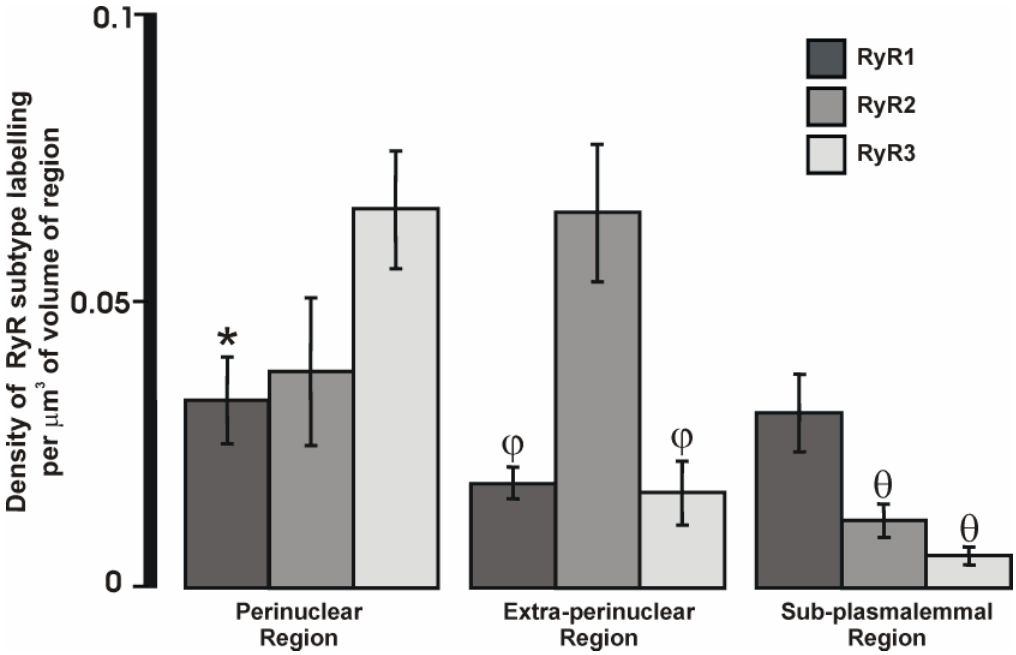

Fig. 4.17 **Comparison of the density (μm³ of labelling per μm³ of region) of RyR subtype labelling within the 3 regions of isolated pulmonary artery smooth muscle cells. * indicates statistical difference ($P = \leq 0.05$) when compared to the density of RyR3 labelling in the perinuclear region. φ indicates statistical difference ($P = \leq 0.05$) when compared to the density of RyR2 labelling in the extra-perinuclear region. θ indicates statistical difference ($P = \leq 0.05$) when compared to RyR1 labelling in the sub-plasmalemmal region (n = 8 for each RyR subtype).**

A further variation was observed with respect to the sub-plasmalemmal region. Here, the densities of labelling for both RyR2 and RyR3 declined markedly relative to that observed in the perinuclear and extra-perinuclear regions of cells. By contrast, there was little change in the density of RyR1 labelling between these regions. Furthermore, comparison between the three

RyR subtypes within the sub-plasmalemmal region of cells indicated that the density of RyR1 labelling was significantly greater than the labelling of either RyR2 ($P = \leq 0.05$; Appendix 2, Table 4.29) or RyR3 ($P = \leq 0.05$; Appendix 2, Table 4.29). Thus, it would appear that the predominant form of RyR within the sub-plasmalemmal region of cells is RyR1.

Differences in the clustering of RyR subtypes in the three regions of pulmonary artery smooth muscle cells is shown in Fig. 4.18, which compares the mean volumes of individual elements of RyR subtype labelling. Statistical analysis of the mean volumes of labelling within the perinuclear region of cells showed that mean volume of RyR3 labelling was significantly larger than those measured for RyR2 ($P = \leq 0.05$; Appendix 2, Table 4.30). The mean volume of areas of RyR3 labelling was also larger than that for RyR1, with this difference being on the verge of statistical significance ($P = 0.06$; Appendix 2, Table 4.30).

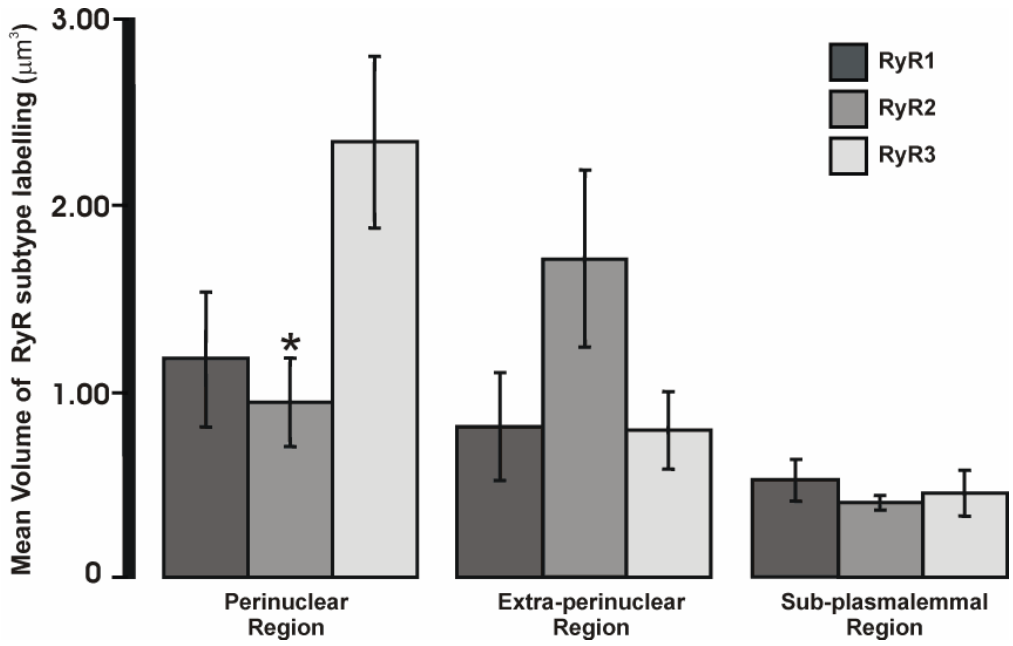

Fig. 4.18 **Comparison of the mean volume (μm^3) of individual elements of RyR subtype labelling within the 3 regions of isolated pulmonary artery smooth muscle cells. * indicates statistical difference ($P = \leq 0.05$) when compared to the density of RyR3 labelling in the perinuclear region (n = 8 for each RyR subtype).**

Within the extra-perinuclear region of cells elements of RyR2 labelling appeared to have a larger mean volume than elements of either RyR1 or RyR3

labelling. However, these differences were not statistically significant ($P > 0.05$; Appendix 2, Table 4.31). Furthermore, statistical comparison of the volumes of labelling for RyR1, RyR2 and RyR3 within the sub-plasmalemmal regions of cells showed there was no difference between the mean volume of labelling between RyR subtypes within this region ($P > 0.05$; Appendix 2, Table 4.32). Therefore, there is no evidence that any of the RyR subtypes show larger clusters of receptors compared to the other subtypes in the sub-plasmalemmal region.

In conclusion, these findings indicate that all 3 RyR subtypes are present within pulmonary artery smooth muscle, and that labelling of each of the subtypes was observed in the perinuclear, extra-perinuclear and sub-plasmalemmal regions. However, volumetric analysis of RyR subtype labelling identified clear differences in regional distribution of the different RyR subtypes. Thus, RyR3 was the predominant subtype of RyR in the perinuclear region, where it formed dense clusters of labelling. Furthermore, RyR3 did not appear to be widely distributed outside this region of the cell. By contrast, RyR2 was the predominant subtype of RyR within the extra-perinuclear region, where it exhibited a higher density and mean volume of labelling than in any other region. The distribution of RyR1 was different still with a similar density and mean volume of labelling across all 3 regions. However, RyR1 appeared to be the predominant subtype of RyR expressed proximal to the plasma membrane of cells. Following this examination of the distribution of RyR subtypes, I proceeded to examine the extent to which each of the RyR subtypes were associated with lysosomes in pulmonary artery smooth muscle cells.

4.2.4 Examination of colocalisation between lysosomes and ryanodine receptor subtypes in pulmonary artery smooth muscle cells

An examination of the colocalisation between αlgp120- and RyR subtype-labelling was carried out to determine which RyR subtype associates with lysosomes to form the trigger zone for NAADP-mediated Ca^{2+} signalling. Volumetric analysis identified marked differences in the degree to which RyR1, RyR2 and RyR3 colocalised with lysosomal labelling in isolated

pulmonary artery smooth muscle cells. These differences are visualised in the examples of the colocalisation between lysosomal-labelling and RyR1-, RyR2- and RyR3-labelling are shown in Figs. 4.19, 4.22 and 4.25, respectively.

4.2.4.1 Colocalisation between ryanodine receptor subtype 1- and lysosomal-labelling in pulmonary artery smooth muscle cells

Fig. 4.19(i) shows a transmitted light image of an isolated pulmonary artery smooth muscle cell. While 4.191(ii) shows a 3D reconstruction of a series of deconvolved Z-sections (focal depth 0.28 μm, Z step 0.2 μm) obtained through the cell shown in (i), showing the distribution of αlgp120-labelling in green and the DAPI labelled nucleus in blue. Fig. 4.19(iii) shows

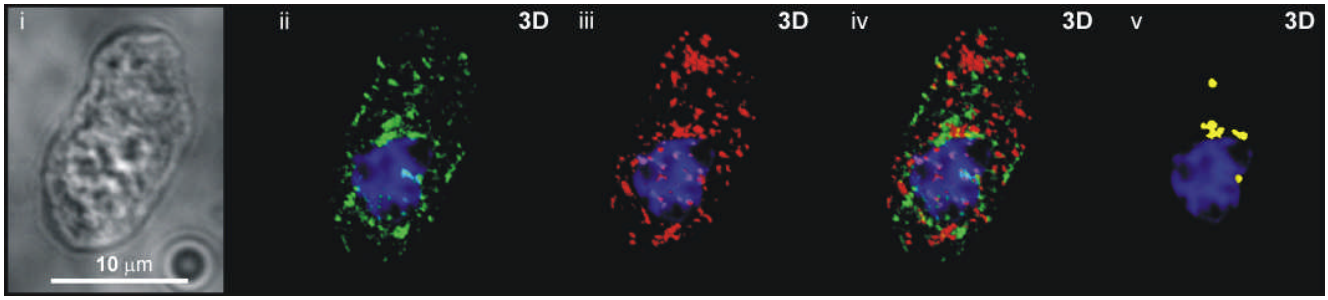

Fig. 4.19 **Visualisation of the colocalisation between RyR1- and lysosomal-labelling within an isolated pulmonary artery smooth muscle cell:** ***(i)*** transmitted light image of an isolated pulmonary artery smooth muscle cell. ***(ii)*** 3D reconstruction of a series of Z-sections (focal depth 0.28 μm, Z step 0.2 μm) obtained through the cell shown in ***(i)*** fluorescently labelled to show the distribution of lysosomal labelling and the nucleus in *green* and *blue*, respectively. ***(iii)*** 3D reconstruction of a series of Z-sections (focal depth 0.28 μm, Z step 0.2 μm) obtained through the cell shown in ***(i)*** fluorescently labelled to show the distribution of RyR1 labelling and the nucleus in *red* and *blue*, respectively.***(iv)*** 3D representation of the distribution of lysosomal- and RyR1-labelling in respect to the nucleus. Areas of colocalisation between lysosomal- and RyR1-labelling are shown in yellow. ***(v)*** individual volumes of colocalisation between lysosomal- and RyR1-labelling, ≥ 0.125 μm^3 (in *yellow*), in the cell shown in ***(i)***, in relation to the nucleus of the cell, shown in *blue*.

a 3D reconstruction of deconvolved Z-sections (focal depth 0.28 μm, Z step 0.2 μm), from the same cell, this time showing the distribution of RyR1- labelling in red, in relation to the DAPI labelled nucleus. The Z-series were then superimposed upon one another to allow comparison of the spatial distribution

of lysosomal- and RyR1-labelling. A 3D reconstruction of the superimposed Z-series is shown in Fig. 4.19(iv). Areas of colocalisation between lysosomal- and RyR1-labelling are visualised in yellow. An example of an area of colocalisation between lysosomal- and RyR1-labelling is indicated by the arrow in Fig. 4.19(iv). Analysis of the colocalisation between lysosomal- and RyR1-labelling, excluding areas of colocalisation < 0.125 μm^3, was then carried out. Fig. 4.19(v) shows a 3D representation of the positioning of each individual element of colocalisation, in yellow, measured within the cell in relation to the nucleus, following removal of all RyR1- and lysosomal-labelling which did not colocalise. Examination of labelled cells showed that there was a volume of 4.22 ± 1.15 μm^3 of colocalisation between lysosomal- and RyR1-labelling (n = 8; Appendix 2, Table 4.33). This equated to a density of 0.003 ± 0.0007 μm^3 of colocalisation per μm^3 of the cell volume (n = 8; Appendix 2, Table 4.33). The distribution of colocalisation between the perinuclear, extra-perinuclear and sub-plasmalemmal regions was then examined. Colocalisation between RyR1- and lysosomal-labelling was seen to occupy a volume of 1.91 ± 0.54 μm^3 in the perinuclear region of cells (n = 8; Appendix 2, Table 4.34), equating to a density of 0.0046 ± 0.0016 μm^3 of colocalisation per μm^3 of the region (n = 8; Fig. 4.20; Appendix 2, Table 4.34). The volume and the density of colocalisation between RyR1- and lysosomal-labelling were both seen to decline in the extra-perinuclear region. Thus, colocalisation was seen to occupy a volume of 0.9 ± 0.36 μm^3 in the extra-perinuclear region (n = 8, Appendix 2, Table 4.35), accounting for a density of 0.0018 ± 0.0007 μm^3 of colocalisation per μm^3 of the region (n = 8; Fig. 4.20; Appendix 2, Table 4.35). Both the volume and the density of colocalisation between RyR1- and lysosomal-labelling in the sub-plasmalemmal region appeared to be smaller than those observed in the extra-perinuclear region. Thus, colocalisation was seen to occupy a volume of 0.58 ± 0.17 μm^3 in the sub-plasmalemmal region, equating to a density of 0.0009 ± 0.0003 μm^3 of colocalisation per μm^3 of the region (n = 8; Fig. 4.20; Appendix 2, Table 4.36). Statistical analysis of the regional distribution of colocalisation between RyR1- and lysosomal-labelling showed that although the density of labelling appeared to decrease from the perinuclear region to the extra-perinuclear region of cells, this decrease was not seen to be

statistically significant (P > 0.05; Appendix 2, Table 4.37). However, the density of colocalisation between RyR1- and lysosomal-labelling within the perinuclear region of cells was significantly larger than the density of colocalisation observed in the sub-plasmalemmal region of cells (P ≤ 0.05; Appendix 2, Table 4.37).

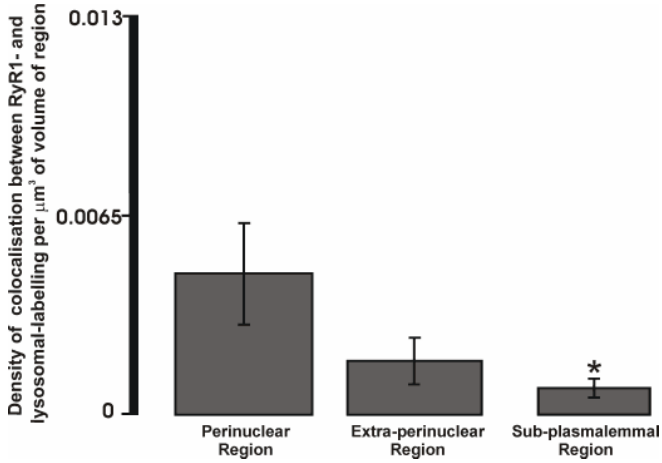

Fig. 4.20 **Comparison of the density (μm³ of labelling per μm³ of region) of colocalisation between RyR1- and lysosomal-labelling within the 3 regions of isolated pulmonary artery smooth muscle cells * indicates statistical difference (P = ≤ 0.05) when compared to the perinuclear region (n = 8).**

The mean volumes of individual elements of colocalisation between RyR1- and lysosomal-labelling were then examined. As described above, the larger the mean volumes of colocalisation within a given region is indicative of a greater degree of clustering of the two fluorescent labels within that region. Measurements of the mean volumes of colocalisation between RyR1- and lysosomal-labelling in the perinuclear region indicated that elements of colocalisation had a mean volume of 0.29 ± 0.04 μm^3 (n = 8; Fig. 4.21; Appendix 2, Table 4.34). The mean volumes of elements of colocalisation between RyR1- and lysosomal-labelling within the extra-perinuclear region were similar to those measured in the perinuclear region. Thus, the mean volume of elements of colocalisation in the extra-perinuclear region of cells was 0.29 ± 0.08 μm^3 (n = 8; Fig. 4.21; Appendix 2, Table 4.35). The smallest elements of colocalisation between RyR1- and lysosomal-labelling appeared to be located in the sub-plasmalemmal region, where the mean volume was

measured at 0.17 ± 0.04 μm^3 (n = 8; Fig. 4.21; Appendix 2, Table 4.36). However, statistical analysis of the mean volumes of colocalisation between RyR1- and lysosomal-labelling showed that there was no difference between the perinuclear, extra-perinuclear or sub-plasmalemmal regions (P = > 0.05; Appendix 2, Table 4.38). Therefore, although there was a greater density of colocalisation between RyR1- and lysosomal-labelling in the perinuclear than in the sub-plasmalemmal, there was little difference between the mean volumes of areas of colocalisation between the perinuclear, extra-perinuclear and sub-plasmalemmal regions.

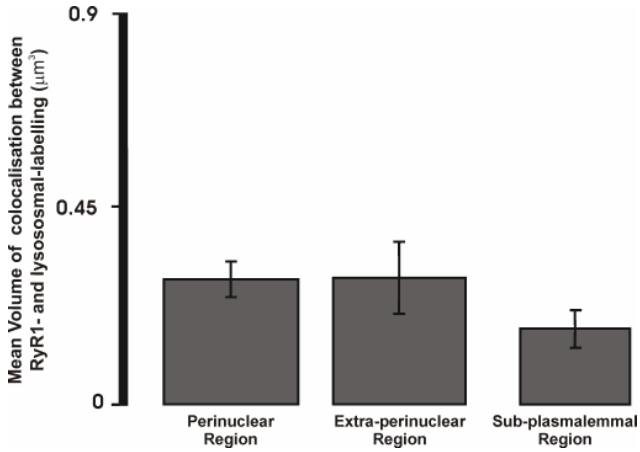

Fig. 4.21 **Comparison of the mean volume (μm^3) of colocalisation between RyR1- and lysosomal-labelling within the 3 regions of isolated pulmonary artery smooth muscle cells.**

4.2.4.2 Colocalisation between ryanodine receptor subtype 2- and lysosomal-labelling in pulmonary artery smooth muscle cells

Fig. 4.22(i) shows a transmitted light image of an isolated pulmonary artery smooth muscle cell. Fig. 4.22(ii) shows a 3D reconstruction of a series of deconvolved Z-sections (focal depth 0.28 μm, Z step 0.2 μm) obtained through the cell in (i), with the distribution of αlgp120-labelling in green and the DAPI labelled nucleus in blue. Fig. 4.22(iii) shows another 3D reconstruction of deconvolved Z-sections (focal depth 0.28 μm, Z step 0.2 μm) which shows the distribution of RyR2-labelling in the cell in red and the nucleus once again in blue. Deconvolved Z-sections through the cell were then superimposed upon

one another and a 3D reconstruction was produced, allowing for comparison of the distribution of lysosomal- and RyR2-labelling. This 3D reconstruction is

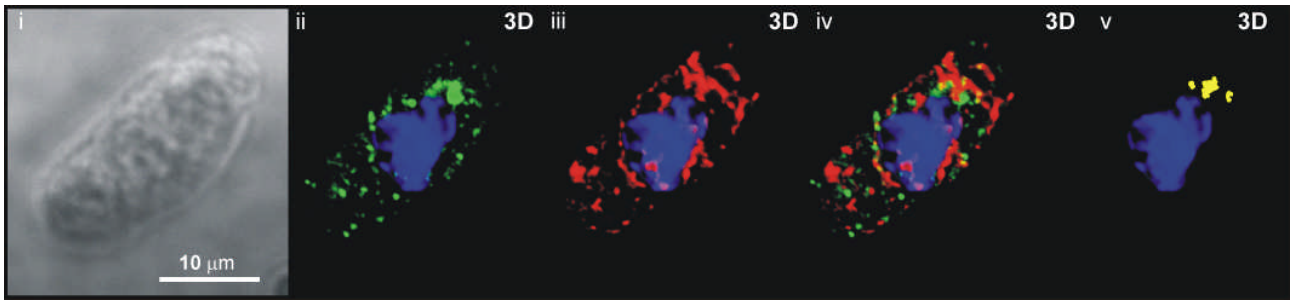

Fig. 4.22 **Visualisation of the colocalisation between RyR2- and lysosomal-labelling within an isolated pulmonary artery smooth muscle cell:** ***(i)*** transmitted light image of an isolated pulmonary artery smooth muscle cell. ***(ii)*** 3D reconstruction of a series of Z-sections (focal depth 0.28 μm, Z step 0.2 μm) obtained through the cell shown in ***(i)*** fluorescently labelled to show the distribution of lysosomal labelling and the nucleus in *green* and *blue*, respectively. ***(iii)*** 3D reconstruction of a series of Z-sections (focal depth 0.28 μm, Z step 0.2 μm) obtained through the cell shown in ***(i)*** fluorescently labelled to show the distribution of RyR2 labelling and the nucleus in *red* and *blue*, respectively.***(iv)*** 3D representation of the distribution of lysosomal- and RyR2-labelling in respect to the nucleus. Areas of colocalisation between lysosomal- and RyR2-labelling are shown in yellow. ***(v)*** individual volumes of colocalisation between lysosomal- and RyR2-labelling, ≥ 0.125 μm^3 (in *yellow*), in the cell shown in ***(i)***, in relation to the nucleus of the cell, shown in *blue*.

shown in Fig. 4.22(iv). Areas of colocalisation between lysosomal- and RyR2-labelling are visualised in yellow. Analysis of the colocalisation between lysosomal- and RyR2-labelling, excluding areas of colocalisation < 0.125 μm^3, was then carried out. Fig. 4.24(v) shows the positioning of each individual element of colocalisation, in yellow, in a 3D reconstruction measured within the cell in relation to the nucleus following removal of all RyR2- and lysosomal-labelling which did not colocalise. Volumetric analysis indicated there was a volume of 4.94 ± 0.81 μm^3 of colocalisation between lysosomal- and RyR2-labelling in cells (n = 8; Appendix 2, Table 4.39), equating to a density of 0.0038 ± 0.0012 μm^3 of colocalisation per μm^3 of the cell volume (n = 8; Appendix 2, Table 4.39). Following this, the regional distribution of colocalisation within cells was examined. Colocalisation between RyR2- and lysosomal-labelling occupied a volume of 2.16 ± 0.43 μm^3 in the perinuclear

region of cells (n = 8; Appendix 2, Table 4.40). This equated to a density of 0.0053 ± 0.0016 μm^3 of colocalisation per μm^3 of the region (n = 8; Fig. 4.23; Appendix 2, Table 4.40). Although the volume of colocalisation between RyR2- and lysosomal-labelling appeared to be comparable between the perinuclear and extra-perinuclear regions, there appeared to be an increase in the density of colocalisation within the region. Thus, while colocalisation occupied a volume of 2.33 ± 0.79 μm^3 in the extra-perinuclear region (n = 8, Appendix 2, Table 4.41), this accounted for a density of 0.0071 ± 0.0031 μm^3 of colocalisation per μm^3 of the region (n = 8; Fig. 4.23; Appendix 2, Table 4.41). There was, however, a marked decline in both the volume and density of colocalisation observed between RyR2- and lysosomal-labelling in the sub-plasmalemmal region, where colocalisation accounted for a volume of 0.42 ± 0.18 μm^3, and a density of 0.0007 ± 0.0002 μm^3 of colocalisation per μm^3 of the region (n = 8; Fig. 4.23; Appendix 2, Table 4.42). Statistical analysis indicated that although there appeared to be an increase in the density of colocalisation between RyR2- and lysosomal-labelling from the perinuclear to the extra-perinuclear region. However, this increase was not statistically significant (P = > 0.05; Appendix 2, Table 4.43), this was most likely due to the large degree of variation between the extent of colocalisation between RyR2- and lysosomal-labelling within this region (Appendix 2, Table 4.41).

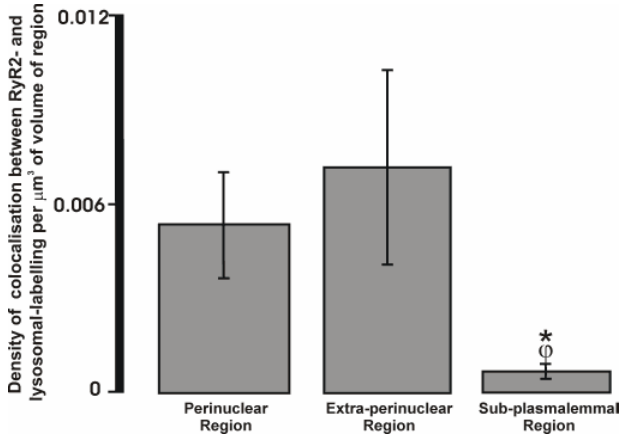

Fig. 4.23 **Comparison of the density (μm^3 of labelling per μm^3 of region) of colocalisation between RyR2- and lysosomal-labelling within the 3 regions of isolated pulmonary artery smooth muscle cells. * indicates statistical difference (P = ≤ 0.05) when compared to the perinuclear region. φ indicates statistical difference (P = ≤ 0.05) when compared to the extra-perinuclear region (n = 8).**

However, the density of labelling within the sub-plasmalemmal region of cells was significantly lower than that measured in either the perinuclear ($P = \leq 0.05$; Appendix 2, Table 4.43) or the extra-perinuclear region ($P = \leq 0.05$; Appendix 2, Table 4.43). Therefore, RyR2- and lysosomal-labelling colocalised to a greater extent within the perinuclear and extra-perinuclear region of pulmonary artery smooth muscle cells.

To examine the degree to which RyR2- and lysosomal-labelling formed clusters of colocalisation, the mean volume of colocalisation was determined. In the perinuclear region, elements of colocalisation had a mean volume of 0.39 ± 0.07 μm^3 (n = 8; Fig. 4.24; Appendix 2, Table 4.40). There was little difference between the mean volume of elements of colocalisation of RyR2- and lysosomal-labelling between the extra-perinuclear region and perinuclear region. Thus, the mean volume of elements of colocalisation in the extra-perinuclear region of cells was 0.47 ± 0.2 μm^3 (n = 8; Fig. 4.24; Appendix 2, Table 4.41). However, the mean volume of elements of colocalisation decreased markedly in the sub-plasmalemmal region of cells, where the mean volume of colocalisation was 0.18 ± 0.05 μm^3 (n = 8; Fig. 4.24; Appendix 2, Table 4.42). Statistical analysis of the mean volumes of colocalisation between

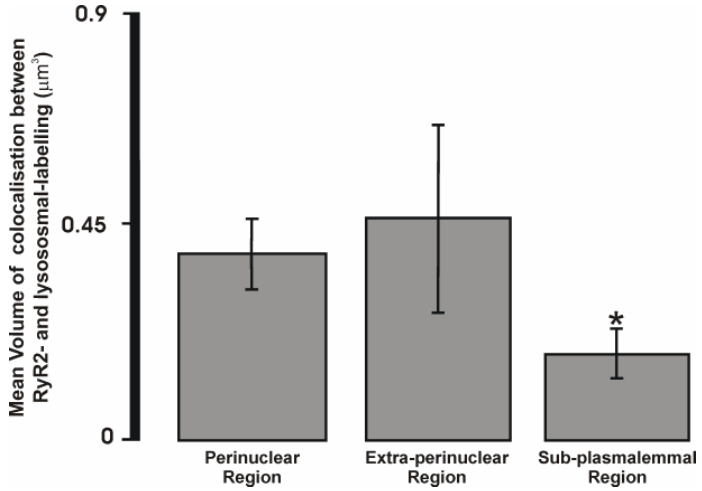

Fig. 4.24 **Comparison of the mean volume (μm^3) of colocalisation between RyR2- and lysosomal-labelling within the 3 regions of isolated pulmonary artery smooth muscle cells. * indicates statistical difference ($P = \leq 0.05$) when compared to the perinuclear region (n = 8).**

RyR2- and lysosomal-labelling showed that, in a similar manner to the density of colocalisation, there was no difference between the mean volume of colocalisation in the perinuclear and extra-perinuclear regions (P = > 0.05; Appendix 2, Table 4.44). However, although the mean volume of colocalisation in the extra-perinuclear region of cells appeared greater than that measured in the sub-plasmalemmal region, the difference between these values was not significant (P = > 0.05; Appendix 2, Table 4.44). Therefore, RyR2- and lysosomal-labelling formed larger clusters of labelling in the perinuclear region of cells than in the sub-plasmalemmal region.

4.2.4.3 Colocalisation between ryanodine receptor subtype 3- and lysosomal-labelling in pulmonary artery smooth muscle cells

Fig. 4.25(i) shows a transmitted light image of an isolated pulmonary artery smooth muscle cell. Fig. 4.25(ii) shows a 3D reconstruction of a series of deconvolved Z-sections (focal depth 0.28 μm, Z step 0.2 μm) obtained through the cell, with the distribution of αlgp120-labelling in green and the DAPI labelled nucleus in blue. A second 3D reconstruction of a deconvolved Z-series obtained through this cell is shown in Fig. 4.25(iii), where the distribution of RyR3-labelling in the cell is visualised in red, while the nucleus is, visualised in blue. Deconvolved Z-sections through the cell were then superimposed upon one another and a 3D reconstruction was produced to enable comparison between the distributions of lysosomal- and RyR3-labelling, as represented in Fig. 4.25(iv). Areas of colocalisation are visualised in Yellow. Fig. 4.25(v) indicates the position of each individual element of colocalisation measured from the cell, in yellow, in a 3D reconstruction measured within the cell in relation to the nucleus following removal of all non-colocalised lysosomal- and RyR3-labelling. This analysis indicated a volume of 8.21 ± 1.44 μm^3 of colocalisation between lysosomal- and RyR3-labelling in cells (n = 8; Appendix 2, Table 4.45), equating to a density of 0.005 ± 0.0008 μm^3 of colocalisation per μm^3 of the cell volume (n = 8; Appendix 2, Table 4.45). The regional distribution of areas of colocalisation between lysosomal- and RyR3-

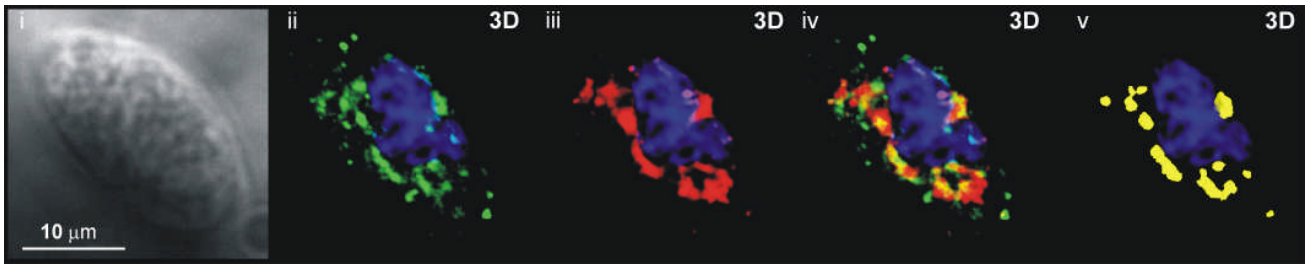

Fig. 4.25 **Visualisation of the colocalisation between RyR3- and lysosomal-labelling within an isolated pulmonary artery smooth muscle cell:** ***(i)*** transmitted light image of an isolated pulmonary artery smooth muscle cell. ***(ii)*** 3D reconstruction of a series of Z-sections (focal depth 0.28 μm, Z step 0.2 μm) obtained through the cell shown in ***(i)*** fluorescently labelled to show the distribution of lysosomal labelling and the nucleus in *green* and *blue*, respectively. ***(iii)*** 3D reconstruction of a series of Z-sections (focal depth 0.28 μm, Z step 0.2 μm) obtained through the cell shown in ***(i)*** fluorescently labelled to show the distribution of RyR3 labelling and the nucleus in *red* and *blue*, respectively.***(iv)*** 3D representation of the distribution of lysosomal- and RyR3-labelling in respect to the nucleus. Areas of colocalisation between lysosomal- and RyR3-labelling are shown in yellow. ***(v)*** individual volumes of colocalisation between lysosomal- and RyR3-labelling, ≥ 0.125 μm^3 (in *yellow*), in the cell shown in ***(i)***, in relation to the nucleus of the cell, shown in *blue*.

labelling within cells was then examined. Colocalisation between RyR3- and lysosomal-labelling occupied a volume of 6.85 ± 1.23 μm^3 in the perinuclear region (n = 8; Appendix 2, Table 4.46). This equated to a density of 0.011 ± 0.0015 μm^3 of colocalisation per μm^3 of the region (n = 8; Fig. 4.26; Appendix 2, Table 4.46). There was a sharp decrease in the incidence of colocalisation between lysosomal- and RyR3-labelling in the extra-perinuclear region where both the volume and density of colocalisation were more than 3-fold lower than those measured in the perinuclear region. Indeed, within the extra-perinuclear region, colocalisation occupied a volume of 1.19 ± 0.56 μm^3 (n = 8, Appendix 2, Table 4.47), accounting for a density of 0.0033 ± 0.0016 μm^3 of colocalisation per μm^3 of the region (n = 8; Fig. 4.26; Appendix 2, Table 4.47). There appeared to be a further decline in both the volume and density of colocalisation in the sub-plasmalemmal region of cells, where colocalisation was measured at a volume of 0.099 ± 0.078 μm^3, and a density of 0.0002 ± 0.0002 μm^3 of colocalisation per μm^3 of the region (n = 8; Fig. 4.26; Appendix 2, Table 4.48). Statistical analysis confirmed that there was a much greater

density of colocalisation between RyR3- and lysosomal-labelling in the perinuclear region of cells than was observed in either the extra-perinuclear (P = ≤ 0.05; Appendix 2, Table 4.49) or the sub-plasmalemmal regions (P = ≤ 0.05; Appendix 2, Table 4.49).

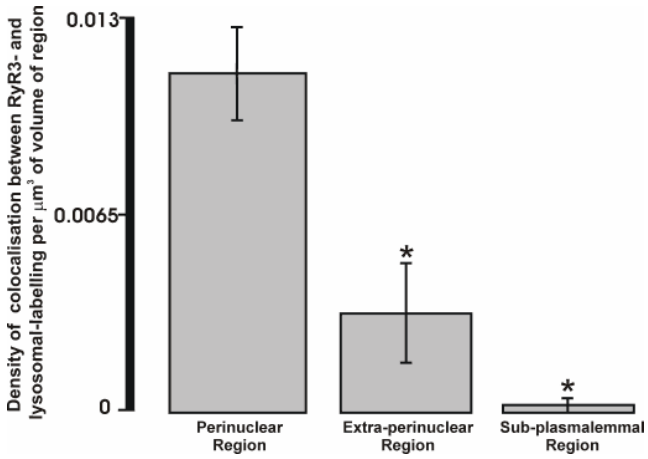

Fig. 4.26 **Comparison of the density (μm^3 of labelling per μm^3 of region) of colocalisation between RyR3- and lysosomal-labelling within the 3 regions of isolated pulmonary artery smooth muscle cells. * indicates statistical difference (P = ≤ 0.05) when compared to the perinuclear region (n = 8).**

Examination of the mean volume of colocalisation between RyR3- and lysosomal-labelling, indicative of the size of clusters of colocalisation, was then carried out. Measurements of the mean volumes of colocalisation between RyR3- and lysosomal-labelling in the perinuclear region indicated that elements of colocalisation had a mean volume of 0.68 ± 0.11 μm^3 (n = 8; Fig. 4.27; Appendix 2, Table 4.46). There appeared to be a decline in the mean volume of areas of colocalisation in the extra-perinuclear region, where the mean volume of colocalisation was 0.4 ± 0.1 μm^3 (n = 8; Fig. 4.27; Appendix 2, Table 4.47). Furthermore, there was a greater than 10-fold decrease in the mean volume of colocalisation in the sub-plasmalemmal region of cells, where the mean volume of colocalisation was 0.034 ± 0.02 μm^3 (n = 8; Fig. 4.27; Appendix 2, Table 4.48). Statistical analysis of the mean volume of colocalisation between RyR3- and lysosomal-labelling showed that although there appeared to be a decrease in mean volume of colocalisation between the perinuclear and extra-perinuclear region of cells, this difference was not statistical significant (P = > 0.05; Appendix 2, Table 4.50). However, the mean

volume of colocalisation between RyR3- and lysosomal-labelling in the sub-plasmalemmal region was significantly smaller than in either the perinuclear region (P = ≤ 0.05; Appendix 2, Table 4.50) or the extra-perinuclear regions (P = ≤0.05; Appendix 2, Table 4.50). These findings suggest that, not only did colocalisation between RyR3- and lysosomal-labelling predominate in the perinuclear region of cells, but areas of colocalisation were much larger in this region of cells than were observed in the extra-perinuclear or sub-plasmalemmal regions.

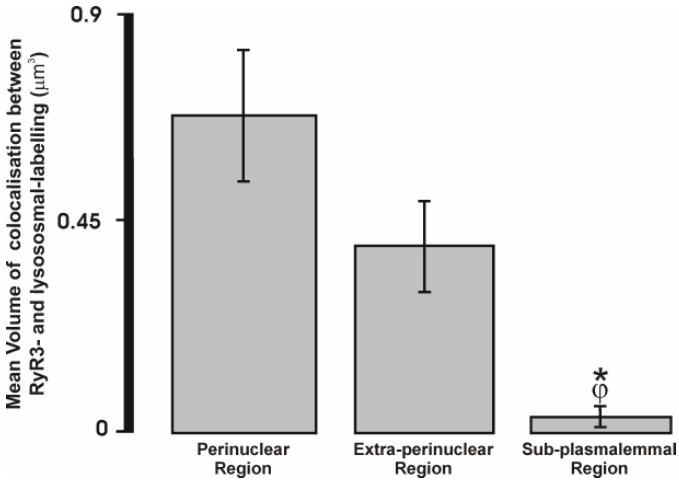

Fig. 4.27 **Comparison of the mean volume (μm^3) of colocalisation between RyR3- and lysosomal-labelling within the 3 regions of isolated pulmonary artery smooth muscle cells. * indicates statistical difference (P = ≤ 0.05) when compared to the perinuclear region. φ indicates statistical difference (P = ≤ 0.05) when compared to the extra-perinuclear region (n = 8).**

4.2.4.4 Comparison of the spatial distribution of colocalisation between lysosomal- and ryanodine receptor subtype-labelling in pulmonary artery smooth muscle cells

A direct comparison of the distribution of areas of colocalisation between the three subtypes of RyR- and lysosomal-labelling in the perinuclear, extra-perinuclear and sub-plasmalemmal regions of cells is shown in the bar chart in Fig. 4.28. The density of colocalisation between the different RyR subtypes and lysosomes in the perinuclear region of cells indicated that there was a considerably greater density of colocalisation observed between RyR3-

and lysosomal-labelling than was observed for either RyR2- and lysosomal-labelling (P = ≤ 0.05, Appendix 2, Table 4.51) or RyR1- and lysosomal-labelling (P = ≤ 0.05, Appendix 2, Table 4.51). Therefore, lysosomes colocalise with RyR3 to a greater extent than with either RyR2 or RyR1 in the perinuclear region of cells.

There was a marked decline in the colocalisation between RyR3- and lysosomal-labelling in the extra-perinuclear region, where the density of colocalisation was not seen to differ from the density of colocalisation between lysosomal labelling and labelling of either RyR2 or RyR1 (P > 0.05; Appendix 2, Table 4.52). Furthermore, there was no statistical difference between the density of colocalisation between lysosomal labelling and labelling for either

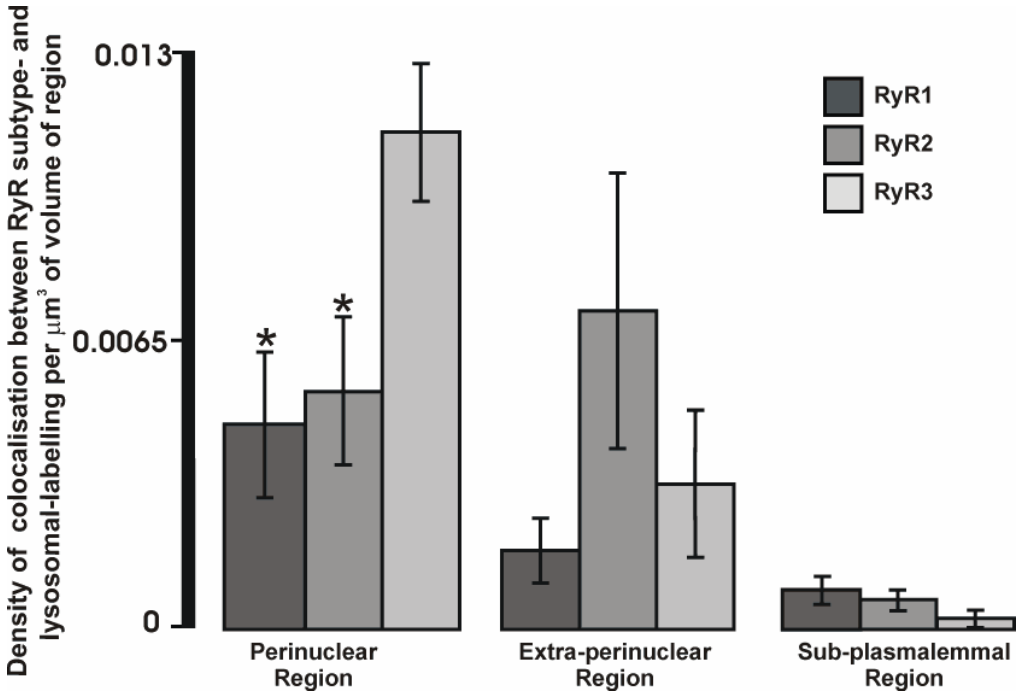

Fig. 4.28 **Comparison of the density (μm³ of colocalisation per μm³ of region) of colocalisation between RyR subtype- and lysosomal-labelling within the 3 regions of isolated pulmonary artery smooth muscle cells. * indicates statistical difference (P = ≤ 0.05) when compared to the density of colocalisation between RyR3- and lysosomal-labelling in the perinuclear region (n = 8 for each RyR subtype).**

RyR1 or RyR2 within this region (P > 0.0.5; Appendix 2, Table 4.52). Thus, lysosomes associate with all 3 RyR subtypes to a similar degree within the extra-perinuclear region of cells. Furthermore, there was little variation between the densities of colocalisation measured between lysosomal labelling

and labelling of RyR1, RyR2 or RyR3 in the sub-plasmalemmal region ($P > 0.05$; Appendix 2, Table 4.53).

Differences among the mean volume of areas of colocalisation between lysosomal labelling, and the labelling of the 3 RyR subtypes in the 3 defined regions of the cell is shown in Fig. 4.29. The mean volume of colocalisation between RyR3- and lysosomal-labelling in the perinuclear region of cells appeared to be greater than the mean volume of colocalisation between lysosomal labelling and labelling of either RyR2 or RyR1. Indeed, statistical analysis of the mean volume of colocalisation RyR3- and lysosomal-labelling was significantly larger than that of colocalisation between RyR1- and lysosomal-labelling ($P = \leq 0.05$; Appendix 2, Table 4.54). Although the mean volume of colocalisation between RyR3- and lysosomal-labelling in the perinuclear region of cells appeared to be larger than the mean volume of colocalisation between RyR2- and lysosomal-labelling in this region, this difference did not appear to be statistically significant ($P = > 0.05$; Appendix 2, Table 4.54).

Examination of the mean volumes of colocalisation between RyR1-, RyR2-, RyR3- and lysosomal-labelling in the extra-perinuclear region of cells indicated that there was no statistical difference between the mean volume of colocalisation within this region ($P > 0.05$; Appendix 2, Table 4.55).

Furthermore, in the sub-plasmalemmal region of cells there was no difference between the mean volume of areas of colocalisation between RyR1- and lysosomal-labelling and the mean volume of areas of colocalisation between RyR2- and lysosomal-labelling ($P > 0.05$; Appendix 2, Table 4.56). However, the mean volume of colocalisation between RyR3- and lysosomal-labelling was significantly smaller than the mean volume of colocalisation between either RyR2- and lysosomal-labelling or RyR1- and lysosomal-labelling in the sub-plasmalemmal region of cells ($P = < 0.05$; Appendix 2, Table 4.56). Thus, it would appear that areas of colocalisation between RyR3- and lysosomal-labelling are marginally smaller than those areas of colocalisation between RyR2- and lysosomal-labelling or RyR1- and lysosomal-labelling.

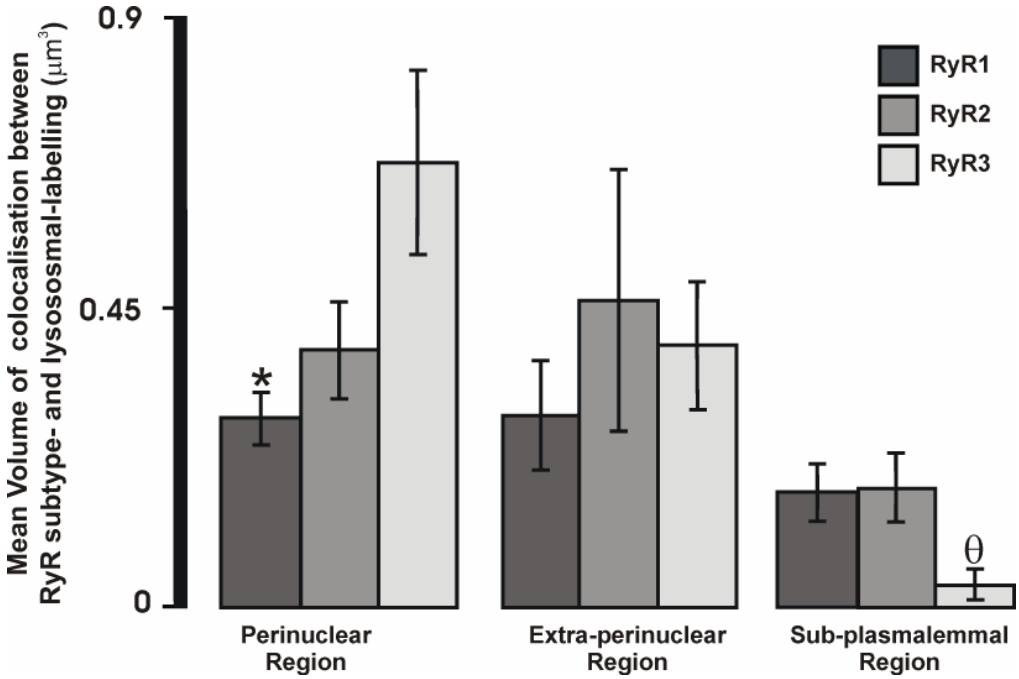

Fig. 4.29 **Comparison of the mean volume (μm^3) of individual elements of colocalisation between RyR subtype- and lysosomal-labelling within the 3 regions of isolated pulmonary artery smooth muscle cells. * indicates statistical difference (P = ≤ 0.05) when compared to the density of RyR3- and lysosomal-labelling in the perinuclear region. θ indicates statistical difference (P = ≤ 0.05) when compared to RyR1- and lysosomal-labelling and RyR2- and lysosomal-labelling in the sub-plasmalemmal region (n = 8 for each RyR subtype).**

In conclusion, these findings indicate that labelling for all 3 RyR subtypes colocalise with labelling of the lysosomal membrane glycoprotein αlgp120, and therefore lysosomes, to some extent in pulmonary artery smooth muscle. It was also clear from these data that colocalisation was evident within the perinuclear, extra-perinuclear and sub-plasmalemmal regions. However, volumetric analysis of the colocalisation between RyR subtypes and lysosomes clearly demonstrated that lysosomes colocalised with portions of the SR expressing RyR3 to a much greater extent than portions of the SR expressing either RyR1, or RyR2. Also, the mean volume of individual elements of colocalisation between RyR3 and lysosomes was larger than those observed between lysosomes and RyR1, or RyR2. Furthermore, out with the perinuclear region, both the density and mean volume of elements of colocalisation between lysosomes and the three RyR subtypes were lower than was measured between lysosomes and RyR3 within the perinuclear region of cells. These data

would, therefore, suggest that the trigger zone for Ca^{2+} signalling by NAADP may be formed between lysosomal clusters closely associated with sections of the SR expressing dense clusters of RyR3.

If this proposed model of a trigger zone for Ca^{2+} signalling by NAADP is indeed accurate, then the close association between RyRs and lysosomes will be important in the initiation of global Ca^{2+} signals. However, any measure of colocalisation between the fluorescent labelling of RyR subtypes and αlgp120 must ultimately be an underestimate of the true extent of colocalisation between areas of lysosomal membrane containing the NAADP receptor and areas of the SR containing RyRs. This must be the case, given that the fluorescent labelling of αlgp120 is merely an indicator of the spatial distribution of a single membrane glycoprotein that is likely to be unrelated to the NAADP receptor and will occupy only a fraction of the area of the lysosomal membrane. Thus, I examined the degree to which lysosomes were associated with areas of RyR subtype labelling. As free Ca^{2+} ions have been estimated to diffuse for maximum distance of less than 5 μm in the cytoplasm of cells (Allbritton *et al.*, 1992), I examined only elements of fluorescent labelling located within the immediate vicinity of the area of colocalisation, in an attempt to identify if there was any structural element underpinning the trigger zone. In order to achieve this I measured the volume of fluorescent labelling of a given RyR subtype and labelling of lysosomes located within ~1 μm, in the X-, Y- and Z-planes, of large areas of colocalisation (> 0.5 μm^3).

4.2.4.5 Volume of labelling associated with colocalisation between ryanodine receptor subtypes and lysosomes

In order to examine the degree to which lysosomes associate with the 3 different RyR subtypes, Volocity software (Improvision, UK) was used to identify all regions of colocalisation ≥ 0.5 μm^3 in the perinuclear region of each cell. Once an area of colocalisation had been identified (Fig. 4.30A), its dimensions were measured in the X-, Y- and Z- planes (Fig. 4.30B). These

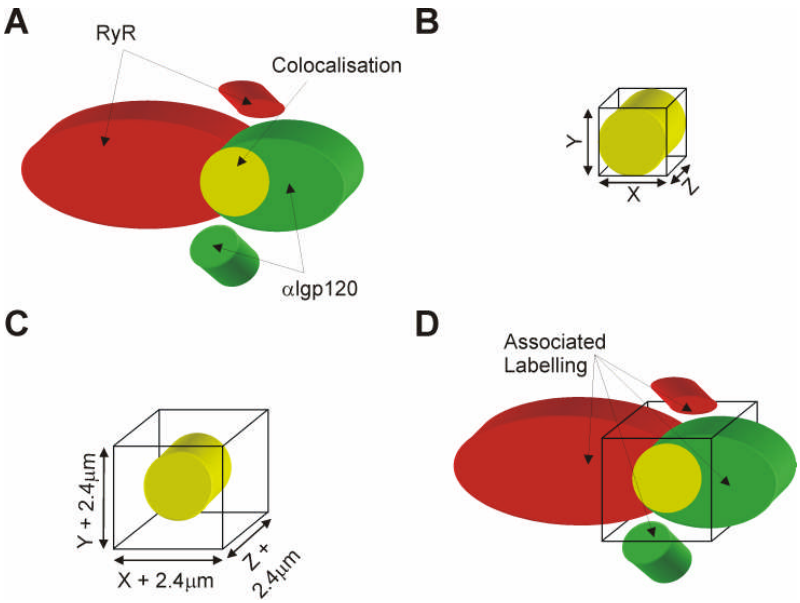

Fig. 4.30 **Volumetric analysis of fluorescent labelling associated with large areas of colocalisation:** ***A:*** An area of colocalisation (Yellow) between RyR-labelling (Red) and αlgp120-labelling (Green) ≥ 0.5 μm^3 was identified in the perinuclear region of cells. ***B:*** following identification, the dimensions of the area of colocalisation were identified in the X-, Y- and Z- planes. ***C:*** These measurements were used to construct a region of interest (ROI) around the area of colocalisation with dimensions ~2.4 μm^3 longer in the X-, Y- and Z- planes than the area of colocalisation. ***D:*** Following construction of the ROI, the volume of all the fluorescent labelling closely associated with the ROI and, therefore, the area of colocalisation were measured.

measurements were used to create an ROI around the area of colocalisation with X-, Y- and Z- dimensions that were ~2.4 μm longer in each of the planes than was measured for the area of colocalisation (Fig. 4.30C). Volume measurements were then obtained of all RyR- or αlgp120-labelling which encroached within the area of the ROI, thus giving a measure of the fluorescent labelling 'associated' with colocalisation (Fig. 4.30D, Appendix 2, Tables 4.57, 4.58 and 4.59).

An example of the determination of fluorescent labelling associated with an area of colocalisation ≥ 0.5 μm^3 is shown in Fig. 4.31. Fig. 4.31A shows a 3D reconstruction of an isolated pulmonary artery smooth muscle cell labelled to show the spatial distribution of αlgp120-labelling (Green), RyR3-

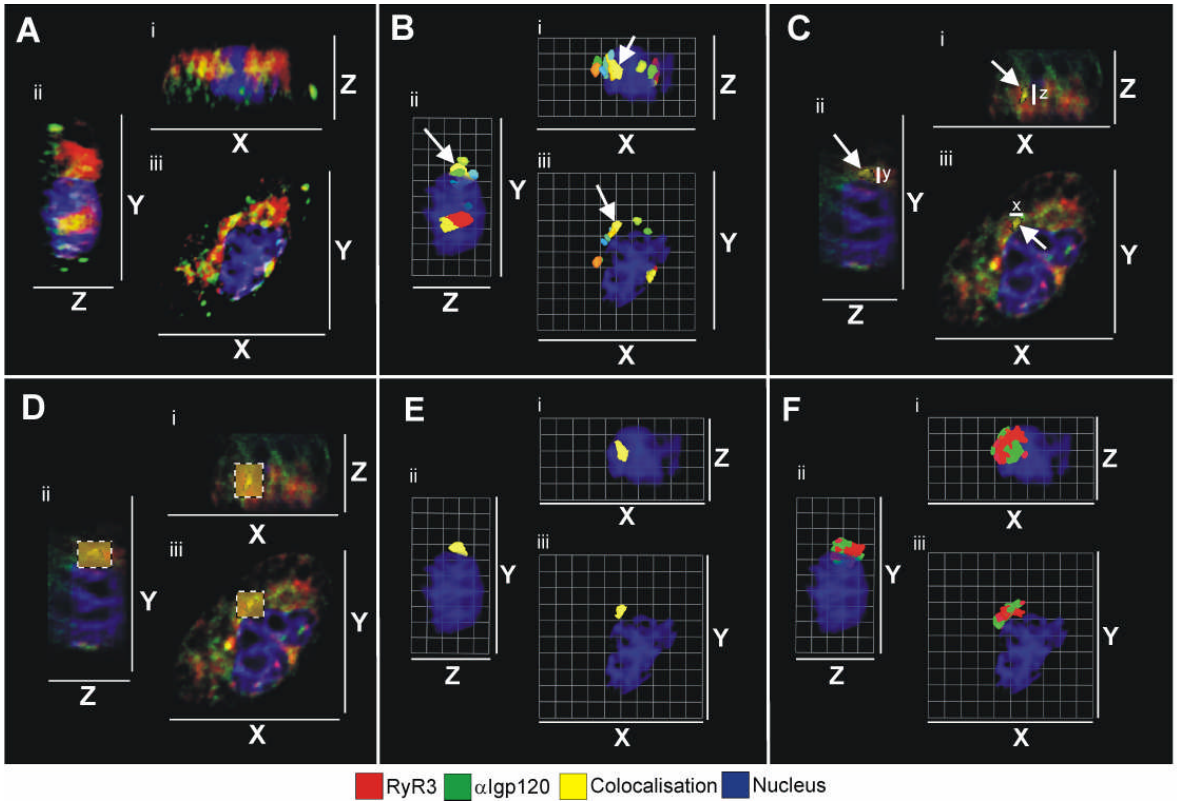

Fig. 4.31 **Representation of the analysis carried out to determine fluorescent labelling closely associated with RyR- and lysosomal-labelling in pulmonary artery smooth muscle cells:** ***A*** 3-dimensional reconstruction of an isolated pulmonary artery smooth muscle cell fluorescently labelled to show the distribution of ryanodine receptor subtype 3 (RyR3), *red*; the distribution of αlgp120, in *green* and the nucleus of the cell, in *blue*. Colocalisation between RyR3 and αlgp120 is shown in *yellow*. ***A(i)*** shows the cell in the X – Z plane as looking down the Y-plane. ***A(ii)*** shows the cell in the Z – Y plane as looking down the X-plane. ***A(iii)*** shows the cell in the X – Y plane as looking down the Z-plane. ***B*** shows the same isolated pulmonary artery smooth muscle cell. The nucleus is indicated as in ***A***. RyR3 and αlgp120 that was not colocalised within the cell has been removed leaving only areas of colocalisation ≥ 0.5 μm^3 within the perinuclear region of the cell. These areas are indicated in different colours to easily identify spatially distinct areas of colocalisation within the cell. The box units in ***B*** are 2.2 x 2.2 μm. ***B(i)***, ***(ii)*** and ***(iii)*** show the cell looking down the Y-, X- and Z-planes, respectively. ***C*** shows the cell in the same planes as ***A***. RyR3- and αlgp120-labelling is shown uncorrected for background fluorescence. An area of colocalisation ≥ 0.5 μm^3 measured in the perinuclear region of the cell is shown as the solid area of yellow, indicated by the arrows in ***(i)***, ***(ii)*** and ***(iii)***. Line Z in ***(i)*** indicates the distance measured in the Z-plane of the colocalised area for use in constructing a region of interest (ROI) in order to determine the closely associated areas of fluorescent labelling. Line Y in ***(ii)*** shows the distance measured for the area of colocalisation in the Y-plane used for ROI measurements. Line X in ***(iii)*** show the distance measured for the area of colocalisation in the X-Plane used for ROI measurements. ***D*** shows the same images of the cell as ***C*** following the construction of an ROI (orange) around the area of colocalisation indicated in ***C***. ***D(i)***, ***(ii)*** and ***(iii)*** show the cell looking down the Y-, X- and Z-planes, respectively. ***E*** Shows a 3D reconstruction of the isolated pulmonary artery smooth muscle cell**.** The nucleus of the cell is indicated in blue. All RyR3- and αlgp120-labelling has been removed to leave the area of perinuclear colocalisation as indicated in **Fig. 4.33*B***, shown in yellow. ***E(i)*** shows the cell in the X – Z plane as looking down the Y-plane. ***E(ii)*** shows the cell in the Z – Y plane as looking down the X-plane. ***E(iii)*** shows the cell in the X – Y plane as looking down the Z-plane. ***F*** shows the same isolated pulmonary artery smooth muscle cell. The nucleus of the cell is indicated as in ***A***. The volumes of RyR3- and αlgp120-labelling closely associated with the area of colocalisation shown in ***E*** are shown in red and green, respectively. ***F(i)***, ***(ii)*** and ***(iii)*** show the cell looking down the Y-, X- and Z-planes, respectively.

labelling (Red) and DAPI-labelling of the nucleus (Blue). Areas of colocalisation between RyR3- and αlgp120-labelling are shown in yellow. Each panel in Fig.4.31 shows three views of the cell; (i) a view of the cell looking along the Y-plane, therefore the X- and Z-planes are visible; (ii) a view looking along the X-plane, thus, the Y- and Z-planes are visible; (iii) a view looking along the Z-plane, in this image the X- and Y-planes are visible. Fig. 4.31B shows a visual representation of each of the areas of colocalisation between RyR3- and αlgp120- labelling ≥ 0.5 μm^3 in volume located within the perinuclear region of the cell. Each of these individual volumes of colocalisation is visualised in different colours to allow easy identification. Fig. 4.31B – F show the determination of the fluorescent labelling associated with the area of colocalisation indicated by the arrows in Fig. 4.31B(i, ii and iii). Fig. 4.31C shows this area of colocalisation in relation to the RyR3-, αlgp120- and DAPI-labelling in sections taken through the Y- (i), X- (ii) and Z-planes (iii), respectively, at the mid-point through the area of colocalisation. These images are uncorrected for background fluorescence. Fig. 4.31C (i, ii and iii) shows the dimensions of the area of colocalisation in the X-, Y- and Z-planes used to construct the ROI to measure fluorescent labelling associated with colocalisation, as indicated by white lines. Fig. 4.31D shows the ROI constructed to measure the volumes of fluorescent labelling associated with this area of colocalisation, while Fig. 4.31E shows the same area of perinuclear colocalisation between RyR3- and αlgp120-labelling, in relation to the nucleus following removal of all other fluorescent labelling. Following measurement, the labelling of RyR3 (red) and αlgp120 (green) associated with this area of colocalisation are shown in Fig. 4.31F.

All 8 cells labelled to show the distribution of RyR3- and αlgp120-labelling displayed areas of colocalisation ≥ 0.5 μm^3 within the perinuclear region, with 4.63 ± 1.07 areas per cell (Fig. 4.32; Appendix 2, Table 4.60). Conversely, only 4 of 8 cells with RyR1- and αlgp120-labelling displayed areas of colocalisation in the perinuclear region of cells with 0.75 ± 0.5 areas per cell (Fig. 4.32; Appendix 2, Table 4.60) and 6 of 8 cells with RyR2- and αlgp120-labelling displaying areas of colocalisation ≥ 0.5 μm^3 in this region,

averaging 1.25 ± 0.37 areas per cell (Fig. 4.32; Appendix 2, Table 4.60). Therefore, cells labelled to show the distribution of RyR3- and αlgp120-labelling displayed significantly more areas of colocalisation ≥ 0.5 μm^3 in the perinuclear region of cells than did in cells labelled to show the distribution of RyR1- and αlgp120-labelling (P = ≤ 0.05; Appendix 2, Table 4.61) or cells labelled to show the distribution of RyR2- and αlgp120-labelling (P = ≤ 0.05; Appendix 2, Table 4.61).

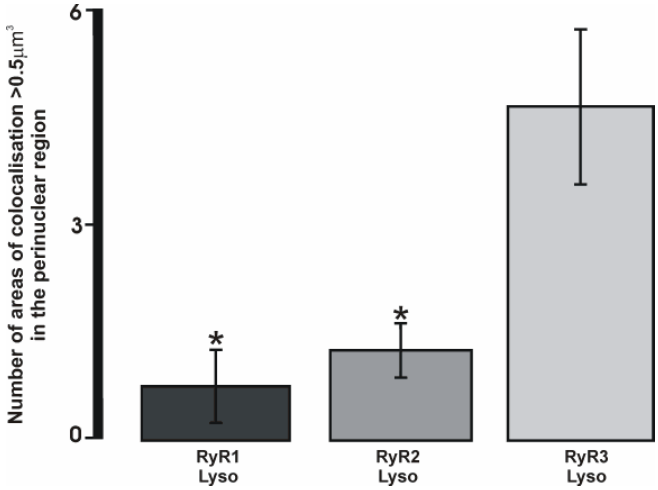

Fig. 4.32 **Comparison of the number of areas of colocalisation ≥ 0.5 μm^3 in the perinuclear region of cells. * indicates statistical difference (P = ≤ 0.05) when compared to the number of areas of colocalisation ≥ 0.5 μm^3 between RyR3- and lysosomal-labelling in the perinuclear region (n = 8 for each RyR subtype- and lysosomal-labelling).**

Although there was a marked difference between the number of areas of colocalisation ≥ 0.5 μm^3 between the different RyR subtypes and lysosomal labelling, there was little difference between the total volumes of fluorescent labelling associated with these areas of colocalisation. Thus, volumetric examination of cells showed that there was 21.64 ± 7.99 μm^3 of fluorescent labelling associated with areas of colocalisation between RyR1- and αlgp120-labelling ≥ 0.5 μm^3 (Appendix 2, Table 4.57), while there was 21.28 ± 1.17 μm^3 of labelling associated with areas of RyR2- and αlgp120-labelling ≥ 0.5 μm^3 (Appendix 2, Table 4.58), and 24.08 ± 1.78 μm^3 of labelling associated with areas of colocalisation between RyR3- and αlgp120-labelling ≥ 0.5 μm^3 (Appendix 2, Table 4.59). Indeed, statistical analysis confirmed that the

differences between the total volumes of fluorescent labelling associated with areas of colocalisation were not significant ($P > 0.05$; Appendix 2, Table 4.62).

However, an examination of the total fluorescent labelling associated with areas of colocalisation $\geq 0.5\ \mu m^3$ may mask differences in the extent of RyR subtype and lysosomal clustering around areas of colocalisation. I therefore proceeded to examine the association of fluorescent labelling of each of the 3 different RyR subtypes with areas of colocalisation $\geq 0.5\ \mu m^3$. Furthermore, I also examined the extent to which lysosomes associated with large areas of colocalisation between lysosomal-labelling and labelling of each of the 3 RyR subtypes.

Examination of the RyR1 labelled cells indicated that there was $17.87 \pm 7.84\ \mu m^3$ of RyR1 labelling associated with areas of colocalisation between RyR1- and lysosomal-labelling (Appendix 2, Table 4.57). In RyR2 labelled cells there appeared to be less of an association of RyR2 labelling with areas of colocalisation between RyR2- and lysosomal-labelling. In these cells the volume of RyR2 labelling associated with areas of colocalisation was $12.47 \pm 1.39\ \mu m^3$ (Appendix 2, Table 4.58). Similar to observations in RyR2 labelled cells, in cells labelled to show the distribution of RyR3 and lysosomes, a volume of $13.38 \pm 1.18\ \mu m^3$ of RyR3 labelling was associated with areas of colocalisation between RyR3- and lysosomal-labelling (Appendix 2, Table 4.59). Although the volume of RyR2- and RyR3-labelling associated with areas of colocalisation between the respective RyR subtypes and lysosomal labelling appeared to be slightly less than the volume detected in RyR1 labelled cells, these differences in volume were not seen to have any statistical significance ($P > 0.05$; Appendix 2, Table 4.63).

There were, however, marked differences in the extent to which lysosomes were associated with areas of colocalisation between labelling of the 3 different RyR subtypes and lysosomes. In cells labelled to show the distribution of RyR3 and lysosomes, it was noted that $11.41 \pm 1.29\ \mu m^3$ of lysosomal labelling was associated with areas of colocalisation between RyR3- and lysosomal-labelling $\geq 0.5\ \mu m^3$ in volume (Fig. 4.33; Appendix 2, Table 4.59). Interestingly, there was a smaller volume of lysosomal labelling associated with areas of colocalisation between RyR2- and lysosomal-labelling

than was observed in RyR3 labelled cells. Thus, 8.81 ± 1.28 μm^3 of lysosomal labelling was associated with areas of RyR2 and lysosomal colocalisation (Fig. 4.33; Appendix 2, Table 4.58). There was a further decrease in the volume of lysosomal labelling associated with areas of colocalisation between RyR1- and lysosomal-labelling ≥ 0.5 μm^3 in volume, measuring only 3.78 ± 1.04 μm^3 (Fig 4.33; Appendix 2, Table 4.57). Statistical analysis of the volume of associated lysosomal labelling with areas of colocalisation between a given RyR subtype- and lysosomal-labelling confirmed that there was a significantly smaller

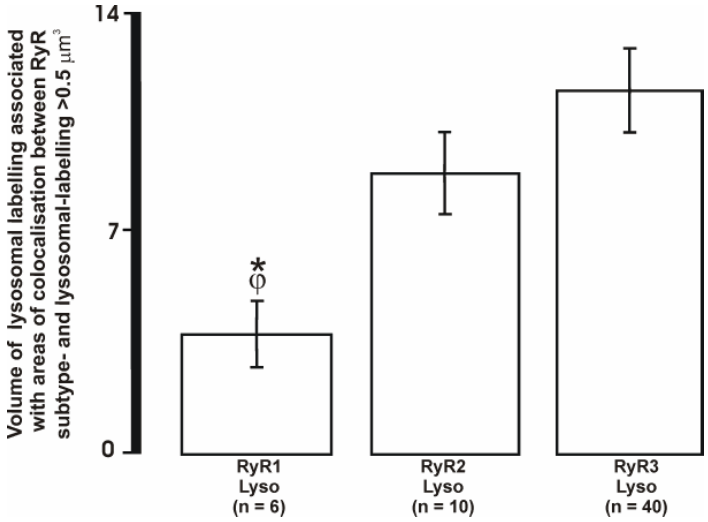

Fig. 4.33 **Comparison of the volume of lysosomal labelling associated with areas of colocalisation ≥ 0.5 μm^3 formed between RyR subtype- and lysosomal-labelling in the perinuclear region of pulmonary artery smooth muscle cells. * indicates statistical difference (P = ≤ 0.05) when compared to RyR3 labelled cells. φ indicates statistical difference (P = ≤ 0.05) when compared to RyR2 labelled cells.**

volume of lysosomal labelling located close to areas of colocalisation ≥ 0.5 μm^3 between RyR1- and lysosomal-labelling than was observed in the cytoplasm immediately surrounding areas of colocalisation ≥ 0.5 μm^3 between either RyR2- and lysosomal-labelling (P = ≤ 0.05; Appendix 2, Table 4.64), or RyR3- and lysosomal-labelling (P = ≤ 0.05; Appendix 2, Table 4.64). However, although there appeared to be a greater volume of lysosomal labelling associated with areas of colocalisation between RyR3 and lysosomes than was observed between RyR2 and lysosomes, this difference was not statistically significant (P = > 0.05; Appendix 2, Table 4.64).

A further difference in the distribution of lysosomes was observed following examination of the mean volume of distinct elements of lysosomal labelling located in the space surrounding areas of colocalisation ≥ 0.5 μm^3 formed between RyR subtype- and lysosomal-labelling. The mean volume of elements of lysosomal labelling located close to large areas of colocalisation between RyR3- and lysosomal-labelling measured 3.8 ± 0.41 μm^3 (Fig. 4.34; Appendix 2, Table 4.59). This was larger than the mean volume of elements of lysosomal labelling located close to areas of RyR2- and lysosomal-colocalisation, measured at 1.65 ± 0.18 μm^3 (Fig. 4.34; Appendix 2, Table 4.58), or the mean volume of lysosomal labelling close to areas of colocalisation between RyR1- and lysosomal-labelling where the mean volume measured 1.31 ± 0.29 μm^3 (Fig. 4.34; Appendix 2, Table 4.57). Indeed, statistical analysis of the mean volume of lysosomal labelling associated with

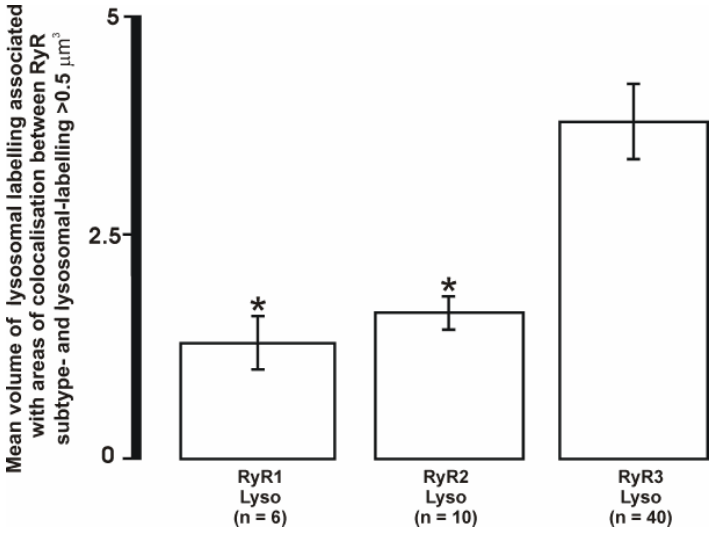

Fig. 4.34 **Comparison of the mean volume of lysosomal labelling associated with areas of colocalisation ≥ 0.5 μm^3 formed between RyR subtype- and lysosomal-labelling in the perinuclear region of pulmonary artery smooth muscle cells. * indicates statistical difference (P = ≤ 0.05) when compared to RyR3 labelled cells.**

areas of colocalisation between RyR subtype- and lysosomal-labelling confirmed that the mean volume of elements of lysosomal labelling, indicative of lysosomal clustering, were observed close to areas of colocalisation ≥ 0.5 μm^3 formed between RyR3- and lysosomal-labelling than was observed surrounding areas of colocalisation formed by either RyR2- and lysosomal

labelling ($P = \leq 0.05$; Appendix 2, Table 4.65), or RyR1- and lysosomal-labelling ($P = \leq 0.05$; Appendix 2, Table 4.65).

Theses data indicate that there was very little difference between the total volume of RyR subtype labelling located within ~1 μm of areas of colocalisation ≥ 0.5 μm^3 formed between the 3 different RyR subtypes and lysosomes. However, a far greater number of discrete elements of colocalisation with a volume ≥ 0.5 μm^3 were observed between RyR3- and lysosomal labelling than were observed between either RyR2- and lysosomal-labelling, or RyR1- and lysosomal-labelling. Furthermore, there was a greater volume of lysosomal labelling associated with areas of colocalisation between RyR3 than RyR1, with the mean volume of lysosomal labelling associated with areas of colocalisation being at least twice as large as that associated with RyR1 or RyR2. Therefore, these findings provide evidence that clustering of lysosomes occurs to a greater extent with portions of the SR expressing RyR3, than portions of the SR expressing either RyR2 or RyR1.

Taken together with the findings presented above that RyR3 colocalised to a significantly greater extent with lysosomes than either RyR2 or RyR1, it would appear that the trigger zone for Ca^{2+} signalling by NAADP is likely formed between portions of the SR expressing a high density of RyR3 and clusters of lysosomes in close proximity to the nucleus of pulmonary artery smooth muscle cells.

4.3 Discussion

In chapter 3 I showed that NAADP elicits spatially restricted Ca^{2+} bursts from lysosome-related Ca^{2+} stores which initiate global Ca^{2+} signals, in an all-or-none manner by CICR from the SR via RyRs, but not via IP_3Rs. The aim of this chapter, therefore, was to examine the spatial organisation of lysosomes and RyRs in pulmonary artery smooth muscle cells in order to determine whether or not lysosomes colocalise with RyRs located on the SR in order to facilitate this process.

4.3.1 Close association between lysosomes and ryanodine receptors in artery smooth muscle, a trigger zone for NAADP-mediated Ca^{2+} signalling?

Examination of the spatial distribution of lysosomes, labelled with LysoTracker Red, and RyRs located on the surface of the SR, labelled with BODIPY-FL ryanodine, was carried out in freshly isolated pulmonary artery smooth muscle cells. Lysosomes, were seen to form spatially segregated clusters throughout the cytoplasm of cells, while RyRs were located throughout the cytoplasm of cells, forming ribbons of labelling within a number of areas, consistent with the distribution of the SR previously observed in pulmonary artery smooth muscle (Devine *et al*., 1972). Importantly, lysosomal clusters were seen to be closely associated with a subpopulation of RyRs and appeared to be separated from these RyRs by a narrow junction or cleft less than 0.4 μm in size. Indeed in the vast majority of cases the distance between lysosomes and BODIPY-labelled RyRs was too small to be accurately resolved using the imaging techniques employed in this study. Thus, the data presented here suggest that lysosomal clusters and RyRs form a highly organised 'trigger zone' in arterial smooth muscle in which spatially restricted Ca^{2+} bursts, induced by NAADP, may raise the cytoplasmic Ca^{2+} concentration in the immediate vicinity of a subpopulation of RyRs on the SR. Thereby, NAADP-dependent Ca^{2+} bursts may breach, in an all-or-none manner, the threshold for

initiation of a propagating, global Ca^{2+} signal that is carried by CICR via RyRs alone (Boittin *et al*., 2002).

The existence of the narrow junction between RyRs and lysosomes within the proposed trigger zone, and the all-or-none generation of global Ca^{2+} waves via this trigger zone, is reminiscent of the well characterised neuromuscular junction and the all-or-none activation of skeletal muscle fibres. The neuromuscular junction is a junctional space formed between motor neurons and skeletal muscle fibres, across which signals are conveyed from the nerve to cause contraction of the muscle fibre via the neurotransmitter acetylcholine (ACh) and consequent activation of nicotinic ACh receptors (nAChRs) located on the surface of the adjacent skeletal muscle fibre. Here, basal release of ACh is not sufficient to induce depolarisation and contraction of muscle fibres (Fatt and Katz, 1952). Rather, there is a margin of safety for initiation of transmission at the neuromuscular junction (Paton and Waud, 1967). Indeed, more than 25 % of nAChRs must be occupied in order to induce depolarisation of the muscle fibre (Waud and Waud, 1972). Below this threshold of receptor activation muscle depolarisation and contraction do not occur. It is not beyond the bounds of possibility, therefore, that the proposed trigger zone for Ca^{2+} signalling by NAADP may, in a similar manner provide for all-or-none Ca^{2+} signalling via an 'intracellular synapse' between lysosomes and RyRs in arterial smooth muscle.

4.3.2 Lysosomes form clusters within the perinuclear region of pulmonary artery smooth muscle cells

Immunocytochemical investigations on methanol-fixed pulmonary artery smooth muscle cells allowed for visualisation of the spatial distribution of lysosomes, via fluorescent labelling of the integral lysosomal membrane glycoprotein αlgp120, in relation to the nucleus of the cell.

In order to examine the cellular distribution of labelled protein the cytoplasmic volume of cells was divided into three regions of interest relative to the nucleus (defined by DAPI labelling), namely the perinuclear (within 1.5 μm of the nucleus), the sub-plasmalemmal (within 1.5 μm of the perimeter of

the cell) and the extra-perinuclear region (defined as the remaining volume of the cytoplasm following definition of the perinuclear and sub-plasmalemmal regions). Volumetric analysis was then carried out to determine the density of labelling for a given protein within each region.

The density of lysosomal labelling was around 2-fold greater in the perinuclear region than in the extra-perinuclear region and 3-fold greater than the density of lysosomal labelling measured in the sub-plasmalemmal region of cells. Furthermore, an examination of the mean volume of lysosomal labelling indicated that dense clusters of lysosomal labelling were present in the perinuclear region, compared to a more diffuse distribution of lysosomal labelling in both the extra-perinuclear and sub-plasmalemmal regions. If lysosomes are the source of NAADP-mediated Ca^{2+} signals, as proposed in Chapter 3, and these signals are generated in trigger zones formed between lysosomes and closely apposed RyRs on the SR, then the predominant distribution of large lysosomal clusters within the perinuclear region of cells suggests that the trigger zone for NAADP-mediated Ca^{2+} signalling is likely to be located in this region. Reaves *et al.* (1996a) have previously used the monoclonal antibody GM10 to visualise the spatial distribution of αlgp120 in normal rat kidney fibroblasts. Consistent with my findings in pulmonary artery smooth muscle, they found that whilst there was punctuate labelling of αlgp120 throughout the cytoplasm of cells, the majority of the labelling of αlgp120 occurred within the cytoplasm surrounding the nucleus of cells (Reaves, *et al.*, 1996a). Furthermore, a predominantly perinuclear distribution of lysosomes has also been noted in a number of other cell types, including vascular smooth muscle (Peters, et al., 1972; James-Kracke, et al., 1979; Robinson, et al., 1986; Matteoni and Kreis, 1987; Pohlmann, et al., 1995).

There was no evidence in immunocytochemical investigations of lysosomal labelling forming a dense ring around the perimeter of cells. In fact, there was a notable decline in the density of lysosomal labelling observed within the sub-plasmalemmal region in comparison to either the perinuclear or extra-perinuclear regions. This is at odds with the findings in cells labelled with LysoTracker Red, which identified a proportion of cells with a ring of lysosomal labelling around the perimeter of the cell. This contradiction may be

explained if a group of cells in the LysoTracker Red studies had contracted and reduced the cytoplasmic space between the nucleus and the plasma membrane. Thus, the contents of the cytoplasm would be concentrated in a confined area around the nucleus and would, therefore, be visualised as being close to the plasma membrane. It is worthy of note that of the two forms of Ca^{2+} burst observed in pulmonary artery smooth muscle cells in response to NAADP, a ring of Ca^{2+} release proximal to the plasma membrane of cells was observed only in those cells which had contracted and 'rounded up' to some extent. In contrast, however, following intracellular dialysis of NAADP, pulmonary artery smooth muscle cells which were more elongated in appearance exhibited spatially restricted, focal Ca^{2+} bursts towards the centre of the cell.

In conclusion, the larger volume of lysosomal labelling located within the perinuclear region of pulmonary artery smooth muscle cells, coupled with the existence of larger clusters of lysosomal labelling in this region, when compared to either the extra-perinuclear or sub-plasmalemmal regions, argues in favour of a functional role for lysosomes within the perinuclear region of cells.

4.3.3 Differences in ryanodine receptor subtype distribution within isolated pulmonary artery smooth muscle cells, an indicator of functional significance?

Examination of the distribution of labelling for the 3 different RyR subtypes indicated that there was no difference between the total densities of RyR1, RyR2 and RyR3 in pulmonary artery smooth muscle cells. However, examination of their relative distribution within the perinuclear, extra-perinuclear and sub-plasmalemmal regions identified significant differences in the spatial organisation of each of the subtypes of RyR.

4.3.3.1 Ryanodine receptor subtype 1 is uniformly distributed throughout the cytoplasm of pulmonary artery smooth muscle cells

Examination of the distribution of RyR1 labelling showed that labelling was evenly distributed throughout the cytoplasm of pulmonary artery smooth

muscle cells. Thus, there was little difference between the density of RyR1 labelling between the perinuclear, extra-perinuclear and sub-plasmalemmal regions. Similarly, an examination of the mean volumes of individual elements of RyR1 labelling showed that there was no difference in the mean volume of elements of RyR1 labelling between the perinuclear, extra-perinuclear or sub-plasmalemmal regions. The uniform distribution of RyR1 labelling provided no evidence of a predominance of RyR1 labelling, or any indication of a predominance of clustering of RyR1, within the perinuclear, extra-perinuclear or sub-plasmalemmal regions of cells.

4.3.3.2 Ryanodine receptor subtype 2 forms large clusters within the extra-perinuclear region of pulmonary artery smooth muscle cells

In contrast to the distribution of RyR1 labelling, RyR2 labelling did not display a uniform distribution across the cytoplasm of pulmonary artery smooth muscle cells. Rather, RyR2 labelling appeared to be predominantly located within the extra-perinuclear region of cells, where the density of RyR2 labelling was around 2-fold greater than that measured in the perinuclear region. Furthermore, RyR2 labelling declined to its lowest levels in the sub-plasmalemmal region of cells, where the density of RyR2 labelling was around 6-fold lower than that observed in the extra-perinuclear region. In a similar manner, the mean volume of elements of RyR2 labelling within the extra-perinuclear region was almost 2-fold larger than was measured in the perinuclear region, and around 4-fold larger than elements of RyR2 labelling detected in the sub-plasmalemmal region. Therefore, it would appear that although RyR2 labelling was evident in the perinuclear, extra-perinuclear and sub-plasmalemmal regions, RyR2 labelling was predominantly observed within the extra-perinuclear region of pulmonary artery smooth muscle cells.

4.3.3.3 Ryanodine receptor subtype 3 forms large clusters in the perinuclear region of pulmonary artery smooth muscle cells

The distribution of RyR3 labelling within pulmonary artery smooth muscle cells was markedly different to the distribution of labelling for either

RyR1 or RyR2. Indeed, RyR3 labelling was predominantly detected within the perinuclear region of cells with a decrease in RyR3 labelling of around 3-fold observed in the extra-perinuclear region, and a decrease of around 6-fold in the sub-plasmalemmal region. There was also a marked decrease in the clustering of RyR3 labelling observed outwith the perinuclear region of cells, with the mean volume of elements of RyR3 labelling being around 3-fold larger than those measured in the extra-perinuclear region and around 5-fold larger than elements of RyR3 labelling measured in the sub-plasmalemmal region of cells. RyR3 labelling, therefore, was predominantly restricted to the perinuclear region of pulmonary artery smooth muscle cells where larger clusters of labelling were evident than were observed in either the extra-perinuclear or sub-plasmalemmal regions of cells.

4.3.3.4 Comparison of the distribution of ryanodine receptor subtypes in pulmonary artery smooth muscle cells

The expression of different RyR subtypes on different portions of the SR throughout cells may be fundamentally important to the regulation of Ca^{2+} signalling within arterial smooth muscle. This proposal is strengthened by a direct comparison of the labelling RyR1, RyR2 and RyR3 within the 3 designated regions of the cytoplasm.

Thus, direct comparison between the 3 RyR subtypes in the perinuclear region of cells showed that both the density, and the mean volume of elements of RyR3 labelling were around 2-fold greater than was measured for either RyR2 or RyR1 within this region. Therefore, RyR3 was the predominant subtype of RyR within the perinuclear region of pulmonary artery smooth muscle cells. Further evidence in support of an important functional role for RyR3 in the regulation of Ca^{2+} signalling proximal to the nucleus of pulmonary artery smooth muscle cells was provided by the finding that labelling of RyR3 declined dramatically within the extra-perinuclear and sub-plasmalemmal regions.

While there was a sharp decline in RyR3 labelling in the extra-perinuclear region of cells, there was a marked increase in the labelling of RyR2 within this region. Indeed, RyR2 was by far the dominant subtype of

RyR observed within the extra-perinuclear region of pulmonary artery smooth muscle cells, where the density of RyR2 labelling was around 4-fold greater than was measured for either RyR1- or RyR3-labelling. RyR2 also appeared to form much larger clusters in the extra-perinuclear region of cells when compared to either RyR1 or RyR3. Thus, the mean volume of elements of RyR2 labelling in the extra-perinuclear region was around 2-fold larger than was measured for either RyR1- or RyR3-labelling. Therefore, as for RyR3 in the perinuclear region of cells, the dominance of RyR2 labelling in the extra-perinuclear region coupled to the greater degree of clustering of RyR2 labelling than was observed for either RyR1- or RyR3-labelling may be indicative of an important function for RyR2 in the extra-perinuclear region.

As described previously, both the density and the mean volume of elements of RyR1 labelling showed little difference across the 3 regions of the cytoplasm. However, the consistency in the extent of labelling of RyR1 across the cell meant that RyR1 was the dominant RyR subtype expressed in the sub-plasmalemmal region, because there was a marked decline in the labelling of both RyR2 and RyR3 within this region. This unexpected, but significant observation suggests that RyR1 may play a fundamental role in the regulation of SR Ca^{2+} signalling proximal to the plasma membrane of pulmonary artery smooth muscle cells. It is quite probable, therefore, that RyR1 is the RyR subtype involved in SR Ca^{2+} release that this laboratory has previously shown to underpin, in part, BK_{Ca}-dependent hyperpolarisation and vasodilation evoked by adenylyl-cyclase coupled receptors in pulmonary arterial smooth muscle cells (Boittin *et al*., 2003).

Consistent with the findings presented here, a recent investigation into the spatial distribution of RyR subtypes in pulmonary artery smooth muscle cells has suggested that different RyR subtypes are located in different regions of the cell (Yang, *et al.*, 2005). In their study, Sham and colleagues showed that RyR3 was mainly located in the perinuclear region of cells with some labelling in the general cytoplasm, whilst RyR2 appeared to be present away from the nucleus and RyR1 was located mainly in the periphery of the cell and around the nucleus (Yang, *et al.*, 2005). However, the study of Yang *et al*. did not contain any quantitative analysis of the distribution of RyR subtypes within

pulmonary artery smooth muscle cells and any comparison with the findings of my investigation, therefore, would be impossible to conduct.

4.3.4 Ryanodine receptor subtype 3, but not ryanodine receptor subtype 1 or 2, associates with lysosomes to form large areas of colocalisation in the perinuclear region of isolated pulmonary artery smooth muscle cells

Examination of the colocalisation between labelling of the 3 different RyR subtypes and lysosomal labelling within cells identified clear differences in the extent to which each of the RyR subtypes associated with lysosomes within pulmonary artery smooth muscle cells.

4.3.4.1 Colocalisation between ryanodine receptor subtype 1 and lysosomes in pulmonary artery smooth muscle cells

RyR1 labelling was seen to form areas of colocalisation with lysosomal labelling across the cytoplasm of pulmonary artery smooth muscle cells. However, there was little difference between the density of colocalisation, and the mean volume of areas of colocalisation between RyR1 and lysosomal labelling in the perinuclear and extra-perinuclear regions. In the sub-plasmalemmal region there was a decrease of around 2-fold in the density, and around 3-fold in the mean volume of elements of colocalisation observed between RyR1 and lysosomal labelling when compared to the perinuclear or extra-perinuclear regions of cells.

4.3.4.2 Colocalisation between ryanodine receptor subtype 2 and lysosomes in pulmonary artery smooth muscle cells

As for RyR1, there was little difference between the density of, and the mean volume of elements of colocalisation between RyR2 and lysosomal labelling between the perinuclear and extra-perinuclear regions of cells. However, there was a decrease of around 6-fold in the density, and around 3-

fold in the mean volume of elements of colocalisation between RyR2- and lysosomal-labelling in the sub-plasmalemmal region of cells.

4.3.4.3 Colocalisation between ryanodine receptor subtype 3 and lysosomes in pulmonary artery smooth muscle

In contrast to my findings with respect to colocalisation between RyR1 or RyR2 and lysosomal labelling, colocalisation between RyR3 and lysosomal labelling was predominantly located in the perinuclear region of cells. Indeed, the density of colocalisation observed between RyR3 and lysosomal labelling within the extra-perinuclear region and sub-plasmalemmal region was around 3-fold and 10-fold lower than that measured in the perinuclear region, respectively. Similarly, examination of the mean volume of areas of colocalisation between RyR3 and lysosomal labelling identified a greater degree of clustering between lysosomes and RyR3 in the perinuclear region than was observed outwith this region. Thus, there was a decrease of around 2-fold in the mean volume of areas of colocalisation between RyR3 and lysosomal labelling in the extra-perinuclear and sub-plasmalemmal regions when compared to the perinuclear region of cells.

4.3.4.4 Lysosomes and ryanodine receptor subtype 3 colocalise to form the trigger zone for NAADP-mediated Ca^{2+} signalling in pulmonary artery smooth muscle cells

Direct comparison of the extent to which each of the 3 RyR subtypes colocalised with lysosomes in each of the 3 regions of the cytoplasm indicated that RyR3 labelling colocalised with lysosomal labelling to a much greater extent than was observed for either RyR2 or RyR1. Indeed the density of colocalisation between RyR3 and lysosomes within the perinuclear region was more than 2-fold greater than the colocalisation observed between RyR2 or RyR1 and lysosomes. Also, there was evidence that the mean volume of colocalisation between RyR3 and lysosomal labelling was around 2-fold larger than that observed between RyR2 or RyR1 and lysosomal labelling, indicative of a much greater association between RyR3 and lysosomes within the

perinuclear region of cells. The predominance of colocalisation between lysosomes and RyR3 over RyR2 or RyR1 was not detected in either the extra-perinuclear or sub-plasmalemmal regions where in addition to the lower incidence of colocalisation, there was little difference between the density of colocalisation, and the mean volume of areas of colocalisation between lysosomes and RyR1, RyR2 or RyR3.

These data provide compelling evidence that RyR3 is a likely candidate for the RyR subtype expressed in tight lysosomal-SR junctions in pulmonary artery smooth muscle cells. However, the lysosomal marker examined in these immunocytochemical studies (αlgp120) may not be targeted to the lysosomal membrane at the lysosome-SR junction. Thus, measurements of colocalisation between RyR subtypes and αlgp120 are likely to be an underestimate of the true degree of colocalisation between lysosomes and RyR3. I therefore examined the distribution of fluorescent labelling in close proximity to the larger volumes of colocalisation ($\geq$ 0.5 μm^3), within the perinuclear region, between each RyR subtype and lysosomal labelling. This provided valuable information on the degree to which lysosomes and RyR subtypes were associated, in that they provided further evidence in support of a preferential association between lysosomes and RyR3 in pulmonary artery smooth muscle cells. It was noted that all the cells examined for RyR3 labelling were seen to display areas of colocalisation $\geq$ 0.5 μm^3 in the perinuclear region, compared to 75% of RyR2 labelled cells and 50% of RyR1 labelled cells. Also, there were around 4 times and 6 times as many areas of colocalisation observed between RyR3 and lysosomal labelling $\geq$ 0.5 μm^3 in cells than were observed in either RyR2 or RyR1 labelled cells, respectively. Furthermore, there was much greater mean volume of elements of lysosomal labelling and thus, a greater degree of lysosomal clustering, around large areas of colocalisation between RyR3 and lysosomal labelling was observed when compared with that for RyR1 or RyR2. Therefore, these data provide further support for my proposal that a trigger zone for Ca^{2+} signalling by NAADP is likely formed between lysosomal clusters and portions of the SR expressing a high density of RyR3 proximal to the nucleus of pulmonary artery smooth muscle cells.

The aforementioned findings raise the question as to why RyR3 may be targeted to the lysosome-SR junctions. A determining factor in this respect may be the relative sensitivity of each RyR subtype to CICR, the maximum gain in response to Ca^{2+} and their relative sensitivity to inactivation by Ca^{2+}. The threshold for activation of RyR1, RyR2 and RYR3 is similar, with channel activation occurring at cytoplasmic Ca^{2+} concentrations > 100 nM (Chen, *et al.*, 1997; Li and Chen, 2001). However, estimates of the EC_{50} (In the absence of Mg^{2+} and ATP) are different, with half maximal activation at ~250 nM for RyR2 (Chen, *et al.*, 1997) and ~400 nM for RyR3 (Li and Chen, 2001). The higher EC_{50} exhibited by RyR3 could be significant, because this would provide for a higher margin of safety with respect to the all-or-none amplification of Ca^{2+} bursts from lysosomal Ca^{2+} stores by CICR via RyRs at the lysosome-SR junction i.e. the probability of false events being initiated would be lower for RyR3 than for RyR2. Another factor that may be of significance is that whilst the mean open time vs. cytoplasmic Ca^{2+} concentration for RyR2 and RyR3 are comparable and increase approximately 10-fold over their activation range, the mean open time for RyR1 is much lower and increases only 2-fold over its activation range (Chen, *et al.*, 1997; Li and Chen, 2001). Furthermore, comparison of the open probability (Po) versus cytoplasmic Ca^{2+} concentration curves shows that RyR3 (0 – 1) exhibits a higher gain in Po than does RyR2 (0 – 0.9), whilst RyR1 (0 – 0.2) exhibits relatively little gain in Po with increasing cytoplasmic Ca^{2+} concentration (Chen, *et al.*, 1997; Li and Chen, 2001). Thus, once the threshold for activation is breached RyR3 would offer greater amplification of Ca^{2+} bursts from lysosomal Ca^{2+} stores than would RyR2, whilst amplification via RyR1 would be marginal. There is also marked variation in the relative sensitivity of each RyR subtype to inactivation by Ca^{2+}. RyR3 exhibits the lowest sensitivity to inactivation by Ca^{2+} with an IC_{50} of 3 mM whilst that for RyR2 is 2 mM; in each case channel activity may still be observed at concentrations > 10 mM (Chen, *et al.*, 1997; Li and Chen, 2001). In marked contrast, RyR1 inactivation occurs within the μM range and full inactivation is achieved by 1 mM Ca^{2+} (Chen, *et al.*, 1997); this may, in part, explain the low gain in Po for RyR1 in response to activation by Ca^{2+}. Its sensitivity to inactivation by Ca^{2+} would

therefore render RyR1 unsuitable for a role in amplification of Ca^{2+} bursts at lysosome-SR junctions because the local Ca^{2+} concentration may exceed the threshold for RyR1 inactivation. Thus, the functional properties of RyR3 make it best suited to a role in the amplification of Ca^{2+} bursts at lysosome-SR junctions.

However, the density of RyR3 labelling declined markedly outwith the perinuclear region of the cell. It seems unlikely, therefore, that RyR3 functions to carry a propagating Ca^{2+} wave far beyond the point of initiation of CICR within the trigger zone for Ca^{2+} signalling by NAADP. Given this finding it may be of significance that the density of labelling for RyR2 increases within the extra-perinuclear region of cells. Indeed the lower EC_{50} for CICR of RyR2 (~250 mM) over RyR3 (~ 400 mM) would help insure that once initiated a propagating Ca^{2+} wave would be less prone to failure. Thus, RyR2 would be best suited for a role in underpinning the wider propagation of a global Ca^{2+} wave.

In conclusion, I propose that lysosomal clusters are primarily located in the perinuclear region pulmonary artery smooth muscle cells where they form junctions with a subsection of the SR that contains a high density of RyR3. These lysosome-SR junctions likely comprise a trigger zone for Ca^{2+} signalling by NAADP, within which CICR via RyR3 is a prerequisite for initiation of a propagating Ca^{2+} wave in response to NAADP-dependent Ca^{2+} bursts from lysosome-related stores. Thereafter, CICR via RyR2 likely carries the propagating wave beyond the perinuclear region of the cell (Fig. 4.35).

Although the evidence in the literature suggests that the affinity-purified sequence-specific antibodies used in my investigations raised against the three distinct RyR subtypes are reliable indicators of the RyR subtype proteins, I cannot rule out the possibility that these antibodies recognise epitopes present on other cellular proteins. Furthermore, misleading discrepancies may be introduced as a result of the harsh conditions encountered in processing proteins/cells for immunoblotting and immunocytochemical investigations, respectively. Therefore, it is worthy of note that although the investigations presented within this thesis may provide a good indication of differences in the spatial distribution of RyR subtypes within pulmonary artery smooth muscle cells, definitive evidence may be provided by future studies

employing a number of more reliable and sensitive diagnostic and visualisation techniques.

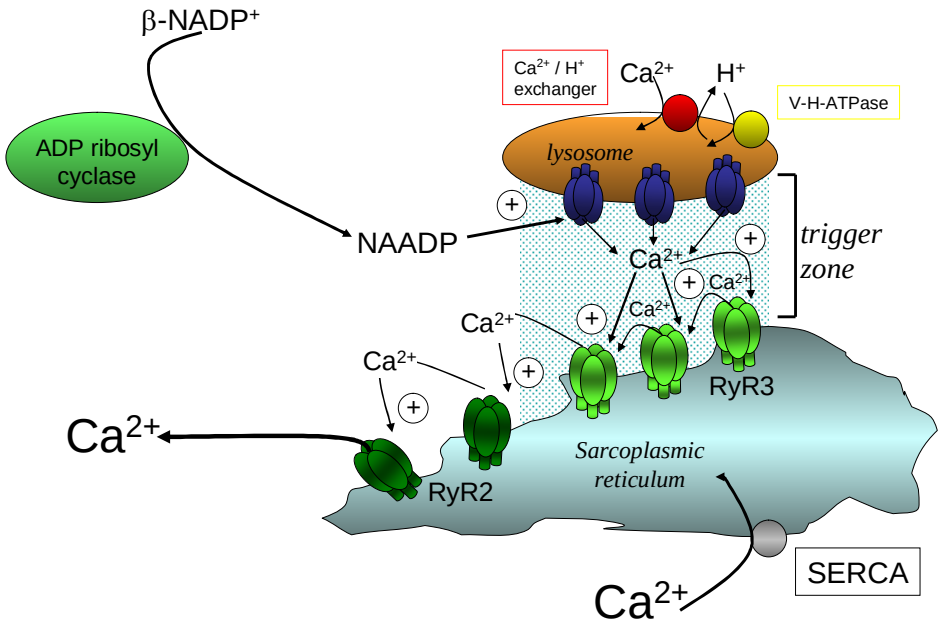

Fig. 4.35 **Schematic representation of the trigger zone for Ca^{2+} signalling by NAADP in arterial smooth muscle:** The trigger zone is formed between closely opposed lysosomes expressing a putative NAADP receptor and portions of the SR expressing clusters of RyR3. NAADP acts on the putative NAADP receptors causing initiation of a Ca^{2+} burst, which is released into the trigger zone. If the Ca^{2+} concentration within the trigger zone rises beyond the threshold for activation of CICR via RyR3, the initial Ca^{2+} burst is amplified via the recruitment of RyR2 located on portions of the SR located outwith the trigger zone, resulting in a global Ca^{2+} wave and contraction of the smooth muscle cell.

Chapter 5: Agonist dependent regulation of NAADP-mediated Ca^{2+} signalling in pulmonary artery smooth muscle

5.1 Introduction

Previous investigations from this laboratory have provided evidence in support of the view that NAADP acts as a Ca^{2+} mobilising messenger in pulmonary artery smooth muscle (Boittin *et al*., 2002). However, one of the fundamental criterions that must be fulfilled by any molecule in order for it to be considered a second messenger is whether or not the molecule mediates responses to known ligand-gated receptors in an agonist-specific manner. Recently, a study from Galione and colleagues provided data in support of a role for NAADP as a Ca^{2+} mobilising second messenger in isolated murine pancreatic acinar cells (Yamasaki, *et al*., 2005). In their study, Galione and colleagues showed that the activation of cholecystokinin receptor A on the surface of pancreatic acinar cells resulted in a marked increase in the levels of NAADP detected within cells (Yamasaki *et al*., 2005). Furthermore, Galione and colleagues had previously determined that cholecystokinin-induced Ca^{2+} signals in pancreatic acinar cells were dependent on NAADP-mediated Ca^{2+} release from an acidic, lysosome-related Ca^{2+} store (Cancela *et al*., 1999; Yamasaki *et al*., 2004).

As a result of the fact that NAADP-dependent Ca^{2+} signals induced contraction of isolated pulmonary artery smooth muscle cells (Chapter 3; Boittin *et al*., 2002), The aim of this chapter, therefore, is to determine whether or not any vasoconstrictor receptors on pulmonary artery smooth muscle may mediate their effects, in part, via NAADP-dependent Ca^{2+} signalling. To this end, three potent vasoconstrictors are examined, namely, phenylepherine (PE), prostaglandin-$F_{2\alpha}$ ($PGF_{2\alpha}$) and endothelin-1 (ET-1). These vasoconstrictors were chosen for investigation due to reported differences in the manner in which they elicit initial Ca^{2+} signals within vascular smooth muscle (Hamada, *et al.*, 1997; Doi, *et al.*, 2000)

5.2 Results

5.2.1 Is there a role for NAADP in agonist-mediated vasoconstriction in pulmonary artery smooth muscle cells?

In chapter 3 of this thesis, I presented data in support of the proposal that NAADP elicits Ca^{2+} signals and contraction of isolated pulmonary arterial smooth muscle cells by triggering Ca^{2+} bursts from a Bafilomycin A1-sensitive Ca^{2+} store, that are subsequently amplified into global waves by CICR from the SR via RyRs. In this chapter, I therefore sought to determine whether or not NAADP could mediate agonist-specific Ca^{2+} signalling in pulmonary arterial smooth muscle. To this end I studied the effect of Bafilomycin A1 on Ca^{2+} signalling by three vasoconstrictors, namely phenylepherine (PE), prostaglandin-$F_{2\alpha}$ ($PGF_{2\alpha}$) and endothelin-1 (ET-1).

5.2.1.1 Ca^{2+} signals induced by phenylepherine and prostoglandin-$F_{2\alpha}$ are not affected by Bafilomycin A1

Extracellular application of the α_1-adrenoceptor agonist PE (3 μM) was seen to induce a global Ca^{2+} wave in isolated pulmonary artery smooth muscle cells, as indicated in a representative record of the Fura-2 fluorescence ratio (F340 / F380) against time (Fig. 5.1A). The Fura-2 fluorescence peaked within ~30 s of application, rising from 0.49 ± 0.09 to 1.57 ± 0.37 (n = 3; Appendix 3, Table 5.1) which equates to a rise in the intracellular Ca^{2+} concentration from ~100 nM to ~700 nM (see calibration curve in Chapter 2, section 2.6.6). Following pre-incubation of cells with Bafilomycin A1 (100 nM), the Ca^{2+} wave induced by PE (3 μM) remained unaffected, the Fura-2 fluorescence ratio increasing from 0.58 ± 0.11 to 1.49 ± 0.28 (n = 3; P = > 0.05; Appendix 3, Table 5.2).

Likewise, extracellular application of $PGF_{2\alpha}$ (2 μM) induced a global Ca^{2+} wave in isolated pulmonary artery smooth muscle cells in a manner that was insensitive to Bafilomycin A1. Fig. 5.1B shows a record of the Fura-2 fluorescence ratio against time from a representative experiment. The increase

in Fura-2 fluorescence ratio induced by $PGF_{2\alpha}$ (2 μM) peaked within ~60 s, rising from 0.54 ± 0.04 to 1.29 ± 0.18 in the absence of Bafilomycin A1 and from 0.59 ± 0.03 to 1.32 ± 0.15 in its presence (n = 5; P = > 0.05; Appendix 3, Tables 5.3 and 5.4). From these data it can be concluded that PE and $PGF_{2\alpha}$ evoke global Ca^{2+} waves in a manner that is independent of bafilomycin-sensitive, acidic Ca^{2+} stores.

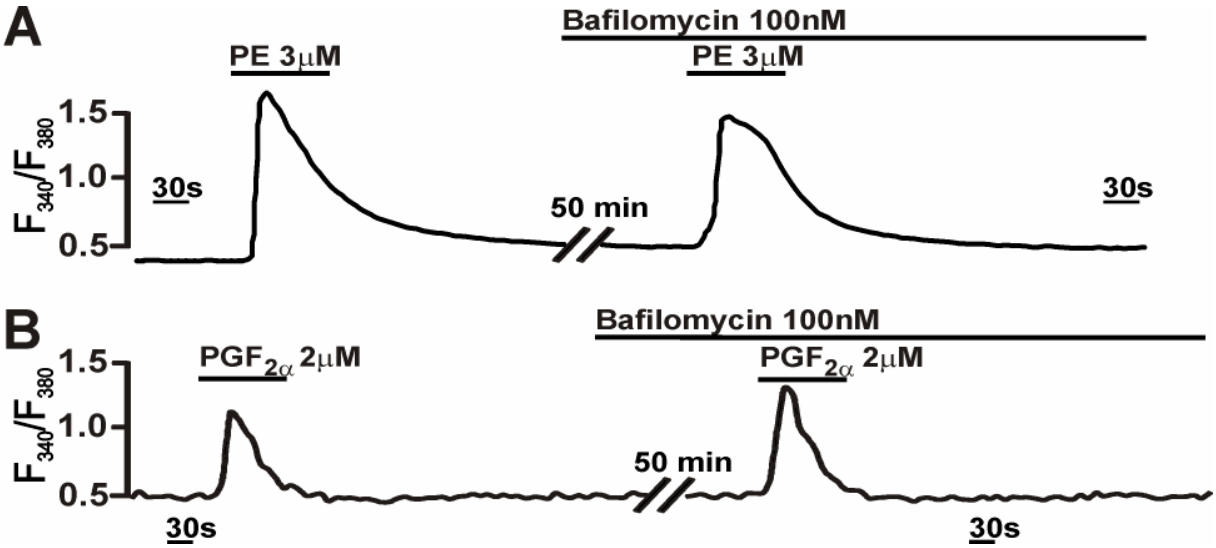

Fig. 5.1: **Bafilomycin A1 is without effect on calcium signalling by phenylepherine or prostaglandin-$F_{2\alpha}$ in isolated pulmonary artery smooth muscle cells: *Panel A*:** shows a record of the F_{340}/F_{380} fluorescence ratio against time recorded in a cell to the extracellular application of PE (3 μM) in the absence and presence of Bafilomycin A1 (100 nM). ***Panel B*:** shows a record of the F_{340}/F_{380} fluorescence ratio against time recorded in a cell to the extracellular application of $PGF_{2\alpha}$ (2 μM) in the absence and presence of Bafilomycin A1 (100 nM).

5.2.1.2 Bafilomycin A1 abolishes intracellular Ca^{2+} signals in response to endothelin-1

Extracellular application of ET-1 (100 nM) induced reproducible and reversible global Ca^{2+} transients in pulmonary artery smooth muscle cells (Fig. 5.2A). The increase in the Fura-2 fluorescence ratio (F340/F380) peaked within 60s of application, rising from 0.52 ± 0.02 to 1.16 ± 0.05 on the first application and from 0.53 ± 0.02 to 1.16 ± 0.04 on the second (n = 16; Appendix 3, Table 5.5). In marked contrast to my findings with respect to PE

and $PGF_{2\alpha}$, however, pre-incubation of cells with Bafilomycin A1 abolished Ca^{2+} signals evoked by ET-1 (100 nM). Fig. 5.2B shows a representative experiment. The upper panel shows a series of pseudocolour images of the

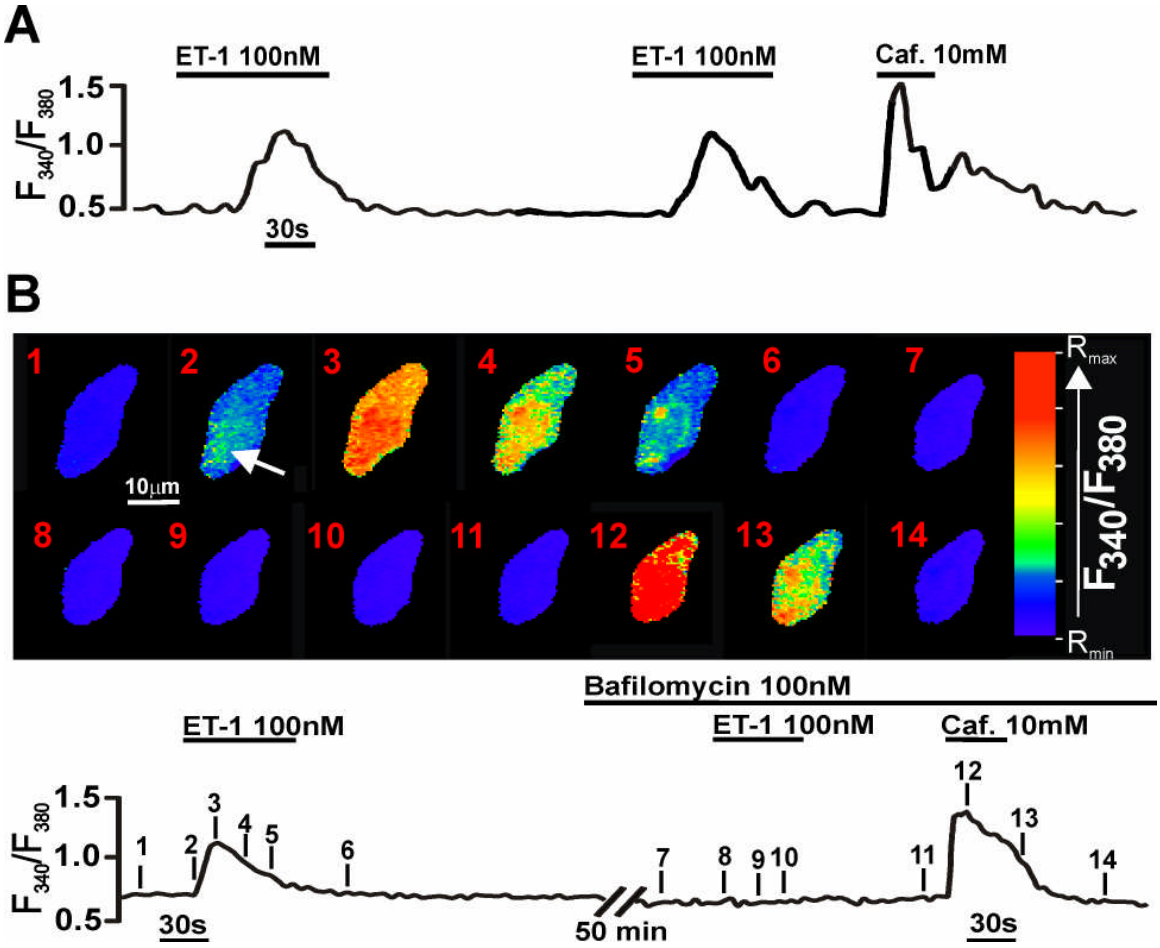

Fig. 5.2: **Bafilomycin A1 abolishes calcium signalling by endothelin-1 in isolated pulmonary artery smooth muscle cells: *Panel A*:** shows a record of the F_{340}/F_{380} fluorescence ratio against time recorded in a cell showing the reproducible nature of Ca^{2+} signals in response to two application of ET-1 (100 nM). ***Panel B , upper panel*:** shows a series of pseudocolour representations of the change in Fura-2 fluorescence ratio (F_{340}/F_{380}) in an isolated pulmonary artery smooth muscle cell to the extracellular dialysis of ET-1 (100 nM) in the absence and presence of Bafilomycin A1 (100 nM). The arrow in image 2 indicates a localised increase in the Fura-2 fluorescence ratio. ***Lower panel*** shows a record of the F_{340}/F_{380} fluorescence ratio against time recorded from the same cell as in the upper panel.

Fura-2 fluorescence ratio, whilst the lower panel shows the record of the fluorescence ratio against time. It is notable that the global Ca^{2+} wave induced by ET-1 in the absence of Bafilomycin A1 is preceded by a spatially restricted

Ca^{2+} release event (image 2, arrow) consistent with the Ca^{2+} bursts generated by NAADP (Chapter 3; Boittin *et al.*, 2002); no such events were observed in response to PE or $PGF_{2\alpha}$. Following pre-incubation (50 min) with Bafilomycin A1 both ET-1 induced Ca^{2+} bursts and global Ca^{2+} waves were abolished. Thus, the Fura-2 fluorescence ratio increased from 0.56 ± 0.09 to 1.17 ± 0.02 in the absence of Bafilomycin A1 (100 nM) and from 0.64 ± 0.03 to 0.65 ± 0.03 in its presence (n = 4; P = < 0.05; Appendix 3, Tables 5.6 and 5.7). Significantly, and consistent with experiments described previously (Chapter 3), global Ca^{2+} waves induced by ryanodine receptor activation by caffeine (10 mM) were observed in the presence of Bafilomycin A1. These data suggest that ET-1 may trigger intracellular Ca^{2+} release and contraction, in part, by mobilising a bafilomycin-sensitive, lysosome-related Ca^{2+} store. One pivotal experiment to examine whether there is a role for NAADP in mediating Ca^{2+} signals in response to ET-1 may be to take advantage of the finding in other cell types that NAADP receptors undergo self-inactivation and desensitiation in response to high concentrations of NAADP (Aarhus, *et al.*, 1996a; Cancela, *et al.*, 1999; Berg, *et al.*, 2000; Billington and Genazzani, 2000b; Churchill and Galione, 2000). Thus, one might be able to determine whether a high, desensitising concentration of NAADP alters the nature of Ca^{2+} signals generated in response to ET-1. However, an investigation from this laboratory has shown that robust Ca^{2+} signals were observed in response to a high concentration of NAADP (100 μM) in pulmonary artery smooth muscle cells (Boittin *et al.*, 2002). Therefore, the NAADP receptor(s) expressed in pulmonary artery smooth muscle do not appear to undergo self-inactivation in a similar manner to those described previously in other cell types.

5.2.1.3 The role of the sarcoplasmic reticulum in endothelin-1-mediated Ca^{2+} signals

I then proceeded to investigate the role of SR Ca^{2+} stores in the generation of ET-1-mediated Ca^{2+} signals. Thus, I carried out a comparison of the pharmacology of ET-1-induced Ca^{2+} waves with that of NAADP- and Bafilomycin A1-induced Ca^{2+} waves. Following preincubation (15 min) of

cells with thapsigargin (1 μM), extracellular application of ET-1 (100 nM) failed to induce global Ca^{2+} waves. Fig. 5.3 shows a representative experiment. The upper panel shows a series of pseudocolour images of the Fura-2 fluorescence ratio, whilst the lower panel shows the record of the fluorescence

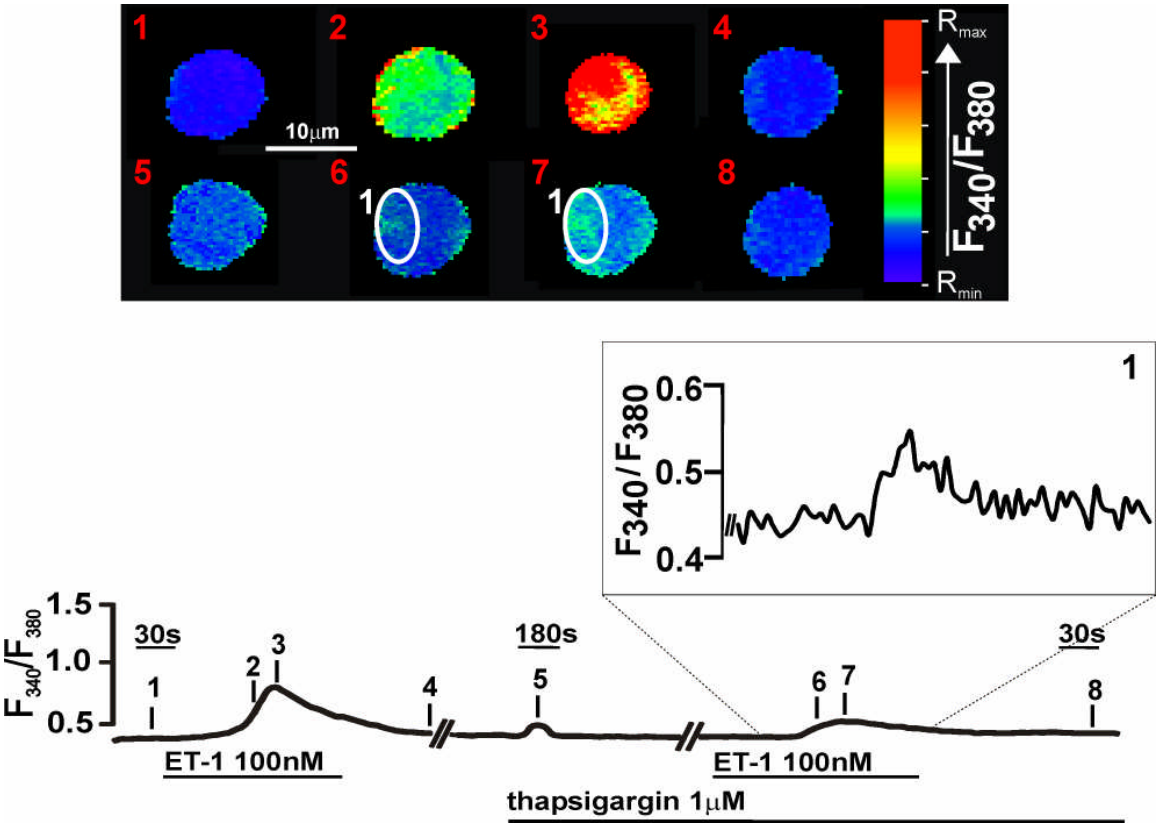

Fig. 5.3: **Thapsigargin abolishes global Ca^{2+} waves in response to ET-1, but not localized release events.** ***Upper panel:*** shows a pseudocolour representation of the changes in Fura-2 fluorescence ratio within an isolated pulmonary artery smooth muscle cell after preincubation (20 min) with thapsigargin (1 μM) in response to the extracellular application of ET-1 (100 nM). Note, the spatially restricted Ca^{2+} burst indicated by the ROI shown as the white circle, 1 in pseudocolour images 6 and 7. ***Lower panel:*** shows the Fura-2 fluorescence ratio against time for the cell in the upper panel, the insert shows the Fura-2 fluorescence ratio for the ROI indicated in pseudocolour representations 6 and 7.

ratio against time. Thus, ET-1 induced an increase in the Fura-2 fluorescence ratio from 0.39 ± 0.01 to 0.8 ± 0.05 in the absence of thapsigargin, and from 0.45 ± 0.01 to 0.49 ± 0.02 in the presence of thapsigargin (n = 9; P = < 0.05; appendix 3, Tables 5.8 and 5.9). However, spatially restricted Ca^{2+} bursts were still observed in 5 out of 9 cells examined (Fig. 5.3, images 6 and 7) with the

increase in Fura-2 fluorescence ratio within a given region of interest of these 5 cells measuring 17 ± 4 %. In the remaining 4 cells a small, non-uniform rise in intracellular Ca^{2+} concentration was observed, but with less than clear spatial definition. The lack of a noticeable Ca^{2+} burst in the remaining 4 cells examined was likely due to the Ca^{2+} burst occurring outwith the focal plane of the microscope. The average rise in Fura-2 fluorescence ratio within a given region of interest in all 9 cells examined was 10 ± 4 % (Fig. 5.5; Appendix 3, Table 5.8). These data suggest that, in a similar fashion to NAADP and Bafilomycin A1, ET-1 induces an initial phase of Ca^{2+} release from a thapsigargin-insensitive, non-SR Ca^{2+} store.

5.2.1.4 The role of the ryanodine receptors in endothelin-1-mediated global Ca^{2+} waves

Given that amplification of NAADP- and Bafilomycin A1-mediated localised Ca^{2+} release events into global Ca^{2+} waves required amplification via CICR from RyRs on the SR (Chapter 3), I next sought to determine whether or not CICR via RyRs was required for the generation of global Ca^{2+} signals in response to ET-1. Following preincubation (20 min) of cells with ryanodine (20 μM), the extracellular application of ET-1 (100 nM) once more failed to induce global Ca^{2+} waves and no cell contraction was observed. Fig. 5.4 shows a representative experiment. The upper panel shows a series of pseudocolour representations of the Fura-2 fluorescence ratio, while the lower panel shows a record of the Fura-2 fluorescence ratio against time in the same cell. Thus, ET-1 caused an increase in the Fura-2 fluorescence ratio within cells from 0.4 ± 0.02 to 0.93 ± 0.08 in the absence of ryanodine, and from only 0.45 ± 0.02 to 0.5 ± 0.03 in the presence of ryanodine (n = 8; P = < 0.05; Appendix 3, Tables 5.10 and 5.11). It is worthy of note that, consistent with NAADP-mediated global Ca^{2+} waves, the extracellular application of ET-1 prior to incubation with ryanodine triggered an initial Ca^{2+} burst event which declined to baseline prior to the initiation of a global Ca^{2+} wave in the example cell shown in Fig 5.4 (image 2, arrow 1). Following preincubation of cells with ryanodine, ET-1 induced low magnitude, spatially restricted Ca^{2+} bursts in 3 out of the 8 cells

examined (Fig. 5.4, image 9, arrow 2). In the three cells which exhibited Ca^{2+} bursts in response to ET-1, a rise in the Fura-2 fluorescence ratio of 24 ± 0.1 % was observed within a given region of interest (Fig. 5.4). In the remaining 5 cells a small, non-uniform rise in the intracellular Ca^{2+} was also observed. However, these increases had less than clear spatial definition. As with thapsigargin, the lack of a discernable Ca^{2+} burst in these remaining cells was likely due to the Ca^{2+} burst occurring outwith the focal plane of the microscope. The average increase in Fura-2 fluorescence ratio within a given

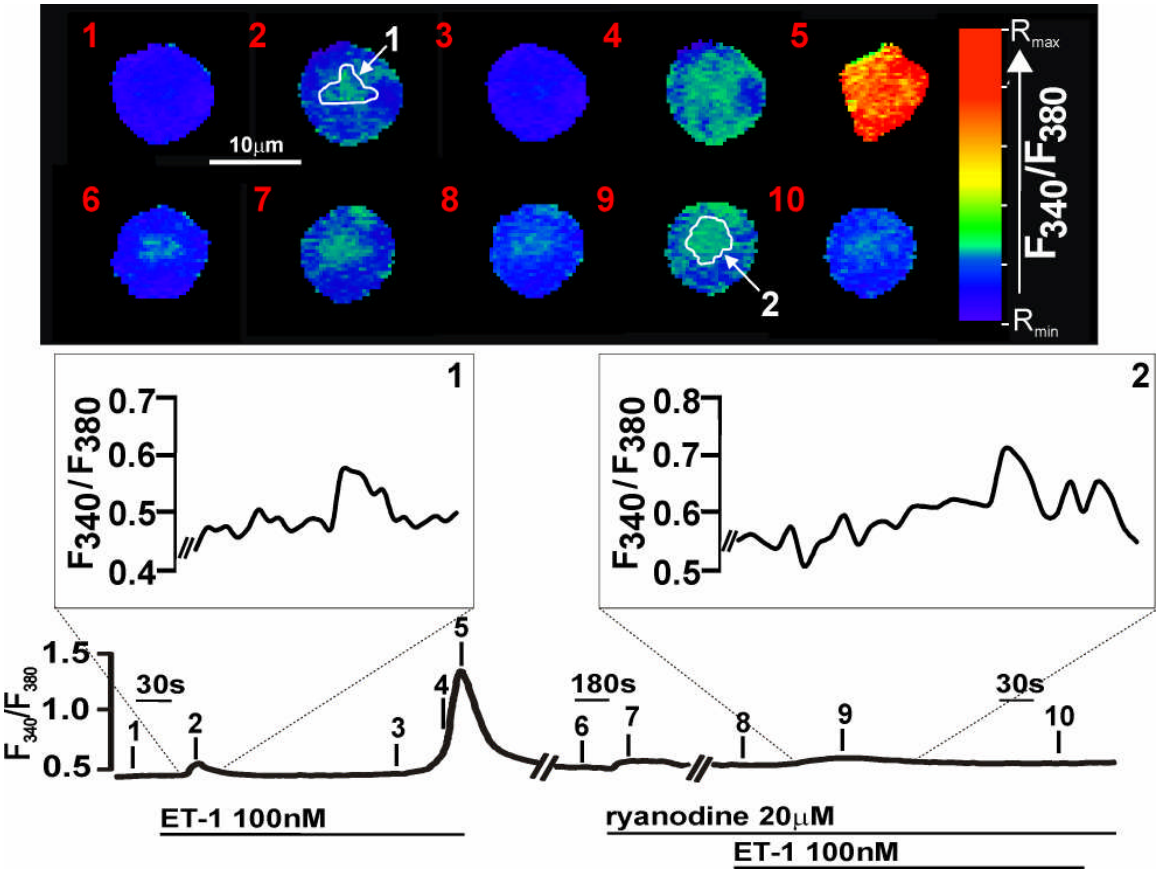

Fig. 5.4: **Ryanodine abolishes global Ca^{2+} waves in response to ET-1, but not localized release events.** ***Upper panel:*** shows a pseudocolour representation of the changes in Fura-2 fluorescence ratio within an isolated pulmonary artery smooth muscle cell after preincubation (20 min) with ryanodine (20 μM) in response to the extracellular application of ET-1 (100 nM). Note, the spatially restricted Ca^{2+} bursts indicated by arrows 1 and 2 in the the ROIs shown in images 2 and 9, respectively. ***Lower panel:*** shows the Fura-2 fluorescence ratio against time for the cell in the upper panel, inserts 1 and 2 show the Fura-2 fluorescence ratio for ROIs 1 and 2 indicated in pseudocolour representations 2 and 9, respectively.

region of interest in all 8 cells examined, following preincubation of cells with ryanodine, was 10 ± 1 % (Fig. 5.5; Appendix 3, Table 5.10). Taken together with the findings presented above, it can be concluded that ET-1 generates spatially restricted Ca^{2+} bursts from a thapsigargin-insensitive Ca^{2+} store which are, in turn, amplified to generate global Ca^{2+} waves by recruitment of RyRs via CICR. Indeed, the striking similarity in the pharmacology underlying the generation of global Ca^{2+} waves in response to NAADP, Bafilomycin A1 and ET-1 (Fig. 5.5), suggests that generation of global Ca^{2+} waves in response to ET-1 may be activated via NAADP-dependent Ca^{2+} release.

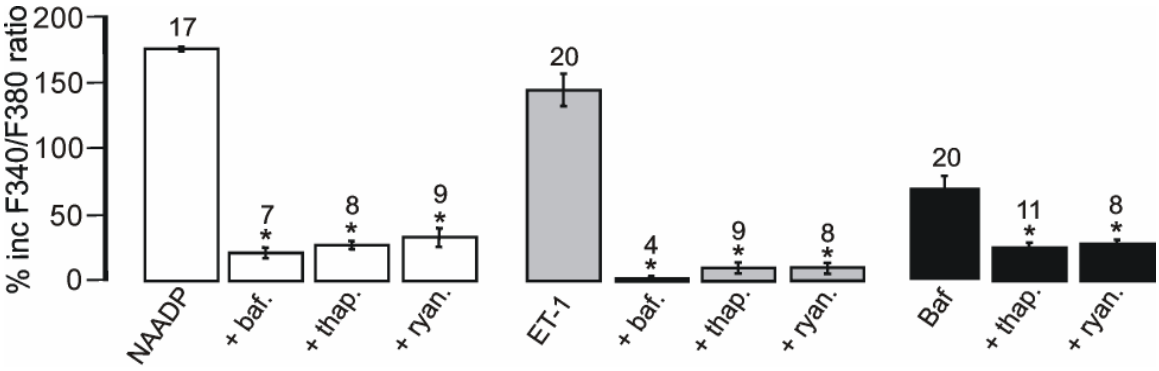

Fig. 5.5: **Comparison of the pharmacology of Ca^{2+} signals generated by NAADP, ET-1 and Bafilomycin A1 in isolated pulmonary artery smooth muscle cells:** ***Bar chart*** shows the percentage change (± S.E.M.) in Fura-2 fluorescence ratio in pulmonary artery smooth muscle cells induced by intracellular dialysis of NAADP (10 nM) before and after incubation of cells with Bafilomycin A1 (baf.; 100 nM), thapsigargin (thap.; 1 μM) and ryanodine (ryan.; 20 μM), respectively (white bars); extracellular application of ET-1 (100 nM) before and after incubation of cells with Bafilomycin A1 (100 nM), thapsigargin (1 μM) and ryanodine (20 μM), respectively (grey bars); extracellular application of Bafilomycin A1 (100 – 300 nM) before and after incubation of cells with thapsigargin (1 μM) and ryanodine (20 μM), respectively (black bars). Asterisk (*) denotes statistical significance of inhibition of Ca^{2+} signals vs. control by means of a one-way ANOVA test, where $p \leq 0.05$.

5.2.2 Endothelin-1 induces an increase in endogenous NAADP levels in pulmonary artery smooth muscle

In order to confirm the proposal that ET-1 initiates NAADP-dependent Ca^{2+} signals in pulmonary artery smooth muscle, in association with Dr. Justyn

Thomas, I investigated the effect of ET-1 on the levels of NAADP within pulmonary artery smooth muscle by means of an NAADP radioligand binding assay. The exposure of pulmonary arteries, denuded of their endothelia, to ET-1 (1 μM) resulted in a significant increase in the level of NAADP in tissue lysates. Thus ET-1 (1 μM) caused a significant increase in the levels of NAADP, from 0.21 ± 0.04 pmol/mg protein in the absence of ET-1 (time matched control), to 1.33 ± 0.19 pmol/mg protein within 30 s of exposure to ET-1 (1 μM; Fig. 5.6A; P = < 0.05; Appendix 3, Tables 5.12 and 5.13). This increase in the level of NAADP declined to baseline within 60s, measuring

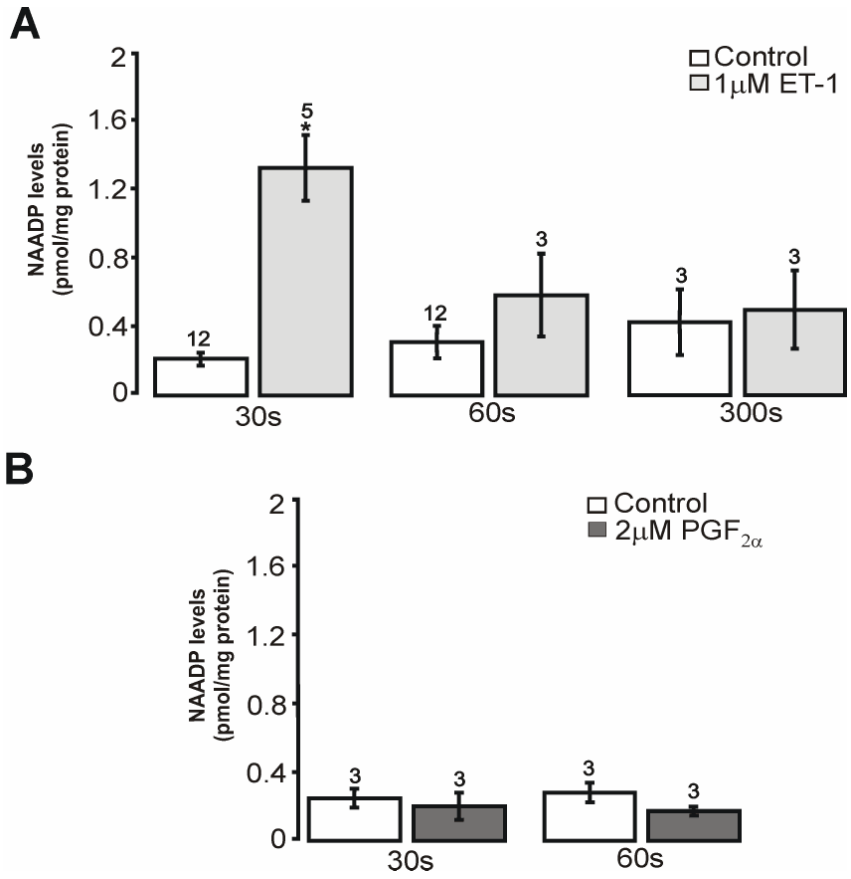

Fig. 5.6: **ET-1 causes a rapid transient in NAADP levels in arterial smooth muscle:** ***Panel A: Bar chart*** shows the effect of ET-1 (1 μM; 30, 60, and 300 s incubation) on the tissue levels of NAADP in the second and third order branches of the pulmonary arterial tree without endothelium, relative to levels in control tissue. Asterisk (*) denotes statistical significant difference when compared to control with a one way ANOVA test (P = ≤ 0.05). ***Panel B: Bar chart*** shows the effect of $PGF_{2\alpha}$ (2 μM; 30 and 60 s incubation) on the tissue levels of NAADP in the second and third order branches of the pulmonary arterial tree without endothelium, relative to levels in control tissue.

0.31 ± 0.09 pmol/mg protein in the absence of ET-1, and 0.58 ± 0.24 pmol/mg protein in the presence of ET-1 (1 μM; Fig. 5.6A; P = > 0.05; Appendix 3, Tables 5.12 and 5.14). Time course analysis showed that levels of NAADP within arteries exposed to ET-1 (1 μM) did not increase again from the basal level over a further incubation period (300 s). Thus, at 300 s, NAADP levels measured 0.43 ± 0.2 pmol/mg protein in the absence of ET-1, and 0.5 ± 0.2 pmol/mg protein in the presence of ET-1 (1 μM; Fig. 5.6A; P = > 0.05; Appendix 3, Tables 5.12 and 5.15). In contrast to the increase in NAADP levels induced by ET-1, the exposure of pulmonary arteries, denuded of endothelia, to $PGF_{2\alpha}$ (2 μM) had little or no effect on the level of NAADP detected, which measured 0.25 ± 0.06 pmol per mg tissue in the absence of $PGF_{2\alpha}$ (time matched control) and 0.2 ± 0.08 pmol per mg tissue in the presence of $PGF_{2\alpha}$ (2 μM) 30 s after exposure (n = 3; P = > 0.05; Appendix 3, Tables 5.16 and 5.17), and 0.28 ± 0.05 pmol/mg protein and 0.17 ± 0.02 pmol/mg protein, respectively, after 60s (Fig. 5.6B; P = > 0.05; Appendix 3, Tables 5.16 and 5.18).

These results suggest that ET-1 causes a rapid, transient increase in the concentration of NAADP in pulmonary artery smooth muscle in an agonist-specific manner. This rapid, transient increase in NAADP levels within pulmonary artery smooth muscle in response to ET-1, is entirely consistent with my proposal that NAADP mediates, at least in part, Ca^{2+} signalling by ET-1.

5.2.3 Endothelin-1 mediates NAADP-dependent Ca^{2+} signalling through activation of ETB receptors, but not ETA receptors, on pulmonary artery smooth muscle

ET-1 is a potent vasoconstrictor and mediates its effects through at least two known subtypes of ET receptor, ETA and ETB (Yanagisawa, *et al.*, 1988; Arai, *et al.*, 1990; Sakurai, *et al.*, 1990; Sakamoto, *et al.*, 1991; Leach, *et al.*, 1994; Yoshida, *et al.*, 1994; MacLean, *et al.*, 1995; Maguire, *et al.*, 1996; McCulloch, *et al.*, 1996). Therefore, I proceeded to examine the possibility that one discrete ET receptor subtype may underpin the generation of Ca^{2+} signals

in isolated pulmonary artery smooth muscle cells. In order to examine the possible roles of the ETA and ETB receptors in the generation of Ca^{2+} signals I co-applied selective antagonists of each of the subtypes of ET receptors, namely, the ETB receptor antagonist BQ-788 (Ishikawa, *et al.*, 1994; Karaki, *et al.*, 1994) and the ETA receptor antagonist BQ-123 (Morel and Godfriand, 1994; Warner, *et al.*, 1994) with ET-1.

Co-application of the ETB receptor antagonist BQ-788 (30 μM) with ET-1 (100 nM) abolished Ca^{2+} signals in isolated pulmonary artery smooth

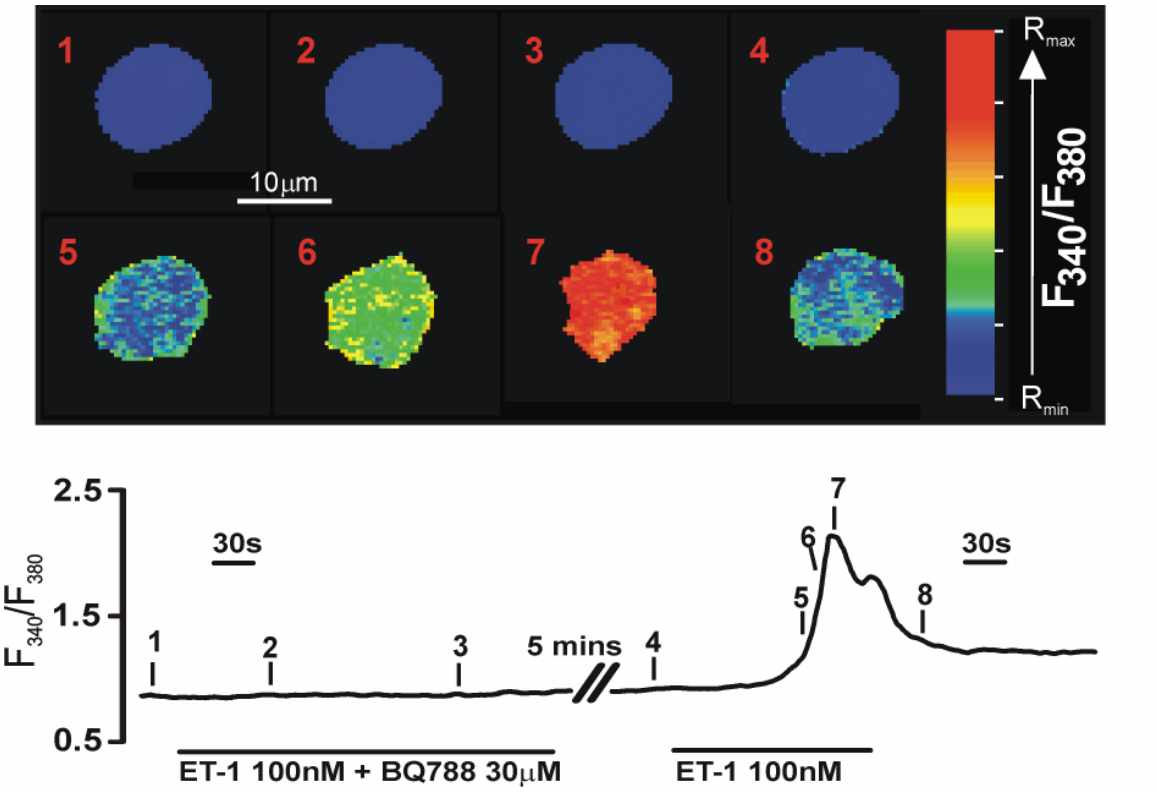

Fig. 5.7: **Activation of ETB receptors are required for the generation of global Ca^{2+} waves in response to ET-1:** ***Upper panel:*** shows a pseudocolour representation of the changes in Fura-2 fluorescence ratio within an isolated pulmonary artery smooth muscle cell in response to the extracellular application of ET-1 (100 nM) in the presence and absence of BQ-788 (30 μM). ***Lower panel:*** shows the Fura-2 fluorescence ratio against time for the cell in the upper panel.

muscle cells. However, following a period of wash (5 min) to remove BQ-788, application of ET-1 was seen to induce global Ca^{2+} signals and contraction of

cells. A representative experiment is shown in Fig 5.7. The upper panel shows a series of pseudocolour images of the Fura-2 fluorescence ratio, whilst the lower panel shows the record of the fluorescence ratio against time. Thus, ET-1 (100 nM) caused no discernable increase in the Fura-2 fluorescence ratio, 0.66 ± 0.05 to 0.66 ± 0.05 in the presence of BQ-788 (30 μM), however, ET-1 caused an increase in the Fura-2 fluorescence ratio from 0.7 ± 0.05 to 1.86 ± 0.23 in the absence of BQ-788 (n = 7, P = < 0.05; Appendix 3, Tables 5.19 and 5.12). These data suggest a role for ETB receptor activation in the generation of Ca^{2+} signals in response to the extracellular application of ET-1 (100 nM) in isolated pulmonary artery smooth muscle cells as the ETB receptor antagonist BQ-788 abolished Ca^{2+} signals in response to ET-1.

I then proceeded to examine a possible role for ETA receptors in the generation of Ca^{2+} signals in response to extracellular application of ET-1 (100 nM) in isolated pulmonary artery smooth muscle cells. It was observed that the ETA receptor antagonist BQ-123 did not affect Ca^{2+} signalling in response to ET-1 (100 nM). Fig. 5.8 shows a representative experiment. The upper panel shows a series of pseudocolour images of the Fura-2 fluorescence ratio, whilst the lower panel shows the record of the fluorescence ratio against time. It can be seen that in this example cell, application of ET-1 causes an initial increase in Ca^{2+} at the perimeter of the cell, indicated by the arrow in Fig. 5.7, images 3 – 5. This initial Ca^{2+} release event precedes the global Ca^{2+} wave and contraction within the cell and is reminiscent of one of the forms of Ca^{2+} bursts observed in response to the intracellular application of NAADP, as described previously (Chapter 3 Fig. 3.1, page 114). Thus, co-application of ET-1 (100 nM) and BQ-123 (30 μM) induced an increase in the Fura-2 fluorescence ratio from 0.59 ± 0.01 to 1.61 ± 0.04 (n = 5, Appendix 3, Table 5.21). These data suggest that the blockade of ETA receptors is without effect on the generation of Ca^{2+} signals in response to ET-1 (100nM). Therefore, it would appear that ETB, but not ETA receptor activation is required in order to initiate Ca^{2+} signalling in response to ET-1 in isolated pulmonary artery smooth muscle cells.

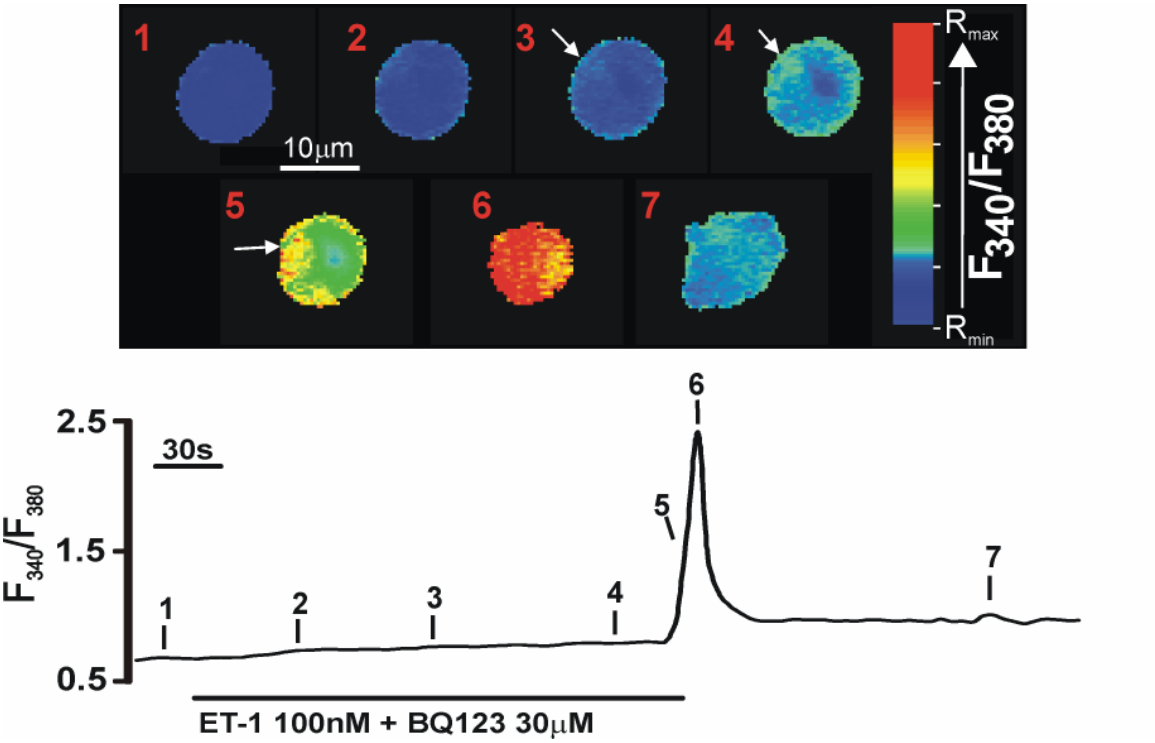

Fig. 5.8: **Activation of ETA receptors is not required for the generation of global Ca^{2+} waves in response to ET-1:** ***Upper panel:*** shows a pseudocolour representation of the changes in Fura-2 fluorescence ratio within an isolated pulmonary artery smooth muscle cell in response to the extracellular application of ET-1 (100 nM) in the presence and absence of BQ-123 (30 μM). ***Lower panel:*** shows the Fura-2 fluorescence ratio against time for the cell in the upper panel.

5.2.4 Endothelin-1-induced increases in endogenous NAADP levels in pulmonary artery smooth muscle occurs via activation of ETB receptors

Given the requirement on ETB receptor activation for initiation of Ca^{2+} signals in response to ET-1, in association with Dr. Justyn Thomas, I proceeded to examine the role of ETB receptors in the regulation of intracellular NAADP levels within pulmonary arterial smooth muscle. Increases in the levels of NAADP within second and third order branches of the pulmonary artery denuded of endothelia in response to ET-1 were not observed in tissue lysates that were exposed to ET-1 and the ETB receptor antagonist BQ-788. Thus, ET-1 (100 nM) caused a significant increase in the levels of NAADP from 0.18 ± 0.02 pmol/mg protein in the absence of ET-1

(time matched control) to 0.82 ± 0.11 pmol/mg protein within 30s exposure to ET-1 (100 nM; Fig. 5.9, P = < 0.05; Appendix 3, Tables 5.22 and 5.23). Consistent with a role for ETB receptors, the increase in NAADP levels in response to ET-1 was abolished in tissue lysates exposed to ET-1 (100 nM) and BQ-788 (30 μM), where NAADP levels were measured at 0.15 ±0.01 pmol/mg protein, when compared to time matched controls (Fig. 5.9; P = < 0.05; Appendix 3, Tables 5.22 and 5.24). Therefore, these data suggest that the increase in NAADP levels measured in pulmonary arteries, in response to ET-1, is initiated via activation of ETB receptors.

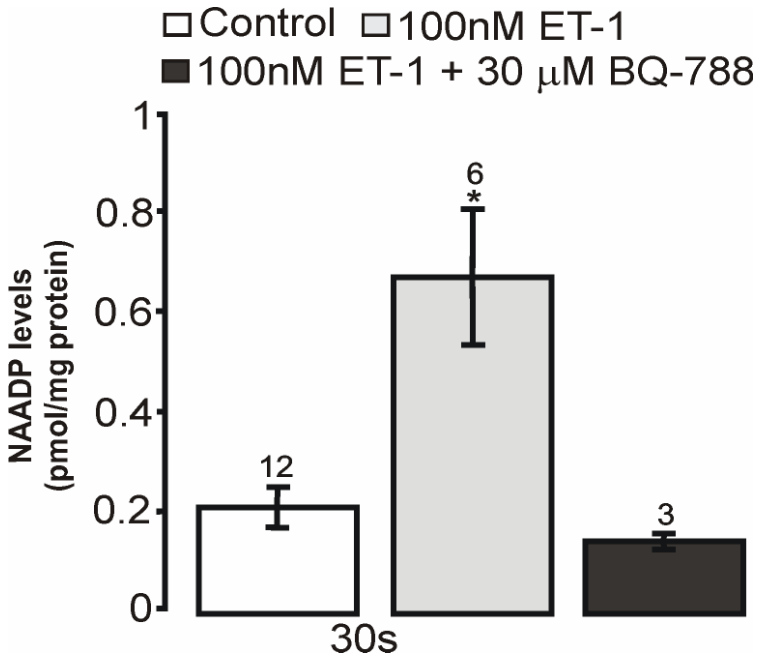

Fig. 5.9: **NAADP levels in pulmonary arterial smooth muscle is increased following activation of ETB receptors by ET-1:** ***Bar chart*** shows the effect of ET-1 (100 nM; 30 s incubation) both in the presence and absence of BQ-788 (20 μM), on the tissue levels of NAADP in the second and third order branches of the pulmonary arterial tree without endothelium, relative to levels in control tissue. Asterisk (*) denotes statistical significance when compared to control with a one way ANOVA test (P = ≤ 0.05).

5.3 Discussion

In this chapter I sought to determine whether or not NAADP elicits agonist- and receptor-specific Ca^{2+} signals in pulmonary arterial smooth muscle cells. To this end the: (1) pharmacology of Ca^{2+} signalling by the vasocontrictors phenylepherine (PE), prostaglandin $F_{2\alpha}$ ($PGF_{2\alpha}$) and endothelin-1 (ET-1) was compared with that of NAADP (2) the effect on NAADP levels in pulmonary arterial smooth muscle was studied.

5.3.1 Bafilomycin A1 abolishes Ca^{2+} signalling in an agonist specific manner

I have previously demonstrated that NAADP-dependent Ca^{2+} signals were abolished by pre-incubation of pulmonary arterial smooth muscle cells with Bafilomycin A1 (see Chapter 3). Consistent with this finding, Ca^{2+} signals in response to the extracellular application of ET-1 were abolished by Bafilomycin A1, whilst those elicited by PE and $PGF_{2\alpha}$ remained unaffected. Of further significance was the finding that global Ca^{2+} waves evoked by ET-1, like those in response to NAADP, were preceded by spatially restricted Ca^{2+} release events akin to Ca^{2+} bursts (see section 5.3.2). In common with NAADP, therefore, Ca^{2+} signals evoked by ET-1, but not PE and $PGF_{2\alpha}$, may be dependent, at least in part, upon the mobilisation of a bafilomycin-sensitive, acidic Ca^{2+} store. Direct support for this conclusion may be taken from a subsequent study on bovine coronary artery smooth muscle cells in which ET-1-induced Ca^{2+} signals were shown to be abolished by Bafilomycin A1 (Zhang, *et al.*, 2006).

5.3.2 Endothelin-1 induces Ca^{2+} bursts from lysosome-related Ca^{2+} stores that are then amplified into global Ca^{2+} signals by ryanodine receptor-mediated sarcoplasmic reticulum Ca^{2+} release

In common with NAADP (see Chapter 3), global Ca^{2+} waves in response to the extracellular application of ET-1 were abolished following

depletion of SR stores Ca^{2+} with the SERCA pump antagonist thapsigargin, while spatially restricted Ca^{2+} bursts were still observed. Thus, SR Ca^{2+} release is a pre-requisite for the generation of global Ca^{2+} waves but not localised Ca^{2+} bursts elicited by ET-1. Furthermore, block of ryanodine receptors by pre-incubation of pulmonary arterial smooth muscle cells with ryanodine abolished global Ca^{2+} waves in response to application of ET-1. Once more this occurred without affect on spatially restricted Ca^{2+} bursts. Direct comparison of the pharmacological profile of NAADP-, Bafilomycin A1- and ET-1-induced Ca^{2+} signals, suggests, therefore, that all three stimuli elicit global Ca^{2+} waves in pulmonary artery smooth muscle cells via a common mechanism, that is by evoking Ca^{2+} bursts from a Bafilomycin-sensitive, acidic Ca^{2+} store other than the SR, which are then amplified into global Ca^{2+} waves by CICR from the SR via RyRs.

5.3.3 Endothelin-1 induces agonist-specific increases in the concentration of NAADP in pulmonary artery smooth muscle

In order to determine whether or not NAADP does indeed mediate, at least in part, Ca^{2+}-mobilisation in response to ET receptors activation I investigated the effects of agonist exposure on the concentration of NAADP in pulmonary artery smooth muscle. Exposure of 2^{nd} and 3^{rd} order branches of the pulmonary arterial tree, denuded of endothelia, to ET-1 for 30s resulted in a significant increase in NAADP levels within tissue lysates. The increase in NAADP levels was both rapid and transient, because it was seen to return to basal levels within 60 s and did not increase again over a further 300 s period of exposure to ET-1. This finding suggests that NAADP likely acts to initiate rather than maintain Ca^{2+} signals in response to ET-1. Importantly, the coupling of NAADP synthesis to cell surface receptors was found to be both agonist- and receptor-specific. Thus, $PGF_{2\alpha}$ elicited no change in NAADP levels in paired pulmonary artery smooth muscle lysates.

In support of my findings, a recent study has shown that exposure of bovine coronary artery homogenates to ET-1 stimulates a significant increase in the conversion of $NADP^+$ to NAADP (Zhang, *et al.*, 2006). It seems likely,

therefore, that NAADP-dependent signalling may play a functional role in mediating agonist-specific Ca^{2+} signalling throughout the vasculature and it is clear that it may function in this way in a variety of cell types. For example, a recent investigations into the mechanisms underpinning NAADP-dependent Ca^{2+} signalling in pancreatic acinar cells (Yamasaki, *et al.*, 2005) demonstrated that the activation of cholecystokinin (CCK) A receptors on the surface of pancreatic acinar cells caused a rapid, transient increase in the cellular levels of NAADP, while the activation of muscarinic acetylcholine receptors (mAChR) by acetylcholine (ACh) did not.

5.3.4 NAADP-dependent Ca^{2+} signalling in pulmonary artery smooth muscle is coupled to ETB but not ETA receptor activation

ET-1 exerts its vasoconstrictor activity through the activation of two subtypes of receptor, namely the endothelin A receptor (ETA) and the endothelin B receptor (ETB; Arai, *et al.*, 1990; Sakurai, *et al.*, 1990). Indeed, the vasoconstrictor actions of ET-1 in the intrapulmonary resistance arteries of rabbit and rat appear to be mediated via both ETA and ETB receptors (Ladouceur, *et al.*, 1993; MacLean, *et al.*, 1994). Significantly in this respect, there is evidence to suggest that each ET receptor subtype may couple to the same or different Ca^{2+}-mobilising second messengers and in some cases in a tissue-dependent manner. For example, in the main branch and 2nd and 3rd order branches of rat pulmonary arteries, ETA receptors have been proposed to couple to IP_3 (Hyvelin, *et al.*, 1998; Zhang, *et al.*, 2003), while ETA receptors may couple to both IP_3 and cADPR in rat peritubular smooth muscle (Barone, *et al.*, 2002). Furthermore, ETB receptors have been proposed to couple to cADPR but not IP_3 in both peritubular smooth muscle (Barone, *et al.*, 2002) and shark vascular smooth muscle (Fellner and Parker, 2004). I therefore sought to determine which of the two endothelin receptor subtypes coupled to NAADP in pulmonary arterial smooth muscle.

When applied in combination with the ETB receptor antagonist BQ-788, ET-1 failed to induce Ca^{2+} signals in pulmonary artery smooth muscle cells. Importantly however, subsequent application of ET-1 in the absence of BQ-788 induced a global Ca^{2+} wave of a similar magnitude to those evoked by

ET-1 in cells which had not been previously exposed to BQ-788. In marked contrast, the ETA receptor antagonist BQ-123 was found to be without effect on Ca^{2+} signalling in response to ET-1. Therefore, NAADP-dependent Ca^{2+} signals induced by 100 nM ET-1 in isolated pulmonary artery smooth muscle cells are likely initiated by activation of ETB receptors, but not via the activation of ETA receptors. Furthermore, the rapid, transient increase in NAADP levels measured in endothelium denuded pulmonary arteries in response to ET-1 was abolished following exposure of tissue to ET-1 in the presence of the ETB receptor antagonist BQ-788. These findings suggest that ET-1 initiates Ca^{2+} signalling via NAADP following activation of ETB receptors in isolated pulmonary artery smooth muscle cells. These findings are in contrast to a previous investigation in smooth muscle cells of 2nd and 3rd order branches of the pulmonary artery which showed ET-1 (0.1 – 10 nM) mediated Ca^{2+} signalling via ETA receptor activation coupled to IP_3 (Zhang, *et al.*, 2003). One possible explanation for this discrepancy is that at the IP_3-dependence of observed responses to ET-1 is not evident at the concentration (100 nM) applied here.

In summary, the findings presented in this chapter suggest that activation by ET-1 of ETB receptors, but not ETA receptors, induces an increase in NAADP levels within pulmonary artery smooth muscle and that this increase in NAADP levels may, in part, underpin global Ca^{2+} signalling and contraction of pulmonary artery smooth muscle cells in response to ET-1. Furthermore, my data suggest that NAADP-dependent Ca^{2+} signalling may be evoked in an agonist-specific manner, since PE and $PGF_{2\alpha}$ evoked signals independent of NAADP and lysosome-related Ca^{2+} stores. These findings provide further evidence in support of the proposal that NAADP is an important and agonist-specific Ca^{2+}-mobilising messenger in mammalian cells (Cancela, *et al.*, 1999; Yamasaki, *et al.*, 2004; Zhang, *et al.*, 2006). A schematic representation of the model I propose to describe the nature of ET-1-mediated Ca^{2+} signalling in arterial smooth muscle is shown in Fig. 5.10. Thus, activation of ETB receptors on the surface of arterial smooth muscle cells induces an increase in NAADP synthesis, which is likely catalysed by ADP-ribosyl cyclase (Wilson, *et al.*, 1998). NAADP then activates putative NAADP

receptors located on the surface of lysosomes to initiate a Ca^{2+} burst. This occurs within a lysosome-SR junction proximal to ryanodine receptors, leading to amplification of the Ca^{2+} burst into a global Ca^{2+} wave by CICR via RyRs.

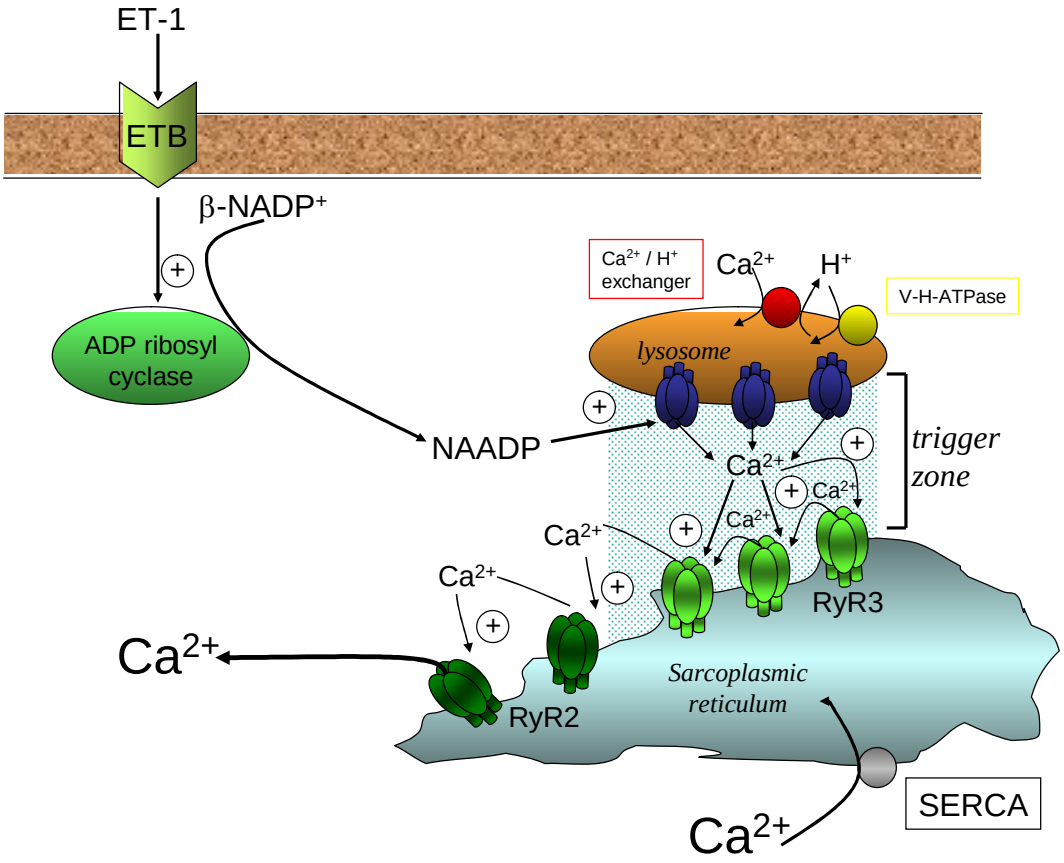

Fig. 5.10 **Schematic representation of proposed model of NAADP-dependent Ca^{2+} signalling induced by ET-1 in pulmonary artery smooth muscle cells:** Activation of ETB receptors on the surface of cells by ET-1 induces an increase in the synthesis of NAADP within pulmonary artery smooth muscle cells. NAADP activates the putative NAADP receptor on the surface of lysosomes to cause an initial Ca^{2+} burst. This initial Ca^{2+} burst is then amplified by calcium-induced calcium-release via ryanodine receptor subtype 3 on the surface of the sarcoplasmic reticulum that lie in close apposition to the lysosomes. Further activation of ryanodine receptor subtype 2 outwith the trigger zone then leads to a global Ca^{2+} wave and contraction of the cell.

Chapter 6: General discussion

The investigations presented within this thesis provide evidence in support of the proposal from this laboratory that NAADP acts as a discrete and potent Ca^{2+}-mobilising messenger in arterial smooth muscle (Boittin *et al.*, 2002). Significantly, I provide the first direct evidence in mammalian smooth muscle in support of the proposal (Churchill, *et al.*, 2002; Yamasaki, *et al.*, 2004; Yamasaki, *et al.*, 2005) that NAADP may selectively elicit Ca^{2+} signals from a lysosome-related Ca^{2+} store alone, which may then be amplified by CICR from the SR/ER via RyRs (Fig. 6.1). Furthermore, my data show that NAADP-dependent signalling is recruited in an agonist-specific manner. Thus, different agonists may evoke discrete and characteristic signalling patterns by selective recruitment of a given Ca^{2+}-mobilising second messenger and its complementary Ca^{2+} storing organelle(s).

6.1 NAADP mobilises Ca^{2+} from a lysosome-related Ca^{2+} store separate to the sarcoplasmic reticulum in pulmonary artery smooth muscle

In this thesis, I showed that selective block by Bafilomycin A1 of the vacuolar proton pump (V-H^+ ATPase; Haller, *et al.*, 1996; Christensen, *et al.*, 2002) discharged lysosome-related Ca^{2+} stores and, thereby, abolished Ca^{2+} signalling by NAADP. Bafilomycin A1 was without effect on SR Ca^{2+} stores as Ca^{2+} signals generated by the activation of Ca^{2+} release through RyRs, via caffeine application, or the activation of IP_3Rs via IP_3 application, remained unaffected following preincubation of pulmonary artery smooth muscle cells with Bafilomycin A1. These findings are entirely consistent with the proposal by Churchill *et al* (2002) that reserve granules in sea urchin eggs may act as an NAADP-sensitive Ca^{2+} store. That an acidic, lysosome-related organelle can act as an accessible Ca^{2+} store is in keeping with previous reports of a role for lysosomes in Ca^{2+} signalling in snail neurones (Sugaya and Onozuka, 1978), Madin-Darby canine kidney cells (Haller, *et al.*, 1996) and a cell-line derived from *Drosophila Melanogaster* (Yagodin, *et al.*, 1999). Further support for this viewpoint may be derived from the finding that non-ER acidic vesicles, which

may be related to lysosomes or secretory vesicles may constitute the NAADP-sensitive Ca^{2+} store in pancreatic acinar cells and clonal pancreatic β cells (MIN6; Yamasaki, *et al.*, 2004), and from the finding that a Bafilomycin A1-sensitive, acidic Ca^{2+} store promotes growth of rat cortical neurons (Brailoiu, *et al.*, 2005). However, my observations are contrary to the proposal that NAADP primarily mobilises Ca^{2+} by direct activation of RyRs on a thapsigargin-sensitive store in skeletal muscle (Hohenegger, *et al.*, 2002) and the nuclear envelope of isolated pancreatic acinar cell nuclei (Gerasimenko, *et al.*, 2003).

Consistent with the amplification by CICR of intracellular Ca^{2+} signals in other cell types (Takasawa, *et al.*, 1998; Cancela, *et al.*, 1999; Cancela, 2001; Patel, *et al.*, 2001), NAADP-dependent Ca^{2+} mobilisation in pulmonary artery smooth muscle is subsequently amplified by Ca^{2+} release from the SR. In fact, the findings presented in this thesis, consistent with previous findings from this laboratory (Boittin *et al.*, 2002), further suggests that in arterial smooth muscle NAADP-dependent Ca^{2+} signalling via lysosome-related Ca^{2+} stores alone is not sufficient to elicit a global Ca^{2+} wave and activation of primary cell function, in this case contraction. This is apparent as NAADP-dependent Ca^{2+} bursts may occur with or without a global Ca^{2+} wave or smooth muscle contraction. Moreover, global Ca^{2+} waves by NAADP may be triggered in an all-or-none fashion by NAADP-dependent Ca^{2+} bursts in a manner dependent on subsequent CICR from the SR via RyRs.

The requirement for amplification of NAADP-dependent Ca^{2+} bursts by CICR via RyRs is apparent from the fact that selective depletion of SR Ca^{2+} stores by thapsigargin, or block of RyRs by ryanodine abolished global Ca^{2+} waves by NAADP, but not spatially restricted Ca^{2+} bursts via lysosomes (Boittin *et al.*, 2002). My investigations provide further support for this viewpoint in that, when lysosome-related Ca^{2+} stores were discharged by Bafilomycin A1, spatially restricted Ca^{2+} release events were seen to precede global Ca^{2+} waves. Furthermore, these global Ca^{2+} waves but not spatially restricted Ca^{2+} release in response to Bafilomycin A1 alone were abolished after depletion of SR Ca^{2+} stores by thapsigargin or by block of RyRs using ryanodine. In short, global Ca^{2+} waves by NAADP and Bafilomycin A1 required amplification of initial Ca^{2+} signals by CICR via RyRs in the SR.

6.2 Lysosomes associate with a subpopulation of ryanodine receptors to form a trigger zone for NAADP-dependent Ca^{2+} signalling in pulmonary artery smooth muscle

In contrast to the findings of others with respect to NAADP (Takasawa, *et al.*, 1998; Cancela, *et al.*, 1999; Cancela, 2001; Patel, *et al.*, 2001), data from this laboratory suggest that Ca^{2+} signalling by IP_3 in arterial smooth muscle occurs in a manner independent of lysosomal Ca^{2+} stores and that IP_3 is able to initiate a global Ca^{2+} wave in the absence of CICR via RyRs (Chapter 3; Boittin et al., 2002). Cells may therefore coordinate and restrict the relationship between lysosomal Ca^{2+} stores and the SR/ER in a manner suited to their function. Consistent with this proposal and in contrast to previous investigations that have shown a diffuse, granular pattern of lysosome-related organelles in both sea urchin eggs (Churchill et al., 2002) and MIN6 (Yamasaki et al., 2004), my data suggests that lysosomes may form highly organised and spatially restricted clusters in freshly isolated pulmonary arterial smooth cells when visualised using the fluorescent probe LysoTracker Red. The organelles were determined to be lysosomes as they lost fluorescence in a time-dependent manner following the addition of glycyl-phenylalanyl-napthylamide (GPN), a known substrate of the lysosomal exopeptidase cathepsin C. Upon entering lysosomes GPN is hydrolysed to free amino acids by the actions of the cathepsin C (Berg, *et al.*, 1994). When the spatial distribution of LysoTracker Red labelled lysosomes and BODIPY-FL ryanodine labelled RyRs were examined in freshly isolated pulmonary artery smooth muscle cells, it was observed that lysosomal clusters were closely associated with a subpopulation of RyRs. These closely associated RyRs and lysosomal clusters appear to be separated by a narrow junction or cleft that is less than 0.4 μm wide. Thus, lysosomal clusters and RyRs may form a highly organised trigger zone for Ca^{2+} signalling by NAADP in arterial smooth muscle (Fig. 6.1). The presence of this trigger zone may explain, in part, why Ca^{2+} bursts by NAADP induce global Ca^{2+} signals in a manner that requires CICR via RyRs in the SR of arterial smooth muscle cells, whereas Ca^{2+} release by IP_3 does not (Chapter 3; Boittin et al., 2002).

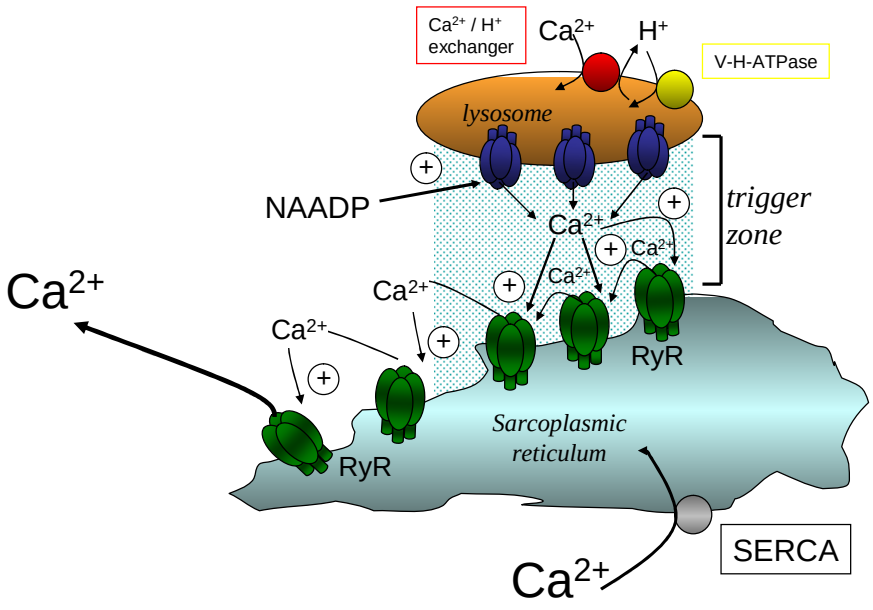

Fig. 6.1 **Schematic diagram of the proposed trigger zone between RyRs and lysosomes in the formation of a trigger zone for NAADP-dependent Ca^{2+} signalling in pulmonary artery smooth muscle cells.** The formation of a trigger zone between lysosomes and RyRs allows for the amplification of NAADP-mediated Ca^{2+} bursts into global Ca^{2+} waves by the recruitment of RyRs located on the Sarcoplasmic Reticulum by the mechanism of Ca^{2+}-induced Ca^{2+}-release.

6.3 Large clusters of lysosomes are located close to the nucleus of pulmonary artery smooth muscle cells

Immunocytochemical investigations carried out on pulmonary artery smooth muscle cells, showed that although labelling of lysosomes was evident throughout the cytoplasm of cells, a greater density of lysosomal labelling and a larger mean volume of elements of lysosomal labelling was observed in the perinuclear region than in either the extra-perinuclear or sub-plasmalemmal regions. The large volumes of lysosomal labelling located in the perinuclear region of pulmonary artery smooth muscle cells resembled the large, spatially restricted clusters of lysosomes visualised using LysoTracker Red, located

close to the centre of elongated pulmonary artery smooth muscle cells. These findings suggest, therefore, that large clusters of lysosomes are located in close proximity to the nucleus of pulmonary artery smooth muscle cells and are consistent with the perinuclear distribution of lysosomes observed in a number of other tissues, including vascular smooth muscle (Peters, *et al.*, 1972; James-Kracke, *et al.*, 1979; Robinson, *et al.*, 1986; Matteoni and Kreis, 1987; Pohlmann, *et al.*, 1995; Reaves, *et al.*, 1996b). Furthermore, spatially restricted clusters of lysosomes were seen to correspond to spatially restricted Ca^{2+} burst events observed in pulmonary artery smooth muscle cells in response to NAADP. The resemblance between the distributions of lysosomes in pulmonary artery smooth muscle cells with one of the forms of spatially restricted Ca^{2+} bursts observed in response to NAADP, combined with the finding that lysosomal clusters are located in the perinuclear region of cells, provides compelling evidence that spatially restricted NAADP-mediated Ca^{2+} bursts are elicited from clusters of lysosomes located in the perinuclear region of cells.

However, the limited lysosomal labelling observed within the sub-plasmalemmal region of elongated pulmonary artery smooth muscle cells examined in immunocytochemical studies appears to be contrary to my earlier observations in live cells that lysosomes may form a ring around the periphery of the cell consistent with the second form of Ca^{2+} burst generated in response to NAADP; namely a ring of Ca^{2+} release observed around the periphery of cells. This discrepancy may be explained due to the contracted state of the subset of cells which displayed either peripheral LysoTracker Red labelling of lysosomes, or peripheral Ca^{2+} bursts in response to NAADP. Thus, as these cells had contracted, the cytoplasmic space between the nucleus and the plasma membrane would be greatly reduced. The contents of the cytoplasm would, therefore, be concentrated into a relatively small area around the nucleus and would be visualised as appearing close to the plasma membrane. It is likely, therefore, that the contracted state of a given pulmonary artery smooth muscle cell could determine whether or not a focal lysosomal cluster proximal to the nucleus is evident and thereby determine the characteristics of a Ca^{2+} burst within such a cell.

6.4 Do lysosomes colocalise with a specific subtype of ryanodine receptor in pulmonary artery smooth muscle cells?

As mentioned previously, LysoTracker Red labelled lysosomes were seen to associate with a subpopulation of RyRs to form lysosome-SR junctions in pulmonary artery smooth muscle cells. To date there have been three distinct subtypes of RyRs identified, all of which have been shown to be present in pulmonary artery smooth muscle (Chapter 4, Hermann-Frank, et al., 1991, Neylon, et al., 1995, Jeyakumar, et al., 1998, Coussin, et al., 2000, Mirroneau, et al., 2001, Yang, et al., 2005, Zheng et al., 2005). That all three subtypes of RyR are expressed in pulmonary artery smooth muscle raises the question as to whether or not lysosomes form a trigger zone for NAADP-mediated Ca^{2+} signalling with one particular subtype of RyR. Therefore, I examined the spatial organisation of RyRs within pulmonary artery smooth muscle cells and the degree to which each subtype associated with lysosomes.

6.4.1 Differences in the distribution of ryanodine receptor subtype 1, 2 and 3 in pulmonary artery smooth muscle cells

Immunocytochemical examination of pulmonary artery smooth muscle cells showed that RyR1 labelling was uniformly distributed throughout the cytoplasm of cells, with little evidence of clustering in the perinuclear, extra-perinuclear or sub-plasmalemmal regions.

In contrast, RyR2 labelling was seen to predominate in the extra-perinuclear region where a greater density and larger clusters of RyR2 labelling was observed than in either the perinuclear or sub-plasmalemmal regions.

RyR3 labelling on the other hand, was seen to predominate in the perinuclear region of cells, where the extensive clustering of RyR3 was reminiscent of the greater clustering of lysosomal labelling in the perinuclear region when compared to either the extra-perinuclear or sub-plasmalemmal regions.

Comparison between the labelling of the three different RyR subtypes identified marked differences in their distributions within cells. Thus, RyR3 was seen to be the dominant subtype of RyR detected in the perinuclear region,

while RyR2 was predominant in the extra-perinuclear region and RyR1 was the predominant subtype of RyR in the sub-plasmalemmal region of cells. Therefore, the profound differences in the distributions of the different RyR subtypes within the cytoplasm of cells may be indicative of functional relevance, with each of the subtypes having an important and distinct role in the regulation of SR Ca^{2+} signalling in different areas of pulmonary artery smooth muscle cells.

6.4.2 Lysosomes and ryanodine receptor subtype 3, but not ryanodine receptor subtype 1 or 2, form large areas of colocalisation in the perinuclear region of pulmonary artery smooth muscle cells

Comparison of the degree to which RyR1, RyR2 and RyR3 associated with lysosomes indicated that RyR3 labelling colocalised with lysosomes to a much greater extent than either RyR1 or RyR2 within the perinuclear region of pulmonary artery smooth muscle cells. Indeed, both the density and the mean volume of areas of colocalisation between RyR3 and lysosomes were significantly larger than was measured for either RyR2 or RyR1 in the perinuclear region. The colocalisation between RyR3 and lysosomes declined considerably outwith the perinuclear region and there was little difference between the extent to which each of the RyR subtypes colocalised with lysosomes in either the extra-perinuclear or sub-plasmalemmal regions. Furthermore, examination of the fluorescent labelling located in close proximity to large areas of colocalisation between the RyR subtypes and lysosomes in the perinuclear region indicated that larger clusters of lysosomes were associated with areas of colocalisation between RyR3 and lysosomes than was observed with RyR2 or RyR1.

Therefore, these findings indicate that the trigger zone for NAADP-mediated Ca^{2+} signalling is formed between clusters of lysosomes and portions of the SR expressing clusters of RyR3 in the perinuclear region of pulmonary artery smooth muscle cells (Fig. 6.2). Furthermore, the dominance of RyR2 within the extra-perinuclear region of cells suggests that RyR2 may function to carry a propagating Ca^{2+} signal away from the trigger zone to the rest of the

cell following amplification of the initial NAADP-mediated Ca^{2+} burst by RyR3 (Fig. 6.2).

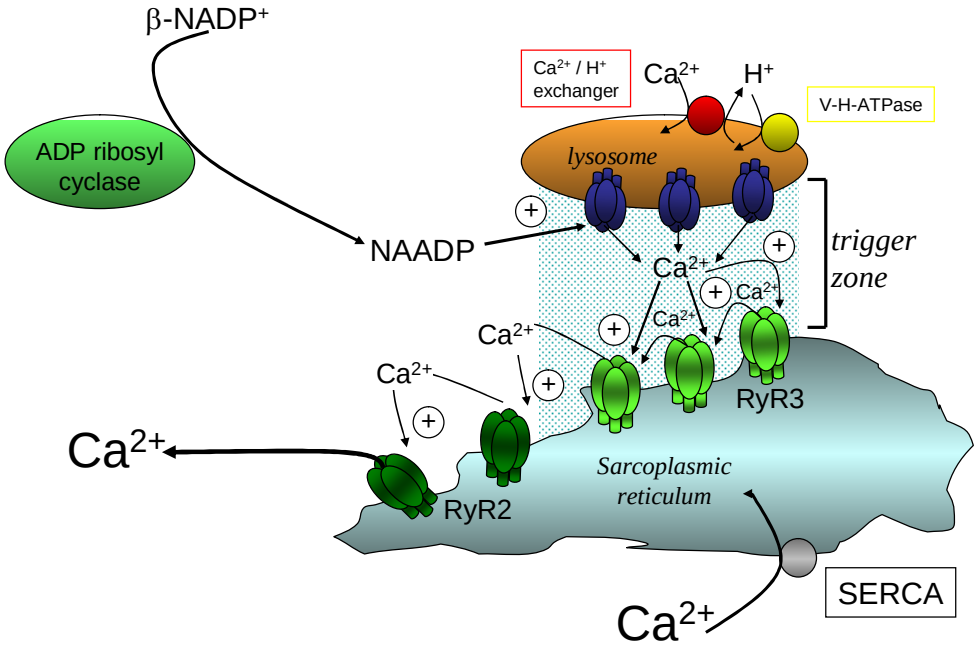

Fig. 6.2 **Schematic diagram of the proposed role for RyR3 and RyR2 in the formation of the trigger zone for NAADP-dependent Ca^{2+} signalling in pulmonary artery smooth muscle cells.** RyR3 on the Sarcoplasmic Reticulum (SR) are located close to putative NAADP receptors on the surface of lysosomes forming the proposed trigger zone for NAADP-dependent Ca^{2+} signalling in the perinuclear region of cells. Ca^{2+} released from lysosomal Ca^{2+} stores activates RyR3s, resulting in an increase in the Ca^{2+} concentration in the trigger zone. Ca^{2+} signals generated in the trigger zone are amplified to global Ca^{2+} signals by the recruitment of RyR2 located through the cytoplasm of the cell by the mechanism of Ca^{2+}-induced Ca^{2+}-release.

6.5 NAADP-mediated Ca^{2+} signalling is activated in an agonist-specific manner in pulmonary artery smooth muscle cells

Significant support for a role for NAADP and lysosomes in a discrete and agonist-specific Ca^{2+}signalling pathway in arterial smooth muscle was derived from my investigation of the effects of three different vasoconstrictors, phenylepherine (PE), prostaglandin-$F_{2\alpha}$ ($PGF_{2\alpha}$) and endothelin-1 (ET-1).

Firstly, depletion of lysosomal Ca^{2+} stores by Bafilomycin A1 abolished Ca^{2+} signalling in response to ET-1. However Bafilomycin A1 was without effect on Ca^{2+} mobilisation by either $PGF_{2\alpha}$, PE or by direct activation of RyRs with caffeine. Furthermore, my data are consistent with the idea that ET-1, like NAADP, evoked spatially restricted Ca^{2+} bursts from lysosomes that were amplified by CICR from the SR via RyRs (Fig. 6.3). Most conclusively, however, I have shown that NAADP levels were raised in pulmonary arterial smooth muscle upon exposure to ET-1 but not $PGF_{2\alpha}$. Further examination of ET-1 evoked Ca^{2+} signals in arterial smooth muscle showed that the generation of Ca^{2+} signals in response to ET-1 in my studies was mediated through the activation of ETB receptors, independent of the activation of ETA receptors (Fig. 6.3). It was also shown that the increase in NAADP levels following treatment of arterial smooth muscle with ET-1 was abolished following incubation of tissue with the ETB receptor antagonist BQ-788.

A previous investigation in peritubular smooth muscle from rat testis has suggested a role for cADPR in the generation of Ca^{2+} signals in response to activation of both ETA and ETB receptors (Barone et al., 2002), while a role for cADPR in the regulation of Ca^{2+} signalling in response to the activation of ETB receptors in shark vascular smooth muscle has also been identified (Fellner and Parker, 2004). Furthermore, a recent study in pancreatic acinar cells has demonstrated an increase in the synthesis of both NAADP and cADPR in response to the activation of cell surface receptors (Yamasaki et al., 2005). Briefly, following initial stimulation of pancreatic acinar cells with the brain-gut peptide (CCK) there is an immediate increase in the cellular levels of NAADP. This immediate increase in NAADP levels mediates initial Ca^{2+} signals. However, this rise in NAADP levels is seen to be transient and as the levels of NAADP decline there is an increase in the cellular levels of cADPR which plays a role in the sustained Ca^{2+} response to CCK by sensitising RyRs to activation by CICR (Yamasaki et al., 2005). There are obvious parallels therefore, between the transient rise in NAADP levels in response to CCK in pancreatic acinar cells (Yamasaki et al., 2005) and the transient increase in NAADP levels in arterial smooth muscle in response to ET-1 described within this thesis. These similarities in the changes in NAADP levels between

pancreatic acinar cells and arterial smooth muscle, coupled with the evidence of an involvement of cADPR in ET-1-mediated Ca^{2+} signalling in smooth muscle cells from different tissues (Barone et al., 2002; Fellner and Parker, 2004) raises the possibility of an involvement of cADPR in mediating Ca^{2+} signalling in response to ET-1 in pulmonary arterial smooth muscle. Thus, ET-1 may initiate transient global Ca^{2+} signals via NAADP-mediated Ca^{2+} release following activation of ETB receptors. The ability of NAADP-mediated Ca^{2+} bursts to generate subsequent, sustained global Ca^{2+} signals may then be governed by the actions of cADPR through modulation of the sensitivity of RyR2 to activation by cytosolic Ca^{2+} (Clementi, *et al.*, 1996; Lukyanenko and Gyorke, 1999; Prakash, *et al.*, 2000). Thereby, an increase in the cellular levels of cADPR, following the initial transient rise in NAADP levels, may shift the threshold Ca^{2+} concentration required for the generation of global Ca^{2+} signals by CICR via RyR2 in such a way that Ca^{2+} signals in response to ET-1 may be maintained in the absence of further NAADP-dependent Ca^{2+} release. Conversely, an immediate increase in cADPR levels following exposure to ET-1 could serve to modulate the threshold for initiation of CICR via RyRs and lower the threshold for NAADP-mediated Ca^{2+} bursts to the point where the failsafe mechanism afforded by the presence of RyR3 in the trigger zone is negated. Indeed, a previous study in bovine and murine skeletal muscle has shown that cADPR increases the Po of RyR3 by 20-fold and that the affinity of RyR3 for Ca^{2+} is increased by around 10-fold (Sonnleitner, *et al.*, 1998). Thus, the actions of cADPR on RyR3 and/or RyR2 may serve to promote both the generation and maintenance of global Ca^{2+} waves in pulmonary artery smooth muscle following initiation of NAADP-mediated Ca^{2+} bursts from lysosomal Ca^{2+} stores (Fig. 6.3). However, such a role for cADPR in the regulation of Ca^{2+} signals in response to ET-1 in smooth muscle of the pulmonary artery remains to be elucidated.

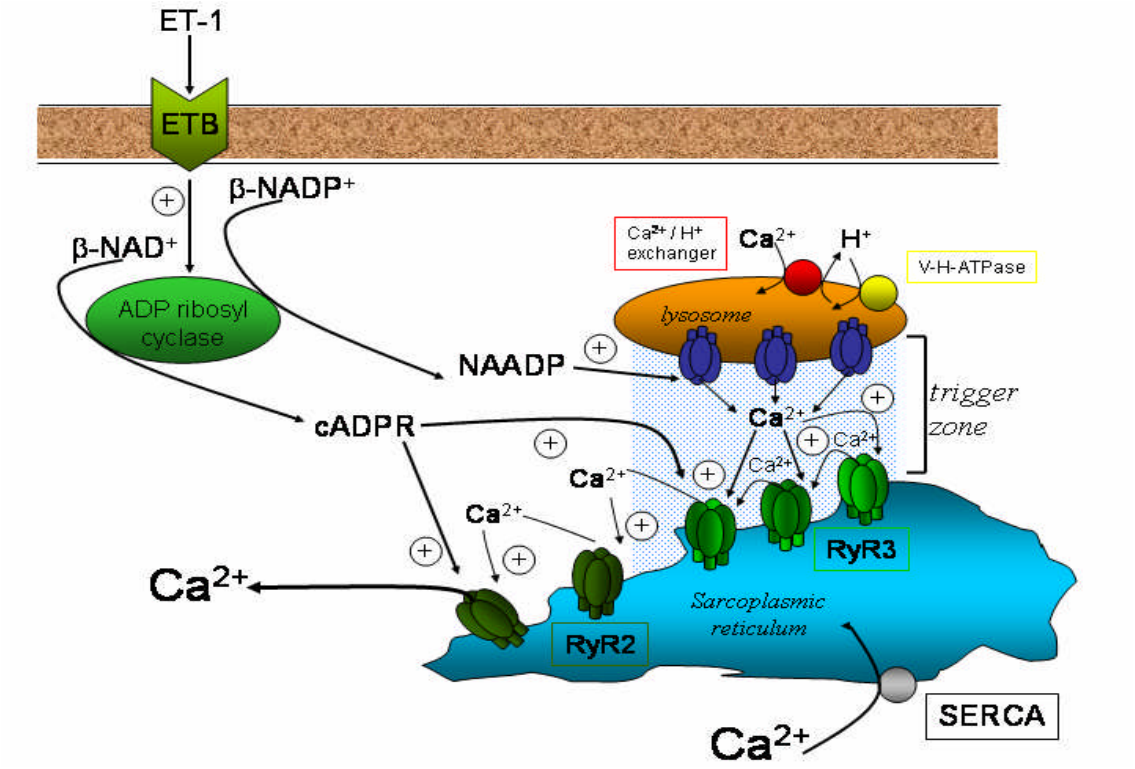

Fig. 6.3 **Schematic diagram of the proposed signalling pathway involved in the generation of global Ca^{2+} signals in response to ET-1 in pulmonary artery smooth muscle cells.** The activation of ETB receptors on the surface of the cell leads to an increase in the cellular production of NAADP. NAADP then activates localised Ca^{2+} release from acidic lysosomal Ca^{2+} stores through putative NAADP-receptors. Ca^{2+} released from lysosomes into the trigger zone acts upon RyR3s on the Sarcoplasmic Reticulum (SR). These increased Ca^{2+} signals are amplified to global Ca^{2+} signals by the recruitment of RyR2 located through the cytoplasm of the cell by the mechanism of Ca^{2+}-induced Ca^{2+}-release. Exposure of cells to ET-1 may also lead to an increase in the cellular levels of cADPR which may act to enhance the sensitivity of RyRs to activation by cytoplasmic Ca^{2+}, thereby promoting the generation of global Ca^{2+} signals in response to initial Ca^{2+} bursts elicited by NAADP.

Given the multitude of cellular mechanisms governed by changes in Ca^{2+} concentration from the fertilisation of eggs to cell death, it is perhaps not surprising that the systems controlling Ca^{2+} signalling are complex. Thus, not all stimuli that generate a specific cellular response do so by initiating Ca^{2+} signals with similar spatiotemporal patterns (Berridge, *et al.*, 2000). Research into the intricate pathways underlying cellular responses to physiological and pharmacological stimuli is vital, therefore, if paradoxes such as these are to be resolved. The results presented in this thesis provide a platform on which we may develop a deeper understanding of how different vasoconstrictors may

trigger smooth muscle contraction while generating their own characteristic signalling patterns through the selective recruitment of a given Ca^{2+} mobilising second messenger and its complimentary storing organelle(s). For example, recent investigations have demonstrated that different Ca^{2+} signals may regulate differential gene expression (Dolmetsch, *et al.*, 1998; Li, *et al.*, 1998) and transcription (Stevenson, *et al.*, 2001), in preparations including native vascular smooth muscle. It seems likely, therefore, that the required code for differential gene expression and transcription could be determined, at least in part, by the discrete mechanisms through which IP_3, cADPR and NAADP trigger Ca^{2+} release and by the spatiotemporal characteristics of the resultant Ca^{2+} signal. Further flexibility could be incorporated into this system by the combinatorial effects of cADPR, NAADP, and/or IP_3. For example, differential activation of these Ca^{2+} signalling pathways by vasoactive agents may trigger an initial contraction of vascular smooth muscle while promoting, over a longer time course, differential gene expression required in the maintenance of normal physiological function. Furthermore, abnormalities in the regulation of these signalling pathways may underlie and promote the development of a range of pathophysiologies associated with, for example, hypertension, angiogenisis and atherogenisis. However, further investigations are required in order to address these questions.

Chapter 7: References

Aarhus, R., Dickey, D. M., Graeff, R. M., Gee, K. R., Walseth, T. F. and Lee, H. C. (1996a). Activation and Inactivation of Ca2+ Release by NAADP. *J. Biol. Chem.* **271,** 8513-8516.

Aarhus, R., Dickey, D. M., Graeff, R. M., Gee, K. R., Walseth, T. F. and Lee, H. C. (1996b). Activation and inactivation of Ca2+ release by NAADP+. *J Biol Chem* **271,** 8513-8516.

Aarhus, R., Graeff, R. M., Dickey, D. M., T.F.;, W. and Lee, H. C. (1995). ADP-ribosyl Cyclase and CD38 Catalyze the Synthesis of a Calcium-mobilizing Metabolite from NADP. *J. Biol. Chem.* **270,** 30327-30333.

Abrenica, B. and Gilchrist, J. S. C. (2000). Nucleoplasmic Ca2+loading is regulated by mobilization of perinuclear Ca2+. *Cell Calcium* **28,** 127-136.

Adebanjo, O. A., Anandatheerthavarada, H. K., Koval, A. P., Moonga, B. S., Biswas, G., Sun, L., Sodam, B. R., Bevis, P. J., Huang, C. L., Epstein, S., Lai, F. A., Avadhani, N. G. and Zaidi, M. (1999). A new function for CD38/ADP-ribosyl cyclase in nuclear Ca2+ homeostasis. *Nature Cell Biol.* **1,** 409-414.

Adebanjo, O. A., Koval, A., Moonga, B. S., Wu, X. B., Yao, S., Bevis, P. J. R., Kumegawa, M., Zaidi, M. and Sun, L. (2000). Molecular Cloning, Expression, and Functional Characterization of a Novel Member of the CD38 Family of ADP-ribosyl Cyclases. *Biochem. Biophys.l Res. Comm.* **273,** 884-889.

Aguilar-Brtyan, L., Clement, J. P., Gonzalez, G., Kunjilwar, K., Babenko, A. and Bryan, J. (1998). Toward Understanding the Assembly and Structure of KATP Channels. *Physiol. Rev.* **78,** 227-245.

Ahern, G. P., Junankar, P. R. and Dulhunty, A. F. (1997). Subconductance states in single-channel activity of skeletal muscle ryanodine receptors after removal of FKBP12. *Biophys. J.* **72,** 146-162.

Aiello, E. A., Walsh, M. P. and Cole, W. C. (1995). Phosphorylation by protein kinase A enhances delayed rectifier K+ current in rabbit vascular smooth muscle cells. *Am. J. Physiol.* **268,** H926-934.

Albert, A. P. and Large, W. A. (2002). Activation of store-operated channels by noradrenaline via protein kinase C in rabbit portal vein myocytes. *J. Physiol.* **544,** 113-125.

Allbritton, N. L., Meyer, T. and Stryer, L. (1992). Range of messenger action of calcium ion and inositol 1,4,5-triphosphate. *Science* **258,** 1812-1815.

Allen, J. M., Iggulden, H. L. and McHale, N. G. (1986). Beta-adrenergic inhibition of bovine mesenteric lymphatics. *J. Physiol.* **374,** 401-411.

Amano, M., Fukata, Y. and Kaibuchi, K. (2000). Regulation and Functions of Rho-Associated Kinase. *Exp. Cell Res.* **261,** 44-51.

Amedee, T., Benham, C. D., Bolton, T. B., Byrne, N. G. and Large, W. A. (1990). Pottasium, chloride and non-selective cation conductances opened by noradrenaline in rabbit ear artery cells. *J. Physiol.* **423,** 551-568.

Anderson, M. E., Braun, A. P., Schulman, H. and Premack, B. A. (1994). Multifunctional Ca2+/calmodulin-dependent protein kinase mediates

Ca(2+)-induced enhancement of the L-type Ca2+ current in rabbit ventricular myocytes. *Circ. Res.* **75,** 854-861.

Arai, H., Hori, S., Aramori, I., Pohkubo, H. and Nakanishi, S. (1990). Cloning and expression of a cDNA encoding an endothelin receptor. *Nature* **348,** 730-732.

Araki, S., Ito, M., Kureishi, Y., Feng, J., Machida, H., Isaka, N., Amano, M., Kaibuchi, K., Hartshorne, D. J. and Nakano, T. (2001). Arachidonic acid-induced Ca^{2+} sensitization of smooth muscle contraction through activation of Rho-kinase. *Pflugers Arch.* **441,** 596-603.

Archer, S., Will, J. A. and Weir, E. K. (1986). Redox status in the control of pulmonary vascular tone. *Herz.* **11,** 127-141.

Archer, S. L., Huang, J., Henry, T., Petersen, D. and Weir, E. K. (1993). A redox-based O2 sensor in rat pulmonary vasculature. *Circ. Res.* **73,** 1100-1112.

Archer, S. L., Nelson, D. P. and Weir, E. K. (1989). Simultaneous measurement of O2 radicals and pulmonary vascular reactivity in rat lung. *J. Appl. Physiol.* **67,** 1903-1911.

Arkin, I. T., Adams, P. D., Brunger, A. T., Smith, S. O. and Engelman, D. M. (1997). Structural perspectives of phospholamban, a helical transmembrane pentamer. *Annu. Rev. Biophys. Biomol. Struct.* **26,** 157-179.

Armant, D. R., Carson, D. D., Decker, G. L., Welply, J. K. and Lennarz, W. J. (1986). Characterization of yolk platelets isolated from developing embryos of Arbacia punctulata. *Dev. Biol.* **113,** 342-355.

Armstrong, D. L. (1989). Calcium channel regulation by calcineurin, a Ca2+-activated phosphatase in mammalian brain. *Trends Neurosci.* **12,** 117-122.

Arnon, A., Hamlyn, J. M. and Blaustein, M. P. (2000). Ouabain augments Ca2+ transients in arterial smooth muscle without raising cytosolic Na+. *Am. J. Physiol.* **279,** H679-691.

Asahi, M., Kurzydlowski, K., Tada, M. and MacLennan, D. H. (2002). Sarcolipin inhibits polymerisation of phospholamban to induce superinhibition of sarco(endo)plasmic reticulum Ca^{2+}-ATPases (SERCAs). *J. Biol. Chem.* **277,** 725-726.

Bak, J., Billington, R. A., Timar, G., Dutton, A. C. and Genazzani, A. A. (2001). NAADP receptors are present and functional in the heart. *Current Biology* **11,** 987-990.

Bak, J., White, P., Timar, G., Missiaen, L., Genazzani, A. A. and Galione, A. (1999). Nicotinic acid adenine dinucleotide phosphate triggers Ca2+ release from brain microsomes. *Curr. Biol.* **9,** 751-754.

Balshaw, D. M., Yamaguchi, M. and Meissner, G. (2002). Modulation of intracellular calcium-release channels by calmodulin. *J. Membr. Biol.* **185,** 1-8.

Barcellona, M. L., Cardiel, G. and Gratton, E. (1990). Time-resolved fluorescence of DAPI in solution and bound to polydeoxynucleotides. *Biochem. Biophys. Res. Commun.* **170,** 270-280.

Barone, F., Genazzani, A. A., Conti, A., Churchill, G. C., Palombi, F., Ziparo, E., Sorrentino, V., Galione, A. and Filippini, A. (2002). A pivotal role for cADPR-mediated Ca2+ signaling: regulation of endothelin-induced contraction in peritubular smooth muscle cells. *FASEB. J.* **16,** 697-705.

Batty, I. R., Nahorski, R. and Irvine, R. F. (1985). Rapid formation of inositol-1,3,4,5- tetrakisphosphate following muscarinic receptor stimulation of rat cerebral cortex slices. *Biochem. J.* **232,** 211-215.

Bean, B. P., Sturek, M., Puga, A. and Hermsmeyer, K. (1986). Calcium channels in muscle cells isolated from rat mesenteric arteries: modulation by dihydropyridine drugs. *Circ. Res.* **59,** 229-235.

Beard, N. A., Sakowska, M. M., Dulhunty, A. F. and Laver, D. R. (2002). Calsequestrin Is an Inhibitor of Skeletal Muscle Ryanodine Receptor Calcium Release Channels. *Biophys. J.* **82,** 310-320.

Beckman, D. L. and Metha, P. (1996). Effects of sympathetic nerve stimulation on pulmonary vascular permeability. *Med. Sci. Res.* **24,** 179-180.

Beech, D. J. and Bolton, T. B. (1989). A voltage-dependent outward current with fast kinetics in single smooth muscle cells isolated from rabbit portal vein. *J. Physiol.* **412,** 397-414.

Beech, D. J., Muraki, K. and Flemming, R. (2004). Non-selective cationic channels of smooth muscle and the mammalian homologues of Drosophila TRP. *J. Physiol.* **559,** 685-706.

Beech, D. J., Zhang, H., Nakao, K. and Bolton, T. B. (1993a). K channel activation by nucleotide diphosphates and its inhibition by glibenclamide in vascular smooth muscle. *Br. J. Pharmacol.* **110,** 573-590.

Beech, D. J., Zhang, H., Nakao, K. and Bolton, T. B. (1993b). Single channel and whole-cell K-currents evoked by levcromakalim in smooth muscle cells from the rabbit portal vein. *Br. J. Pharmacol.* **110,** 583-590.

Benham, C. D. and Bolton, T. B. (1986). Spontaneous transient outward currents in single visceral and vascular smooth muscle cells of the rabbit. *J. Physiol.* **381,** 385-406.

Benham, C. D. and Tsien, R. W. (1987). Calcium- permeable channels in vascular smooth muscle: Voltage- activated, receptor- operated, and leak channels. *Soc. Gen. Physiol. Ser.* **42,** 45-64.

Berg, I., Potter, B. V. L., Mayr, G. W. and Guse, A. H. (2000). Nicotinic Acid Adenine Dinucleotide Phosphate (NAADP+) Is an Essential Regulator of T-lymphocyte Ca2+-signaling. *J. Cell Biol.* **150,** 581-588.

Berg, T. O., Stromhaug, E., Lovdal, T., Seglen, O. and Berg, T. (1994). Use of glycyl-L-phenylalanine 2-naphthylamide, a lysosome-disrupting cathepsin C substrate, to distinguish between lysosomes and prelysosomal endocytic vacuoles. *Biochem. J.* **300,** 229-236.

Bergdahl, A., Gomez, M. F., Dreja, K., Xu, S.-Z., Adner, M., Beech, D. J., Broman, J., Hellstrand, P. and Sward, K. (2003). Cholesterol depletion impairs vascular reactivity to endothelin-1 by reducing store- operated Ca2+ entry dependent on TRPC1. *Circ. Res.* **93,** 839-847.

Berne, R. M., Levy, M. N., Koeppen, B. M. and Stanton, B. A. (2004). *Physiology*, 5th edn. Mosby.

Bernofsky, C. (1980). Nicotinic acid adenine dinucleotide phosphate (NAADP+). *Methods Enzymol.* **66,** 105-112.

Berridge, G., Dickinson, G., Parrington, J., Galione, A. and Patel, S. (2002). Solubilization of Receptors for the Novel Ca2+-mobilizing Messenger, Nicotinic Acid Adenine Dinucleotide Phosphate. *J. Biol. Chem.* **277,** 43717-43723.

Berridge, M. J. (1982). 5-hydroxytryptamine stimulation of phosphatidylinositol hydrolysis and calcium signalling in the blowfly salivary gland. *Cell Calcium* **3,** 385-397.

Berridge, M. J., Dawson, R. M., Downes, C. P., Heslop, J. P. and Irvine, R. F. (1983). Changes in the levels of inositol phosphates after agonist-dependent hydrolysis of membrane phospholipids. *Biochem J* **212,** 473-482.

Berridge, M. J., Lipp, P. and Bootman, M. D. (2000). The versatility and universality of calcium signalling. *Nat Rev Mol Cell Biol.* **1,** 11-21.

Berruet, L., Muller-Steffner, H. and Schuber, F. (1998). Occurrence of bovine spleen CD38/NAD+ glycohydrolase disulfide-linked dimers. *Biochem. Mol. Biol. Int.* **46,** 847-855.

Billington, R. A. and Genazzani, A. A. (2000a). Characterization of NAADP(+) binding in sea urchin eggs. *Biochem. Biophys.l Res. Comm.* **276,** 112-116.

Billington, R. A. and Genazzani, A. A. (2000b). Characterization of NAADP+ Binding in Sea Urchin Eggs. *Biochem. Biophys.l Res. Comm.* **276,** 112-116.

Blaustein, M. P. and Lederer, W. J. (1999). Sodium/Calcium Exchange: Its Physiological Implications. *Physiol. Rev.* **79,** 763-854.

Boittin, F.-X., Dipp, M., Kinnear, N. P., Galione, A. and Evans, A. M. (2003). Vasodilation by the Calcium-mobilizing Messenger Cyclic ADP-ribose. *J. Biol. Chem.* **278,** 9602-9608.

Boittin, F.-X., Galione, A. and Evans, A. M. (2002). Nicotinic Acid Adenine Dinucleotide Phosphate Mediates Ca2+ Signals and Contraction in Arterial Smooth Muscle via a Two-Pool Mechanism. *Circ. Res.* **91,** 1168-1175.

Bonev, A. D. and Nelson, M. T. (1996). Vasoconstrictors inhibit ATP-sensitive K^+ channels in arterial smooth muscle through protein kinase C. *J. Gen. Physiol.* **108,** 315-323.

Boulay, G., Zhu, X., Peyton, M., Jian, M., Hurst, R., Stefani, E. and Birnbaumber, L. (1997). Cloning and expression of a novel mammalian homolog of *Drosophila transient receptor potential* (Trp) involved in calcium entry secondary to activation of receptors coupled by the Gq class of G protein. *J. Biol. Chem* **272,** 29672-29680.

Bowman, E. J., Siebers, A. and Altendorf, K. (1988). Bafilomycins: A Class of Inhibitors of Membrane ATPases from Microorganisms, Animal Cells, and Plant Cells. *Proc. Natl. Acad. Sci.* **85,** 7972-7976.

Bradford, J. R. and Dean, H. P. (1894). The pulmonary circulation. *J. Physiol.* **16,** 34-96.

Bradford, M. M. (1976). A rapid and sensitive method for the quantitation of microgram quantities of protein utilizing the principle of protein-dye binding. *Anal. Biochem.* **72,** 248-254.

Bradley, A. B. and Morgan, K. G. (1987). Alterations in cytoplasmic calcium sensitivity during porcine coronary artery contractions as detected by aequorin. *J. Physiol.* **385,** 437-448.

Bradley, K. K., Jaggar, J. H., Bonev, A. D., Heppner, T. J., Flynn, E. R. M., Nelson, M. T. and Horowitz, B. (1999). Kir2.1 encodes the inward rectifier potassium channel in rat arterial smooth muscle cells. *J. Physiol.* **515,** 639-651.

Bradley, K. N., Currie, S., MacMillan, D., Muir, T. C. and McCarron, J. G. (2003). Cyclic ADP-ribose increases Ca2+ removal in smooth muscle. *J Cell Sci* **116,** 4291-4306.

Brailoiu, E., Hoard, J. L., Filipeanu, C. M., Brailoiu, G. C., Dun, S. L., Patel, S. and Dun, N. J. (2005). Nicotinic Acid Adenine Dinucleotide Phosphate Potentiates Neurite Outgrowth. *J. Biol. Chem.* **280,** 5646-5650.

Briggs, F. N., Lee, K. F., Weschler, A. W. and Jones, L. R. (1992). Phospholamban expressed in slow-twich and chronically stimulated fast-twitch muscles minimally affects calcium affinity of sarcoplasmic reticulum Ca^{2+}-ATPase. *J. Biol. Chem.* **267,** 26056-56061.

Brillantes, A. B., Ondrias, K., Scott, A., Kobrinsky, E., Ondriasova, E., Moschella, M. C., Jayaraman, T., Landers, M., Ehrlich, B. E. and Marks, A. R. (1994). Stabilization of calcium release channel (ryanodine receptor) function by FK506-binding protein. *Cell* **77,** 513-523.

Brock, R. C. (1942). The use of silver nitrate in the production of aseptic obliterative pleuritis. *Guy's Hosp. Res.* **91,** 111-130.

Brueggemann, L. I., Martin, B. L., Barakat, J., Byron, K. L. and Cribbs, L. L. (2005). Low voltage-activated calcium channels in vascular smooth muscle: T-type channels and AVP-stimulated calcium spiking. *Am. J. Physiol.* **288,** H923-935.

Buhling, F., Fengler, A., Brandt, W., Welte, T., Ansorge, S. and Nagler, D. (2000). Review: novel cysteine proteases of the papain family. *Adv. Exp. Med. Biol* **477,** 241-254.

Bultynck, G., Rossi, D., Callewaert, G., Missiaen, L., Sorrentino, V., Parys, J. B. and De Smedt, H. (2001). The Conserved Sites for the FK506-binding Proteins in Ryanodine Receptors and Inositol 1,4,5-Trisphosphate Receptors Are Structurally and Functionally Different. *J. Biol. Chem.* **276,** 47715-47724.

Burridge, K. and Wennerberg, K. (2004). Rho and Rac Take Center Stage. *Cell* **116,** 167-179.

Byrne, N. G. and Large, W. A. (1988). Membrane ionic mechanisms activated by noradrenaline in cells isolated from the rabbit portal vein. *J. Physiol.* **404,** 557-573.

Campbell, K. P., MacLennan, D. H., Jorgensen, A. O. and Mintzer, M. C. (1983). Purification and characterization of calsequestrin from canine cardiac sarcoplasmic reticulum and identification of the 53,000 dalton glycoprotein. *J. Biol. Chem.* **258,** 1197-1204.

Cancela, J., Churchill, G. and Galione, A. (1999). Coordination of agonist-induced Ca2+-signalling patterns by NAADP in pancreatic acinar cells. *Nature* **398,** 74-76.

Cancela, J. M. (2001). Specific Ca2+ signaling evoked by cholecystokinin and acetylcholine: the roles of NAADP, cADPR, and IP3. *Ann. Rev. Physiol.* **63,** 99-117.

Cancela, J. M., Gerasimenko, O. V., Gerasimenko, J. V., Tepikin, A. V. and Petersen, O. H. (2000). Two different but converging messenger pathways to intracellular Ca2+ release: the roles of nicotinic acid adenine dinucleotide phosphate, cyclic ADP-ribose and inositol trisphosphate. *EMBO J.* **19,** 2549-2557.

Cancela, J. M., Van Coppenolle, F., Galione, A., Tepikin, A. V. and Petersen, O. H. (2002). Transformation of local Ca2+ spikes to global Ca2+ transients: the combinatorial roles of multiple Ca2+ releasing messengers. *EMBO J.* **21,** 909-919.

Carafoli, E. (1991). Calcium pump of the plasma membrane. *Physiol. Rev.* **71,** 129-153.

Carafoli, E., Garcia-Martin, E. and Guerini, D. (1996). The plasma membrane calcium pump: recent developments and future perspectives. *Experentia* **52,** 1091-1100.

Carbone, E. and Lux, H. D. (1984). A low voltage-activated, fully inactivating Ca channel in vertebrate sensory neurons. *Nature* **310,** 501-502.

Carrington, W. A., Lynch, R. M., Moore, E. D., Isenberg, G., Fogarty, K. E. and Fay, F. S. (1995). Superresolution three-dimensional images of fluorescence in cells with minimal light exposure. *Science* **268,** 1483-1487.

Catterall, W. A. (1993). Structure and function of voltage-gated ion channels. *Trends Neurosci.* **16,** 500-506.

Cervetto, L., Lagnado, L., Perry, R. J., Robinson, D. W. and McNaughton, P. A. (1989). Extrusion of calcium from rod outer segments is driven by both sodium and potassium gradients. *Nature* **337,** 740-743.

Chad, J. E. and Eckert, R. (1986). An enzymatic mechanism for calcium current inactivation in dialysed Helix neurones. *J. Physiol.* **378,** 31-51.

Chemin, J., Patel, A. J., Duprat, F., Lauritzen, I., Lazdunski, M. and Honore, E. (2005). A phospholipid sensor controls mechanogating of the K+ channel TREK-1. *EMBO J.* **24,** 44-53.

Chen, S. R. W., Li, X., Ebisawa, K. and Zhang, L. (1997a). Functional Characterization of the Recombinant Type 3 Ca2+ Release Channel (Ryanodine Receptor) Expressed in HEK293 Cells. *J. Biol. Chem.* **272,** 24234-24246.

Cheng, H., Lederer, W. J. and Cannell, M. B. (1993). Calcium sparks: elementary events underlying excitation-contraction coupling in heart muscle. *Science* **262,** 740-744.

Cheng, J., Yusufi, A. N. K., Thimpson, M. A., Chini, E. N. and Grande, J. P. (2001). Nicotinic Acid Adenine Dinucleotide Phosphate: A New Ca2+ Releasing Agent in Kidney. *J. Am. Soc. Nephrol.* **12,** 54-60.

Cheung, D. W. (2003). Modulation of spontaneous transient Ca2+-activated K+ channel currents by cADP-ribose in vascular smooth muscle cells. *Eur. J. Pharmacol.* **458,** 57-59.

Chicka, M. C. and Strehler, E. E. (2003). Alternative Splicing of the First Intracellular Loop of Plasma Membrane Ca2+-ATPase Isoform 2 Alters Its Membrane Targeting. *J. Biol. Chem.* **278,** 18464-18470.

Chidambaram, N. and Chang, C. F. (1998). Functional role of glycosylation on the recombinant CD38/ADP-ribosyl cyclase in CHO cells. *Int. J. Biochem. & Cell Biol.* **30,** 1011-1018.

Ching, L. L., Williams, A. J. and Sitsapesan, R. (2000). Evidence for Ca2+ Activation and Inactivation Sites on the Luminal Side of the Cardiac Ryanodine Receptor Complex. *Circ. Res.* **87,** 201-206.

Chini, E. N., Beers, K. W. and Dousa, T. P. (1995). Nicotinate Adenine Dinucleotide Phosphate (NAADP) Triggers a Specific Calcium Release System in Sea Urchin Eggs. *J. Biol. Chem.* **270,** 3216-3223.

Chini, E. N. and Dousa, T. P. (1995). Enzymatic synthesis and degradation of nicotinate adenine dinucletide phosphate (NAADP), a Ca2+-releasing agonist, in rat tissues. *Biochem. Biophys. Res. Commun.* **209,** 167-174.

Chini, E. N. and Dousa, T. P. (1996). Nicotinate-adenine dinucleotide phosphate-induced Ca2+ release does not behave as a Ca2+-induced Ca2+-release system. *Biochem. J.* **316,** 709-711.

Chini, E. N., Liang, M. and Dousa, T. P. (1998). Differential effect of pH upon cyclic-ADP-ribose and nicotinate-adenine dinucleotide phosphate-induced Ca2+ release systems. *Biochem. J.* **335,** 499-504.

Christensen, K. A., Myers, J. T. and Swanson, J. A. (2002). pH-dependent regulation of lysosomal calcium in macrophages. *J. Cell Sci.* **115,** 599-607.

Chu, A., Fill, M., Stefani, E. and Entman, M. L. (1993). Cytoplasmic Ca2+ does not inhibit the cardiac muscle sarcoplasmic reticulum ryanodine receptor Ca2+ channel, although Ca(2+)-induced Ca2+ inactivation of Ca2+ release is observed in native vesicles. *J. Membr. Biol.* **135,** 49-59.

Churchill, G. C. and Galione, A. (2000). Spatial Control of Ca2+ Signalling by Nicotinic Acid Adenine Dinucleotide Phosphate Diffusion and Gradients. *J. Biol. Chem.* **275,** 38687-38692.

Churchill, G. C. and Galione, A. (2001). NAADP induces Ca2+ oscillations via a two-pool mechanism by priming IP3- and cADPR-sensitive Ca2+ stores. *EMBO J.* **20,** 2666-2671.

Churchill, G. C., Okada, Y., Thomas, J. M., Genazzani, A. A., Patel, S. and Galione, A. (2002). NAADP mobilizes Ca(2+) from reserve granules, lysosome-related organelles, in sea urchin eggs. *Cell* **111,** 703-708.

Chutkow, W. A., Pu, J., Wheeler, M. T., Wada, T., Makielski, J. C., Burant, C. F. and McNally, E. M. (2002). Episodic coronary artery vasospasm and hypertension develop in the absence of Sur2 KATP channels. *J. Clin. Invest.* **110,** 203-208.

Clapper, D., Walseth, T., Dargie, P. and Lee, H. (1987). Pyridine nucleotide metabolites stimulate calcium release from sea urchin egg microsomes desensitised ti inositol trisphosphate. *J. Biol. Chem* **262,** 9561-9568.

Clementi, E., Riccio, M., Sciorati, C., Nistico, G. and Meldolesi, J. (1996). The Type 2 Ryanodine Receptor of Neurosecretory PC12 Cells Is Activated by Cyclic ADP-ribose. Role of the nitric oxide/cGMP pathway. *J. Biol. Chem.* **271,** 17739-17745.

Coburn, R. F. and Baron, C. B. (1990). Coupling mechanisms in airway smooth muscle. *Am. J. Physiol.* **258,** L119-L133.

Cockayne, D. A., Muchamuel, T., Grimaldi, J. C., Muller-Steffner, H., Randall, T. D., Lund, F. E., Murray, R., Schuber, F. and Howard, M. C. (1998). Mice Deficient for the Ecto-Nicotinamide Adenine Dinucleotide Glycohydrolase CD38 Exhibit Altered Humoral Immune Responses. *Blood* **92,** 1324-1333.

Coffey, J. W. and de Duve, C. (1968). Digestive Activity of Lysosomes. I. THE DIGESTION OF PROTEINS BY EXTRACTS OF RAT LIVER LYSOSOMES. *J. Biol. Chem.* **243,** 3255-3263.

Copello, J. A., Qi, Y., Jeyakumar, L. H., Ogunbunmi, E. and Fleischer, S. (2001). Lack of effect of cADP-ribose and NAADP on the activity of skeletal muscle and heart ryanodine receptors. *Cell Calcium* **30,** 269-284.

Coussin, F., Macrez, N., Morel, J.-L. and Mironneau, J. (2000). Requirement of Ryanodine Receptor Subtypes 1 and 2 for Ca2+-induced Ca2+ Release in Vascular Myocytes. *J. Biol. Chem.* **275,** 9596-9603.

Cox, D. H. and Aldrich, R. W. (2000). Role of the {beta}1 Subunit in Large-Conductance Ca2+-activated K+ Channel Gating Energetics: Mechanisms of Enhanced Ca2+ Sensitivity. *J. Gen. Physiol.* **116,** 411-432.

Crane, G. J. and Garland, C. J. (2004). Thromboxane receptor stimulation associated with the loss of SKCa activity and reduced EDHF responses in the rat isolated mesenteric artery. *Br. J. Pharmacol.* **142,** 43-50.

Craven, M., Sergeant, G. P., Hollywood, M. A., McHale, N. G. and Thornbury, K. D. (2004). Modulation of spontaneous Ca2+-activated Cl- currents in the rabbit corpus cavernosum by the nitric oxide-cGMP pathway. *J. Physiol.* **556,** 495-506.

Cui, Y., Galione, A. and Terrar, D. A. (1999). Effects of photoreleased cADP-ribose on calcium transients and calcium sparks in myocytes isolated from guinea-pig and rat ventricle. *Biochem. J.* **342,** 269-273.

Dai, Y. P., Bongalon, S., Hatton, W. J., Hume, J. R. and Yamboliev, I. A. (2005). ClC-3 chloride channel is upregulated by hypertrophy and inflammation in rat and canine pulmonary artery. *Br. J. Pharmacol.* **145,** 5-14.

Dammermann, W. and Guse, A. H. (2005). Functional Ryanodine Receptor Expression Is Required for NAADP-mediated Local Ca2+ Signaling in T-lymphocytes. *J. Biol. Chem.* **280,** 21394-21399.

Dargie, P. J., Agre, M. C. and Lee, H. C. (1990). Comparison of Ca2+ mobilizing activities of cyclic ADP-ribose and inositol trisphosphate. *Cell Regulation* **1,** 279-290.

Dart, C. and Standen, N. B. (1993). Adenosine-activated potassium current in smooth muscle cells isolated from the pig coronary artery. *J. Physiol.* **471,** 767-786.

Dart, C. and Standen, N. B. (1995). Activation of ATP-dependent K^+ channels by hypoxia in smooth muscle cells isolated from the pig coronary artery. *J. Physiol.* **483,** 29-39.

Daut, J., Klieber, H. G., Cyrys, S. and Noack, T. (1994). KATP channels and basal coronary vascular tone. *Cardiovasc. Res.* **28,** 811-817.

De Flora, A., Franco, L., Guida, L., Bruzzone, S., Usai, C. and Zocchi, E. (2000). Topology of CD38. *Chem. Immunol.* **75,** 79-98.

De Flora, A., Guida, L., Franco, L., Zocchi, E., Pestarino, M., Usai, C., Marchetti, C., Fedele, E., Fontana, G. and Raiteri, M. (1996). Ectocellular in vitro and in vivo metabolism of cADP-ribose in cerebellum. *Biochem J.* **320,** 665-671.

de Meiss, L. and Vianna, A. L. (1979). Energy interconversion by the Ca2+-dependent ATPase of the Sarcoplasmic Reticulum. *Annu. Rev. Biochem.* **48,** 275-292.

de Toledo, F. G. S., Cheng, J. and Dousa, T. P. (1997). Retinoic Acid and Triiodothyronine Stimulate ADP-Ribosyl Cyclase Activity in Rat Vascular Smooth Muscle Cells. *Biochem. Biophys.l Res. Comm.* **238,** 847-850.

Deaglio, S., Zubiaur, M., Gregorini, A., Bottarel, F., Ausiello, C. M., Dianzani, U., Sancho, J. and Malavasi, F. (2002). Human CD38 and CD16 are

functionally dependent and physically associated in natural killer cells. *Blood* **99,** 2490-2498.

DeMarco, S. J. and Strehler, E. E. (2001). Plasma Membrane Ca2+-ATPase Isoforms 2b and 4b Interact Promiscuously and Selectively with Members of the Membrane-associated Guanylate Kinase Family of PDZ (PSD95/Dlg/ZO-1) Domain-containing Proteins. *J. Biol. Chem.* **276,** 21594-21600.

Devine, C. E., Somlyo, A. V. and Somlyo, A. P. (1972). Sarcoplasmic reticulum and excitation- contraction coupling in mammalian smooth muscle. *J. Cell Biol.* **52,** 690-718.

Dickinson, G. D. and Patel, S. (2003). Modulation of NAADP (nicotinic acid-adenine dinucleotide phosphate) receptors by K+ ions: evidence for multiple NAADP receptor conformations. *Biochem. J.* **375,** 805-812.

Dillon, P. F., Oksoy, M. O., Driska, S. P. and Murphy, R. A. (1981). Myosin phosphorylation and the cross-bridge cycle in arterial smooth muscle. *Science* **211,** 495-497.

Dipp, M. and Evans, A. M. (2001). Cyclic ADP-Ribose Is the Primary Trigger for Hypoxic Pulmonary Vasoconstriction in the Rat Lung In Situ. *Circ. Res.* **89,** 77-83.

Dipp, M., Nye, P. C. G. and Evans, A. M. (2001). Hypoxic release of calcium from the sarcoplasmic reticulum of pulmonary artery smooth muscle. *Am. J. Physiol.* **281,** L318-325.

Docampo, R. and Moreno, S. N. (1999). Acidocalcisome: A novel Ca2+ storage compartment in trypanosomatids and apicomplexan parasites. *Parasitol. Today* **15,** 443-448.

Dode, L., Andersen, J. P., Leslie, N., Dhitavat, J., Vilsen, B. and Hovnanian, A. (2003). Dissection of the Functional Differences between Sarco(endo)plasmic Reticulum Ca2+-ATPase (SERCA) 1 and 2 Isoforms and Characterization of Darier Disease (SERCA2) Mutants by Steady-state and Transient Kinetic Analyses. *J. Biol. Chem.* **278,** 47877-47889.

Doi, S., Damron, D. S., Horibe, M. and Murray, P. A. (2000). Capacitative Ca2+ entry and tyrosine kinase activation in canine pulmonary arterial smooth muscle cells. *Am. J. Physiol.* **278,** L118-130.

Dolmetsch, R. E., Xu, K. and Lewis, R. S. (1998). Calcium oscillations increase the efficiency and specificity of gene expression. *Nature* **392,** 933-936.

Dong, H., Light, P. E., French, R. J. and Lytton, J. (2001). Electrophysiological Characterization and Ionic Stoichiometry of the Rat Brain K+-dependent Na+/Ca2+ Exchanger, NCKX2. *J. Biol. Chem.* **276,** 25919-25928.

Downes, C. P., Mussatt, M. C. and Michell, R. H. (1982). The inositol trisphosphate phosphomonoesterase of the human erythrocyte membrane. *Biochem. J.* **203,** 169-177.

Driska, S. P., Stein, P. G. and Porter, R. (1989). Myosin dephosphorylation during rapid relaxation of hog carotid artery smooth muscle. *Am. J. Physiol.* **256,** C315-C321.

Duan, D., Winter, C., Cowley, S., Hume, J. R. and Horowitz, B. (1997). Molecular identification of a volume-regulated chloride channel. *Nature* **390,** 417-421.

Duchen, M. R. (1992). Ca(2+)-dependent changes in the mitochondrial energetics in single dissociated mouse sensory neurons. *Biochem. J.* **283,** 41-50.

Duchen, M. R. and Biscoe, T. J. (1992a). Mitochondrial function in type I cells isolated from rabbit arterial chemoreceptors. *J. Physiol.* **450,** 13-31.

Duchen, M. R. and Biscoe, T. J. (1992b). Relative mitochondrial membrane potential and $[Ca^{2+}]_i$ in type I cells isolated from the rabbit carotid body. *J. Physiol.* **450,** 33-61.

Dufour, J.-F., Arias, I. M. and Turner, T. J. (1997). Inositol 1,4,5- trisphosphate and calcium regulate the calcium channel function of the hepatic inositol 1,4,5- trisphosphate receptor. *J. Biol. Chem.* **272,** 2675-2681.

Dzhura, I., Wu, Y., Colbran, R. J., Balser, J. R. and Anderson, M. E. (2000). Calmodulin kinase determines calcium-dependent facilitation of L-type calcium channels. *Nat. Cell Biol.* **2,** 173-177.

Ebashi, S. (1991). Excitation-contraction coupling and the mechanism of muscle contraction. *Annu. Rev. Physiol.* **53,** 1-16.

Edwards, F. R., Hirst, G. D. and Silverberg, G. D. (1988). Inward rectification in rat cerebral arterioles; involvement of potassium ions in autoregulation. *J. Physiol.* **404,** 455-466.

Endo, M., Tanaka, M. and Ogawa, Y. (1970). Calcium induced release of calcium from the sarcoplasmic reticulum of skinned skeletal muscle fibres. *Nature* **228,** 34-36.

Ertel, E. A., Campbell, K. P., Harpold, M. M., Hoffmann, F., Mori, Y., Perez-Reyes, E., Schwartz, A., Snutch, T. P., Tanabe, T. and Birnbaumer, L. (2000). Nomenclature of voltage-gated calcium channels. *Neuron.* **25,** 1185-1193.

Etienne-Manneville, S. and Hall, A. (2002). Rho GTPases in cell biology. *Nature* **420,** 629-635.

Evans, A. M. and Dipp, M. (2002). Hypoxic pulmonary vasoconstriction: cyclic adenosine diphosphate-ribose, smooth muscle Ca2+ stores and the endothelium. *Resp. Physiol. Nerobiol.* **132,** 3-15.

Evans, A. M., Mustard, K. J. W., Wyatt, C. N., Peers, C., Dipp, M., Kumar, P., Kinnear, N. P. and Hardie, D. G. (2005). Does AMP-activated Protein Kinase Couple Inhibition of Mitochondrial Oxidative Phosphorylation by Hypoxia to Calcium Signaling in O2-sensing Cells? *J. Biol. Chem.* **280,** 41504-41511.

Evans, A. M., Osipenko, O. N. and Gurney, A. M. (1996). Properties of a novel K^+ current that is active at resting potential in rabbit pulmonary artery smooth muscle cells. *J. Physiol.* **496,** 407-420.

Fabiato, A. (1983). Calcium-induced release of calcium from the cardiac sarcoplasmic reticulum. *Am. J. Physiol.* **245,** C1-C14.

Fabiato, A. and Fabiato, F. (1975). Contractions induced by a calcium-triggered release of calcium from the sarcoplasmic reticulum of single skinned cardiac cells. *J. Physiol.* **249,** 469-495.

Fagan, K. A., Oka, M., Bauer, N. R., Gebb, S. A., Ivy, D. D., Morris, K. G. and McMurtry, I. F. (2004). Attenuation of acute hypoxic pulmonary vasoconstriction and hypoxic pulmonary hypertension in mice by inhibition of Rho-kinase. *Am. J. Physiol.* **287,** L656-664.

Fatt, P. and Katz, B. (1952). Spontaneous subthreshold activity at motor nerve endings. *J. Physiol.* **117,** 109-128.

Fatt, P. and Katz, B. (1953). The electrical properties of crustacean muscle fibres. *J. Physiol.* **120,** 171-204.

Fellner, S. K. and Parker, L. A. (2004). Endothelin B receptor Ca2+ signaling in shark vascular smooth muscle: participation of inositol trisphosphate and ryanodine receptors. *J. Exp. Biol.* **207,** 3411-3417.

Filo, R. S., Bohr, D. F. and Ruegg, J. C. (1965). Glycerinated skeletal and smooth muscle: Calcium and Magnesium dependence. *Science* **147,** 1581-1583.

Finlay, M., Barer, G. R. and Suggert, A. J. (1986). Quantitative changes in the rat pulmonary vasculature in chronic hypoxia - relation to haemodynamic changes. *Q. J. Exper. Physiol.* **71,** 151-163.

Fleischmann, B. K., Wang, Y. X. and Kotlikoff, M. I. (1997). Muscarinic activation and calcium permeation of nonselective cation currents in airway myocytes. *Am. J. Physiol.* **272,** C341-349.

Ford, L. E. and Podolsky, R. J. (1970). Regenerative calcium release within muscle cells. *Science* **167,** 58-59.

Franco, L., Guida, L., Bruzzone, S., Zocchi, E., Usai, C. and Flora, A. D. (1998). The transmembrane glycoprotein CD38 is a catalytically active transporter responsible for generation and influx of the second messenger cyclic ADP-ribose across membranes. *FASEB J.* **12,** 1507-1520.

Franco, L., Zocchi, E., Usai, C., Guida, L., Bruzzone, S., Costa, A. and De Flora, A. (2001). Paracrine Roles of NAD+ and Cyclic ADP-ribose in Increasing Intracellular Calcium and Enhancing Cell Proliferation of 3T3 Fibroblasts. *J. Biol. Chem.* **276,** 21642-21648.

Fried, R., Meyrick, B., Rabinovitch, M. and Reid, L. (1983). Polycythemia and the acute hypoxic response in awake rats following chronic hypoxia. *J. Appl. Physiol.* **55,** 1167-1172.

Fruen, B. R., Bardy, J. M., Byrem, T. M., Strasburg, G. M. and Louis, C. F. (2000). Differential Ca2+ sensitivity of skeletal and cardiac muscle ryanodine receptors in the presence of calmodulin. *Am. J. Physiol.* **279,** C724-733.

Fujimoto, T. (1993). Calcium pump of the plasma membrane is localized in caveolae. *J. Cell Biol.* **120,** 1147-1157.

Fukushi, Y., Kato, I., Takasawa, S., Sasaki, T., Ong, B. H., Sato, M., Ohsaga, A., Sato, K., Shirato, K., Okamoto, H. and Maruyama, Y. (2001). Identification of Cyclic ADP-ribose-dependent Mechanisms in Pancreatic Muscarinic Ca2+ Signaling Using CD38 Knockout Mice. *J. Biol. Chem.* **276,** 649-655.

Fung, Y. C. and Sobin, S. S. (1972). Pulmonary alveolar blood flow. *Circ. Res.* **30,** 470-490.

Furchgott, R. F. and Zawadski, J. V. (1980). The obligatory role of endothelial cells in the realxation of arterial smooth muscle by acetylcholine. *Nature* **288,** 373-376.

Furuichi, T., Yoshikawa, S., Miyawaki, A., Wada, K., Maeda, N. and Mikoshiba, K. (1989). Primary structure and functional expression of the inositol 1,4,5- trisphosphate- binding protein P400. *Nature* **342,** 32-38.

Galione, A., Lee, H. C. and Busa, W. B. (1991). Ca2+-induced Ca2+ release in sea urchin egg homogenates: modulation by cyclic ADP-ribose. *Science* **253,** 1143-1146.

Galione, A., Thomas, J. and Churchill, G. (2000). Pharmacological studies of new calcium release mechanisms. in Tepikin, A. (Ed), *Calcium signalling, a practical approach*, IRL Press.

Galione, A., White, A., Willmott, N., Turner, M., Potter, B. V. and Watson, S. P. (1993). cGMP mobilizes intracellular Ca2+ in sea urchin eggs by stimulating cyclic ADP-ribose synthesis. *Nature* **365,** 388-389.

Ganitkevich, V. Y. and Isenberg, G. (1995). Efficacy of peak Ca2+ currents (ICa) as trigger of sarcoplasmic reticulum Ca2+ release in myocytes from the guinea-pig coronary artery. *J. Physiol.* **484,** 287-306.

Gardiner, S. M., Kemp, P. A., March, J. E., Fallgren, B. and Bennett, T. (1996). Effects of glibenclamide on the regional haemodynamic actions of alpha-inositol and its influence on responses to vasodilators in concious rats. *Br. J. Pharmacol.* **117,** 507-515.

Ge, Z.-D., Zhang, D. X., Chen, Y.-F., Yi, F.-X., Zou, A.-P., Campbell, W. B. and Li, P.-L. (2003). Cyclic ADP-Ribose Contributes to Contraction and Ca 2+ Release by M 1 Muscarinic Receptor Activation in Coronary Arterial Smooth Muscle. *J. Vasc. Res.* **40,** 28-36.

Geiger, J., Zou, A.-P., Campbell, W. B. and Li, P.-L. (2000). Inhibition of cADP-Ribose Formation Produces Vasodilation in Bovine Coronary Arteries. *Hypertension* **35,** 397-402.

Genazzani, A. A., Bak, J. and Galione, A. (1996a). Inhibition of cADPR-Hydrolase by ADP-Ribose Potentiates cADPR Synthesis from [beta]-NAD+. *Biochem. Biophys. Res. Commun.* **223,** 502-507.

Genazzani, A. A., Empson, R. M. and Galione, A. (1996b). Unique inactivation properties of NAADP-sensitive Ca2+ release. *J. Biol. Chem* **271,** 11599-11602.

Genazzani, A. A. and Galione, A. (1996). Nicotinic acid-adenine dinucleotide phosphate mobilises Ca2+ from a thapsigargin-insensitive pool. *Biochem. J.* **315,** 721-725.

Genazzani, A. A., Mezna, M., Dickey, D. M., Michelangeli, F., Walseth, T. F. and Galione, A. (1997). Pharmacological properties of the Ca2+-release mechanism sensitive to NAADP in the sea urchin egg. *Br. J. Pharmacol.* **121,** 1489-1495.

Gerasimenko, J. V., Maruyama, Y., Yano, K., Dolman, N. J., Tepikin, A. V., Petersen, O. H. and Gerasimenko, O. V. (2003). NAADP mobilizes Ca2+ from a thapsigargin-sensitive store in the nuclear envelope by activating ryanodine receptors. *J. Cell Biol.* **163,** 271-282.

Gerasimenko, J. V., Tepikin, A. V., Petersen, O. H. and Gerasimenko, O. V. (1998). Calcium uptake via endocytosis with rapid release from acidifying endosomes. *Curr. Biol.* **8,** 1335-1338.

Giannini, G., Clementi, E., Ceci, R., Marziali, G. and Sorrentino, V. (1992). Expression of a ryanodine receptor-Ca2+ channel that is regulated by TGF-beta. *Science* **257,** 91-94.

Gilchrist, J., Belcastro, A. and Katz, S. (1992). Intraluminal Ca2+ dependence of Ca2+ and ryanodine-mediated regulation of skeletal muscle sarcoplasmic reticulum Ca2+ release. *J. Biol. Chem.* **267,** 20850-20856.

Ginsborg, B. L., House, C. R. and Mitchell, M. R. (1980). A calcium readmission response recorded from Nauphotea salivary gland acinar cells. *J. Physiol.* **304,** 437-447.

Golovina, V. A., Platoshyn, O., Bailey, C. L., Wang, J., Limsuwan, A., Sweeney, M., Rubin, L. J. and Yuan, J. X.-J. (2001). Upregulated TRP and enhanced capacitative Ca2+ entry in human pulmonary artery myocytes during proliferation. *Am. J. Physiol.* **280,** H746-H755.

Gong, M. C., Cohen, P., Kitazawa, T., Ikebe, M., Masuo, M., Somlyo, A. P. and Somlyo, A. V. (1992). Myosin light chain phosphatase activities and the effects of phosphatase inhibitors in tonic and phasic smooth muscle. *J. Biol. Chem.* **267,** 14662-14668.

Gong, M. C., Fujihara, H., Somlyo, A. V. and Somlyo, A. P. (1997). Translocation of rhoA Associated with Ca2+ Sensitization of Smooth Muscle. *J. Biol. Chem.* **272,** 10704-10709.

Gordienko, D. V., Greenwood, I. A. and Bolton, T. B. (2001). Direct visualisation of sarcoplasmic reticulum regions discharging Ca2+ sparks in vascular myocytes. *Cell Calcium* **29,** 13-28.

Graeff, R. M., Walseth, T. F., Fryxell, K., Branton, W. D. and Lee, H. C. (1994). Enzymatic synthesis and characterizations of cyclic GDP-ribose. A procedure for distinguishing enzymes with ADP-ribosyl cyclase activity. *J. Biol. Chem.* **269,** 30260-30267.

Gray, H. (1858). *Gray's anatomy*, 2002 edn. Paragon Books.

Gray, H. (1995). *Gray's anatomy*. Livingstone.

Greenwood, I. A., Ledoux, J. and Leblanc, N. (2001). Differential regulation of Ca2+-activated Cl- currents in rabbit arterial and portal vein smooth muscle cells by Ca2+-calmodulin-dependent kinase. *J. Physiol.* **534,** 395-408.

Greenwood, I. A., Ledoux, J., Sanguinetti, A., Perrino, B. A. and Leblanc, N. (2004). Calcineurin A{alpha} but Not A{beta} Augments ICl(Ca) in Rabbit Pulmonary Artery Smooth Muscle Cells. *J. Biol. Chem.* **279,** 38830-38837.

Grimaldi, K. A., Hutton, J. C. and Siddle, K. (1987). Production and characterisation of monoclonal antibodies to insulin secretory granule membranes. *Biochem. J.* **245,** 557-566.

Gros, R., Afroze, T., You, X.-M., Kabir, G., Van Wert, R., Kalair, W., Hoque, A. E., Mungrue, I. N. and Husain, M. (2003). Plasma Membrane Calcium ATPase Overexpression in Arterial Smooth Muscle Increases Vasomotor Responsiveness and Blood Pressure. *Circ. Res.* **93,** 614-621.

Gross, S. S. and Wolin, M. S. (1995). Nitric oxide: pathophysiological mechanisms. *Annu. Rev. Physiol.* **57,** 737-769.

Grynkiewicz, G., Poenie, M. and Tsien, R. Y. (1985). A new generation of Ca2+ indicators with greatly improved fluorescence properties. *J. Biol. Chem.* **260,** 3440-3450.

Guia, A., Wan, X., Courtemanche, M. and Leblanc, N. (1999). Local Ca2+ Entry Through L-Type Ca2+ Channels Activates Ca2+-Dependent K+ Channels in Rabbit Coronary Myocytes. *Circ. Res.* **84,** 1032-1042.

Gurney, A. M., Osipenko, O. N., MacMillan, D., McFarlane, K. M., Tate, R. J. and Kempsill, F. E. J. (2003). Two-Pore Domain K Channel, TASK-1, in Pulmonary Artery Smooth Muscle Cells. *Circ. Res.* **93,** 957-964.

Guse, A. H., da Silva, C. P., Berg, I., Skapenko, A. L., Weber, K., Heyer, P., Hohenegger, M., Ashamu, G. A., Schulze-Koops, H., Potter, B. V. and Mayr, G. W. (1999). Regulation of calcium signalling in T lymphocytes by the second messenger cyclic ADP-ribose. *Nature* **398,** 70-73.

Gyorke, I. and Gyorke, S. (1998). Regulation of the Cardiac Ryanodine Receptor Channel by Luminal Ca2+ Involves Luminal Ca2+ Sensing Sites. *Biophys. J.* **75,** 2801-2810.

Hakamata, Y., Nakai, J., Takeshima, H. and Imoto, K. (1992). Primary structure and distribution of a novel ryanodine receptor/calcium release channel from rabbit brain. *FEBS Lett.* **312,** 229-235.

Haller, T., Dietl, P., Deetjen, P. and Volkl, H. (1996). The lysosomal compartment as intracellular calcium store in MDCK cells: a possible involvement in InsP3-mediated Ca2+ release. *Cell Calcium* **19,** 157-165.

Halliday, F. C., Aaronson, P. I., Evans, A. M. and Gurney, A. M. (1995). The pharmacological properties of K^+ currents from rabbit isolated aortic smooth muscle cells. *Br. J. Pharmacol.* **116,** 3139-3148.

Hamada, H., Damron, D. S., Hong, S. J., Van Wagoner, D. R. and Murray, P. A. (1997). Phenylephrine-Induced Ca2+ Oscillations in Canine Pulmonary Artery Smooth Muscle Cells. *Circ. Res.* **81,** 812-823.

Hamill, O. P., Marty, A., Neher, E., Sakmann, B. and Sigworth, F. J. (1981). Improved patch-clamp techniques for high-resolution current recording from cells and cell-free membrane patches. *Pflugers Arch.* **391,** 85-100.

Hammes, A., Oberdorf-M.S.;, Rother, T., Nething, K., Gollnick, F., Linz, K. W., Meyer, R., Hu, K., Han, H., Gaudron, P., Ertl, G., Hoffmann, S., Ganten, U., Vetter, R., Schuh, K., Benkwitz, C., Zimmer, H. G. and Neyses, L. (1998). Overexpression of the Sarcolemmal Calcium Pump in the Myocardium of Transgenic Rats. *Circ Res* **83,** 877-888.

Hardie, D. G. (2005). New roles for the LKB1-->AMPK pathway. *Curr. Opin. Cell Biol.* **17,** 167-173.

Hardie, D. G., Hawley, S. A. and Scott, J. W. (2006). AMP-activated protein kinase - development of the energy sensor concept. *J. Physiol.* **574,** 7-15.

Harding, M. W., Galat, A., Uehling, D. E. and Schreiber, S. L. (1989). A receptor for the immunosuppressant FK506 is a cis-trans peptidyl-prolyl isomerase. *Nature* **341,** 758-760.

Heppner, T. J., Bonev, A. D. and Nelson, M. T. (1997). Ca(2+)-activated K+ channels regulate action potential repolarization in urinary bladder smooth muscle. *Am. J. Physiol.* **273,** C110-117.

Herrmann-Frank, A., Darling, E. and Meissner, G. (1991). Functional characterization of the Ca(2+)-gated Ca2+ release channel of vascular smooth muscle sarcoplasmic reticulum. *Pflugers Arch.* **418,** 353-359.

Hess, P., Lansman, J. B. and Tsien, R. W. (1984). Different modes of Ca channel gating behaviour favoured by dihydropyridine Ca agonists and antagonists. *Nature* **311,** 538-544.

Himpens, B. and Casteels, R. (1990). Different effects of depolarisation and muscarinic stimulation on the Ca2+/force relationship during the contraction-relaxation cycle in the guinea pig ileum. *Pflugers Arch.* **416,** 28-35.

Hirata, M., Suematsu, E., Hashimoto, T., Hamachi, T. and Koga, T. (1984). Release of Ca2+ from non-mitochondrial store sites in perotoneal macrophages treated with saponin by inositol 1,4,5- trisphosphate. *Biochem. J.* **223,** 229-236.

Hirata, Y., Kimura, N., Sato, K., Ohsugi, Y., Takasawa, S., Okamoto, H., Ishikawa, J., Kaisho, T., Ishihara, K. and Hirano, T. (1994). ADP ribosyl cyclase activity of a novel bone marrow stromal cell surface molecule, BST-1. *FEBS Lett.* **356,** 244-248.

Hislop, A. and Reid, L. (1976). New findings in pul;monary arteries of rats with hypoxia-induced pulmonary hypertension. *Br. J. Exp. Pathol.* **57,** 542-554.

Hislop, A. and Reid, L. (1977). Changes in the pulmonary arteries of the rat during recovery from hypoxia-induced pulmonary hypertension. *Br. J. Exp. Pathol.* **58,** 653-662.

Hoffmann, F., Biel, M. and Flockerzi, V. (1994). Molecular basis for Ca2+ channel diversity. *Annu. Rev. Neurosci.* **17,** 399-418.

Hogg, R. C., Wang, Q., Helliwell, R. M. and Large, W. A. (1993a). Properties of spontaneous inward currents in rabbit pulmonary artery smooth muscle cells. *Pflugers Arch.* **425,** 233-240.

Hogg, R. C., Wang, Q. and Large, W. A. (1993b). Time course of spontaneous calcium-activated chloride currents in smooth muscle cells from the rabbit portal vein. *J. Physiol.* **464,** 15-31.

Hogue, D., Michalak, M. and Fliegel, l. (1991). The role of ion antiporters in the maintenance of intracellular pH in rat vascular smooth muscle cells. *Mol. Cell Biochem.* **10,** 125-137.

Hohenegger, M., Suko, J., Gscheidlinger, R., Drobny, H. and Zidar, A. (2002). Nicotinic acid-adenine dinucleotide phosphate activates the skeletal muscle ryanodine receptor. *Biochem. J.* **367,** 423-431.

Holz, G. G., Leech, C. A., Heller, R. S., Castonguay, M. and Habener, J. F. (1999). cAMP-dependent Mobilization of Intracellular Ca2+ Stores by Activation of Ryanodine Receptors in Pancreatic beta -Cells. A Ca2+ SIGNALING SYSTEM STIMULATED BY THE INSULINOTROPIC HORMONE GLUCAGON-LIKE PEPTIDE-1-(7-37). *J. Biol. Chem.* **274,** 14147-14156.

Horowitz, A., Menice, C. B., Laporte, R. and Morgan, K. G. (1996). Mechanisms of smooth muscle contraction. *Physiol. Rev.* **76,** 967-1003.

Hoth, M. and Penner, R. (1992). Depletion of intracellular calcium stores activates a calcium curent in mast cells. *Nature* **355,** 353-356.

Howard, M., Grimaldi, J. C., Bazan, J. F., Lund, F. E., Santos-Argumedo, L., Parkhouse, R. M., Walseth, T. F. and Lee, H. C. (1993). Formation and hydrolysis of cyclic ADP-ribose catalyzed by lymphocyte antigen CD38. *Science* **262,** 1056-1059.

Howe, C. L., Granger, B. L., Hull, M., Green, S. A., Gabel, C. A., Helenius, A. and Mellman, I. (1988). Derived protein sequence, oligosaccharides, and membrane insertion of the 120-kDa lysosomal membrane glycoprotein (1gp120): identification of a highly conserved family of lysosomal membrane glycoproteins. *Proc. Natl. Acad. Sci.* **85,** 7577-7581.

Howell, K., Preston, R. J. and McLoughlin, P. (2003). Chronic hypoxia causes angiogenesis in addition to remodelling in the adult rat pulmonary circulation. *J .Physiol.* **547,** 133-145.

Hugnot, J. P., Salinas, M., Lesage, F., Guillemare, E., de Weilles, J., Heurteaux, C., Meattei, M. G. and Lazdunski, M. (1996). Kv8.1, a new neuronal potassium channel subunit with specific inhibitory properties towards Shab and Shaw channels. *EMBO J.* **15,** 332-3331.

Humerickhouse, R. A., Bidasee, K. R., Gerzon, K., Emmick, J. T., Kwon, S., Sutko, J. L., Ruest, L. and Besch, H. R. (1994). High affinity C10-Oeq ester derivatives of ryanodine. Activator- selective agonists of the sarcoplasmic reticulum calcium release channel. *J. Biol. Chem.* **269,** 30243-30253.

Hyvelin, J. M., Guibert, C., Marthan, R. and Savineau, J. P. (1998). Cellular mechanisms and role of endothelin-1-induced calcium oscillations in pulmonary arterial myocytes. *Am. J. Physiol.* **275,** L269-L282.

Hyvelin, J. M., O'Connor, C. and McLoughlin, P. (2004). Effect of changes in pH on wall tension in isolated rat pulmonary artery: role of the RhoA/Rho-kinase pathway. *Am. J. Physiol.* **287,** L673-684.

Ignarro, L. J., Buga, G. M., Wood, K. S., Byrns, R. E. and Chaudhuri, G. (1987). Endothelium-Derived Relaxing Factor Produced and Released from Artery and Vein is Nitric Oxide. *Proc. Natl. Acad. Sci.* **84,** 9265-9269.

Iino, M. (1990). Biphasic Ca2+ depepndence of inositol 1,45- trisphosphate-induced Ca release in smooth muscle cells of the Guinae-pig taenia caeci. *J. Gen. Physiol.* **95,** 1103-1122.

Iino, M. and Endo, M. (1992). Calcium-dependent immediate feedback control of inositol 1,4,5- trisphosphate-induced Ca2+ release. *Nature* **360,** 76-78.

Inesi, G. and Asai, H. (1968). Trypsin digestion of fragmented sarcoplasmic reticulum. *Arch. Biochem. Biophys.* **126,** 469-477.

Inesi, G., Sumbilla, C. and Kirtley, M. E. (1990). Relationships of molecular structure and function in Ca2(+)-transport ATPase. *Physiol. Rev.* **70,** 749-760.

Inoue, R., Okada, T., Onoue, H., Hara, Y., Shimizu, S., Naitoh, S., Ito, Y. and Mori, Y. (2001). The transient receptor potential protein homologue TRP6 is the essential component of vascular alpha1- adrenoceptor-activated Ca2+- permeable cation channel. *Circ. Res.* **88,** 325-332.

Inui, M., Saito, A. and Fleischer, S. (1987a). Isolation of the ryanodine receptor from cardiac sarcoplasmic reticulum and identity with the feet structures. *J. Biol. Chem.* **262,** 15637-15642.

Inui, M., Saito, A. and Fleischer, S. (1987b). Purification of the ryanodine receptor and identity with feet structures of junctional terminal cisternae of sarcoplasmic reticulum from fast skeletal muscle. *J. Biol. Chem.* **262,** 1740-1747.

Ishikawa, K., Ihara, M., Noguchi, K., Mase, T., Mino, N., Saeki, T., Fukuroda, T., Fukami, T., Ozaki, S., Nagase, T., Nishikibe, M. and Yano, M. (1994). Biochemical and Pharmacological Profile of a Potent and Selective Endothelin B-Receptor Antagonist, BQ-788. *Proc. Natl. Acad. Sci.* **91,** 4892-4896.

Itoh, M., Ishihara, K., Tomizawa, H., Tanaka, H., Kobune, Y., Ishikawa, J., Kaisho, T. and Hirano, T. (1994). Molecular Cloning of Murine BST-1 Having Homology with CD38 and Aplysia ADP-Ribosyl Cyclase. *Biochem. Biophys.l Res. Comm.* **203,** 1309-1317.

Jabr, R. I., Toland, H., Gelband, C. H., Wang, X. X. and Hume, J. R. (1997). Prominent role of intracellular Ca2+ release in hypoxic pulmonary vasoconstriction of canine pulmonary artery. *Br. J. Pharmacol.* **122,** 21-30.

Jadot, M., Colmant, C., Wattiaux-De Conick, S. and Wattiaux, R. (1984). Intralysosomal hydrolysis of glycyl-L-phenylalanine 2-napthylamide. *Biochem. J.* **219,** 965-970.

Jadot, M. and Wattiaux, R. (1995). Effect of glycyl-L-phenylalanine 2-napthylamide on invertase endocytosed by rat liver. *Biochem. J.* **225,** 645-648.

Jaggar, J. H., Porter, V. A., Lederer, W. J. and Nelson, M. T. (2000). Calcium sparks in smooth muscle. *Am. J. Physiol.* **278,** C235-C256.

James-Kracke, M. R., Sloane, B. F., Shuman, H. and Somlyo, A. P. (1979). Lysosomal composition in cultured vascular smooth muscle cells. *Proc. Natl. Acad. Sci.* **76**.

Jan, L. Y. and Jan, Y. N. (1992). Tracing the roots of ion channels. *Cell* **69,** 715-718.

Jencks, W. P. (1992). On the mechanism of ATP-driven Ca2+ transport by the calcium ATPase of sarcoplasmic reticulum. *Ann. N.Y. Acad. Sci.* **671,** 49-56.

Jentsch, T. J., Stein, V., Weinreich, F. and Zdebik, A. A. (2002). Molecular structure and physiological function of chloride channels. *Physiol. Rev.* **82,** 503-568.

Jeyakumar, L. H., Ballester, L., Cheng, D. S., McIntyre, J. O., Chang, P., Olivey, H. E., Rollins-Smith, L., Barnett, J. V., Murray, K., Xin, H.-B. and Fleischer, S. (2001). FKBP Binding Characteristics of Cardiac Microsomes from Diverse Vertebrates. *Biochem. Biophys.l Res. Comm.* **281,** 979-986.

Jeyakumar, L. H., Copello, J. A., O'Malley, A. M., Wu, G.-M., Grassucci, R., Wagenknecht, T. and Fleischer, S. (1998). Purification and Characterization of Ryanodine Receptor 3 from Mammalian Tissue. *J. Biol. Chem.* **273,** 16011-16020.

Ji, G., Barsotti, R. J., Feldman, M. E. and Kotlikoff, M. I. (2002). Stretch-induced Calcium Release in Smooth Muscle. *J. Gen. Physiol.* **119,** 533-544.

Jiang, Z., Wallner, M., Meera, P. and Toro, L. (1999). Human and rodent maxiK channel beta1-subunit genes: cloning and characterisation. *Genomics* **55,** 57-67.

Johnson, J. D. and Misler, S. (2002). Nicotinic acid-adenine dinucleotide phosphate-sensitive calcium stores initiate insulin signaling in human beta cells. *Proc. Natl. Acad. Sci.* **99,** 14566-14571.

Jones, A. W. (1981). Vascular smooth muscle and alterations during hypertension. in Bulbring, E., Brading, A. F., Jones, A. W. and Tomita, T. (Eds), *Smooth muscle: an assessment of current knowledge.*, Edward Arnold, pp. 397-431.

Joshi, S., Balan, P. and Gurney, A. M. (2006). Pulmonary vasoconstrictor action of KCNQ potassium channel blockers. *Resp. Res.* **7,** 31.

Juhaszova, M., Ambesi, A., Lindenmayer, G. E., Bloch, R. J. and Blaustein, M. P. (1994). Na(+)-Ca2+ exchanger in arteries: identification by immunoblotting and immunofluorescence microscopy. *Am. J. Physiol.* **266,** C234-242.

Kajioka, S., Kitamura, K. and HKuriyama, H. (1991). Guanosine diphosphate activates an adenosine 5'-triphosphate-sensitive K^+ channel in the rabbit portal vein. *J. Physiol.* **444,** 397-418.

Kamishima, T., Davies, N. W. and Standen, N. B. (2000). Mechanisms that regulate [Ca2+]i following depolarization in rat systemic arterial smooth muscle cells. *J Physiol* **522,** 285-295.

Kamishima, T. and McCarron, J. G. (1996). Depolarization-evoked increases in cytosolic calcium concentration in isolated smooth muscle cells of rat portal vein. *J. Physiol.* **492,** 61-74.

Kamishima, T. and McCarron, J. G. (1997). Regulation of the cytosolic Ca2+ concentration by Ca2+ stores in single smooth muscle cells from rat cerebral arteries. *J. Physiol.* **501,** 497-508.

Kamouchi, M., Van Den Bremt, K., Eggermont, J., Droogmans, G. and Nilius, B. (1997). Modulation of inwardly rectifying potassium channels in cultured bovine pulmonary artery endothelial cells. *J. Physiol.* **504,** 545-556.

Kang, T. M., Park, M. K. and Uhm, D. Y. (2003). Effects of hypoxia and mitochondrial inhibition on the capacitative calcium entry in rabbit pulmonary arterial smooth muscle cells. *Life Sci.* **72,** 1467-1479.

Kannan, M. S., Fenton, A. M., Prakash, Y. S. and Sieck, G. C. (1996). Cyclic ADP-ribose stimulates sarcoplasmic reticulum calcium release in porcine coronary artery smooth muscle. *Am. J. Physiol.* **270,** H801-H806.

Kannan, M. S., Prakash, Y. S., Brenner, T., Mickelson, J. R. and G.C., S. (1997). Role of ryanodine receptor channels in Ca2+ oscillations of porcine tracheal smooth muscle. *Am. J. Physiol.* **272,** L659-L664.

Kao, J. P. (1994). Practical aspects of measuring [Ca2+] with fluorescent indicators. *Methods Cell Biol.* **40,** 155-181.

Karaki, H., Sudjarwo, S. A. and Hori, M. (1994). Novel Antagonist of Endothelin ETB1 and ETB2 Receptors, BQ-788: Effects on Blood Vessel and Small Intestine. *Biochem. Biophys. Res. Commun.* **205,** 168-173.

Karolin, J., B.-A.;, J. L., Strandberg, L. and Ny, T. (1994). Fluorescence and Absorption Spectroscopic Properties of Dipyrrometheneboron Difluoride (BODIPY) Derivatives in Liquids, Lipid Membranes, and Proteins. *J. Am. Chem. Soc.* **116,** 7801-7806.

Kato, I., Yamamoto, Y., Fujimura, M., Noguchi, N., Takasawa, S. and Okamoto, H. (1999). CD38 Disruption Impairs Glucose-induced Increases in Cyclic ADP-ribose, [Ca2+]i, and Insulin Secretion. *J. Biol. Chem.* **274,** 1869-1872.

Kato, M. and Staub, N. C. (1966). Response of small pulmonary arteries to unilobar hypoxia and hypercania. *Circ. Res.* **19,** 426-440.

Kay, J. M., Suyama, K. L. and Keane, P. M. (1982). Failure to show decrease in small pulmonary blood vessels in rats with experimental pulmonary hypertension. *Thorax* **37,** 927-930.

Khoo, K. M., Han, M.-K., Park, J. B., Chae, S. W., Kim, U.-H., Lee, H. C., Bay, B. H. and Chang, C. F. (2000). Localization of the Cyclic ADP-ribose-dependent Calcium Signaling Pathway in Hepatocyte Nucleus. *J. Biol. Chem.* **275,** 24807-24817.

Kiechle, F. L. and Malinski, T. (1993). Nitric oxide. Biochemistry, pathophysiology, and detection. *Am. J. Clin. Pathol.* **100,** 567-575.

Kim, D., Fujita, A., Horio, Y. and Kurachi, Y. (1998). Cloning and Functional Expression of a Novel Cardiac Two-Pore Background K+ Channel (cTBAK-1). *Circ. Res.* **82,** 513-518.

Kim, H., Jacobson, E. L. and Jacobson, M. K. (1993). Synthesis and degredation of cyclic ADP-ribose by NAD glycohydrolases. *Science* **261,** 1330-1333.

Kim, H. W., Steenaart, N. A., Ferguson, D. G. and Kranias, E. G. (1990). Functional reconstruction of the cardiac sarcoplasmic reticulum Ca^{2+}-ATPase with phospholamban in phospholipid vesicles. *J. Biol. Chem.* **265,** 1702-1709.

Kim, U. H., Fink, D. J., Kim, H. S., Park, D. J., Contreras, M. L., Guroff, G. and Rhee, S. G. (1991). Nerve growth factor stimulates phosphorylation of phospholipase C-gamma in PC12 cells. *J. Biol. Chem.* **266,** 1359-1362.

Kimura, N., Ito, M., Amano, M., Chihara, K., Fukata, Y., Nakafuku, M., Yamamori, B., Feng, J., Nakano, T., Okawa, K., Iwamatsu, A. and Kaibuchi, K. (1996). Regulation of myosin phosphatase by Rho and Rho-associated kinase (Rho-kinase). *Science* **273,** 245-248.

Kinnear, N. P., Boittin, F.-X., Thomas, J. M., Galione, A. and Evans, A. M. (2004). Lysosome-Sarcoplasmic reticulum junctions: A trigger zone for calcium signalling by NAADP and endothelin-1. *J. Biol. Chem.* **279,** 54319-54326.

Kirber, M. T., Ordway, R. W., Clapp, L. H., Walsh, J. V. and Singer, J. J. (1992). Both membrane stretch and fatty acids directly activate large conductance Ca2+-activated K+ channels in vascular smooth muscle cells. *FEBS Letters* **297,** 24-28.

Kitazawa, T., Kobayashi, S., Horiuti, K., Somlyo, A. V. and Somlyo, A. P. (1989). Receptor-coupled, permeabilized smooth muscle. Role of the phosphatidylinositol cascade, G-proteins, and modulation of the contractile response to Ca2+. *J. Biol. Chem.* **264,** 5339-5342.

Kleppisch, T. and Nelson, M. T. (1995). Adenosine activates ATP sensitive potassium channels in arterial myocytes via A2 receptors and cAMP-dependent protein kinase. *Proc. Natl. Acad. Sci.* **92,** 12441-12445.

Klockner, U. and Isenberg, G. (1985). Action potentials and net membrane currents of isolated smooth muscle cells (urinary bladder of the guinea-pig). *Pflugers Arch.* **405,** 329-339.

Knot, H. J. and Nelson, M. T. (1995). Regulation of membrane potential and diameter by voltage-dependent K+ channels in rabbit myogenic cerebral arteries. *Am. J. Physiol.* **269,** H348-355.

Knot, H. J., Standen, N. B. and Nelson, M. T. (1998a). Ryanodine receptors regulate arterial diameter and wall [Ca2+] in cerebral arteries of rat via Ca2+-dependent K+ channels. *J. Physiol.* **501,** 211-221.

Knot, H. J., Standen, N. B. and Nelson, M. T. (1998b). Ryanodine receptors regulate arterial diameter and wall [Ca^{2+}] in cerebral arteries of rat via Ca^{2+}-dependent K^{+} channels. *J. Physiol.* **508,** 211221.

Koh, S. D., Ward, S. M., Dick, G. M., Epperson, A., Bonner, H. P., Sanders, K. M., Horowitz, B. and Kenyon, J. L. (1999). Contribution of delayed rectifier potassium currents to the electrical activity of murine colonic smooth muscle. *J. Physiol.* **515,** 475-487.

Kohler, M., Hirschberg, B., Band, C. T., Kinie, J. M., Marrion, N. V., Maylie, J. and Adelman, J. P. (1996). Small-conductance, calcium-activated potassium channels from mammalian brain. *Science* **273,** 1709-1714.

Kontani, K., Nishina, H., Ohoka, Y., Takahashi, K. and Katada, T. (1993). NAD glycohydrolase specifically induced by retinoic acid in human leukemic HL-60 cells. Identification of the NAD glycohydrolase as leukocyte cell surface antigen CD38. *J. Biol. Chem.* **268,** 16895-16898.

Koyama, M., Ito, M., Feng, J., Seko, T., Shiraki, K., Takase, K., Hartshorne, D. J. and Nakano, T. (2000). Phosphorylation of CPI-17, an inhibitory phosphoprotein of smooth muscle myosin phosphatase, by Rho-kinase. *FEBS Lett.* **475,** 197-200.

Kramer, J. W., Post, M. A., Brown, A. M. and Kirsch, G. E. (1998). Modulation of potassium channel gating by coexpression of Kv2.1 with regulatory Kv5.1 or Kv6.1 alpha -subunits. *Am. J. Physiol.* **274,** C1501-1510.

Krause, E., Gobel, A. and Schulz, I. (2002). Cell Side-specific Sensitivities of Intracellular Ca2+ Stores for Inositol 1,4,5-Trisphosphate, Cyclic ADP-ribose, and Nicotinic Acid Adenine Dinucleotide Phosphate in Permeabilized Pancreatic Acinar Cells from Mouse. *J. Biol. Chem.* **277,** 11696-11702.

Krause, K. H. and Michalak, M. (1997). Calrecticulin. *Cell* **88,** 439-443.

Krause, K. H., Milos, M., Luan-Rilliet, Y., Lew, D. P. and Cox, J. A. (1991). Thermodynamics of cation binding to rabbit skeletal muscle calsequestrin. Evidence for distinct Ca(2+)- and Mg(2+)-binding sites. *J. Biol. Chem.* **266,** 9453-9459.

Kubista, M., Akerman, B. and Norden, B. (1987). Characterization of interaction between DNA and 4',6-diamidino-2-phenylindole by optical spectroscopy. *Biochemistry* **26,** 4545-4553.

Kuemmerle, J. F. and Makhlouf, G. M. (1995). Agonist-stimulated Cyclic ADP Ribose. *J. Biol. Chem.* **270,** 25488-25494.

Kume, H., Hall, I. P., Washabau, R. J., Takagi, K. and Koltikoff, M. I. (1994). Beta-adrenergic agonists regulate KCa channels in airway smooth muscle by cAMP-dependent and -independent mechanisms. *J. Clin. Invest.* **93,** 371-379.

Kume, H., Takai, A., Tokuno, H. and Tomita, T. (1989). Regulation of Ca2+-dependent K+-channel activity in tracheal myocytes by phosphorylation. *Nature* **341,** 152-154.

Kureishi, Y., Kobayashi, S., Amano, M., Kimura, K., Kanaide, H., Nakano, T., Kaibuchi, K. and Ito, M. (1997). Rho-associated Kinase Directly

Induces Smooth Muscle Contraction through Myosin Light Chain Phosphorylation. *J. Biol. Chem.* **272,** 12257-12260.
Ladouceur, D. M., Flynn, M. A., Keiser, J. A., Reynolds, E. and Haleen, S. J. (1993). ETA and ETB Receptors Coexist on Rabbit Pulmonary Artery Vascular Smooth Muscle Mediating Contraction. *Biochem. Biophys. Res. Commun.* **196,** 209-215.
Lai, F. A., Erickson, H. P., Rousseau, E., Liu, Q. Y. and Meissner, G. (1988). Purification and reconstitution of the calcium release channel from skeletal muscle. *Nature* **331,** 315-319.
Lamb, F. S., Clayton, G. H., Liu, B. X., Smith, R. L., Barna, T. J. and Schutte, B. C. (1999). Expression of CLCN voltage-gated chloride channel genes in human blood vessels. *J. Mol. Cell. Cardiol.* **31,** 657-666.
Langhorst, M. F., Schwarzmann, N. and Guse, A. H. (2004). Ca2+ release via ryanodine receptors and Ca2+ entry: major mechanisms in NAADP-mediated Ca2+ signaling in T-lymphocytes. *Cell. Sig.* **16,** 1283-1289.
Langton, P. D. (1993). Calcium channel currents recorded from isolated myocytes of rat basilar artery are stretch sensitive. *J. Physiol.* **471,** 1-11.
Lassen, N. A., Ingvar, D. H. and Skinhoj, E. (1978). Brain function and blood flow. *Sci. Am.* **239,** 62-71.
Lazor, R., Feihl, F., Waeber, B., Kucera, P. and Perret, C. (1996). Endothelin-1 does not mediate the endothelium-dependent hypoxic contractions of small pulmonary arteries in rats. *Chest* **110,** 189-197.
Leach, R. M., H.M.;, H., Snetkov, V. A., Robertson, T. P. and Ward, J. P. (2001). Divergent roles of glycolysis and the mitochondrial electron transport chain in hypoxic pulmonary vasoconstriction of the rat: identity of the hypoxic sensor. *J. Physiol.* **536,** 211-224.
Leach, R. M., Robertson, T. P., Twort, C. H. and Ward, J. P. (1994). Hypoxic vasoconstriction in rat pulmonary and mesenteric arteries. *Am. J. Physiol.* **266,** L223-L231.
Leblanc, N. and Hume, J. R. (1990). Sodium current-induced release of calcium from cardiac sarcoplsmic reticulum. *Science* **248,** 372-376.
Ledoux, J., Greenwood, I., Villeneuve, L. R. and Leblanc, N. (2003). Modulation of Ca2+-dependent Cl- channels by calcineurin in rabbit coronary arterial myocytes. *J. Physiol.* **552,** 701-714.
Lee, A. G. (2002). A calcium pump made visible. *Curr. Opin. Struct. Biol.* **12,** 547-554.
Lee, H. C. (1991). Specific binding of cyclic ADP-ribose to calcium-storing microsomes from sea urchin eggs. *J. Biol. Chem.* **266,** 2276-2281.
Lee, H. C. (1997). Mechanisms of calcium signaling by cyclic ADP-ribose and NAADP. *Physiol. Rev.* **77,** 1133-1164.
Lee, H. C. and Aarhus, R. (1991). ADP-ribosyl cyclase: an enzyme that cyclizes NAD+ into a calcium-mobilizing metabolite. *Cell Reg.* **2,** 203-209.
Lee, H. C. and Aarhus, R. (1993). Wide Distribution of an enzyme that catalyses the hydrolysis of cyclic ADP-ribose. *Biochim. Biophys. Acta* **24,** 68-74.
Lee, H. C. and Aarhus, R. (1995). A derivative of NADP mobilises calcium stores insensitive to inositol trisphosphate and cyclic ADP-ribose. *J. Biol. Chem* **270,** 2152-2157.

Lee, H. C. and Aarhus, R. (2000). Functional visualisation of the seperate but interacting calcium stores sensitive to NAADP and cyclic ADP-ribose. *J. Cell Sci.* **113,** 4413-4420.

Lee, H. C., Aarhus, R. and Graeff, R. M. (1995). Sensitization of Calcium-induced Calcium Release by Cyclic ADP-ribose and Calmodulin. *J. Biol. Chem.* **270,** 9060-9066.

Lee, H. C., Aarhus, R., Graeff, R. M. and Walseth, T. F. (1994a). Cyclic ADP-ribose activation of the ryanodine receptor is mediated by calmodulin. *Nature* **370,** 307-309.

Lee, H. C., Aarhus, R. and Levitt, D. (1994b). The crystal structure of cyclic ADP-ribose. *Nature Struct. Biol.* **1,** 143-144.

Lee, H. C., Walseth, T. F., Bratt, G. T., Hayes, R. N. and Clapper, D. L. (1989). Structural determination of a cyclic metabolite of NAD+ with intracellular Ca2+-mobilizing activity. *J. Biol. Chem.* **264,** 1608-1615.

Lee, J. H., Gomora, J. C., Cribbs, L. L. and Perez-Reyes, E. (1999). Nickel Block of Three Cloned T-Type Calcium Channels: Low Concentrations Selectively Block alpha 1H. *Biophys. J.* **77,** 3034-3042.

Lee, S. L., Yu, A. S. and Lytton, J. (1994c). Tissue-specific expression of Na(+)-Ca2+ exchanger isoforms. *J. Biol. Chem.* **269,** 14849-14852.

Lesh, R. A., Marks, A. R., Somlyo, A. V., Fleischer, S. and Somlyo, A. P. (1992). Anti- ryanodine receptor antibody binding. *Circ. Res.* **72,** 481-488.

Lesh, R. A., Marks, A. R., Somlyo, A. V., Fleischer, S. and Somlyo, A. P. (1993). Anti- ryanodine receptor antibody binding. *Circ. Res.* **72,** 481-488.

Lesh, R. E., Nixon, G. F., Fleischer, S., Airey, J. A., Somlyo, A. P. and Somlyo, A. V. (1998). Localization of Ryanodine Receptors in Smooth Muscle. *Circ. Res.* **82,** 175-185.

Levesque, P. C., Leblanc, N. and Hume, J. R. (1991). Role of reverse-mode Na(+)-Ca2+ exchange in excitation-contraction coupling in the heart. *Ann. N.Y. Acad. Sci.* **639,** 386-397.

Lewis, V., Green, S. A., Marsh, M., Vihko, P., Helenius, A. and Mellman, I. (1985). Glycoproteins of the lysosomal membrane. *J. Cell Biol.* **100,** 1839-1847.

Li, N., Teggatz, E. G., Li, P.-L., Allaire, R. and Zou, A.-P. (2000). Formation and Actions of Cyclic ADP-Ribose in Renal Microvessels. *Microvas. Res.* **60,** 149-159.

Li, P. and Chen, S. R. W. (2001). Molecular Basis of Ca2+ Activation of the Mouse Cardiac Ca2+ Release Channel (Ryanodine Receptor). *J. Gen. Physiol.* **118,** 33-44.

Li, P., Zou, A. P. and Campbell, W. B. (1997). Metabolism and actions of ADP-riboses in coronary arterial smooth muscle. *Adv. Exp. Med. Biol* **419,** 437-441.

Li, P. L., Chen, C.-L., Bortell, R. and Campbell, W. B. (1999). 11,12-Epoxyeicosatrienoic Acid Stimulates Endogenous Mono-ADP-Ribosylation in Bovine Coronary Arterial Smooth Muscle. *Circ. Res.* **85,** 349-356.

Li, P. L., Lee, H. C., Nelson, M. T., Meininger, G. A. and Van Breemen, C. (2003). Novel Ca2+ signalling mechanisms in vascular myocytes: symposium overview. *Acta Physiol. Scand.* **179,** 339-352.

Li, P.-L., Zhang, D. X., Ge, Z.-D. and Campbell, W. B. (2002a). Role of ADP-ribose in 11,12-EET-induced activation of KCa channels in coronary arterial smooth muscle cells. *Am. J. Physiol.* **282,** H1229-H1236.

Li, P.-L., Zhang, D. X., Ge, Z.-D. and Campbell, W. B. (2002b). Role of ADP-ribose in 11,12-EET-induced activation of KCa channels in coronary arterial smooth muscle cells. *Am. J. Physiol.* **282,** H1229-1236.

Li, P. L., Zou, A.-P. and Campbell, W. B. (1998). Regulation of KCa-channel activity by cyclic ADP-ribose and ADP-ribose in coronary arterial smooth muscle. *Am. J. Physiol.* **275,** H1002-1010.

Lindemann, J. P., Jones, L. R., Hathaway, D. R. H., B.G.; and Watanabe, A. M. (1983). beta-Adrenergic stimulation of phospholamban phosphorylation and Ca2+-ATPase activity in guinea pig ventricles. *J. Biol. Chem.* **258,** 464-471.

Liu, J. Q., Sham, J. S. K., Shimoda, L. A., Kuppusamy, P. and Sylvester, J. T. (2003). Hypoxic constriction and reactive oxygen species in porcine distal pulmonary arteries. *Am. J. Physiol.* **285,** L322-333.

Liu, Q., Sham, J. S. K., Shimoda, L. A. and Sylvester, J. T. (2001). Hypoxic constriction of porcine distal pulmonary arteries: endothelium and endothelin dependence. *Am. J. Physiol.* **280,** L856-865.

Lockhart, A., Zelter, M., Mensch-Dechene, J., Antezana, G., Paz-Zamora, M., Varga, E. and Coudert, J. (1976). Pressure-flow-volume relationships in pulmonary circulation of normal highlanders. *J. Appl. Physiol.* **41,** 449-456.

Luik, R. M., Wu, M. M., Buchanan, J. and Lewis, R. S. (2006). The elementary unit of store-operated Ca2+ entry: local activation of CRAC channels by STIM1 at ER-plasma membrane junctions. *J. Cell Biol.* **174,** 815-825.

Lukyanenko, V. and Gyorke, S. (1999). Ca2+ sparks and Ca2+ waves in saponin-permeabilized rat ventricular myocytes. *J. Physiol.* **521,** 575-585.

Lytton, J., Westlin, M., Burk, S. E., Shull, G. E. and MacLennan, D. H. (1992). Functional comparisons between isoforms of the sarcoplasmic or endoplasmic reticulum family of calcium pumps. *J. Biol. Chem.* **267,** 14483-14489.

Lytton, J., Westlin, M. and Hanley, M. R. (1991). Thapsigargin inhibits the sarcoplasmic or endoplasmic reticulum Ca- ATPase family of calcium pumps. *J. Biol. Chem.* **266,** 17067-17071.

Ma, H. T., Patterson, R. L., Van Rossum, D. B., Birnbaumber, L., Mikoshiba, K. and Gill, D. L. (2000). Requirement of the inositol trisphosphate receptor for activation of store-operated Ca2+ channels. *Science* **287,** 1647-1651.

MacLean, M. R., McCulloch, K. M. and Baird, M. (1994). Endothelin ETA- and ETB-recpetor-mediated vasoconstriction in rat pulmonary arteries and arterioles. *J. Cardiovasc. Pharmacol.* **23,** 838-845.

MacLean, M. R., McCulloch, K. M. and Baird, M. (1995). Effects of pulmonary hypertension on vasoconstrictor responses to endothelin-1 and sarafotoxin S6C and on inherent tone in rat pulmonary arteries. *J. Cardiovasc. Pharmacol.* **26,** 822-830.

Maekawa, M., Ishizaki, T., Boku, S., Watanabe, N., Fujita, A., Iwamatsu, A., Obinata, T., Ohashi, K., Mizuno, K. and Narumiya, S. (1999).

Signaling from Rho to the Actin Cytoskeleton Through Protein Kinases ROCK and LIM-kinase. *Science* **285,** 895-898.

Maguire, J. J., Kuc, R. F., Rous, B. A. and Davenport, A. P. (1996). Failure of BQ123, a more potent antagonist of sarafotoxin 6b than of endothelin-1, to distinguish between these agonists in binding experiments. *Br. J. Pharmacol.* **118,** 335-342.

Marchant, J. S. and Taylor, C. W. (1997). Cooperative activation of IP3 receptors by sequential binding of IP3 and Ca2+ safeguards against spontaneous activity. *Curr. Biol.* **7,** 510-518.

Marshall, C., Mamary, A. J., Verhoeven, A. J. and Marshall, B. E. (1996). Pulmonary artery NADPH-oxidase is activated in hypoxic pulmonary vasoconstriction. *Am. J. Physiol.* **15,** 633-644.

Marshall, I. C. B. and Taylor, C. W. (1993). Regulation of inositol 1,4,5-trisphosphate receptors. *J. Exp. Biol.* **184,** 161-182.

Martin, R. L., Lee, J. H., Cribbs, L. L., Perez-Reyes, E. and Hanck, D. A. (2000). Mibefradil Block of Cloned T-Type Calcium Channels. *J Pharmacol. Exp. Ther.* **295,** 302-308.

Marx, S. O., Ondrias, K. and Marks, A. R. (1998). Coupled Gating Between Individual Skeletal Muscle Ca2+ Release Channels (Ryanodine Receptors). *Science* **281,** 818-821.

Masgrau, R., Churchill, G. C., Morgan, A. J., Ashcroft, S. J. H. and Galione, A. (2003). NAADP: A New Second Messenger for Glucose-Induced Ca2+ Responses in Clonal Pancreatic [beta] Cells. *Curr. Biol.* **13,** 247-251.

Masuda, W., Takenaka, S., Tsuyama, S., Inui, H., Miyatake, K. and Nakano, Y. (1999). Purification and characterization of ADP-ribosyl cyclase from Euglena gracilis. *J. Biochem.* **125,** 449-453.

Matsumura, N. and Tanuma, S.-i. (1998). Involvement of Cytosolic NAD+Glycohydrolase in Cyclic ADP-Ribose Metabolism,. *Biochem. Biophys.l Res. Comm.* **253,** 246-252.

Matteoni, R. and Kreis, T. E. (1987). Translocation and clustering of endosomes and lysosomes depends on microtubules. *J. Cell Sci.* **105,** 1253-1265.

McCulloch, K. M., Docherty, C. C., Morecroft, I. and MacLean, M. R. (1996). EndothelinB receptor-mediated contraction in human pulmonary resistance arteries. *Br. J. Pharmacol.* **119,** 1125-1130.

McDaniel, S. S., Platoshyn, O., Wang, J., Yu, Y., Sweeney, M., Krick, S., Rubin, L. J. and Yuan, J. X.-J. (2001). Capacitive Ca2+ entry in agonist- induced pulmonary vasoconstriction. *Am. J. Physiol.* **280,** L870-L880.

McLean, J. R., Twarog, B. M. and Bergofsky, E. H. (1985). The adrenergic innervation of pulmonary vasculature in the normal and hypertensive rat. *J. Auton. Nerv. Syst.* **14,** 111-123.

McManus, O. B., Helms, L. M., Pallanck, L., Ganetzky, B., Swanson, R. and Leonard, R. J. (1995). Functional role of the beta-subunit of high conductance calcium-activated potasium channels. *Neuron* **14,** 645-650.

McNeil, P. L., Vogel, S. S., Miyake, K. and Terasaki, M. (2000). Patching plasma membrane disruptions with cytoplasmic membrane. *J. Cell Sci.* **113,** 1891-1902.

McNeish, A. J., Sandow, S. L., Neylon, C. B., Chen, M. X., Dora, K. A. and Garland, C. J. (2006). Evidence for Involvement of Both IKCa and SKCa Channels in Hyperpolarizing Responses of the Rat Middle Cerebral Artery. *Stroke* **37,** 1277-1282.

Meissner, G. and Henderson, J. S. (1987). Rapid calcium release from cardiac sarcoplasmic reticulum vesicles is dependent on Ca2+ and is modulated by Mg2+, adenine nucleotide, and calmodulin. *J. Biol. Chem.* **262,** 3065-3073.

Meszaros, L. G., Bak, J. and Chu, A. (1993). Cyclic ADP-ribose as an endogenous regulator of the non-skeletal type ryanodine receptor Ca2+ channel. *Nature* **364,** 76-79.

Meszaros, L. G., Wrenn, R. W. and Varadi, G. (1997). Sarcoplasmic Reticulum-Associated and Protein Kinase C-Regulated ADP-Ribosyl Cyclase in Cardiac Muscle. *Biochem. Biophys.l Res. Comm.* **234,** 252-256.

Meyer, T., Holowaka, D. and Stryer, L. (1988). Highly cooperative opening of calcium channels by inositol 1,4,5- trisphosphate. *Science* **240,** 653-656.

Michalak, M., Corbett, E. F., Mesaeli, N., Nakamura, K. and Opas, M. (1999). Calrecticulin: one protein, one gene, many functions. *Biochem. J.* **344,** 281-292.

Michalak, M., Milner, R. E., Burns, K. and Opas, M. (1992). Calrecticulin. *Biochem. J.* **285,** 681-692.

Michelakis, E. D., Thebaud, B., Weir, E. K. and Archer, S. L. (2004). Hypoxic pulmonary vasoconstriction: redox regulation of O_2-sensitive K^+ channels by a mitochondrial O_2-sensor in resistance artery smooth muscle cells. *J. Mol. Cell. Cardiol.* **37,** 1119-1136.

Michels, G., Matthes, J., Handrock, R., Kuchinke, U., Groner, F., Cribbs, L. L., Pereverzev, A., Schneider, T., Perez-Reyes, E. and Herzig, S. (2002). Single-Channel Pharmacology of Mibefradil in Human Native T-Type and Recombinant Cav3.2 Calcium Channels. *Mol. Pharmacol.* **61,** 682-694.

Michikawa, T., Hamanaka, H., Otsu, H., Yamamoto, A., Miyawaki, A., Furuichi, T., Tashiro, Y. and Mikoshiba, K. (1994). Transmembrane topology and sites of N- glycosylation of inositol 1,4,5- trisphosphate receptor. *J. Biol. Chem.* **269,** 9184-9189.

Mignery, G. A. and Sudhof, T. C. (1990). The ligand binding site and transduction mechanism in the inositol-1,4,5-triphosphate receptor. *EMBO J.* **9,** 3893-3898.

Miki, T., Suzuki, M., Shibasaki, T., Uemura, H., Sato, T., Yamaguchi, K., Koseki, H., Iwanaga, T., Nakaya, H. and Seino, S. (2002). Mouse model of prinzmetal angina by disruption of the inward rectifier Kir6.1. *Nat. Med.* **8,** 466-472.

Millar, J. A., Barratt, L., Southan, A. P., Page, K. M., Fyffe, R. E. W., Robertson, B. and Mathie, A. (2000). A functional role for the two-pore domain potassium channel TASK-1 in cerebellar granule neurons. *Proc. Natl. Acad. Sci.* **97,** 3614-3618.

Mills, E. and Jobsis, F. F. (1972). Mitochondrial respiratory chain of carotid body and chemoreceptor response to changes in oxygen tension. *J. Neurophysiol.* **35,** 405-428.

Milnor, W. R. (1982). *Hemodynamics*. William & Wilkins.
Mironneau, J., Coussin, F., Jeyakumar, L. H., Fleischer, S., Mironneau, C. and Macrez, N. (2001). Contribution of Ryanodine Receptor Subtype 3 to Ca2+ Responses in Ca2+-overloaded Cultured Rat Portal Vein Myocytes. *J. Biol. Chem.* **276,** 11257-11264.
Mitchell, K. J., Lai, F. A. and Rutter, G. A. (2003). Ryanodine Receptor Type I and Nicotinic Acid Adenine Dinucleotide Phosphate Receptors Mediate Ca2+ Release from Insulin-containing Vesicles in Living Pancreatic beta -Cells (MIN6). *J. Biol. Chem.* **278,** 11057-11064.
Miyakawa, T., Maeda, A., Yamazawa, T., Hirose, K., Kurosaki, T. and Iino, M. (1999). Encoding of Ca2+ signals by differential expression of IP3 receptor subtypes. *EMBO J.* **18,** 1303-1308.
Mojzisova, A., Krizanova, O., Zacikova, L., Kominkova, V. and Ondrias, K. (2001). Effect of nicotinic acid adenine dinucleotide phosphate on ryanodine calcium release channel in heart. *Pflugers Arch.* **441,** 674-677.
Moncada, S., Palmer, R. M. and Higgs, E. A. (1991). Nitric Oxide: physiology, pathophysiology and pharmacology. *Pharmacol. Rev.* **43,** 109-142.
Moon, S. Y. and Zheng, Y. (2003). Rho GTPase-activating proteins in cell regulation. *Trends in Cell Biology* **13,** 13-22.
Moore, E. D., Etter, E. F., Philipson, K. D., Carrington, W. A., Fogarty, K. E., Lifshitz, L. M. and Fay, F. S. (1993). Coupling of the Na+/Ca2+ exchanger, Na+/K+ pump and sarcoplasmic reticulum in smooth muscle. *Nature* **365,** 657-660.
Morano, I. (2003). Tuning smooth muscle contraction by molecular motors. *J. Molec. Med.* **81,** 481-487.
Morel, N. and Godfriand, T. (1994). The ETA receptor antagonist, BQ-123, normalises the response of SHR aorta to Ca2+ channel activator. *Eur. J. Pharmacol.* **252,** R3-4.
Morgan, J. P. and Morgan, K. G. (1982). Vascular smooth muscle: the first recorded Ca2+ transients. *Pflugers Arch.* **395,** 75-77.
Morio, Y. and McMurtry, I. F. (2002). Ca^{2+} release from ryanodine-sensitive store contributes to mechanism of hypoxic vasoconstriction in rat lungs. *J. Appl. Physiol.* **92,** 527-534.
Murayama, T., Kurebayashi, N. and Ogawa, Y. (2000). Role of Mg2+ in Ca2+-Induced Ca2+ Release through Ryanodine Receptors of Frog Skeletal Muscle: Modulations by Adenine Nucleotides and Caffeine. *Biophys. J.* **78,** 1810-1824.
Murray, R. K., Fleischmann, B. K. and Kotlikoff, M. I. (1993). Receptor-activated Ca influx in human airway smooth muscle: use of Ca imaging and perforated patch-clamp techniques. *Am. J. Physiol.* **264,** C485-C490.
Murray, R. K. and Kotlikoff, M. I. (1991). Receptor-activated calcium influx in human airway smooth muscle cells. *J. Physiol.* **435,** 123-144.
Nakamura, K., Robertson, M., Liu, G., Dickie, P., Nakamura, K., Guo, J. Q., Duff, H. J., Opas, M., Kavanagh, K. and Michalak, M. (2001). Complete heart block and sudden death in mice overexpressing calreticulin. *J. Clin. Invest.* **107,** 1245-1253.
Nakazawa, H., Hori, M., Murata, T., Ozaki, H. and Karaki, H. (2001). Contribution of chloride channel activation to the elevated muscular

tone of the pulmonary artery in monocrotaline-induced pulmonary hypertensive rats. *Jpn. J. Pharmacol.* **86,** 310-315.
Narumiya, S., Ishizaki, T. and Watanabe, N. (1997). Rho effectors and reorganization of actin cytoskeleton. *FEBS Letters* **410,** 68-72.
Navazio, L., Bewell, M., Siddiqua, A., Dickinson, G. D., Galione, A. and Sanders, D. (2000). Calcium release from the endoplasmic reticulum of higher plants elicited by the NADP metabolite nicotinic acid adenine dinucleotide phosphate. *Proc. Natl. Acad. Aci.* **97,** 8693-8698.
Nelson, M. T., Cheng, H., Rubart, M., Santana, L. F., Bonev, A. D., Knot, H. J. and Lederer, W. J. (1995). Relaxation of arterial smooth muscle by calcium sparks. *Science* **270,** 633-637.
Nelson, M. T. and Quayle, J. M. (1995). Physiological roles and properties of potassium channels in arterial smooth muscle. *Am. J. Physiol.* **268,** C799-822.
Newton, C., Mignery, G. and Sudhof, T. (1994). Co-expression in vertebrate tissues and cell lines of multiple inositol 1,4,5-trisphosphate (InsP3) receptors with distinct affinities for InsP3. *J. Biol. Chem.* **269,** 28613-28619.
Neylon, C. B., Richards, S. M., Larsen, M. A., Agrotis, A. and Bobik, A. (1995). Multiple Types of Ryanodine Receptor/Ca2+ Release Channels Are Expressed in Vascular Smooth Muscle. *Biochem. Biophys. Res. Commun.* **215,** 814-821.
Ng, L. C., Wilson, S. M. and Hume, J. R. (2005). Mobilisation of sarcoplasmic reticulum stores by hypoxia leads to consequent activation of capacitative Ca^{2+} entry in isolated canine pulmonary artery smooth muscle cells. *J. Physiol.* **563,** 409-419.
Nicoll, D. A., Quednau, B. D., Qui, Z., Xia, Y. R., Lusis, A. J. and Philipson, K. D. (1996). Cloning of a Third Mammalian Na+-Ca2+ Exchanger, NCX3. *J. Biol. Chem.* **271,** 24914-24921.
Niggli, E. (1999). Localized intracellular calcium signaling in muscle: calcium sparks and calcium quarks. *Annu. Rev. Physiol.* **61,** 311-335.
Nissel, O. (1948). Effects of oxygen and carbon dioxide on the circulation of isolated and perfused lungs of cats. *Acta Physiol. Scand.* **16,** 121-127.
Nixon, G. F., Mignery, G. A. and Somlyo, A. V. (1994). Immunoglod localization of inositol 1,4,5- trisphosphate receptors and characterization of ultra-structural features of the sarcoplasmic reticulum in phasic and tonic smooth muscle. *J. Muscle Res. Cell Motil.* **15,** 682-700.
Nobes, C. D. and Hall, A. (1995). Rho, Rac, and Cdc42 GTPases regulate the assembly of multimolecular focal complexes associated with actin stress fibers, lamellipodia, and filopodia. *Cell* **81,** 53-62.
Noguchi, N., Takasawa, S., Nata, K., Tohgo, A., Kato, I., Ikehata, F., Yonekura, H. and Okamoto, H. (1997). Cyclic ADP-ribose Binds to FK506-binding Protein 12.6to Release Ca2+ from Islet Microsomes. *J. Biol. Chem.* **272,** 3133-3136.
Noma, A. (1983). ATP-regulated K+ channels in cardiac muscle. *Nature* **305,** 147-148.
Nowycky, M. C., Fox, A. P. and Tsien, R. W. (1985). Long-opening mode of gating of neuronal calcium channels and its promotion by the

dihydropyridine calcium agonist Bay K 8644. *Proc. Natl. Acad. Sci.* **82,** 2178-2182.

Ochocka, A. M. and Pawelczyk, T. (2003). Isozymes delta of phosphoinositide-specific phospholipase C and their role in signal transduction in the cell. *Acta Biochim. Pol.* **50,** 1097-1110.

Odermatt, A., Becker, S., Khanna, V. K., Kurzydlowski, K., Leisner, E., Pette, D. and MacLennan, D. H. (1998). Sarcolipin regulates the activity of SERCA1, the fast-twitch skeletal muscle sarcoplasmic reticulum Ca^{2+}-ATPase. *J. Biol. Chem.* **273,** 12360-12369.

Olschewski, A., Li, Y., Tang, B., Hanze, J., Eul, B., Bohle, R. M., Wilhelm, J., Morty, R. E., Brau, M. E., Weir, E. K., Kwapiszewska, G., Klepetko, W., Seeger, W. and Olschewski, H. (2006). Impact of TASK-1 in Human Pulmonary Artery Smooth Muscle Cells. *Circ. Res.* **98,** 1072-1080.

Orallo, F. (1996). Regulation of cytosolic calcium levels in vascular smooth muscle. *Pharmacol. Ther.* **69,** 153-171.

Paky, A., Michael, J. R., Burke-Wolin, T. M., Wolin, M. S. and Gurtner, G. H. (1993). Endogenous production of superoxide by rabbit lungs: effects of hypoxia or metabolic inhibitors. *J. Appl. Physiol.* **74,** 2868-2874.

Palmer, R. M., Ferrige, A. G. and Moncada, S. (1987). Nitric oxide release accounts for the biological activity of endothelium-derived relaxing factor. *Nature* **327,** 524-526.

Panfoli, I., Burlando, B. and Viarengo, A. (1999). Cyclic ADP-Ribose-Dependent Ca2+Release Is Modulated by Free [Ca2+] in the Scallop Sarcoplasmic Reticulum. *Biochem. Biophys. Res. Commun.* **257,** 57-62.

Parekh, A. B. and Penner, R. (1997). Store-operated calcium influx. *Physiol. Rev.* **77,** 901-930.

Parekh, A. B. and Putney, J. W. (2005). Store-Operated Calcium Channels. *Physiol. Rev.* **85,** 757-810.

Partida-Sanchez, S., Cockayne, D. A., Monard, S., Jacobson, E. L., Oppenheimer, N., Garvy, B., Kusser, K., Goodrich, S., Howard, M., Harmsen, A., Randall, T. D. and Lund, F. (2001). Cyclic ADP-ribose production by CD38 regulates intracellular calcium release, extracellular calcium influx and chemotaxis in neutrophils and is required for bacterial clearance in vivo. *Nature Med.* **7,** 1209-1216.

Partovian, C., Adnot, S., Raffestin, B., Louzier, V., Levame, M., Mavier, I. M., Lemarchand, P. and Eddahibi, S. (2000). Adenovirus-mediated lung vascular endothelial growth factor overexpression protects against hypoxic pulmonary hypertension in rats. *Am. J. Physiol.* **23,** 762-771.

Pate, P., Mochca-M.J.;, Wu, Y., Zhang, J. Z., Rodney, G. G., Serysheva, I. I., Williams, B. Y., Anderson, M. E. and Hamilton, S. L. (2000). Determinants for Calmodulin Binding on Voltage-dependent Ca2+ Channels. *J. Biol. Chem.* **275,** 39786-39792.

Patel, A. J. and Honore, E. (2001). Properties and modulation of mammalian 2P domain K+ channels. *Trends Neurosci.* **24,** 339-346.

Patel, S. (2004). NAADP-induced Ca2+ Release - A new signalling pathway. *Biology of the Cell* **96,** 19-28.

Patel, S., Churchill, G. C. and Galione, A. (2000a). Unique kinetics of nicotinic acid-adenine dinucleotide phosphate (NAADP) binding enhance the

sensitivity of NAADP receptors for their ligand. *Biochem. J.* **352,** 725-729.
Patel, S., Churchill, G. C. and Galione, A. (2001). Coordination of Ca2+ signalling by NAADP. *Trends Biochem. Sci.* **26,** 482-489.
Patel, S., Churchill, G. C., Sharp, T. and Galione, A. (2000b). Widespread Distribution of Binding Sites for the Novel Ca2+-mobilizing Messenger, Nicotinic Acid Adenine Dinucleotide Phosphate, in the Brain. *J. Biol. Chem.* **275,** 36495-36497.
Patel, S., Joseph, S. K. and Thomas, A. P. (1999). Molecular properties of inositol 1,4,5-trisphosphate receptors. *Cell Calcium* **25,** 247-264.
Paton, W. D. and Waud, D. R. (1967). The matgin of safety of neuromuscular transmission. *J. Physiol.* **191,** 59-90.
Perez, G. J., Bonev, A. D., Patlak, J. B. and Nelson, M. T. (1999). Functional coupling of ryanodine receptors to KCa channels in smooth muscle cells from rat cerebral arteries. *J. Gen. Physiol.* **113,** 229-238.
Perez-Reyes, E. (2003). Molecular physiology of low-voltage-activated T-type calcium channels. *Physiol. Rev.* **83,** 117-161.
Peters, T. J., Muller, M. and de Duve, A. C. (1972). Lysosomes of the arterial wall: I. Isolation and subcellular fractionation of cells from normal rabbit aorta. *J. Exp. Med.* **136,** 1117-1139.
Peterson, B. Z., DeMaria, C. D., Adelman, J. P. and Yue, D. T. (1999). Calmodulin is the Ca2+ sensor for the Ca2+- dependent inactivation of L-type calcium channels. *Neuron* **22,** 549-558.
Peterson, B. Z., Lee, J. S., Mulle, J. G., Wang, Y., de Leon, M. and Yue, D. T. (2000). Critical Determinants of Ca2+-Dependent Inactivation within an EF-Hand Motif of L-Type Ca2+ Channels. *Biophys. J.* **78,** 1906-1920.
Petkov, G. V., Heppner, T. J., Bonev, A. D., Herrera, G. M. and Nelson, M. T. (2001). Low levels of KATP channel activation decrease excitability and contractility of urinary bladder. *Am. J. Physiol.* **280,** R1427-1433.
Pohlmann, R., Boeker, M. W. C. and von Figura, K. (1995). The Two Mannose 6-Phosphate Receptors Transport Distinct Complements of Lysosomal Proteins. *J. Biol. Chem.* **270,** 27311-27318.
Pongs, O., Leicher, T., Berger, M., Roeper, J., Bahring, R., Wray, D., Giese, K. P., Silva, A. J. and Storm, J. F. (1999). Functional and Molecular Aspects of Voltage-Gated K+ Channel beta Subunits. *Ann. N.Y. Acad. Sci.* **868,** 344-355.
Porter, V. A., Bonev, A. D., Knot, H. J., Heppner, T. J., Stevenson, A. S., Kleppisch, T., Lederer, W. J. and Nelson, M. T. (1998). Frequency modulation of Ca2+ sparks is involved in regulation of arterial diameter by cyclic nucleotides. *Am. J. Physiol.* **274,** C1346-1355.
Pozzan, T., Rizzuto, R., Volpe, P. and Meldolesi, J. (1994). Molecular and cellular physiology of intracellular calcium stores. *Physiol. Rev.* **74,** 595-636.
Prakash, Y. S., Kannan, M. S. and G.C., S. (1997). Regulation of intracellular calcium oscillations in porcine tracheal smooth muscle cells. *Am. J. Physiol.* **272,** C966-C975.
Prakash, Y. S., Kannan, M. S., Walseth, T. F. and Sieck, G. C. (1998). Role of cyclic ADP-ribose in the regulation of [Ca2+]i in porcine tracheal smooth muscle. *Am. J. Physiol.* **274,** C1653-C1660.

Prakash, Y. S., Kannan, M. S., Walseth, T. F. and Sieck, G. C. (2000). cADP ribose and [Ca2+]i regulation in rat cardiac myocytes. *Am. J. Physiol.* **279,** H1482-1489.

Prakriya, M., Feske, S., Gwack, Y., Srikanth, S., Rao, A. and Horgan, P. G. (2006). Orai1 is an essential pore subunit of the CRAC channel. *Nature* **443,** 230-233.

Prieto, D., Simonsen, U., Hernadez, M. and Garcia-Sacristan, A. (1998). Contribution of K^+ channels and ouabain-sensitive mechanisms to the endothelium-dependent relaxations of horse penile small arteries. *Br. J. Pharmacol.* **123,** 1609-1620.

Pugsley, M. K. and Tabrizchi, R. (2000). The vascular system: An overview of structure and function. *J. Pharmacol. Toxicol. Methods* **44,** 333-340.

Putney, J. W. J. (1986). A model for receptor regulated calcium entry. *Cell Calcium* **7,** 1-12.

Quayle, J. M., Dart, C. and Standen, N. B. (1996). The properties and distribution of inward rectifier pottsium currents in pig coronary arterial smooth muscle. *J. Physiol.* **494,** 715-726.

Quayle, J. M., McCarron, J. G., Brayden, J. E. and Nelson, M. T. (1993). Inward rectifier K+ currents in smooth muscle cells from rat resistance-sized cerebral arteries. *Am. J. Physiol.* **265,** C1363-1370.

Quayle, J. M., Nelson, M. T. and Standen, N. B. (1997). ATP-sensitive and inwardly rectifying potassium channels in smooth muscle. *Physiol. Rev.* **77,** 1165-1232.

Quednau, B. D., Nicoll, D. A. and Philipson, K. D. (2004). The Sodium/Calcium exchanger family- SLC8. *Pflugers Arch.* **447,** 543-548.

Rabinovitch, M. (2001). Pathobiology of pulmonary hypertension. Extracellular matrix. *Clin. Chest Med.* **22,** 433-449.

Rabinovitch, M., Gamble, W., Nadas, A. S., Miettinen, O. S. and Reid, L. (1979). Rat pulmonary circulation after chronic hypoxia: hemodynamic and structural features. *Am. J. Physiol.* **236,** H818-827.

Rakovic, S., Cui, Y., Iino, S., Galione, A., Ashamu, G. A., Potter, B. V. L. and Terrar, D. A. (1999). An Antagonist of cADP-ribose Inhibits Arrhythmogenic Oscillations of Intracellular Ca2+ In Heart Cells. *J. Biol. Chem.* **274,** 17820-17827.

Rakovic, S., Galione, A., Ashamu, G. A., Potter, B. V. and Terrar, D. A. (1996). A specific cyclic ADP-ribose antagonist inhibits cardiac excitation-contraction coupling. *Curr. Biol.* **6,** 989-996.

Rapoport, R. M. and Murad, F. (1983). Agonist-induced endothelium-dependent relaxation in rat thoracic aorta may be mediated through cGMP. *Circ. Res.* **52,** 352-357.

Reaves, B., Bright, N., Mullock, B. and Luzio, J. (1996a). The effect of wortmannin on the localisation of lysosomal type I integral membrane glycoproteins suggests a role for phosphoinositide 3-kinase activity in regulating membrane traffic late in the endocytic pathway. *J. Cell Sci.* **109,** 749-762.

Reaves, B. J., Bright, N. A., Mullock, B. M. and Luzio, J. P. (1996b). The effect of wortmannin on the localisation of lysosomal type I integral membrane glycoproteins suggests a role for phosphoinositide 3-kinase

activity in regulating membrane traffic late in the endocytic pathway. *J. Cell Sci.* **109,** 749-762.
Rebecchi, M. J. and Pentyala, S. N. (2000). Structure, Function, and Control of Phosphoinositide-Specific Phospholipase C. *Physiol. Rev.* **80,** 1291-1335.
Reeve, H. L., Weir, E. K., Nelson, D. P., Peterson, D. A. and Archer, S. L. (1995). Opposing effects of oxidants and antioxidants on K+ channel activity and tone in rat vascular tissue. *Exp. Physiol.* **80,** 825-834.
Reeves, J. P. and Hale, C. C. (1984). The stoichiometry of the cardiac sodium-calcium exchange system. *J. Biol. Chem.* **259,** 7733-7739.
Remillard, C. V. and Leblanc, N. (1996). Mechanism of inhibition of delayed rectifier K^+ current by 4-aminopyridine in rabbit coronary myocytes. *J. Physiol.* **491,** 383-400.
Ridley, A. J. and Hall, A. (1992). The small GTP-binding protein rho regulates the assembly of focal adhesions and actin stress fibers in response to growth factors. *Cell* **70,** 389-399.
Ridley, A. J., Paterson, H. F., Johnston, C. L., Diekmann, D. and Hall, A. (1992). The small GTP-binding protein rac regulates growth factor-induced membrane ruffling. *Cell* **70,** 401-410.
Robertson, T., Hashmi-Hill, M., Vandenplas, M. L. and Lewis, S. J. (2005). Endothelium-dependent activation of Rho-kinase during hypoxic pulmonary vasoconstriction in rat intrapulmonary arteries. *FASEB J.* **19,** A1277.
Robertson, T. P., Aaronson, P. I. and Ward, J. P. (1995). Hypoxic vasoconstriction and intracellular Ca2+ in pulmonary arteries: evidence for PKC-independent Ca2+ sensitization. *Am. J. Physiol.* **268,** H301-307.
Robertson, T. P., Aaronson, P. I. and Ward, J. P. T. (2003). Ca2+ sensitization during sustained hypoxic pulmonary vasoconstriction is endothelium dependent. *Am. J. Physiol.* **284,** L1121-1126.
Robertson, T. P., Ward, J. P. and aaronson, P. I. (2001). Hypoxia induces the release of a pulmonary-selective, Ca^{2+}-sensitising, vasoconstrictor from the perfused rat lung. *Cardiovasc. Res.* **50,** 145-150.
Robinson, J., Okada, T., Castellot, J., Jr and Karnovsky, M. (1986). Unusual lysosomes in aortic smooth muscle cells: presence in living and rapidly frozen cells. *J. Cell Biol.* **102,** 1615-1622.
Rodney, G. G., Moore, C. P., Williams, B. Y., Zhang, J.-Z., Krol, J., Pedersen, S. E. and Hamilton, S. L. (2001). Calcium Binding to Calmodulin Leads to an N-terminal Shift in Its Binding Site on the Ryanodine Receptor. *J. Biol. Chem.* **276,** 2069-2074.
Romanin, C., Gamsjaeger, R., Kahr, H., Schaufler, D., Carlson, O., Abernethy, D. R. and Soldatov, N. M. (2000). Ca2+ sensors of L-type Ca2+ channel. *FEBS Letters* **487,** 301-306.
Rooney, E. K. and Gross, J. D. (1992). ATP-Driven Ca2+/H+ Antiport in Acid Vesicles from Dictyostelium. *Proc. Natl. Acad. Sci.* **89,** 8025-8029.
Rounds, S. and McMurtry, I. F. (1981). Inhibitors of oxidative ATP production cause transient vasoconstriction and block subsequent pressor responses in rat lungs. *Circ. Res.* **48,** 393-400.
Roy, C. S. and Sherrington, C. S. (1890). The regulation of blood supply to the brain. *J. Physiol.* **11,** 85.

Ruppersberg, J. P. (2000). Intracellular regulation of inward rectifier K+ channels. *Pflugers Arch.* **441,** 1-11.

Rusinko, N. and Lee, H. C. (1989). Widespread occurrence in animal tissues of an enzyme catalysing the conversion of NAD+ into a cyclic metabolite with intracellular Ca2+ mobilising activity. *J. Biol. Chem* **264,** 11725-11731.

Saitoh, M., Naka, M. and Hidaka, H. (1986). The modulatory role of myosin light chain phosphorylation in human platelet activation. *Biochem. Biophys. Res. Commun.* **140,** 280-287.

Sakamoto, A., Yanagisawa, M., Sakurai, T., Takuwa, Y., Yanagisawa, H. and Masaki, T. (1991). Cloning and functional expression of human cDNA for the ETB endothelin receptor. *Biochem. Biophys. Res. Commun.* **178,** 656-663.

Sakurai, T., Yanagisawa, M., Takuwa, Y., Miyazaki, H., Kimura, S., Goto, K. and Masaki, T. (1990). Cloning of a cDNA encoding a non-isopeptide-selective subtype of the endothelin receptor. *Nature* **348,** 673.

Salinas, M., Duprat, F., Heurteaux, C., Hugnot, J. P. and Lazdunski, M. (1997). New Modulatory alpha Subunits for Mammalian Shab K+ Channels. *J. Biol. Chem.* **272,** 24371-24379.

Salvaterra, C. G. and Goldman, W. F. (1993). Acute hypoxia increases cytosolic calcium in cultured pulmonary arterial myocytes. *Am. J. Physiol.* **264,** L323-328.

Samso, M. and Wagenknecht, T. (2002). Apocalmodulin and Ca2+-Calmodulin Bind to Neighboring Locations on the Ryanodine Receptor. *J. Biol. Chem.* **277,** 1349-1353.

Sanders, K. M. and Koh, S. D. (2006). Two-pore-domain potassium channels in smooth muscles: new components of myogenic regulation. *J. Physiol.***,** jphysiol.2005.098897.

Santella, L., De Riso, L., Gragnaniello, G. and Kyozuka, K. (1998). Separate Activation of the Cytoplasmic and Nuclear Calcium Pools in Maturing Starfish Oocytes,. *Biochem. Biophys. Res. Commun.* **252,** 1-4.

Santella, L., Kyozuka, K., Genazzani, A. A., De Riso, L. and Carafoli, E. (2000). Nicotinic Acid Adenine Dinucleotide Phosphate-induced Ca2+ Release. Interactions among distinct Ca(2+) mobilizing mechanisms in starfish oocytes. *J. Biol. Chem.* **275,** 8301-8306.

Sanz, E., Monge, L., Fernandez, N., Climent, B., Dieguez, G. and Garcia-Villalon, A. L. (2003). Mechanisms of relaxation by urocortin in renal arteries from male and female rats. *Br. J. Pharmacol.* **140,** 1003-1007.

Satake, N., Shibata, M. and Sibata, S. (1996). The inhibitory effects of iberiotoxin and 4-aminopyridine on the relaxation induced by beta 1- and beta 2-adrenoceptor activation in rat aortic rings. *Br. J. Pharmacol.* **119,** 505-510.

Sato, K., Morio, Y., Morris, K. G., Rodman, D. M. and McMurtry, I. F. (2000). Mechanism of hypoxic pulmonary vasoconstriction involves ETA receptor-mediated inhibition of KATP channel. *Am. J. Physiol.* **278,** L434-442.

Schnetkamp, P. P. M. (1995). Calcium homeostasis in vertebrate retinal rod outer segments. *Cell Calcium* **18,** 322-330.

Schnetkamp, P. P. M. (2004). The SLC24 Na+/Ca2+- K+ exchanger family: vision and beyond. *Pflugers Arch.* **447,** 683-688.

Schuh, K., Uldrijan, S., Telkamp, M., Rothlein, N. and Neyses, L. (2001). The plasmamembrane calmodulin-dependent calcium pump: a major regulator of nitric oxide synthase I. *J. Cell Biol.* **155,** 201-206.

Schuhmann, K., Romanin, C., Baumgartner, W. and Groschner, K. (1997). Intracellular Ca2+ Inhibits Smooth Muscle L-Type Ca2+ Channels by Activation of Protein Phosphatase Type 2B and by Direct Interaction with the Channel. *J. Gen. Physiol.* **110,** 503-513.

Segal, S. S., Brett, S. E. and Sessa, W. C. (1999). Codistribution of NOS and caveolin throughout peripheral vasculature and skeletal muscle of hamsters. *Am. J. Physiol.* **277,** H1167-1177.

Sethi, J. K., Empson, R. M., Bailey, V. C., Potter, B. V. L. and Galione, A. (1997). 7-Deaza-8-bromo-cyclic ADP-ribose, the First Membrane-permeant, Hydrolysis-resistant Cyclic ADP-ribose Antagonist. *J. Biol. Chem.* **272,** 16358-16363.

Shieh, C. C., Petrini, M. F., Dwyer, T. M. and Farley, J. M. (1991). Concentration-dependence of acetylcholine-induced changes in calcium and tension in swine trachealis. *J. Pharmacol. Exp. Ther.* **256,** 141-148.

Shigemori, K., Ishizaki, T., Matsukawa, S., Sakai, A., Nakai, T. and Miyabo, S. (1996). Adenine nucleotides via activation of ATP-sensitive K^+ channels modulate hypoxic responses in rat pulmonary arteries. *Am. J. Physiol.* **270,** L803-809.

Shimizu, H., Borin, M. L. and Blaustein, M. P. (1997). Use of La3+ to distinguish activity of the plasmalemmal Ca2+ pump from Na+/Ca2+ exchange in arterial myocytes. *Cell Calcium* **21,** 31-41.

Shimoda, L. A., Sylvester, J. T. and Sham, J. S. K. (2000). Mobilization of intracellular Ca2+ by endothelin-1 in rat intrapulmonary arterial smooth muscle cells. *Am. J. Physiol.* **278,** L157-164.

Shin, D. W., Ma, J. and Kim, D. H. (2001). The asp-rich region at the carboxyl-terminus of calsequestrin binds to Ca2+ and interacts with triadin. *FEBS lett.* **486,** 178-182.

Sierralta, J., Fill, M. and Suarez-Isla, B. A. (1996). Functionally Heterogenous Ryanodine Receptors in Avian Cerebellum. *J. Biol. Chem.* **271,** 17028-17034.

Sime, F., Penaloza, D. and Riz, L. (1971). Bradycardia, increased cardiac output, and reversal of pulmonary hypertension in altitude natives living at sea level. *Br. Heart J.* **33,** 647-657.

Sims, S. M., Jiao, Y. and Zheng, Z. G. (1996). Intracellular calcium stores in isolated tracheal smooth muscle cells. *Am. J. Physiol.* **271,** L300-L309.

Sitsapesan, R. and Williams, A. J. (1995). The gating of the sheep skeletal sarcoplasmic reticulum Ca(2+)-release channel is regulated by luminal Ca2+. *J. Membr. Biol.* **146,** 133-144.

Slodzinski, M. K., Juhaszova, M. and Blaustein, M. P. (1995). Antisense inhibition of Na+/Ca2+ exchange in primary cultured arterial myocytes. *Am. J. Physiol.* **269,** C1340-1345.

Smirnov, S. V., Beck, R., Tammaro, P., Ishii, T. and Aaronson, P. I. (2002). Electrophysiologically distinct smooth muscle cell subtypes in rat conduit and resistance pulmonary arteries. *J. Physiol.* **538,** 867-878.

Somlyo, A. P. and Himpens, B. (1989). Cell calcium and its regulation in smooth muscle. *FASEB J.* **3,** 2266-2276.

Somlyo, A. P. and Somlyo, A. V. (1990). Flash photolysis studies of excitation-contraction coupling, regulation, and contraction in smooth muscle. *Annu. Rev. Physiol.* **52,** 857-874.
Somlyo, A. P. and Somlyo, A. V. (1991). Smooth muscle structure and function. in Fozzard, H. A., Haber, E., Jennings, R. B., Katzand, A. M. and Morgan, H. E. (Eds), *The heart and the cardiovascular system.*, Raven, pp. 845-864.
Somlyo, A. P. and Somlyo, A. V. (1994). Signal transduction and regulation in smooth muscle. *Nature* **372,** 231-236.
Somlyo, A. P. and Somlyo, A. V. (2003). Ca2+ Sensitivity of Smooth Muscle and Nonmuscle Myosin II: Modulated by G Proteins, Kinases, and Myosin Phosphatase *Physiol. Rev.* **83,** 1325-1358.
Somlyo, A. P., Wu, X., Walker, L. A. and Somlyo, A. V. (1999). Pharmacomechanical coupling: the role of calcium, G-proteins, kinases and phosphatases. *Rev. Physiol. Biochem. Pharmacol.* **134,** 201-234.
Somlyo, A. V. and Somlyo, A. P. (1968). Elecromechanical and pharmacomechanical coupling in vascular smooth muscle. *J. Pharmacol. Exp. Ther.* **159,** 129-154.
Sonnleitner, A., Conti, A., Bertocchini, F., Schindler, H. and Sorrentino, V. (1998). Functional properties of the ryanodine receptor type 3 (RyR3) Ca2+ release channel. *EMBO J.* **17,** 2790-2798.
Sorrentino, V., Giannini, G., Malzac, P. and Mattei, M. G. (1993). Localization of a Novel Ryanodine Receptor Gene (RYR3) to Human Chromosome 15q14-q15 by in Situ Hybridization. *Genomics* **18,** 163-165.
Standen, N. B., Quayle, J. M., Davies, N. W., Brayden, J. E., Huang, Y. and Nelson, M. T. (1989). Hyperpolarizing vasodilators activate ATP-sensitive K+ channels in arterial smooth muscle. *Science* **245,** 177-180.
States, D. J., T.F.;, W. and H.C., L. (1992). Similarities in amino acid sequences of *Aplysia* ADP-ribosyl cyclase and human lymphocyte antigen CD38. *Trends Biochem. Sci.* **17,** 495.
Stenmark, K. R. and Mecham, R. P. (1997). Cellular and molecular mechanisms of pulmonary vascular remodelling. *Annu. Rev. Physiol.* **59,** 89-144.
Stevenson, A. S., Gomez, M. F., Hill-Eubanks, D. C. and Nelson, M. T. (2001). NFAT4 Movement in Native Smooth Muscle. A ROLE FOR DIFFERENTIAL Ca2+ SIGNALING. *J. Biol. Chem.* **276,** 15018-15024.
Stocker, M., Hellwig, M. and Kerschensteiner, D. (1999). Subunit Assembly and Domain Analysis of Electrically Silent K+ Channel alpha-Subunits of the Rat Kv9 Subfamily. *J. Neurochem.* **72,** 1725-1734.
Streb, H., Irvine, R. F., Berridge, M. J. and Schulz, I. (1983). Release of Ca2+ from a nonmitochondrial intracellular store in pancreatic acinar cells by inositol-1,4,5-trisphosphate. *Nature* **306,** 67-69.
Strehler, E. E. and Zacharias, D. A. (2001). Role of Alternative Splicing in Generating Isoform Diversity Among Plasma Membrane Calcium Pumps. *Physiol. Rev.* **81,** 21-50.
Sugaya, E. and Onozuka, M. (1978). Intracellular calcium: its release from granules during bursting activity in snail neurons. *Science* **202,** 1195-1197.

Sugiyama, T., Matsuda, Y. and Mikoshiba, K. (2000). Inositol 1,4,5-trisphosphate receptor associated with focal contact ctyoskeletal proteins. *FEBS lett.* **466,** 29-34.

Sumbilla, C., Cavagna, M., Zhong, L., Ma, H., Lewis, D., Farrance, I. and Inesi, G. (1999). Comparison of SERCA1 and SERCA2a expressed in COS-1 cells and cardiac myocytes. *Am. J. Physiol.* **277,** H2381-H2391.

Sun, L., Adebanjo, O. A., Moonga, B. S., Corisdeo, S., Anandatheerthavarada, H. K., Biswas, G., Arakawa, T., Hakeda, Y., Koval, A., Sodam, B., Bevis, P. J. R., Moser, A. J., Lai, F. A., Epstein, S., Troen, B. R., Kumegawa, M. and Zaidi, M. (1999). CD38/ADP-Ribosyl Cyclase: A New Role in the Regulation of Osteoclastic Bone Resorption. *J. Cell Biol.* **146,** 1161-1172.

Sutko, J. L. and Airey, J. A. (1996a). Ryanodine receptor Ca2+ release channels: does diversity in form equal diversity in function? *Physiol. Rev.* **76,** 1027-1071.

Sutko, J. L. and Airey, J. A. (1996b). Ryanodine receptor Ca^{2+} release channels: does diversity in form equal diversity in function? *Physiol. Rev.* **76,** 1027-1060.

Suzuki, M., Li, R. A., Miki, T., Uemura, H., Sakamoto, N., Ohmoto-Sekine, Y., Tamagawa, M., Ogura, T., Seino, S., Marban, E. and Nakaya, H. (2001). Functional Roles of Cardiac and Vascular ATP-Sensitive Potassium Channels Clarified by Kir6.2-Knockout Mice. *Circ. Res.* **88,** 570-577.

Sweeney, H. L., Yang, Z., Zhi, G., Stull, J. T. and Trybus, K. M. (1994). Charge Replacement Near the Phosphorylatable Serine of the Myosin Regulatory Light Chain Mimics Aspects of Phosphorylation. *Proc. Natl. Acad. Sci.* **91,** 1490-1494.

Sweeney, M., Yu, Y., Platoshyn, O., Zhang, O., McDaniel, S. S. and Yuan, J. X.-J. (2002). Inhibition of endogenous TRP1 decreases capacitive Ca2+ entry and attenuates pulmonary hypertension in guinea pigs. *J. Appl. Physiol.* **66,** 920-928.

Szerencsei, R. T., Tucker, J. E., Cooper, C. B., Winkfein, R. J., Farrell, P. J., Iatrou, K. and Schnetkamp, P. P. M. (2000). Minimal Domain Requirement for Cation Transport by the Potassium-dependent Na/Ca-K Exchanger. COMPARISON WITH AN NCKX PARALOG FROM CAENORHABDITIS ELEGANS. *J. Biol. Chem.* **275,** 669-676.

Szidon, J. P., Cherniak, N. S. and Fishman, A. P. (1969). Traube-Hering waves in the pulmonary circulation of the dog. *Science* **164,** 75-76.

Takahashi, J., Kagaya, Y., Kato, I., Ohta, J., Isoyama, S., Miura, M., Sugai, Y., Hirose, M., Wakayama, Y. and Ninomiya, M. (2003). Deficit of CD38/cyclic ADP-ribose is differentially compensated in hearts by gender. *Biochem. Biophys.l Res. Comm.* **312,** 434-440.

Takai, Y., Sasaki, T., Tanaka, K. and Nakanishi, H. (1995). Rho as a regulator of the cytoskeleton. *Trends Biochem. Sci.* **20,** 227-231.

Takasawa, S., Akiyama, T., Nata, K., Kuroki, M., Tohgo, A., Noguchi, N., Kobayashi, S., Kato, I., Katada, T. and Okamoto, H. (1998). Cyclic ADP-ribose and Inositol 1,4,5-Trisphosphate as Alternate Second Messengers for Intracellular Ca2+ Mobilization in Normal and Diabetic beta -Cells. *J. Biol. Chem.* **273,** 2497-2500.

Takeshima, H., Ikemoto, T., Nishi, M., Nishiyama, N., Shimuta, M., Sugitani, Y., Kuno, J., Saito, I., Saito, H., Endo, M., Iino, M. and Noda, T. (1996). Generation and Characterization of Mutant Mice Lacking Ryanodine Receptor Type 3. *J. Biol. Chem.* **271,** 19649-19652.

Takeshima, H., Komazaki, S., Hirose, K., Nishi, M., Noda, T. and Iino, M. (1998). Embryonic lethality and abnormal cardiac myocytes in mice lacking ryanodine receptor type 2. *EMBO J.* **17,** 3309-3316.

Takeshima, H., Yamazawa, T., Ikemoto, T., Takekura, H., Nishi, M., Noda, T. and Iino, M. (1995). Ca(2+)-induced Ca2+ release in myocytes from dyspedic mice lacking the type-1 ryanodine receptor. *EMBO J.* **14,** 2999-3006.

Tanaka, Y. and Tashjian, A. H. (1995). Calmodulin is a Selective Mediator of Ca2+-Induced Ca2+ Release via the Ryanodine Receptor-Like Ca2+ Channel Triggered by Cyclic ADP- Ribose. *Proc. Natl. Acad. Sci.* **92,** 3244-3248.

Tanaka, Y. M., Aida, H., Tanaka, K., Shigenobu, K. and Toro, L. (1998). *Naunym-Scmiedebergs Arch. Pharmakol.* **357,** 705-708.

Tang, W. X., Chen, Y. F., Zou, A. P., Campbell, W. B. and Li, P. L. (2002). Role of FKBP12.6 in cADPR-induced activation of reconstituted ryanodine receptors from arterial smooth muscle. *Am. J. Physiol.* **282,** H1304-H1310.

Tasker, P. N., Michelangeli, F. and Nixon, G. F. (1999). Expression and distribution of the type 1 and type 3 inositol 1,4,5- trisphosphate receptor in developing vascular smooth muscle. *Circ. Res.* **84,** 536-542.

Tasker, P. N., Taylor, C. W. and Nixon, G. F. (2000). Expression and Distribution of InsP3 Receptor Subtypes in Proliferating Vascular Smooth Muscle Cells. *Biochem. Biophys.l Res. Comm.* **273,** 907-912.

Taylor, C. W., Genazzani, A. A. and Morris, S. A. (1999). Expression of inositol trisphosphate receptors. *Cell Calcium* **26,** 237-251.

Taylor, C. W. and Laude, A. J. (2002). IP3 receptors and their regulation by calmodulin and cytosolic Ca2+. *Cell Calcium* **32,** 321-334.

Thastrup, O., Cullen, P. J., Drobak, B. K., Hanley, M. R. and Dawson, A. P. (1990). Thapsigargin, a Tumor Promoter, Discharges Intracellular Ca2+ Stores by Specific Inhibition of the Endoplasmic Reticulum Ca2+-ATPase. *Proc. Natl. Acad. Sci.* **87,** 2466-2470.

Thomas, J. M., Masgrau, R., Churchill, G. C. and Galione, A. (2001). Pharmacological characterization of the putative cADP-ribose receptor. *Biochem. J.* **359,** 451-457.

Tiaho, F., Piot, C., Nargeot, J. and Richard, S. (1994). Regulation of the frequency-dependent facilitation of L-type Ca2+ currents in rat ventricular myocytes. *J. Physiol.* **477,** 237-251.

Timerman, A. P., Ogunbumni, E., Freund, E., Wiederrecht, G., Marks, A. R. and Fleischer, S. (1993). The calcium release channel of sarcoplasmic reticulum is modulated by FK-506-binding protein. Dissociation and reconstitution of FKBP-12 to the calcium release channel of skeletal muscle sarcoplasmic reticulum. *J. Biol. Chem.* **268,** 22992-22999.

Timerman, A. P., Wiederrecht, G., Marcy, A. and Fleischer, S. (1995). Characterization of an Exchange Reaction between Soluble FKBP-12 and the FKBPbulletRyanodine Receptor Complex. *J. Biol. Chem.* **270,** 2451-2459.

Trebak, M., Bird, G. S. J., McKay, R. R. and Putney, J. W. J. (2002). Comparison of human TRPC3 channels in receptor-activated and store-operated modes. Differential sensitivity to channel blockers suggests differences in channel composition. *J. Biol. Chem* **277,** 21617-21623.

Trepakova, E. S., Gericke, M., Hirakawa, Y., Weisbrod, R. M., Cohen, R. A. and Bolotina, V. M. (2001). Properties of a Native Cation Channel Activated by Ca2+ Store Depletion in Vascular Smooth Muscle Cells. *J. Biol. Chem.* **276,** 7782-7790.

Tripathy, A. and Meissner, G. (1996). Sarcoplasmic reticulum lumenal Ca2+ has access to cytosolic activation and inactivation sites of skeletal muscle Ca2+ release channel. *Biophys. J.* **70,** 2600-2615.

Tucker, A. (1979). Pulmonary and systemic vascular responses to hypoxia after chemical sympathectomy. *Cardiovasc. Res.* **13,** 469-476.

Uebele, V. N., Lagrutta, A., Wade, T., Fiqueroa, D. J., Liu, Y., McKenna, E., Austin, C. P., Bennett, P. B. and Swanson, R. (2000). Cloning and functional expression of two families of beta-subunits of the large conductance calcium-activated K+ channel. *J. Biol. Chem.* **275,** 23211-23218.

Valdivia, H. H., Kaplan, J. H., Ellis-Davies, G. C. and Lederer, W. J. (1995). Rapid adaptation of cardiac ryanodine receptors: modulation by Mg2+ and phosphorylation. *Science* **267,** 1997-2000.

Van Aelst, L. and D'Souza-Schorey, C. (1997). Rho GTPases and signaling networks. *Genes Dev.* **11,** 2295-2322.

Van Breemen, C. and Saida, K. (1989). Cellular mechanisms regulating [Ca2+]i smooth muscle. *Annu. Rev. Physiol.* **51,** 315-329.

Vasquez, G., Lievremont, J.-P., Bird, G. S. J. and Putney, J. W. J. (2001). Human Trp3 forms both inositol trisphosphate receptor-dependent and receptor-independent store-operated cation channels in DT40 avian B lymphocytes. *Proc. Natl. Acad. Sci.* **98,** 11777-11782.

Verboomen, H., Wuytack, F., De Smedt, H., Himpens, B. and Casteels, R. (1992). Functional difference between SERCA2a and SERCA2b Ca2+ pumps and their modulation by phospholamban. *Biochem. J.* **286,** 591-595.

Verboomen, H., Wuytack, F., Van den Bosch, L., Mertens, L. and Casteels, R. (1994). The functional importance of the extreme C-terminal tail in the gene 2 organellar Ca(2+)-transport ATPase (SERCA2a/b). *Biochem. J.* **303,** 979-984.

Verderio, C., Bruzzone, S., Zocchi, E., Fedele, E., Schenk, U., De Flora, A. and Matteoli, M. (2001). Evidence of a role for cyclic ADP-ribose in calcium signalling and neurotransmitter release in cultured astrocytes. *J. Neurochem.* **78,** 646-657.

Villa, A., Podini, P., Panzeri, M. C., Soling, H. D., Volpe, P. and Meldolesi, J. (1993). The endoplasmic-sarcoplasmic reticulum of smooth muscle immunocytochemistry of vas deferens fibers reveals specialised sub-compartments differnetly equipped for the control of Ca2+ homeostasis. *J. Cell Biol.* **121,** 1041-1051.

Vogalis, F., Vincent, T., Quershi, I., Schmalz, F., Ward, M. W., Sanders, K. M. and Horowitz, B. (1996). Cloning and expression of the large-conductance Ca(2+)-activated K+ channels from colonic smooth muscle. *Am. J. Physiol.* **271,** G629-639.

von Euler, U. S. and Liljestrand, G. (1946). Observations on the pulmonary arterial blood pressure in the cat. *Acta Physiol. Scand.* **12,** 301-320.

Wahl, M. I., Nishibe, S., Suh, P. G., Rhee, S. G. and Carpenter, G. (1989a). Epidermal Growth Factor Stimulates Tyrosine Phosphorylation of Phospholipase C-II Independently of Receptor Internalization and Extracellular Calcium. *Proc. Natl. Acad. Sci.* **86,** 1568-1572.

Wahl, M. I., Olashaw, N. E., Nishibe, S., Rhee, S. G., Pledger, W. J. and Carpenter, G. (1989b). Platelet-derived growth factor induces rapid and sustained tyrosine phosphorylation of phospholipase C-gamma in quiescent BALB/c 3T3 cells. *Mol. Cell. Biol.* **9,** 2934-3943.

Wallner, M., Meera, P. and Toro, L. (1996). Determinant for beta-subunit regulation in high-conductance voltage-activated and Ca(2+)-sensitive K+ channels: an additional transmembrane region at the N terminus. *Proc. Natl. Acad. Sci.* **93,** 14922-14927.

Walseth, T. F., Aarhus, R., Gurnack, M. E., Wong, L., Breitinger, H. G., Gee, K. R. and Lee, H. C. (1997). Preparation of cyclic ADP-ribose antagonists and caged cyclic ADP-ribose. *Methods Enzymol.* **280**.

Walseth, T. F., Aarhus, R., Zeleznicker, R. J. and Lee, H. C. (1991). Determination of endogenous levels of cyclic ADP-ribose in rat tissue. *Biochim. Biophys. Acta* **1094,** 113-120.

Walseth, T. F. and Lee, H. C. (1993). Synthesis and characterization of antagonists of cyclic-ADP-ribose-induced Ca2+ release. *Biochim. Biophys. Acta* **1178,** 235-242.

Wang, G. L., Wang, X. R., Lin, M. J., Hr, H., Lan, X. J. and Guan, Y. Y. (2002). Deficiency in ClC-3 chloride channels prevents rat aortic smooth muscle cell proliferation. *Circ. Res.* **91**.

Wang, J., Shimoda, L. A., Weigand, L., Wang, W., Sun, D. and Sylvester, J. T. (2005). Acute hypoxia increases intrcellular [Ca^{2+}] in pulmonary arterial smooth muscle by enhancing capacatative Ca^{2+} entry. *Am. J. Physiol.* **288,** L1059-1069.

Wang, Y. X. and Kotlikoff, M. I. (1996a). Activation of KCa channels in airway smooth muscle cells by endogenous protein kinase A. *Am. J. Physiol.* **271,** L100-105.

Wang, Y. X. and Kotlikoff, M. I. (2000). Signalling pathway for histamine activation of non-selective cation channels in equine tracheal myocytes. *J. Physiol.* **523,** 131-138.

Wang, Z., Jin, N., Ganguli, S., Swartz, D. R., Li, L. and Rhoades, R. A. (2001). Rho-Kinase Activation Is Involved in Hypoxia-Induced Pulmonary Vasoconstriction. *Am. J. Respir. Cell Mol. Biol.* **25,** 628-635.

Wang, Z. W. and Kotlikoff, M. I. (1996b). Activation of KCa channels in airway smooth muscle cells by endogenous protein kinase A. *Am. J. Physiol.* **271,** L100-L105.

Ward, J. P. and Robertson, T. P. (1995). The role of the endothelium in hypoxic pulmonary vasoconstriction. *Exp. Physiol.* **80,** 793-801.

Ward, J. P. T., Knock, G. A., Snetkov, V. A. and Aaronson, P. I. (2004). Protein kinases in vascular smooth muscle tone--role in the pulmonary vasculature and hypoxic pulmonary vasoconstriction. *Pharmacol. Therap.* **104,** 207-231.

Warner, T. D., Allcock, G. H. and Vane, J. R. (1994). Reversal of established responses to endothelin-1 in vivo and in vitro by the endothelin receptor antagonists, BQ-123 and PD 145065. *Br. J. Pharmacol.* **112,** 207-213.

Waud, B. E. and Waud, D. R. (1972). The margin of safety of neuromuscular transmission in the muscle of the diaphragm. *Anesthesiology* **37,** 417-422.

Waypa, G. B., Chandel, N. S. and Schumacker, P. T. (2001). Model for Hypoxic Pulmonary Vasoconstriction Involving Mitochondrial Oxygen Sensing. *Circ. Res.* **88,** 1259-1266.

Weibel, E. R. (1963). *Morphometry of the human lung.* Academic Press.

Wellman, G. C., Santana, L. F., Bonev, A. D. and Nelson, M. T. (2001). Role of phospholamban in the modulation of arterial Ca(2+) sparks and Ca(2+)-activated K(+) channels by cAMP. *Am. J. Physiol.* **281,** C1029-C1037.

Wellner, M. C. and Isenberg, G. (1993). Properties of stretch-activated channels in myocytes from the guinea-pig urinary bladder. *J. Physiol.* **466,** 213-227.

White, T. A., Walseth, T. F. and Kannan, M. S. (2002). Nitric oxide inhibits ADP-ribosyl cyclase through a cGMP-independent pathway in airway smooth muscle. *Am. J. Physiol.* **283,** L1065-1071.

Wilson, H. L., Dipp, M., Thomas, J. M., Lad, C., Galione, A. and Evans, A. M. (2001). ADP-ribosyl cyclase and cyclic ADP-ribose hydrolase act as a redox sensor: a primary role for cADPR in hypoxic pulmonary vasoconstriction. *J. Biol. Chem.* **276,** 11180-11188.

Wilson, H. L., Evans, A. M. and Galione, A. (1998). Cyclic AMP and cGMP differentially regulate the production of the calcium-mobilising metabolites, nicotinic acid adenine dinucleotide phosphate and cyclic ADP-ribose. *Br. J. Pharmacol.* **124,** 30P.

Wojcikiewicz, R. J. (1995). Type I, II and III inositol 1,4,5- trisphosphate receptors are unequally susceptible to down- regulation and are expressed in markedly different proportions in different cell types. *J. Biol. Chem.* **270,** 11678-11683.

Wong, L., Aarhus, R., Cheung Lee, H. and Walseth, T. F. (1999). Cyclic 3-deaza-adenosine diphosphoribose: a potent and stable analog of cyclic ADP-ribose. *Biochim. Biophys. Acta* **1472,** 555-564.

Wu, K. D., Lee, W. S., Wey, J., Bungard, D. and Lytton, J. (1995). Localization and quantification of endoplasmic reticulum Ca(2+)-ATPase isoform transcripts. *Am. J. Physiol.* **269,** C775-C784.

Wu, M. W., Buchanan, J., Luik, R. M. and Lewis, R. S. (2006). Ca2+ store depletion causes STIM1 to accumulate in ER regions closely associated with the plasma membrane. *J. Cell Biol.* **174,** 803-813.

Wu, X. and Davis, M. J. (2001). Characterization of stretch-activated cation current in coronary smooth muscle cells. *Am. J. Physiol.* **280,** H1751-1761.

Wu, Y., MacMillan, L. B., McNeill, R. B., Colbran, R. J. and Anderson, M. E. (1999). CaM kinase augments cardiac L-type Ca2+ current: a cellular mechanism for long Q-T arrhythmias. *Am. J. Physiol.* **276,** H2168-H2178.

Wyatt, C. N. and Buckler, K. J. (2004). The effect of mitochondrial inhibitors on membrane currents in isolated neonatal rat carotid body type I cells. *J. Physiol.* **556,** 175-191.

Xia, X. M., Fakler, B., Rivard, A., Waymen, A., Johnsonm-Pais, T., Keen, J. E., Hirschberg, B., Bond, C. T., Lutsenko, S., Maylie, J. and Adelman, J. P. (1998). Mechanism of calcium gating in small-conductance calcium-activated potassium channels. *Nature* **395,** 503-507.

Xin, H. B., Senbonmatsu, T., Cheng, D. S., Wang, Y. X., Copello, J. A., Ji, G. J., Collier, M. L., Deng, K. Y., Jeyakumar, L. H., Magnuson, M. A., Inagami, T., Kotlikoff, M. I. and Fleischer, S. (2002). Oestrogen protects FKBP12.6 null mice from cardiac hypertrophy. *Nature* **416,** 273-274.

Xu, W. X., Kim, S. J., So, I., Kang, T. M., Rhee, J. C. and Kim, K. W. (1997). Volume-sensitive chloride current activated by hyposmotic swelling in antral gastric myocytes of the guinea-pig. *Pflugers Arch.* **435,** 9-19.

Yagodin, S., Pivovarova, N. B., Andrews, S. B. and Sattelle, D. B. (1999). Functional characterization of thapsigargin and agonist-insensitive acidic Ca2+stores in Drosophila melanogaster S2 cell lines. *Cell Calcium* **25,** 429-438.

Yamada, M., Mizuguchi, M., Otsuka, N., Ikeda, K. and Takahashi, H. (1997). Ultrastructural localization of CD38 immunoreactivity in rat brain. *Brain Res.* **756,** 52-60.

Yamasaki, M., Masgrau, R., Morgan, A. J., Churchill, G. C., Patel, S., Ashcroft, S. J. and Galione, A. (2004). Organelle selection determines agonist-specific Ca2+ signals in pancreatic acinar and beta cells. *J. Biol. Chem.* **279,** 7234-7240.

Yamasaki, M., Thomas, J. M., Churchill, G. C., Garnham, C., Lewis, A. M., Cancela, J. M., Patel, S. and Galione, A. (2005). Role of NAADP and cADPR in the Induction and Maintenance of Agonist-Evoked Ca2+ Spiking in Mouse Pancreatic Acinar Cells. *Curr. Biol.* **15,** 874-878.

Yamashita, K., Discher, D. J., Hu, J., Bishopric, N. H. and Webster, K. A. (2001). Molecular Regulation of the Endothelin-1 Gene by Hypoxia. CONTRIBUTIONS OF HYPOXIA-INDUCIBLE FACTOR-1, ACTIVATOR PROTEIN-1, GATA-2, AND p300/CBP. *J. Biol. Chem.* **276,** 12645-12653.

Yamazaki, J., Duan, D., Janiak, R., Kuenzli, K., Horowitz, B. and Hume, J. R. (1998). Functional and molecular expression of volume-regulated chloride channels in canine vascular smooth muscle cells. *J. Physiol.* **507,** 729-736.

Yamazawa, T., Takeshima, H., Sakurai, T., Endo, M. and Iino, M. (1996). Subtype specificity of the ryanodine receptor for Ca2+ signal amplification in excitation-contraction coupling. *EMBO J.* **15,** 6172-6177.

Yanagisawa, M., Kurihara, H., Kimura, S., Tomobe, Y., Kobayashi, M., Mitsui, Y., Yakazi, Y., Goto, K. and Masaki, T. (1988). A novel potent vasoconstrictor peptide produced by vascular endothelial cells. *Nature* **332,** 411-415.

Yang, X.-R., Lin, M.-J., Yip, K.-P., Jeyakumar, L. H., Fleischer, S., Leung, G. P. H. and Sham, J. S. K. (2005). Multiple ryanodine receptor subtypes

and heterogeneous ryanodine receptor-gated Ca2+ stores in pulmonary arterial smooth muscle cells. *Am. J. Physiol.* **289,** L338-L348.

Yonekura, K., Stokes, D. L., Sasabe, H. and Toyoshima, C. (1997). The ATP-binding site of Ca(2+)-ATPase revealed by electron image analysis. *Biophys. J.* **72,** 997-1005.

Yoshida, M., Suzuki, A. and Itoh, T. (1994). Mechanisms of vasoconstriction induced by endothelin-1 in smooth muscle of rabbit mesenteric artery. *J. Physiol.* **477,** 253-265.

Yoshikawa, F., Iwasaki, H., Michikawa, T., Furuichi, T. and Mikoshiba, K. (1999). Cooperative Formation of the Ligand-binding Site of the Inositol 1,4,5-Trisphosphate Receptor by Two Separable Domains. *J. Biol. Chem.* **274,** 328-334.

Youngson, C., Nurse, C., Yeger, H. and Katz, E. (1993). Oxygen sensing in airway chemoreceptors. *Nature* **356,** 153-155.

Yu, J.-Z., Zhang, D. X., Zou, A.-P., Campbell, W. B. and Li, P.-L. (2000). Nitric oxide inhibits Ca2+ mobilization through cADP-ribose signaling in coronary arterial smooth muscle cells. *Am. J. Physiol.* **279,** H873-H881.

Yu, Y., Sweeney, M., Zhang, S., Platoshyn, O., Landsberg, J., Rothman, A. and Yuan, J. X.-J. (2003). PDGF stimulates pulmonary vascular smooth muscle cell proliferation by upregulating TRPC6 expression. *Am. J. Physiol.* **284,** C316-C330.

Yuan, W. and Bers, D. M. (1994). Ca-dependent facilitation of cardiac Ca current is due to Ca-calmodulin-dependent protein kinase. *Am. J. Physiol.* **267,** H982-H993.

Yuan, X. J. (1997). Role of calcium-activated chloride current in regulating pulmonary vasomotor tone. *Am. J. Physiol.* **272,** L959-968.

Yusufi, A. N., Cheng, J., Thompson, M. A., Burnett, J. C. and Grande, J. P. (2002). Differential mechanisms of Ca(2+) release from vascular smooth muscle cell microsomes. *Exp. Biol. Med.* **227,** 36-44.

Yusufi, A. N., Cheng, J., Thompson, M. A., Chini, E. N. and Grande, J. P. (2001). Nicotinic acid-adenine dinucleotide phosphate (NAADP) elicits specific microsomal Ca2+ release from mammalian cells. *Biochem. J.* **353,** 531-536.

Zar, J. H. (1999). *Biostatistical analysis*, 4th edn. Prentice-Hall International (UK) limited.

Zhang, D. X., Harrison, M. D. and Li, P.-L. (2002). Calcium-induced calcium release and Cyclic ADP-Ribose-mediated signalling in the myocytes from small coronary arteries. *Microvas. Res.* **64,** 339-348.

Zhang, F., Zhang, G., Zhang, A. Y., Koeberl, M. J., Wallander, E. and Li, P. L. (2006). Production of NAADP and its role in Ca^{2+} mobilization associated with lysosomes in coronary artery smooth muscle myocytes. *Am. J. Physiol.* **291,** H274-282.

Zhang, H. L. and Bolton, T. B. (1996). Two types of ATP-sensitive potassium channels in rat portal vein smooth muscle cells. *Br. J. Pharmacol.* **118,** 105-114.

Zhang, S., Yuan, J. X., Barrett, K. E. and Dong, H. (2005). Role of Na+/Ca2+ exchange in regulating cytosolic Ca2+ in cultured human pulmonary artery smooth muscle cells. *Am. J. Physiol.* **288,** C245-252.

Zhang, W. M., Yip, K. P., Lin, M. J., Shimoda, L. A., Li, W. H. and Sham, J. S. K. (2003). ET-1 activates Ca2+ sparks in PASMC: local Ca2+ signaling between inositol trisphosphate and ryanodine receptors. *Am. J. Physiol.* **285,** L680-L690.

Zhong, J., Wang, G. X., Hatton, W. J., Yamboliev, I. A., Walsh, M. P. and Hume, J. R. (2002). Regulation of volume-sensitive outwardly rectifying anion channels in pulmonary arterial smooth muscle cells by PKC. *Am. J. Physiol.* **283,** C1627-1636.

Ziegler, M., Jorcke, D. and Schweiger, M. (1997). Identification of bovine liver mitochondrial NAD+ glycohydrolase as ADP-ribosyl cyclase. *Biochem. J.* **326,** 401-405.

Zocchi, E., Daga, A., Usai, C., Franco, L., Guida, L., Bruzzone, S., Costa, A., Marchetti, C. and De Flora, A. (1998). Expression of CD38 Increases Intracellular Calcium Concentration and Reduces Doubling Time in HeLa and 3T3 Cells. *J. Biol. Chem.* **273,** 8017-8024.

Zocchi, E., Franco, L., Guida, L., Piccini, D., Tacchetti, C. and De Flora, A. (1996). NAD+-dependent internalization of the transmembrane glycoprotein CD38 in human Namalwa B cells. *FEBS Lett.* **396,** 327-332.

Zuhlke, R. D., Pitt, G. S., Deisseroth, K., Tsien, R. W. and Reuter, H. (1999). Calmodulin supports both inactivation and facilitation of L-type calcium channels. *Nature* **399,** 159-162.

Zuhlke, R. D., Pitt, G. S., Tsien, R. W. and Reuter, H. (2000). Ca2+-sensitive Inactivation and Facilitation of L-type Ca2+ Channels Both Depend on Specific Amino Acid Residues in a Consensus Calmodulin-binding Motif in thealpha 1C subunit. *J. Biol. Chem.* **275,** 21121-21129.

Zuhlke, R. D. and Reuter, H. (1998). Ca2+-sensitive inactivation of L-type Ca2+ channels depends on multiple cytoplasmic amino acid sequences of the alpha 1C subunit. *Proc. Natl. Acad. Sci.* **95,** 3287-3294.

Appendix 1:

Results Tables Chapter 3:

	Resting F_{340}/F_{380}	Maximum F_{340}/F_{380}	Increase in F_{340}/F_{380}	% increase in F_{340}/F_{380}
	0.76	1.11	0.35	46
	0.73	1.4	0.67	92
	0.81	2.89	2.08	257
	0.78	1.75	0.97	124
	0.4	1.28	0.88	220
	0.56	1.2	0.64	114
	0.38	2.34	1.96	516
	0.36	2.36	2	556
	0.7	1.69	0.99	141
	0.76	1.78	1.02	134
	0.67	2.94	2.27	339
	0.73	1.74	1.01	138
	0.86	1.5	0.64	74
	0.83	1.86	1.03	124
	0.72	1.83	1.11	154
	0.9	2.67	1.77	197
	0.66	2.6	1.94	294
Mean	**0.7**	**1.9**	**1.3**	**207**
S.E.M. ±	**0.1**	**0.1**	**0.2**	**35**

Table 3.1: **Fura-2 fluorescence ratio measurements in all experiments involving intracellular dialysis of NAADP into isolated pulmonary artery smooth muscle cells.** The resting F_{340}/F_{380} ratio was determined before the intracellular dialysis of NAADP from the patch pipette. The maximum F_{340}/F_{380} ratio value is the peak ratio value recorded during the global Ca^{2+} wave generated in response to the intracellular dialysis of NAADP (10 nM). The increase in F_{340}/F_{380} ratio was measured as the overall increase in Fura-2 fluorescence ratio within the cell as a result of NAADP dialysis and was determined by subtracting the resting F_{340}/F_{380} value in column 2 from the maximum F_{340}/F_{380} value in column 3. The % increase in F_{340}/F_{380} ratio was determined by expressing the value of the increase in F_{340}/F_{380} ratio for each experiment as a percentage of the resting F_{340}/F_{380} ratio, when the resting F_{340}/F_{380} ratio value is taken to be 100%.

	Resting F_{340}/F_{380}	Maximum F_{340}/F_{380}	Increase in F_{340}/F_{380}	% increase in F_{340}/F_{380}
	0.54	1.02	0.48	89
	0.54	1.00	0.46	86
	0.62	0.96	0.34	55
	0.9	1.17	0.27	30
	0.66	1.01	0.35	53
	0.61	0.99	0.38	62
	0.68	1.14	0.46	68
	0.58	0.88	0.3	52
	0.61	0.95	0.34	58
	1.28	2.1	0.86	64
	0.72	1.06	0.36	47
	0.75	0.99	0.24	32
	0.64	1.04	0.4	63
	0.60	1.17	0.57	95
	0.42	1.21	0.79	188
	0.87	1.18	0.31	36
	0.49	0.77	0.28	57
	0.38	0.75	0.37	97
	0.37	0.78	0.41	111
	0.35	0.69	0.34	97
Mean	**0.63**	**1.04**	**0.42**	**72**
S.E.M. ±	**0.05**	**0.06**	**0.04**	**8**

Table 3.2: **Fura-2 fluorescence ratio measurements in all experiments involving the extracellular application of Bafilomycin A1 to isolated pulmonary artery smooth muscle cells.** The resting F_{340}/F_{380} ratio was determined before the extracellular application of Bafilomycin A1 (100 – 300 nM) to cells. The maximum F_{340}/F_{380} ratio value is the peak ratio value recorded during the global Ca^{2+} wave generated in response to the extracellular application of Bafilomycin A1. The increase in F_{340}/F_{380} ratio was measured as the overall increase in Fura-2 fluorescence ratio within the cell as a result of Bafilomycin A1 and was determined by subtracting the resting F_{340}/F_{380} value in column 2 from the maximum F_{340}/F_{380} value in column 3. The % increase in F_{340}/F_{380} ratio was determined by expressing the value of the increase in F_{340}/F_{380} ratio for each experiment as a percentage of the resting F_{340}/F_{380} ratio, when the resting F_{340}/F_{380} ratio value is taken to be 100%.

	Resting F_{340}/F_{380}	Maximum F_{340}/F_{380}	Increase in F_{340}/F_{380}	% increase in F_{340}/F_{380}
	0.6	0.86	0.26	43*
	0.66	0.85	0.19	29*
	0.79	0.96	0.17	22*
	0.81	0.98	0.17	21*
	0.86	0.99	0.13	15*
	0.64	0.87	0.23	36*
	0.68	0.89	0.21	31*
	0.7	0.82	0.12	17*
	0.37	0.44	0.07	19
	0.48	0.65	0.17	35
	0.42	0.43	0.01	2
Mean	**0.64**	**0.79**	**0.16**	**25**
S.E.M. ±	**0.05**	**0.06**	**0.02**	**4**

Table 3.3 **Fura-2 fluorescence ratio measurements in all experiments involving the extracellular application of Bafilomycin A1 to isolated pulmonary artery smooth muscle cells following preincubation of cells with thapsigargin.** The resting F_{340}/F_{380} ratio was determined before the extracellular application of Bafilomycin A1 (100 – 300 nM) to cells following preincubation (20 min) with thapsigargin (1 μM). The maximum F_{340}/F_{380} ratio value is the peak ratio value recorded during the global Ca^{2+} wave generated in response to the extracellular application of Bafilomycin A1. The increase in F_{340}/F_{380} ratio was measured as the overall increase in Fura-2 fluorescence ratio within the cell as a result of Bafilomycin A1 and was determined by subtracting the resting F_{340}/F_{380} value in column 2 from the maximum F_{340}/F_{380} value in column 3. The % increase in F_{340}/F_{380} ratio was determined by expressing the value of the increase in F_{340}/F_{380} ratio for each experiment as a percentage of the resting F_{340}/F_{380} ratio, when the resting F_{340}/F_{380} ratio value is taken to be 100%. The Asterisk (*) denotes cells that exhibited spatially restricted increases in Fura-2 fluorescence ratio.

	Bafilomycin A1	Bafilomycin A1 + Thapsigargin		
Mean	0.42	0.16	**P value**	<0.0001
S.E.M. ±	0.04	0.02	**F**	25.21
n	20	11		

Table 3.4: **Summary of the mean increases in Fura-2 fluorescence ratio in isolated pulmonary artery smooth muscle cells in response to Bafilomycin A1 (100 – 300 nM) in the presence and absence of thapsigargin (1 μM):** Means were calculated from changes in Fura-2 fluorescence ratio measured by subtracting the resting Fura-2 fluorescence ratio value from the peak Fura-2 fluorescence ratio value measured in each experiment. The P value determining statistical significance was calculated by means of a one-way ANOVA test.

	Resting F_{340}/F_{380}	Maximum F_{340}/F_{380}	Increase in F_{340}/F_{380}	% increase in F_{340}/F_{380}
	0.6	0.78	0.18	30*
	0.7	0.91	0.21	30*
	0.71	0.89	0.18	25
	0.77	1.01	0.24	31*
	0.77	1.12	0.35	46*
	0.38	0.46	0.08	21
	0.44	0.56	0.12	27*
	0.48	0.56	0.08	17
Mean	**0.61**	**0.79**	**0.18**	**28**
S.E.M. ±	**0.05**	**0.08**	**0.03**	**3**

Table 3.5: **Fura-2 fluorescence ratio measurements in all experiments involving the extracellular application of Bafilomycin A1 to isolated pulmonary artery smooth muscle cells following preincubation of cells with ryanodine.** The resting F_{340}/F_{380} ratio was determined before the extracellular application of Bafilomycin A1 (100 – 300 nM) to cells following the preincubation (20 min) with ryanodine (20 μM). The maximum F_{340}/F_{380} ratio value is the peak ratio value recorded during the global Ca^{2+} wave generated in response to the extracellular application of Bafilomycin A1. The increase in F_{340}/F_{380} ratio was measured as the overall increase in Fura-2 fluorescence ratio within the cell as a result of Bafilomycin A1 and was determined by subtracting the resting F_{340}/F_{380} value in column 2 from the maximum F_{340}/F_{380} value in column 3. The % increase in F_{340}/F_{380} ratio was determined by expressing the value of the increase in F_{340}/F_{380} ratio for each experiment as a percentage of the resting F_{340}/F_{380} ratio, when the resting F_{340}/F_{380} ratio value is taken to be 100%. The Asterisk (*) denotes cells that exhibited spatially restricted increases in Fura-2 fluorescence ratio.

	Bafilomycin A1	Bafilomycin A1 + ryanodine		
Mean	0.42	0.18	**P value**	<0.0001
S.E.M.	0.04	0.03	**F**	14.99
n	20	8		

Table 3.6: **Summary of the mean increases in Fura-2 fluorescence ratio in isolated pulmonary artery smooth muscle cells in response to Bafilomycin A1 in the presence and absence of ryanodine:** Means were calculated from changes in Fura-2 fluorescence ratio measured by subtracting the resting Fura-2 fluorescence ratio value from the peak Fura-2 fluorescence ratio value measured in each experiment. The P value determining statistical significance was calculated by means of a one-way ANOVA test.

	Resting F_{340}/F_{380}	Maximum F_{340}/F_{380}	Increase in F_{340}/F_{380}	% increase in F_{340}/F_{380}
	0.79	0.9	0.21	14
	0.76	1	0.24	32
	0.66	0.86	0.2	30
	0.85	1.14	0.29	34
	0.63	0.67	0.04	6
	0.74	0.81	0.07	9
	0.59	0.73	0.14	23
Mean	**0.72**	**0.87**	**0.17**	**21**
S.E.M. ±	**0.04**	**0.06**	**0.03**	**4**

Table 3.7: **Fura-2 fluorescence ratio measurements in all experiments involving the intracellular dialysis of NAADP to isolated pulmonary artery smooth muscle cells following preincubation of cells with Bafilomycin A1.** The resting F_{340}/F_{380} ratio was determined before the intracellular dialysis of NAADP (10 nM) to cells following preincubation of cells with Bafilomycin A1 (100 nM). The maximum F_{340}/F_{380} ratio value is the peak ratio value recorded during the global Ca^{2+} wave generated in response to the intracellular dialysis of NAADP. The increase in F_{340}/F_{380} ratio was measured as the overall increase in Fura-2 fluorescence ratio within the cell as a result of NAADP and was determined by subtracting the resting F_{340}/F_{380} value in column 2 from the maximum F_{340}/F_{380} value in column 3. The % increase in F_{340}/F_{380} ratio was determined by expressing the value of the increase in F_{340}/F_{380} ratio for each experiment as a percentage of the resting F_{340}/F_{380} ratio, when the resting F_{340}/F_{380} ratio value is taken to be 100%.

	NAADP	NAADP + Bafilomycin A1		
Mean	1.3	0.17	**P value**	<0.0001
S.E.M.	0.02	0.03	**F**	21.59
n	17	7		

Table 3.8: **Summary of the mean increases in Fura-2 fluorescence ratio in isolated pulmonary artery smooth muscle cells in response to NAADP (10 nM) in the presence and absence of Bafilomycin A1 (100 nM):** Means were calculated from changes in Fura-2 fluorescence ratio measured by subtracting the resting Fura-2 fluorescence ratio value from the peak Fura-2 fluorescence ratio value measured in each experiment. The P value determining statistical significance was calculated by means of a one-way ANOVA test.

	Resting F_{340}/F_{380}	Maximum F_{340}/F_{380}	Increase in F_{340}/F_{380}	% increase in F_{340}/F_{380}
	0.75	2.77	2.02	269
	0.78	2.09	1.31	168
	0.51	1.9	1.39	273
	0.68	2.11	1.43	210
Mean	**0.68**	**2.22**	**1.54**	**230**
S.E.M. ±	**0.06**	**0.2**	**0.16**	**25**

Table 3.9: **Fura-2 fluorescence ratio measurements in all experiments involving the extracellular application of caffeine to isolated pulmonary artery smooth muscle cells.** The resting F_{340}/F_{380} ratio was determined before the extracellular application of caffeine (2.5 mM) to cells. The maximum F_{340}/F_{380} ratio value is the peak ratio value recorded during the global Ca^{2+} wave generated in response to the extracellular application of caffeine. The increase in F_{340}/F_{380} ratio was measured as the overall increase in Fura-2 fluorescence ratio within the cell as a result of caffeine and was determined by subtracting the resting F_{340}/F_{380} value in column 2 from the maximum F_{340}/F_{380} value in column 3. The % increase in F_{340}/F_{380} ratio was determined by expressing the value of the increase in F_{340}/F_{380} ratio for each experiment as a percentage of the resting F_{340}/F_{380} ratio, when the resting F_{340}/F_{380} ratio value is taken to be 100%.

	Resting F_{340}/F_{380}	Maximum F_{340}/F_{380}	Increase in F_{340}/F_{380}	% increase in F_{340}/F_{380}
	0.72	2.15	1.4	199
	0.75	2.37	1.62	216
	0.68	2.09	1.41	207
	0.68	2.12	1.44	212
Mean	**0.71**	**2.18**	**1.47**	**209**
S.E.M. ±	**0.02**	**0.06**	**0.05**	**4**

Table 3.10: **Fura-2 fluorescence ratio measurements in all experiments involving the extracellular application of caffeine to isolated pulmonary artery smooth muscle cells following preincubation of cells with Bafilomycin A1.** The resting F_{340}/F_{380} ratio was determined before the extracellular application of caffeine (2.5 mM) to cells following the preincubation with Bafilomycin A1 (100 nM). The maximum F_{340}/F_{380} ratio value is the peak ratio value recorded during the global Ca^{2+} wave generated in response to the extracellular application of caffeine. The increase in F_{340}/F_{380} ratio was measured as the overall increase in Fura-2 fluorescence ratio within the cell as a result of caffeine and was determined by subtracting the resting F_{340}/F_{380} value in column 2 from the maximum F_{340}/F_{380} value in column 3. The % increase in F_{340}/F_{380} ratio was determined by expressing the value of the increase in F_{340}/F_{380} ratio for each experiment as a percentage of the resting F_{340}/F_{380} ratio, when the resting F_{340}/F_{380} ratio value is taken to be 100%.

	Caffeine	Caffeine + Bafilomycin A1		
Mean	1.54	1.47	**P value**	0.7
S.E.M. ±	0.16	0.05	**F**	17
n	4	4		

Table 3.11: **Summary of the mean increases in Fura-2 fluorescence ratio in isolated pulmonary artery smooth muscle cells in response to caffeine (2.5 mM) in the presence and absence of Bafilomycin A1 (100 nM):** Means were calculated from changes in Fura-2 fluorescence ratio measured by subtracting the resting Fura-2 fluorescence ratio value from the peak Fura-2 fluorescence ratio value measured in each experiment. The P value determining statistical significance was calculated by means of a one-way ANOVA test.

	Resting F_{340}/F_{380}	**Maximum F_{340}/F_{380}**	**Increase in F_{340}/F_{380}**	**% increase in F_{340}/F_{380}**
	0.57	2.5	1.93	339
	0.72	2.44	1.72	239
	0.64	1.34	0.7	109
	0.52	1.03	0.51	98
Mean	**0.61**	**1.83**	**1.22**	**196**
S.E.M. ±	**0.04**	**0.38**	**0.36**	**57**

Table 3.12: **Fura-2 fluorescence ratio measurements in all experiments involving the intracellular dialysis of IP_3 into isolated pulmonary artery smooth muscle cells.** The resting F_{340}/F_{380} ratio was determined before the intracellular dialysis of IP_3 (1 μM) into cells. The maximum F_{340}/F_{380} ratio value is the peak ratio value recorded during the global Ca^{2+} wave generated in response to the intracellular dialysis of IP_3. The increase in F_{340}/F_{380} ratio was measured as the overall increase in Fura-2 fluorescence ratio within the cell as a result of IP_3 and was determined by subtracting the resting F_{340}/F_{380} value in column 2 from the maximum F_{340}/F_{380} value in column 3. The % increase in F_{340}/F_{380} ratio was determined by expressing the value of the increase in F_{340}/F_{380} ratio for each experiment as a percentage of the resting F_{340}/F_{380} ratio, when the resting F_{340}/F_{380} ratio value is taken to be 100%.

	Resting F_{340}/F_{380}	Maximum F_{340}/F_{380}	Increase in F_{340}/F_{380}	% increase in F_{340}/F_{380}
	0.75	2.77	2.72	269
	0.78	2.09	1.31	170
	0.51	1.9	1.39	273
	0.68	2.11	1.43	211
Mean	**0.68**	**2.22**	**1.71**	**231**
S.E.M. ±	**0.06**	**0.19**	**0.34**	**25**

Table 3.13: **Fura-2 fluorescence ratio measurements in all experiments involving the intracellular dialysis of IP_3 to isolated pulmonary artery smooth muscle cells following preincubation of cells with Bafilomycin A1.** The resting F_{340}/F_{380} ratio was determined before the intracellular dialysis of IP_3 to cells following the preincubation with Bafilomycin A1. The maximum F_{340}/F_{380} ratio value is the peak ratio value recorded during the global Ca^{2+} wave generated in response to the intracellular dialysis of IP_3. The increase in F_{340}/F_{380} ratio was measured as the overall increase in Fura-2 fluorescence ratio within the cell as a result of IP_3 and was determined by subtracting the resting F_{340}/F_{380} value in column 2 from the maximum F_{340}/F_{380} value in column 3. The % increase in F_{340}/F_{380} ratio was determined by expressing the value of the increase in F_{340}/F_{380} ratio for each experiment as a percentage of the resting F_{340}/F_{380} ratio, when the resting F_{340}/F_{380} ratio value is taken to be 100%.

	IP_3	IP_3 + Bafilomycin A1		
Mean	1.22	1.71	**P value**	0.4
S.E.M. ±	0.36	0.34	**F**	1.03
N	4	4		

Table 3.14: **Summary of the mean increases in Fura-2 fluorescence ratio in isolated pulmonary artery smooth muscle cells in response to IP_3 (1 μM) in the presence and absence of Bafilomycin A1 (100 nM):** Means were calculated from changes in Fura-2 fluorescence ratio measured by subtracting the resting Fura-2 fluorescence ratio value from the peak Fura-2 fluorescence ratio value measured in each experiment. The P value determining statistical significance was calculated by means of a one-way ANOVA test.

	Volume (μm^3)
	7.84
	31.59
	42.83
Mean	**27.42**
S.E.M. ±	**10**

Table 3.15: **Volume of distinct clusters of lysosomes in isolated pulmonary artery smooth muscle cells:** Measurements of volume (μm^3) of the large, distinct lysosomal clusters observed in pulmonary artery smooth muscle cells. To obtain these measures cells were rotated through 0^0, 90^o, 180^o and 270^o of rotation around either the X- or Y- axis.

Appendix 2:

Results Tables Chapter 4:

Area of close association	Degree of rotation	distance (μm)
1	229	0.25
2	176	0.25
3	237	0.16
4	279	0.32
5	265	0.25
6	90	0.34
7	90	0.11
8	284	0.11
9	246	0.34
10	59	0.34
11	222	0.25
12	90	0.36
MEAN		**0.26**
S.E.M. +/-		**0.03**

Table 4.1 **Measurements of distance between distinct lysosomal clusters and RyRs in isolated pulmonary artery smooth muscle cells.** All distance measurements obtained on Deltavision imaging system using SoftWorx software (Applied Precision, USA).

	Volume of cells (μm^3)	Volume of nucleus (μm^3)	Volume of perinuclear ROI (μm^3)	Volume of extra-perinuclear region (μm^3)	Volume of sub-plasmalemmal region (μm^3)
	2089.31	140.27	570.75	616.57	901.99
	927.2	78.15	253.72	225.44	368.13
	1507.29	74.01	453.68	316.91	662.69
	4206.95	95.3	1237.26	751.28	2218.41
	729.16	47.72	235.66	171.92	329.92
	1879.62	133.73	616.13	494.84	768.65
	1701.72	142.01	460.13	715.44	513.17
	2208.73	125.81	554.25	1017.2	637.28
	1472.71	85.3	438.72	455.17	633.47
	1366.61	101.57	283.73	401.6	641.56
	741.59	71.74	178.63	210.36	285.09
	1429.76	173.61	282.09	458.06	514.44
	2551.58	130.03	1131.17	425.68	958.68
	1959.04	145.07	840.18	318.82	652.62
	2076.69	150.5	758.86	411.12	801.96
	1688.99	80.37	719.56	354.95	569.38
	2300.8	130.21	584.03	555.19	1071.32
	1090.41	61.5	309.18	275.59	444.15
	846.87	58.7	266.9	178.52	376.58
	2073.08	92.31	649.4	83.35	540.33
	2215.08	59.63	950.76	590.71	626.81
	1934.38	74.33	948.97	300.32	642.8
	1557.8	108.35	750.38	313.7	443.05
	1542.94	175.38	498.46	387.95	554.32
MEAN	**1754.1**	**105.65**	**380.41**	**417.95**	**673.2**
S.E.M. +/-	**258.4**	**13.36**	**103.9**	**75.04**	**135.16**

Table 4.2 **Measurements of Volume occupied by the perinuclear, extra-perinuclear and sub-plasmalemmal regions in relation to the total volume occupied by isolated pulmonary artery smooth muscle cells** (n = 40)

	Volume Lysosomal label in cells (μm^3)	Mean volume of labelling within cells (μm^3)	Volume of cells (μm^3)	Volume occupied, per μm^3 of cell, by lysosomal labelling
	26.14	0.42	2089.31	0.013
	10.6	0.46	927.2	0.011
	8.68	0.33	1507.29	0.006
	34.78	0.32	4206.95	0.008
	23.59	0.62	729.16	0.032
	34.68	0.41	1879.62	0.019
	28.53	0.66	1701.72	0.017
	31.5	0.42	2208.73	0.014
	42.52	0.58	1472.71	0.029
	33.9	0.62	1366.61	0.025
	24.87	0.83	741.59	0.034
	29.73	0.52	1429.76	0.021
	33.15	0.64	2551.58	0.013
	24.46	1.34	1959.04	0.013
	29.13	0.74	2076.69	0.014
	21.28	0.4	1688.99	0.013
	31.58	0.53	2300.8	0.014
	29.77	0.88	1090.41	0.027
	22.68	0.55	846.87	0.027
	22.43	0.7	2073.08	0.011
	38.1	1.53	2215.08	0.017
	35.64	0.7	1934.38	0.018
	51.51	1.61	1557.8	0.033
	46.93	1.36	1542.94	0.03
MEAN	**29.84**	**0.72**	**1754.1**	**0.019**
S.E.M. +/-	**3.47**	**0.13**	**258.4**	**0.003**

Table 4.3 **Measurements of αlgp120 labelling obtained from pulmonary artery smooth muscle cells** (n = 24)

	Nuclear volume in cells (μm^3)	Volume of perinuclear lysosomal labelling (μm^3)	Mean volume of perinuclear lysosomal labelling (μm^3)	Volume of perinuclear region of cell (μm^3)	Volume of lysosomal labelling per μm^3 of perinuclear regiopn
	140.27	8.73	0.42	570.75	0.015
	78.15	3.76	0.58	253.72	0.015
	74.01	3.08	0.55	453.68	0.007
	95.3	15.15	0.33	1237.26	0.012
	47.72	11.12	0.93	192.94	0.058
	133.73	10.04	0.42	616.13	0.016
	142.01	9.55	0.4	460.13	0.021
	125.81	13.86	0.43	554.25	0.025
	85.3	20.79	0.54	438.72	0.047
	101.57	16.05	0.68	283.73	0.057
	71.74	6.59	0.51	178.63	0.037
	173.61	16.57	0.67	282.09	0.059
	130.03	17.12	0.63	1131.17	0.015
	145.07	22.6	1.5	840.18	0.027
	150.5	19.36	0.82	758.86	0.026
	80.37	12.64	0.47	719.56	0.018
	130.21	20.15	0.64	584.03	0.035
	61.5	16.18	0.87	309.18	0.05
	58.7	14.31	0.59	266.9	0.054
	92.31	16.54	0.85	649.4	0.026
	59.63	24.61	1.51	950.76	0.026
	74.33	25.72	0.83	948.97	0.027
	108.35	47.77	1.9	750.38	0.064
	175.38	17.71	1.13	498.46	0.036
MEAN	**105.65**	**16.25**	**0.76**	**580.41**	**0.032**
S.E.M. +/-	**13.36**	**3.18**	**0.14**	**103.91**	**0.006**

Table 4.4 **Measurements of αlgp120 labelling within the perinuclear region of isolated pulmonary artery smooth muscle cells** (n = 24)

	Volume extra-perinuclear lysosomal labelling (μm^3)	Mean volume of extra-perinuclear lysosomal labelling (μm^3)	Volume of extra-perinuclear region (μm^3)	Volume of lysosomal labelling per μm^3 of the extra-perinuclear region
	7.98	0.43	616.57	0.013
	0.85	0.22	225.44	0.004
	2.6	0.21	316.91	0.008
	9.97	0.3	751.28	0.013
	8.36	1.19	171.91	0.049
	9.83	0.41	494.84	0.02
	2.35	0.9	715.44	0.003
	6.75	0.29	1017.2	0.007
	15.34	0.72	455.17	0.034
	12.56	0.59	401.6	0.031
	14.21	1.8	210.36	0.068
	7.36	0.33	458.06	0.016
	5.28	0.55	425.68	0.012
	1.09	0.52	318.82	0.003
	6.16	0.44	411.12	0.015
	3.91	0.33	354.95	0.011
	4.27	0.27	555.19	0.008
	10.8	0.78	275.59	0.039
	2.87	0.47	178.52	0.016
	1.73	0.57	83.35	0.002
	10	1.13	590.71	0.017
	5.9	0.4	300.32	0.019
	2.55	0.58	313.7	0.008
	8.57	0.73	387.95	0.022
MEAN	**6.72**	**0.59**	**417.95**	**0.018**
S.E.M.+/-	**1.47**	**0.13**	**75.04**	**0.006**

Table 4.5 **Measurements of lysosomal labelling within the extra-perinuclear region of isolated pulmonary artery smooth muscle cells** (n = 24)

	Volume sub-plasmalemmal lysosomal labelling (μm^3)	Mean volume of lysosomal labelling (μm^3)	Volume of sub-plasmalemmal region (μm^3)	Volume of lysosomal labelling per μm^3 of sub-plasmalemmal region
	9.43	0.31	902.99	0.011
	2.15	0.21	368.13	0.006
	3	0.22	662.69	0.005
	7.52	0.27	2218.41	0.003
	4.11	0.22	329.92	0.013
	13.19	0.27	768.65	0.017
	15.46	0.24	513.17	0.03
	9.09	0.32	637.28	0.014
	3.72	0.19	633.47	0.006
	4.33	0.24	641.56	0.007
	3.94	0.26	285.09	0.014
	4.75	0.25	514.44	0.009
	8.47	0.52	958.68	0.009
	0.77	0.25	652.62	0.001
	3.3	0.37	801.96	0.004
	3.26	0.24	569.38	0.006
	6.1	0.21	1071.32	0.006
	2.79	0.28	444.15	0.006
	5.46	0.27	376.58	0.015
	3.61	0.56	540.33	0.007
	2.86	0.43	626.81	0.005
	3.44	0.28	642.8	0.005
	1.19	0.3	443.05	0.003
	20.46	0.9	554.32	0.037
MEAN	**5.93**	**0.32**	**673.2**	**0.0099**
S.E.M.+/-	**1.68**	**0.05**	**135.16**	**0.003**

Table 4.6 **Measurements of lysosomal labelling within the sub-plasmalemmal region of isolated pulmonary artery smooth muscle cells** (n = 24)

	P value	F value
Perinuclear vs. Extra-perinuclear	0.005	8.51
Perinuclear vs. Sub-plasmalemmal	<0.0001	32.44
Extra-perinuclear vs. Sub-plasmalemmal	0.027	5.21

Table 4.7 **Record of P and F values obtained from statistical analysis between the density of lysosomal labelling in a given region of the cell, by means of a 1-way ANOVA test. P value considered significant if $P \leq 0.05$** (n = 24)

	P value	F value
Perinuclear vs. Extra-perinuclear	0.13	2.33
Perinuclear vs. Sub-plasmalemmal	<0.0001	25.85
Extra-perinuclear vs. Sub-plasmalemmal	0.002	11.21

Table 4.8 **Record of P and F values obtained from statistical analysis between the mean volume of lysosomal labelling in a given region of the cell, by means of a 1-way ANOVA test. P value considered significant if $P \leq 0.05$** (n = 24)

	Volume RyR1 label in cells (μm^3)	Volume of cells (μm^3)	Volume occupied, per μm^3 of cell, by RyR1labelling
	47.78	2089.31	0.0229
	19.2	847.29	0.0227
	28.39	1430.7	0.0198
	77.61	4206.95	0.0184
	34.41	729.16	0.0472
	64.48	1879.62	0.0343
	64.22	1701.72	0.0377
	70.07	2208.73	0.0317
MEAN	**50.77**	**1886.69**	**0.029**
S.E.M. +/-	**7.60**	**382.45**	**0.004**

Table 4.9 **Measurements of RyR1 labelling obtained from pulmonary artery smooth muscle cells** (n = 8)

	Nuclear volume in cells (μm^3)	Volume of perinuclear RyR1 labelling (μm^3)	Mean volume of perinuclear RyR1 labelling (μm^3)	Volume of perinuclear region of cell (μm^3)	Volume of RyR1 labelling per μm^3 of perinuclear regiopn
	140.27	13.54	1.03	1518.56	0.024
	78.15	6	0.67	593.57	0.024
	74.01	3.93	0.56	981.06	0.009
	95.3	23.06	0.56	2969.69	0.019
	47.72	13.52	0.65	501.84	0.07
	133.73	26.6	1.34	1263.49	0.043
	142.01	7.55	0.93	1228.61	0.016
	125.81	31.97	3.61	1654.48	0.058
MEAN	**104.63**	**15.77**	**1.17**	**1338.91**	**0.033**
S.E.M. +/-	**12.63**	**3.65**	**0.36**	**273.65**	**0.008**

Table 4.10 **Measurements of RyR1 labelling within the perinuclear region of isolated pulmonary artery smooth muscle cells** (n = 8)

	Volume extra-perinuclear RyR1 labelling (μm^3)	Mean volume of extra-perinuclear RyR1 labelling (μm^3)	Volume of extra-perinuclear region (μm^3)	Volume of RyR1 labelling per μm^3 of the extra-perinuclear region
	6.52	0.31	616.57	0.011
	4.45	0.74	225.44	0.02
	3.87	0.35	312.49	0.012
	22.52	0.51	751.28	0.03
	2.87	0.26	171.92	0.017
	14.03	1.11	494.84	0.028
	8.13	0.45	715.44	0.011
	12.64	2.72	1017.2	0.012
MEAN	**9.38**	**0.81**	**538.15**	**0.018**
S.E.M.+/-	**2.36**	**0.29**	**103.27**	**0.003**

Table 4.11 **Measurements of RyR1 labelling within the extra-perinuclear region of isolated pulmonary artery smooth muscle cells** (n = 8)

	Volume sub-plasmalemmal RyR1 labelling (μm^3)	Mean volume of RyR1 labelling (μm^3)	Volume of sub-plasmalemmal region (μm^3)	Volume of RyR1 labelling per μm^3 of sub-plasmalemmal region
	20.7	0.63	901.99	0.023
	6.87	0.32	368.13	0.019
	18.52	0.37	668.57	0.028
	28.62	0.4	2218.41	0.013
	14.19	0.43	329.92	0.043
	16.33	0.48	768.65	0.021
	36.73	1.27	513.17	0.072
	16.57	0.33	637.28	0.026
MEAN	**19.82**	**0.53**	**800.77**	**0.031**
S.E.M.+/-	**3.24**	**0.11**	**213.67**	**0.007**

Table 4.12 **Measurements of RyR1 labelling within the sub-plasmalemmal region of isolated pulmonary artery smooth muscle cells** (n = 8)

	P value	F value
Perinuclear vs. Extra-perinuclear	0.09	3.38
Perinuclear vs. Sub-plasmalemmal	0.83	0.05
Extra-perinuclear vs. Sub-plasmalemmal	0.1	3.18

Table 4.13 **Record of P and F values obtained from statistical analysis between the density of RyR1 labelling in a given region of the cell, by means of a 1-way ANOVA test. P value considered significant if $P \leq 0.05$** (n = 8)

	P value	F value
Perinuclear vs. Extra-perinuclear	0.45	0.61
Perinuclear vs. Sub-plasmalemmal	0.11	2.86
Extra-perinuclear vs. Sub-plasmalemmal	0.39	0.8

Table 4.14 **Record of P and F values obtained from statistical analysis between the mean volume of RyR1 labelling in a given region of the cell, by means of a 1-way ANOVA test. P value considered significant if $P \leq 0.05$** (n = 8)

	Volume RyR2 label in cells (μm^3)	Volume of cells (μm^3)	Volume occupied, per μm^3 of cell, by RyR2labelling
	64.61	1472.71	0.044
	53.54	1366.61	0.039
	45.39	741.59	0.061
	58.83	1429.76	0.041
	44.3	2551.58	0.017
	36.47	1959.04	0.019
	36.07	2076.69	0.017
	52.13	1688.99	0.031
MEAN	**48.92**	**1660.87**	**0.034**
S.E.M. +/-	**3.61**	**192.56**	**0.006**

Table 4.15 **Measurements of RyR2 labelling obtained from pulmonary artery smooth muscle cells** (n = 8)

	Nuclear volume in cells (μm^3)	Volume of perinuclear RyR2 labelling (μm^3)	Mean volume of perinuclear RyR2 labelling (μm^3)	Volume of perinuclear region of cell (μm^3)	Volume of RyR2 labelling per μm^3 of perinuclear regiopn
	85.3	15.01	1.23	438.72	0.034
	101.57	10.45	0.49	283.75	0.037
	71.74	21.61	2.3	178.63	0.12
	173.61	12.16	0.64	282.09	0.043
	130.03	5.33	0.4	1131.17	0.005
	145.07	13.14	0.63	840.18	0.016
	150.5	10.98	0.49	758.86	0.015
	80.37	24.05	1.33	719.56	0.033
MEAN	**117.27**	**14.09**	**0.94**	**579.12**	**0.038**
S.E.M. +/-	**13.31**	**2.16**	**0.23**	**118.06**	**0.013**

Table 4.16 **Measurements of RyR2 labelling within the perinuclear region of isolated pulmonary artery smooth muscle cells** (n = 8)

	Volume extra-perinuclear RyR2 labelling (μm^3)	Mean volume of extra-perinuclear RyR2 labelling (μm^3)	Volume of extra-perinuclear region (μm^3)	Volume of RyR2 labelling per μm^3 of the extra-perinuclear region
	47.12	2.55	455.17	0.104
	32.48	1.91	401.6	0.081
	22.36	4.24	210.36	0.106
	35.27	1.21	458.06	0.077
	30.76	2.3	425.68	0.072
	5.42	0.45	318.82	0.017
	17.27	0.62	411.12	0.042
	9.25	0.36	354.95	0.026
MEAN	**24.99**	**1.71**	**379.47**	**0.066**
S.E.M.+/-	**4.97**	**0.47**	**29.4**	**0.012**

Table 4.17 **Measurements of RyR2 labelling within the extra-perinuclear region of isolated pulmonary artery smooth muscle cells** (n = 8)

	Volume sub-plasmalemmal RyR2 labelling (μm^3)	Mean volume of RyR2 labelling (μm^3)	Volume of sub-plasmalemmal region (μm^3)	Volume of RyR2 labelling per μm^3 of sub-plasmalemmal region
	2.23	0.36	633.47	0.004
	10.23	0.38	641.56	0.016
	0.79	0.27	285.09	0.003
	10.93	0.27	514.44	0.021
	7.94	0.47	958.68	0.008
	9.77	0.41	652.62	0.015
	4	0.48	801.96	0.005
	12.97	0.56	569.38	0.023
MEAN	**7.36**	**0.4**	**632.15**	**0.012**
S.E.M.+/-	**1.58**	**0.036**	**69.98**	**0.003**

Table 4.18 **Measurements of RyR2 labelling within the sub-plasmalemmal region of isolated pulmonary artery smooth muscle cells** (n = 8)

	P value	F value
Perinuclear vs. Extra-perinuclear	0.14	2.52
Perinuclear vs. Sub-plasmalemmal	0.05	3.99
Extra-perinuclear vs. Sub-plasmalemmal	0.001	19.26

Table 4.19 **Record of P and F values obtained from statistical analysis between the density of RyR2 labelling in a given region of the cell, by means of a 1-way ANOVA test. P value considered significant if $P \leq 0.05$** (n = 8)

	P value	F value
Perinuclear vs. Extra-perinuclear	0.17	2.15
Perinuclear vs. Sub-plasmalemmal	0.04	5.34
Extra-perinuclear vs. Sub-plasmalemmal	0.02	7.68

Table 4.20 **Record of P and F values obtained from statistical analysis between the mean volume of RyR2 labelling in a given region of the cell, by means of a 1-way ANOVA test. P value considered significant if $P \leq 0.05$** (n = 8)

	Volume RyR3 label in cells (μm^3)	Volume of cells (μm^3)	Volume occupied, per μm^3 of cell, by RyR3labelling
	66.94	2300.8	0.029
	37.66	1090.41	0.035
	29.8	846.87	0.035
	33.43	2073.08	0.016
	72.06	2215.08	0.033
	37.3	1934.38	0.019
	39.2	1557.8	0.025
	60.67	1542.94	0.039
MEAN	**47.13**	**1695.17**	**0.029**
S.E.M. +/-	**5.88**	**187.3**	**0.003**

Table 4.21 **Measurements of RyR3 labelling obtained from pulmonary artery smooth muscle cells** (n = 8)

	Nuclear volume in cells (μm^3)	Volume of perinuclear RyR3 labelling (μm^3)	Mean volume of perinuclear RyR3 labelling (μm^3)	Volume of perinuclear region of cell (μm^3)	Volume of RyR3 labelling per μm^3 of perinuclear regiopn
	130.21	61.8	4.74	584.03	0.11
	61.5	23.1	1.54	309.18	0.075
	58.7	22.51	2.23	266.9	0.084
	92.31	24.67	1.37	649.4	0.037
	59.63	48.57	1.37	950.76	0.051
	74.33	38.36	3	948.97	0.035
	108.35	30.63	1.03	750.38	0.041
	175.38	48.37	3.35	498.46	0.097
MEAN	**95.05**	**37.25**	**2.33**	**619.76**	**0.066**
S.E.M. +/-	**14.64**	**5.13**	**0.45**	**91.89**	**0.01**

Table 4.22 **Measurements of RyR3 labelling within the perinuclear region of isolated pulmonary artery smooth muscle cells** (n = 8)

	Volume extra-perinuclear RyR3 labelling (μm^3)	Mean volume of extra-perinuclear RyR3 labelling (μm^3)	Volume of extra-perinuclear region (μm^3)	Volume of RyR3 labelling per μm^3 of the extra-perinuclear region
	1.87	0.38	555.19	0.004
	10.56	1.29	275.59	0.038
	6.27	0.35	178.52	0.035
	1.01	0.51	883.35	0.001
	18.09	1.99	590.71	0.031
	1.79	0.45	300.32	0.006
	4.31	0.75	313.7	0.014
	2.09	0.58	387.95	0.005
MEAN	**5.75**	**0.79**	**435.67**	**0.017**
S.E.M.+/-	**2.09**	**0.2**	**80.84**	**0.005**

Table 4.23 **Measurements of RyR3 labelling within the extra-perinuclear region of isolated pulmonary artery smooth muscle cells** (n = 8)

	Volume sub-plasmalemmal RyR3 labelling (μm^3)	Mean volume of RyR3 labelling (μm^3)	Volume of sub-plasmalemmal region (μm^3)	Volume of RyR3 labelling per μm^3 of sub-plasmalemmal region
	2.62	0.19	1071.32	0.0030
	3.6	0.54	444.15	0.0080
	1.02	0.34	376.58	0.0027
	5.53	0.38	540.33	0.01
	1.35	0.39	626.81	0.0020
	0.78	0.32	642.8	0.0012
	2.92	0.22	443.05	0.0065
	7.27	1.21	554.32	0.0130
MEAN	**3.14**	**0.45**	**587.42**	**0.006**
S.E.M.+/-	**0.81**	**0.12**	**76.52**	**0.002**

Table 4.24 **Measurements of RyR3 labelling within the sub-plasmalemmal region of isolated pulmonary artery smooth muscle cells** (n = 8)

	P value	F value
Perinuclear vs. Extra-perinuclear	0.001	18.03
Perinuclear vs. Sub-plasmalemmal	<0.0001	33.65
Extra-perinuclear vs. Sub-plasmalemmal	0.07	3.74

Table 4.25 **Record of P and F values obtained from statistical analysis between the density of RyR3 labelling in a given region of the cell, by means of a 1-way ANOVA test. P value considered significant if $P \leq 0.05$** (n = 8)

	P value	F value
Perinuclear vs. Extra-perinuclear	0.008	9.67
Perinuclear vs. Sub-plasmalemmal	0.001	16.21
Extra-perinuclear vs. Sub-plasmalemmal	0.17	2.12

Table 4.26 **Record of P and F values obtained from statistical analysis between the mean volume of RyR3 labelling in a given region of the cell, by means of a 1-way ANOVA test. P value considered significant if $P \leq 0.05$** (n = 8)

	P value	F value
RyR1 Perinuclear vs, RyR2 Perinuclear	0.73	0.12
RyR1 Perinuclear vs, RyR3 Perinuclear	0.02	6.76
RyR2 Perinuclear vs, RyR3 Perinuclear	0.11	2.98

Table 4.27 **Record of P and F values obtained from statistical analysis between the densities of the labelling of RyR1, RyR2 and RyR3 in the perinuclear region of the cells, by means of a 1-way ANOVA test. P value considered significant if $P \leq 0.05$** (n = 8)

	P value	F value
RyR1 Extra-Perinuclear vs, RyR2 Extra-Perinuclear	0.002	15.32
RyR1 Extra-Perinuclear vs, RyR3 Extra-Perinuclear	0.88	0.02
RyR2 Extra-Perinuclear vs, RyR3 Extra-Perinuclear	0.002	13.89

Table 4.28 **Record of P and F values obtained from statistical analysis between the densities of the labelling of RyR1, RyR2 and RyR3 in the extra-perinuclear region of the cells, by means of a 1-way ANOVA test. P value considered significant if P ≤ 0.05** (n = 8)

	P value	F value
RyR1 Sub-plasmalemmal vs, RyR2 Sub-plasmalemmal	0.021	6.72
RyR1 Sub-plasmalemmal vs, RyR3 Sub-plasmalemmal	0.003	13.17
RyR2 Sub-plasmalemmal vs, RyR3 Sub-plasmalemmal	0.08	3.54

Table 4.29 **Record of P and F values obtained from statistical analysis between the densities of the labelling of RyR1, RyR2 and RyR3 in the sub-plasmalemmal region of the cells, by means of a 1-way ANOVA test. P value considered significant if P ≤ 0.05** (n = 8)

	P value	F value
RyR1 Perinuclear vs, RyR2 Perinuclear	0.6	0.29
RyR1 Perinuclear vs, RyR3 Perinuclear	0.06	4.01
RyR2 Perinuclear vs, RyR3 Perinuclear	0.02	7.5

Table 4.30 **Record of P and F values obtained from statistical analysis between the mean volumes of elements of labelling of RyR1, RyR2 and RyR3 in the perinuclear region of the cells, by means of a 1-way ANOVA test. P value considered significant if P ≤ 0.05** (n = 8)

	P value	F value
RyR1 Extra-Perinuclear vs, RyR2 Extra-Perinuclear	0.13	2.65
RyR1 Extra-Perinuclear vs, RyR3 Extra-Perinuclear	0.96	0.00
RyR2 Extra-Perinuclear vs, RyR3 Extra-Perinuclear	0.094	3.22

Table 4.31 **Record of P and F values obtained from statistical analysis between the mean volumes of elements of labelling of RyR1, RyR2 and RyR3 in the extra-perinuclear region of the cells, by means of a 1-way ANOVA test. P value considered significant if P ≤ 0.05** (n = 8)

	P value	F value
RyR1 Sub-plasmalemmal vs, RyR2 Sub-plasmalemmal	0.29	1.21
RyR1 Sub-plasmalemmal vs, RyR3 Sub-plasmalemmal	0.63	0.25
RyR2 Sub-plasmalemmal vs, RyR3 Sub-plasmalemmal	0.69	0.16

Table 4.32 **Record of P and F values obtained from statistical analysis between the mean volumes of elements of labelling of RyR1, RyR2 and RyR3 in the sub-plasmalemmal region of the cells, by means of a 1-way ANOVA test. P value considered significant if P ≤ 0.05** (n = 8)

	Volume of colocalisation (RyR1- and Lysosomal-labelling) label in cells (μm^3)	Volume of cells (μm^3)	Volume occupied, per μm^3 of cell, by colocalisation (RyR1- and Lysosomal-labelling)
	1.61	2089.31	0.0008
	1.02	847.29	0.0011
	0.13	1430.7	0.0001
	4.61	4206.95	0.0011
	3.69	729.16	0.0051
	5.85	1879.62	0.0031
	9.51	1701.72	0.0056
	7.3	2208.73	0.0033
MEAN	**4.22**	**1886.69**	**0.0025**
S.E.M. +/-	**1.15**	**382.45**	**0.0007**

Table 4.33 **Measurements of colocalisation between RyR1- and lysosomal-labelling obtained from pulmonary artery smooth muscle cells** (n = 8)

	Nuclear volume in cells (μm^3)	Volume of perinuclear colocalisation (RyR1- and Lysosomal-labelling) (μm^3)	Mean volume of perinuclear colocalisation (RyR1- and Lysosomal-labelling) (μm^3)	Volume of perinuclear region of cell (μm^3)	Volume of colocalisation (RyR1- and Lysosomal-labelling) per μm^3 of perinuclear region
	140.27	0.57	0.19	1518.56	0.0010
	78.15	0.87	0.29	593.57	0.0034
	74.01	0.13	0.13	981.06	0.0003
	95.3	2.41	0.21	2969.69	0.0019
	47.72	2.65	0.44	501.84	0.0137
	133.73	1.42	0.39	1263.49	0.0023
	142.01	2.37	0.26	1228.61	0.0052
	125.81	4.89	0.4	1654.48	0.0088
MEAN	**104.63**	**1.91**	**0.29**	**1338.91**	**0.0046**
S.E.M. +/-	**12.63**	**0.54**	**0.04**	**273.65**	**0.0016**

Table 4.34 **Measurements of the colocalisation between RyR1- and lysosomal-labelling within the perinuclear region of isolated pulmonary artery smooth muscle cells** (n = 8)

	Volume extra-perinuclear colocalisation (RyR1- and lysosomal-labelling) (μm^3)	Mean volume of extra-perinuclear colocalisation (RyR1- and lysosomal-labelling) (μm^3)	Volume of extra-perinuclear region (μm^3)	volume of colocalisation (RyR1- and lysosomal-labelling) per μm^3 of the extra-perinuclear region
	0.15	0.14	616.57	0.0002
	0	0	225.44	0
	0	0	312.49	0
	1.6	0.4	751.28	0.0021
	0.57	0.29	171.92	0.0033
	2.94	0.25	494.84	0.0059
	1.19	0.78	715.44	0.0017
	0.75	0.32	1017.2	0.0007
MEAN	**0.9**	**0.29**	**538.15**	**0.0018**
S.E.M.+/-	**0.36**	**0.08**	**103.27**	**0.0007**

Table 4.35 **Measurements of the colocalisation between RyR1- and lysosomal-labelling within the extra-perinuclear region of isolated pulmonary artery smooth muscle cells** (n = 8)

	Volume colocalisation (RyR1- and lysosomal-labelling) in sub-plasmalemmal labelling (μm^3)	Mean volume colocalisation (RyR1- and lysosomal-labelling) (μm^3)	Volume of sub-plasmalemmal region (μm^3)	Volume of colocalisation (RyR1- and lysosomal-labelling) per μm^3 of sub-plasmalemmal region
	0.42	0.15	901.99	0.0005
	0	0	368.13	0.0000
	0	0	668.57	0.0000
	0.86	0.3	2218.41	0.0004
	0.47	0.24	329.92	0.0014
	0.56	0.19	768.65	0.0007
	0.98	0.33	513.17	0.0019
	1.34	0.2	637.28	0.0021
MEAN	**0.58**	**0.18**	**800.77**	**0.0009**
S.E.M.+/-	**0.17**	**0.04**	**213.67**	**0.0003**

Table 4.36 **Measurements of the colocalisation between RyR1- and lysosomal-labelling within the sub-plasmalemmal region of isolated pulmonary artery smooth muscle cells** (n = 8)

	P value	F value
Perinuclear vs. Extra-perinuclear	0.13	2.66
Perinuclear vs. Sub-plasmalemmal	0.04	5.16
Extra-perinuclear vs. Sub-plasmalemmal	0.3	1.15

Table 4.37 **Record of P and F values obtained from statistical analysis between the density of colocalisation between RyR1- and lysosomal-labelling in a given region of the cell, by means of a 1-way ANOVA test. P value considered significant if $P \leq 0.05$** (n = 8)

	P value	F value
Perinuclear vs. Extra-perinuclear	0.98	0.00
Perinuclear vs. Sub-plasmalemmal	0.08	3.65
Extra-perinuclear vs. Sub-plasmalemmal	0.24	0.24

Table 4.38 **Record of P and F values obtained from statistical analysis between the mean volume of colocalisation between RyR1- and lysosomal-labelling in a given region of the cell, by means of a 1-way ANOVA test. P value considered significant if $P \leq 0.05$** (n = 8)

	Volume of colocalisation (RyR2- and Lysosomal-labelling) label in cells (μm^3)	Volume of cells (μm^3)	Volume occupied, per μm^3 of cell, by colocalisation (RyR2- and Lysosomal-labelling)
	7.03	1472.71	0.0048
	6.81	1366.61	0.0050
	8.52	741.59	0.0115
	2.41	1429.76	0.0017
	4.13	2551.58	0.0016
	3.72	1959.04	0.0019
	2.24	2076.69	0.0011
	4.65	1688.99	0.0028
MEAN	**4.94**	**1660.87**	**0.0038**
S.E.M. +/-	**0.81**	**192.56**	**0.0012**

Table 4.39 **Measurements of colocalisation between RyR2- and lysosomal-labelling obtained from pulmonary artery smooth muscle cells** (n = 8)

	Nuclear volume in cells (μm^3)	Volume of perinuclear colocalisation (RyR2- and Lysosomal-labelling) (μm^3)	Mean volume of perinuclear colocalisation (RyR2- and Lysosomal-labelling) (μm^3)	Volume of perinuclear region of cell (μm^3)	Volume of colocalisation (RyR2- and Lysosomal-labelling) per μm^3 of perinuclear region
	85.3	2.42	0.35	438.72	0.0055
	101.57	1.67	0.34	283.73	0.0059
	71.74	2.82	0.71	178.63	0.0158
	173.61	0.88	0.18	282.09	0.0031
	130.03	0.3	0.15	1131.17	0.0003
	145.07	3.4	0.38	840.18	0.0040
	150.5	1.9	0.35	758.86	0.0025
	80.37	3.92	0.69	719.56	0.0054
MEAN	**117.27**	**2.16**	**0.39**	**579.12**	**0.0053**
S.E.M. +/-	**13.31**	**0.43**	**0.073**	**118.06**	**0.0016**

Table 4.40 **Measurements of the colocalisation between RyR2- and lysosomal-labelling within the perinuclear region of isolated pulmonary artery smooth muscle cells** (n = 8)

	Volume extra-perinuclear colocalisation (RyR2- and lysosomal-labelling) (μm^3)	Mean volume of extra-perinuclear colocalisation (RyR2- and lysosomal-labelling) (μm^3)	Volume of extra-perinuclear region (μm^3)	volume of colocalisation (RyR2- and lysosomal-labelling) per μm^3 of the extra-perinuclear region
	4.47	0.41	455.17	0.0098
	4.73	0.53	401.6	0.0118
	5.41	1.8	210.36	0.0257
	0.85	0.31	458.06	0.0019
	2.32	0.25	425.68	0.0055
	0.32	0.32	318.82	0.0010
	0.34	0.14	411.12	0.0008
	0.2	0.13	354.95	0.0006
MEAN	**2.33**	**0.47**	**379.47**	**0.0071**
S.E.M.+/-	**0.79**	**0.2**	**29.4**	**0.0031**

Table 4.41 **Measurements of the colocalisation between RyR2- and lysosomal-labelling within the extra-perinuclear region of isolated pulmonary artery smooth muscle cells** (n = 8)

	Volume colocalisation (RyR2- and lysosomal-labelling) in sub-plasmalemmal labelling (μm^3)	Mean volume colocalisation (RyR2- and lysosomal-labelling) (μm^3)	Volume of sub-plasmalemmal region (μm^3)	Volume of colocalisation (RyR2- and lysosomal-labelling) per μm^3 of sub-plasmalemmal region
	0.14	0.14	633.47	0.0002
	0.41	0.2	641.56	0.0006
	0.29	0.29	285.09	0.0010
	0.68	0.15	514.44	0.0013
	1.51	0.43	958.68	0.0016
	0	0	652.62	0.0000
	0	0	801.96	0.0000
	0.3	0.25	569.38	0.0005
MEAN	**0.42**	**0.18**	**632.15**	**0.0007**
S.E.M.+/-	**0.18**	**0.05**	**69.98**	**0.0002**

Table 4.42 **Measurements of the colocalisation between RyR2- and lysosomal-labelling within the sub-plasmalemmal region of isolated pulmonary artery smooth muscle cells** (n = 8)

	P value	F value
Perinuclear vs. Extra-perinuclear	0.61	0.28
Perinuclear vs. Sub-plasmalemmal	0.01	7.98
Extra-perinuclear vs. Sub-plasmalemmal	0.05	4.48

Table 4.43 **Record of P and F values obtained from statistical analysis between the density of colocalisation between RyR2- and lysosomal-labelling in a given region of the cell, by means of a 1-way ANOVA test. P value considered significant if $P \leq 0.05$** (n = 8)

	P value	F value
Perinuclear vs. Extra-perinuclear	0.72	0.13
Perinuclear vs. Sub-plasmalemmal	0.03	5.59
Extra-perinuclear vs. Sub-plasmalemmal	0.18	1.97

Table 4.44 **Record of P and F values obtained from statistical analysis between the mean volume of colocalisation between RyR2- and lysosomal-labelling in a given region of the cell, by means of a 1-way ANOVA test. P value considered significant if $P \leq 0.05$** (n = 8)

	Volume of colocalisation (RyR3- and Lysosomal-labelling) label in cells (μm^3)	Volume of cells (μm^3)	Volume occupied, per μm^3 of cell, by colocalisation (RyR3- and Lysosomal-labelling)
	8.31	2300.8	0.004
	9.4	1090.41	0.0086
	3.76	846.87	0.004
	3.53	2073.08	0.002
	15.21	2215.08	0.007
	12.13	1934.38	0.0063
	8.19	1557.8	0.0053
	5.16	1542.94	0.003
MEAN	**8.21**	**1695.17**	**0.005**
S.E.M. +/-	**1.44**	**187.3**	**0.0008**

Table 4.45 **Measurements of colocalisation between RyR3- and lysosomal-labelling obtained from pulmonary artery smooth muscle cells** (n = 8)

	Nuclear volume in cells (μm^3)	Volume of perinuclear colocalisation (RyR3- and Lysosomal-labelling) (μm^3)	Mean volume of perinuclear colocalisation (RyR3- and Lysosomal-labelling) (μm^3)	Volume of perinuclear region of cell (μm^3)	Volume of colocalisation (RyR3- and Lysosomal-labelling) per μm^3 of perinuclear region
	130.21	8.31	0.63	584.03	0.014
	61.5	5.89	1.63	309.18	0.019
	58.7	3	0.43	266.9	0.011
	92.31	3.53	0.44	649.4	0.005
	59.63	11.44	0.61	950.76	0.01
	74.33	11.34	0.63	948.97	0.012
	108.35	8.03	0.46	750.38	0.011
	175.38	3.28	0.62	498.46	0.007
MEAN	**95.05**	**6.85**	**0.68**	**619.76**	**0.011**
S.E.M. +/-	**14.64**	**1.23**	**0.14**	**91.89**	**0.002**

Table 4.46 **Measurements of the colocalisation between RyR3- and lysosomal-labelling within the perinuclear region of isolated pulmonary artery smooth muscle cells** (n = 8)

	Volume extra-perinuclear colocalisation (RyR3- and lysosomal-labelling) (μm^3)	Mean volume of extra-perinuclear colocalisation (RyR3- and lysosomal-labelling) (μm^3)	Volume of extra-perinuclear region (μm^3)	volume of colocalisation (RyR3- and lysosomal-labelling) per μm^3 of the extra-perinuclear region
	0.68	0.68	555.19	0.001
	3.51	0.75	275.59	0.013
	0.13	0.35	178.52	0.0007
	0	0	883.35	0
	3.61	0.68	590.71	0.006
	0.24	0.24	300.32	0.0008
	0.16	0.21	313.7	0.0005
	1.88	0.3	387.95	0.005
MEAN	**1.19**	**0.4013**	**435.67**	**0.0033**
S.E.M.+/-	**0.56**	**0.0958**	**80.84**	**0.0016**

Table 4.47 **Measurements of the colocalisation between RyR3- and lysosomal-labelling within the extra-perinuclear region of isolated pulmonary artery smooth muscle cells** (n = 8)

	Volume colocalisation (RyR3- and lysosomal-labelling) in sub-plasmalemmal labelling (μm^3)	Mean volume colocalisation (RyR3- and lysosomal-labelling) (μm^3)	Volume of sub-plasmalemmal region (μm^3)	Volume of colocalisation (RyR3- and lysosomal-labelling) per μm^3 of sub-plasmalemmal region
	0	0	1071.32	0.0000
	0	0	444.15	0.0000
	0.63	0.11	376.58	0.0017
	0	0	540.33	0
	0.16	0.16	626.81	0.0002
	0	0	642.8	0.0000
	0	0	443.05	0.0000
	0	0	554.32	0.0000
MEAN	**0.099**	**0.034**	**587.42**	**0.0002**
S.E.M.+/-	**0.078**	**0.023**	**76.52**	**0.0002**

Table 4.48 **Measurements of the colocalisation between RyR3- and lysosomal-labelling within the sub-plasmalemmal region of isolated pulmonary artery smooth muscle cells** (n = 8)

	P value	F value
Perinuclear vs. Extra-perinuclear	0.003	12.69
Perinuclear vs. Sub-plasmalemmal	<0.0001	51.32
Extra-perinuclear vs. Sub-plasmalemmal	0.09	3.4

Table 4.49 **Record of P and F values obtained from statistical analysis between the density of colocalisation between RyR3- and lysosomal-labelling in a given region of the cell, by means of a 1-way ANOVA test. P value considered significant if $P \leq 0.05$** (n = 8)

	P value	F value
Perinuclear vs. Extra-perinuclear	0.12	2.75
Perinuclear vs. Sub-plasmalemmal	<0.0001	21.09
Extra-perinuclear vs. Sub-plasmalemmal	0.002	13.95

Table 4.50 **Record of P and F values obtained from statistical analysis between the mean volume of colocalisation between RyR3- and lysosomal-labelling in a given region of the cell, by means of a 1-way ANOVA test. P value considered significant if $P \leq 0.05$** (n = 8)

	P value	F value
RyR1Lyso Perinuclear vs, RyR2Lyso Perinuclear	0.74	0.12
RyR1Lyso Perinuclear vs, RyR3Lyso Perinuclear	0.009	9.08
RyR2Lyso Perinuclear vs, RyR3Lyso Perinuclear	0.02	6.83

Table 4.51 **Record of P and F values obtained from statistical analysis between the densities of colocalisation between the labelling of RyR1, RyR2 and RyR3 and lysosomes in the perinuclear region of the cells, by means of a 1-way ANOVA test. P value considered significant if $P \leq 0.05$** (n = 8)

	P value	F value
RyR1Lyso Extra-Perinuclear vs, RyR2Lyso Extra-Perinuclear	0.11	3
RyR1Lyso Extra-Perinuclear vs, RyR3Lyso Extra-Perinuclear	0.4	0.77
RyR2Lyso Extra-Perinuclear vs, RyR3Lyso Extra-Perinuclear	0.28	1.26

Table 4.52 **Record of P and F values obtained from statistical analysis between the densities of colocalisation between the labelling of RyR1, RyR2 and RyR3 and lysosomes in the extra-perinuclear region of the cells, by means of a 1-way ANOVA test. P value considered significant if $P \leq 0.05$** (n = 8)

	P value	F value
RyR1Lyso Sub-plasmalemmal vs, RyR2Lyso Sub-plasmalemmal	0.54	0.39
RyR1Lyso Sub-plasmalemmal vs, RyR3Lyso Sub-plasmalemmal	0.098	3.15
RyR2Lyso Sub-plasmalemmal vs, RyR3Lyso Sub-plasmalemmal	0.19	1.91

Table 4.53 **Record of P and F values obtained from statistical analysis between the densities of colocalisation between the labelling of RyR1, RyR2 and RyR3 and lysosomes in the sub-plasmalemmal region of the cells, by means of a 1-way ANOVA test. P value considered significant if $P \leq 0.05$** (n = 8)

	P value	F value
RyR1Lyso Perinuclear vs, RyR2Lyso Perinuclear	0.23	1.59
RyR1Lyso Perinuclear vs, RyR3Lyso Perinuclear	0.009	7.36
RyR2Lyso Perinuclear vs, RyR3Lyso Perinuclear	0.02	3.34

Table 4.54 **Record of P and F values obtained from statistical analysis between the mean volumes of elements of colocalisation between the labelling of RyR1, RyR2 and RyR3 and lysosomes in the perinuclear region of the cells, by means of a 1-way ANOVA test. P value considered significant if P ≤ 0.05** (n = 8)

	P value	F value
RyR1Lyso Extra-Perinuclear vs, RyR2Lyso Extra-Perinuclear	0.42	0.69
RyR1Lyso Extra-Perinuclear vs, RyR3Lyso Extra-Perinuclear	0.39	0.76
RyR2Lyso Extra-Perinuclear vs, RyR3Lyso Extra-Perinuclear	0.76	0.1

Table 4.55 **Record of P and F values obtained from statistical analysis between the mean volumes of elements of colocalisation between the labelling of RyR1, RyR2 and RyR3 and lysosomes in the extra-perinuclear region of the cells, by means of a 1-way ANOVA test. P value considered significant if P ≤ 0.05** (n = 8)

	P value	F value
RyR1Lyso Sub-plasmalemmal vs, RyR2Lyso Sub-plasmalemmal	0.93	0.01
RyR1Lyso Sub-plasmalemmal vs, RyR3Lyso Sub-plasmalemmal	0.01	8.41
RyR2Lyso Sub-plasmalemmal vs, RyR3Lyso Sub-plasmalemmal	0.02	7.05

Table 4.56 **Record of P and F values obtained from statistical analysis between the mean volumes of elements of colocalisation between the labelling of RyR1, RyR2 and RyR3 and lysosomes in the sub-plasmalemmal region of the cells, by means of a 1-way ANOVA test. P value considered significant if P ≤ 0.05** (n = 8)

	Volume RyR1 labelling associated with areas of colocalisation ≥ 0.5 μm^3	Mean volume of RyR1 labelling associated with areas of colocalisation ≥ 0.5 μm^3	Volume Lysosomal labelling associated with areas of colocalisation ≥ 0.5 μm^3	Mean volume of Lysosomal labelling associated with areas of colocalisation ≥ 0.5 μm^3	Total volume of fluorescent labelling associated with areas of colocalisation ≥ 0.5 μm^3	Mean volume of fluorescent labelling associated with areas of colocalisation ≥ 0.5 μm^3
	3.78	0.76	4.7	1.18	8.48	0.94
	9.28	0.62	7.66	1.91	16.94	0.89
	3.31	3.31	1.54	0.77	4.85	1.62
	42.4	42.4	2.28	2.28	44.68	22.34
	5.82	2.91	1.15	0.38	6.97	1.39
	42.62	21.31	5.32	1.33	47.94	7.99
MEAN	**17.87**	**11.88**	**3.78**	**1.31**	**21.64**	**5.86**
S.E.M. +/-	**7.84**	**6.89**	**1.04**	**0.29**	**7.99**	**3.48**

Table 4.57 **Measurements of the RyR1- and lysosomal-labelling associated with areas of colocalisation between RyR1- and lysosomal-labelling ≥ 0.05 μm^3 in the perinuclear region of cells** (n = 6 from 8 cells)

	Volume RyR2 labelling associated with areas of colocalisation ≥ 0.5 μm^3	Mean volume of RyR2 labelling associated with areas of colocalisation ≥ 0.5 μm^3	Volume Lysosomal labelling associated with areas of colocalisation ≥ 0.5 μm^3	Mean volume of Lysosomal labelling associated with areas of colocalisation ≥ 0.5 μm^3	Total volume of fluorescent labelling associated with areas of colocalisation ≥ 0.5 μm^3	Mean volume of fluorescent labelling associated with areas of colocalisation ≥ 0.5 μm^3
	11.96	1.5	4.56	1.14	16.52	1.38
	4.27	0.53	11.14	2.23	15.41	1.19
	13.01	1.18	6.52	1.09	19.53	1.15
	8.47	1.06	14.58	1.62	23.05	1.36
	8.87	1.27	15.42	2.2	24.29	1.74
	19.54	1.5	5.37	0.9	24.91	1.31
	16.21	1.8	4.57	1.14	20.78	1.6
	15.87	15.87	10.81	1.55	26.68	3.34
	13.45	13.45	9.25	2.31	22.7	4.54
	13.07	6.54	5.88	2.28	18.95	2.71
MEAN	**12.47**	**4.47**	**8.81**	**1.65**	**21.28**	**2.03**
S.E.M. +/-	**1.39**	**1.79**	**1.28**	**0.18**	**1.17**	**0.36**

Table 4.58 **Measurements of the RyR2- and lysosomal-labelling associated with areas of colocalisation between RyR2- and lysosomal-labelling ≥ 0.05 μm^3 in the perinuclear region of cells** (n = 10 from 8 cells)

	Volume RyR3 labelling associated with areas of colocalisation ≥ 0.5 μm^3	Mean volume of RyR3 labelling associated with areas of colocalisation ≥ 0.5 μm^3	Volume Lysosomal labelling associated with areas of colocalisation ≥ 0.5 μm^3	Mean volume of Lysosomal labelling associated with areas of colocalisation ≥ 0.5 μm^3	Total volume of fluorescent labelling associated with areas of colocalisation ≥ 0.5 μm^3	Mean volume of fluorescent labelling associated with areas of colocalisation ≥ 0.5 μm^3
	12.7	1.27	5.64	2.82	18.34	1.53
	8.73	1.46	5.91	5.91	14.64	2.09
	15.9	3.18	8.06	4.03	23.96	3.42
	10.07	1.44	5.91	5.91	15.98	2
	9.48	1.58	5.2	5.2	14.68	2.1
	12.38	1.55	5.2	5.2	17.58	1.95
	11.16	1.86	12.31	4.1	23.47	2.61
	9.94	1.66	1.95	1.95	11.89	1.7
	18.06	2.58	7.93	7.93	25.99	3.25
	8.3	1.38	5.91	5.91	14.21	2.03
	8.73	1.46	5.91	5.91	14.64	2.09
	5.21	1.3	5.9	5.9	11.11	2.22
	11.98	1.5	30.9	7.73	42.88	3.57
	10.76	2.15	31.74	5.29	42.5	3.86
	17.13	2.45	29.98	7.5	47.11	4.28
	10.72	3.57	3.35	0.84	14.07	2.01
	17.85	2.23	29.98	7.5	47.83	3.99
	10.72	3.57	22.79	3.8	33.51	3.72
	5.98	1.5	11.58	5.79	17.56	2.93
	16.65	1.85	20.9	2.09	37.55	1.98
	7.09	2.36	14.38	1.11	21.47	1.34
	6	1.5	12.47	3.12	18.47	2.31
	10.39	2.6	13.98	1.17	24.37	1.52
	10.39	2.6	12.84	1.43	23.23	1.79
	4	2	14.43	2.41	18.43	2.3
	10.39	2.6	13.43	1.49	23.82	1.83
	1.42	1.42	0.99	0.99	2.41	1.21
	29.52	7.38	2.01	0.29	31.53	2.87
	31.51	6.3	15.68	1.43	47.19	2.95
	27.46	5.49	3.9	0.78	31.36	3.14
	31.16	10.39	14.58	1.46	45.74	3.52
	13.33	4.45	9.29	1.55	22.62	2.51
	19.95	3.99	13.98	2.80	33.93	3.39
	20.39	20.39	8.53	2.84	28.92	7.23
	21.35	5.34	9.39	0.85	30.74	2.05
	2.49	2.49	12.21	4.07	14.7	3.68
	22.99	22.99	0.75	0.38	23.74	7.91
	11.63	3.88	8.07	4.03	19.7	3.94
	10.51	2.1	9.31	9.31	19.82	3.3
	10.86	1.55	9.31	9.31	20.17	2.52
MEAN	**13.38**	**3.78**	**11.41**	**3.8**	**24.8**	**2.87**
S.E.M. +/-	**1.18**	**0.72**	**1.29**	**0.41**	**1.78**	**0.22**

Table 4.59 **Measurements of the RyR3- and lysosomal-labelling associated with areas of colocalisation between RyR3- and lysosomal-labelling ≥ 0.05 μm^3 in the perinuclear region of cells** (n = 40 from 8 cells)

	Number of cells	Number of areas of colocalisation ≥ 0.5 μm^3 in perinuclear region	Mean number of areas per cell	SEM number of areas per cell
RyR1Lyso	8	6	0.75	0.5
RyR2Lyso	8	10	1.25	0.37
RyR3Lyso	8	40	4.63	1.07

Table 4.60 **Number of areas of colocalisation between RyR1, RyR2, RyR3 and lysosomal labelling ≥ 0.5 μm^3 in the perinuclear region of pulmonary artery smooth muscle cells**

	P value	F value
No. Areas Colocalisation RyR1 cells vs. No. Areas Colocalisation RyR2 cells	0.35	0.93
No. Areas Colocalisation RyR1 cells vs. No. Areas Colocalisation RyR3 cells	0.004	11.78
No. Areas Colocalisation RyR2 cells vs. No. Areas Colocalisation RyR3 cells	0.01	8.94

Table 4.61 **Record of P and F values obtained from statistical analysis between the number of areas of colocalisation between the labelling of RyR1, RyR2, RyR3 and lysosomes ≥ 0.5 μm^3 in the perinuclear region of cells, by means of a 1-way ANOVA test. P value considered significant if P ≤ 0.05**

	P value	F value
Vol. fluorescent labelling RyR1 cells vs. Vol. fluorescent labelling RyR2 cells	0.75	0.1
Vol. fluorescent labelling RyR1 cells vs. Vol. fluorescent labelling RyR3 cells	0.75	0.1
Vol. fluorescent labelling RyR2 cells vs. Vol. fluorescent labelling RyR3 cells	0.32	1.03

Table 4.62 **Record of P and F values obtained from statistical analysis between the total volume of fluorescent labelling associated with areas of colocalisation between the labelling of RyR1, RyR2, RyR3 and lysosomes ≥ 0.5 μm^3 in the perinuclear region of cells, by means of a 1-way ANOVA test. P value considered significant if P ≤ 0.05**

	P value	F value
Vol. assoc. RyR labelling RyR1 cells vs. Vol. assoc. RyR labelling RyR2 cells	0.3	1.15
Vol. assoc. RyR labelling RyR1 cells vs. Vol. assoc. RyR labelling RyR3 cells	0.21	1.65
Vol. assoc. RyR labelling RyR2 cells vs. Vol. assoc. RyR labelling RyR3 cells	0.68	0.17

Table 4.63 **Record of P and F values obtained from statistical analysis between the volume of RyR1, RyR2 or RyR3 labelling associated with areas of colocalisation between the labelling of RyR1, RyR2, RyR3 and lysosomes ≥ 0.5 μm^3 in the perinuclear region of cells, by means of a 1-way ANOVA test. P value considered significant if P ≤ 0.05**

	P value	F value
Vol. assoc. Lyso. labelling RyR1 cells vs. Vol. assoc. Lyso. labelling RyR2 cells	0.04	5.16
Vol. assoc. Lyso. labelling RyR1 cells vs. Vol. assoc. Lyso. labelling RyR3 cells	0.04	4.31
Vol. assoc. Lyso. labelling RyR2 cells vs. Vol. assoc. Lyso. labelling RyR3 cells	0.33	0.98

Table 4.64 **Record of P and F values obtained from statistical analysis between the volume of lysosomal labelling associated with areas of colocalisation between the labelling of RyR1, RyR2, RyR3 and lysosomes ≥ 0.5 μm^3 in the perinuclear region of cells, by means of a 1-way ANOVA test. P value considered significant if P ≤ 0.05**

	P value	F value
Mean vol. assoc. Lyso. labelling RyR1 cells vs. Mean vol. assoc. Lyso. labelling RyR2 cells	0.14	2.45
Mean vol. assoc. Lyso. labelling RyR1 cells vs. Mean vol. assoc. Lyso. labelling RyR3 cells	0.02	5.91
Mean vol. assoc. Lyso. labelling RyR2 cells vs. Mean vol. assoc. Lyso. labelling RyR3 cells	0.02	6.24

Table 4.65 **Record of P and F values obtained from statistical analysis between the mean volume of elements of lysosomal labelling associated with areas of colocalisation between the labelling of RyR1, RyR2, RyR3 and lysosomes ≥ 0.5 μm^3 in the perinuclear region of cells, by means of a 1-way ANOVA test. P value considered significant if P ≤ 0.05**

Appendix 3:

Results Tables Chapter 5:

	Resting F340/F380	Maximum F340/F380 + PE	Increase F340/F380 + PE	% increase F340F380 + PE	Resting F340/F380 + Bafilomycin	Maximum F340/F380 + Bafilomycin + PE	Increase F340/F380 + Bafilomycin + PE	% increase F340/F380 + Bafilomycin + PE
	0.4	0.89	0.49	122	0.43	0.99	0.56	129
	0.39	1.64	1.25	317	0.5	1.49	0.99	198
	0.68	2.17	1.49	219	0.8	1.98	1.17	146
MEAN	**0.49**	**1.57**	**1.08**	**219**	**0.58**	**1.49**	**0.91**	**158**
S.E.M +/-	**0.09**	**0.37**	**0.3**	**56**	**0.11**	**0.28**	**0.18**	**21**

Table 5.1 **Fura-2 fluorescence ratio measurements in all experiments involving the extracellular application of phenylepherine (3 μM), in the presence and absence of Bafilomycin A1 (100 nM), in isolated pulmonary artery smooth muscle cells:** The resting F_{340}/F_{380} ratio was determined before the extracellular application of PE to cells in the presence and absence of Bafilomycin A1. The maximum F_{340}/F_{380} ratio value is the peak ratio value recorded after exposure of cells to PE. The Increase in F_{340}/F_{380} ratio was determined by subtracting the resting F_{340}/F_{380} ratio value from the maximum F_{340}/F_{380} ratio value. The % increase in F_{340}/F_{380} ratio was determined by expressing the increase in F_{340}/F_{380} ratio for each experiment as a percentage of the resting F_{340}/F_{380} ratio value, when the resting F_{340}/F_{380} ratio value was taken to equal 100 %.

	PE	PE + Bafilomycin A1		
Mean	1.08	0.91	**P value**	0.65
S.E.M.	0.3	0.18	**F**	0.23
n	3	3		

Table 5.2: **Summary of the mean increases in Fura-2 fluorescence ratio in isolated pulmonary artery smooth muscle cells in response to PE in the presence and absence of Bafilomycin A1:** The P value determining statistical significance was calculated by means of a one-way ANOVA test.

	Resting F340/F380	Maximum F340/F380 + PGF	Increase F340/F380 + PGF	% increase F340F380 + PGF	Resting F340/F380 + Bafilomycin	Maximum F340/F380 + Bafilomycin + PGF	Increase F340/F380 + Bafilomycin + PGF	% increase F340/F380 + Bafilomycin + PGF
	0.61	1.79	1.18	193	0.647	1.593	0.95	146
	0.59	1.39	0.8	137	0.606	1.35	0.74	123
	0.52	1.15	0.63	119	0.619	1.304	0.69	111
	0.41	0.68	0.27	66	0.455	0.746	0.29	64
	0.58	1.41	0.83	143	0.6	1.586	0.99	164
MEAN	**0.54**	**1.28**	**0.74**	**132**	**0.59**	**1.32**	**0.73**	**122**
S.E.M +/-	**0.04**	**0.18**	**0.15**	**21**	**0.03**	**0.15**	**0.12**	**17**

Table 5.3 **Fura-2 fluorescence ratio measurements in all experiments involving the extracellular application of prostaglandin-$F_{2\alpha}$ (2 μM), in the presence and absence of Bafilomycin A1 (100 nM), in isolated pulmonary artery smooth muscle cells:** The resting F_{340}/F_{380} ratio was determined before the extracellular application of $PGF_{2\alpha}$ to cells in the presence and absence of Bafilomycin A1. The maximum F_{340}/F_{380} ratio value is the peak ratio value recorded after exposure of cells to $PGF_{2\alpha}$. The Increase in F_{340}/F_{380} ratio was determined by subtracting the resting F_{340}/F_{380} ratio value from the maximum F_{340}/F_{380} ratio value. The % increase in F_{340}/F_{380} ratio was determined by expressing the increase in F_{340}/F_{380} ratio for each experiment as a percentage of the resting F_{340}/F_{380} ratio value, when the resting F_{340}/F_{380} ratio value was taken to equal 100 %.

	$PGF_{2\alpha}$	$PGF_{2\alpha}$ + Bafilomycin A1		
Mean	0.74	0.73	**P value**	0.96
S.E.M.	0.15	0.12	**F**	0.00
n	5	5		

Table 5.4: **Summary of the mean increases in Fura-2 fluorescence ratio in isolated pulmonary artery smooth muscle cells in response to $PGF_{2\alpha}$ in the presence and absence of Bafilomycin A1:** The P value determining statistical significance was calculated by means of a one-way ANOVA test.

	Resting F340/F380	Maximum F340/F380 + ET-1 (1st application)	Increase F340/F380 + ET-1	% increase F340F380 + ET-1	Resting F340/F380	Maximum F340/F380 + ET-1 (2nd application)	Increase F340/F380 + ET-1	% increase F340/F380 + ET-1
	0.48	0.95	0.47	98	0.53	0.96	0.43	81
	0.52	1.24	0.72	139	0.55	1.2	0.65	118
	0.43	1.19	0.76	177	0.41	1.23	0.82	200
	0.65	1.13	0.48	74	0.6	1.17	0.57	95
	0.66	1.74	1.08	164	0.67	1.69	1.02	152
	0.51	1.23	0.72	141	0.55	1.27	0.72	131
	0.39	0.97	0.58	149	0.44	0.99	0.55	125
	0.44	0.99	0.55	125	0.45	1.02	0.57	127
	0.68	1.22	0.54	79	0.65	1.23	0.58	89
	0.45	1.1	0.65	144	0.47	1.13	0.66	140
	0.48	1.09	0.61	127	0.45	1.1	0.65	144
	0.43	1.02	0.59	137	0.43	1.1	0.67	156
	0.49	1.11	0.62	127	0.49	1.01	0.52	106
	0.6	1.31	0.71	118	0.58	1.27	0.69	119
	0.54	0.99	0.45	83	0.57	0.96	0.39	68
	0.56	1.27	0.71	127	0.59	1.24	0.65	110
MEAN	**0.52**	**1.16**	**0.64**	**126**	**0.53**	**1.16**	**0.63**	**123**
S.E.M +/-	**0.02**	**0.05**	**0.04**	**7**	**0.02**	**0.04**	**0.04**	**8**

Table 5.5 **Endothelin-1 induces reproducible global calcium release events in isolated pulmonary artery smooth muscle cells:** The resting F_{340}/F_{380} ratio was determined before the 1st or 2nd extracellular application of ET-1 to cells. The maximum F_{340}/F_{380} ratio value is the peak ratio value recorded after exposure of cells to ET-1. The Increase in F_{340}/F_{380} ratio was determined by subtracting the resting F_{340}/F_{380} ratio value from the maximum F_{340}/F_{380} ratio value. The % increase in F_{340}/F_{380} ratio was determined by expressing the increase in F_{340}/F_{380} ratio for each experiment as a percentage of the resting F_{340}/F_{380} ratio value, when the resting F_{340}/F_{380} ratio value was taken to equal 100 %

	Resting F340/F380	Maximum F340/F380 + ET-1	Increase F340/F380 + ET-1	% increase F340F380 + ET-1	Resting F340/F380 + Bafilomycin	Maximum F340/F380 + Bafilomycin + ET-1	Increase F340/F380 + Bafilomycin + ET-1	% increase F340/F380 + Bafilomycin + ET-1
	0.71	1.14	0.43	61	0.65	0.65	0	0
	0.73	1.21	0.49	67	0.61	0.63	0.02	3
	0.43	1.13	0.7	163	0.62	0.65	0.03	5
	0.38	1.19	0.81	213	0.46	0.48	0.01	2
MEAN	**0.56**	**1.17**	**0.61**	**126**	**0.64**	**0.65**	**0.02**	**2**
S.E.M +/-	**0.09**	**0.02**	**0.09**	**37**	**0.03**	**0.03**	**0.01**	**1**

Table 5.6 **Fura-2 fluorescence ratio measurements in all experiments involving the extracellular application of endothelin-1 (100 nM), in the presence and absence of Bafilomycin A1 (100 nM), in isolated pulmonary artery smooth muscle cells:** The resting F_{340}/F_{380} ratio was determined before the extracellular application of ET-1 to cells in the presence and absence of Bafilomycin A1. The maximum F_{340}/F_{380} ratio value is the peak ratio value recorded after exposure of cells to ET-1. The Increase in F_{340}/F_{380} ratio was determined by subtracting the resting F_{340}/F_{380} ratio value from the maximum F_{340}/F_{380} ratio value. The % increase in F_{340}/F_{380} ratio was determined by expressing the increase in F_{340}/F_{380} ratio for each experiment as a percentage of the resting F_{340}/F_{380} ratio value, when the resting F_{340}/F_{380} ratio value was taken to equal 100 %.

	ET-1	ET-1 + Bafilomycin A1		
Mean	0.61	0.02	**P value**	0.001
S.E.M.	0.09	0.01	**F**	44.17
n	4	4		

Table 5.7: **Summary of the mean increases in Fura-2 fluorescence ratio in isolated pulmonary artery smooth muscle cells in response to ET-1 in the presence and absence of Bafilomycin A1:** The P value determining statistical significance was calculated by means of a one-way ANOVA test.

	Resting F340/F380	Maximum F340/F380 + ET-1	Increase F340/F380 + ET-1	% increase F340F380 + ET-1	Resting F340/F380 + Thapsigargin	Maximum F340/F380 + Thapsigargin +ET-1	Increase F340/F380 + Thapsigargin +ET-1	% increase F340/F380 + Thapsigargin +ET-1
	0.35	1.06	0.71	203	0.4	0.44	0.04	10*
	0.41	0.72	0.31	76	0.45	0.46	0.01	2
	0.38	0.64	0.26	68	0.48	0.53	0.05	10*
	0.4	0.79	0.39	98	0.51	0.52	0.01	2
	0.4	0.93	0.53	133	0.42	0.44	0.02	5
	0.43	0.94	0.51	119	0.47	0.48	0.01	2
	0.4	0.81	0.41	103	0.41	0.54	0.13	32*
	0.35	0.75	0.40	114	0.4	0.45	0.05	13*
	0.35	0.58	0.23	66	0.5	0.59	0.09	18*
MEAN	**0.39**	**0.80**	**0.42**	**109**	**0.45**	**0.49**	**0.05**	**10**
S.E.M +/-	**0.01**	**0.05**	**0.05**	**14**	**0.01**	**0.02**	**0.01**	**3**

Table 5.8 **Fura-2 fluorescence ratio measurements in all experiments involving the extracellular application of endothelin-1 (100 nM), in the presence and absence of thapsigargin (1 μM), in isolated pulmonary artery smooth muscle cells:** The resting F_{340}/F_{380} ratio was determined before the extracellular application of ET-1 to cells in the presence and absence of thapsigargin. The maximum F_{340}/F_{380} ratio value is the peak ratio value recorded after exposure of cells to ET-1. The Increase in F_{340}/F_{380} ratio was determined by subtracting the resting F_{340}/F_{380} ratio value from the maximum F_{340}/F_{380} ratio value. The % increase in F_{340}/F_{380} ratio was determined by expressing the increase in F_{340}/F_{380} ratio for each experiment as a percentage of the resting F_{340}/F_{380} ratio value, when the resting F_{340}/F_{380} ratio value was taken to equal 100 %. Asterisk (*) denotes those cells which displayed clear, spatially restricted Ca^{2+} release event in response to ET-1 following pre-incubation with thapsigargin.

	ET-1	ET-1 + thapsigargin		
Mean	0.42	0.05	**P value**	<0.0001
S.E.M.	0.05	0.01	**F**	51.22
n	9	9		

Table 5.9: **Summary of the mean increases in Fura-2 fluorescence ratio in isolated pulmonary artery smooth muscle cells in response to ET-1 in the presence and absence of thapsigargin:** The P value determining statistical significance was calculated by means of a one-way ANOVA test.

	Resting F340/F380	Maximum F340/F380 + ET-1	Increase F340/F380 + ET-1	% increase F340F380 + ET-1	Resting F340/F380 + ryanodine	Maximum F340/F380 + ryanodine +ET-1	Increase F340/F380 + ryanodine +ET-1	% increase F340/F380 + ryanodine +ET-1
	0.49	1.19	0.7	143	0.51	0.66	0.15	29*
	0.38	0.64	0.26	68	0.38	0.45	0.07	18*
	0.38	1.08	0.7	184	0.47	0.52	0.05	11
	0.37	1.03	0.66	178	0.41	0.44	0.03	7*
	0.37	1.05	0.68	184	0.45	0.47	0.02	4
	0.36	0.67	0.31	86	0.42	0.43	0.01	2
	0.44	0.68	0.24	55	0.51	0.53	0.02	4
	0.41	0.92	0.51	124	0.47	0.49	0.02	4
MEAN	**0.4**	**0.93**	**0.51**	**134**	**0.45**	**0.5**	**0.05**	**10**
S.E.M +/-	**0.02**	**0.08**	**0.07**	**19**	**0.02**	**0.03**	**0.02**	**3**

Table 5.10 **Fura-2 fluorescence ratio measurements in all experiments involving the extracellular application of endothelin-1 (100 nM), in the presence and absence of ryanodine (20 μM), in isolated pulmonary artery smooth muscle cells:** The resting F_{340}/F_{380} ratio was determined before the extracellular application of ET-1 to cells in the presence and absence of ryanodine. The maximum F_{340}/F_{380} ratio value is the peak ratio value recorded after exposure of cells to ET-1. The Increase in F_{340}/F_{380} ratio was determined by subtracting the resting F_{340}/F_{380} ratio value from the maximum F_{340}/F_{380} ratio value. The % increase in F_{340}/F_{380} ratio was determined by expressing the increase in F_{340}/F_{380} ratio for each experiment as a percentage of the resting F_{340}/F_{380} ratio value, when the resting F_{340}/F_{380} ratio value was taken to equal 100 %.

	ET-1	ET-1 + ryanodine		
Mean	0.51	0.07	**P value**	<0.0001
S.E.M.	0.05	0.02	**F**	57.86
n	8	8		

Table 5.11: **Summary of the mean increases in Fura-2 fluorescence ratio in isolated pulmonary artery smooth muscle cells in response to ET-1 in the presence and absence of ryanodine:** The P value determining statistical significance was calculated by means of a one-way ANOVA test.

	NAADP levels control 30s incubation (pmol per mg tissue)	NAADP levels ET-1 (1 μM) 30s incubation (pmol per mg tissue)	NAADP levels control 60s incubation (pmol per mg tissue)	NAADP levels ET-1 (1 μM) 60s incubation (pmol per mg tissue)	NAADP levels control 300s incubation (pmol per mg tissue)	NAADP levels ET-1 (1 μM) 300s incubation (pmol per mg tissue)
	0.25	1.08	0.94	1.05	0.79	0.94
	0.24	1.74	0.7	0.4	0.27	0.26
	0.5	1.69	0.65	0.3	0.22	0.3
	0.32	1.37	0.24			
	0.13	0.75	0.38			
	0.3		0.23			
	0.18		0.06			
	0.07		0.05			
	0.17		0.05			
	0.16		0.19			
	0.21		0.13			
	0.03		0.09			
MEAN	**0.21**	**1.33**	**0.31**	**0.58**	**0.43**	**0.5**
S.E.M +/-	**0.04**	**0.19**	**0.09**	**0.24**	**0.2**	**0.2**

Table 5.12: **Comparison of NAADP levels untreated control and ET-1 treated branches of the pulmonary arterial tree.**

	Control 30s	**ET-1 30s**		
Mean	0.21	1.33	**P value**	<0.0001
S.E.M.	0.04	0.19	**F**	75.49
N	12	5		

Table 5.13: **Summary of the mean increases in NAADP levels in second and third order branches of the pulmonary arterial tree in response to 30 s exposure to ET-1:** The P value determining statistical significance was calculated by means of a one-way ANOVA test.

	Control 60s	**ET-1 60s**		
Mean	0.31	0.58	**P value**	0.2
S.E.M.	0.09	0.24	**F**	1.8
N	12	3		

Table 5.14: **Summary of the mean increases in NAADP levels in second and third order branches of the pulmonary arterial tree in response to 60 s exposure to ET-1:** The P value determining statistical significance was calculated by means of a one-way ANOVA test.

	Control 300s	**ET-1 300s**		
Mean	0.43	0.5	**P value**	0.81
S.E.M.	0.2	0.2	**F**	0.07
N	3	3		

Table 5.15: **Summary of the mean increases in NAADP levels in second and third order branches of the pulmonary arterial tree in response to 300 s exposure to ET-1:** The P value determining statistical significance was calculated by means of a one-way ANOVA test.

	NAADP levels control 30 s incubation (pmol per mg tissue)	NAADP levels PGF_{2a} (2 μM) 30 s incubation (pmol per mg tissue)	NAADP levels control 60 s incubation (pmol per mg tissue)	NAADP levels PGF_{2a} (2 μM) 60 s incubation (pmol per mg tissue)
	0.32	0.29	0.24	0.14
	0.13	0.05	0.38	0.19
	0.3	0.27	0.23	0.2
MEAN	**0.25**	**0.2**	**0.28**	**0.17**
S.E.M +/-	**0.06**	**0.08**	**0.05**	**0.02**

Table 5.16: **Comparison of NAADP levels between $PGF_{2\alpha}$ treated and untreated branches of the pulmonary arterial tree.**

	Control 30s	$PGF_{2\alpha}$ 30s		
Mean	0.25	0.2	**P value**	0.658
S.E.M.	0.06	0.05	**F**	0.23
N	3	3		

Table 5.17: **Summary of the mean increases in NAADP levels in second and third order branches of the pulmonary arterial tree in response to 30 s exposure to $PGF_{2\alpha}$:** The P value determining statistical significance was calculated by means of a one-way ANOVA test.

	Control 30s	$PGF_{2\alpha}$ 30s		
Mean	0.28	0.17	**P value**	0.11
S.E.M.	0.05	0.02	**F**	4.23
N	3	3		

Table 5.18: **Summary of the mean increases in NAADP levels in second and third order branches of the pulmonary arterial tree in response to 60 s exposure to $PGF_{2\alpha}$:** The P value determining statistical significance was calculated by means of a one-way ANOVA test.

	Resting F340/F380	Maximum F340/F380 + ET-1 +BQ-788	Increase F340/F380 + ET-1 + BQ-788	% increase F340F380 + ET-1 +BQ-788	Resting F340/F380	Maximum F340/F380 +ET-1	Increase F340/F380 +ET-1	% increase F340/F380 +ET-1
	0.71	0.73	0.02	3	0.78	1.76	0.98	126
	0.78	0.78	0	0	0.78	2.7	1.92	246
	0.8	0.83	0.03	4	0.86	2.25	1.39	162
	0.69	0.71	0.02	3	0.75	1.33	0.58	77
	0.66	0.66	0	0	0.67	2.04	1.37	205
	0.51	0.51	0	0	0.56	2.09	1.53	273
	0.49	0.5	0.01	2	0.49	0.85	0.36	74
MEAN	**0.66**	**0.67**	**0.01**	**2**	**0.70**	**1.86**	**1.16**	**166**
S.E.M +/-	**0.05**	**0.05**	**0.005**	**1**	**0.05**	**0.23**	**0.21**	**30**

Table 5.19 **Fura-2 fluorescence ratio measurements in all experiments involving the extracellular application of ET-1, in the presence and absence of BQ-788, in isolated pulmonary artery smooth muscle cells:** The resting F_{340}/F_{380} ratio was determined before the extracellular application of ET-1 (100 nM) to cells in the presence and absence of BQ-788 (30 μM). The maximum F_{340}/F_{380} ratio value is the peak ratio value recorded after exposure of cells to ET-1. The Increase in F_{340}/F_{380} ratio was determined by subtracting the resting F_{340}/F_{380} ratio value from the maximum F_{340}/F_{380} ratio value. The % increase in F_{340}/F_{380} ratio was determined by expressing the increase in F_{340}/F_{380} ratio for each experiment as a percentage of the resting F_{340}/F_{380} ratio value, when the resting F_{340}/F_{380} ratio value was taken to equal 100 %.

	Increase in F340/F380 ET-1 +BQ-788	Increase in F340/F380 ET-1		
Mean	0.01	1.16	**P value**	<0.0001
S.E.M.	0.005	0.21	**F**	30.5
n	7	7		

Table 5.20: **Summary of the mean increases in Fura-2 fluorescence ratio in isolated pulmonary artery smooth muscle cells in response to ET-1 in the presence and absence of BQ-788:** The P value determining statistical significance was calculated by means of a one-way ANOVA test.

Cell	Resting F340/F380	Maximum F340/F380 + ET-1 +BQ-123	Increase F340/F380 + ET-1 + BQ-123	% increase F340F380 + ET-1 +BQ-123
1	0.66	2.4	1.74	263.64
2	0.55	1.44	0.89	161.82
3	0.56	1.38	0.82	146.43
4	0.55	1.39	0.84	152.73
5	0.62	1.45	0.83	133.87
MEAN	**0.59**	**1.61**	**1.02**	**171.7**
S.E.M +/-	**0.01**	**0.04**	**0.04**	**6.5**

Table 5.21 **Fura-2 fluorescence ratio measurements in all experiments involving the extracellular application of ET-1, in the presence and absence of BQ-123, in isolated pulmonary artery smooth muscle cells:** The resting F_{340}/F_{380} ratio was determined before the extracellular application of ET-1 (100 nM) to cells in the presence and absence of BQ-123 (30 μM). The maximum F_{340}/F_{380} ratio value is the peak ratio value recorded after exposure of cells to ET-1. The Increase in F_{340}/F_{380} ratio was determined by subtracting the resting F_{340}/F_{380} ratio value from the maximum F_{340}/F_{380} ratio value. The % increase in F_{340}/F_{380} ratio was determined by expressing the increase in F_{340}/F_{380} ratio for each experiment as a percentage of the resting F_{340}/F_{380} ratio value, when the resting F_{340}/F_{380} ratio value was taken to equal 100 %.

	NAADP levels control (pmol per mg tissue)	NAADP levels ET-1 (1 μM) (pmol per mg tissue)	NAADP levels ET-1 (1 μM) + BQ-788 (20 μM) (pmol per mg tissue)
	0.17	1.04	0.17
	0.16	0.73	0.13
	0.21	0.69	0.14
MEAN	**0.18**	**0.82**	**0.15**
S.E.M +/-	**0.02**	**0.11**	**0.01**

Table 5.22: **Comparison of NAADP levels between untreated control, ET-1 treated and ET-1 + BQ-788 treated branches of the pulmonary arterial tree.**

	Control NAADP levels	NAADP levels + ET-1		
Mean	0.18	0.82	**P value**	<0.0001
S.E.M ±.	0.02	0.11	**F**	33.82
n	3	3		

Table 5.23: **Summary of the mean increases in NAADP levels in second and third order branches of the pulmonary arterial tree in response to ET-1:** The P value determining statistical significance was calculated by means of a one-way ANOVA test.

	NAADP levels ET-1	NAADP levels ET-1+BQ-788		
Mean	0.82	0.15	**P value**	0.004
S.E.M ±.	0.11	0.01	**F**	36.63
n	3	3		

Table 5.24: **Summary of the mean increases in NAADP levels in second and third order branches of the pulmonary arterial tree in response to ET-1 and ET-1 + BQ-788:** The P value determining statistical significance was calculated by means of a one-way ANOVA test.

Appendix 4:

Future experiments:

1. Identification of the NAADP receptor:

One approach could be to identify candidate receptors (e.g. TRPML (mucolipins) or TPC1 channels) and then stably transfect them into an expression system (i.e. a clonal cell line, such as HEK-293 or CHO cells) that lack the receptor in question. Thereby calcium signals (Fura-2 fluorescence ratio) in response to intracellular dialysis of NAADP from a patch-pipette in the whole cell configuration could be studied in transfected and non-transfected (control) cells. Alternatively, protein purification and sequencing or cloning techniques could be employed to identify novel Ca^{2+} channels, and whether these channels are targeted to lysosomal membranes and function as NAADP receptors.

2. Cellular localisation of the NAADP receptor:

Once the NAADP receptor has been identified, sequence-specific antibodies could be generated in order to allow for detailed quantitative immunocytochemistry. Thus, I could determine whether or not; (1) the NAADP receptor, like αlgp120, is targeted to lysosomes, or (2) the NAADP receptor selectively co-localises with ryanodine receptor subtype 3 (RyR3) in pulmonary artery smooth muscle cells.

3. Functional examination of the involvement of RyR3 in NAADP-mediated Ca^{2+} signalling in pulmonary artery smooth muscle cells

The examinations presented in this thesis suggest that lysosomes colocalise with RyR3, in the perinuclear region of pulmonary artery smooth muscle cells, to form a trigger zone for NAADP-mediated Ca^{2+} signalling. However, further examinations must be carried out to examine the functional role of each of the 3 different RyR subtypes in the amplification by CICR of Ca^{2+} bursts evoked by NAADP.

- My findings suggest that RyR3 colocalises with lysosomes to a significantly greater degree than is observed for either RyR1 or RyR2. These findings suggest, therefore, that the trigger zone for NAADP-mediated Ca^{2+} signalling in pulmonary artery smooth muscle cells is formed between RyR3 and lysosomes. The relative lack of association between RyR1 and lysosomes, coupled with the relative lack of sensitivity to CICR of RyR1, when compared to RyR3, argues against a role for RyR1 in the amplification of localised NAADP-mediated Ca^{2+} bursts into global Ca^{2+} waves. To determine whether RyR3 or RyR2 contribute to the amplification of Ca^{2+} bursts within the trigger zone the effects of dantrolene on

NAADP-mediated Ca^{2+} signals in isolated pulmonary artery smooth muscle cells could be examined. Dantrolene is known to inhibit RyR1 and RyR3 without affecting Ca^{2+} signals generated via activation of RyR2. Therefore, if preincubation of pulmonary artery smooth muscle cells with dantrolene abolishes global Ca^{2+} waves in response to the intracellular dialysis of NAADP, then RyR2 can be excluded as being involved in the initial amplification of NAADP-mediated Ca^{2+} bursts into global Ca^{2+} waves.

As dantrolene is an inhibitor of both RyR1 and RyR3, its use in the above experiment would not provide conclusive evidence that initial NAADP-mediated Ca^{2+} bursts are amplified via activation of RyR3. Therefore, I could distinguish between RyR3 and RyR1 in the following manner:

- Sequence specific antibodies raised against conserved sequences in the pore regions of each of the different RyR subtypes could be used to examine the involvement of each of the RyR subtypes in amplifying NAADP-mediated Ca^{2+} signalling. Caged NAADP and anti-RyR subtype antibodies could be introduced to pulmonary artery smooth muscle cells by means of a patch-pipette. Then, following a period of incubation to allow the antibodies to associate with their target, a comparison could be carried out on the profile of Ca^{2+} signals generated by photorelease of caged NAADP. The profile of these Ca^{2+} responses could then be compared to Ca^{2+} signals generated in response to NAADP under control conditions, in the absence of anti-RyR antibodies.

- The generation of short interfering RNA (siRNA) against each of the RyR subtypes would allow for examination of NAADP-mediated Ca^{2+} signalling following knockout of a given RyR subtype. Thus, isolated pulmonary artery smooth muscle cells could be cultured and transfected with siRNA specific for a given RyR subtype. Following confirmation that the siRNA had knocked down expression of a given RyR subtype, via western blot and immunocytochemical analysis, the profile of NAADP-mediated Ca^{2+} signals in transfected cells could be compared to the profiles of Ca^{2+} signals in non-transfected cells to gauge the contribution of each RyR subtype to NAADP-mediated Ca^{2+} signals.

4. How does the ET-B receptor promote an increase in NAADP levels?

Investigations in sea urchin eggs have shown that the phosphorylation of ADP-ribosyl cyclase by protein kinase A (PKA) and protein kinase G (PKG) drives the production of NAADP and cADPR, respectively (Galione, *et al.*, 1993; Wilson, *et al.*, 1998). Although the ADP-ribosyl cyclase responsible for the production of cADPR and NAADP in mammalian cells remains to be elucidated, the findings of this thesis indicate that the activation of ETB receptors, by exposure to ET-1, in pulmonary artery smooth muscle causes an

increase in the cellular levels of NAADP. Therefore, as ETB receptors in mammalian cells have been shown to activate a number of different intracellular kinases, including PKA (da Cunha, *et al.*, 2004), PKG (Mullaney, *et al.*, 2000), protein kinase C (PKC) ((da Cunha, *et al.*, 2004) and the ERK2, JNK1 p38 MAP kinase signalling pathways (Aquilla, *et al.*, 1996; Henriksson, *et al.*, 2004), it is possible that the production of NAADP in pulmonary artery smooth muscle, following activation of ETB receptors, may be dependent upon the actions of one or other of these kinases. The requirement for a kinase to drive NAADP production in pulmonary artery smooth muscle could be examined in the following manner:

PKA:

- A role for PKA in promoting NAADP production by activating ADP-ribosyl cyclase could be assessed by utilising an assay designed to examine the ability of ADP-ribosyl cyclase to synthesise NAADP from its substrate β-$NADP^+$. This assay allows for examination of the enzymatic activity of ADP-ribosyl cyclase and examination of the effect of pharmacological intervention on this activity. Thus, I could examine the effect of PKA on NAADP production by ADP-ribosyl cyclase enzyme by determining the rate of synthesis of NAADP in homogenates of pulmonary arteries incubated with NAADP substrates, β-NADP and nicotinic acid, +/- constitutively active PKA. The rate of synthesis of NAADP within pulmonary artery homogenates would then be assessed, over time, by HPLC, using an anion exchange column with a 1mg/ml flow rate over an increasing trifluoroacetic acid gradient. By comparison of the absorbance spectra of the NAADP-containing eluate against standards of known NAADP concentration (measured at 254 nm), I would be able to assess whether constitutively active PKA serves to activate ADP-ribosyl cyclase-mediated production of NAADP in pulmonary artery homogenates. If there was an increase in the rate of NAADP synthesis within pulmonary artery homogenates in the presence of constitutively active PKA, I would then need to assess whether activation of endogenous PKA in pulmonary arteries serves to increase the rate of NAADP synthesis via ADP-ribosyl cyclase. To examine this, I could examine the rate of NAADP synthesis in pulmonary artery homogenates +/- the PKA activator cAMP in the presence of the phosphodiesterase inhibitor (to prevent breakdown of cAMP). Thus, an increase in the rate of synthesis of NAADP observed in cAMP treated homogenates would indicate a role for PKA in promoting NAADP synthesis by activation of ADP-ribosyl cyclase. In order to confirm that the increase in the rate of synthesis of NAADP in response to cAMP was due to an action of PKA, the assay would be repeated in the presence of PKA inhibitors, such as H89 or KT5720.

- If the above experiments indicated a role for PKA in increasing the rate at which ADP-ribosyl cyclase synthesises NAADP in homogenates of pulmonary arteries, it would be pertinent to

examine the role of endogenous PKAs in mediating ET-1 induced increases in NAADP levels in intact pulmonary arteries. Examination of the levels of NAADP in pulmonary arteries +/- the membrane permeant cAMP analogue, 8-Br-cAMP, could be carried out using the competitive NAADP radioreceptor assay described in chapter 5 of this thesis. An increase in NAADP levels in response to 8-Br-cAMP would suggest a role for PKA in promoting NAADP synthesis. A possible role for PKA in mediating the increase in NAADP could be further examined by incubation of arteries with PKA antagonists prior to exposure of 8-Br-cAMP. If the findings of these experiments provide evidence in support of a role for PKA-mediated promotion of an increase in the levels of NAADP within cells, then an investigation of the possible role of PKA in the ET-1-mediated increase in NAADP levels in pulmonary arteries would be required. To examine this I could examine the effect of preincubation of pulmonary arteries of PKA inhibitors on the increase in NAADP levels detected in response to exposure of arteries to ET-1 by use of the radioreceptor assay mentioned previously.

PKG:

- The pulmonary artery homogenate assay described above could be used to examine the effect of PKG on ADP-ribosyl cyclase activity by monitoring the rate of NAADP synthesis. Thus, examination, by HPLC of the rate of NAADP synthesis in pulmonary artery homogenates, +/- constitutively active PKG would indicate whether PKG altered the enzymatic activity of ADP-ribosyl cyclase. If there was an increase in the rate of NAADP synthesis, indicative of an increase in ADP-ribosyl cyclase activity, in response to constitutively active PKG then I would proceed to examine the effect of activation of endogenous PKG on ADP-ribosyl cyclase activity in the assay system. This could be achieved by adding cGMP to homogenates of pulmonary arteries to activate PKG. These experiments would be carried out in the presence of phosphodiesterase inhibitors and any changes in the rate of NAADP synthesis within artery homogenates would be examined via HPLC. These experiments could be repeated in the presence of PKG inhibitors, such as KT5823, to confirm that any increase in the rate of NAADP synthesis in response to application of cGMP was due to the activity of PKG.

- A role for PKG in mediating increases in the levels of NAADP within whole tissue preparation of pulmonary arteries could be assessed by means of the competitive NAADP radioreceptor assay described in chapter 5 of this thesis. Initially, the effect on NAADP levels within pulmonary arteries could be assessed +/- the membrane permeant analogue of cGMP, 8-Br-cGMP. An increase in tissue NAADP levels in response to 8-Br-cGMP would indicate a possible role for PKG in promoting this increase. The

involvement of PKG could be assessed by preincubation of pulmonary arteries with PKG inhibitors prior to exposure with 8-Br-cGMP. Abolition of the 8-Br-cGMP-mediated increase in NAADP levels within pulmonary arteries by PKG inhibitors would confirm that 8-Br-cGMP promotes an increase in tissue NAADP levels by activation of PKG. A possible role for PKG in mediating ET-1 induced increases in NAADP levels within pulmonary arteries could be examined through application of the competitive radioreceptor assay described previously. Thus, the levels of NAADP within pulmonary arteries exposed to ET-1 could be determined +/- preincubation of arteries with PKG inhibitors.

PKC:

- The effect of PKC activators, such as the phorbol ester PMA, on the rate of NAADP synthesis in homogenates of pulmonary arteries could be assessed by HPLC in order to examine whether or not PKC altered the enzymatic activity of ADP-ribosyl cyclase. That any observed increase in the rate of NAADP synthesis was due to PKC could be examined by the preincubation of homogenates with PKC inhibitors, such as staurosporine. If the increase in the rate of NAADP synthesis was abolished, this would provide compelling evidence that PKC regulates the enzymatic activity of ADP-ribosyl cyclase. The PKC family of serine threonine kinases is subdivided into three groups on the basis of structural and biophysical properties: the conventional (α, $\beta1$, $\beta2$, γ), novel (δ, ε, η, θ, μ, ν) and atypical (ζ and ι/λ) isoforms. A number of the PKC isoforms have been shown to mediate contraction of smooth muscle, including PKCα, β, δ, ε, and ζ (Lee, *et al.*, 1999; Dallas and Khalil, 2003). Therefore, if there was an increase in the rate of NAADP production in pulmonary artery homogenates in response to PKC activation, then I could proceed to screen constitutively active isoforms of PKC to identify which isoform were responsible for the activation of NAADP production by ADP-ribosyl cyclase.

- If activation of PKC increased the rate of NAADP synthesis in homogenates of pulmonary arteries, then a role for PKC in mediating increases in NAADP levels following activation of ETB receptors in whole tissue preparations of pulmonary arteries could be examined. I could investigate this by measuring the levels of NAADP in pulmonary arteries, using the radioreceptor assay described previously, +/- PKC activators. That any observed increase was due to PKC could then be examined by repeating the experiments following preincubation of arteries with PKC inhibitors. Any involvement for PKC in ET-1-mediated increases in NAADP levels in pulmonary arteries could then be investigated by incubating pulmonary arteries with PKC inhibitors prior to exposure to ET-1.

MAPK:

- MAPK signalling pathways involve a cascade of kinases. Thus, by systematically screening the effect of the members of a given signalling cascade one would be able to identify whether or not any one of these kinases is responsible for phosphorylating, and thereby activating, the ADP-ribosyl cyclase present in pulmonary artery smooth muscle. ETB receptor activation has been shown to activate the ERK, p38 and JNK MAPK signalling pathways. The effect of each of these signalling pathways on the rate of synthesis of NAADP in homogenates of pulmonary arteries could be assessed via the addition of constitutively active forms of initial signalling kinases, the MAP kinase kinase kinase (MAPKKK), within these signalling cascades (i.e. Raf-1 for ERK pathway, and MEKK-1 for p38 and JNK pathways). HPLC analysis of the rate of NAADP synthesis within homogenates of pulmonary arteries would indicate whether any of the kinases involved in these signalling pathways mediated an increase in the rate of NAADP synthesis by phosphorylation of ADP-ribosyl cyclase. If an increase in the rate of NAADP synthesis was evident after addition of constitutively active MAPKKK (i.e Raf-1), one would proceed to examine the effect on the rate of NAADP on the next kinase in that particular kinase cascade. I would then proceed to add a constitutively active form of the downstream MAP kinase kinase (MAPKK; in the case of Raf-1, I would add a constitutively active form of MEK) and the effects of this kinase on the rate of NAADP synthesis would be examined. If there was no effect on the rate of NAADP synthesis in response to the constitutively active MAPKK, then one would assume that the upstream MAPKKK was the candidate kinase involved in regulation of NAADP synthesis. However, an increase in the rate of NAADP synthesis would suggest a role for this MAPKK in phosphorylating ADP-ribosyl cyclase. One would then examine the role of the downstream MAPK on the effect of NAADP synthesis via addition of a constitutively active MAPKK (ERK in this example). Thus, by measuring the effect of a constitutively active form of MAPK on the rate of NAADP synthesis one would be able to identify whether or not a member of the MAPK cascade is the kinase responsible for the phosphorylation, and thereby activation of ADP-ribosyl cyclase. There are a number of commercially available specific inhibitors of each of the kinases within the MAPK cascades (e.g. PD 98059 for ERK and U 0126 for MEK). These inhibitors could be employed in the homogenate assay, along with constitutively active kinases, to confirm the identity of the kinase responsible for the phosphorylation of ADP-ribosyl cyclase.

- A role for MAPK pathways in coupling the activation of ETB receptors to the observed increase in NAADP levels within pulmonary artery smooth muscle could be examined in the following manner. Pulmonary arteries could be incubated with

specific inhibitors of the MAPK kinase pathway identified from the homogenate assay to activate ADP-ribosyl cyclase. Radio ligand bindings assays would then be carried out following exposure to ET-1, +/- specific MAPK inhibitors to examine their effect on the ET-1-mediated increase in NAADP levels.

5. Do NAADP and cADPR act in concert to modulate the temporal pattern of Ca^{2+} signalling in response to ET-1 in pulmonary arterial smooth muscle?

A recent investigation by Galione and colleagues has shown in murine pancreatic acinar cells that activation of CCK A receptors causes an initial, transient increase in cellular levels of NAADP. Following decline of the initial NAADP transient, Ca^{2+} signalling is maintained by a sustained increase in the cellular levels of cADPR. Thus, these two Ca^{2+} mobilising messengers act synergistically to govern prolonged Ca^{2+} signalling in response to CCK (Yamasaki, *et al.*, 2005). Significantly, therefore, there is compelling evidence in the literature that cADPR is involved in the mediation of Ca^{2+} signals in response to ET-1 in a number of smooth muscle types, including vascular smooth muscle (Giulumian, *et al.*, 2000; Barone, *et al.*, 2002; Fellner and Parker, 2004). Thus, investigations are required which would examine whether NAADP and cADPR act synergistically to mediate responses to ET-1. This could be assessed in the following manner:

- I have shown in Chapter 5 of this thesis that activation of ETB receptors stimulates a rapid, transient increase in the levels of NAADP in pulmonary arteries. This increase in NAADP was seen to peak after 30s and declined to baseline within 60s. Radioligand binding assays could be used to determine the cellular levels of NAADP over a longer time course of exposure to ET-1 (i.e. 0, 0.5, 1, 2.5, 5, 10, 15, 30 mins). Parallel studies into the effects of exposure of pulmonary arteries to ET-1 on the levels of cADPR could then be carried out to examine whether ET-1 promotes an increase in the cellular levels of cADPR. If cADPR levels are seen to increase in response to ET-1, comparison between the results obtained for NAADP and cADPR would indicate whether increases in NAADP and cADPR occurred simultaneously or whether, as is the case in pancreatic acinar cells (Yamasaki *et al.*, 2005), they occur independently of one another with NAADP mediating initial Ca^{2+} signals and cADPR mediating longer lasting signals.

- If cADPR binding studies identify an increase in cADPR levels, relative to control, in pulmonary arteries, then it will be important to examine which of the endothelin receptors (ETA or ETB) is responsible for initiating this increase. Therefore, the endothelin receptor antagonists BQ-123 (ETA antagonist) and BQ-788 (ETB antagonist) could be used in conjunction with ET-1, in parallel studies, to examine whether the increase in cADPR production is coupled to activation of ETA, or whether activation of ETB is

responsible for the increase in production of both NAADP and cADPR.

Functional Ca^{2+} imaging experiments would then be required to examine the precise role cADPR plays in Ca^{2+} signalling initiated by NAADP. Thus, it would be of importance to examine whether cADPR has an involvement in; (1) sensitising RyRs to activation by Ca^{2+}, thereby lowering the threshold for amplification of NAADP-mediated Ca^{2+} bursts; (2) altering the degree to which initial Ca^{2+} bursts are amplified; (3) altering the speed at which Ca^{2+} signals are propagated through the cytoplasm of cells; (4) altering the frequency of subsequent Ca^{2+} oscillations; (5) increasing the sensitivity of RyRs to activation by Ca^{2+}, such that global Ca^{2+} waves are maintained in the absence of any further requirement for NAADP-mediated Ca^{2+} signals. These possible roles for cADPR in pulmonary artery smooth muscle cells could be assessed in the following ways:

- An examination of the possible involvement of basal cADPR levels in facilitating global Ca^{2+} waves generated by NAADP in pulmonary artery smooth muscle cells could be carried out. This could be achieved by comparing the profiles of Ca^{2+} signals generated in response to NAADP in the absence and presence of the cADPR antagonist 8-Br-cADPR.

- Although the above experiment may serve to indicate a requirement of basal cADPR concentrations in the generation of Ca^{2+} signals in response to NAADP, the effects of cADPR may be lost due to dilution basal cADPR concentrations within the cell by the addition of pipette solution. Thus, the above experiments could be repeated with the addition of various concentrations of cADPR in the patch-pipette (i.e. 3, 10, 30 and 100 μM). Comparison would then be carried out between the profiles of Ca^{2+} signals generated in response to NAADP alone and those generated in response to NAADP and varying concentrations of cADPR.

- The effect of cADPR on Ca^{2+} signals could also be examined by introducing caged NAADP into a cell via a patch pipette +/- varying concentrations of cADPR. Ca^{2+} signals in response to the flash photolysis of NAADP +/- cADPR could be analysed and compared.

- Functional experiments may also be carried out to examine the role of cADPR in mediating Ca^{2+} responses to ET-1 in isolated pulmonary artery smooth muscle cells. Thus, a comparison of Ca^{2+} signals generated in response to ET-1 in the absence and the presence of 8-Br-cADPR would be carried out.

6. Does NAADP play a role in the initiation of HPV?

Our laboratory has previously shown that the initial, transient constriction (Phase 1) of HPV observed in isolated pulmonary artery rings is dependent on

RyR-mediated SR Ca^{2+} release that is unaffected by the cADPR antagonist 8-Br-cADPR, whilst the maintained phase 2 constriction is abolished by this antagonist (Dipp, *et al.*, 2001; Wilson, *et al.*, 2001). Therefore, it is not beyond the realms of possibility that the initial SR Ca^{2+} release underpinning the transient phase 1 constriction in isolated pulmonary artery rings may be mediated by the actions of NAADP. It is therefore important to investigate whether or not NAADP has a combinatorial role with cADPR in HPV. This could be achieved in the following manner:

- Radioligand binding assays have shown that the tissue levels of cADPR in pulmonary arteries are significantly increased by exposure to hypoxia (Wilson, *et al.*, 2001). Radioligand binding assays similar to those described in chapter 5 of this thesis could be used to examine whether hypoxia induces an increase in the levels of NAADP within pulmonary arteries and systemic arteries. Furthermore, by carrying out parallel investigations on the effects of hypoxia on levels of cADPR, it would be possible to examine whether there were differences in the time course over which alterations in the levels of NAADP and cADPR occur. By utilising this approach, one could examine whether a transient increase in NAADP was responsible, in part, for the transient phase 1 constriction, while a delayed increase in the production of cADPR underpins phase 2 constriction in isolated pulmonary arterial rings.

- If NAADP levels were seen to rise in pulmonary arteries in response to hypoxia, a series of small vessel myography experiments could be carried out to provide functional evidence in support of the findings of the radioligand binding assays. This could be achieved by incubating isolated pulmonary arterial rings with known antagonists of NAADP-mediated Ca^{2+} signalling (e.g. Bafilomycin A1 and GPN) before exposure to hypoxia and the resultant contractile responses could be compared to control responses elicited by hypoxia in the same tissue preparations in the absence of antagonists.

Recent investigations from this laboratory have identified that AMP-activated protein kinase (AMPK) serves to link mitochondrial inhibition by hypoxia to Ca^{2+} signalling in pulmonary artery smooth muscle cells (Evans, *et al.*, 2005). Thus, if the investigations described above indicated that NAADP and cADPR are involved in HPV it will be of importance to investigate whether AMPK couples to the production of NAADP and cADPR in pulmonary artery smooth muscle.

- Radioligand binding assays could be used to measure the increase in NAADP and cADPR levels within pulmonary arteries in response to hypoxia in the absence and presence of the AMPK inhibitor Compound C.

- A direct link between the production of both NAADP and cADPR and AMPK activation could be provided by use of the AMPK

mimetic AICA-riboside. Thus, assaying of the levels of NAADP and cADPR in pulmonary arteries in the absence and presence of AICA-riboside would give a clear indication as to whether the production of NAADP and cADPR was coupled to activation of AMPK in pulmonary artery smooth muscle cells.

7. What anchors lysosomes to the SR to form the trigger zone for NAADP signalling?

Junctophilins (JPs) are structural proteins which were first described in skeletal muscle where they serve a pivotal role in excitation-contraction coupling by maintaining a close association between the plasma membrane and the SR (Nishi, *et al.*, 2000; Takeshima, *et al.*, 2000). JPs are now believed to be important in maintaining junctional membrane complexes in a number of excitable cells. Indeed, to date there have been four JP subtypes identified (JP-1, JP-2, JP-3 and JP-4), with JP-1 expressed predominantly in skeletal muscle, JP-2 expressed in a number of muscle cells and JP-3 and JP-4 predominantly expressed in the brain (Nishi, *et al.*, 2003). Given the important role that JPs have in maintaining junctional complexes required for coherent Ca^{2+} signalling it is of importance to examine the possibility that one of the JP subtypes may be important in maintaining the structural integrity of the trigger zone for NAADP-dependent Ca^{2+} signalling in pulmonary artery smooth muscle.

- Initial studies would be required to examine which of the JP subtypes are expressed in pulmonary artery smooth muscle cells. This could be achieved through the use of sequence-specific antibodies raised to conserved sequences on each of the JP subtypes in Western blotting and immunocytochemical analysis.

- Once the identity of the JP subtypes present in pulmonary artery smooth muscle cells has been identified, quantitative immunocytochemical investigations could be carried out in order to examine the spatial distribution of those JP subtypes which are expressed within cells. Results presented within this thesis (Chapter 4) suggest that the trigger zone for NAADP-mediated Ca^{2+} signalling is likely located in the perinuclear region of pulmonary artery smooth muscle cells. Thus, a predominance of a given subtype of JP within the perinuclear region of cells may be indicative of a role in maintenance of the trigger zone.

- Immunocytochemical investigations could then be carried out to determine whether a given JP subtype associates with large areas of colocalisation between RyR3 and lysosomes, thus providing further evidence of a role for JPs in maintaining the structural integrity of the trigger zone.

8. Does NAADP alter the lysosomal or cytoplasmic pH in pulmonary artery smooth muscle cells?

It is clear from our investigations that NAADP causes Ca^{2+} release from lysosomal Ca^{2+} stores in pulmonary artery smooth muscle cells. It is not yet known, however, whether NAADP causes an alteration in the luminal pH within lysosomes in these cells, or indeed, whether NAADP results in an alteration of the cytoplasmic pH immediately surrounding NAADP-sensitive acidic Ca^{2+} stores. While alterations in the luminal pH of lysosomes may have important implications in proteolysis (Busch, *et al.*, 1996), alterations in cytoplasmic pH close to the trigger zone may have functional effects on the gating properties of RyRs, located in the trigger zone, which are involved in the amplification of initial Ca^{2+} bursts mediated by NAADP.

- Fluorescence imaging experiments could be designed to determine the effects of NAADP on the luminal pH of lysosomes using fluorescent indicator dyes which selectively partition into acidic stores as a function of their pH (i.e. Acridine orange, Lysosensor Green). These dyes undergo self-quenching upon aggregation, therefore monitoring their fluorescence intensity would provide information on the pH state of lysosomes. Thus, the effects of NAADP on lysosomal pH could be compared against known inhibitors of lysosomal function (such as Bafilomycin A1), protonophores (FCCP) and Ca^{2+} mobilising messengers (IP_3 and cADPR) which do not target lysosomal Ca^{2+} stores.

- Fluorescence imaging experiments could also be undertaken to examine the effects of NAADP upon the cytoplasmic pH in pulmonary artery smooth muscle cells by examining the effects of agents on the fluorescence of the pH indicator dye 5-FAM (carboxyfluorescein). These experiments could be performed in conjunction with Fura-2 fluorescence imaging to monitor Ca^{2+} signals generated within cells to examine whether Ca^{2+} signals are generated in areas of the cytoplasm where there are alterations in the cytoplasmic pH.

9. Why are IP_3Rs not involved in NAADP-mediated Ca^{2+} signalling in pulmonary artery smooth muscle cells?

Findings from this laboratory indicate that IP_3R-mediated Ca^{2+} release is not involved in the generation of global Ca^{2+} waves following intracellular dialysis of NAADP (Boittin, *et al.*, 2002; Chapter 3 of this thesis). The lack of involvement of IP_3Rs in the amplification of NAADP-generated Ca^{2+} bursts may be explained if IP_3Rs expressed in pulmonary artery smooth muscle were insensitive to activation by Ca^{2+}. The sensitivity of IP_3Rs to activation by Ca^{2+} could be examined in the following manner:

- The profile (i.e. the kinetics and amplitude) of Ca^{2+} signals generated by the liberation of caged Ca^{2+} by flash photolysis in

pulmonary artery smooth muscle cells preincubated with ryanodine could be analysed and compared to the profile of the Ca^{2+} signals generated following flash photolysis of caged Ca^{2+} after preincubation of cells with ryanodine +/- xestospongin C. If the presence of the IP_3R antagonist xestospongin C caused an inhibition of the Ca^{2+} signals observed in its absence then one could conclude that IP_3Rs in pulmonary artery smooth muscle cells were sensitive to CICR.

The lack of involvement of IP_3Rs in amplifying spatially restricted, NAADP-mediated Ca^{2+} bursts from lysosome-related Ca^{2+} stores into global Ca^{2+} waves may, therefore, be due to spatial separation of NAADP receptors and IP_3Rs in pulmonary artery smooth muscle cells. It is clear from the evidence presented in this thesis that lysosomes and portions of the SR expressing RyR3 form tight junctions proximal to the nucleus of pulmonary artery smooth muscle cells (Chapter 4; Kinnear, *et al.*, 2004). Thus, the ability of IP_3Rs to contribute to CICR could be limited by spatial compartmentalisation of cells. I could determine whether or not this is the case by examining the degree to which lysosomes associate with IP_3Rs in pulmonary artery smooth muscle cells:

- Western blotting using sequence-specific antibodies raised against the 3 known IP_3Rs could be used to identify the IP_3R subtypes present in pulmonary artery smooth muscle cells.

- Immunocytochemical investigations could then be used to determine the spatial distribution of those IP_3R subtypes identified as being present in pulmonary artery smooth muscle and the degree to which these subtypes colocalise with the lysosomal membrane glycoprotein αlgp120.

References Appendix 4:

Aquilla, E., Whelchel, A., Knot, H. J., Nelson, M. T. and Posada, J. (1996). Activation of Multiple Mitogen-activated Protein Kinase Signal Transduction Pathways by the Endothelin B Receptor Requires the Cytoplasmic Tail. *J. Biol. Chem.* **271,** 31572-31579.

Barone, F., Genazzani, A. A., Conti, A., Churchill, G. C., Palombi, F., Ziparo, E., Sorrentino, V., Galione, A. and Filippini, A. (2002). A pivotal role for cADPR-mediated Ca2+ signaling: regulation of endothelin-induced contraction in peritubular smooth muscle cells. *FASEB. J.* **16,** 697-705.

Boittin, F.-X., Galione, A. and Evans, A. M. (2002). Nicotinic Acid Adenine Dinucleotide Phosphate Mediates Ca2+ Signals and Contraction in Arterial Smooth Muscle via a Two-Pool Mechanism. *Circ. Res.* **91,** 1168-1175.

Busch, G. L., Lang, H. J. and Lang, F. (1996). Studies on the mechanism of swelling-induced lysosomal alkalinization in vascular smooth muscle cells. *Pflugers Arch.* **V431,** 690-696.

da Cunha, J. M., Rae, G. A., Ferreira, S. H. and Cunha, F. Q. (2004). Endothelins induce ETB receptor-mediated mechanical hypernociception in rat hindpaw: roles of cAMP and protein kinase C. *Eur. J. Pharmacol.* **501,** 87-94.

Dallas, A. and Khalil, R. A. (2003). Ca2+ antagonist-insensitive coronary smooth muscle contraction involves activation of epsilon-protein kinase C-dependent pathway. *Am. J. Physiol.* **285,** C1454-C1463.

Dipp, M., Nye, P. C. G. and Evans, A. M. (2001). Hypoxic release of calcium from the sarcoplasmic reticulum of pulmonary artery smooth muscle. *Am. J. Physiol.* **281,** L318-L325.

Evans, A. M., Mustard, K. J. W., Wyatt, C. N., Peers, C., Dipp, M., Kumar, P., Kinnear, N. P. and Hardie, D. G. (2005). Does AMP-activated Protein Kinase Couple Inhibition of Mitochondrial Oxidative Phosphorylation by Hypoxia to Calcium Signaling in O2-sensing Cells? *J. Biol. Chem.* **280,** 41504-41511.

Fellner, S. K. and Parker, L. A. (2004). Endothelin B receptor Ca2+ signaling in shark vascular smooth muscle: participation of inositol trisphosphate and ryanodine receptors. *J Exp Biol* **207,** 3411-3417.

Galione, A., White, A., Willmot, N., Turner, M., Potter, B. V. and Watson, S. P. (1993). cGMP mobilises intracellular Ca2+ in sea urchin eggs by stimlating cyclic ADP-ribose synthesis. *Nature* **365,** 388-389.

Giulumian, A. D., Meszaros, L. G. and Fuchs, L. C. (2000). Endothelin-1-induced contraction of mesenteric small arteries is mediated by ryanodine receptor Ca2+ channels and cyclic ADP-ribose. *J. Cardiovasc. Pharmacol.* **36,** 758-763.

Henriksson, M., Xu, C. B. and Edvinsson, L. (2004). Importance of ERK1//2 in upregulation of endothelin type B receptors in cerebral arteries. *British Journal of Pharmacology* **142,** 1155-1161.

Kinnear, N. P., Boittin, F.-X., Thomas, J. M., Galione, A. and Evans, A. M. (2004). Lysosome-Sarcoplasmic reticulum junctions: A trigger zone for calcium signalling by NAADP and endothelin-1. *J. Biol. Chem.* **279,** 54319-54326.

Lee, Y. H., ;, Kim, I., Laporte, R., Walsh, M. P. and Morgan, K. G. (1999). Isozyme-specific inhibitors of protein kinase C translocation: effects on contractility of single permeabilized vascular muscle cells of the ferret. *J. Physiol.* **517,** 709-720.

Mullaney, I., Vaughan, D. M. and MacLean, M. R. (2000). Regional modulation of cyclic nucleotides by endothelin-1 in rat pulmonary arteries: direct activation of Gi2-protein in the main pulmonary artery. *British Journal of Pharmacology* **129,** 1042-1048.

Nishi, M., Mizushima, A., Nakagawara, K. and Takeshima, H. (2000). Characterization of Human Junctophilin Subtype Genes. *Biochem. Biophys. Res. Commun.* **273,** 920-927.

Nishi, M., Sakagami, H., Komazaki, S., Kondo, H. and Takeshima, H. (2003). Coexpression of junctophilin type 3 and type 4 in brain. *Mol. Brain Res.* **118,** 102-110.

Takeshima, H., Komazaki, S., Nishi, M., Iino, M. and Kangawa, K. (2000). Junctophilins: A Novel Family of Junctional Membrane Complex Proteins. *Mol. Cell* **6,** 11-22.

Wilson, H. L., Dipp, M., Thomas, J. M., Lad, C., Galione, A. and Evans, A. M. (2001). ADP-ribosyl cyclase and cyclic ADP-ribose hydrolase act as a redox sensor: a primary role for cADPR in hypoxic pulmonary vasoconstriction. *J. Biol. Chem.* **276,** 11180-11188.

Wilson, H. L., Evans, A. M. and Galione, A. (1998). Cyclic AMP and cGMP differentially regulate the production of the calcium-mobilising metabolites, nicotinic acid adenine dinucleotide phosphate and cyclic ADP-ribose. *British Journal of Pharmacology* **124,** 30P.

Yamasaki, M., Thomas, J. M., Churchill, G. C., Garnham, C., Lewis, A. M., Cancela, J. M., Patel, S. and Galione, A. (2005). Role of NAADP and cADPR in the Induction and Maintenance of Agonist-Evoked Ca2+ Spiking in Mouse Pancreatic Acinar Cells. *Current Biology* **15,** 874-878.

Appendix 5:

Publications associated with this thesis:

Peer reviewed papers:

- Boittin, F.X., Dipp, M., Kinnear, N.P., Galione, A. and Evans, A.M. (2003) Vasodilation by the calcium-mobilising messenger cyclic ADP-ribose. *J. Biol. Chem.* **278**, 9602-9608.

- Kinnear, N.P., Boittin, F.X., Thomas, J.M., Galione, A. and Evans, A.M. (2004) Lysosome-sarcoplasmic reticulum junctions. A trigger zone for calcium signalling by nicotinic acid adenine dinucleotide phosphate and endothelin-1. *J. Biol. Chem.* **279**, 54319-54326.

- Evans, A.M., Wyatt, C.N., Kinnear, N.P., Clark, J.H. and Blanco, E.A. (2005) Pyridine nucleotides and calcium signalling in arterial smooth muscle: from cell physiology to pharmacology. *Pharmacol. Ther.* **107**, 286- 313.

- Evans, A.M., Mustard, K.J., Wyatt, C.N., Peers, C., Dipp, M., Kumar, P., Kinnear, N.P. and Hardie D.G. (2005) Does AMP-activated protein kinase couple inhibition of mitochondrial oxidative phosphorylation by hypoxia to calcium signalling in O2-sensing cells? *J. Biol. Chem.* **280**, 41504-41511.

- Evans, A.M., Mustard, K.J., Wyatt, C.N., Dipp, M., Kinnear, N.P. and Hardie D.G. (2006) Does AMP-activated protein kinase couple inhibition of mitochondrial oxidative phosphorylation by hypoxia to pulmonary artery constriction? *Adv. Exp. Med. Biol.* **580**, 147-154.

Published abstracts of oral presentations to learned societies:

- Kinnear, N.P., Boittin, F.X., Galione, A. and Evans, A.M. (2003) NAADP triggers 'Ca^{2+} bursts' by mobilising lysosome-related calcium stores in isolated rat pulmonary artery smooth muscle cells. *J. Physiol.* **552P**, C70

- Kinnear, N.P., Galione, A. and Evans, A.M. (2004) Lysosomes and Ryanodine receptors co-localise to form a 'trigger zone' for Ca^{2+} signalling by NAADP in isolated rat pulmonary artery smooth muscle cells. *J. Physiol.* **555P**, C139

- Kinnear, N.P., Thomas, J.M., Galione, A. and Evans, A.M. (2004) NAADP mediates Ca^{2+} signals by endothelin-1 in isolated rat pulmonary artery smooth muscle cells. *J. Physiol.* **560P**, C46

Published abstracts of poster presentations to learned societies:

- Kinnear, N.P., Wyatt, C.N., Jeyakumar, L.H., Fleischer, S., Nixon, G.F. and Evans, A.M. (*in press*) Lysosomes and ryanodine receptor subtype 3 colocalise to form a trigger zone for calcium signalling by NAADP in rat pulmonary artery smooth muscle cells. *Presented at the Winter Meeting of the British Pharmacological Society, University of Oxford, December 2006*